Peering into the Dark: Investigating dark matter and neutrinos with cosmology and astrophysics

Markus Rasmussen Mosbech
School of Physics
Faculty of Science
The University of Sydney

A thesis submitted in fulfilment of the requirements for the degree of Doctor of Philosophy

Year of award: 2023
Supervisors: Celine Boehm and Yvonne Y. Y. Wong

School of Physics
The University of Sydney
Physics Road
Camperdown NSW 2006
Australia
Email: markus.mosbech@sydney.edu

2023

Typesetting done with LaTeX 2$_\varepsilon$, BibLaTeX and the MEMOIR class.
Compiled using luaLaTeX.

Authorship and Originality

Parts of this thesis have previously been published in, or submitted to, scientific journals. They make up the chapters of Part II, presented with a short preamble for context, and only minor stylistic changes to match the rest of the thesis.

Chapter 5 is published as Ref. [1].

- Markus R. Mosbech et al. "The Full Boltzmann Hierarchy for Dark Matter-Massive Neutrino Interactions". In: *Journal of Cosmology and Astroparticle Physics* 2021.03 (Mar. 2021), p. 066. ISSN: 1475-7516. DOI: 10.1088/1475-7516/2021/03/066. arXiv: 2011.04206. URL: http://arxiv.org/abs/2011.04206 (visited on 26/05/2021)

I performed the derivations with input from co-authors, I also did the majority of the code implementation with some input from Julia Stadler, as well as the MCMC analysis. All co-authors participated in the writing of the final manuscript.

Chapter 6 is published as Ref. [2].

- Markus R. Mosbech, Celine Boehm and Yvonne Y. Y. Wong. "Probing Dark Matter Interactions with 21cm Observations". In: *Journal of Cosmology and Astroparticle Physics* 2023.03 (1st Mar. 2023), p. 047. ISSN: 1475-7516. DOI: 10.1088/1475-7516/2023/03/047. arXiv: 2207.03107. URL: http://arxiv.org/abs/2207.03107 (visited on 23/03/2023)

I performed all simulations and other calculations, and all authors contributed to discussions and writing the paper.

Chapter 7 is submitted to a journal, at the time of writing, an earlier draft is publicly released in the form of a preprint, Ref. [3].

- Markus R. Mosbech et al. *Gravitational-Wave Event Rates as a New Probe for Dark Matter Microphysics*. 2nd Aug. 2022. DOI: 10.48550/arXiv.2207.14126. arXiv: 2207.14126. URL: http://arxiv.org/abs/2207.14126 (visited on 03/08/2022). preprint

I performed the cosmological simulations and halo mass function analysis. All authors contributed to discussions and writing the paper.

Chapter 8 is published as Ref. [4].

- Markus R. Mosbech and Zachary S. C. Picker. "Effects of Hawking Evaporation on PBH Distributions". In: *SciPost Physics* 13.4 (25th Oct. 2022), p. 100. ISSN: 2542-4653. DOI: 10.21468/SciPostPhys.13.4.100. arXiv: 2203.05743. URL: http://arxiv.org/abs/2203.05743 (visited on 14/12/2022)

The paper is based on an idea by Zachary Picker, and the final content is the result of our discussions. I performed all calculations. We both participated equally in the writing.

Declaration of authorship

In addition to the statements above, in cases where I am not the corresponding author of a published item, permission to include the published material has been granted by the corresponding author.

Markus R. Mosbech
April 28, 2023

As supervisor for the candidature upon which this thesis is based, I can confirm that the authorship attribution statements above are correct.

Statement of originality

This is to certify that to the best of my knowledge, the content of this thesis is my own work. This thesis has not been submitted for any degree or other purposes.

I certify that the intellectual content of this thesis is the product of my own work and that all the assistance received in preparing this thesis and sources have been acknowledged.

Markus R. Mosbech
April 28, 2023

Acknowledgements

First of all, I would like to thank my scientific supervisors Celine Boehm and Yvonne Wong, for their support, guidance, and mentorship. They have made me the scientist I am today, and it is because of them that I am able to submit this work.

In like to extend this thanks the astroparticle group at The University of Sydney for providing a friendly, supportive, and above all fun environment. You have taught me a lot, and broadened my scientific horizons, Ciaran O'Hare, Zac Picker, Theresa Fruth, Ellen Sirks, Joseph Allingham, and everyone else who has passed through the group. This also includes my scientific collaborators near and far. It has been a pleasure to work with you, and I have learned a lot.

I would also like to thank my friends, and particularly the PhD student community at the School of Physics. You have made lunch (and the associated coffee break) a highlight of the day, and a compelling reason to leave the home office behind. So thanks for all the lunch breaks, coffee breaks, and trips to the pub. It's been great.

Finally, above all I would like to thank Cecilie, for coming with me on this journey and supporting me all the way through it. I could not have done this without you.

Moving across the world is never easy, especially when a global pandemic strikes, but you have all made it easier.

Thank you.

Abstract

The ΛCDM model of modern cosmology provides a highly accurate description of our universe. However, it relies on two mysterious "dark" components, dark matter and dark energy. The cold dark matter paradigm does not provide a satisfying description of its particle nature, nor any link to the Standard Model of particle physics. In this thesis, I will investigate the consequences for cosmological structure formation in models with a coupling between dark matter and Standard Model neutrinos, as well as probes of primordial black holes as dark matter.

Open questions still remain regarding the neutrinos of the Standard Model, in particular how they gain mass, and the exact values of their masses. Any interaction between neutrinos and dark matter would also be very difficult to probe in the lab, due to their weak coupling to other Standard Model particles. This provides motivation to investigate the possibility of such couplings through their impact on cosmological observables.

In the work presented in this thesis, I examine the impact that such an interaction would have through both linear perturbation theory and nonlinear N-body simulations. I present limits on the possible interaction strength from cosmic microwave background, large scale structure, and galaxy population data, as well as forecasts on the sensitivity of future observatories. I provide an analysis of what is necessary to distinguish the cosmological impact of interacting dark matter from similar effects, such as the free-streaming of warm dark matter. Intensity mapping of the 21 cm line of neutral hydrogen at high redshift using next generation observatories, such as the SKA, would provide the strongest constraints yet on such interactions, and may be able to distinguish between different scenarios causing suppressed small scale structure. I also present a novel type of probe of structure formation, using the cosmological gravitational wave signal of high redshift compact binary mergers to provide information about structure formation, and thus the behaviour of dark matter. Such observations would also provide competitive constraints.

Finally, I investigate primordial black holes as an alternative dark matter candidate, presenting an analysis and framework for the evolution of extended mass populations over cosmological time and computing the present day gamma ray signal, as well as the allowed local evaporation rate. This is used to set constraints on the allowed population of low mass primordial black holes, and the likelihood of witnessing an evaporation.

Contents

Authorship and Originality v

Acknowledgements vii

Abstract ix

Contents x

I Review 1

1 A brief introduction to modern cosmology 3
1.1 A simple universe: The ΛCDM model . . . 4
1.2 The expansion of the universe . . . 5
1.3 The history of the universe . . . 8
1.4 The evidence for dark matter . . . 15
1.5 Challenges to ΛCDM . . . 19

2 The dark matter model zoo 23
2.1 Thermal particle dark matter . . . 24
2.2 Axions and ultralight dark matter . . . 38
2.3 Primordial Black Holes . . . 44

3 Linear Cosmology 51
3.1 The perturbed Einstein equations . . . 52
3.2 The Boltzmann equation . . . 53
3.3 Collisionless species . . . 55
3.4 Interacting species . . . 61
3.5 Observables . . . 68
3.6 Initial Conditions . . . 75

4 Non-linear Structure Formation 77
4.1 N-body Simulations . . . 77
4.2 The Halo Model . . . 81
4.3 Halos in Simulations . . . 86
4.4 Beyond Cold Dark Matter . . . 88
4.5 Neutrinos and other hot dark matter . . . 90
4.6 Beyond Dark Matter . . . 91

II Research Works **93**

5 A linear treatment of dark matter-neutrino scattering **95**
5.1 Introduction . . . 96
5.2 The Boltzmann equation . . . 98
5.3 Modified Boltzmann equations in presence of neutrino-dark matter interactions . 99
5.4 Numerical results . . . 100
5.5 Conclusions . . . 105
5.A Derivation . . . 107
5.B Fluid Approximation . . . 113
5.C Parameter correlations . . . 114

6 Investigating the nature of dark matter with 21cm signals **119**
6.1 Introduction . . . 120
6.2 Dark matter scenarios . . . 122
6.3 The 21cm emission line . . . 124
6.4 Comparing interacting and warm dark matter scenarios . . . 127
6.5 Simulation results . . . 128
6.6 Conclusions . . . 131

7 Probing the nature of dark matter with gravitational waves **135**
7.1 Introduction . . . 136
7.2 Interacting dark matter . . . 138
7.3 Simulating structure formation . . . 139
7.4 Gravitational-wave event rates . . . 143
7.5 Summary and conclusion . . . 150

8 The evolution of extended primordial black hole distributions **153**
8.1 Introduction . . . 154
8.2 Evolving PBH distributions . . . 155
8.3 γ-ray constraints . . . 158
8.4 Black hole explosions . . . 162
8.5 Conclusions . . . 164

9 Conclusions **167**

Bibliography **169**

Part I

Review

CHAPTER 1

A brief introduction to modern cosmology

When speaking of physical cosmology it is commonly quoted that around 70% of the energy in the universe is some mysterious substance called 'dark energy', 25% is another similarly mysterious substance called 'dark matter', and finally, only 5% is the normal matter we know from our everyday life [5]. This sort of number might lead the mind to the quote from Socrates, oft paraphrased that he was the wisest of the Greeks, for only he knew that he knew nothing [6]. And indeed, most cosmologists would be under no illusions of what we know about our universe, but this 'well-known ignorance' does represent a much better understanding of the universe than we used to have. Dark matter would not become an accepted part of our standard picture of cosmology until the 1970s with rotation curve measurements from Vera Rubin, Albert Bosma, and others [7–13]. Dark energy was included again in the late 1990s when supernova observations showed evidence of the universe expanding at an accelerating rate [14, 15], after having previously falled out of favour as its initial purpose of counteracting cosmic expansion became redundant. This revealed to us yet more mysteries, and showed us how much we did not know.

However, knowing our ignorance about these components also presents us with an exciting challenge as scientists. What is an unknown component, but a question waiting for an answer? In particular, this thesis will focus on the question of what the dark matter could be, and how we can find an answer, questions to which I will be presenting my own contributions.

This thesis is presented in two distinct parts. In the first, I will present the context of my research, providing a brief overview of our picture of cosmology and the breadth of possible dark matter scenarios, as well as an introduction to some important techniques for cosmological research that I have made use of. The second part presents my own contributions to the field, consisting of four manuscripts, three of which have been published [1, 2, 4] and the fourth currently in review [3], each with a short introduction to place it in the context of this thesis.

The rest of this chapter will present a brief overview of ΛCDM cosmology, key pieces of evidence for the model, and the challenges facing it. This will be followed by chapters on different types of dark matter models (Chapter 2) as well as the methods used to compute predictions for these models in the linear and nonlinear regimes (Chapters 3 and 4). This forms a solid base for the presentation of my own work to investigate the nature of dark matter in Part II.

1.1 A simple universe: The ΛCDM model

Despite its marvellous complexity, the universe is in fact, perhaps surprisingly, very well described by a remarkably simple model, the so-called ΛCDM model of cosmology [16, 17]. The model can be fitted to large scale observables, such as the CMB and BAO to great precision using only six parameters, with modern experiments constraining several of these to percent-level precision [5]. Of course, the model was proposed to fit the data, so one could argue that it is behaving as expected, however it has made several successful predictions including the detection of polarisation in the CMB with the DASI experiment in 2002 [18], and later in Planck data [19], as well as the presence and location of the BAO in large scale structure with SDSS [20] and 2dFGRS [21] in 2005.

While the base ΛCDM model is fully described with only six parameters, $\{\omega_b, \omega_{dm}, \theta_s, \tau, A_s, n_s\}$, meaning respectively the baryon density, dark matter density, the angular size of the acoustic scale, the optical depth to reionisation, the amplitude of the primordial power spectrum, and the scalar spectral index. Other common parameters used to describe the model are H_0, the current value of the Hubble parameter, and σ_8 which quantifies the amplitude of matter fluctuation.

While this is the technical definition of the parameters used to define the model, it is perhaps useful to present the content and basic assumptions of the model. As the name implies, the model describes a universe whose matter budget today is dominated by two components: Λ, dark energy treated as a cosmological constant, and CDM, cold dark matter. Of course, the universe contains also baryonic ("normal") matter, as well as radiation, but as illustrated in Fig. 1.1, these components make up only a small part of the total energy content today.

The dark matter has been a generally accepted part of our models since the 1970–80s [13], and was theorised at least as early as 1904 by Lord Kelvin [22]. The concept of dark matter, meaning matter in space that is invisible to us, was investigated through the 20th century, early studies involved examining the motion of stars in the Milky Way, such as by Kapteyn [23], Lundmark [24], and Oort [25]. Fritz Zwicky applied the same thinking to larger scales, measuring the motion of galaxies in the Coma cluster [26–28]. Another key piece of evidence for the existence of dark matter was the rotation curves of galaxies, measured as early as 1939 [29], but in particular the work of Vera Rubin and others in the 1970s [7–12, 30] was key to showing that there was more matter in galaxies than could be seen.

The cosmological constant, despite its later acceptance into our current model, also has a long history, beginning with Einstein's inclusion of it to counteract a natural conclusion of general relativity: an expanding universe [31, 32]. However, with the discovery that the universe was indeed expanding [32–35], its inclusion seemed superfluous. The advent of quantum field theory brought the idea back, as the vacuum energy could indeed produce such a term, but the lack of observational evidence meant that its value would be many orders of magnitude smaller than predicted [36]. The cosmological constant would not be brought back until the late 1990s, when observational evidence for its effect on cosmic expansion was found [14, 15], despite its lack of concordance with the vacuum energy of quantum field theory. Since then, it has been a generally accepted, although mysterious, part of the cosmological model.

The exact natures of these two dominant components are still unknown and a large research effort goes into learning more about them, including the search for deviations from the non-interacting cold dark matter and cosmological constant paradigms. My own work, as found in Part II concerns the deviations from the cold dark matter paradigm in particular.

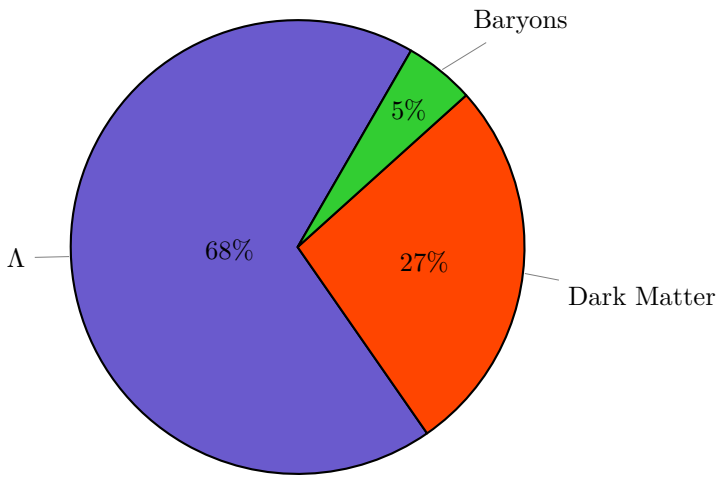

Figure 1.1: *The contents of the universe today, as inferred from the measurements of the Planck satellite [16]. It is evident that the energy density of the universe is dominated by dark energy (Λ) and dark matter, with baryons having a smaller contribution. The contribution from radiation is vanishingly small.*

1.2 The expansion of the universe

Since the observations by Hubble in the late 1920s [34], it has been widely accepted that the universe is expanding, as had indeed been predicted as a natural consequence of a non-empty universe in general relativity [31–33]. It follows by solving the Einstein field equations, written in tensor form as

$$G_{\mu\nu} - \Lambda g_{\mu\nu} = 8\pi G T_{\mu\nu}, \tag{1.1}$$

where $g_{\mu\nu}$ is the metric tensor, Λ is the cosmological constant, G is Newton's gravitational constant, $T_{\mu\nu}$ is the stress-energy tensor, and $G_{\mu\nu}$ is the Einstein tensor, given as

$$G_{\mu\nu} = R_{\mu\nu} - \frac{1}{2} R g_{\mu\nu}, \tag{1.2}$$

where $R_{\mu\nu}$ and R are the Ricci tensor and scalar, respectively, both of which are given from the metric tensor and its derivatives (via the Riemann tensor). In that sense, everything on the left hand side of Eq. (1.1) is determined by metric, i.e. the shape of spacetime, whereas the right hand side is given by the contents of the spacetime, as expressed by the stress-energy tensor.

The Friedmann-Lemaître-Robertson-Walker (FLRW) metric describes a spacetime with a maximally symmetric spatial part, and is given by

$$ds^2 = dt^2 - a(t)^2 \left[\frac{dr^2}{1 - kr^2} + r^2 \left(d\theta^2 + \sin^2 \theta d\phi^2 \right) \right], \tag{1.3}$$

where r, θ, and ϕ are the spatial coordinates, $a(t)$ is the cosmological scale factor, and k is a curvature parameter. It is motivated by the Cosmological Principle, which states that our universe is homogeneous and isotropic on large scales ($\gtrsim$100 Mpc). Specifically r is the comoving radial coordinate, with the physical radial coordinate given as $r_{\text{phys}} = a(t)r$. Sometimes, for convenience, the radial coordinate is reparameterised as $d\chi \equiv dr/\sqrt{1 - kr^2}$, giving the metric the form

$$ds^2 = dt^2 - a(t)^2 \left[d\chi^2 + f^2(\chi) \left(d\theta^2 + \sin^2 \theta d\phi^2 \right) \right], \tag{1.4}$$

For a flat ($k = 0$), open ($k < 0$), or closed ($k > 0$) universe, the function $f(\chi)$ is χ, $\sqrt{k}^{-1} \sinh\left(\sqrt{k}\chi\right)$, or $\sqrt{k}^{-1} \sin\left(\sqrt{k}\chi\right)$ respectively.

A homogeneous and isotropic universe, filled with a perfect fluid will have a stress-energy tensor given as

$$T_{\mu\nu} = (\rho + p)u_\mu u_\nu + p g_{\mu\nu}, \tag{1.5}$$

where ρ is the rest energy density of the fluid, and p is its pressure. It is common to express the relationship between ρ and p in terms of an equation of state parameter w, which is $1/3$ for relativistic fluids like photons, and 0 for cold, "dust like", species. Sometimes, the cosmological constant is absorbed into the stress-energy tensor with an equation of state $w = -1$. It is easy to see that inserting this into Eq. (1.5) yields only a scalar multiplied with the metric tensor, just as the cosmological constant term in Eq. (1.1).

Evaluating the time-time component of the Einstein equation for a homogeneous and isotropic universe will yield the well-known Friedmann equation,

$$\left(\frac{\dot{a}}{a}\right)^2 = \frac{8\pi G}{3}\rho - \frac{k}{a^2}, \tag{1.6}$$

while the spatial components yield the acceleration equation,

$$\frac{\ddot{a}}{a} = -\frac{4\pi G}{3}\left(\rho + 3P\right), \tag{1.7}$$

where ρ and P are the sum of energy density and pressure respectively, for all components in the universe, including the cosmological constant. The expansion rate is generally described in terms of the Hubble parameter, $H \equiv \frac{\dot{a}}{a}$.

Another common expression of the Friedmann equation is component-wise in terms of dimensionless density parameters normalised to the critical density today. The critical density is defined as the energy density required to have a flat universe, meaning $k = 0$,

$$\rho_{\mathrm{crit},0} = \frac{3H_0^2}{8\pi G}, \tag{1.8}$$

and the density of component i is then given as

$$\Omega_{i,0} \equiv \frac{\rho_{i,0}}{\rho_{\mathrm{crit},0}}, \tag{1.9}$$

where the subscript 0 signifying 'today' is often omitted for simplicity and only implied. This parameterisation is useful, since the density of most components have a simple evolution in terms of the scale factor. Matter (both dark and baryonic) has an energy density dominated by its rest mass, its energy density will therefore be proportional to the number density of particles which scales inversely to the volume, hence $\rho_m \propto a^{-3}$. Since the energy density of radiation is dominated by the kinetic energy of the particles, which is redshifted, its energy density scales as $\rho_r \propto a^{-4}$. The a^{-2} scaling of curvature is already evident in Eq. (1.6), and the cosmological constant does not scale, as implied by the name. Using the common convention that $a_0 = 1$, the Friedmann equation can thus be written as,

$$\frac{H^2}{H_0^2} = \frac{\Omega_{r,0}}{a^4} + \frac{\Omega_{m,0}}{a^3} + \Omega_{\Lambda,0} - \frac{k}{H_0^2 a^2}, \tag{1.10}$$

where sometimes the curvature is expressed in terms of a "curvature energy density", defined as $\Omega_{k,0} \equiv -k/H_0^2$. Another way of expressing the curvature term is through a "radius of curvature" R_0 and a curvature sign κ, with $k = \kappa/R_0^2$.

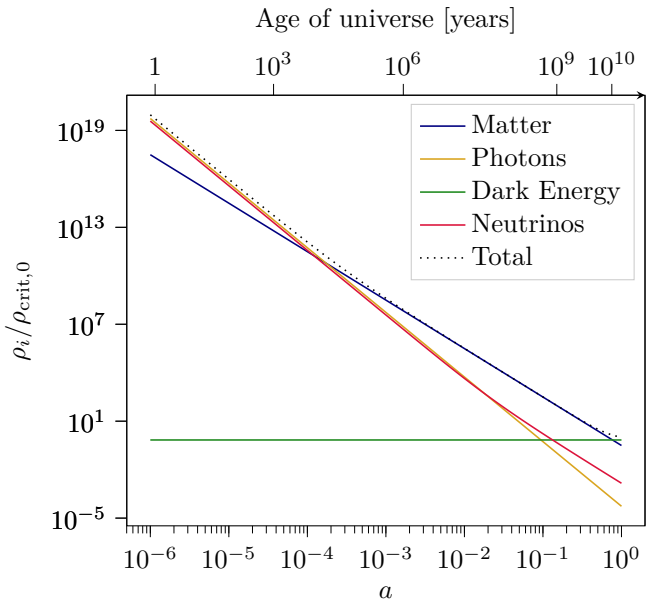

Figure 1.2: *The evolution of the density of various components of the universe. The neutrinos are included using the approximation of two massless species, and one of $m_\nu = 0.06$ eV.*

As implied by the different scalings with the scale factor, these components will generally be dominant at different points in the history of the universe, as illustrated in Fig. 1.2. Here it is also evident from how the photon and neutrino lines deviate at late times that, unlike the other species, neutrinos do not have a simple power law evolution.[1] This is due to having a small, but nonzero mass, as implied by the measurement of neutrino oscillations [37, 38]. In the early universe, their kinetic energy will be much larger than their mass, and they will therefore behave as radiation, however, as the universe expands and the neutrinos lose kinetic energy to redshift, their mass will become the dominant component of their energy, and they will behave like matter.

Another implication of Eq. (1.10) it that the expansion rate can be roughly separated into different epochs, depending on which component dominates the energy budget. If the universe is dominated by a single component, the expansion rate will generally be a simple function of time, i.e. $a \propto t^{2/3}$ in a matter-only universe, $a \propto t^{1/2}$ in a radiation-only universe, and exponential expansion in a Λ-only universe. This expansion rate will affect how global processes in the universe proceed. The extent to which these components dominate at a given time is illustrated in Fig. 1.3, assuming parameters similar to our universe.

Our universe is either spatially flat, or with only a very small curvature component [5], its evolution after inflation is therefore generally separated into three epochs: radiation domination until $a \sim 3 \cdot 10^{-4}$, when the universe was roughly fifty thousand years old. This point in time is called matter-radiation equality, and is followed by a long period of matter domination, until $a \sim 0.77$, when the age of the universe was around ten billion years, the matter density was overtaken by dark energy, though they are still of the same order of magnitude. Some argue that this means we are at a special time in cosmic history, which they find problematic, dubbing it the "coincidence problem" [39]. If the universe keeps expanding as expected, this means that we are on the cusp of an epoch truly dominated by the dark energy component, leading to an

[1] In principle this is true for any species transitioning from being relativistic to nonrelativistic, but for baryons this happens too early to be included here, and is generally neglected for dark matter in the cold dark matter paradigm.

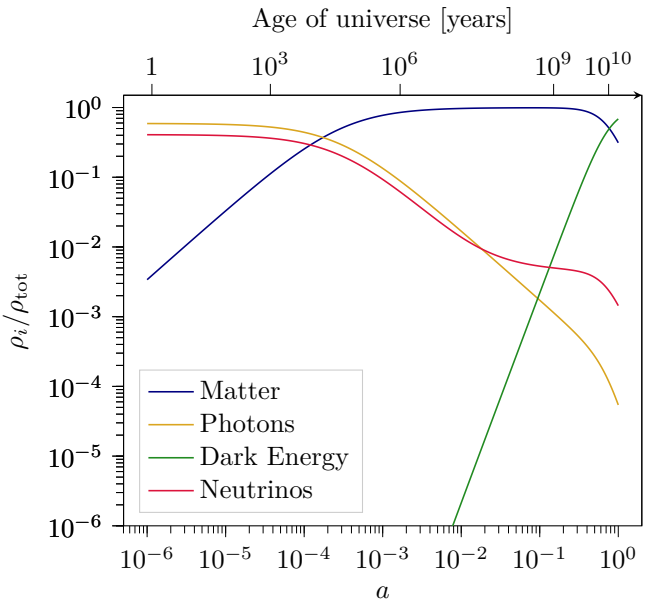

Figure 1.3: *The evolution of the relative density of various components of the universe.*

exponential increase of the scale factor over time.

1.3 The history of the universe

Many stories can be neatly divided into a beginning, a middle, and an end. This is not so straightforward with a universe like ours. If you look at "events" that significantly affect the makeup of the universe, these initially happen very quickly in succession, before the universe remains essentially unchanged, except for expansion, for quite a while before the next "event". In a universe such as ours, without a "big crunch" or "big rip", expansion may just continue forever. Astrophysical processes will continue over the next trillions of years [40], dynamical systems will continue to lose energy to gravitational waves over very long timescales, and black holes may emit Hawking radiation for even longer [41], and in the absence of proton decay, dense, cold remnants of white dwarfs may end as supernovae in the very far future [42]. While these scenarios are theoretically interesting, they are by definition not accessible to observations without waiting extremely long, therefore, this section will mainly be concerned with the history of our universe from its beginning until the present day.

1.3.1 Inflation and Reheating

It is extraordinarily hard to say anything definite about the beginnings of the universe. The generally accepted baseline model is that of a "hot big bang", where the universe started in a very hot, dense state, as would indeed be implied by Fig. 1.2. This idea was championed by Georges Lemaître, who argued that it was not unnatural for the universe to have a beginning [43–45].

The first "event" is often taken to be inflation. The content of the universe is generally described as having been in a very dense state of quantum fluctuations before this, but the energy scale is too high and the epoch too inaccessible to observations to make meaningful statements. Inflation then, is a period of rapid expansion at very early times, which was proposed to solve several puzzles of cosmology [46–49], including the horizon problem and the flatness problem.

The horizon problem is the fact that the universe is very homogeneous on large scales, for example the CMB temperature being constant to one part in ten thousand across the whole sky, despite the fact that these regions could not have been in causal contact in the past, assuming a "normal" expansion history without inflation.

The flatness problem is the fact that our universe appears to be very close to flatness, if not completely without curvature. Some argue that this is a problem of fine tuning, because as close as we are to flatness today, the deviation from flatness must have been even smaller in the past, and values so close to zero would not be "natural". Specifically, the deviation from flatness is given from Eq. (1.10) as

$$1 - \Omega(t) = -\frac{k}{a^2 H^2}, \tag{1.11}$$

with the evolution of a and H implying that the deviation from flatness scales as $\propto t$ during radiation domination and $\propto t^{2/3}$ during matter domination. This means that if the deviation from flatness today is $|1 - \Omega_0| \leq 0.2$, then it would be $\lesssim 10^{-4}$ at matter-radiation equality, $\lesssim 10^{-14}$ at big bang nucleosynthesis, and $\lesssim 10^{-60}$ when the age of the universe was the Planck time, $\sim 10^{-32}$ seconds [50].

Both of these problems are neatly solved by inflation. The very rapid expansion of space by several orders of magnitude would allow the whole observable universe to have been in causal contact prior to this, and the observed homogeneity is thus no longer an issue.

If the expansion of space during inflation is dominated by a component with an equation of state parameter $w \leq -1/3$, the deviation from flatness will decrease. For the case of exponential expansion, it will decrease as $\propto e^{-2Ht}$. If the expansion is fast enough, meaning a large enough H, it will suppress $|1 - \Omega_0|$ by many orders of magnitude, leaving the observable universe close to flatness even if it had fairly strong curvature prior to inflation.

How exactly inflation happened (if it is the correct solution) remains an open question, though. I will here present a simple example of slow-roll inflation, as shown in e.g. Ref. [51]. In the simplest models, only a single scalar field ϕ, the inflaton, is introduced. The density and pressure of the fluid are given by

$$\rho_{\bar{\phi}} = \frac{\dot{\bar{\phi}}^2}{2} + V\left(\bar{\phi}\right), \tag{1.12a}$$

$$p_{\bar{\phi}} = \frac{\dot{\bar{\phi}}^2}{2} - V\left(\bar{\phi}\right), \tag{1.12b}$$

where homogeneity and isotropy dictate that the main component of the scalar field, $\bar{\phi}$ is only time dependent.

Following the acceleration equation, Eq. (1.7), for positive acceleration we must have $\rho_{\bar{\phi}} + 3p_{\bar{\phi}} < 0$, i.e.

$$\dot{\bar{\phi}}^2 - V\left(\bar{\phi}\right) < 0, \tag{1.13a}$$

$$\dot{\bar{\phi}}^2 < V\left(\bar{\phi}\right), \tag{1.13b}$$

for inflation to occur. If the inflaton is the dominant component of the universe, as expected in inflation, this then gives the Friedmann equation

$$H^2 = \frac{8\pi G}{3}\left(\frac{\dot{\bar{\phi}}^2}{2} + V\left(\bar{\phi}\right)\right), \tag{1.14}$$

and the equation of motion of the inflaton field,

$$\ddot{\bar{\phi}} + 3H\dot{\bar{\phi}} + \frac{\partial V\left(\bar{\phi}\right)}{\partial \phi} = 0. \tag{1.15}$$

The next step is ensuring that inflation continues long enough to actually solve our cosmological problems, requiring a great enough expansion of the universe. This is usually measured in e-folds, how many factors of e the universe grows during inflation.

Unless the universe contains phantom energy (dark energy with equation of state parameter $w < -1$), for a universe containing matter or radiation, the Hubble parameter will always decrease as the universe expands. The requirement for inflation is therefore that this decrease is slow enough to allow the requisite number of e-folds. The condition for inflation can be parameterised in terms of

$$\epsilon_H \equiv -\frac{\dot{H}}{H^2}, \tag{1.16}$$

and since the acceleration of the scale factor can be written as $\ddot{a} = a\left(\dot{H} + H^2\right)$, ϵ_H must be less than 1 to have positive acceleration, and $\epsilon_H = 1$ is thus the condition for the end of inflation.

The timescale of one e-fold is the Hubble time, H^{-1}. The condition $\epsilon_H < 1$ thus implies that the timescale over which the Hubble parameter changes appreciably is significantly longer than a Hubble time. The requisite number of e-folds is ~ 40–60, for which ϵ_H must be kept less than 1.

The rate of change of ϵ_H can be parameterised as

$$\eta_H \equiv \frac{\dot{\epsilon_H}}{H\epsilon_H} = \frac{\mathrm{d}\ln\epsilon_H}{\mathrm{d}N}, \tag{1.17}$$

the logarithmic change in ϵ_H per e-fold. For a slow enough change to ϵ_H, it is therefore necessary that $|\eta_H| \ll 1$, meaning a roughly constant Hubble parameter during inflation, leading to a roughly exponential expansion similar to a universe dominated by a cosmological constant. Observations put the limits on these parameters at $\epsilon_H < 0.1$ and $\eta_H \sim 0.03 \pm 0.01$ [51, 52].

In standard show-roll inflation, the initial conditions of the rest of the universe's evolution is set by this exponential expansion imprinting the pre-inflation quantum fluctuations, leading to the so-called primordial curvature perturbations being described by the dimensionless power spectrum,

$$\Delta^2_{\mathcal{R}}(k) = \left(\frac{H^2}{2\pi\dot{\phi}^2}\right)^2\Bigg|_{k=aH} = \frac{1}{8\pi^2\epsilon_H}\frac{H^2}{M^2_{\mathrm{Pl}}}\Bigg|_{k=aH}, \tag{1.18}$$

the power spectrum being the RMS fluctuation squared of the (density) field. It is described in greater detail in Chapters 3 and 4. Since H changes slightly as different scales k cross the horizon, a slight time dependece is introduced, leading to a tilt of the power spectrum given by the scalar spectral index n_s,

$$n_s - 1 \equiv \frac{d\ln\Delta^2_{\mathcal{R}}(k)}{d\ln k}, \tag{1.19}$$

which can be computed from the slow roll parameters,

$$n_s - 1 = -2\epsilon_H - \eta_H. \tag{1.20}$$

Defining our quantities in terms of the pivot scale k_*, and neglecting any k-dependence in n_s (usually called running), the quantities used to describe the primordial power spectrum can be defined,

$$A_s \equiv \frac{1}{8\pi^2}\frac{H^2_*}{\epsilon_{H*}M^2_{\mathrm{Pl}}}, \tag{1.21a}$$

$$n_s \equiv 1 - 2\epsilon_{H*} - \eta_{H*}, \tag{1.21b}$$

where the subscript $*$ indicates that the quantity is evaluated when the pivot scale k_* exits the horizon, yielding an initial power spectrum given as,

$$\Delta^2_{\mathcal{R}}(k) = A_s \left(\frac{k}{k_*}\right)^{n_s - 1} . \tag{1.22}$$

More complicated inflation models, such as multi-field inflation or ultra slow roll can have more complicated initial power spectra.

As inflation comes to an end, it is generally assumed to be followed by a period of reheating. The inflaton field will decay, the energy release from which heats up the universe after the cooling induced by the inflationary expansion. This decay could also account for the creation of the current particle content of our universe [51].

1.3.2 Big Bang Nucleosynthesis

To end up with a population of baryons, an asymmetry between baryons and antibaryons must be introduced. This can happen in a multitude of ways, the viabilities of which depend on the exact conditions of reheating, including via Grand Unified Theory interactions, the electroweak phase transition, or leptogenesis, where lepton flavour violations can induce baryon number violations.

As the universe cools down, the temperature drops below the QCD scale, leading to the quark confinement and the formation of nucleons. With the temperature dropping even further, the conditions for producing stable atomic nuclei arose, as the density was large enough for nuclear interactions, but the temperature was low enough that any formed nuclei were not instantly destroyed by gamma rays or other energetic particles. This epoch is known as big bang nucleosynthesis (BBN) [53–63].

At early times, the temperature of the universe was large compared to the mass difference between protons and neutrons, their densities were essentially the same, as they were coupled the neutrinos and so kept in equilibrium, given through the usual [62, 63]

$$\left(\frac{n_n}{n_p}\right)_{\text{eq}} = \left(\frac{m_n}{m_p}\right)^{3/2} e^{-(\overbrace{m_n - m_p}^{\equiv Q})/T}, \tag{1.23}$$

the mass difference between being $Q = 1.30$ MeV. The processes maintaining this equilibrium are,

$$n + \nu_e \leftrightarrow p^+ + e^-, \tag{1.24a}$$
$$n + e^+ \leftrightarrow p^+ + \bar{\nu}_e, \tag{1.24b}$$

which are efficient until the temperature drops below ≈ 0.7 MeV.

When the neutrinos decouple around $T \sim 1$ MeV, the balance has started to tilt slightly in the favour of protons, but neutrino decoupling happens before the neutron population becomes completely Boltzmann suppressed, and a relic population is frozen in,[2] with around 15% of the nucleons being neutrons. However, had the conditions not been right for nucleosynthesis at this time, the neutrons would all have disappeared anyway, as they are unstable, decaying through,

$$n \to p^+ + e^- + \bar{\nu}_e, \tag{1.25}$$

with a lifetime around 15 minutes. While this does not sound like much cosmologically speaking (or conversely, an incredibly long time for particle physics processes and the very early universe), it is in fact roughly the same timescale as BBN happens on.

[2] To avoid repeating myself too much, I will not go into great detail on freeze-out here. A more detailed description of freeze-out is presented in the context of dark matter production in Section 2.1.

Fortunately for our existence, this means that stable nuclei are able to form before the neutrons all decay away, with the free neutrons and protons able to form stable deuterium,

$$n + p^+ \leftrightarrow \mathrm{D} + \gamma \tag{1.26}$$

which then acts as a building block for heavier elements, via helium,

$$\mathrm{D} + p^+ \leftrightarrow {}^3\mathrm{He} + \gamma \tag{1.27a}$$

$${}^3\mathrm{He} + \mathrm{D} \leftrightarrow {}^4\mathrm{He} + p^+, \tag{1.27b}$$

with nearly all the neutrons in the universe ending up in helium nuclei in the end.

Since formation of all heavier nuclei relies on deuterium, the production of deuterium forms the bottleneck to their production rates. A key ingredient to determining how much is produced of any element is thus determining the balance between deuterium production and neutron decay. What determines this balance is the rate at which the deuterium will get destroyed by photons, which is governed by the baryon-to-photon ratio, $\eta \approx 6 \cdot 10^{-10}$. Because this is such a small number, the high-energy tail of the photon distribution will still comprise enough photons to keep the deuterium population down until the temperature is significantly lower than the deuterium binding energy, $B_\mathrm{D} = 2.22$ MeV, with the equilibrium density given through,

$$\left(\frac{n_\mathrm{D}}{n_p}\right)_\mathrm{eq} \approx \eta \left(\frac{T}{m_p}\right)^{3/2} e^{B_\mathrm{D}/T}. \tag{1.28}$$

Once the left-hand side reaches unity[3], which happens at $T_\mathrm{nuc} \sim 0.07$ MeV, deuterium production becomes very efficient, with knock-on effects for helium and the heavier nuclei, as illustrated in Fig. 1.4. This corresponds to a time of $t_\mathrm{nuc} \sim 250$ s. This is not too large compared to the neutron lifetime, but large enough that neutron decay reduces the number of free neutrons by $\sim 25\%$ between freeze-out and t_nuc.

It is useful to describe the abundances of different isotopes as fractions of the total nucleon density,

$$X_i = \frac{n_i}{\sum_j A_j n_j}, \tag{1.29}$$

where A_j is the nucleon number of isotope j, such that the mass fraction of an isotope is (to good approximation) $A_i X_i$. At early times, the sum can be simply approximated as $n_p + n_n$, and after BBN as $n_p + 4n_\mathrm{He}$. Since (nearly) all the neutrons end up in ^{4}He, the helium abundance will be roughly half the neutron abundance at t_nuc, yielding a helium mass fraction $\sim 25\%$, which is very close to the result of a more careful calculation solving the coupled Boltzmann equations for all involved species, [62, 65]

$$Y_\mathrm{P} = 0.2262 + 0.0135 \ln\!\left(\eta/10^{-10}\right), \tag{1.30}$$

with a larger baryon-to-photon ratio leading to a larger helium abundance, as this lets protons and neutrons form deuterium earlier.

Since BBN predictions are based on fairly well-known nuclear physics, and the abundances of isotopes can be measured observationally, BBN provides an independent probe of cosmology, and can be used to set constraints on e.g. the number of relativistic species.

BBN results generally agree with other cosmological measurements, such as CMB, but notably the predicted lithium abundance does not match measurements. This is known as the lithium problem, and proposed solutions include observational systematics, unknown nuclear physics resonances, or new physics [66].

[3] Slightly more accurately $\mathcal{O}(10^{-3})$, as this is already large enough to begin efficient helium production. In fact, the deuterium fraction never becomes much larger than that because its further conversion into helium happens so quickly [62].

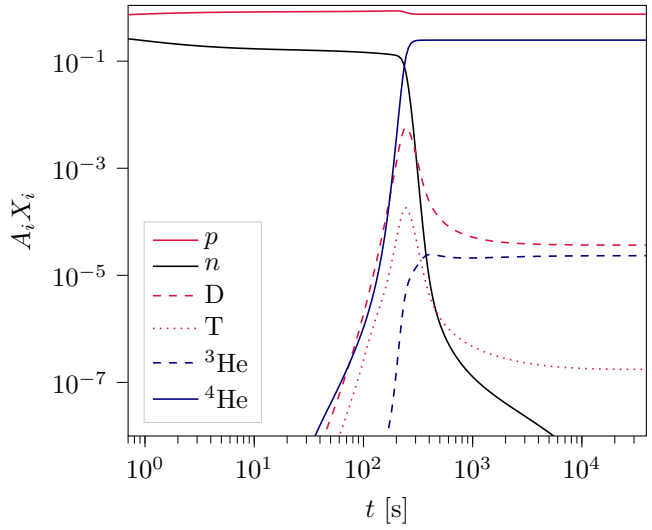

Figure 1.4: *The evolution of the abundances of different elements during BBN. It is clear that production of helium starts as soon as deuterium is formed, and that this quickly depletes the deuterium abundance. abundances computed with PRIMAT [64, 65].*

1.3.3 Recombination

In terms of learning about the contents of our universe, recombination is perhaps the most significant epoch of its evolution, as this is what gives rise to the cosmic microwave background.

In terms of basic processes, recombination is conceptually similar to BBN. As the temperature of the cosmic fluid drops, it becomes possible for electrons and nuclei to form neutral atoms that are not immediately ionised by the background photons. In another parallel with BBN, this happens well below the temperature one would naively expect from the electronic binding energies of hydrogen and helium, again because of the small baryon-to-photon ratio.

In a simplified description, neglecting helium, the free electron fraction can be defined as [62],[4]

$$x_e = \frac{n_e}{n_e + n_{\mathrm{H}}}. \tag{1.31}$$

Since the electrons and protons are strongly coupled via the photons, the neutral hydrogen density will follow its equilibrium value,

$$\left(\frac{n_{\mathrm{H}}}{n_e^2}\right)_{\mathrm{eq}} \approx \left(\frac{2\pi}{m_e T}\right)^{3/2} e^{E_I/T}, \tag{1.32}$$

where $E_I = 13.6$ eV is the ionisation energy of hydrogen. Recombination is therefore well described by the Saha equation,

$$\left(\frac{1-x_e}{x_e^2}\right)_{\mathrm{eq}} = \frac{2\zeta(3)}{\pi^2}\eta\left(\frac{2\pi T}{m_e}\right)^{3/2} e^{E_I/T}, \tag{1.33}$$

which has the analytical solution for x_e,

$$x_e = \frac{\sqrt{1+4f}-1}{2f}, \tag{1.34}$$

with the auxillary function f,

$$f(T,\eta) = \frac{2\zeta(3)}{\pi^2}\eta\left(\frac{2\pi T}{m_e}\right)^{3/2} e^{E_I/T}. \tag{1.35}$$

[4] Since the universe is neutral, $n_e = n_p$.

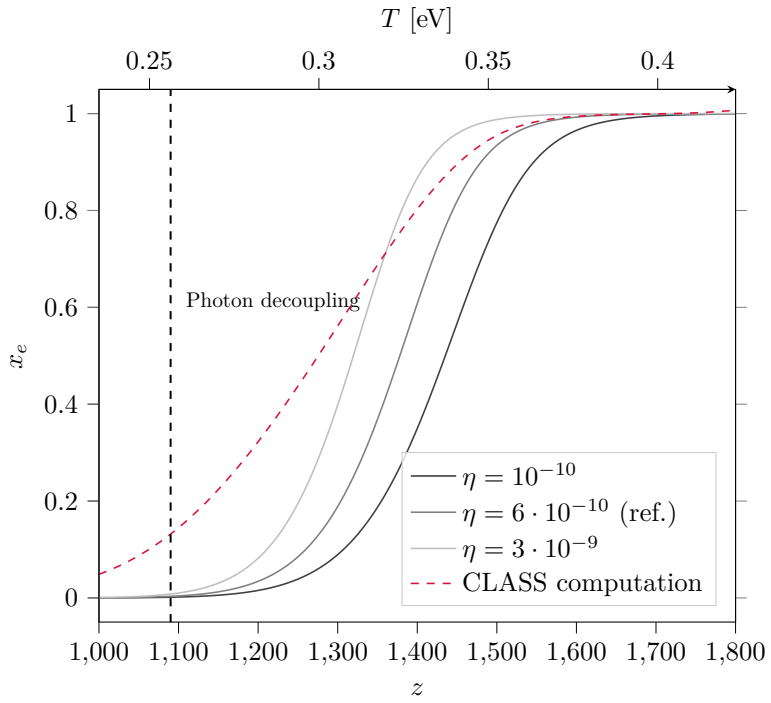

Figure 1.5: *The free electron fraction for a simplified recombination considering only hydrogen, as computed from the Saha equation, Eq.* (1.33)*. It is clear that the baryon-to-photon ratio η is a key parameter in determining the time of recombination. Full Boltzmann treatment from CLASS [67] (using HyREC [68]) included for comparison. The latter includes a treatment of the most relevant energy levels in the hydrogen and helium atoms, using effective transition operators to model absorption and emission of photons at multiple energies.*

This makes recombination a gradual process, the timing of which depends on η, illustrated in Fig. 1.5.

As the universe becomes dominated by neutral hydrogen rather than charged protons and electrons, with the latter dominating the interaction with photons through Thomson scattering, the photons will decouple and begin free-streaming, like the neutrinos did around the start of BBN. As recombination is not instantaneous, neither is photon decoupling. However, the latter is usually defined as when the scattering rate, $\Gamma_\gamma = n_e \sigma_T$, drops below the Hubble rate, where $\sigma_T = 6.65 \cdot 10^{-25}\,\mathrm{cm}^2$ is the Thomson cross-section. The full calculation yields a decoupling redshift around $z_{\mathrm{dec}} \approx 1090$. Photon decoupling corresponds well to the last scattering surface of CMB photons, observing the CMB can therefore give great insight into what the universe was like at this time.

To obtain the high-precision recombination predictions needed for sub-percent-level accuracy in CMB predictions, a more careful treatment of recombination is required [62]. Beyond including helium, this involves taking the multiple energy levels of different electron excitations into account, as well as their different modes of decay. This would naively entail solving a large number of coupled Boltzmann equations, one for each electronic state. However, a simple three-level atom approximation was proposed by Peebles in the 1960s [69]. This was followed by a more thorough treatment of multiple states, where degenerate states were approximated to be in equilibrium [70, 71]. An even more accurate treatment that retains the computational efficiency tracks only the few most relevant states, and compensates by using effective transition rates rather than the true physical ones. There are multiple modern implementations of this effective multi-level atom

approximation, such as HyREC [68, 72] and CosmoRec [73]. For a more detailed treatment of computing CMB predictions, see Chapter 3.

1.3.4 Reionisation and Cosmic Dawn

Directly after recombination comes the so-called dark ages, generally referred to this way because not much new light is being emitted, although the background radiation that is to become the CMB remains ever present. These cosmological relic photons have decoupled and are free-streaming, the baryons will decouple from the photons not too long after, and the matter overdensities are still relatively modest. However, just because it is "dark" does not mean that nothing is happening. Dark matter overdensities continue to grow, while the baryons, now free of the photon pressure, are free to fall into these increasingly deep gravitational wells.

Here we transition from the regime of linear structure formation described in detail in Chapter 3 into the nonlinear regime covered in Chapter 4.

Eventually, around $z \sim 30$ to ~ 15, enough gas has fallen into the dark matter potential wells that the first proto-galaxies can start to form, and on even smaller scales, the gas has cooled down enough to form molecular hydrogen, and may further collapse to form the first stars. This is rapidly followed by the first supernovae, and the first quasars beginning to accrete gas, further bringing new light to the universe, the cosmic dawn [74–81]. All these local processes bring a departure from the comparatively simple physics that has dominated the universe until this point. Suddenly, the "messy" physics of star formation, radiative feedback, and galaxies become the drivers of cosmological evolution in a universe that is highly inhomogeneous and can no longer be described by nice global properties. Even so, we like to try.

The cosmic dawn eventually brings about the epoch of reionisation, generally thought to have lasted until $z \sim$ 5-6, where the radiation emitted from bright stars, supernovae and quasars ionise the intergalactic medium, leading it to once again scatter CMB photons, albeit at a highly reduced rate, compared to pre-recombination. Nevertheless, reionisation leaves a significant signature on the observed CMB, as described in Section 3.5.2.

Probing these eras is a key goal for several current and upcoming experiments, such as HERA, SKA, and JWST [80–85], and may be crucial for distinguishing between different dark matter models, as described in Chapter 6, which also contains a description of the neutral hydrogen 21cm signal, an important observable of these epochs.

After reionisation is completed, we are essentially in the modern universe of stars, galaxies, and all the other weird and wonderful things we observe. Of course, the mysterious components of the ΛCDM model are still at work, with the universe entering its Λ dominated era at $z \sim 0.3$, and dark matter remaining key to the evolution of galaxies.

1.4 The evidence for dark matter

Despite its elusive nature, there is a wealth of evidence for the existence of dark matter on a variety of scales, from universe-wide effects such as the CMB [5] down to the size of dwarf galaxies [86] and within our own galaxy [87], however, the fact that dark matter is only detected through its gravitational effects have led some to suggest that our theory of gravity should be modified instead [88–90]. I will keep the focus on the evidence for the existence of dark matter rather than delving deeper into these alternative theories.

1.4.1 CMB evidence for dark matter

The cosmic microwave background was emitted when the universe was $\sim 370,000$ years old, as the density and temperature of the universe dropped enough for the photons and baryons to decouple. A characteristic length scale was imprinted in the CMB based on how far the coupled plasma managed to travel before this decoupling[5], via the baryon acoustic oscillations. This imprint is measured in the anisotropy of the CMB, despite its incredible uniformity, there are fluctuations on the order of $\sim 10^{-4}$ K, which are left by the over- and underdensities around the recombination era. The amplitude, in addition to the aforementioned size, can tell us a lot about the content of the universe.

The structures found in the CMB anisotropies are perhaps best described through the angular power spectrum, illustrating the strength and scales of the correlations across the sky. The temperature autocorrelation (TT) power spectrum looks remarkably different, depending on the dark matter content of the universe, as illustrated in Figs. 1.6 and 1.7. It is evident that changing the dark matter content $\Omega_{\rm cdm}$, substituting either Ω_b or Ω_Λ leads to drastically different sprectra. It is clear that the CMB can tell us not just how much matter, or how much baryonic matter, is in the universe, but actually give us an accurate picture of the amounts of both baryonic and dark matter. This is of course dependent on having accurate enough measurements of the CMB power spectrum, but such measurements have been firmly established [5, 16, 17, 19, 91, 92].

The baryons and dark matter thus have different effects on the physics of baryon acoustic oscillations, as one might expect. Changing the baryon to photon ratio will change the sound speed of the coupled plasma, which affects the ratio of the height of odd peaks to even peaks. This is because the odd peaks correspond to oscillation modes that have experienced one more contraction than expansions (the large first peak being one contraction only, no expansions), while even peaks represent models that have experienced an equal number. With a significant baryon fraction, an asymmetry is introduced, leading to a greater contraction than expansion, thus leading to the difference between odd and even peaks. The baryon to photon ratio can also be determined from BBN with high precision measurements of the deuterium abundance [93–95], providing an independent check on the value inferred from the CMB.

Unlike the baryons, the dark matter does not couple directly to the photons, and is thus not part of the oscillating plasma. Instead, the dark matter contributes to the matter to radiation ratio, and the gravitational potential. In particular, the amount of dark matter will determine when matter radiation equality happens. This is important because the baryon acoustic oscillations will behave differently in radiation and matter dominated epochs, namely, the amplitude of oscillations is enhanced during radiation domination, and a larger dark matter density thus decreases the overall amplitude. It is distinguishable from the effect of changing the baryon density in how it affects odd and even peaks, namely the fact that the measured second and third peak are of roughly even height, as illustrated in Fig. 1.6, is a clear piece of evidence for the existence of dark matter.

With the level of precision measurements of the CMB temperature and polarisation power spectra obtained from WMAP [91, 96–98] and Planck [5, 92, 99–101], one piece of very compelling evidence for the existence of dark matter is firmly established. The different effects of baryonic and non-baryonic batter is also key to the conclusion that the dark matter is not just non-luminous baryons, such as dark gas or rogue planets. This is backed up by big bang nucleosynthesis, which places strong bounds on the amount of baryons, which agree with CMB results. It really must be a different type of matter.

[5] There are some additional subtleties to this epoch, which will be presented in more detail in Chapter 3

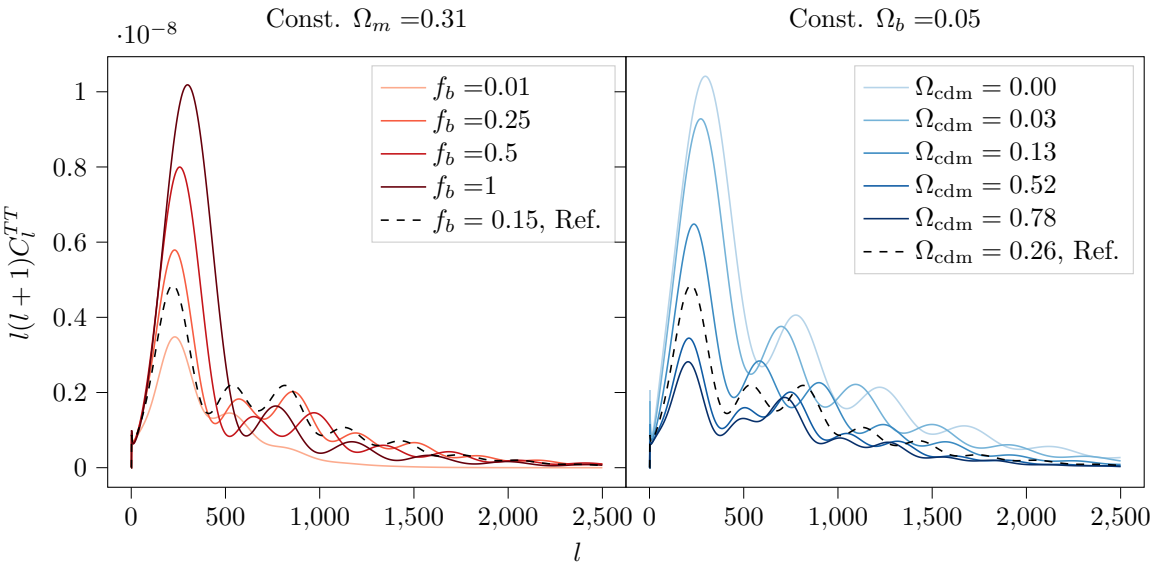

Figure 1.6: *The impact on the CMB TT spectrum of changing the baryon fraction while keeping the total matter density constant (left) as well as changing the dark matter density while keeping the baryon density constant (right). In the latter, the Hubble rate today is kept constant, while Ω_Λ varies to maintain flatness. Ref. notes the values inferred from observations [5].*

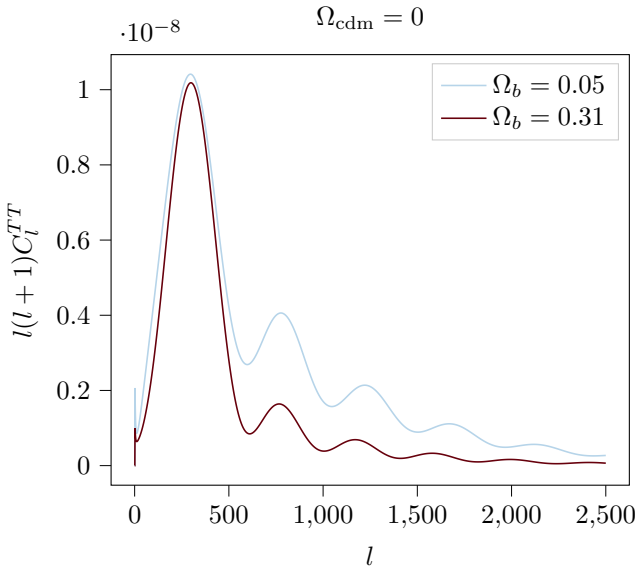

Figure 1.7: *Comparison of the CMB TT spectrum for two universes with no dark matter, light blue has baryon density equal to our universe, dark red has baryon density equal to our universe's matter density.*

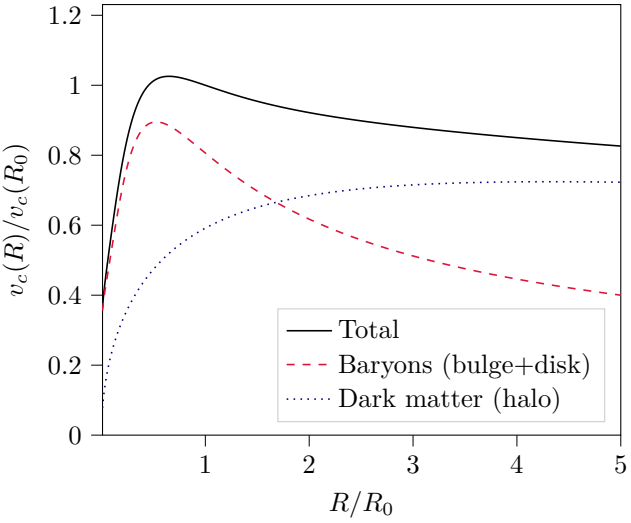

Figure 1.8: *A normalised rotation curve for a Milky Way-like galaxy consisting of a baryonic bulge+disk and a dark matter halo, computed using galpy [103]. It is clear that the contribution from the dark matter halo dominates at large radii.*

1.4.2 Dynamics as evidence for dark matter

One of the first pieces of evidence for dark matter was in the form of galactic rotation curves, as measured by Vera Rubin [7, 8] and Albert Bosma [9, 10, 12]. The gist of their finding was that outer parts of galaxies showed much larger mass-to-light rations than expected, essentially, the outer parts of galaxies had dynamics dominated by non-luminous matter. This conclusion is of course also backed up by modern observations of rotation curves [102]. A rotation curve for a Milky Way-like galaxy is illustrated in Fig. 1.8.

Galactic rotation curves using the circular velocities of spiral galaxies are not the only type of whose kinematics provide evidence for the existence of dark matter. Other examples includes the motion of galaxies in clusters [28], as well as Milky Way satellites [104], and velocity dispersions in dwarf galaxies [105–108], providing dynamical evidence for dark matter at multiple scales.

1.4.3 Lensing as evidence for dark matter

Following the evidence for the presence of dark matter from CMB and kinematics, the mass inferred from other types of measurements can be predicted. Fortunately for the ΛCDM model, measurements of gravitational lensing confirm the existence of dark matter on the scales that can be probed, with the cluster 1E0657-558[6], perhaps better known as the Bullet Cluster, acting as a particularly photogenic piece of evidence [109–111]. Some authors even go so far as to call it "direct empirical proof" that dark matter exists [111].

Gravitational lensing, the "bending" of light by gravity, is an important prediction of general relativity. If the magnitude of this effect can be measured, the mass of the "lens" can be inferred [112–114]. Going beyond point-masses, this also makes it possible to measure a mass distribution. A suitably placed light source behind a galaxy or cluster will therefore enable a mass measurement independent of the dynamics, thus lending more credence to any findings, if they agree.

[6] Also has the designation 1E0657-56.

There are two main avenues for determining the mass of astrophysical structures using gravitational lensing, known as weak and strong lensing, respectively. Conveniently, this designation just denotes whether the effect of the lensing is strong enough to be immediately recognisable. Strong lensing yields visibly distorted images, multiple images of sources, or both [115–125]. Weak lensing only slightly perturbs the visible shapes of background sources, and while their intrinsic shapes are unknown, the correlation between these distortions versus random alignments allows the lensing to be inferred statistically [109, 113, 126–129].

1.5 Challenges to ΛCDM

One could argue that the unknown quantities, the cold dark matter and dark energy of ΛCDM ought to pose a challenge to the model. However, in the context of a phenomenological description of the universe, it does not really matter that the model provides no explanation. The non-interacting cold dark matter and cosmological constant dark energy serve as a baseline for further studies of both, as any true particle physics model can be quantified by its differences from the standard CDM or cosmological constant predictions, and both can be compared with data, so the better fit can be determined. The ΛCDM model does not purport to be the correct theory, merely a miminal model to accurately describe cosmological observations, to be replaced when a better model is found.

There are, however, a few real challenges to the model [130–132], namely observations that do not fit the ΛCDM predictions, or sets of observations that are in conflict if the underlying model is ΛCDM. These offer an interesting opportunity for testing alternative cosmological models, as these might ease the tensions or explain away the so-called problems.

1.5.1 The Hubble Tension

One of the most discussed challenges is the so-called Hubble tension, where late universe measurements of the cosmological expansion rate (e.g. from supernovae) do not match the value inferred from early universe measurements (e.g. CMB) [130, 133–136]. This could also be an indication of a deeper problem with the FLRW metric, which the ΛCDM is generally assumed to rely on.

The main two measurements in tension are the value inferred from Planck measurements of the CMB [5], and the supernova-based measurements of the SH0ES collaboration [137–139],

$$H_0 = 67.44 \pm 0.58\,\mathrm{km\,s^{-1}\,Mpc^{-1}} \qquad \text{(Planck)} \tag{1.36a}$$

$$H_0 = 74.03 \pm 1.42\,\mathrm{km\,s^{-1}\,Mpc^{-1}} \qquad \text{(SH0ES)}, \tag{1.36b}$$

These measurements offer two fundamentally different ways of probing the Hubble parameter, and it is therefore difficult to disentangle whether it is new physics or systematics at play.

The local measurements of the SH0ES collaboration represent a direct measurement of the Hubble parameter today from the luminosity distance to type 1a supernovae. Such measurements rely on both the observational model for the supernovae as standardizable candles, and the Cepheid-based distance ladder. This type of measurements is therefore independent of cosmological model, but may be subject to observational systematics.

The CMB experiments on the other hand, do not directly measure H_0, but rather the angular size of the sound horizon at recombination, which can be used to compute the Hubble parameter today based on a cosmological model. This has been a testing bed for a multitude of models changing early universe physics to give a sound horizon at recombination consistent with the H_0 measured today. This includes a variety of models introducting modified dark energy,

dark matter, or additional radiation, as well as time-varying "constants"[134, 136]. Of course, the Planck CMB measurement is not immune to unknown systematics either.

The problem does go deeper than just these two measurements, with several other late-universe measurements not based on Cepheids agreeing with the SH0ES measurement, and measurements of baryon acoustic oscillations (the scale of which is also set by the sound horizon at recombination) combined with BBN agreeing with the Planck measurement, as well as non-Planck CMB measurements [134].

Many of the proposed models have shown some ability to ease the tension, though in some cases just by increasing the error bars, or at the cost of inconsistency with other observations. In particular, many solutions would make the σ_8 tension worse. So far none have been convincing enough to replace the base ΛCDM model, but searching for solutions to this problem remains an active area of research.

1.5.2 The σ_8 tension

A similar tension between different experiments appears in the σ_8 parameter[7], a measure of the matter power spectrum smoothed on a scale of 8 Mpc, given through,

$$\sigma_8^2 = \int_0^\infty \frac{dk}{k} \Delta^2(k) W^2(k \cdot 8\,\mathrm{Mpc}), \tag{1.37}$$

where W_8 is a window function, generally taken to be a real space tophat.

This tension is mainly between the value inferred from the Planck measurements [5] of the CMB, and the value from cosmic shear measurements of large scale structure [131, 140–142].

Similarly to the Hubble parameter, the σ_8 inferred from CMB measurements is not a direct observable, but rather a model dependent inferred parameter. It is found by fitting a cosmological model to the observed CMB anisotropies, and computing its structure formation predictions at late times. This means that the tension can generally be alleviated by models that suppress structure on the relevant scales, such as the dark matter-neutrino interaction model described in Chapter 5.[8]

1.5.3 The "small scale crisis"

Finally, there are a variety of small-scale (sub-galactic) challenges to ΛCDM that have collectively been termed the "small scale crisis" [143–145]. These problems are known as the "missing satellites", "cusp-core", and "too-big-to-fail" problems [146, 147].

The missing satellites problem refers to a mismatch between the number of satellite galaxies predicted by numerical simulations for a Milky Way-like galaxy, and the number of Milky Way satellites actually observed. Simulations using standard cold dark matter would overpredict the number, leading to them being claimed "missing". As with many such issues, the problem could have several types of solution. Perhaps least interesting is the possibility of the problem being numeric in nature, maybe our simulations were just not accurate enough, neglecting some effect or making improper approximations. In particular, it is possible that these structures are blown apart by supernovae. Another explanation for the problem would be observational in nature, perhaps the satellites are there, but we just haven't been able to see them yet due to the limitations of our instruments, similarly, it is predicted that many are very faint and thus not yet expected to be detectable. This solution is be backed up by the steady increase of detected Milky

[7] Sometimes reparameterised as $S_8 \equiv \sigma_8 \sqrt{\Omega_m/0.3}$.

[8] The interaction strengths required to solve the σ_8 tension would eventually be ruled out, as described in Chapter 7.

Way satellites. Finally, and perhaps most interesting, is the possibility that this problem offers a hint to the true physics of the dark matter, beyond the noninteracting cold approximation. Indeed, several types of models, such as warm dark matter, and dark matter interacting with relativistic species, yield lower predictions for the Milky Way satellite count [148, 149].

The cusp-core problem refers to the structure of the inner dark matter halo, namely, if the density profile is "cuspy" or "cored." Cold dark matter simulations predict that the cores of halos will have a steep, "cuspy", density profile, such as an NFW, with $\rho(r) \propto r^{-\gamma}$ and $\gamma \approx 0.8$-1.4 (for more detail on simulations and halo profiles see Chapter 4). However, measurements of the rotation curves of low-mass dark matter dominated systems seem to indicate a much flatter, "cored", central density profile with $\gamma \approx 0$-0.5. Again, there are proposed solutions both within ΛCDM and by introducing new physics. Within ΛCDM a likely culprit is expected to be baryonic effects. Many simulations include only collisionless matter, including baryons only as through their gravitational contribution. With baryonic matter making up a significant part of the density at the centres of halos, it is very possible that feedback from the baryons would alter the potential, giving rise to cored halos. The inclusion of more accurate modelling baryons in simulations is also a field of active research, with the different implementations yielding different results [150, 151]. There are also dark matter models offering to solve this problem, in particular models of warm or self-interacting dark matter have been put forth as solutions, with simulations showing flatter, shallower central densities.

The too-big-to-fail problem is in some sense related to that of missing satellites. Namely, accepting that we might not be able to observe all the Milky Way satellites, the most massive satellite halos should host galaxies. Thus, the central masses of the most massive satellite halos predicted by simulations should match the halos of massive satellite galaxies that we observe. Essentially, these simulated dark matter halos would be too big to fail to have star formation to produce an observable satellite galaxy. Unfortunately for ΛCDM, the most massive satellites we observe do not match with those predicted by simulations, not just for the Milky Way, but also Andromeda [147]. Again, a likely culprit is missing baryon physics in simulations, which could include tidal stripping and shocks, which would reduce the satellites' central mass. Again, warm and self interacting dark matter have both been put forward as possible solutions, as they will both help to lower the central masses.

CHAPTER 2

The dark matter model zoo

Based on our observations and understanding of gravity, the majority of matter in our universe must be invisible, or in other words, dark. This poses a challenge to our model of particle physics, since none of the known particles can satisfy the requirements. A simplified list of these requirements could be stated as [152, 153],

- Dark matter must exist in the right abundance to explain observations, $\sim 27\%$ of the total energy budget today [16].
- Dark matter must be produced in the early universe, so it can leave its imprints on e.g. CMB and structure formation.
- Any dark matter cross-section with Standard Model particles must be small enough to escape direct and indirect detection, as well as collider constraints. This implies a scattering cross-section $\sigma \lesssim 10^{-41}$ cm^2 for GeV-scale particles, although it can be much larger for very heavy dark matter candidates [154].
- Dark matter must be long-lived enough that it still exists today, to explain local phenomena such as galactic rotation curves.

The whole truth is of course more complicated than this. For instance, it could be proposed that the role of dark matter could be played by Standard Model neutrinos. These were produced in copious amounts in the early universe, are stable, and interact only weakly with the rest of the Standard Model. Indeed, this very idea has been suggested [155, 156], though it runs into problems with the neutrinos being too light [157] and their fast motion preventing the formation of the structures we observe in the universe [158], though it was long theorised that such a "hot" component could be a significant part of a mixed dark matter scenario [159–165].

More recent results show that the role played by massive Standard Model neutrinos, and hot dark matter in general, must be fairly modest when it comes to the makeup of the universe today, letting cosmology set very tight bounds on the sum of neutrino masses [166–170], and future observations are set to improve this [171–176].

It would have been nice to have an explanation for dark matter already in the Standard Model. However, this is unfortunately not the case for the universe we live in. Instead, it is necessary to think up something else to explain the unseen mass. This generally necessitates new particle species, though primordial black holes have also been suggested as an option [177–180],

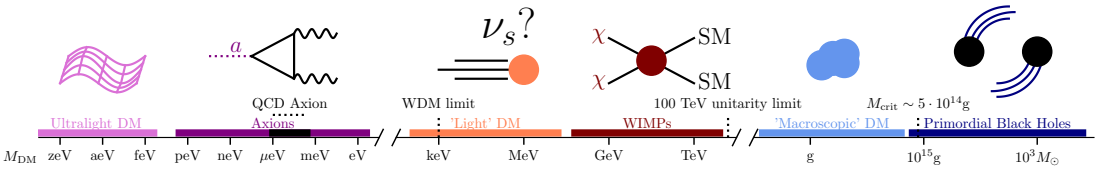

Figure 2.1: *The wide spectrum of possible dark matter masses, encompassing a range of different model types. The cartoons illustrate possible candidates in these regimes.*

as well as modifications to our theory of gravity [88]. In this chapter, I will attempt to provide a broad overview of the different types of proposed dark matter model. I will in general describe classes of models with similar cosmological phenomenology, rather than present the minute details of every single particle physics model.

One of the key properties of a dark matter model is the mass of the associated particle(s). There is an extremely wide spectrum of possible masses for different types of model, which is illustrated in Fig. 2.1, showing the range of possible masses from ultralight "wave-like" dark matter, to the extremely heavy models, such as primordial black holes, where the dark matter is no longer described as traditional particles.

2.1 Thermal particle dark matter

The typical idea of dark matter is some heavy particle that does not interact too much. However, it needs to somehow be produced in the early universe, and end up with the correct relic density. One of the simplest ways of doing this is through thermal production, where the dark matter is produced from some particle in thermal equilibrium, which can either be through freeze-out of dark matter particles initially in equilibrium with the standard model, or the annihilation or decay of a particle in thermal equilibrium, i.e. freeze-in [154].

Perhaps the most widely assumed type of model is the so-called WIMP, an acronym for Weakly Interactive Massive Particle [152, 153, 181]. The clue is in the name here, that it does exactly what we need from dark matter: have mass without interacting too strongly. The slightly stronger term "thermal WIMP" implies production through thermal mechanisms, leading to stronger constraints on allowed masses and cross-sections.

One of the most popular types of WIMPs, historically has been the lightest neutralino, a term for a neutral fermionic superpartner of the gauge Bosons in a supersymmetric model [152, 182], however, this stems mainly from "convenience". If you already have a well motivated theory extension, such as supersymmetry, which provides you with a particle fulfilling your needs, there is no need to make up new particles or theories [183–189]. A similar argument can be made for axions as dark matter, since their existence is motivated by solutions to the CP problem, they also offer a convenient dark matter candidate [190, 191], which will be covered in Section 2.2.

2.1.1 Production Mechanisms

An important reason for the popularity of the WIMP is the so-called "WIMP miracle". This describes the fact that a particle with a weak-scale mass and coupling to the Standard Model would provide the correct relic density to be the dark matter, if thermally produced[1] in the early universe via freeze-out[152, 153, 181, 192–196].

[1] In this case, production is perhaps a bit of a misnomer, as the dark matter particle is assumed to already exist in copious amounts in the thermal plasma, continually being produced and destroyed as it remains in equilibrium.

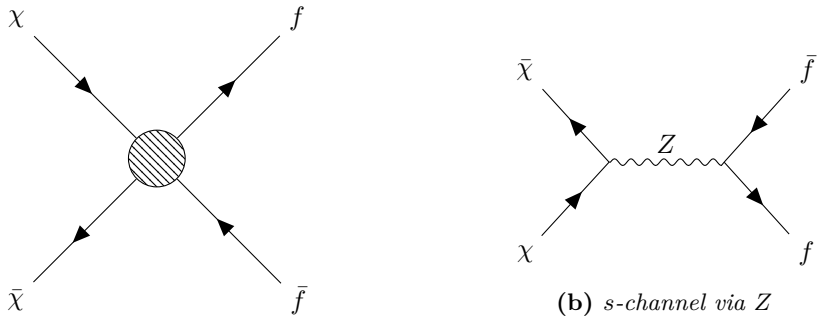

(a) *Generic* **(b)** *s-channel via Z*

Figure 2.2: *Feynman diagrams showing the process of WIMP annihilation to Standard Model Fermions, through generic (Fig. 2.2a) or s-channel (Fig. 2.2b) interactions.*

This can easily be shown using the Boltzmann equation for particle number density. We assume a simple model where dark matter particles χ can annihilate into Standard Model Fermions f,

$$\chi\bar{\chi} \to f\bar{f}, \tag{2.1}$$

as shown with the Feynman diagram in Fig. 2.2, which proceeds with some interaction rate Γ. In general, this can be computed using the annihilation cross-section times velocity, using the squared matrix element [197],

$$\sigma_{\chi\chi} v = \frac{1}{16\pi s} \sum_{s_i, s_j} \frac{|\mathcal{M}|^2}{(2s_i+1)(2s_j+1)}, \tag{2.2}$$

where $s_{i,j}$ are the spins of the incoming particles. The matrix element depends on the exact annihilation channel, and how it is mediated. An overview of different possibilities is presented in Ref. [197]. For simplicity, I will just use a single possibility as an example, the Z-Boson s-channel annihilation as presented in Ref. [198], but other commonly suggested channels are through W-bosons, or new bosons e.g. Z'.

For an s-channel annihilation process, the non-relativistic annihilation cross-section via a Z-Boson is [198]

$$\sigma_{\chi\chi}(T \ll m_\chi) = \frac{\pi\alpha^2 m_\chi^2}{c_w^4 m_Z^4}, \tag{2.3}$$

where α is the fine structure constant $\approx 1/137$, and since the dark matter particles are assumed to be non-relativistic, their velocity can be roughly approximated to be

$$v_\chi = \sqrt{\frac{2T}{m_\chi}}, \tag{2.4}$$

using the standard kinetic energy relation.[2]

In a freeze-out scenario, the WIMP starts out coupled to the thermal bath of the Standard Model particles. The number density of WIMPs will therefore follow the equilibrium density, as long as this coupling remains efficient. The condition for efficient coupling being $\Gamma > H$, where H is the Hubble parameter. Generally, as the temperature and density decrease due to

The important condition is maintaining equilibrium until the population is suppressed the right amount to end up with the correct relic density.

[2]The quantity $\sigma_{\chi\chi} v$ should not generally be split, but the approximation works out in this case.

cosmic expansion, the ratio Γ/H will also decrease, and the WIMP will decouple once it reaches $\Gamma(T_{\rm dec}) = H(T_{\rm dec})$, thus also defining the decoupling temperature $T_{\rm dec}$.

The interaction rate before freeze-out is given as

$$\Gamma \equiv \sigma_{\chi\chi} v_\chi n_\chi = \sigma_{\chi\chi} \sqrt{\frac{2T}{m_\chi}} \left(\frac{m_\chi T}{2\pi}\right)^{3/2} e^{-m_\chi/T}, \tag{2.5}$$

with the WIMP number density being the equilibrium density of a non-relativistic particle

$$n^{(\rm eq)}(T) = g \int \frac{d^3p}{(2\pi)^3} \frac{1}{e^{E/T} \pm 1} \overset{\text{non-rel.}}{=} g \left(\frac{mT}{2\pi}\right)^{3/2} e^{-m/T}, \tag{2.6}$$

where g is the number of degrees of freedom and the $\pm$ being for Fermions/Bosons respectively, but is irrelevant for non-relativistic decoupling. The velocity comes from Eq. (2.4).

The dark matter freeze-out would be happening deep in the radiation dominated era, such that $\rho_{\rm tot} \approx \rho_{\rm r}$ (species that normally count as matter may even be relativistic enough to contribute as radiation). The energy density of radiation can be expressed in terms of temperature and the effective degrees of freedom as,

$$\rho_{\rm r} = \frac{\pi^2}{30} g_{\rm eff}(T) T^4, \tag{2.7}$$

so the Hubble rate can be expressed in terms of the Planck mass $M_{\rm Pl}$ as

$$H^2 = \frac{\pi g_{\rm eff}}{90} \frac{T^4}{M_{\rm Pl}}. \tag{2.8}$$

Thus, having both the interaction rate and the Hubble parameter in terms of temperature, equating these makes it possible to identify the decoupling (freeze-out) temperature $T_{\rm dec}$. It is useful to express this in terms of the inverse temperature parameter $x \equiv m_\chi/T$, yielding

$$e^{-x_{\rm dec}} = \frac{\pi^{5/3}}{m_\chi M_{\rm Pl} \sigma_{\chi\chi}} \sqrt{\frac{g_{\rm eff}(T_{\rm dec})}{10}}, \tag{2.9}$$

which for the electroweak cross-section Eq. (2.3) gives

$$e^{-x_{\rm dec}} = \frac{\pi^{3/2}}{3\alpha^2} \frac{c_w^4 M_Z^4}{m_\chi^3 M_{\rm Pl}} \sqrt{\frac{g_{\rm eff}(T_{\rm dec})}{10}}. \tag{2.10}$$

For a decoupling temperature on the order of tens of GeV, the number of relativistic degrees of freedom is $\sim \mathcal{O}(100)$, taking the Standard Model particles into account. A rough estimate of the decoupling temperature and x is shown in Fig. 2.3, and an analytic approximation was presented in Ref. [199] for particle masses with mass MeV–$\mathcal{O}$(GeV),

$$x_{\rm dec} \approx 17.2 + \ln\left(\frac{g}{\sqrt{g_{\rm eff}}}\right) + \ln\left(\frac{m_\chi}{\rm GeV}\right) + \ln\sqrt{x_{\rm dec}}, \tag{2.11}$$

where g is the dark matter particle's number of internal degrees of freedom.

From knowing the decoupling temperature this makes it possible to compute the number density at decoupling using Eq. (2.6), and thus also the energy density, as $\rho_\chi = m_\chi n_\chi$ in the non-relativistic case. Namely,

$$n_\chi(T_{\rm dec}) \approx 10^3 \frac{m_Z^4}{M_{\rm Pl}} \left(\frac{T(T_{\rm dec})}{M_\chi}\right)^{3/2}. \tag{2.12}$$

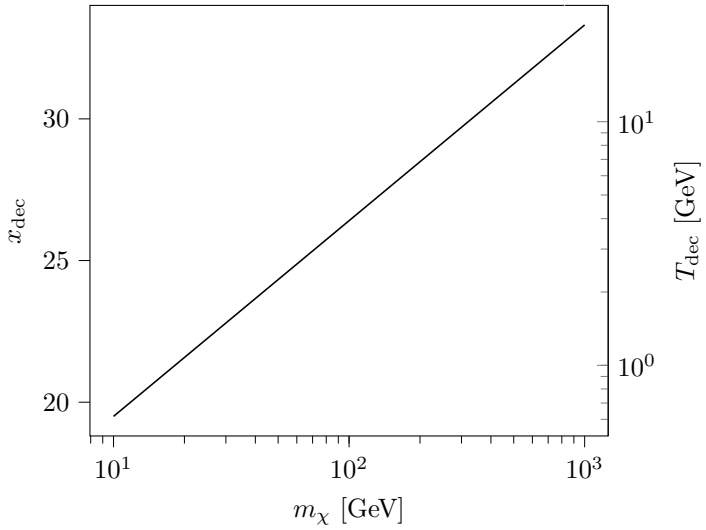

Figure 2.3: *A rough estimate of the decoupling temperature as a function of mass for a massive relic interacting via the electroweak force.*

Being a standard non-relativistic species, once the dark matter decouples from the thermal bath and no more particles are created or annihilated, the energy density will just evolve as a^{-3}, however it is tricky to a priori determine the scale factor a at decoupling. Instead, one can use the adiabatic cooling of the thermal bath, and its temperature today, T_0, as $aT \sim$ const.. This relation holds as long as the number of degrees of freedom is constant, over such a large change in temperature, this yields a factor

$$\left(\frac{a_{\mathrm{dec}}T_{\mathrm{dec}}}{a_0T_0}\right)^3 = \frac{g_{\mathrm{eff}}(T_0)}{g_{\mathrm{eff}}(T_{\mathrm{dec}})} \approx \frac{1}{28}. \tag{2.13}$$

With this correction, the energy density today can be computed to be

$$\rho_\chi(T_0) = \left(\frac{a_{\mathrm{dec}}T_{\mathrm{dec}}}{a_0T_0}\right)^3 \frac{T_0^3}{T_{\mathrm{dec}}^3} m_\chi n_\chi(T_{\mathrm{dec}}), \tag{2.14}$$

which combined with Eq. (2.12) yields a density parameter today depending only on m_χ,

$$\Omega_\chi h^2 \approx 0.12 \left(\frac{13\,\mathrm{GeV}}{m_\chi}\right)^2. \tag{2.15}$$

This tells us that a particle interacting through a completely standard electroweak coupling, with a weak-scale mass (13 GeV) neatly gives us the exact right dark matter density, which is measured to be $\Omega_{\mathrm{cdm}}h^2 \approx 0.12$ to percent precision [5].

This is of course not the only possible interaction. Indeed, if the coupling to the gauge Bosons was slightly different, i.e. changing the cross-section, the mass that would yield the correct relic abundance would be different as well. The key parameters to think of are the mass and the annihilation cross-section. A larger mass means that the equilibrium number density will become Boltzmann suppressed at an earlier time, while a larger cross-section lets the species stay coupled to the thermal bath for longer, thus maintaining its density at the equilibrium value, leading to a lower relic density. Requiring that the species ends up at the correct relic density for dark matter thus puts strong constraints on the cross-section to avoid over- or underproduction.

It can also be useful to describe the evolution of the density in terms of the Boltzmann equation. The Boltzmann equation for number density can be expressed in terms of the equilibrium

density,

$$a^{-3}\frac{d(n_1 a^3)}{dt} = n_1^{(\mathrm{eq})} n_2^{(\mathrm{eq})} \langle \sigma v \rangle \left(\frac{n_3 n_4}{n_3^{(\mathrm{eq})} n_4^{(\mathrm{eq})}} - \frac{n_1 n_2}{n_1^{(\mathrm{eq})} n_2^{(\mathrm{eq})}} \right), \tag{2.16}$$

for a particle process

$$(1)(2) \rightarrow (3)(4), \tag{2.17}$$

which the process described by Eq. (2.1) fits. The factors of a simplify the expression, such that the right-hand side only contains the change in number density from interaction, and not the dilution from cosmic expansion. The equation can be further simplified due to the fact that the Standard Model Fermions are all strongly coupled to the thermal bath, and are thus kept at their equilibrium density, $n_f = n_f^{(\mathrm{eq})}$. It can be even further simplified by making the assumption that either the density of WIMPs and anti-WIMPs are the same, or that the WIMP is a Majorana Fermion and its own antiparticle. In this case Eq. (2.16) simplifies to

$$a^{-3}\frac{d(n_\chi a^3)}{dt} = \langle \sigma v \rangle \, ((n_\chi^{(\mathrm{eq})})^2 - n_\chi^2), \tag{2.18}$$

it becomes evident that the number density will be driven towards equilibrium as long as the interaction is efficient. It can also be worth making both the annihilation and the dilution more explicit, with

$$\frac{dn}{dt} = -\underbrace{3H(t)n}_{\text{dilution}} - \underbrace{\langle \sigma v \rangle \, (n_\chi^2 - (n_\chi^{(\mathrm{eq})})^2)}_{\text{creation/annihilation}}, \tag{2.19}$$

making it clear that at equilibrium, the density will be dropping as the universe expands. Another thing to note is that the annihilation term is $\propto n^2$, thus, unless the cross-section increases dramatically as the temperature drops, the annihilation term will always decrease faster than the dilution term. Eventually, the particle density will be low enough that annihilation is no longer going to happen efficiently, and dn/dt will be dominated by the Hubble expansion term. The key question is whether this happens before or after the number density has been Boltzmann suppressed.

This differential equation cannot be solved analytically, so a numerical treatment is necessary. However, it can be useful to express it in terms of the quantity

$$Y_\chi = \frac{n_\chi}{T^3}, \tag{2.20}$$

which is proportional to the comoving number density, as the a scalings of n and T^3 cancel out. It is also helpful to define the dimensionless interaction rate parameter,[3]

$$\lambda = \frac{\Gamma}{H(x=1)} = \frac{m_\chi^3 \langle \sigma v \rangle}{H(x=1)}, \tag{2.21}$$

which lets the Boltzmann equation for Y_χ be express as

$$\frac{dY_\chi}{dx} = -\frac{\lambda}{x^2}((Y_\chi^{(\mathrm{eq})})^2 - Y_\chi^2), \tag{2.22}$$

which can be solved using standard methods. Example solutions for constant λ are presented in Fig. 2.4. However, there are a few more observations that can be made, allowing for a simple analytical approximation.

[3] Remembering the definition $x \equiv m_\chi/T$.

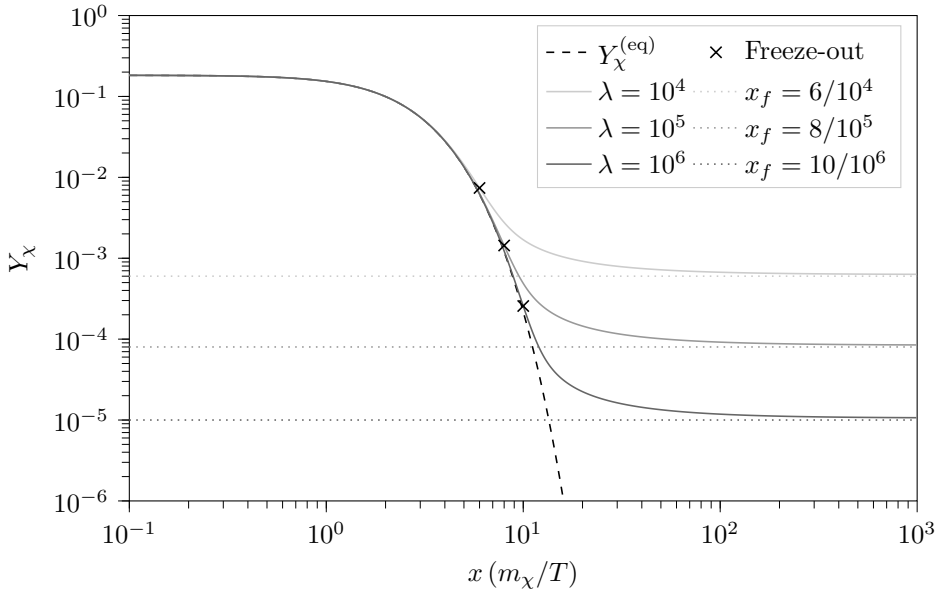

Figure 2.4: *An example of the freeze-out of a dark matter species for different values of the dimensionless interaction rate parameter λ. Note the good agreement with the approximated relic density of Eq.* (2.25)*, with the freeze-out x chosen by eye.*

If freeze-out happens after Boltzmann suppression has begun, i.e. at $x \gtrsim 1$, the parenthesis on the right-hand side of Eq. (2.22) becomes completely dominated by Y_χ^2, as the equilibrium density is suppressed exponentially. In this regime the differential equation thus reduces to,

$$\frac{dY_\chi}{dx} \approx -\frac{\lambda Y_\chi^2}{x^2}, \tag{2.23}$$

which can be integrated from freeze-out $x = x_{\mathrm{dec}}$ to $x = \infty$ (today), yielding

$$\frac{1}{Y_\chi^\infty} - \frac{1}{Y_\chi^{\mathrm{dec}}} = \frac{\lambda}{x_{\mathrm{dec}}}. \tag{2.24}$$

Since freeze-out is not an instantaneous process, there would still be a significant drop in Y_χ from freeze-out begins at x_{dec} before the annihilation term is completely suppressed, hence $Y_\chi^{\mathrm{dec}} \gg Y_\chi^\infty$, and the relic density in terms of Y_χ can be approximated with

$$Y_\chi^\infty \approx \frac{x_{\mathrm{dec}}}{\lambda}. \tag{2.25}$$

The only thing left then, is to identify x_{dec}. This can generally be approximated to be $x_{\mathrm{dec}} \sim 10$, which gives the correct Y_χ^∞ up to a factor of $\sim \mathcal{O}(1)$, as illustrated in Fig. 2.4.

This can be translated to a physical relic density,

$$\Omega_\chi h^2 = m_\chi \frac{Y_\chi^\infty T_0^3}{28} \frac{h^2}{3M_{\mathrm{Pl}}^2 H_0^2} \tag{2.26a}$$

$$= \frac{\pi\sqrt{g_{\mathrm{eff}}} T_0^3}{252\sqrt{10} M_{\mathrm{Pl}}^3} \frac{x_{\mathrm{dec}}}{\langle\sigma v\rangle} \frac{h^2}{H_0^2} \tag{2.26b}$$

$$\approx 0.12 \frac{x_{\mathrm{dec}}}{23} \frac{\sqrt{g_{\mathrm{eff}}}}{10} \frac{2.04 \cdot 10^{-26}\,\mathrm{cm}^3/s}{\langle\sigma v\rangle}. \tag{2.26c}$$

Assuming the electroweak cross-section Eq. (2.3) and the non-relativistic approximation for velocity,

$$\Omega_\chi h^2 \approx 0.12 \left(\frac{x_{\text{dec}}}{23}\right)^{3/2} \frac{\sqrt{g_{\text{eff}}}}{10} \left(\frac{35\,\text{GeV}^2}{m_\chi}\right), \tag{2.27}$$

giving the correct relic density $\Omega h^2 \sim 0.12$ for a WIMP mass of ~ 35 GeV depending on the exact x_{dec} and g_{eff}. This is the same order of magnitude as predicted by Eq. (2.15) with its more simplified assumptions. This calculation shows the WIMP miracle, the $\mathcal{O}$(10–100) GeV particle interacting via the weak force directly predicting the correct relic density. Versions of this calculation can be found in a variety of places in the literature, e.g. Refs. [62, 63, 152, 181, 198, 200]. However, this type of model is facing some challenges, as ever more sensitive experiments rule out parts of the parameter space via both direct detection [201–206], collider searches [206–215], and indirect detection [216–219].

If the assumption that the WIMP is annihilating via the standard weak interaction is loosened, much higher particle masses are possible. With the generic cross-section

$$\langle \sigma v \rangle \approx \frac{g^4}{16\pi m_\chi^2}, \tag{2.28}$$

and assuming that the scales of x_{dec} and g_{eff} are the same as in Eq. (2.26c), so must the thermally averaged cross-section be, to achieve the correct relic density. This yields the relationship for the coupling

$$\frac{g^4}{16 m_\chi^2} = 1.9 \cdot 10^{-9}\,\text{GeV}^{-2} \quad \Leftrightarrow g^2 \approx \frac{m_\chi}{3.4\,\text{TeV}}, \tag{2.29}$$

which can in turn be used to set an upper limit on the WIMP mass using the unitarity condition,

$$g^2 \lesssim 4\pi \Rightarrow m_\chi \lesssim 54\,\text{TeV}, \tag{2.30}$$

several orders of magnitude larger than the mass expected from a particle coupled through the Standard Model weak interaction.

Of course, this has all been a much simplified picture using either a velocity-independent scattering, or an approximated thermally averaged cross-section $\langle \sigma v \rangle$ that is just a constant $\sigma_{\chi\chi}$ times the thermal velocity. Generally, the thermally averaged cross-section can be expressed in terms of powers of the velocity, with a velocity-independent leading-order term,

$$\langle \sigma v \rangle = \left\langle s_0 + s_1 v^2 + \mathcal{O}(v^4) \right\rangle, \tag{2.31}$$

where the higher orders will be suppressed for non-relativistic WIMPs, as $v \ll 1$. The exact type of dark matter particle and annihilation channel determine which contributions are important. For the specifics, see e.g. [197, 198, 220]

If the cross-section is much smaller than the classic WIMP coupling, it is quite possible that the dark matter species would never have been in thermal equilibrium with the Standard Model particles, and would essentially begin with a number density of zero. These are sometimes called feebly interactive massive particles, or "FIMP", with the implication that a "feeble" interaction is even weaker than "weak".

If these dark matter particles can be produced through the decay of a heavy Standard Model particle, their number density will gradually increase until the Standard Model parent particle becomes Boltzmann suppressed, at which point the comoving density of the dark matter particle gets "frozen in". These types of models are therefore termed freeze-in production. [198, 221–223]

For a heavy Standard Model particle P decaying to two DM particles through a process $P \to \chi\bar{\chi}$, the Boltzmann equation for the dark matter number density can be expressed, similarly to the case of production through annihilation in Eq. (2.19), as,

$$\frac{dn_\chi}{dt} = -\underbrace{3Hn_\chi}_{\text{dilution}} + \underbrace{\frac{g_P^* m_P^2}{2\pi^2}\Gamma_{P\to\chi\bar{\chi}} T K_1(m_P/T)}_{\text{production via decay}}, \tag{2.32}$$

where m_P and g_P^* are the P mass and its internal degrees of freedom respectively, $\Gamma_{P\to\chi\bar{\chi}}$ is the partial decay width of P into $\chi\bar{\chi}$, and $K_1(x)$ is a modified Bessel function of the second kind. This is the part of the term that captures the suppression of the interaction when the parent particle becomes Boltzmann suppressed. The inverse decay can be neglected, as with the relevant cross-sections, the dark matter particle never reaches a number density where the process becomes relevant. It can also be useful to express this in terms of the equilibrium density of P, which can be computed to be,

$$n_P^{(eq)} = \frac{g_P^* m_P^2}{2\pi^2} T K_2(m_P/T), \tag{2.33}$$

where $K_2(x)$ is likewise a modified Bessel function of the second kind. The production term of Eq. (2.32) can then be rewritten as

$$\frac{K_1(m_P/T)}{K_2(m_P/T)}\Gamma_{P\to\chi\bar{\chi}} n_P^{(eq)}, \tag{2.34}$$

getting rid of the explicit temperature dependence.

As in Eq. (2.22), it can be useful to express the evolution in terms of the temperature-scaled quantities x and Y_χ.[4] However, as the dark matter is not following its equilibrium density, the previous definition of x is not useful. However, the parent particle being in equilibrium with the thermal bath, it can be used instead, $x_P \equiv m_P/T$. The analogous equation then becomes,

$$\frac{dY_\chi}{dx_b} = \frac{g_P^*}{2\pi^2}\frac{\Gamma_{P\to\chi\bar{\chi}}}{H(x_P = 1)} x^3 K_1(x). \tag{2.35}$$

The temperature dependent part of the equation, $x^3 K_1(x)$ has a maximum around $x = 1$, so this is where production will be most efficient. This equation can be integrated just like the freeze-out case to find the relic density for a given model, yielding

$$\Omega_\chi h^2 = \frac{3\sqrt{10}h^2}{112\pi^2}\frac{g_P^2}{\sqrt{g_{\text{eff}}}}\frac{m_\chi}{m_P^2}\frac{T_0^3}{H_0^2 M_{\text{Pl}}}\Gamma_{P\to\chi\bar{\chi}}. \tag{2.36}$$

Expressing the partial decay width in terms of a dimensionless parameter y, $\Gamma_{P\to\chi\bar{\chi}} = y^2 m_P/8\pi$, the relic density can be written simply as,

$$\Omega_\chi h^2 = 0.12\left(\frac{y}{2\cdot 10^{-12}}\right)^2 \frac{g_P^*}{2}\frac{m_\chi}{m_P}, \tag{2.37}$$

which is clearly capable of producing the correct relic density with a small enough coupling. Note that for freeze-in, a larger coupling leads to a larger relic density, as more dark matter is produced before the interaction decouples.

Freeze-in is not only possible through the decay of a Standard Model particle to $\chi\bar{\chi}$, but also through annihilation processes $P\bar{P} \to \chi\bar{\chi}$, or "mixed" decays $P \to P_2\chi$. The important thing is that the DM density starts low and only briefly experiences thermal equilibrium before the production mechanism becomes suppressed and the relic density is frozen in. These types

[4] A reminder for convenience, $x \equiv m_\chi/T$ and $Y_\chi = n_\chi/T^3$.

of interactions are often termed to happen via a "Portal" e.g. a Higgs portal, and there exist a variety of models for freeze-in of FIMPs [221–232].

A similar type of dark matter candidate with a different production mechanism is sterile neutrinos. These are essentially a proposed new uncharged lepton, which unlike the three standard neutrinos does not have a charged counterpart. With some mixing with the Standard Model neutrinos, they can be produced in the early universe via oscillations,the so-called Dodelson-Widrow mechanism [162, 165, 233–236]. With a Boltzmann equation for the sterile neutrino,

$$\left(\frac{\partial}{\partial t} - HE\frac{\partial}{\partial E}\right) f_S(E,t) = \left(\frac{1}{2}\sin^2\left(2\theta_M(E,t)\right)\Gamma(E,t)\right) f_A(E,t), \tag{2.38}$$

where f_i are the distribution function for sterile (S) and active (A) neutrinos respectively, E is the neutrino energy, θ_M is the mixing angle, and Γ is the collision rate. If the interaction rate of the sterile neutrinos is large enough to maintain equilibrium, it will freeze-out similarly to WIMPs, and the sterile neutrino relic density will be [233, 237],

$$\Omega_S h^2 \simeq 0.12 \left(\frac{10.75}{g_{\text{eff}}}\right)\left(\frac{M_S}{1\,\text{keV}}\right)\left(\frac{87.5}{S}\right), \tag{2.39}$$

where g_{eff} is the number of relativistic degrees of freedom at freeze-out, M_S is the sterile neutrino mass, and S is the entropy released after the sterile neutrino freezes out. The relic abundance can also be enhanced through resonant production mechanisms. If thermally produced, this type of dark matter would be relativistic at the time of production and become non-relativistic at a later (but not too late) time due to its ∼keV-scale mass. This type of model is therefore called warm dark matter [238].

There are also a wealth of non-thermal production mechanisms for dark matter, which greatly expands the number possible particle models, at the cost of the "neatness" of simple thermal production [239–243].

The question of course remains which of these models (if any), is the correct one, and there is much ongoing research into finding out. So far, what has been achieved is limited to ruling out models, or at least constraining the allowed parameter space. Perhaps the simplest and most fundamental test of a dark matter model is whether it is capable of producing the correct relic abundance. However, there is no law stating that the entirety the dark matter must consist of the same particle type, as long as the different components are not mutually exclusive. This weakens the production requirement to only ensuring that the given model does not overproduce dark matter (though it leaves open the question of what the rest of the dark matter is).

Having satisfied the requirement that the particle is not overproduced, its expected observational signatures can be investigated. There are three general approaches to this: direct detection, indirect detection, and collider searches. All of these generally assume some non-gravitational coupling to the Standard Model (although there are efforts to search for ultra-heavy dark matter through only its gravitational coupling [244, 245]).

The principle behind direct detection is very simple. If the dark matter particle has some interaction cross-section with nuclei or electrons, we should observe these scatterings in a detector, as the Earth is located in the Milky Way dark matter halo, provided that the detector is sensitive enough [152, 200, 223, 246, 247].

In indirect detection, the objective is to observe the signals emitted by dark matter particles, rather than the dark matter itself, hence the name. This generally relies on astronomical observations of high energy radiation from areas of high dark matter densities, such as the galactic centre [248, 249]. These methods rely on the assumption that the dark matter particles are able to either annihilate (which gives a signal $\propto \int \rho_\chi^2$) or decay (which gives a signal $\propto \int \rho_\chi$). A famous

example of this type of search is the research into the 511 keV line emission from the galactic bulge, although the WIMP origin has eventually been deemed unlikely [152, 200, 223, 250–252].

Finally, colliders are also able to set constraints on possible particles, as they should exist as possible end states in particle interactions, if they have a coupling to the particles in question and the centre of mass energy of the collision is large enough. Of course, we do not expect the detector instruments of the colliders to pick up the dark matter particles. Instead, they are inferred through the mass-energy they carry away from the interaction, which is specifically not detected. This is the so-called "missing energy" [152, 200, 223, 253].

2.1.2 Direct detection searches

In a direct detection experiment, the differential rate of dark matter particles scattering off a nucleus with mass m_N is given by

$$\frac{dR}{dE_{\rm nr}} = \frac{\rho_\chi M_T}{m_N m_\chi} \int_{v_{\rm min}}^{v_{\rm esc}} dv v f(v) \frac{d\sigma}{dE_{\rm nr}}, \tag{2.40}$$

where $E_{\rm nr}$ is the nuclear recoil energy, v is the dark matter particle velocity in the detector frame, $f(v)$ is the dark matter velocity distribution, and σ is the scattering cross-section. The velocity distribution is often approximated with a Maxwellian distribution [247], possibly with some offset if the Earth is not exactly comoving with the dark matter halo. The minimum velocity required to reach a nuclear recoil energy $E_{\rm nr}$ is given as,

$$v_{\rm min} = \sqrt{\frac{E_{\rm nr} m_N}{2\mu^2}}, \tag{2.41}$$

and dark matter particles faster than the galactic escape velocity $v_{\rm esc} \approx 544$ km/s [254] will escape the galaxy and thus not show up in the experiment. μ is the reduced mass of the dark matter-nucleus system

$$\mu = \frac{m_N m_\chi}{m_N + m_\chi}. \tag{2.42}$$

The number of events observed in an experiment running for a time T is then,

$$N_{\rm event} = T \int_{E_{\rm low}}^{E_{\rm high}} dE_{\rm nr} \epsilon(E_{\rm nr}) \frac{dR}{dE_{\rm nr}}, \tag{2.43}$$

where ϵ is the detector efficiency, $E_{\rm low}$ is the threshold energy of the experiment and $E_{\rm high}$ is the recoil energy corresponding to a velocity[5] $v = v_{\rm esc}$ [247].

The dark matter-nucleus differential scattering cross-section is often expressed in terms of a spin-dependent part (denoted with subscript SD) and a spin-independent part(denoted with subscript SI),

$$\frac{d\sigma}{dE_{\rm nr}} = \frac{m_N}{2v^2\mu^2} \left(\sigma_{\rm SI} F_{\rm SI}^2(E_{\rm nr}) + \sigma_{\rm SD} F_{\rm SD}^2(E_{\rm nr}) \right), \tag{2.44}$$

where σs are again cross-sections, and Fs are form factors. For spin-independent interactions, the dark matter-nucleon cross-section is often described as,

$$\sigma_{\rm SI} = \frac{\sigma_n \mu^2}{\mu_n^2} A^2, \tag{2.45}$$

assuming equal coupling to protons and neutrons. However, there is a range of possible effective field theory operators which may e.g. introduce a velocity dependence in σ_n, depending on the type of mediator [255, 256].

[5] This can be computed by replacing $v_{\rm min}$ with $v_{\rm esc}$ in Eq. (2.41) and inverting.

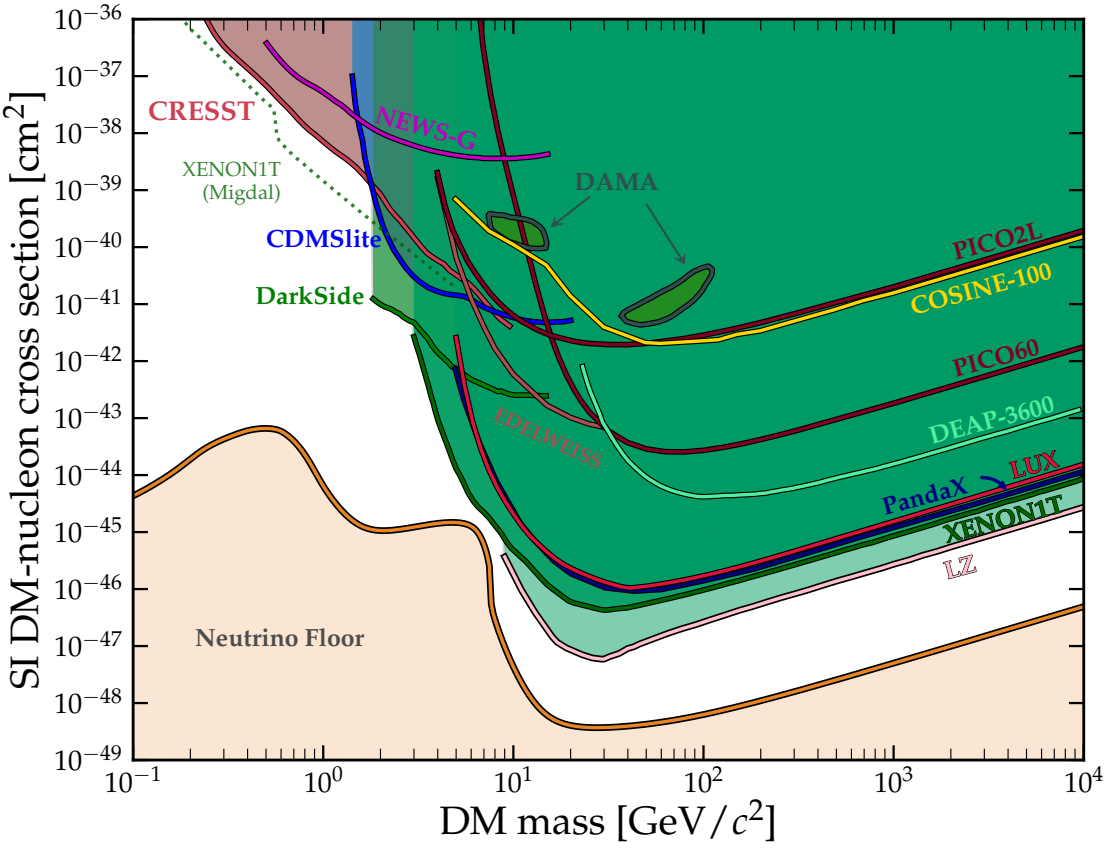

Figure 2.5: *An overview of the limits on the spin-independent scattering cross-section from a variety of direct detection experiments [205, 257–274]. Figure adapted from Ref. [271].*

For spin-dependent interactions coupling to unpaired nuclear spins, the cross-section will generally depend on the momentum transfer $|\vec{q}|$,

$$\frac{d\sigma_{\mathrm{SD}}}{d|\vec{q}|^2} = \frac{8G_F^2}{\pi v^2}\left(a_p\langle S_P\rangle + a_n\langle S_n\rangle\right)^2 \frac{J+1}{J}\frac{S(|\vec{q}|)}{S(0)}, \tag{2.46}$$

where a_i and $\langle S_i\rangle$ are the coupling to, and spin expectation values for protons (p) and neutrons (n) respectively, J is the total nuclear spin, and $S(|\vec{q}|)$ is the spin structure function of the target.

Direct detection of dark matter is quite a challenge. Because of the small (expected) cross-section, events will be quite rare, and any experiment to detect them will want to maximise their detection potential. How to do this can be summed up with a few general aims. Ideally, the experiment's energy threshold should be as low as possible, to ensure no low-energy scattering events are missed. A larger detector mass is also desirable, as this will have more potential for scattering events. Finally, the background should be as low as possible, so the few events from a dark matter signal are not lost in a sea of background events.

A great number of different experiments have been built to attempt a measurement of dark matter through direct detection. A selection of their results is presented in Fig. 2.5,[6] which shows limits on the spin-independent cross-section for dark matter-nucleon scattering. Limits on spin-dependent scattering are similar. The figure also shows the so-called "neutrino-floor" or "neutrino fog". This indicates the regime where the direct detection experiments will start to pick

[6]The plotting code from Ref. [271] is available at `https://github.com/cajohare/NeutrinoFog`.

up neutrinos, which would be difficult to distinguish from dark matter scattering events [266, 271, 275–281]. As is evident from the figure, different experiments, and in particular different *types* of experiments, have different strengths and weaknesses, and several types of detectors are in use or in development [247, 265].

The current strongest limits on dark matter-nucleon scattering in the mass range above a few GeV are set using liquid noble gas detectors, the strongest limits at this time being set by LZ [205], XENON1T [202, 262, 263, 282], and XENONnT [283], all (as implied by the name) using tons of liquid xenon, making use of both the scintillation light and the ionisation signal from scattering events. Liquid noble gas, and in particular xenon, detectors are very powerful in this range, due to the large nuclear masses and low background, as well as the fact that they can be readily scaled up [265]. However, due to the large nuclear masses, they have comparatively high energy thresholds, which limits their potential at low dark matter masses. Future experiments will be even larger and more sensitive [201, 203]. Even with better technology and larger masses, the sensitivity of nuclear recoil experiments will never be great for "low" dark matter masses, as the energy transfer in scatterings with nucleons becomes inefficient at $m_\chi < m_p \sim 1$ GeV.

At the lower end of the mass scale is cryogenic bolometers, such as CRESST [269], which win out here due to their lower energy thresholds. However, they are much harder to scale up, than the liquid noble gas detectors.

The motion of the Earth around the Sun is also expected to impact the event rate. This is exploited by a type of experiment using NaI crystal based detectors. These are scintillating crystals, which are very sensitive to spin-independent interactions, coupled to photomultiplier tubes. They are easy to operate stably for long periods of time, but suffer from high background, and are therefore only able to detect dark matter via the expected annual modulation of the signal. As the Earth moves around the sun over the course of a year, the relative velocity between the detector and the dark matter wind changes (i.e. the velocity distribution $f(v)$ in Eq. (2.40) is shifted), leading to a changing event rate. This oscillating event rate enables a detection of dark matter scattering with even a fairly low signal-to-noise ratio, as long as the modulation is significant [284–287]. One of the main challenges for building these detectors is growing large, pure crystals [247, 265]. This type of detector was also used by the very first experiment to directly detect dark matter, in 1987 with the USC/PNL Germanium Spectrometer, although this used a high purity germanium crystal as implied by the name, rather than NaI [288]. It is interesting to note that the DAMA/LIBRA experiment reports observing such a modulation [264, 272, 284, 289–295], however, as illustrated in Fig. 2.5, the cross-section required to explain the DAMA/LIBRA signal is strongly ruled out by other experiments. Further experiments are underway to test the DAMA/LIBRA claim using similar types of detectors, to replicate the experiment as closely as possible, e.g. SABRE [296–300], COSINUS [301–305], PICOLON [306, 307], ANAIS [308–312], and the COSINE experiments [257, 313–320].

A big question in a dark matter detection experiment will always be how to determine that what is detected is actually dark matter and not just some previously unknown background. This can be dealt with in a variety of ways, including by removing backgrounds statistically.

As the sensitivity of experiments increases, the neutrino fog will become a significant background [271]. One way of solving this problem is through directional detection, as knowing the direction of incoming particles can help discriminate between dark matter and particles of e.g. terrestrial or solar origin, due to the directionality of the dark matter wind. This can be done with gas-filled time projection chambers, such as the proposed CYGNUS experiment [321–324], or other more exotic detector types [325].

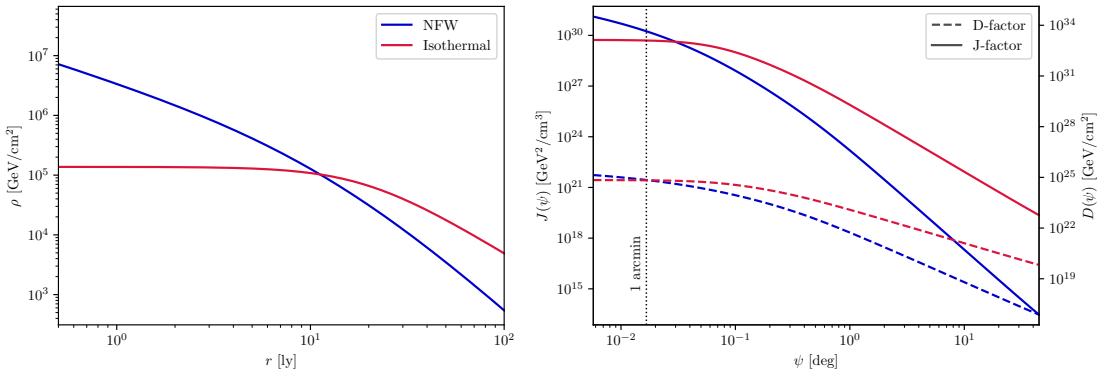

Figure 2.6: Left: *A rough approximation of the density profile of the globular cluster ωCentauri using two different types of halo profiles, a cuspy NFW profile, and a cored isothermal profile.* Right: *The J- and D-factors (Eq.* (2.48)*) associated with these halo profile with a line of sight angle ψ away from the centre of the cluster. Note the sharp rise in the J-factor compared to the D-factor.*

2.1.3 Indirect searches

Indirect detection follows a different path. If the dark matter is not showing up in our detectors, we have to look where the dark matter is, hoping to see some signature. The types of dark matter subject to these searches broadly fall into two similar categories: annihilating dark matter and decaying dark matter. It is usually assumed (or perhaps rather hoped) that these interactions will emit Standard Model particles that are more easily detectable to us.

The expected signal will be larger from locations with higher dark matter densities, with the received flux spectrum $d\phi/dE$ described by

$$\frac{d\phi}{dE} = \frac{d\Phi_{\text{ann}}}{dE} J, \tag{2.47a}$$

$$\frac{d\phi}{dE} = \frac{d\Phi_{\text{dec}}}{dE} D, \tag{2.47b}$$

for annihilation (Eq. (2.47a)) and decay (Eq. (2.47b)) respectively, where $d\Phi/dE$ is the emitted flux spectrum, as determined by the particle physics model, while J and D are the so-called J- and D-factors, which capture the (line of sight integrated) spatial dark matter distribution. Sometimes the instrument resolution is also included in these [248, 326]. The "pointlike" equations are given through

$$J(\psi) = \int_{\text{los}} \rho_\chi^2(\psi, l) dl, \tag{2.48a}$$

$$D(\psi) = \int_{\text{los}} \rho_\chi(\psi, l) dl, \tag{2.48b}$$

where l is the distance along the line of sight, and ψ is the observing direction. To get a prediction for an actual observation, the angular size of needs to be included as determined by the instrument,

$$J(\Delta\Omega) = \int_{\Delta\Omega} \int_{\text{los}} \rho_\chi^2(\Omega, l) dl d\Omega, \tag{2.49a}$$

$$D(\Delta\Omega) = \int_{\Delta\Omega} \int_{\text{los}} \rho_\chi(\Omega, l) dl d\Omega, \tag{2.49b}$$

where $\Delta\Omega$ is the solid angle covered by the instrument.

Due to the ρ^2 dependence in Eqs. (2.48a) and (2.49a), searches for annihilating dark matter are more reliant on density spikes than with decaying dark matter. It is also advantageous to look at sources nearby, for all the usual distance-square law reasons.[7] For an example of J- and D-factors, see Fig. 2.6. Indirect dark matter searches therefore often focus on the galactic centre, which intriguingly does present a GeV-scale gamma ray excess [217, 251, 327–332], as well as dwarf spheroidals with large mass-to-light ratios [216, 326, 333–335]. However, the problem with some targets, such as the galactic centre, is the presence of astrophysical backgrounds. It can be difficult, if not impossible, to disentangle a possible dark matter signal from other astrophysical sources of emission [248]. There is also some sensitivity to the exact shape of the dark matter density profile, especially the central region, which may bring some uncertainty to predicting signals for various dark matter models [248, 326]. These issues can be remedied by investigating the diffuse flux from the Milky Way halo, at the cost of a lower expected signal, as in Refs. [336–339], as well as the extragalactic cosmological flux, as in Refs. [340–345]. Other targets of indirect searches include galaxy clusters, nearby galaxies, or the sun (in neutrinos). Ref. [248] provides an overview.

There is a lot of particle physics hidden in the $d\Phi/dE$, capturing which exact particle spectrum is emitted from the annihilation or decay process. Often, the dark matter will have annihilation or decay channels into unstable standard model particles, which will then further decay and contribute to the final prompt spectrum of stable particles. The produced energy spectrum for particle i per annihilation/decay is thus given as,

$$\frac{dN_i}{dE} = \sum_f B_f \frac{dN_{i,f}}{dE}, \tag{2.50}$$

summing over the production from all possible annihilation/decay final states f, weighted by their branching ratios B_f. Example photon spectra from different decay channels are shown in Fig. 2.7. Similar predictions can be made for fluxes in neutrinos, electrons, and protons (and their antiparticles, assuming they don't annihilate on the way here). Determining whether a gamma ray (or other cosmic ray) signal is caused by dark matter then involves comparing the observed spectrum to those predicted by the particle physics models.

There is another wrinkle to this, however. Namely, the fact that interstellar space is not an exact vacuum, indeed, the cosmic rays have to propagate through the interstellar medium and the galactic magnetic field, which will affect the received signal through e.g. energy loss. An overview of the computation of the fluxes and their propagations can be found in Ref. [346].

An interesting note is that the D-factor used for decaying dark matter is actually applicable to any signal proportional to the integrated dark matter density, and is therefore also used for constraining the fraction of dark matter constituted by light primordial black holes, as described in Section 2.3 and Chapter 8.

Finally, it is possible to investigate a particle physics model of dark matter, not by its emissions from annihilation or decay, but by its effects on other observables through interactions. It is a natural consequence of any coupling between dark matter and the Standard Model, such as would be required for annihilation or decay signals, that scattering would also be possible. An advantage of this approach is that it also applies to models that are unable to annihilate, such as e.g. asymmetric dark matter.

Depending on the exact model, dark matter may scatter with one or more Standard Model species, or with other dark matter particles. These scenarios can yield different observational

[7] However, this is to some extent countered by the finite width of the line-of-sight, as the same solid angle $\Delta\Omega$ will correspond to a larger volume when more distant.

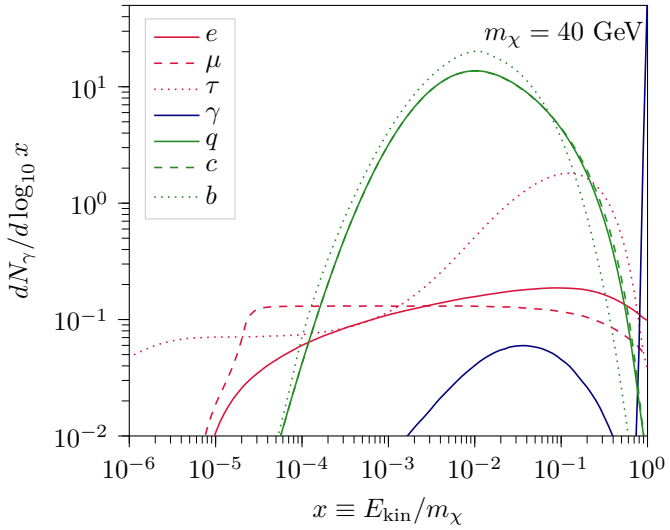

Figure 2.7: *The photon spectrum from annihilating dark matter of mass $m_\chi = 40$ GeV, via several decay channels, light quarks $q = u$, d, s, heavy quarks c and b, as well as the leptons $e^\pm$, $\mu^\pm$, $\tau^\pm$, and directly into photons. Spectra also correspond to decaying dark matter with twice the mass, 80 GeV. The actual photon emission spectrum would then be calculated by weighting these contributions by their branching fraction in the original dark matter annihilation/decay. Data from PPPC4DMID [346–351].*

signatures, although some may be similar. They can be investigated in various ways, in particular using the cosmic microwave background and structure formation, as such interacting models generally show damped small-scale structure. This can be probed both through the matter power spectrum, and through the halo mass function, including the number of Milky Way satellites [1, 2, 143, 144, 148, 149, 220, 352–379]. Similarly to the models of interacting dark matter, warm dark matter will also have damped small scale structure, but for a different reason. Rather than collisional damping, warm dark matter will free-stream at early times due to being relativistic, and will therefore not collapse to form structures smaller than the free-streaming scale. The same type of cosmological constraints setting upper limtis on scattering cross-sections can therefore be used to set lower limits on the mass of thermally produced warm dark matter [2, 3, 145, 237, 380–392].

A large part of my own work has been focused on constraining dark matter models in this way, which is presented in Chapters 5 to 7, including a novel way of constraining suppressed small-scale structure through the rate of gravitational wave events [3]. The methods for constraining such models generally involve computing their linear or non-linear structure formation predictions, using the techniques described in Chapters 3 and 4.

2.2 Axions and ultralight dark matter

Another model that has been gaining popularity as dark matter is axions, or axion-like particles. Such particles and their implications for cosmology are described in a multitude of reviews, e.g. Refs. [191, 253, 393–395]. The origin of these models is the CP problem of the strong force, which refers to the fact that the strong force seems to preserve CP symmetry despite no terms in the Lagrangian ensuring this conservation [393]. A solution to this problem was proposed in the form of the Peccei-Quinn mechanism, introducing a new scalar field [396–399].

Expressing this in terms of the Lagrangian, QCD allows the addition of a term [191]

$$\Delta\mathcal{L}_{\theta\mathrm{QCD}} = \frac{\theta_{\mathrm{QCD}}}{32\pi^2}\mathrm{Tr}G_{\mu\nu}\tilde{G}^{\mu\nu}, \tag{2.51}$$

where $G_{\mu\nu}$ is the gluon field strength tensor, and $\tilde{G}^{\mu\nu} = \epsilon^{\mu\nu\alpha\beta}G_{\alpha\beta}/2$ is its dual. The QCD "vacuum angle" θ_{QCD} could in principle have any value, however, it shows up in the calculation of the neutron electric dipole moment [400, 401]

$$d_n \approx 3.6 \cdot 10^{-16}\bar{\theta}_{\mathrm{QCD}}\, e\,\mathrm{cm}, \tag{2.52}$$

although, rather than θ_{QCD}, the measured quantity is in fact $\bar{\theta}_{\mathrm{QCD}} = \theta_{\mathrm{QCD}} + \mathrm{Arg}\,\mathrm{Det}M_uM_d$, where M_i are the quark mass matrices, but this complication does not meaningfully change the argument. Experiments place an upper limit on the neutron electric dipole moment at $\lesssim 10^{-26}\, e\,\mathrm{cm}$ [253, 402, 403], requiring a QCD vacuum angle smaller than 10^{-10}. This extremely small value is problematic, as it could receive $\mathcal{O}(1)$ contributions from electroweak CP-symmetry breaking. Fortunately, the Peccei-Quinn solution proposes a method of dynamically setting the vacuum angle to zero, thus solving the strong CP problem.

This is done by introducing a new spontaneously broken $U(1)$ chiral symmetry, leading to a new field a: the axion, which transforms under this symmetry as,

$$a(x) \to a(x) + \alpha f_a \tag{2.53}$$

The addition of this symmetry means that Eq. (2.51) is modified to include a contribution from the axion field,[8]

$$\Delta\mathcal{L}_{\theta\mathrm{QCD}+a} = \frac{1}{32\pi^2}\left(\bar{\theta}_{\mathrm{QCD}} + N\frac{a}{f_a}\right)\mathrm{Tr}G_{\mu\nu}\tilde{G}^{\mu\nu}, \tag{2.54}$$

where f_a is the Peccei-Quinn scale, also known as the axion decay constant, and N is a model dependent parameter which is sometimes absorbed into the definition of f_a [404].

The interaction between axions and gluons yields an effective potential for the axions,

$$V_{\mathrm{eff},ax} \propto -\cos\left(\bar{\theta}_{\mathrm{QCD}} + N\frac{\langle a\rangle}{f_a}\right), \tag{2.55}$$

which clearly has a minimum at

$$\langle a\rangle = -\frac{f_a}{N}\bar{\theta}_{\mathrm{QCD}}, \tag{2.56}$$

neatly cancelling out the CP-violation of QCD, following Eq. (2.54).

The axion's interaction with Standard Model particles are all suppressed by the Peccei-Quinn scale f_a, which also sets the axion mass [398, 399],

$$m_a \approx 6\,\mu\mathrm{eV}\left(\frac{10^{12}\,\mathrm{GeV}}{f_a}\right), \tag{2.57}$$

suggesting that the axion is a fairly low-mass particle.

Unfortunately, the simplest version of the QCD axion, the so called Peccei-Quinn-Weinberg-Wilczek (PQWW) axion has been ruled out. However, there are still two other popular models for the QCD axion both introducing additional particles on top of the Peccei-Quinn scalar [191]. These and are the Kim-Shifman-Vainshtein-Zakharov (KSVZ) axion, which introduces heavy quarks [405, 406], and the Dine-Fischler-Srednicki-Zhitnitsky (DFSZ) axion [407, 408], which

[8] While the addition of an axion with only this term solves the strong CP problem at the EFT level, a fully renormalisable and UV complete theory would lead to more terms. I am omitting those for simplicity.

introduces an additional Higgs field. These two models predict slightly different relatinoships between the axion mass and its couplings, but more the allowed parameter space is more than ten orders of magnitude in m_a [409], and experiments are only just beginning to reach the sensitivity required to probe these models [409–423], and many more experiments are underway that might reach the required sensitivity. Of course, it is also perfectly possible that an axion exists without making up any significant portion of the dark matter. Indeed, if the dark matter is composed entirely of QCD axions, it puts stringent limits on the mass to avoid overclosing the universe [190, 395, 424–426].

Following the proposition of the axion to solve the strong CP-problem, a multitude of other extensions have been suggested, many of which predict additional particles with similar behaviour, so they often also get the label of axion [393]. To distinguish, the axion that solves the strong-CP problem is often referred to as the QCD axion. These other axions are also sometimes referred to as axion-like particles or ALPs.

2.2.1 Axion production

Like thermal freeze-out or freeze-in production, axion-like particles also have a well motivated production mechanism, although this has a fundamentally different nature. Indeed, for a huge range of the mass parameter space, the axions would be far too hot to make up the dark matter if thermally produced. Instead, they can be produced through a process called the "misalignment", or "realignment" mechanism [191, 427, 428]. For the "canonical" case, the homogeneous axion field,

$$a(t) = f_a \theta(t), \tag{2.58}$$

and its cosmological evolution is given through,

$$\ddot{\theta} + 3H(t)\dot{\theta} + m_a^2 \sin\theta = 0, \tag{2.59}$$

where the initial value of θ is usually taken to be some random number in the range $[-\pi, \pi]$, and $\dot{\theta}$ is initially taken to be zero, as the solution otherwise diverges for $t \to 0$. The high-temperature instanton potential relevant at these early times is,

$$V(\theta) = f_a^2 m_a^2 \left(1 - \cos\theta\right). \tag{2.60}$$

At early times, the large Hubble parameter, $H \gg m_a$, means that $\dot{\theta}$ is damped and the field does not change. At later times when the Hubble parameter drops, so $H \ll m_a$, the field will oscillate rapidly, giving it a mean equation of state $\langle w \rangle = 0$, meaning it will behave like cold matter. For reference, the Hubble parameter at matter-radiation equality is $\sim 10^{-28}$ eV, so axions heavier than this will begin to oscillate in the radiation dominated epoch, and can thus act as dark matter [191]. To find the relic density, Eq. (2.59) must be evolved, for examples see e.g. Refs. [190, 424, 425, 429, 430], yielding, as a rough estimate,

$$\Omega_a h^2 \sim 0.12 \left(\frac{f_a}{10^{12}\,\mathrm{GeV}}\right)^{7/6} \langle \theta_i^2 \rangle, \tag{2.61}$$

where the square of the average misalignment angle $\langle \theta_i^2 \rangle$ depends on whether the Peccei-Quinn symmetry is broken before or after inflation.

If the symmetry breaks before inflation, the whole observable universe is assumed to have the same uniform misalignment angle θ_i, as it would have been in causal contact at the time of the symmetry breaking. This would yield a value $\theta_i \in [-\pi, \pi]$. An upper bound on value of θ_i

is set by f_a, to avoid an axion density much larger than the observed matter density, or even overclosing the universe.

If the symmetry breaking happens after inflation, the observable universe would initially be made up of many different patches with different values of θ_i (each randomly picked, as in the pre-inflation scenario). There is therefore no longer a dependence on a specific value of θ_i, but rather an average over all possible values, $\langle\theta_i^2\rangle = \pi^2/3$, so the final axion relic density just depends on f_a.

In both cases, the symmetry breaking may cause topological defects (cosmic strings, domain walls, etc.) [431], which in the pre-inflation scenario are inflated away, but may have important consequences if the symmetry breaking happens after inflation. For a more detailed overview, see e.g. Refs. [191, 427] and references therein.

Axions can in principle also be thermally produced in the early universe through their coupling to Standard Model particles. However, for the sub-eV masses generally considered, the axions would act as dark radiation, or at the very least as hot dark matter. The temperature of the CMB today is $\mathcal{O}(10^{-4})$ eV, so any axion lighter than this would still be relativistic if thermally produced, and an axion of $m_a \sim 0.1$ eV would have been relativistic at recombination. These would therefore not be able to form the bulk of the dark matter.

One of the problems of the Standard Model has thus been solved, and all it took was introducing a new particle, and a dark matter candidate at that!

2.2.2 Axion searches

There are several ways to search for axions, perhaps the most popular is through the axion-photon coupling $g_{a\gamma\gamma}$. The coupling Lagrangian is,

$$\mathcal{L}_{a\gamma\gamma} = g_{a\gamma\gamma} a \vec{E} \cdot \vec{B}, \tag{2.62}$$

where a is the axion field, and E and B are the respective electric and magnetic fields of two propagating photons. The coupling constant is given through,

$$g_{a\gamma\gamma} = \frac{\alpha g_\gamma}{2\pi f_a}, \tag{2.63}$$

where α is the fine structure constant and g_γ is a model-dependent factor, generally $\mathcal{O}(1)$. For the aforementioned two QCD axion models, the coupling is,

$$g_{a\gamma\gamma} = \begin{cases} 0.38 \frac{m_a}{\mathrm{GeV}^2} & \text{(KSVZ)} \\ 0.14 \frac{m_a}{\mathrm{GeV}^2} & \text{(DFSZ)} \end{cases} \tag{2.64}$$

Following Eq. (2.62), there are two important interactions that can be used to probe the axion coupling: decay into two photons, and the inverse Primakoff effect, as illustrated by the Feynman diagrams in Fig. 2.8.

The inverse Primakoff effect is when an axion passes through an electric or magnetic field, and through the coupling in Eq. (2.62) is converted into a photon, as illustrated in Fig. 2.8b. This makes it possible to probe the axion-photon coupling in a variety of ways. One way to do this is through halo- and helioscopes [432, 433]. These work in similar ways, using a cavity with a strong magnetic field. A haloscope relies on the assumption that at least some fraction of the dark matter halo consists of axions. As these pass through the cavity, they may be converted to photons due to the magnetic field, and if that happens, they will excite cavity modes, which can be measured, while non-detection can place limits on the coupling. Rather than direct limits on the axion photon coupling, however, the haloscopes place limits on the product $g_{a\gamma\gamma}\sqrt{\tilde{\rho}_a}$, where

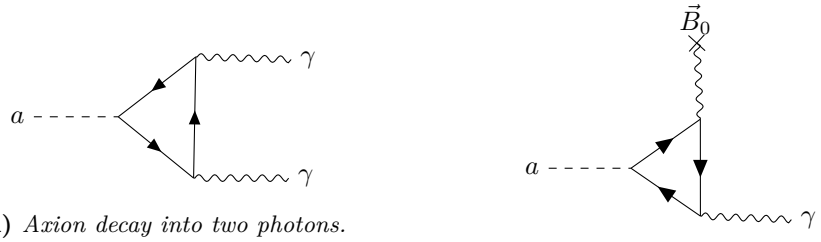

(a) *Axion decay into two photons.*

(b) *Inverse Primakoff.*

Figure 2.8: *Feynman diagrams for two important axion-photon interactions, the axion decay (2.8a) and the inverse Primakoff effect (2.8b).*

$\tilde{\rho}_a$ is the fraction of the local dark matter density made up of axions. This allows comparatively strong limits on the coupling, assuming that the dark matter halo is primarily axions.

Helioscopes, in contrast, make no such assumption. Indeed, all they require is the existence of the axions. If the axions exist with a coupling as in Eq. (2.62), some photons will be converted to axions in the Sun, and these may be reconverted back to photons in the cavity of the helioscope, where a photodetector is often used for single x-ray photons from relativistic axions. These bounds are generally "weaker" than those than can be reached by haloscopes, as the small coupling enters both in the production of axions by the Sun, and in the conversion back to photons in the experiment, however, it could be argued that they are more model independent, since they do not make any assumptions about a background population.

A third method of searching for axions is through so-called "light shining through wall"-experiments[9] [433–436], which works similarly to the helioscope, except the part of the Sun is played by another cavity with a magnetic field. The photons are directed at an opaque wall with a detector on the other side, so the detector will only pick them up if they are converted to axions (which can pass through the wall unhindered) and then reconverted to photons on the other side.

Assuming that axions make up a significant fraction of the dark matter, the axion-photon coupling can also be constrained through its decay into two photons (Fig. 2.8a) using the same indirect detection techniques as for heavier dark matter candidates, as described in Section 2.1, except that the emitted photons will have much lower energies than with MeV to GeV scale dark matter particles.

There are also other "indirect" methods of constraining the axion-photon coupling through astrophysics. The existence of this coupling would give additional avenues from astrophysical systems such as stars and supernovae, and the size of the coupling can thus be constrained based on observations and the modelling of these systems [428]. A comprehensive overview of limits on the axion-photon coupling is shown in Fig. 2.9.

As structure formation begins, light axions will also have qualitatively different behavior than the "standard" particle dark matter models described in Section 2.1. Since they are cold, and their masses are small, the de Broglie wavelength will be on the same order of magnitude as the interparticle separation (or larger!) for densely clustered environments like galaxies [394].

[9] Less colloquially, "resonant regeneration" or "photon regeneration".

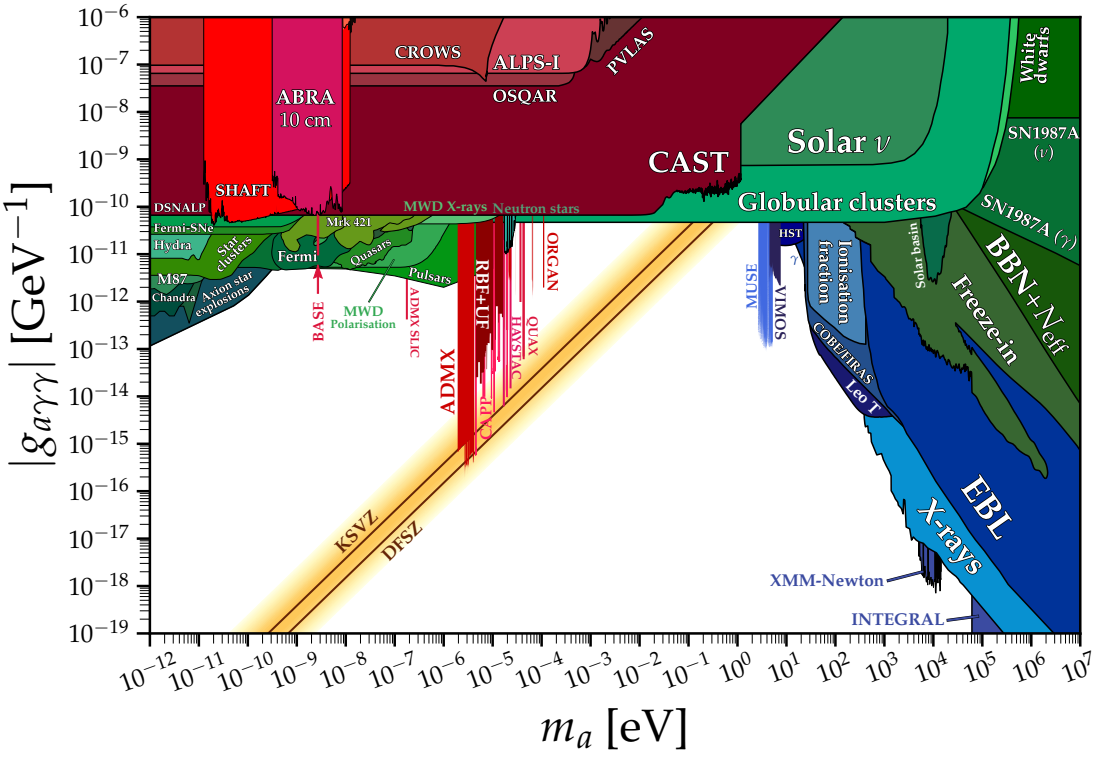

Figure 2.9: *A comprehensive overview of limits on the axion-photon coupling. Figure from [409]. For a full list of of the references used to produce the figure, see the list at* `https://cajohare.github.io/AxionLimits/`.

The de Broglie wavelength is,

$$\begin{aligned}\lambda_{\rm dB} &\equiv \frac{2\pi\hbar}{mv}, \\ &= 1.49\,{\rm km}\left(\frac{10^{-6}\,{\rm eV}}{m}\right)\left(\frac{250\,{\rm km/s}}{v}\right), \\ &= 0.48\,{\rm kpc}\left(\frac{10^{-22}\,{\rm eV}}{m}\right)\left(\frac{250\,{\rm km/s}}{v}\right).\end{aligned} \tag{2.65}$$

Because the wave effects are relevant for these types of models, they are sometimes called wave- or wavelike dark matter. As hinted in Fig. 2.1, axion and axion-like models are sometimes referred to as ultralight dark matter, with the largest mass to still qualify as ultralight varying by author, with some including classic axions. The similar term "fuzzy dark matter" is generally reserved for masses $m_a \lesssim 10^{-20}$ eV, where the wavelike quantum effects are relevant on astrophysical scales [394]. In particular, ultralight models with masses $\sim 10^{-22}$ eV has seen interest [437, 438]. An important note here is that any dark matter candidate of these low masses must be bosonic, as it would otherwise be prevented to collapse to the correct densities due to Pauli blocking.

However, even in the absence of Pauli blocking, quantum pressure will still prevent ultralight dark matter from collapsing on small scales, despite behaving like other cold matter on large scales. This means that the linear matter power spectrum is suppressed on small scales, as with the interacting or warm dark matter models described in Section 2.1, even if the mechanism behind the suppression is qualitatively different. For a given axion mass, the scale where the

linear matter power spectrum is suppressed by 50% is given by [394, 437, 439–441],

$$k_{1/2} = 4.5 \left(\frac{m_a}{10^{-22}\,\mathrm{eV}}\right)^{4/9} \mathrm{Mpc}^{-1}. \tag{2.66}$$

An axion with a mass of $\sim 10^{-22}$ eV would thus suppress structure on similar scales as a thermal warm dark matter particle of mass ~ 1 keV.

When the quantum pressure of the axions balances out the gravitational force, stable objects can be formed.[10] This condition,

$$\frac{GM}{R} \sim \frac{1}{m_a^2 R^2}, \tag{2.67}$$

where M is the object mass, and R is its size, leads to stable objects on scales depending on the axion mass,

$$R \sim \begin{cases} 100\,\mathrm{pc}\,\frac{10^9\,M_\odot}{M}\left(\frac{10^{-22}\,\mathrm{eV}}{m_a}\right)^2, \\ 300\,\mathrm{km}\,\frac{10^{-10}\,M_\odot}{M}\left(\frac{10^{-6}\,\mathrm{eV}}{m_a}\right)^2. \end{cases} \tag{2.68}$$

Ultralight axions can thus form large solitons, which could be found in the centres of galaxies [394, 445, 446], where μeV-scale axions would form smaller structures often referred to as "axion stars", which are essentially smaller versions of the fuzzy dark matter solitons, as well as "miniclusters" which are just gravitationally bound clusters of axions on much smaller scales than regular dark matter halos[442, 443, 447–455], depending on how likely they are to be disrupted, this could have implications for direct detection experiments relying on the local axion density [442–444]. Investigating the nonlinear behaviour requires specific simulations, due to the wavelike nature of the axions. This means that unlike the standard N-body framework described in Chapter 4, the Schrödinger-Poisson equations must be evolved cosmologically, as described in e.g. Refs. [445, 456–462].

The signatures of the wavelike nature of axion models are key to differentiating them from other models of dark matter. Especially as long as a laboratory detection remains elusive.

2.3 Primordial Black Holes

An entirely different type of dark matter candidate is primordial black holes. These are black holes formed, not from collapsing massive stars, but from overdensities in the early universe. At first glance, they do also seem to fulfil all the requirements of being a good dark matter candidate: They interact gravitationally, but otherwise not strongly. They were formed in the early universe, and will still be around today (assuming they are heavy enough). The idea of primordial black holes has been around for more than 50 years [463, 464], and has been suggested as a dark matter candidate for almost as long [465, 466]. Primordial black holes have especially been a popular candidate for dark matter in recent times [179, 180, 467–469], and they are described in a multitude of reviews, in particular how their existence can be constrained [470–472].

Primordial black holes have the "advantage" that they, in principle, do not need any extensions to the standard model, beyond those already required to explain inflation. However, the kind of blue tilted primordial power spectrum usually required for primordial black hole formation needs an inflation more complicated than the standard single field solution. There is strong evidence for the existence of black holes from gravitational wave events [473–482], and direct imaging of supermassive black holes with very long baseline interferometry [483–486]. It

[10] At least stable in isolation. Research is ongoing into how stable these are to being disrupted by external forces, e.g. Refs [442–444].

is a compelling argument for the model that it is not necessary to invent new particles, though this does mean that it will not solve problems with the standard model either. Primordial black holes are in principle indistinguishable from those formed later, except in the cases where such a black hole could not have formed from the collapse of a massive star, i.e. masses below the Tolman-Oppenheimer-Volkoff limit of $\sim 3M_\odot$ [487, 488]. There are no confirmed observations of primordial black holes, though primordial origins have been considered for some gravitational wave events and searches are ongoing [489–491]. Some possible subsolar events may have been observed, but none have been statistically significant enough to claim detection [492, 493], and NANOGrav observations are consistent with primordial black hole formation [494]. It is possible that future instruments, such as LISA [495] can shed further light on this [496–499]. It has also been suggested that the supermassive black holes observed at the centres of galaxies could have primordial origins [500–506]

In this section, I will present a brief overview of primordial black holes, and how it may be possible to detect them, or at least constrain their existence through non-detection. Of course, there is the possibility that they exist, but form only a vanishingly small part of the dark matter, or that they did exist but have since evaporated. This would not help solve the question of dark matter, but primordial black holes are still interesting in their own right, due to what they could tell us about the early universe and gravity. Their evaporation has even been suggested as a possible production mechanism for other types of dark matter [507–511].

2.3.1 Primordial black hole formation

Primordial black holes have a variety of possible exotic formation mechanisms, including from bubble collisions and cosmic strings [502, 512–517], but they can also just form from the collapse of overdensities in the early universe [518]. In a simplified description, if the amplitude of a density perturbation is large enough as it enters the horizon, it will collapse and form a black hole. An overdensity above the critical collapse limit entering the horizon later will enclose more mass, and thus lead to a more massive primordial black hole. That is, the mass within the horizon needs to be at least as large as the mass needed for a horizon-sized Schwarzschild radius (at the time of formation). During radiation domination when these would form, the horizon mass scales as,

$$M_H = \frac{c^3}{2GH} \sim 10^{15}\,\mathrm{g}\left(\frac{t}{10^{-23}\,\mathrm{s}}\right), \tag{2.69}$$

where t is the age of the universe. For reference, a black hole with the same mass as the Sun would form at $t \sim 10^{-6}$ s, corresponding to the QCD phase transition.

In reality, the physics of collapse to a black hole is a bit more complicated, and the relation between black home mass and horizon mass can be parameterised as $M_{\mathrm{PBH}} = \gamma M_H$, where the proportionality factor γ can be approximated as the sound speed squared, $\gamma \approx c_s^2$. In the radiation dominated era, the sound speed is roughly a third of the speed of light, so $\gamma \approx 0.2$ [518].

Having an estimate of the formation mass as a function of time, the question is then how many will form. The initial abundance of primordial black holes of a given mass M is denoted with $\beta(M)$, defined through the horizon mass and the density at formation,

$$\beta(M_H) = \frac{\rho_{\mathrm{PBH}}(t_f)}{\rho_{\mathrm{tot}}(t_f)}, \tag{2.70}$$

with t_f being the formation time. Assuming the initial perturbations δ follow a probability distribution $P(\delta)$. The abundance of black holes formed is then given as the fraction of perturbations

with an amplitude larger than the critical value δ_c [468, 470, 519],

$$\beta(M_{\rm PBH}) \approx \gamma \int_{\delta_c}^{\infty} P(\delta) d\delta, \tag{2.71}$$

which for a Gaussian distribution with width $\sigma(M_{\rm PBH}) \ll \delta_c$ is,

$$\beta(M_{\rm PBH}) \approx \gamma \sqrt{\frac{2}{\pi}} \frac{\sigma(M_{\rm PBH})}{\delta_c} \exp\left(-\frac{\delta_c^2}{2\sigma^2(M_{\rm PBH})}\right). \tag{2.72}$$

This makes it quite difficult to produce primordial black holes in standard cosmology, as the basic scale invariant power spectrum has $\sigma \sim 10^{-5}$, leading to a black hole abundance $\beta \lesssim 10^{-4 \cdot 10^9}$, much too small to be relevant [520].

While it is useful to approximate the critical collapse threshold as $\delta_c \approx 0.3$, reality is a bit more complicated [519]. For a uniform overdensity surrounded by an underdense area, the critical value would be $\delta_c = \sin^2(\pi\sqrt{w})/(1+3w)$, where w is the equation of state parameter [521, 522]. In the end, however, there is not a single answer to this question, and the threshold will vary in the range 0.3–0.6 [519, 521–528], but this wiggle room in δ_c is not sufficient to produce an appreciable abundance of primordial black holes. It is necessary to somehow modify the initial conditions.

A variety of different inflation models exist which modifies the initial spectrum of perturbations, and thus could lead to populations of primordial black holes [468, 469, 519, 529]. In single field inflation models, a simple tilt to enhance small scale perturbations is in violation of observations. It is necessary to introduce more complex features, such as a running of the spectral index, and indeed a "running of the running", inflection inflation where the inflaton potential temporarily plateaus, or chaotic inflation [519]. The formation would also be affected by alternative early universe scenarios such as early matter domination, which would greatly increase β for models with a variance of initial perturbations $\sigma \lesssim 0.01$ [530–534]. Another option is multi field inflation, which allows for multiple peaks in the power spectrum and thus makes it possible to produce black holes while evading e.g. CMB constraints [501, 519, 535–541]. Finally, there are other exotic production mechanisms as previously mentioned [502, 512–517].

2.3.2 Constraining primordial black hole populations

Having established that they could theoretically be produced, it is time to consider how we can tell if they actually were. In practice, this means constraining which possible primordial black hole populations are allowed by data. These theoretical populations can be separated into two distinct categories, depending on whether they would still exist today.

Black holes are, in general, expected to evaporate via Hawking radiation [542–547], emitting particles of species i and particle energy E at a rate[11]

$$\frac{d^2 N_i}{dt dE} = \frac{1}{2\pi} \sum_{\rm dof} \frac{\Gamma_i(E, M)}{e^{E/T} \pm 1}, \tag{2.73}$$

where the black hole temperature T is given as,

$$T = \frac{\hbar c^3}{8\pi G k_{\rm B} M_{\rm BH}}, \tag{2.74}$$

[11] For a nonrotating, uncharged (Schwarzschild) black hole. The formula requires slight modification for Kerr or Reissner-Nordström black holes, but is qualitatively similar.

The parameter Γ is the greybody factor which determines the exact rate of emission for a given particle, and can be calculated with the Teukolsky equations [548–553]. This leads to a mass-loss rate of

$$\frac{dM}{dt} = -\frac{\hbar c^4}{G^2}\frac{\alpha}{M^2}, \tag{2.75}$$

where the α parameter is determined by the number of different particles the black hole can emit at its current temperature. This gives the black hole a finite lifetime of

$$t_{\rm evap} = \frac{5120\pi G^2 M_{\rm BH}^3}{\hbar c^4}, \tag{2.76}$$

assuming it does not absorb any energy from its surroundings. If primordial black holes are formed with a mass corresponding to a lifetime shorter than the current age of the universe, they would have already fully evaporated at the present time, and their existence would have to be probed through their energy injection at previous epochs. The formation mass that corresponds to a lifetime of the age of the universe is often termed the critical mass, and is $M_{\rm crit} \sim 10^{15}$ g. It is therefore also customary to cut off monochromatic constraint plots for extant black holes (such as Fig. 2.10) at this mass, as having a surviving population below the critical mass requires an incredibly fine-tuned initial mass or an extended initial mass distribution [4].

Reference [180] provides a very thorough overview of the constraints on primordial black hole populations, both evaporated and extant. The constraints on evaporated populations come from energy injection and late decaying particles at BBN [177, 554, 555], CMB spectral distortions [555–557] and anisotropies [555, 557–559] from energy injection, the extragalactic γ-ray background [177], extragalactic antiprotons [177], and neutrinos [177, 560].

Primordial black holes with masses $\sim 10^9$–10^{13} will be injecting large amounts of energy into the cosmic fluid around the time of BBN. This changes the production ratios of different isotopes, and the primordial black hole population at these masses can be strongly constrained with the deuterium to hydrogen ratio [180].

Similarly, if enough energy is emitted into the cosmic bath, shortly before photon decoupling (or after decoupling), it will not have had time to thermalize and thus shows up as spectral distortions in the CMB. Such energy injection will also affect the CMB anisotropies in a similar fashion to any other exotic energy injection, leading to a higher freeze-out fraction, meaning the CMB photons experience increased Thomson scattering, causing damping on small scales. If enough energy is injected, recombination may also be delayed, causing a shift in the acoustic peaks [180, 558, 561].

If they were formed not too much below the critical mass ($M \gtrsim 5 \cdot 10^{13}$ g), they can also be constrained by the extragalactic γ-ray background via their Hawking emission, especially the secondary photon signal from decay of unstable emitted particles [177, 180].

Primordial black holes formed at masses larger than $M_{\rm crit}$ will still exist today, and may therefore be observable in the local universe, or conversely, if they remain unobserved, limits can be placed on their existence. For these potentially extant primordial black holes, the convention is using $f_{\rm PBH} = \Omega_{\rm PBH}/\Omega_{\rm DM}$, rather than β. Local observations let us probe $f_{\rm PBH}$ directly, and there are some subtleties in mapping $f_{\rm PBH}$ to β. However, a rough approximation, assuming a monochromatic mass distribution and a standard history of the universe, e.g. no early matter domination, can be expressed as [180],

$$\Omega_{\rm PBH} \sim 10^9 \beta \left(\frac{M}{M_\odot}\right)^{-1/2}. \tag{2.77}$$

Black holes with masses not much larger than $M_{\rm crit}$ would still have non-negligible Hawking emission, which severely limits their existence due to non-observation. These constraints form the

bulk of the low-mass end of Fig. 2.10, including both constraints from galactic and extragalactic emissions, as well as CMB. However, this constraint quickly drops off at higher masses for two compounding reasons. As the mass increases, the emission from each individual black hole decreases sharply, as implied by Eq. (2.75). Additionally, due to the higher mass of each individual black hole,

Primordial black holes at the large end of the spectrum can also be constrained by some non-local measurements such as CMB and the EDGES experiment, from the energy injection due to accretion that such a heavy ($M \gtrsim 100 M_\odot$) primordial black hole would cause in the much denser environment of e.g. the CMB epoch.

Another way of constraining the galactic population of primordial black holes (which should be indicative of the global population), is through microlensing. Indeed, primordial black holes are the quintessential MACHO, they are massive, compact, and distributed in the halo (if they form a fraction of the dark matter) [562, 563]. As shown in Fig. 2.10, microlensing can constrain primordial black holes over an incredibly wide mass range, from $\sim 10^{-10} M_\odot$ to $\sim 10^4 M_\odot$, more than ten orders of magnitude. The constraints relying on the galactic population of primordial black holes are not entirely independent, as they rely on assumptions regarding their distribution in the halo. They are generally assumed to follow the dark matter distribution, for which an NFW profile or similar is often used [180].

Another avenue for constraining primordial black holes has been introduced in recent years, as the technology has become available. Since the detection of gravitational waves, these have also been used to set limits on the primordial black hole abundance. As they are formed in the early universe, these black holes would form binary systems [564, 565] which will coalesce over cosmic timescales.[12] Such binaries could also form through dynamic interactions in dark matter halos [568], and these formation mechanisms would all lead to an expected merger rate if these primordial black holes constitute a fraction of the dark matter. Such mergers would be detectable from their gravitational wave emission, either as individual events [491, 569], or as part of the stochastic gravitational wave background [570], which sets strong limits on a range of black hole masses. Future experiments will be able to further constrain new regions at lower masses [571].

A multitude of different constraints are presented in Fig. 2.10, which neatly illustrates how much work the community has put into looking for primordial black holes. Assuming existing limits not requiring any reevaluation, as has happened before [468, 566], the only mass range where primordial black holes are able to make up the entirety of the dark matter is in the so-called "asteroid range", with masses $\lesssim 10^{18}$ g, where they are heavy enough for their Hawking radiation to be undetectable, but not so heavy as to be readily detectable through other methods.

These constraints have generally been derived for monochromatic mass distributions, though it could be argued that they may be applicable if the distribution width is much smaller than the mean mass [180]. Such a distribution is by no means a generic prediction, and indeed many models may predict extended distributions [467]. Such distributions are trickier to constrain, as not all black holes will contribute equally to the observable in question due to their different masses. However, it has been suggested that the constraints on monochromatic distributions can be mapped to extended distributions, essentially by viewing the extended distribution as a sum of monochromatic ones, and indeed work has gone into investigating such scenarios [613–618], and determining likely mass distributions [619–621]. Limits on such distributions are also slightly harder to communicate, as the parameter space becomes multidimensional, necessitating parameter scans for constrains to cover the possible space (see for example Fig. 8.4).

[12] Assuming the black holes behave as described by a Schwarzschild metric embedded in an FLRW spacetime. This may not be an accurate description of the early universe as described in Refs. [566, 567].

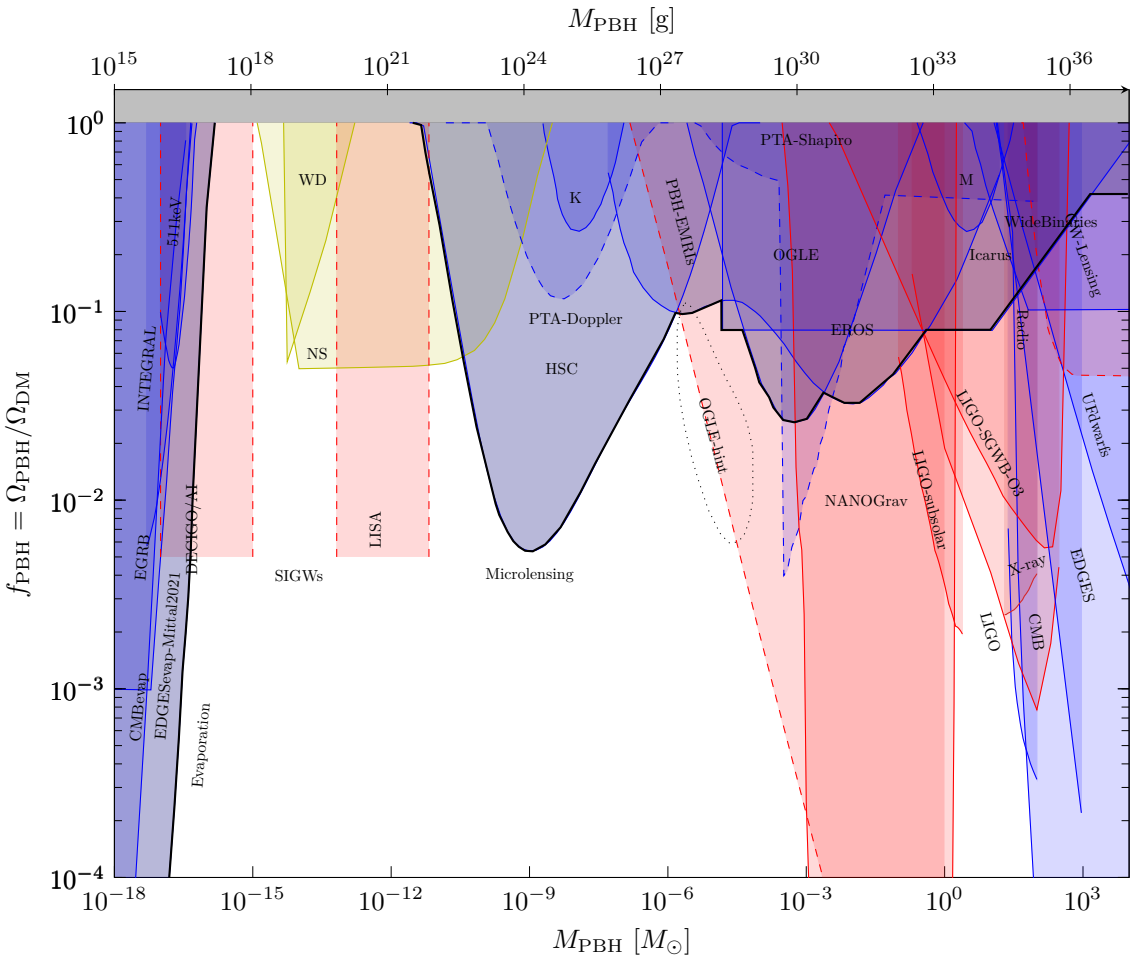

Figure 2.10: *A multitude of different constraints on monochromatic primordial black hole populations, as collated and presented in Ref. [572], using results from Refs. [177, 477, 491, 560, 569, 573–612]. Blue curves indicate limits from "traditional" photon observations, red curves indicate gravitational wave observations, and the yellow curves are indirect constraints from white dwarfs and neutrons stars not being disrupted. Dashed lines are projections.*

In my own research, I have also worked on constraining extended mass distributions of primordial black holes, an in particular on developing a simple formalism for determining the mass distribution today from an initial distribution [4]. This work is included here as Chapter 8.

CHAPTER 3

Linear Cosmology

In ΛCDM and other cosmological models whose matter budget is dominated by dark matter, the dark matter is generally responsible for the formation of structure through its impact on the gravitational potential. An important tool for investigating a dark matter model is thus to predict its impact on cosmological structure formation, both to ensure that it is consistent with existing observations, and to determine distinguishing features of the model that can be used to discriminate between different scenarios, and thus ultimately help discover the nature of dark matter.

Linear perturbation theory is often the first port of call to compute structure formation predictions, and generally a very useful tool for cosmology. The term linear here means that we only go to first order in our perturbation theory, with zeroth order just referring to the global mean values of parameters such as densities, described in Section 1.2.

When the evolution of our universe as we understand it starts, the initial conditions set by inflation are incredibly homogeneous with only tiny fluctuations around the mean density. However, when allowed to grow, these fluctuations eventually form the basis of all structures in the universe. As long as these fluctuations remain small relative to the mean density,

Many of the conventions of the field are based on those used in Ref. [163], which forms the basis of much of this chapter.

If we want to describe how the primordial fluctuations evolve in a quantitative way, we need a mathematical framework to do so. The various components of the universe, photons, baryons, dark matter, etc. are essentially ensembles of particles. There are of course far too many particles to model them individually, but kinetic theory allows us to model their phase space distributions and track their evolution. For this, we use the Boltzmann equation, which can be expressed schematically as,

$$\frac{Df}{dt} = C\left[f\right]. \tag{3.1}$$

Here $f\left(x, p, t\right)$ is the phase space (generalised position + momentum conjugate) distribution function, D/dt is the full time derivative, also known as the Liouville operator, and C is the collision operator. It gives the number of particles in a differential phase-space volume at a given time,

$$f(x, p, t) d^3x\, d^3p = dN, \tag{3.2}$$

and Liouville's theorem states that this is constant along the trajectories of the system, that is, as long as the collision operator is zero.

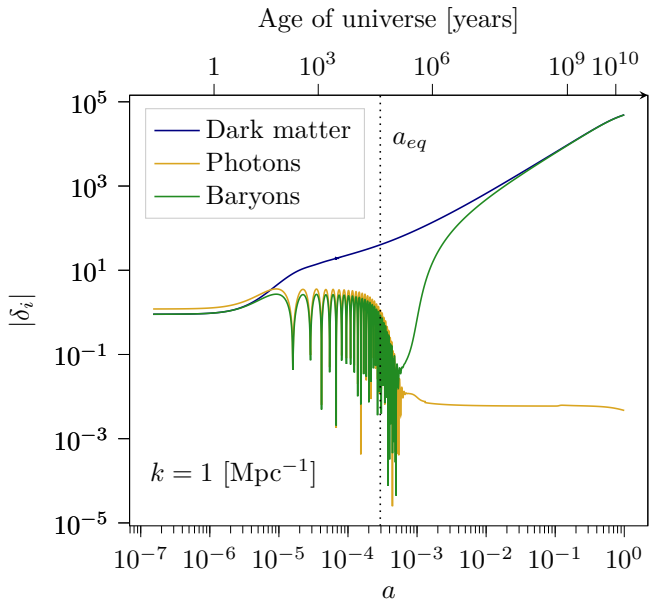

Figure 3.1: *The evolution of the density perturbations of various components of the universe at scales $k = 1$ Mpc^{-1}. Densities are plotted normalised to initial curvature perturbation amplitude $A_s = 1$, as is convention. Observations find $A_s = \left(2.101^{+0.031}_{-0.034}\right) \cdot 10^{-9}$ [5]. The perturbations should be scaled with $\sqrt{A_s}$, firmly putting them $\ll 1$ for most of this range.*

In the context of cosmology, this means that the left-hand side governs the evolution of the distribution function due to gravity and the current momentum, while the collision operator on the right-hand side describes non-gravitational interparticle interactions. A species with $C = 0$ will simply evolve on its existing trajectory under gravity, while interacting species will have more complicated evolution.

3.1 The perturbed Einstein equations

Since we are interested in doing cosmology, we are looking at cosmological scales for both space and time, meaning that we need to use a relativistic framework. This introduces another wrinkle, namely that of gauge freedom. General relativity contains redundant degrees of freedom, and it is therefore necessary to pick a gauge, essentially a set of coordinates, in order to unambiguously define a perturbation: the difference in a given quantity at a specific set of coordinates [622]. Two of the gauges most commonly used for cosmological perturbation theory are the synchronous and Newtonian gauges. The perturbed metrics are respectively defined as

$$ds^2 = a^2 \left\{ -d\tau^2 + (\delta_{ij} + h_{ij})\, dx^i dx^j \right\}, \tag{3.3}$$

for the synchronous gauge, and

$$ds^2 = a^2 \left\{ -(1 + 2\psi)\, d\tau^2 + (1 - 2\phi)\, dx^i dx_j \right\}, \tag{3.4}$$

for the Newtonian gauge[1] in the case of scalar perturbations. The synchronous gauge is defined as the rest frame of a freely falling observer, and the Newtonian gauge is defined such that the expansion rate is shear free [622]. The Newtonian gauge has the pedagogical benefit that

[1] Sometimes, a distinction is drawn between the *conformal* Newtonian gauge, which uses conformal time, and the Newtonian gauge which does not. This is in fact the former, but the prefix is omitted for brevity.

the scalar potential ψ is the equivalent of the gravitational potential when in the Newtonian limit. Additionally, while not generally true, $\psi = \phi$ in a universe with no anisotropic stress. For simplicity, I will be using only the Newtonian gauge for the rest of this chapter. Since the time coordinate used is conformal time, overdots will represent derivatives with respect to conformal time.

The next step is determining ψ and ϕ, and to do this, we can use the Einstein equation, Eq. (1.1). It turns out that the equations simplify greatly by going to Fourier space. In a flat universe, we get

$$k^2\phi + 3\frac{\dot{a}}{a}\left(\dot{\phi} + \frac{\dot{a}}{a}\psi\right) = 4\pi G a^2 \delta T^0{}_0\,, \tag{3.5a}$$

$$k^2\left(\dot{\phi} + \frac{\dot{a}}{a}\psi\right) = 4\pi G a^2\left(\bar{\rho} + \bar{P}\right)\theta, \tag{3.5b}$$

$$\ddot{\phi} + \frac{\dot{a}}{a}\left(\dot{\psi} + 2\dot{\phi}\right) + \left(2\frac{\ddot{a}}{a} - \frac{\dot{a}^2}{a^2}\right)\psi = \frac{4\pi}{3} G a^2 \delta T^i{}_i\,, \tag{3.5c}$$

$$k^2(\phi - \psi) = 12\pi G a^2\left(\bar{\rho} + \bar{P}\right)\sigma, \tag{3.5d}$$

where δT^μ_ν is the perturbation to the stress-energy tensor, and the parameters θ and σ are defined through the relations

$$\left(\bar{\rho} + \bar{P}\right)\theta \equiv ik^j \delta T^0{}_j\,, \tag{3.6a}$$

$$\left(\bar{\rho} + \bar{P}\right)\sigma \equiv -\left(\hat{k}_i\hat{k}^j - \frac{\delta_i{}^j}{3}\right)\Sigma^i{}_j, \tag{3.6b}$$

where $\Sigma^i{}_j \equiv T^i{}_j - \delta^i{}_j T^k{}_k$ is the traceless component of the stress-energy tensor. The quantities $\left(\bar{\rho} + \bar{P}\right)\theta$ and $\left(\bar{\rho} + \bar{P}\right)\sigma$ are summed over each component of the universe, meaning baryons, photons etc.

Defining the perturbations $\delta P = P - \bar{P}$ and $\delta\rho = \rho - \bar{\rho}$, and the coordinate velocity $v^i = dx^i/d\tau$ of a fluid, which can be treated as a perturbation as long as it is small, the linear perturbed stress-energy tensor is given as

$$T^0{}_0 = -\left(\bar{\rho} + \delta\rho\right), \tag{3.7a}$$

$$T^0{}_i = \left(\bar{\rho} + \bar{P}\right)v_i = -T^i{}_0\,, \tag{3.7b}$$

$$T^i{}_j = \left(\bar{P} + \delta P\right)\delta^i{}_j + \Sigma^i{}_j, \quad \Sigma^i{}_i = 0. \tag{3.7c}$$

Comparing Eqs. (3.6a) and (3.7b), we can see that θ is the divergence of the fluid velocity, $\theta = ik^j v_j$. It is also useful to define the dimensionless density perturbation $\delta = \delta\rho/\bar{\rho}$.

Using the fact that the stress-energy tensor is conserved under covariant derivatives, $T^\mu{}_{\nu;\mu}$, we can write equations of motion for these perturbations,

$$\dot{\delta} = -(1+w)\left(\theta - 3\dot{\phi}\right) - 3\frac{\dot{a}}{a}\left(\frac{\delta P}{\delta\rho} - w\right)\delta, \tag{3.8}$$

$$\dot{\theta} = -\frac{\dot{a}}{a}(1-3w)\theta - \frac{\dot{w}}{1+w}\theta + \frac{\delta P\delta\rho}{1+w}k^2\delta - k^2\sigma + k^2\psi, \tag{3.9}$$

which hold for the total mass-averaged content of the universe, or for a single non-interacting component. As implied earlier, things get a bit more complicated once interactions are involved.

3.2 The Boltzmann equation

Remembering our definition of the distribution function Eq. (3.2), we can now express it in terms of the relativistic conjugate momentum, rather than proper momentum. The conjugate

momentum is the spatial part of the 4-momentum, $P_i = mU_i$ with $U_i = dx_i/\sqrt{-ds^2}$. The relationship between conjugate and proper momentum is given in the Newtonian gauge as

$$P_i = a(1-\phi)p_i, \tag{3.10}$$

so again we can write

$$f(x^i, P_j, \tau)dx^1\, dx^2\, dx^3\, dP_1\, dP_2\, dP_3 = dN. \tag{3.11}$$

However, while the conjugate momentum is necessary to define the phase space volume, it may not be the most intuitive or convenient momentum coordinate. We therefore also introduce the comoving momentum $q_i \equiv ap_i$, which can itself be separated into a magnitude q and a directional unit vector n_i as $q_i = qn_i$. The Boltzmann equation in terms of conformal time and comoving momentum, is the written as

$$\frac{Df}{d\tau} = \frac{\partial f}{\partial \tau} + \frac{dx^i}{d\tau}\frac{\partial f}{\partial x^i} + \frac{dq}{d\tau}\frac{\partial f}{\partial q} + \frac{dn_i}{d\tau}\frac{\partial f}{\partial n_i} = \left(\frac{\partial f}{\partial \tau}\right)_C. \tag{3.12}$$

Analogously to the comoving momentum q, it can be useful to define a "comoving energy" $\epsilon = \sqrt{q^2 + a^2m^2}$, which in the Newtonian gauge is related to the conjugate momentum through $P_0 = -(1+\psi)\epsilon$. Having thus fully defined our conjugate 4-momentum, we can write the stress-energy tensor in terms of the distribution function,

$$T_{\mu\nu}\int dP_1 dP_2 dP_3 \sqrt{-g}\frac{P_\mu P_\nu}{P^0} f(x^i, P_j, \tau), \tag{3.13}$$

with g being the determinant of the metric tensor.

We can describe the full distribution in terms of a sum of the unperturbed distribution function and a perturbation,

$$f\left(x^i, q, n_j, \tau\right) = f_0(q)\left[1 + \Psi\left(x^i, q, n_j, \tau\right)\right], \tag{3.14}$$

where the unperturbed distribution function $f_0(q)$ is just the Bose-Einstein distribution for Bosons, and the Fermi-Dirac distribution for Fermions (or the Maxwell-Boltzmann distribution, if you do not want to account for quantum statistics). This allows us to write the stress-energy tensor in terms of the perturbation,

$$T^0{}_0 = -a^{-4}\int q^2 dq\, d\Omega\, \epsilon f_0(q)(1+\Psi) \tag{3.15a}$$

$$T^0{}_i = a^{-4}\int q^3 dq\, d\Omega\, n_i f_0(q)\Psi \tag{3.15b}$$

$$T^i{}_j = a^{-4}\int q^4 dq\, d\Omega\, \frac{n_i n_j}{\sqrt{\epsilon}} f_0(q)(1+\Psi) \tag{3.15c}$$

Since $f_0(q)$ is a well known quantity, we only need to worry about how to evolve Ψ. It would therefore be useful to rewrite Eq. (3.12) in terms of Ψ rather than f.

The first term $\partial f/\partial\tau$ is just $f_0\dot{\Psi}$, since the unperturbed distribution depends only on q. For the second term, remember how going to Fourier space greatly simplifies dealing with spatial derivatives, meaning that $\partial f/\partial x^i = ik_i f_0\Psi$ (f_0 having no spatial dependence), and $dx^i/d\tau = n^i q/\epsilon$. The third term is a bit more tricky, but via the geodesic equation, we can find that

$$\frac{dq}{d\tau} = q\dot{\phi} - \epsilon n_i \frac{\partial\psi}{\partial x^i}. \tag{3.16}$$

The other derivative in this term evaluates to

$$\frac{\partial f}{\partial q} = \frac{df_0}{dq}(1+\Psi) + f_0\frac{\partial\Psi}{\partial q}.$$

This could quickly get very messy. However, now is a good time to invoke that we are only interested in the linear terms, meaning that if two (or more) small quantities get multiplied, we can throw the resulting term away. Luckily for the simplicity of the final equation, both terms in Eq. (3.16) contains a small quantity, and we are therefore left with just Eq. (3.16) multiplied with $\frac{df_0}{dq}$. The linearity criterion is even more powerful for the fourth term since both $dn_i/d\tau$ and $\partial f/\partial n_i$ are first order quantities, allowing the entire term to be dropped.

Having thus expressed each of the terms via Ψ (except the collision term, which will depend on the particular species), we can put them together and divide by f_0 for simplicity, to arrive at

$$\frac{\partial\Psi}{\partial\tau} + i\frac{q}{\epsilon}(\vec{k}\cdot\hat{n})\Psi + \frac{d\ln f_0}{d\ln q}\left(\dot{\phi} - i\frac{\epsilon}{q}(\vec{k}\cdot\hat{n})\psi\right) = \frac{1}{f_0}\left(\frac{\partial f}{\partial\tau}\right)_C, \tag{3.17}$$

remembering that $\frac{d\ln f_0}{d\ln q} = \frac{q}{f_0}\frac{df_0}{dq}$.

It is evident that Eq. (3.17) does not have any inherent dependence on the direction of momentum $\hat{n}$, which only enters via its dot product, and thus angle, with the Fourier wave vector $\vec{k}$, meaning that a phase space perturbation whose momentum dependence is axially symmetric around $\vec{k}$ will retain this symmetry. This is usually assumed to be the case, because any collisionless species whose initial perturbation is not axially asymmetric would not give rise to scalar metric perturbations and hence no effect on other species. Thus, another advantage of Fourier space is that the momentum dependence of Ψ is simpler; rather than depending on the three components of a vector $\vec{q} = q\hat{n}$, the dependence is only on the two scalars q and $(\hat{k}\cdot\hat{n})$.

3.3 Collisionless species

It is prudent to first present the species requiring the simplest treatment, as an introduction, before grappling with the more complicated case of interactions. Of course, some (if not all) of these species are not truly non-interacting, but their coupling strengths are small enough that for the relevant regime, they can be treated as such.

3.3.1 Cold dark matter

The simplest possible case is the textbook example of cold, collisionless dark matter (CDM). If dark matter is a particle like those we know from the standard models, it must have some non-zero interactions, e.g. in order to be produced in the early universe. However, so far, the non-interacting approximation has been good enough that it has remained the standard prescription, even if it is theoretically flawed.

Because of the assumption of coldness, that is, the particle momentum is generally small compared to the mass, the equation of state parameter for CDM is $w = 0$, hence it is also pressureless $P = 0$. Using Eq. (3.8) leaves us with the simple evolution equation for the energy density,

$$\dot{\delta}_{\rm cdm} = -\theta_{\rm cdm} + 3\dot{\phi}, \tag{3.18}$$

denoting that the change in energy density of CDM is governed just by the bulk flow (as described by the velocity divergence $\theta_{\rm cdm}$) and the change in the gravitional potential. To get the evolution of the velocity divergence $\theta_{\rm cdm}$, we just use Eq. (3.9),

$$\dot{\theta}_{\rm cdm} = -\frac{\dot{a}}{a}\theta + k^2\psi. \tag{3.19}$$

This simple expression is fairly easy to interpret. The first term denotes that the velocity gets redshifted as the universe expands, and the second term is just acceleration due to gravity. Exactly the behaviour we would expect from a non-relativistic, non-interacting species.

The linear evolution of the cold dark matter distribution is completely described by Eqs. (3.18) and (3.19), their continuity and Euler equation respectively.

3.3.2 Massless neutrinos

While neutrino oscillation experiments indicate that at least two of the three neutrino mass states associated with standard model neutrinos have nonzero mass, the neutrino mass is sometimes neglected in cosmology, especially when the desired information is not related to high-precision predictions of the neutrino sector. After all, cosmology has not yet been able to detect the presence of neutrino masses, but can only set bounds on the upper limit on their sum. A bound which grows ever tighter, and which may result in a "detection" of a non-zero mass-sum with the next generation of experiments [166, 623–628].

However in the meantime, unless we are interested in the observables specifically connected to neutrinos having mass, the error introduced by neglecting it is generally small, after all, if it had a strong effect, it would have been detected already, rather than only constrained. This also serves as a good pedagogical example of a massless species, similar to photons, but without the complications introduces by the scattering with baryons.[2]

Having no rest mass, the energy density of massless neutrinos is entirely kinetic, and the mean energy and pressure are hence related as,

$$\bar{\rho}_\nu = 3\bar{P}_\nu = a^{-4}\int q^3 dq d\Omega f_0(q), \tag{3.20}$$

as implied by Eq. (3.15a) with $\epsilon = q$. Note that in this section, the subscript ν refers to neutrinos and is not a 4-index.

The perturbations are then given, following Eq. (3.15) and Eq. (3.20), as

$$\delta\rho_\nu = 3\delta P_\nu = a^{-4}\int q^3 dq d\Omega\, f_0(q)\Psi \tag{3.21a}$$

$$\delta T_\nu{}^0{}_i = a^{-4}\int q^3 dq d\Omega\, n_i\, f_0(q)\Psi \tag{3.21b}$$

$$\Sigma_\nu{}^i{}_j = a^{-4}\int q^3 dq d\Omega\, (n_i n_j - \frac{\delta_{ij}}{3})\, f_0(q)\Psi, \tag{3.21c}$$

with the unperturbed $T_\nu{}^0{}_i$ and shear stress $\Sigma_\nu{}^i{}_j$ both being zero.

Since the massless neutrinos are always relativistic, these integrals are analytically possible. It therefore makes sense to define the integrated quantity,

$$F_\nu(\vec{k}, \hat{n}, \tau) \equiv \frac{\int q^3 dq\, f_0(q)\Psi}{\int q^3 dq\, f_0(q)}, \tag{3.22}$$

which can be expanded into a Legendre series of functions $F_{\nu l}(\vec{k}, \tau)$,

$$F_\nu(\vec{k}, \hat{n}, \tau) \equiv \sum_{l=0}^{\infty}(-i)^l(2l+1)F_{\nu l}(\vec{k}, \tau)P_l(\hat{k}\cdot\hat{n}), \tag{3.23}$$

[2] Of course, neutrinos do scatter with standard model particles, we have neutrino detectors after all, but neutrinos decouple earlier than these linear Boltzmann treatments begin, when the thermal bath of the universe was around a few MeV in temperature, and essentially never interact again under cosmological densities [629–631].

where P_l is the lth Legendre polynomial. This basis lets us simply express the perturbations,

$$\delta_\nu = \frac{1}{4\pi}\int d\Omega\, F_\nu(\vec{k},\hat{n},\tau) = F_{\nu 0}, \tag{3.24a}$$

$$\theta_\nu = \frac{3i}{16\pi}\int d\Omega\, k(\hat{k}\cdot\hat{n})F_\nu(\vec{k},\hat{n},\tau) = \frac{3k}{4}F_{\nu 1}, \tag{3.24b}$$

$$\sigma_\nu = -\frac{3}{16\pi}\int d\Omega\, \left((\hat{k}\cdot\hat{n})^2 - \frac{1}{3}\right) F_\nu(\vec{k},\hat{n},\tau) = \frac{1}{2}F_{\nu 2}, \tag{3.24c}$$

for the density, velocity and anisotropic stress. We can perform an integral as in Eq. (3.22) on the perturbation evolution equation, Eq. (3.17), yielding the evolution of F_ν,

$$\frac{\partial F_\nu}{\partial\tau} + ik\mu F_\nu = 4(\dot{\phi} - ik\mu\psi), \tag{3.25}$$

where $\mu \equiv (\hat{k}\cdot\hat{n})$. The Legendre decomposition can also be applied here to yield evolution equations for δ_ν, θ_ν, etc. following Eq. (3.24). This gives,

$$\dot{\delta}_\nu = -\frac{4}{3}\theta_\nu + 4\dot{\phi}, \tag{3.26a}$$

$$\dot{\theta}_\nu = k^2\left(\frac{\delta_\nu}{4} - \sigma_\nu\right) + k^2\psi, \tag{3.26b}$$

$$\dot{F}_{\nu l} = \frac{k}{2l+1}\left(lF_{\nu(l-1)} - (l+1)F_{\nu(l+1)}\right), \quad l \geq 2, \tag{3.26c}$$

using the recursion relation for Legendre polynomials

$$(l+1)P_{l+1}(\mu) = (2l+1)\mu P_l(\mu) - lP_{l-1}(\mu). \tag{3.27}$$

This is all well and good mathematically, however, when in comes to actually computing this evolution, we run into the issue that there is technically an infinite hierarchy of functions $F_{\nu l}$ to evolve, each depending on the two neighboring ls. Practically, some truncation scheme must be used to do any computations.

The most naive solution is to select some $l_{\max}$ and set $F_{\nu(l>l_{\max})} = 0$. This does not work well in practice, unless some incredibly large l is chosen, as the coupling to higher ls in Eq. (3.26c) will uphysically reflect power at the hard boundary, and this introduced error will propagate down through the hierarchy, reaching $l = 0$ in a time $\tau \sim l_{\max}/k$, meaning that for the error to only reach δ_ν at $z = 0$ and $k = 1$, it is necessary to have $l_{\max} = \mathcal{O}(10^4)$, which even then would still leave all higher multipoles with the introduced error. It would hence be preferable to choose some smarter truncation scheme.

Luckily, it turns out that the higher multipole moments are gauge invariant, and they show behaviour similar to spherical Bessel functions. Indeed, for $\partial(\phi+\psi)/\partial\tau = 0$, the spherical Bessel functions will be exact solutions for multipoles $l > 0$, up to some factor,

$$F_{\nu l} \propto j_l(k\tau). \tag{3.28}$$

As demonstrated in [163], this means that we can use the properties of the Bessel functions to make the approximation

$$F_{\nu(l_{\max}+1)} \approx \frac{2l_{\max}+1}{k\tau}F_{\nu l_{\max}} - F_{\nu(l_{\max}-1)}. \tag{3.29}$$

This approximation greatly improves the accuracy compared to setting $F_{\nu(l_{\max}+1)} = 0$, but it is still necessary to be careful not to select a too small $l_{\max}$ due to the effects of time variation

of the potentials during radiation dominating, as indeed Eq. (3.28) does not hold then. For an accurate prediction of the CMB spectrum, it is necessary to have $l_{\max} = \mathcal{O}(30)$. The matter power spectrum $P(k)$ may need a higher $l_{\max}$, denpending in the scales of interest, with $l_{\max}$ proportional to the maximum k desired [67].

However, there are further approximations that could be made for the sake of computational efficiency without sacrificing too much accuracy. Indeed, Ref. [67] implements an Ultra-relativistic Fluid Approximation, based on the notion that the $l_{\max}$ required for the desired accuracy is not necessarily constant throughout the history of the universe. In practice, the k-space is separated into two (time dependent) regimes: sub-horizon wavelengths, and horizon-sized to super-horizon wavelengths. The transition between the regimes occurs for a given wavelength when $k\tau = (k\tau)_{\text{ufa}}$, where $(k\tau)_{\text{ufa}}$ is usually chosen to be between 10 and 50, depending on desired precision. While in the $k\tau \leq (k\tau)_{\text{ufa}}$ regime, the higher multipoles ($l > k\tau$) are negligible (per the Bessel approximation), so it is enough to have $l_{\max} \sim (k\tau)_{\text{ufa}}$. In the other regime, where $k\tau \geq (k\tau)_{\text{ufa}}$, the first three multipoles, δ_ν, θ_ν, and σ_ν, are effectively decoupled from the $l > 2$ multipoles, so $l_{\max}$ can be set to 2, and the the massless neutrinos can be described by three equations for a non-perfect fluid. Ref. [67] introduces the modified equation for σ_ν,

$$\dot{\sigma}_\nu^{(\text{ufa})} = -\frac{3}{\tau}\sigma_\nu + \frac{2}{3}\theta_\nu - 6\dot{\phi}, \tag{3.30}$$

where the standard truncation scheme Eq. (3.29) would give,

$$\dot{\sigma}_\nu^{(\text{ufa})} = -\frac{3}{\tau}\sigma_\nu + \frac{2}{3}\theta_\nu. \tag{3.31}$$

A third option was presented in ref. [632] as part of a generalised framework for the cosmological evolution of a viscous fluid, using the equation

$$\dot{\sigma}_\nu^{(\text{ufa})} = -3\frac{\dot{a}}{a}\sigma_\nu + \frac{2}{3}\theta_\nu. \tag{3.32}$$

It was found in Ref. [67] that the truncation Eq. (3.30) is slightly more precise than the other two options.

At late times, it is possible to go even further. In the "late" universe, after photons have decoupled and the universe is matter or Λ dominated, the massless neutrino contribution to the total energy density is almost negligible and it is not as important to track their evolution with the same accuracy as during radiation domination, where they contributed significantly to the Einstein equations. Here we can use the so-called Radiation Streaming Approximation.

The oscillations of the Bessel functions will have died down on small enough scales at these late times ($k\tau \gg l$), and the standard truncation schemes may lead to spurious oscillations. An analytic approximation to δ and θ will therefore be beneficial at late times, both by lowering computational load, and by avoiding spurious oscillations from truncation. An spproximate analytic equation for δ_ν can be found by combining Eqs. (3.26a) and (3.26b), yielding

$$\delta_\nu^{(\text{rsa})} = -4\phi, \tag{3.33}$$

using $\phi \approx \psi$, $\ddot{\phi} \approx 0$, and neglecting other terms since $|\delta_\nu| \gg |\sigma_\nu|$ and $k^2|\delta_\nu| \gg |\ddot{\delta}_\nu|$ [67, 633], then using energy conservation and the Einstein equations, the velocity divergence is

$$\theta_\nu^{(\text{rsa})} = 6\dot{\phi}, \tag{3.34}$$

allowing for computation at late times without the need to evolve a differential equation.

3.3.3 Massive neutrinos

Massive neutrinos are a bit more complicated to deal with than in the massless approximation, due to the fact that they transition from highly relativistic in the early universe to non-relativistic in the late universe. From neutrino oscillations, we can infer that at least two neutrinos have a mass $m_\nu \gtrsim 8.6 \cdot 10^{-3}$ eV [253], which seems small, but not compared to the current energy of a CMB photon $\sim 2.5 \cdot 10^{-4}$ eV. Indeed, based on the mass splittings calculated from neutrino oscillation data, we can conclude that at least two of the standard model neutrino species are nonrelativistic today.

This is rather troublesome, because that takes away the powerful approximation $E \approx M \gg p$, as for cold dark matter, and the equality $E = p$ of massless neutrinos. This means that we are generally unable to analytically perform the integral over momentum, as in Eqs. (3.15) and (3.24). It is necessary, instead, to evolve the momentum dependent perturbation to the distribution function, Ψ, if we want to compute the evolution of perturbations. The mean background quantities are not quite as challenging, being given by

$$\bar{\rho}_\nu = a^{-4} \int q^2 dq d\Omega \epsilon f_0(q), \tag{3.35a}$$

$$\bar{P}_\nu = \frac{-4}{3} \int q^2 dq d\Omega \frac{q^2}{\epsilon} f_0(q), \tag{3.35b}$$

and while we need a numerical treatment to compute the integrals to obtain the perturbed quantities, we can fortunately still express them,

$$\delta\rho_\nu = a^{-4} \int q^2 dq d\Omega \epsilon f_0(q) \Psi, \tag{3.36a}$$

$$\delta P_\nu = \frac{a^{-4}}{3} \int q^4 dq d\Omega \frac{f_0(q)}{\epsilon} \Psi, \tag{3.36b}$$

$$\delta T_\nu{}^0{}_i = a^{-4} \int q^3 dq d\Omega \, n_i \, f_0(q) \Psi, \tag{3.36c}$$

$$\Sigma_\nu{}^i{}_j = a^{-4} \int q^4 dq d\Omega \, \frac{n_i n_j - \frac{\delta_{ij}}{3}}{\epsilon} \, f_0(q) \Psi, \tag{3.36d}$$

generally similar, but not always equal to the equations for massless neutrinos, since the presence of mass leads to $\epsilon \neq q$. However, to make the system numerically tractable, we can perform a similar Legendre decomposition as with the massless neutrinos, Eq. (3.23), though in this case it must be performed on the momentum dependent perturbation Ψ. We can define the multipole moments Ψ_l,

$$\Psi\left(\vec{k}, \hat{n}, q, \tau\right) = \sum_{l=0}^{\infty} (-i)^l (2l+1) \Psi_l(\vec{k}, q, \tau) P_l(\hat{k} \cdot \hat{n}), \tag{3.37}$$

which can also also be used to compute the perturbation quantities,

$$\delta\rho_\nu = 4\pi a^{-4} \int q^2 dq \epsilon f_0(q) \Psi_0, \tag{3.38a}$$

$$\delta P_\nu = \frac{4\pi a^{-4}}{3} \int q^2 dq \frac{f_0(q)}{\epsilon} \Psi_0, \tag{3.38b}$$

$$\left(\bar{\rho}_\nu + \bar{P}_\nu\right) \theta_\nu = 4\pi k a^{-4} \int q^3 dq f_0(q) \Psi_1, \tag{3.38c}$$

$$\left(\bar{\rho}_\nu + \bar{P}_\nu\right) \sigma_\nu = \frac{8\pi a^{-4}}{3} \int q^4 \frac{f_0(q)}{\epsilon} \Psi_2. \tag{3.38d}$$

The equations for the evolution of perturbation multipole moments can be obtained following the same method as with the massless neutrinos, and are,

$$\dot{\Psi}_0 = -\frac{qk}{\epsilon}\Psi_1 - \dot{\phi}\frac{d\ln f_0}{d\ln q}, \tag{3.39a}$$

$$\dot{\Psi}_1 = \frac{qk}{3\epsilon}\left(\Psi_0 - 2\Psi_2\right) - \frac{\epsilon k}{3q}\psi\frac{d\ln f_0}{d\ln q}, \tag{3.39b}$$

$$\dot{\Psi}_l = \frac{qk}{(2l+1)\epsilon}\left(l\Psi_{l-1} - (l+1)\Psi_{l+1}\right), \quad l \geq 2. \tag{3.39c}$$

The fact that the Ψ_l multipole moments are momentum dependent means that, rather than evolving one equation per multipole, the equation must be split into momentum bins, which are evolved separately, as in Refs. [163, 634–636]. This makes massless each massive neutrino multipole significantly more computationally expensive than their massless counterparts. Again, the technically infinite hierarchy must be truncated, which can be done in a similar fashion to the case of massless neutrinos,

$$\Psi_{(l_{\max}+1)} \approx \frac{(2l_{\max}+1)\epsilon}{qk\tau}\Psi_{l_{\max}} - \Psi_{(l_{\max}-1)}, \tag{3.40}$$

though the presence of mass means that the higher multipoles will quickly be suppressed once the neutrinos become non-relativistic. Hence, a smaller $l_{\max}$ is sufficient.

For the sake of computational efficiency, there have been a variety of approximations suggested in the literature [632, 635, 637–639]. It is possible to introduce a Fluid Approximation, similar to the Ultra-relativistic Fluid Approximation of the massive neutrinos, using the fact that, in the relativistic regime, there is an effective decoupling between low and high multipoles after a mode enters the horizon. In the non-relativistic regime, the massive neutrinos will behave more like a pressureless fluid, in which case a fluid approximation is also applicable. The first two fluid equations can thus be written as,

$$\dot{\delta}_\nu = -(1+w_\nu)\left(\theta_\nu - 3\dot{\phi}\right) - 3\frac{\dot{a}}{a}\left(c^2_{\text{eff}} - w_\nu\right)\delta_\nu, \tag{3.41a}$$

$$\dot{\theta}_\nu = -\frac{\dot{a}}{a}\left(1 - 3c^2_{\text{a}}\right)\theta_\nu + \frac{c^2_{\text{eff}}}{1+w_\nu}k^2\delta_\nu - k^2\sigma_\nu + k^2\psi, \tag{3.41b}$$

where $w_\nu = \bar{P}_\nu/\bar{\rho}_\nu$ is the equation of state parameter, $c^2_{\text{a}} \equiv \dot{P}_\nu/\dot{\rho}_\nu$ is the adiabatic sound speed squared, and c^2_{eff} is the effective sound speed squared. Ref. [635] uses the approximation that $c^2_{\text{a}} \approx c^2_{\text{eff}}$, and computes it through

$$c^2_{\text{a}} = \frac{w}{3(1+w)}\left(5 - \frac{\mathfrak{p}}{p}\right), \tag{3.42}$$

with $\mathfrak{p}$ being the "pseudo-pressure" defined as

$$\mathfrak{p} \equiv \frac{4\pi}{3}\left(\frac{T_{\nu,0}}{a}\right)^4 \int_0^\infty dq f_0(q)\frac{q^6}{\epsilon^3}, \tag{3.43}$$

where $T_{\nu,0}$ is the neutrino temperature today. The same reference presents an approximate equation for $\dot{\sigma}_\nu$,

$$\dot{\sigma}_\nu = -3\left(\frac{\dot{a}}{a}\left(\frac{2}{3} - c^2_{\text{a}} - \frac{\mathfrak{p}}{p}\right) + \frac{1}{\tau}\right)\sigma_\nu + \frac{8}{3}\frac{3w_\nu c^2_{\text{a}}}{1+w_\nu}\left(\theta_\nu - 6\dot{\phi}\right), \tag{3.44}$$

as well as two other similar formulations,

$$\dot{\sigma}_\nu = -3\left(\frac{\dot{a}}{a}\left(\frac{2}{3} - c^2_{\text{a}} - \frac{\mathfrak{p}}{p}\right) + \frac{1}{\tau}\right)\sigma_\nu + \frac{8}{3}\frac{3w_\nu c^2_{\text{a}}}{1+w_\nu}\theta_\nu, \tag{3.45a}$$

$$\dot{\sigma}_\nu = -3\frac{\dot{a}}{a}\frac{c^2_{\text{a}}}{w_\nu}\sigma_\nu + \frac{8}{3}\frac{w_\nu}{1+w_\nu}\theta_\nu, \tag{3.45b}$$

where Eq. (3.45a) is a more naive version of Eq. (3.44), and Eq. (3.45b) is equivalent to the method proposed in Ref. [632]. All three different formulations of the fluid approximation recovers the CMB and $P(k)$ observables to sub-percent level for neutrino masses $m_\nu \leq 0.1$ eV compared to no approximation, with larger masses increasing the discrepancy [635].

The prescription for massive neutrinos can also be used for other species, since the only parameters that identify this species as standard model neutrinos are the mass (implicit in ϵ), temperature $T_{\nu,0}$, and distribution function $f_0(q)$. The prescription can in fact be used to describe any other non-cold, non-interacting species, such as warm dark matter or sterile neutrinos, as long as these parameters are set appropriately according to the given model.

3.4 Interacting species

Having run the gamut of non-interacting species, the time has finally come to confront the collision term, which allows the interaction between species. In standard ΛCDM cosmology, there are only two of these: photons and baryons. However, this interaction is responsible for both the CMB anisotropy spectrum, and baryon acoustic oscillations, not to mention the fact that we even exist, and are able to observe anything at all.

3.4.1 Baryons

In the linear description, baryons act much like cold dark matter, except the fact that they interact with photons. The regime covered here is much later than baryogenesis and BBN, so the baryons are nonrelativistic and their comoving energy density does not change, as no further baryonic matter is created or destroyed, and the energy transfer to and from photons is negligible compared to the energy density.

We can therefore write the Boltzmann hierarchy for baryons using only the continuity and Euler equations, just as for cold dark matter,

$$\dot{\delta}_b = -\theta_b + 3\dot{\phi} \tag{3.46a}$$

$$\dot{\theta}_b = -\frac{\dot{a}}{a}\theta_b + k^2\psi + c_s^2 k^2 \delta_b + \frac{4\bar{\rho}_\gamma}{3\bar{\rho}_b} a n_e \sigma_T (\theta_\gamma - \theta_b), \tag{3.46b}$$

where the amplitude of the baryon-photon scattering rate is sometimes expressed as the derivative of an optical depth, $\dot{\kappa} \equiv a\sigma_T n_e$.

It is clear that the energy density evolves just like cold dark matter, as seen in Eq. (3.18). The difference enters in the Euler equation, which has two unfamiliar terms. The first of these is the sound speed term, as sound waves can propagate through the baryon fluid. The sound speed c_s is given through

$$c_s^2 = \frac{\dot{P}_b}{\dot{\rho}_b} = \frac{k_\mathrm{B} T_b}{\mu_b}\left(1 - \frac{1}{3}\frac{d\ln T_b}{d\ln a}\right), \tag{3.47}$$

where μ_b is the mean molecular weight, including H and He ions, as well as free electrons, T_b is the baryon temperature, and k_B is the Boltzmann constant. The time variation in μ_b is small enough to be negligible for this calculation, even during recombination when it is largest. The baryon temperature, however, complicates things, as this is another evolving parameter needing its own equation.

The final term of Eq. (3.46b) is the baryon-photon momentum exchange term. The ratio $4\bar{\rho}_\gamma/3\bar{\rho}_b$ follows from momentum conservation, $\sigma_\mathrm{T} = 6.65 \cdot 10^{-29}$ m^2 is the Thomson scattering cross section, and n_e is the free electron number density. It is evident that this term is is similar to the population change terms seen in the Boltzmann equations of dark matter freeze-in/freeze-out

or in BBN (see Sections 1.3.2 and 2.1). There is a difference, in this case between the baryon and photon velocity divergences, θ_b and θ_γ, driving the coupled system towards equilibrium, and a prefactor determining the rate at which the process happens. The factor of a exactly cancels out the change over time in $\bar{\rho}_\gamma/\bar{\rho}_b$, so the evolution of the prefactor is determined entirely by n_e. For most of cosmic history, it behaves as a simple density, scaling as a^3, however there are two events where it exhibits a significantly different behaviour, namely recombination and reionization, where the free electron density significantly drops and rises, respectively, due to the formation and ionization of neutral atoms. Recombination essentially "turns off" the scattering term, and the universe goes from being opaque to transparent for the photons, creating the CMB. This means that it is very important to accurately model recombination, in order to make precise predictions. In addition to Ref. [163], this has been described in Refs. [69, 640–645]. There are several efficient and accurate software packages for computing recombination, such as RECFAST [70, 71, 646, 647] and HyRec [68, 72].

Returning to the question of the baryon temperature, from the first law of thermodynamics, it follows that the baryon temperature evolves according to

$$\dot{T}_b = -2\frac{\dot{a}}{a}T_b + \frac{8}{3}\frac{\mu_b}{m_e}\frac{\bar{\rho}_\gamma}{\bar{\rho}_b}an_e\sigma_T(T_\gamma - T_b), \tag{3.48}$$

which is quite similar to Eq. (3.46b). This makes sense, as the baryons' temperature is a measure of their kinetic energy, which non-relativistic particles is proportional to the thermal velocity squared. The factor 2 in front of the $\dot{a}/a$ term means that the temperature would scale as a^{-2} in the absence of interactions, in contrast to the bulk velocity, as described by θ_b, which scales as a^{-1}, or relativistic particles whose kinetic energy also scales as a^{-1}. The second term is similar to the momentum exchange term of Eq. (3.46b), with a few extra factors due to the specifics of energy vs. momentum transfer. It is worth noting that the reservoir of entropy in the photon fluid is much larger than in the baryons, meaning that no matter their temperature, it is essentially impossible for this energy transfer to significantly affect the global photon temperature. This means that as long as the coupling is strong, i.e. before recombination, the baryon temperature will be kept at the photon temperature, after which it will drop until some later time when reionization happens, which is generally inserted by hand. The evolution of temperature and ionization fraction can be seen in Fig. 3.2, where it is clear that the ionization drops during recombination at $z \sim 1000$, and rises again with reionization at $z \sim 10$. A more thorough description of recombination can be found in Section 1.3.3.

With only the three differential equations to evolve to describe the evolution of baryons, one would not expect there to be much need for further approximations. However, before recombination, when the interaction rate between the baryon and photon fluids is large, the system of equations becomes very stiff. To remedy this, a tight-coupling approximation is used, as described in e.g. Refs. [163, 648]. This will be further described in Section 3.4.2.

3.4.2 Photons

One of the main observables that can be predicted directly from linear theory is the CMB, which is just the redshifted cosmological photon fluid. It could therefore be argued that the accurate computation of the photons is one of the key goals of cosmological perturbation theory.

As a massless species, the Boltzmann hierarchy for photons is similar to that of massless neutrinos. However, like comparing baryons to cold dark matter, the presence of interactions complicates things. In a further wrinkle, we are also interested in the polarization states of the photons, which gives us an additional set of equations to track.

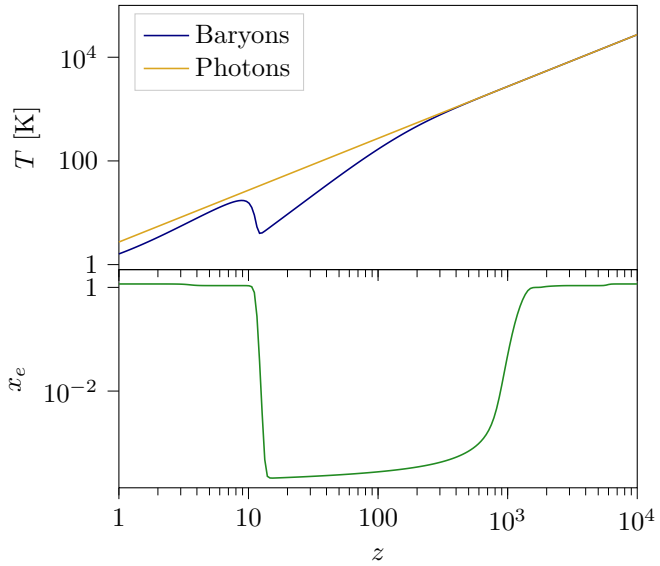

Figure 3.2: Upper: *The evolution of the baryon and photon temperatures, respectively, as a function of redshift z.* Lower: *The ionization fraction x_e as a function of redshift z.*

The momentum integrated collision operators of the Boltzmann equations are [649–652],

$$\left(\frac{\partial F_\gamma}{\partial \tau}\right)_C = a n_e \sigma_T \left(-F_\gamma + F_{\gamma 0} + \hat{n}\cdot\vec{v}_e - \frac{(F_{\gamma 2} + G_{\gamma 0} + G_{\gamma 2})P_2}{2}\right), \tag{3.49a}$$

$$\left(\frac{\partial G_\gamma}{\partial \tau}\right)_C = a n_e \sigma_T \left(-G_\gamma + \frac{(F_{\gamma 2} + G_{\gamma 0} + G_{\gamma 2})(1 - P_2)}{2}\right), \tag{3.49b}$$

where F_γ is the total phase space photon density summed over polarizations, just as F_ν for massless neutrinos, and G_γ is the difference between the two linear polarizations. The prefactor should be recognisable from the baryon equations, Eqs. (3.46b) and (3.48), $\vec{v}_e$ is the bulk velocity of the electrons, and the Legendre polynomial P_2 comes from integrating over the angular dependence of the Thomson cross section, $1 + \cos^2\theta'$ (where θ' is the scattering angle). Simplified versions were originally covered by e.g. [648, 653, 654].

Just as for the other species, these are expanded into a Legendre series, yielding,

$$\left(\frac{\partial F_\gamma}{\partial \tau}\right)_C = a n_e \sigma_T \left(\frac{4iP_1}{k}(\theta_\gamma - \theta_b) + \left(9\sigma_\gamma - \frac{G_{\gamma 0}}{2} - \frac{G_{\gamma 2}}{2}\right)P_2 - \sum_{l\geq 3}^{\infty}(-i)^l(2l+1)F_{\gamma l}P_l\right) \tag{3.50a}$$

$$\left(\frac{\partial G_\gamma}{\partial \tau}\right)_C = a n_e \sigma_T \left(\frac{(F_{\gamma 2} + G_{\gamma 0} + G_{\gamma 2})(1 - P_2)}{2} - \sum_{l\geq 0}^{\infty}(-i)^l(2l+1)G_{\gamma l}P_l\right), \tag{3.50b}$$

using $F_{\gamma 1} = 4\theta_\gamma/3k$ and $F_{\gamma 2} = 2\sigma_\gamma$ as for massless neutrinos (see Eqs. (3.24b) and (3.24c)), as well as $\hat{n}\cdot\vec{v}_e = -(i\theta_b/k)P_1(\hat{h}\cdot\hat{n})$.

The part of the Boltzmann hierarchy not determined by scattering is exactly the same as

for massless neutrinos, so the interaction terms can simply be added, giving the hierarchy,

$$\dot{\delta}_\gamma = -\frac{4}{3}\theta_\gamma + 4\dot{\phi}, \tag{3.51a}$$

$$\dot{\theta}_\gamma = k^2\left(\frac{\delta_\gamma}{4} - \sigma_\gamma\right) + k^2\psi + an_e\sigma_T(\theta_b - \theta_\gamma), \tag{3.51b}$$

$$\dot{F}_{\gamma 2} = 2\dot{\sigma}_\gamma = \frac{8}{15}\theta_\gamma - \frac{3}{5}kF_{\gamma 3} - \frac{9}{5}an_e\sigma_T\sigma_\gamma + \frac{an_e\sigma_T}{10}(G_{\gamma 0} + G_{\gamma 2}), \tag{3.51c}$$

$$\dot{F}_{\gamma l} = \frac{k}{2l+1}\left(lF_{\gamma(l-1)} - (l+1)F_{\gamma(l+1)}\right) - an_e\sigma_T F_{\gamma l}, \quad l \geq 3, \tag{3.51d}$$

$$\dot{G}_{\gamma l} = \frac{k}{2l+1}\left(lG_{\gamma(l-1)} - (l+1)G_{\gamma(l+1)}\right) + an_e\sigma_T\left(-G_{\gamma l} + \frac{(F_{\gamma 2} + G_{\gamma 0} + G_{\gamma 2}}{2}\left(\delta_{l0} + \frac{\delta_{l2}}{5}\right)\right), \tag{3.51e}$$

where the δ_{ij}s in Eq. (3.51e) are Kronecker deltas.

Just as for the other light species, the hierarchy must be truncated at some finite l if anything is to be computed. Due to the interactions, the truncation looks slightly different, with the terms

$$\dot{F}_{\gamma l_{\max}} = kF_{\gamma(l_{\max}-1)} - \frac{l_{\max}+1}{\tau}F_{\gamma l_{\max}} - an_e\sigma_T F_{\gamma l_{\max}}, \tag{3.52a}$$

$$\dot{G}_{\gamma l_{\max}} = kG_{\gamma(l_{\max}-1)} - \frac{l_{\max}+1}{\tau}G_{\gamma l_{\max}} - an_e\sigma_T G_{\gamma l_{\max}}, \tag{3.52b}$$

closing out the hierarchy.

As mentioned at the end of Section 3.4.1, a tight-coupling approximation is generally used prior to recombination. The (conformal) scattering rate is much larger than the (conformal) Hubble rate, $\tau_c^{-1} \equiv an_e\sigma_T \gg \dot{a}/a \sim \tau^{-1}$. The approximation was introduced in Ref. [648], and has since been improved, including going beyond first-order, see e.g. Refs. [67, 163, 633, 655–657].

The first step is combining the Euler equations for baryons and photons, Eqs. (3.46b) and (3.51b),

$$(1+R)\dot{\theta}_b + \frac{\dot{a}}{a}\theta_b - c_s^2k^2\delta_b - k^2R\left(\frac{\delta_\gamma}{4} - \sigma_\gamma\right) + R(\dot{\theta}_\gamma - \dot{\theta}_b) = (1+R)k^2\psi, \tag{3.53}$$

defining $R \equiv 4\bar{\rho}_\gamma/3\bar{\rho}_b$ for simplicity. It is also worth defining $\Theta \equiv (\theta_\gamma - \theta_b)$, the time derivative of which, $\dot{\Theta}$, is often called the baryon-photon slip. The two species behave as one coupled fluid with sound speed $c_{\gamma b}$ (which is distinct from the baryon sound speed c_s), and factors proportional to $\dot{\Theta}$ and σ_γ may be neglected to lowest order in $\max(k\tau_c, \tau_c/\tau)$ [163]. From Eq. (3.51b), we can write,

$$-\Theta = \tau_c\left(\dot{\theta}_\gamma - k^2\left(\frac{\delta_\gamma}{4} - \sigma_\gamma\right) - k^2\psi\right), \tag{3.54}$$

and combining with Eq. (3.53) yields,

$$-\Theta = \frac{\tau_c}{1+R}\left(-\frac{\dot{a}}{a}\theta_b + k^2\left(c_s^2\delta_b - \frac{\delta_\gamma}{4} + \sigma_\gamma\right) + \dot{\Theta}\right), \tag{3.55}$$

while Eq. (3.51c) gives,

$$\sigma_\gamma = \frac{\tau_c}{9}\left(\frac{8}{3}\theta_\gamma - 10\dot{\sigma}_\gamma - 3kF_{\gamma 3}\right). \tag{3.56}$$

Higher multipole moments of the photon hierarchy are smaller by additional powers of $k\tau_c$ and can therefore be neglected.

An equation for the slip can then be obtained by differentiating Eq. (3.55),

$$-\dot{\Theta} = -\frac{2R}{1+R}\frac{\dot{a}}{a}\Theta + \frac{\tau_c}{1+R}\left(-\frac{\ddot{a}}{a}\theta_b - \frac{\dot{a}}{a}k^2\left(\frac{\delta_\gamma}{2}+\psi\right) + k^2\left(c_s^2\dot{\delta}_b - \frac{\dot{\delta}_b}{4}\right)\right) + \mathcal{O}(\tau_c^2), \quad (3.57)$$

where $\dot{\delta}_\gamma$ and $\dot{\delta}_b$ are computed with the standard equations, and the gas is assumed to be nearly fully ionized with $T_b \approx T_\gamma$. An direct equation for $\dot{\theta}_\gamma$ can be obtained by insertion,

$$\dot{\theta}_\gamma = -R^{-1}\left(\dot{\theta}_b + \frac{\dot{a}}{a}\theta_b - c_s^2k^2\delta_b\right) + k^2\left(\frac{1}{4}\delta_\gamma - \sigma_\gamma\right) + \frac{1+R}{R}k^2\psi, \quad (3.58)$$

which lets the evolution be computed (to first order) in a more computationally efficient way.

Various higher-order solutions exist, though some, such as those of Refs. [67, 656] have only been presented in the synchronous gauge. They generally involve computing a second order slip, Θ, as well as a modified equation for σ_γ.

3.4.3 Beyond cold dark matter

The non-interacting cold dark matter of Section 3.3.1 is of course just an effective description that does not assume any particle physics model, other than the fact it acts like nonrelativistic matter, and its interactions are weak enough to be safely neglected. While this provides a good baseline model for ascertaining the impact of nonbaryonic matter on linear observables, it does not help with investigating any models of dark matter interactions, and how they might affect the observables. For this, the interactions would have to be included in the calculations. This is not a new concept, and it is even possible to make an analytic estimate of the effects [352, 357].

A species of dark matter interacting with photons can have the scattering rate expressed as the derivative of an optical depth, analogously to photon-baryon scattering, $\dot{\mu}_{\gamma\chi} \equiv a\sigma_{\gamma\chi}n_\chi$. The subscript χ refers to the interacting dark particle, and n_χ is its number density. There will be four distinct regimes, although two are quite similar. In the small k (large wavelength), $k < \mathcal{H}$, limit, the interaction will decouple before the mode enters the horizon, and therefore has no impact. In the very weak coupling (termed no coupling in in Ref. [357]) regime where the interaction rate is much smaller than the expansion rate $(1 + 4\rho_\gamma/3\rho_\chi)\dot{\mu}_{\gamma\chi} < \mathcal{H} < k$, the interaction can also safely be neglected.

In the strong coupling regime, $\mathcal{H} < k < (1 + 4\rho_\gamma/3\rho_\chi)\dot{\mu}_{\gamma\chi}$, the photons and dark matter will thus behave like a coupled fluid, similar to the baryon-photon plasma. It can therefore be evolved using a coupled fluid velocity and a dark matter-photon slip, similarly to the tight coupling approximation for baryons. In this regime, the photon perturbations, including their Silk damping, are directly imprinted on the dark matter.

Between the strong and very weak coupling regimes, there is an intermediate coupling regime (termed weak coupling in Ref. [357]), $\mathcal{H} < (1 + 4\rho_\gamma/3\rho_\chi)\dot{\mu}_{\gamma\chi} < k$. This regime does not occur for the baryon photon interactions in our universe, as the baryon-photon decoupling happens due to recombination rather than a gradual dilution of the free electron density. The photons therefore go from strongly coupled to the baryons to free streaming "almost instantaneously" (in cosmological terms), bypassing this regime. For these couplings, damping occurs from the photon perturbations averaged over several oscillations, with the effects being stronger the longer the weak coupling regime lasts.

Assuming a dark matter-photon decoupling before recombination (a reasonable assumption for realistic values of the coupling), the strong coupling regime can occur at two distinct times: for relatively small cross-sections decoupling early, and for larger cross-sections decoupling later. With early decoupling, the main effect is inhibiting the logarithmic growth of structure during

radiation domination, leading to a modest but still significant suppression of structure at later times. For late decoupling, the fluid undergoes multiple oscillations before the structure is suppressed, followed by a much greater suppression.

In the intermediate coupling regime, the coupling is not large enough to enforce $\theta_\chi \approx \theta_\gamma$, however, it is still large enough for the photons to drive oscillations in the dark matter fluid such that

$$\dot{\theta}_\chi \approx \frac{4\rho_\gamma}{3\rho_\chi}\dot{\mu}_{\gamma\chi}\theta_\gamma \propto k\theta_\chi, \tag{3.59}$$

as long as the gravitational potential is weak enough to be negligible.

Solving the differential equation, this means that the dark matter density contrast will be,

$$\delta_\chi \sim \frac{4\rho_\gamma}{3\rho_\chi}\frac{\dot{\mu}_{\gamma\chi}}{\mathcal{H}}\frac{\sin\left(k\tau/\sqrt{3}\right)}{k\tau/\sqrt{3}}\exp\left(-\frac{2k^2\tau}{15\dot{\mu}_{\gamma\chi}}\right), \tag{3.60}$$

for $k\tau \gg 1$. That is, the damping of the dark matter structure follows a spherical Bessel function. For the full analysis, see Ref. [357].

For dark matter interacting with relativistic species, such as photons or neutrinos, it is useful to parameterise the cross-section with a particle i, $\sigma_{i\chi}$, in terms of the dark matter particle mass and the Thomson cross-section,

$$u_{i\chi} = \frac{\sigma_{i\chi}}{\sigma_T}\left(\frac{m_\chi}{100\,\mathrm{GeV}}\right)^{-1}, \tag{3.61}$$

where 100 GeV is an arbitrarily chosen scale. This is because, when trying to constrain such interactions through structure formation, there is a degeneracy between $\sigma_{i\chi}$ and m_χ via n_χ, as keeping ρ_χ constant, $n_\chi \propto m_\chi^{-1}$. A lighter dark matter particle means a higher number density, hence more scatterings, similar to a larger cross-section. For velocity-dependent cross-sections, it is common to express this in terms of the current interaction strength and an scale factor dependence, $u_{i\chi}(a) = u_{i\chi,0}a^{-n}$, expressing some power law dependence.

A full Boltzmann treatment has been done for both photons [357, 379, 658, 659], massless neutrinos [220, 376, 659–662], and dark radiation [659, 663, 664].

The modifications to the dark matter equations is fairly simple, impacting only the Euler equation,

$$\dot{\theta} = [\dots] - \frac{4\rho_i}{3\rho_\chi}\dot{\mu}_{i\chi}\left(\theta_\chi - \theta_i\right), \tag{3.62}$$

where the bracket $[\dots]$ represents the standard cold dark matter terms of Eq. (3.19). The modifications to the light particles equations are a bit more involved, with the modified photon equations,

$$\dot{\theta}_\gamma = [\dots] - \dot{\mu}_{\gamma\chi}\left(\theta_\gamma - \theta_\chi\right), \tag{3.63a}$$

$$\dot{F}_{\gamma 2} = [\dots] + \frac{\dot{\mu}_{\gamma\chi}}{10}\left(G_{\gamma 0} + G_{\gamma 2}\right), \tag{3.63b}$$

$$\dot{F}_{\gamma l} = [\dots] - \dot{\mu}_{\gamma\chi}F_{\gamma l}, \tag{3.63c}$$

and the polarisation equations for $G_{\gamma l}$, as well as the truncation scheme likewise having being changed $\dot{\kappa} \to \dot{\kappa} + \dot{\mu}_{\gamma\chi}$.[3]

[3] With $\dot{\kappa} \equiv an_e\sigma_T$.

The massless neutrino case is similar, even slightly simpler due to the lack of polarisation concerns,

$$\dot{\theta}_\nu = [\dots] - \dot{\mu}_{\nu\chi}\left(\theta_\nu - \theta_\chi\right), \tag{3.64a}$$

$$\dot{\sigma}_\nu = [\dots] - \frac{9}{10}\dot{\mu}_{\nu\chi}\sigma_\nu, \tag{3.64b}$$

$$\dot{F}_{\nu l} = [\dots] - \dot{\mu}_{\nu\chi}F_{\nu l}. \tag{3.64c}$$

In the simplest case, dark radiation is essentially equivalent to the massless neutrinos, but may also have self interactions, as described in detail in Refs. [663, 664].

The massive neutrino case is a bit more tricky, as it cannot generally be described in terms of θ. A detailed description and derivation of the equations for this scenario is presented in Chapter 5 (published as Ref. [1]).

Interactions between dark matter and baryons are treated slightly differently, since the mass of a baryon ~ 1 GeV is not necessarily negligible compared to the dark matter mass. In addition, unlike the massless species, the baryons do not have a comparatively "infinite" reservoir of entropy, so their temperature may be affected by their interactions with dark matter. Dark matter baryon interactions have been treated in e.g. Refs. [355, 370, 375, 665–671]. The modifications to the Boltzmann equations are thus,

$$\dot{\theta}_\chi = [\dots] + c_\chi^2 k^2 \delta_\chi - R_\chi\left(\theta_\chi - \theta_b\right), \tag{3.65a}$$

$$\dot{\theta}_b = [\dots] - \frac{\rho_\chi}{\rho_b}R_\chi\left(\theta_b - \theta_\chi\right), \tag{3.65b}$$

where the scattering rate R_χ for a velocity-dependent cross section $\sigma_{b\chi} = \sigma_{b\chi,0}v^n$ is given as,

$$R_\chi \equiv \frac{a\rho_b\sigma_{b\chi,0}c_n}{m_\chi + m_b}\left(\frac{T_b}{m_b} + \frac{T_\chi}{m_\chi} + \frac{V_{\rm rms}^2}{3}\right)^{\frac{n+1}{2}}\mathcal{F}_{\rm He}, \tag{3.66}$$

showing a dependence on the baryon- and dark matter temperatures, and c_n is a factor depending on n,

$$c_n = \frac{2^{\frac{n+5}{2}}\Gamma\left(3 + \frac{n}{2}\right)}{3\sqrt{\pi}}, \tag{3.67}$$

where $\mathcal{F}_{\rm He}$ is a factor accounting for the primordial helium fraction. In the case of no scattering with helium, $\mathcal{F}_{\rm He} = 1 - Y_{\rm He}$. $V_{\rm rms}$ is the RMS bulk velocity between the dark matter and baryon fluids. It is often approximated as,

$$V_{\rm rms}^2 \approx \begin{cases} 10^{-8} & z > 10^4 \\ 10^{-8}\left(\frac{1+z}{10^3}\right)^2 & z \leq 10^3 \end{cases}. \tag{3.68}$$

A deeper investigation of this component is conducted in Ref. [666].

The interaction with baryons also induces a sound speed term in the dark matter, similar to the baryons (Eq. (3.47)),

$$c_\chi^2 = \frac{k_{\rm B}T_\chi}{m_\chi}\left(1 - \frac{1}{3}\frac{d\ln T_\chi}{d\ln a}\right), \tag{3.69}$$

although the impact of this is generally small compared to the scattering term.

The modification to the baryon temperature equation Eq. (3.48) is,

$$\dot{T}_b = [\dots] + \frac{2\mu_b}{m_\chi + m_b}\frac{\rho_\chi}{\rho_b}R_\chi\left(T_\chi - T_b\right), \tag{3.70}$$

with the dark matter obtaining a very similar equation,[4]

$$\dot{T}_\chi = -2\frac{\dot{a}}{a}T_\chi + \frac{2m_\chi}{m_\chi + m_b}R_\chi\left(T_b - T_\chi\right), \tag{3.71}$$

with dark matter strongly coupled to the baryons at early times having an initial temperature $T_{\chi,i} \approx T_{b,i}$.

Models with $n = -4$ can have a significant impact on the baryon temperature at late times, since baryon-dark matter coupling can occur after photon decoupling. This n corresponds to a Coulomb-like interaction, e.g. millicharged dark matter. $n = -2$ will have a weaker late time effect and corresponds to a dipole interaction, and $n = -1$ corresponds to a Yukawa coupling.

Generally the effects of coupling to light species will serve to suppress small scale structure as the dark matter is prevented from collapsing gravitationally until decoupling, similarly to the baryon-photon case. The dark matter-photon case will have the greatest impact on the CMB for a given coupling $u_{i\chi}$, as it is directly coupled, while couplings to neutrinos will have only an indirect effect through the modified gravitational evolution. Coupling to baryons will also have a significant effect on the CMB, effectively acting as additional baryon mass without extra charge, suppressing the temperature power spectrum on scales l larger than a few hundred.

The distinct effects on the CMB, structure formation, and the baryon temperature could be used to distinguish between different interaction scenarios.

3.5 Observables

Unfortunately, we cannot directly probe the density and velocity perturbations of these different species, not even for baryons. Instead, we must use them to compute observables, which can then be used to constrain the cosmological parameters. While the linear theory described in this chapter breaks down once densities get too large, and is thus not applicable to "small" scales, such as galaxies, at late times, it works great for other observables. In particular, it can accurately predict large scale structure above certain length scales, where nonlinearities have not yet set in, as well as the CMB, which was emitted while the universe was still linear and does not experience nonlinear evolution.

3.5.1 The matter power spectrum and baryon acoustic oscillations

One of the simplest quantities to predict is the matter power spectrum, which also has an easy to understand physical interpretation, namely as the Fourier transform of the two-point correlation function, $\xi(r)$. The two-point density correlation function is essentially a measure of how well the densities at two points separated by a distance r match, averaged over all space. Any "special" scales will then appear as peaks or dips in the correlation function. With space being three-dimensional, the correlation function can be written as

$$\xi(|\vec{x} - \vec{y}\,|) = \langle \delta(\vec{x})\delta(\vec{y})\rangle\,, \tag{3.72}$$

where the brackets denote a spatial average.

This is all well and good, but we have solved our (linear) density evolution in Fourier space, so we define the power spectrum,

$$P(k) = \int d^3r e^{i\vec{k}\cdot\vec{r}}\xi(r), \tag{3.73}$$

[4]The dark matter would have such an equation with the other types of interactions covered, but since the dark matter temperature is generally neglected in these cases, the temperature evolution is usually not included. Ref. [659] includes these in their treatment.

which is equal to the Fourier space average $\langle\delta(\vec{k_1})\delta(\vec{k_2})\rangle$ up to a Dirac delta $\delta_D(\vec{k_1}-\vec{k_2})$ and factors of π depending on Fourier conventions.

Looking back at the previous sections, one might realize that the equations only describe the evolution of δ, rather than give its exact value. Indeed, it is necessary to correctly set the initial conditions for the equations to compute their values at later times. By convention, the initial conditions are often separated from the evolving δs, where the normalised $\delta(k,t)$ functions are termed transfer functions, as they are used to compute the perturbation at a given time k from a given initial perturbation. These initial perturbations are termed the *primordial* power spectrum, $\mathcal{P}(k)$. The power spectrum at redshift z can then be expressed as,

$$P(k,z) = \delta^2(k,z)\mathcal{P}(k) \tag{3.74}$$

Generally, it is assumed that these initial conditions are set by inflation (for more detail on inflation, see Section 1.3.1). In the case of simple slow-roll inflation, the primordial power spectrum is expressed as,

$$\mathcal{P}(k) = k^{-3}A_s\left(\frac{k}{k_*}\right)^{n_s-1}, \tag{3.75}$$

where A_s is the amplitude of primordial fluctuations at a reference scale k_*, termed the pivot scale. This is usually taken to be $k_* = 0.05$ Mpc^{-1}. The final parameter n_s is the scalar spectral index, or tilt, which parameterises the deviation from perfect scale invariance in the dimensionless power spectrum $k^3\mathcal{P}(k)$ (Eq. (1.22)), which would be constant in k for $n_s = 1$.

The total matter power spectrum, often presented with the matter subscript $P_m(k)$, generally comprises all matter, meaning all particles with nonzero mass, baryons, dark matter, and massive neutrinos. It therefore uses a sum of their δs, weighted by their relative abundance. In the context on non-linear simulations, it is also commmon to use $P_{cb}(k)$, the dark matter+baryon power spectrum, as massive neutrinos only cluster weakly and are therefore often omitted from the non-linear modeling. For realistic neutrino masses, the difference between P_m and P_{cb} is on the percent level. A sum of neutrino masses around the Planck upper limit, $\sum M_\nu = 0.3$ eV [5], yields a difference of 4% at $k \gtrsim 0.1$, while a mass matching the Planck+BAO limit $\sum M_\nu = 0.12$ eV [5] only shows a difference of 2% on roughly the same scales[5].

The matter power spectrum has a big problem, however. It is very hard to actually observe, because most of the matter in question is dark matter, which is not visible. Instead, it is necessary to use a proxy. On large scales, the commonly used observable is instead the galaxy power spectrum, as the galaxies are a tracer of the underlying matter distribution with some bias, since the baryons are gravitationally coupled to the dark matter [672–676]. The measured galaxy power spectrum is thus related to the underlying matter power spectrum through

$$P_{\rm gal}(k,z) = b^2(k,z)P_m(k,z), \tag{3.76}$$

where b can taken to be the linear bias on large enough scales. In general, the galxy-matter bias is defined through $\delta_{\rm gal} = b\delta_m$, which can be expressed as the series,

$$\delta_{\rm gal} = \sum_k \frac{1}{k!}b_k\delta^k, \tag{3.77}$$

with b_1 being the linear bias. It is possible to estimate this bias through the use of semi-analytical tools, such as halo models or perturbation theory [677–682] (for more detail on halo models, see Section 4.2), which yields different results depending on the underlying dark matter model. It

[5]The suppression affects slightly larger scales for the lower mass, as the free-streaming scale is larger. However, this difference is small, and the lower mass leads to lower Ω_ν and thus smaller suppression.

can also be estimated directly from data, as the two-point and three-point correlation functions have different bias dependence, however, this probe is sensitive to noise in the data [683–685]. As implied by Eq. (3.76), the bias is also subject to redshift evolution, in particular, it is generally found to decrease with time, becoming less biased [686–690]. The bias may also depend on additional parameters, such as the luminosity and stellar mass of the galaxy [691–693].

Matters are also further complicated by another factor, namely the fact that we do not quite observe galaxies in normal position-space. Because of the distances at play in large scale structure, the effects of redshift must be taken into account. This is termed redshift-space distortions [674, 675, 694].

Historically, some of the key goals of measuring the matter power spectrum has been to check the assumptions oflarge scale isotropy and homogeneity, and later to check the prediction of baryon acoustic oscillations, and thus verify an important prediction of the ΛCDM hot big bang model. This was observed in SDSS [20] and 2dFGRS [21] data in 2005, and further surveys since then [170, 695–697].

The baryon acoustic oscillations come about as a result of the strong coupling between baryons and photons in the early universe, as described in Sections 3.4.1 and 3.4.2. There are a few ways to express this, one is in terms of a simple Jeans analysis in Fourier space. The density evolution of a fluid with sound speed c_s obeys the equation [698],

$$\ddot{\delta} + 2\frac{\dot{a}}{a}\dot{\delta} + \left(c_s^2 k^2 - 4\pi G\bar{\rho}a^2\right)\delta = 0, \tag{3.78}$$

which a keen eye will notice looks a lot like a harmonic oscillator. Indeed, this defines the Jeans wavenumber,

$$k_J^2 \equiv \frac{4\pi G\bar{\rho}a^2}{c_s^2}, \tag{3.79}$$

where small scale modes $k \gg k_J$ will oscillate as sound waves, while large scale modes $k \ll k_J$ have a growing, and a vanishing solution. However, a key point is that the Jeans scale is larger than the horizon until recombination, where is suddenly drops. In this framework, this comes about due to the drop in sound speed from baryon-photon decoupling. The result is that all sub-horizon modes experience acoustic oscillations until recombination, which are then frozen into the matter power spectrum. The sudden cessation of oscillations is clearly visible in Fig. 3.1.

Another description is grounded in the real-space realisation of primordial overdensities [699, 700]. Since the overdensities of baryons and photons are coincident, the pressure of the photons will force the baryons to expand as a wavefront, a commonly used analogy is like rings in water, until recombination causes their decoupling, and the baryon wavefront stops (after some residual drag). Since the distance traveled until decoupling is the same across the universe, this imprints a specific length scale, which shows up as a peak in the correlation function. When taking the Fourier transform to obtain the power spectrum, such a peak corresponds to oscillations.

The imprinted baryon acoustic oscillation features are extremely useful for estimating the content of our universe [701], and when combined with CMB data gives some of the most precise measurements of the ΛCDM model parameters [5], as well as additions such as neutrino masses. This is because the scale imprinted in the structure, the sound horizon at decoupling, can be computed to great precision using these parameters. It is essentially a cosmic ruler.

3.5.2 The CMB power spectrum

At roughly the same time as the baryon acoustic oscillations were frozen into the large scale structure, the photons were suddenly allowed to propagate freely without scattering with matter,

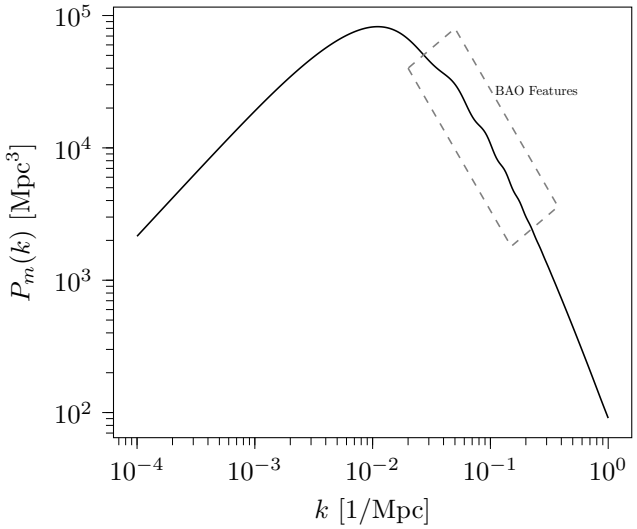

Figure 3.3: *The linear matter power spectrum at $z = 0$ for a ΛCDM cosmology, with the baryon acoustic oscillation features highlighted.*

as the baryons had undergone recombination and become neutral atoms [69]. The vast majority of these photons have been propagating unobstructed ever since, in the form of the cosmic microwave background, and observing these thus gives us a window to what the universe looked like. It shows an extremely isotropic temperature of $T_{cmb} \sim 2.7$ K [702–704], however, it has some small anisotropies on the order of 10^{-4} K. These anisotropies tell us which regions had over- and underdensities at the time the CMB was emitted. Fig. 3.4 shows a synthetic realisation of the CMB temperature anisotropy for a realistic ΛCDM universe.

In the end, however, it is less interesting which exact regions on the sky exhibit these over- and underdensities, as this is just the result of the random quantum fluctuations during inflation at a particular distance from our location in the universe. The important part is the statistical properties of the CMB as a whole, as this can tell us about the general state of the universe at photon decoupling. Similarly to the matter power spectrum and baryon acoustic oscillations, it is irrelevant where exactly a given galaxy is, the important part is the patterns of separation between galaxies. Just like with the matter distribution, we are therefore interested in a power spectrum.

However, comparing to the three-dimensional distribution of matter, the cosmic microwave background does present a wrinkle. Because it is formed of the light just reaching us now from decoupling, it is essentially a spherical shell, rather than a three-dimensional distribution. Instead of performing a standard Fourier transformation, the CMB is instead expressed as a series of spherical harmonics.

The perturbation to the photon brightness temperature, $\Delta \equiv \Delta T/T$, can be defined via the distribution function[163],

$$f(x^i, q, n_j, \tau) = f_0\left(\frac{q}{1+\Delta}\right), \tag{3.80}$$

where f_0 is the Bose-Einstein distribution, as photons are spin-1 particles. Using Eq. (3.14), it follows that,

$$\Delta = -\left(\frac{d\ln f_0}{d\ln q}\right)^{-1}\Psi, \tag{3.81}$$

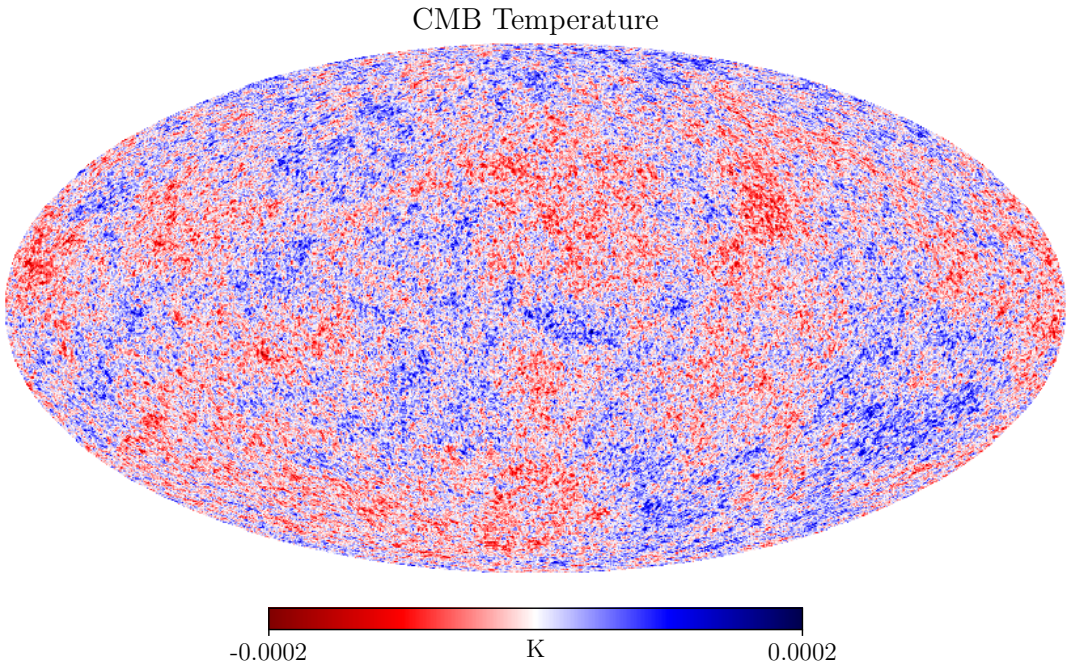

Figure 3.4: *Synthetic CMB temperature anisotropy map, computed with CLASS [67, 635] and realised with healPy [705, 706].*

to linear order. As it happens, the q dependence of both the gravitational and Thomson scattering terms in the Boltzmann equations for photons depend on q through $d\ln f_0/d\ln q$ at the linear level, so in the end, the perturbations will not change the shape of the photon distribution from blackbody spectrum, but rather shift the spectrum to higher or lower temperatures. Deviations from a blackbody spectrum, dubbed spectral distortions, are possible through effects beyond linear perturbation theory, such as the Sunyaev-Zel'dovich effect [70, 163, 557, 707–714].

In the absence of spectral distortions, the temperature perturtbation Δ is related to the phase space density perturbation through,

$$\Delta = \frac{F_\gamma}{4}. \tag{3.82}$$

This makes sense, as the energy density of a thermal population of photons is simply related to its temperature.[6] The temperature anisotropy at a given point can then be expressed in terms of plane waves,

$$\Delta(\vec{x},\hat{n},\tau) = \int d^3k e^{i\vec{k}\cdot\vec{x}}\Delta(\vec{k},\hat{n},\tau) \equiv \int d^3k e^{i\vec{k}\cdot\vec{x}}\sum_{l=0}^{\infty}(-i)^l(2l+1)\Delta_l(\vec{k},\tau)P_l(\hat{k}\cdot\hat{n}), \tag{3.83}$$

where, following Eq. (3.82), $\Delta_l = F_{\gamma l}/4$.

Selecting a given point as the origin, the anisotropy here may be expressed in terms of a series of spherical harmonics,

$$\Delta(\hat{n}) = \sum_{l=0}^{\infty}\sum_{m=-l}^{l} a_{lm}Y_{lm}(\hat{n}), \tag{3.84}$$

[6] Note that some authors use the convention $\Delta = F_\gamma$. In this case, everything is the same except for a factor 4.

with the coefficients a_{lm} given through,

$$a_{lm} = (-i)^l 4\pi \int d^3k\, Y^*_{lm}(\hat{k})\Delta_l(\vec{k},\tau). \tag{3.85}$$

These coefficients can be used to construct the angular power spectrum C_ls,

$$C_l\delta_{ll'}\delta_{mm'} = \langle a_{lm}a^*_{l'm'}\rangle, \tag{3.86}$$

where the δs are Kronecker deltas, and the brackets denote an ensemble average. The angular power spectrum is related to the angular correlation function through,

$$C(\theta) \equiv \langle\Delta(\hat{n}_1)\Delta(\hat{n}_2)\rangle = \frac{1}{4\pi}\sum_{l=0}^{\infty}(2l+1)C_lP_l(\hat{n}_1\cdot\hat{n}_2), \tag{3.87}$$

where $\cos\theta = \hat{n}_1\cdot\hat{n}_2$.

As implied in the beginning of this section, the $\Delta_l(\vec{k},\tau)$ coefficients are set by the random initial conditions of the perturbations. They can therefore be expressed in terms of the initial perturbations to the Newtonian gauge potential ψ_i,

$$\Delta_l(\vec{k},\tau) = \psi_i(\vec{k})\Delta_l(k,\tau), \tag{3.88}$$

with the initial gauge potential power spectrum,

$$\langle\psi_i(\vec{k}_1)\psi_i(\vec{k}_2)\rangle = P_{\psi_i}(k)\delta_D(\vec{k}_1+\vec{k}_2), \tag{3.89}$$

and the C_ls can be expressed as,

$$C_l = 4\pi\int d^3k\, P_{\psi_i}(k)\Delta^2_l(k,\tau). \tag{3.90}$$

The same expression can be used to obtain the polarisation C_ls, by using the polarisation perturbation, rather than Δ_l.

Calculating the C_ls by explicitly computing Eqs. (3.88) to (3.90) requires the evolution of a significant number of differential equations, as a fine sampling in k is needed. This number can be reduced from a few thousand to a few tens by using a line of sight approach, as the higher multipoles are generated from free-streaming, the behaviour of which is well captured by a spherical Bessel function [715].

Although the major features of the cosmic microwave background are imprinted at photon decoupling, the photons are affected by their journey to some degree. Either through the gravitational potential they pass through, or for a minority, another scattering on their way to us. Of course, recombination was not quite an instantaneous process, although this is generally a good approximation. This can be quantified in terms of the visibility function g, defined as [62],

$$g(\tau) = \frac{d}{d\tau}e^{-\kappa} = -\dot{\kappa}e^{-\kappa}, \tag{3.91}$$

with κ being the optical depth. The function describes the probability distribution of time of last scattering, i.e. $g(\tau_0)d\tau$ is the probability that a photon was last scattered in the conformal time interval $[\tau_0, \tau_0 + d\tau]$. The visibility function is plotted in Fig. 3.5 for a standard ΛCDM cosmology. It is clear that by far the majority of CMB photons arrive unscattered from the time of recombination, the peak in the visibility function being orders of magnitude larger than the smaller peak at the time of reionization. Despite this, the effect of reionization is clearly visible in the CMB temperature power spectrum, suppressing power across all scales.

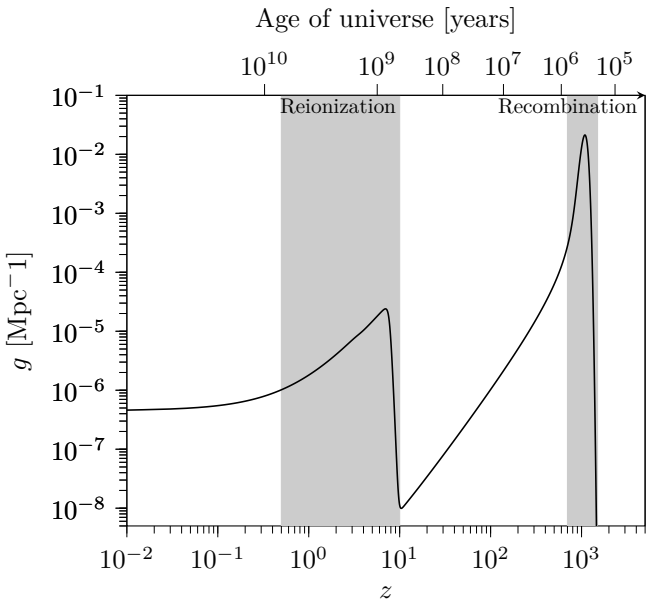

Figure 3.5: *The CMB photon visibility function g as a function of redshift. In particular note the large peak at recombination, and the smaller, less steep, peak at reionization.*

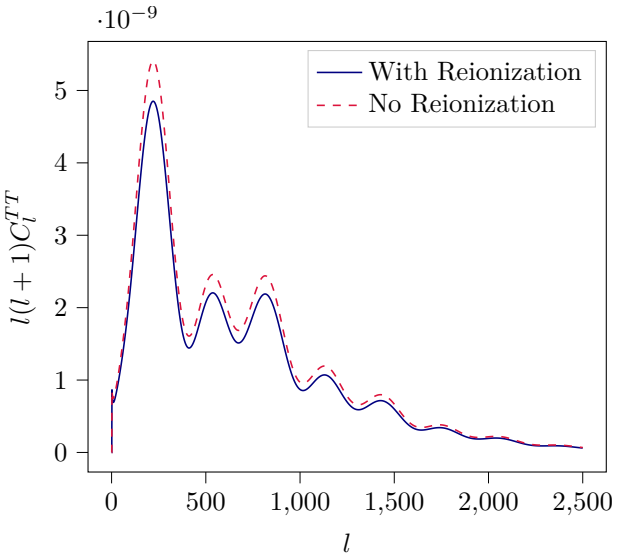

Figure 3.6: *The CMB temperature power spectrum, computed with and without reionization. It is evident that reionization suppresses power across all scales.*

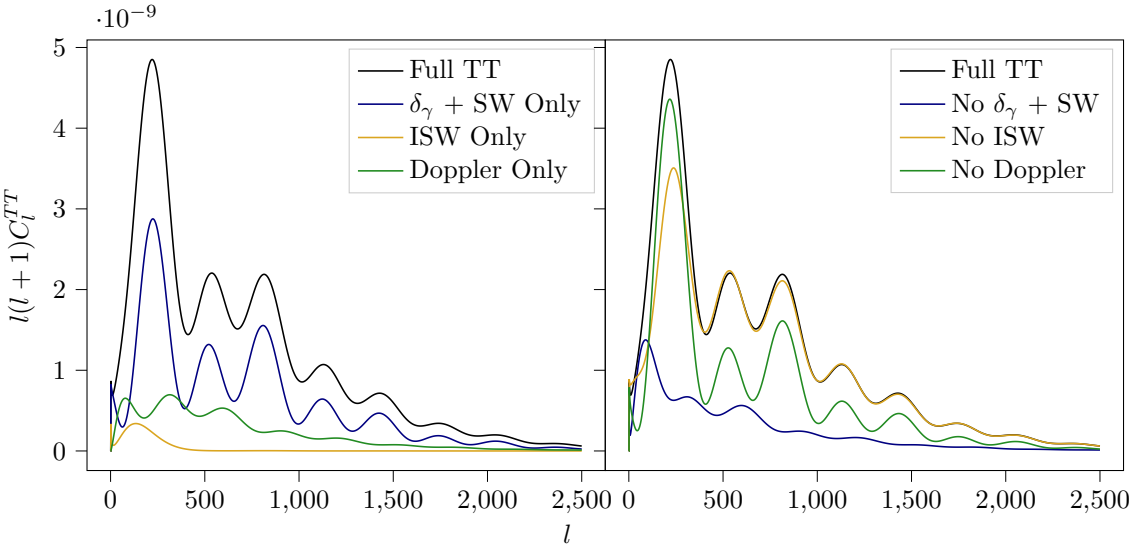

Figure 3.7: *The CMB temperature power spectrum, computed with and without the components of Eq.* (3.92).

The observed temperature perturbation in a given direction $\Delta(\hat{n})$ can be understood in a simplified manner as a sum of three components if scattering after recombination is neglected [62],

$$\Delta(\hat{n}) = \underbrace{\left(\frac{\delta_\gamma}{4} + \psi\right)_*}_{\delta_\gamma+\text{SW}} \underbrace{-(\hat{n}\cdot\vec{v}_b)_*}_{\text{Doppler}} + \underbrace{\int_{\tau_*}^{\tau_0} d\tau\, \dot{\phi} + \dot{\psi}}_{\text{ISW}}, \tag{3.92}$$

where the subscript $*$ denotes the value at recombination. SW is an abbreviation of Sachs-Wolfe [716], while ISW is integrated Sachs-Wolfe.

The first term contains δ_γ, which is the photon density at recombination, as set by the evolution described by the Boltzmann equation. However, overdensities of photons are often associated with matter overdensities, leading to a gravitational potential well. Escaping from this well causes the photons to lose energy, which is the Sachs-Wolfe effect [716]. The second term is the so-called Doppler term. It is related to the electron bulk velocity where the last scattering happened. If the scattering electron had a non-zero velocity along the line of sight to the observer, this would essentially induce a Doppler shift of the photon. Finally, the integrated Sachs-Wolfe term is similar to the first term, in that it deals with the effects of gravity on photons. However, rather than the instantaneous potential at last scattering, the integrated Sachs-Wolfe effect describes the effect of the potentials changing as a photon passes through them. This is zero in a purely matter dominated universe, however, the radiation density at recombination leads to the so-called early integrated Sachs-Wolfe, while the presence of dark energy at late times causes a late integrated Sachs-Wolfe effect.

By far the largest contribution to the temperature power spectrum comes from the δ_γ + Sachs-Wolfe term, as is illustrated in Fig. 3.7.

3.6 Initial Conditions

So far, this chapter has described how to evolve the distributions of various particle species, as well as how to compute observables from this. Now, only the final piece of the puzzle remain,

namely, the initial conditions used to initialize the perturbations' evolution equations.

In numerical treatments, the evolution of each k-mode starts while it is still outside the Hubble horizon, i.e. $k\tau \ll 1$. As these modes are larger than the horizon, they are not observable, and their density evolution can therefore be gauge-dependent [163, 654, 717]. The numerical evolution will always be started in the radiation dominated era, so the the energy density of the universe is to a very good approximation, $\bar{\rho}_{\rm tot} \approx \bar{\rho}_\gamma + \bar{\rho}_\nu$, leading to an expansion rate $\dot{a}/a = \tau^{-1}$. This means we can obtain initial conditions analytically from the evolution equations. For the photons, higher moments $l \geq 2$ of $F_{\gamma l}$ as well as $G_{\gamma l}$ are driven to zero by collisional damping. For massless neutrinos, $F_{\nu l}$ with $l \geq 3$ are suppressed by powers of $k\tau$, and can thus also safely be set to zero. This yields the initial conditions for density perturbations,

$$\delta_\gamma = \delta_\nu = -2\psi, \tag{3.93}$$

$$\delta_{\rm cdm} = \delta_b = \frac{3\delta_\gamma}{4}, \tag{3.94}$$

velocity perturbations,

$$\theta_\gamma = \theta_\nu = \theta_{\rm cdm} = \theta_b = \frac{k^2\tau\psi}{2}, \tag{3.95}$$

neutrino anisotropic stress,

$$\sigma_\nu = \frac{k^2\tau\psi}{15}, \tag{3.96}$$

and the gauge potentials,

$$\psi = \frac{20C}{15 + 4R_\nu}, \tag{3.97}$$

$$\phi = \left(1 + \frac{2R_\nu}{5}\right)\psi, \tag{3.98}$$

where,

$$R_\nu = \frac{\bar{\rho}_\nu}{\bar{\rho}_\gamma}, \tag{3.99}$$

and C is an arbitrary dimensionless constant. CLASS takes it to be 1/2 [635]. The massive neutrino hierarchy can be calculated from the massless neutrinos, and the perturbed distribution function,

$$\psi_0 = -\frac{\delta_\nu}{4}\frac{d\ln f_0}{d\ln q}, \tag{3.100}$$

$$\psi_1 = -\frac{\epsilon\theta_\nu}{3qk}\frac{d\ln f_0}{d\ln q}, \tag{3.101}$$

$$\psi_0 = -\frac{\sigma_\nu}{2}\frac{d\ln f_0}{d\ln q}, \tag{3.102}$$

$$\tag{3.103}$$

again, higher moments are negligible at these early times.

CHAPTER 4

Non-linear Structure Formation

At early times, the density of the universe is quite uniform, with only small perturbations, as described in the previous chapter. However, as these perturbations start to grow, so does their gravitational impact, leading to even faster growth in a continuing cycle. This is the nonlinear growth.

Linear perturbation theory is a great tool for early times, but it can only take you so far, its core assumption being that the perturbations are small compared to the average. As the density perturbations begin to grow, this becomes less and less true. At some point the approximation will break down completely, as illustrated in Fig. 4.1. This means that to accurately model the late universe, non-linear tools are necessary.

This modelling can take a variety of shapes, but one thing that most approaches have in common is that they are much more computationally expensive than making linear predictions. For example, even a relatively modest gravity-only N-body simulation can take hours, if not days, on a computing cluster, while a linear Einstein-Boltzmann solver like CLASS can run in $\mathcal{O}(1)$ second on a regular laptop.

This presents a challenge for non-linear cosmology, which is overcome in part by ever larger computation facilities, and in part by developing new tools to make predictions less computationally expensive. In this chapter I aim to provide a brief overview of different techniques to model the non-linear universe, and how they connect to observables.

4.1 N-body Simulations

Gravity only N-body simulations have long been a workhorse for cosmologists interested in non-linear structure formation, with the first such computations done using an analog optical computer more than 80 years ago [151, 719–724], where a near passage of two "nebulae" was computed by representing the two with 37 lightbulbs each, while the first N-body on digital computers in the 1960s used up to 100 particles, and the first truly cosmological simulation was done in the 1970s with 1000 particles.

This can be contrasted with the largest modern simulations, such as Uchuu, using 12800^3 (2.1 trillion) particles [725]. Many modern simulations also go beyond pure gravity (also called dark matter only) N-body simulations and include a hydrodynamical treatment of the baryonic matter, which can be done using smoothed particle hydrodynamics (SPH) [726–728].

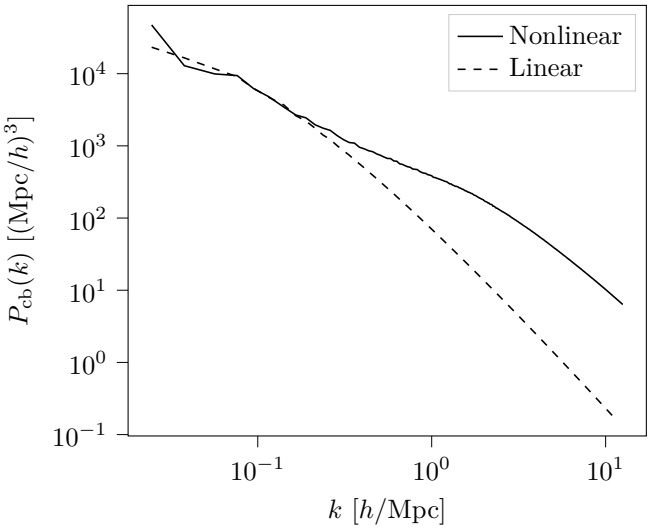

Figure 4.1: *The matter power spectrum computed for the same cosmology using both linear perturbation theory and nonlinear N-body simulation. Note that power on small scales is greatly enhanced in the nonlinear treatment, indicating that a linear treatment is insufficient at these scales at late times. Simulation performed with CONCEPT [718]*

These simulations require advanced software packages taking advantage of the computation infrastructure available. To this end, there are a wealth of public codes with different implementations [718, 729–746]. Many of these use only Newtonian gravity, and therefore require some fixes to ensure that the large scale behaviour is consistent with general relativity. However, some codes, such as CO*N*CEPT [718, 733] and GrGadget [736] model relativistic effects.

The basic idea of N-body simulations is rather simple. Rather than modelling the matter density as a continuous quantity across space, it is discretized into N particles, the spatial distribution of which should approximate the real matter distribution. The larger the number of particles, the better the approximation.

The simplest (and most computationally expensive) way to compute the gravitational acceleration of an N-body particle is to simply sum over the gravitational forces on it from all other particles in the simulation, which is called the direct summation or particle-particle (PP) method,

$$\vec{a}_i = \sum_{j \neq i}^{N} -\frac{G m_j \left(\vec{x}_j - \vec{x}_i\right)}{\left|\vec{x}_j - \vec{x}_i\right|^3}, \tag{4.1}$$

where $\vec{a}_i$ is the acceleration of the ith particle, m_j is the mass of the jth particle, x_i and x_j are particle positions, and G is Newton's gravitational constant. This is a computational problem with an unfortunate scaling of the ever larger simulations being performed, as the number of operations needed per timestep grows as $\propto N^2$. Cosmological simulations have an extra wrinkle. Namely, because we want to accurately simulate cosmology, it would not yield acceptable results to merely truncate the simulated universe at the edge of the simulation box. The solution to this is generally using periodic boundary conditions, which means that the sum in Eq. (4.1) would need to be conducted over an infinite number of "copies" of the particles in the simulated box. This is of course not computationally feasible, so a different solution is needed.

The direct summation technique for a periodic box yields the potential felt by particle i at

position $\vec{x}_i$ is given as,

$$\phi(\vec{x}_i) = -\frac{1}{a} \sum_{\vec{n}\in\mathbb{Z}^3} \left(\sum_{j\neq i}^{N} \frac{Gm_j}{|\vec{x}_i - \vec{x}_j - \vec{n}L|} + \varphi_{\mathrm{box},L}(\vec{x}_i - \vec{n}L) \right), \tag{4.2}$$

where L is the box side length, the integer vector $\vec{n}$ coresponding to the infinite lattice of boxes, and $\varphi_{\mathrm{box},L}$ the potential of a box of uniform density, such that the integrated potential vanishes. Unfortunately, this sum only converges slowly in $\vec{n}$. However, this can be solved by using the Ewald summation [747, 748], originally developed for electrostatic potentials in lattices, which is a similar problem to gravity in a periodic box. The force is split into the contribution from the local particles, which is non-periodic, and the long-range part, which is periodic. The latter can be solved quickly in Fourier space, while the former is only one set of particles. Unfortunately, the $\mathcal{O}(N^2)$ scaling remains, making this method unfeasible for large simulations. An additional factor that needs to be taken into account for direct summation gravity is the fact that the individual N-body particles each correspond to an extended mass distribution rather than very heavy point-particles, as otherwise the particles would exhibit spurious behaviour when interparticle distances become small, in addition to becoming very computationally expensive to simulate. This can be done by instead of a delta function density, using a spline kernel function with some smoothing length, or a softening of the force by a regulatisation $1/r^2 \to 1/(r+\epsilon)^2$ [151, 740, 742, 749].

A more computationally efficient method is the particle-mesh (PM) method. This takes advantage of the periodic matter distribution to compute the periodic potential on a grid [151, 750, 751]. The periodicity means that the computation of the grid can be done efficiently using the Fourier transform, reducing the scaling of the problem to $\mathcal{O}(N \log N)$. However, some care must be taken in how the particle mass contributes to the potential, and how the force is calculated to avoid the individual particles being affected by their own contribution to the potential [151, 718], similarly to how force softening is necessary in PP simulations.

Generally, both of these methods have shortcomings. The PP method is exact, but prohibitively expensive for larger simulations, whereas the PM method is computationally reasonable but loses accuracy when the particle spacing becomes small compared to the gravity mesh grid. Fortunately, they can be combined in a method that combines the best of both, generally referred to as $\mathrm{P^3M}$, in which gravity is split into a short range force and a long range force. The former is then computed using direct summation, and the latter is computed using the PM method. One example of a code using this method is CONCEPT [718, 733], which also uses innovative methods to efficiently split the forces and compute the PP part.

Finally, a popular modern method is the so-called tree method, where the mass distribution is partitioned into local volumes in a hierarchical tree structure [151, 752]. The force on a given particle i thus does not need to be computed for each other particle, but rather the joint force from groups of particles. The trees can be constructed using different principle, one popular example being the octree, where each volume is divided into 8 equally sized sub-volumes. This is done hierarchically until each sub-volume contains no more than some maximum K number of particles. This speeds up the gravity calculation, so the scaling again reaches $\mathcal{O}(N \log N)$.

Unlike PP, this method is by definition not exact (to machine precision). Rather, it can be tuned to the desired precision, as the approximated pairwise interaction between volumes can be expanded to arbitrary order, with modern implementations using a fast multipole method [151, 742]. Similarly to $\mathrm{P^3M}$, it can also be combined with a PM method for the long range forces in a so-called TreePM method [151, 753, 754].

Of course, the calculation of gravity is only one part, albeit the most computationally demanding, of an N-body simulation. It does not matter how accurate the gravity calculation is, if the timestepping algorithm is insufficient.

Generally the timestepping is done using successive applications of the "Kick" and "Drift" operators, the former referring to applying gravitational acceleration to particles, and the latter evolving their position due to their velocity. The timestepping integration needs to be symplectic, meaning that it satisfies the conservation laws of Hamiltonian dynamics. The most widely used method is the second order leapfrog [151], where the kicks and drifts are successively applied half-way through each others' timesteps. This method also has the advantage that it is possible, and fairly simple, to perform split time-stepping, where particles with large velocities or accelerations are assigned smaller timesteps to preserve accuracy, without wasting computational resources by applying these short timesteps to slow particles in less dense regions that do not need them [151]. An example of such a timestepping system is described in detail in e.g. Ref. [718].

The final ingredient to a succesful N-body simulation is the initial conditions. It is easy to say that these can be generated from linear theory, but this generally just means the one-dimensional matter power spectrum. This needs to somehow be translated into a three-dimensional matter distribution, and particles need to be assigned their appropriate initial velocities. In particular, if the matter power spectrum or transfer functions to generate the initial conditions for the simulations were computed using an Einstein-Boltzmann solver, they generally need to be translated from the Eulerian framework to the Lagrangian framework of the N-body simulation.

A traditional way of doing this is through the Zel'Dovich approximation [151, 755], where particles are initially assigned a Lagrangian coordinate $\vec{q}$. With the assumption that the universe was initially extremely homogenous, these are chosen to be uniformly spaced, often chosen as a grid for N-body simulations. At the starting time of the simulation, z_i, each particle have a displacement from their Lagrangian coordinate, this can be computed from the δ and θ output of a Boltzmann solver to obtain the initial position $\vec{x}$ and velocity $\vec{v}$,

$$\vec{x}(\vec{q}, z_i) = \vec{q} - \vec{\nabla}\nabla^{-2}\delta(\vec{q}, z_i), \tag{4.3a}$$

$$\vec{v}(\vec{q}, z_i) = \vec{\nabla}\nabla^{-2}\theta(\vec{q}, z_i). \tag{4.3b}$$

Where the real-space δ and θ fields are obtained via a Fourier transform and drawing a random realisation.

However, many N-body simulations use only Newtonian gravity (in expanding space and non-relativistic particles), while Einstein-Boltzmann solvers generally include both radiation and relativistic effects, which means that on large scales, the results of the N-body simulation will not match that of linear theory. This can be taken care of in multiple ways, such as by including the relativistic effects in the simulation [151, 718], or by scaling back the linear results from the target redshift z_t (e.g. $z = 0$), where results are desired, to the initial z_i. Back-scaling can be done simply with the linear growth factor D_+,

$$\delta^{\mathrm{bs}}(k, z_i) = \frac{D_+(z_i)}{D_+(z_t)}\delta(k, z_t). \tag{4.4}$$

The linear growth factor describes how much the density perturbation has grown relative to some normalised time. Using the growth factor computed for the N-body cosmology (i.e. matter + Λ only, in many cases), $\delta^{\mathrm{bs}}(k, z_i)$ is obtained such that if it was evolved linearly in this cosmology, it would match the fully relativistic Einstein-Boltzmann result. In cold matter + Λ only universes, the growth factor can be computed analytically and is independent of scale. However, if more species are included, such as massive neutrinos, the growth factor becomes scale-dependent.

The Zel'Dovich approximation is the first order of Lagrangian perturbation theory. The Lagrangian picture tracks each particle's displacement from its initial position (in phase space) rather than evolving the densities at fixed positions. The initial position, i.e. at the starting time of the simulation, is given as,

$$\vec{x}(\vec{q},\tau) = \vec{q} + \vec{\Psi}(\vec{q},\tau), \tag{4.5}$$

with the velocity simply obtained as $\dot{\vec{\Psi}}$. Going beyond the first order, the displacement is calculated via a Taylor series up to nth order,

$$\vec{\Psi}(\vec{q},\tau) = \sum_{j}^{n} D_+(\tau)^j \vec{\Psi}^{(j)}(\vec{q}), \tag{4.6}$$

where each order of Ψ can be used to compute the next. However, this quickly gets complicated. Second order is commonly used (2LPT), and occasionally third order (3LPT), however software for computing arbitrarily high orders has recently been released [151, 756]. Using higher-order Lagrangian perturbation theory to generate the initial conditions makes it possible to start the simulations at later initial times without loss of accuracy, thus saving computation time. However, the Lagrangian perturbation theory framework is not as well-developed beyond standard ΛCDM, compared to the Eulerian framework used in Einstein-Boltzmann solvers.

The initial conditions themselves can also be used to maximise what can be learned from simulations. In particular, multi-scale initial conditions allow zoom-in simulations, increasing the dynamical resolution range of the simulation. If the initial conditions of a simulation are generated appropriately, it is possible to resimulate it, but with increased particle resolution in a selected area. This makes use of a second grid of particles, with finer spacing and therefore lower particle mass, in a specific part of the simulation volume. This volume, which could e.g. be a specific galaxy, is then simulated with high resolution, with only a modest increase in computational cost, compared to running the entire simulation at this resolution. A minor issue that needs to be taken into account is, that direct gravitational interaction between the light particles and the heavier particles of the background volume can lead to spurious effects. It is therefore necessary to have some padding region around the region of interest, to ensure it remains unaffected by such effects [151, 757, 758].

4.2 The Halo Model

The halo model approach is nearly as old as the N-body simulations, having been pioneered in the 1950s as a tool to model the distribution of galaxies [759–762], before it was known that the matter budget of the universe was dominated by dark matter. However, it still serves as an important supplement to the N-body method, and is particularly useful due to its much lower computational requirements, as it can be dealt with semi-analytically.

One goal of the halo model framework is to compute any order of n-point correlation function (where the power spectrum described in Chapter 3 is the 2-point correlation). An advantage over N-body methods here is, that not only is the N-body simulation expensive, the higher n-point correlation function estimators are as well. The bispectrum B has been of particular interest, as it is the 3-point Fourier space correlation function, so the next level beyond the power spectrum. It is defined through the density perturbations,

$$(2\pi)^3\delta_D(\vec{k}_1+\vec{k}_2+\vec{k}_3)B(\vec{k}_1,\vec{k}_2,\vec{k}_3) = \langle\delta(\vec{k}_1)\delta(\vec{k}_2)\delta(\vec{k}_3)\rangle, \tag{4.7}$$

where the δs are the usual density perturbations. While the power spectrum will contain all information at the linear level if there are no primordial nongaussianity, nonlinear evolution and

scenarios with nongaussianity will have information requiring higher order correlation functions to capture fully [763–771].

An important quantity for halo model computations is the variance of the smoothed density field, given as[1],

$$\sigma^2(z,R) = \int_0^\infty \frac{dk}{k}\Delta^2(z,k)W^2(kR) \tag{4.8}$$

where Δ^2 is the dimensionless matter power spectrum,

$$\Delta^2(k) \equiv \frac{k^3 P(k)}{2\pi^2}, \tag{4.9}$$

and W is a window function, and R is a real-space length-scale. The standard choice of window function is a real-space tophat, yielding the Fourier-space representation,

$$W(x) = \frac{3}{x^3}\left(\sin x - x\cos x\right), \tag{4.10}$$

however, it has been suggested that a sharp Fourier-space filter may be more accurate for models beyond standard cold dark matter, at the expense of the losing the well-defined real space volume associated by the usual tophat, [772, 774, 775],

$$W(k) = \begin{cases} 1, & \text{for } k \leq k_s, \\ 0, & \text{for } k > k_s, \end{cases} \tag{4.11}$$

where the cutoff scale k_s is given through the real-space filtering-scale R,

$$k_s = \frac{a}{R}, \tag{4.12}$$

with the a parameter calibrated with N-body simulations, yielding a value $a \approx 2.5$ [772, 775].

In the context of halo models, the smoothing scale R is generally connected to a halo mass M via the mean matter density of the universe,

$$R = \left(\frac{3M}{4\pi\bar{\rho}_m}\right)^{1/3}, \tag{4.13}$$

with R being the radius of a sphere containing a total mass M, assuming uniform matter density.

The basic halo model relies on the concept of spherical collapse. A primordial overdensity (approximated to be spherical) will collapse to form a dark matter halo if the density contrast is large enough. This leads to a distribution of halos of different masses, making up the matter content in the universe. An early simple model for this is the Press-Schechter halo mass function [722], which is generally expressed as,

$$\frac{m^2 n(m,z)}{\tilde{\rho}_m}\frac{dm}{m} = \nu f(\nu)\frac{d\nu}{\nu}, \tag{4.14}$$

where $\tilde{\rho}_m$ is the comoving mean matter density, m is the halo mass, n is the comoving density of halos with mass m at redshift z. This definition is such that,

$$\int_0^\infty m\, n(m)\, dm = \tilde{\rho}_m, \tag{4.15}$$

and equivalently

$$\int_0^\infty f(\nu)\, d\nu = 1, \tag{4.16}$$

[1] Up to factors of π, depending on normalisation, see e.g. differences in Refs. [762, 772, 773].

meaning that all clustering matter is contained in halos.

The function $f(\nu)$ is what gives the shape of the halo mass function via the cosmology, which is captured in ν. These are given as,

$$\nu f(\nu) = \sqrt{\frac{\nu}{2\pi}} e^{-\nu/2}, \tag{4.17}$$

and,[2]

$$\nu \equiv \frac{\delta_{\rm sc}^2(z)}{\sigma^2(m)}, \tag{4.18}$$

where part of the cosmology dependence is given through σ computed from the linear matter power spectrum[3], as defined in Eq. (4.8), since this is computed from the matter power spectrum. The parameter $\delta_{\rm sc}(z)$ is the density contrast threshold for spherical collapse at redshift z, extrapolated to today. [762]. In an Einstein-de Sitter (matter only) universe, the critical density has the value $\delta_{\rm sc}(z=0) = 1.6868$, otherwise it will depend (weakly) on Ω_m and Ω_Λ.

While the Press-Schechter framework building on an excursion set formalism works fairly well, the Sheth-Tormen mass function provides an even better fit to simulation results [762, 776]. The halo mass function is still defined as in Eq. (4.14), but the Press-Schecthter definition of $f(\nu)$ (Eq. (4.17)) is replaced with,

$$\nu f(\nu) = A(p)\left(1 + (q\nu)^{-p}\right)\sqrt{\frac{q\nu}{2\pi}} e^{-q\nu/2}, \tag{4.19}$$

with the fitting parameters having the values $p \approx 0.3$ and $q \approx 0.75$, and the function A being,

$$A(p) = \left(1 + \frac{2^{-p}\Gamma(0.5-p)}{\sqrt{\pi}}\right)^{-1}, \qquad A(p \approx 0.3) \approx 0.3222, \tag{4.20}$$

while setting the fitting parameters to $p = 1/2$ and $q = 1$ recovers Eq. (4.17). Simulations show that the dimensionless halo mass function $f(\nu)$ is approximately "universal" when expressed in terms of σ,[4]

$$f(\sigma, z) = \frac{m}{\bar{\rho}_m}\frac{dn(m,z)}{d\ln\sigma^{-1}} \tag{4.21}$$

with simulation results agreeing to $\pm 10\%$ even with slight modifications to standard ΛCDM cosmology, such as massive neutrinos [762, 773, 777–779]. The changes to the cosmology are neatly captured through σ.

With the matter content in the universe distributed in halos, these halos can then be used as the basis of calculating the matter power spectrum (and the higher correlation functions). As the matter making up the halos has undergone nonlinear collapse, this makes it possible to compute the non-linear power spectrum. The matter power spectrum can be decomposed into two components,

$$P(k) = P^{1h}(k) + P^{2h}(k), \tag{4.22}$$

namely the 1-halo and 2-halo power spectra. The former captures the density correlations within a single halo, while the latter captures the correlations between halos. To compute these, it is therefore necessary to know both the shape of individual halos and the spatial distribution of the halo population.

[2] There are (confusingly) varying definitions of ν, e.g. Ref. [773] defines the quantity in Eq. (4.18) as ν^2.

[3] Technically the dark matter-baryon power spectrum, as only clustering matter will collapse like this. Massive neutrinos will not contribute to critical collapse, although they do have an effect on the nonlinear structure inferred from the halo model [773]

[4] Or equivalently with the definition of ν used in e.g. [773].

Starting with the distribution of halos, the halo density contrast can be defined analogously to those of different species, via

$$\frac{M}{V} \equiv \tilde{\rho}(1+\delta), \tag{4.23}$$

where M is the mass contained within a specific comoving volume V. Then the halo density contrast can be written as,

$$\delta_{\rm h}(m, z_1|M, V, z_0) \equiv \frac{N(m, z_1|M, V, z_0)}{n(m, z_1)V} - 1, \tag{4.24}$$

which looks a bit complicated with all the variables $\delta_{\rm h}$ and N depend on. Here $N(m, z_1|M, V, z_0)$ denotes the number of halos of mass m that collapsed at a redshift z_1 in the comoving volume V, which contains total mass M at redshift z_0.

Through considerations of nonlinear collapse, and how the collapse of structures changes the comoving volume containing M over time, and estimate of $\delta_{\rm h}$ can be obtained to linear order in δ [677, 762, 776, 780, 781], as a simple estimate $n(m, z_1|M, V, z_0)$ can be taken to be given through,

$$\frac{m^2 n(m, z_1|M, V, z_0)}{\tilde{\rho}} \frac{dm}{m} = \nu_{10} f(\nu 10) \frac{d\nu_{10}}{n u_{10}}, \tag{4.25}$$

with

$$\nu_{10} \equiv \frac{\left(\delta_{\rm sc}(z_1) - \delta_0(\delta, z_0)\right)^2}{\sigma^2(m) - \sigma^2(M)}, \tag{4.26}$$

where $\delta_0(\delta, z_0)$ is the initial density required to collapse to a density δ as z_0 (as extrapolated back in time using linear theory). For a large volume, the contained mass M would be large enough that it is unlikely for any halos to form with that mass, thus $\sigma(M) \ll \sigma(m)$. Hence, n can be obtained perturbatively,

$$n(m, z_1|M, V, z_0) \approx n(m, z_1) - \delta_0(\delta, z_0) \left(\frac{\partial n(m, z_1)}{\partial \delta_{\rm sc}}\right)_{\delta_{\rm sc}(z_1)} + \ldots, \tag{4.27}$$

giving a perturbative expression for $\delta_{\rm h}$,

$$\delta_{\rm h}(m, z_1|M, V, z_0) \approx \delta - (1+\delta)\delta_0(\delta, z_0) \left(\frac{\partial \ln n(m, z_1)}{\partial \delta_{\rm sc}}\right)_{\delta_{\rm sc}(z_1)}. \tag{4.28}$$

Inserting the Sheth-Tormen formula for $f(\nu)$ then yields,

$$\delta_{\rm h}(m, z_1|M, V, z_0) \approx \delta \left(1 + \frac{q\nu - 1}{\delta_{\rm sc}(z_1)} + \frac{2p/\delta_{\rm sc}(z_1)}{1 + (q\nu)^p}\right) = b_1(m, z_1)\delta, \tag{4.29}$$

where the b_1 parameter is called the linear bias. Being linear, it is only accurate at large scales. To get the accurate small-scale behaviour, orders beyond the linear are required, such that the full halo density contrast can be written as a sum,

$$\delta_{\rm h}(m, z_1|M, V, z_0) = \sum_{i>0} b_i(m, z_1)\delta^i, \tag{4.30}$$

where the higher order bias parameters can be obtained by inserting Eq. (4.25) in Eq. (4.24) and expanding to higher order [762, 782, 783]. For an overview of the higher order biases, see e.g. Ref. [762]. An interesting note however is, to preserve the normalisation,

$$\int_0^\infty dm \frac{m n(m, z)}{\tilde{\rho}} b_i(m, k) = \begin{cases} 1, & \text{for } i = 1 \\ 0, & \text{for } i > 1, \end{cases} \tag{4.31}$$

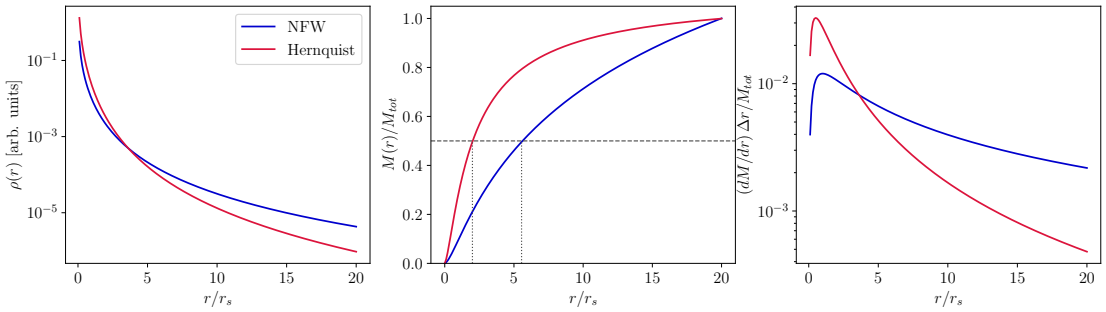

Figure 4.2: *An illustration of the mass distribution in a halo with concentration $c = 20$, showing both a NFW and a Hernquist profile normalised to the same total mass. Left panel shows the density profile, middle panel shows the total mass contained within radius r, right panel shows the mass contained in a shell of radius r and thickness $\sim 0.1 r_s$.*

meaning that higher order biases only "shuffle around" the halo population to different masses.

Having a framework for the distribution of halos, it is also necessary to describe the distribution of matter within each halo. This is done with the halo density profile, the shape of which has been extensively studied, including in numerical simulations (e.g. Refs. [784–793]). Often, the halo density profile is parameterised in the form,

$$\rho(r|m) = \frac{\rho_s}{(r/r_s)^\alpha (1 + r/r_s)^\beta}, \tag{4.32}$$

where parameter sets $[\alpha = 1, \beta = 2]$ yields the well-known Navarro-Frenk-White (NFW) profile [790], and yields $[\alpha = 1, \beta = 3]$ yields the Hernquist profile[784].

In order to have a well-defined halo mass, it is necessary to choose a cutoff to serve as the edge of the halo, since the mass of e.g. a NFW halo diverges if the density is integrated to infinity. A common choice is the virial radius, letting the halo mass be given as,

$$m = \int_0^{r_{vir}} dr\, 4\pi r^2 \rho(r|m), \tag{4.33}$$

letting the mass of an NFW halo be expressed as,

$$m = 4\pi \rho_s r_s \left(\ln(1 + c) - \frac{c}{1 + c} \right), \tag{4.34}$$

where $c \equiv r_{vir}/r_s$ is the so-called concentration parameter, the virial radius expressed in terms of the scale radius r_s. Studies have found that halos with a larger mass generally have a lower concentration. Using the virial radius as cutoff keeps this definition of the halo mass consistent with the one used in the halo mass function [762].

Most of the mass is located in the centre of the halo, as illustrated in Fig. 4.2, therefore the best-fit r_s for a given halo does not depend strongly on the estimated r_{vir}. Halos are of course not all the same, even at a given virial mass. Indeed, simulations show that the concentration parameter of halos with the same mass is approximately distributed according to a log-normal function,

$$p(c|m, z)dc = \frac{d \ln c}{\sqrt{2\pi\sigma^2_{\ln c}}} \exp\left(-\frac{\ln^2 (c/barc(m, z))}{2\sigma^2_{\ln c}} \right), \tag{4.35}$$

with the width $\sigma_{\ln c} \approx 0.25$, and the mean concentration $\bar{c}$ depending weakly on mass,

$$\bar{c}(m, z) = \frac{9}{1 + z} \left(\frac{m}{m_*(z)} \right)^{-0.13}, \tag{4.36}$$

with the mass scale m_* being defined through $\nu(m_*, z) = 1$.

This gives us everything we need to compute the matter power spectrum, Eq. (4.22), using the halo model. The 1-halo power spectrum captures the density correlations inside individual halos,

$$P^{1h}(k) = \int dm\, n(m) \left(\frac{m}{\tilde{\rho}}\right)^2 |u(k|m)|^2 , \tag{4.37}$$

where $u(k|m)$ is the Fourier transform of the halo density profile for halo mass m. The 2-halo power spectrum needs to take into account both the inner structure of the halo, and the halos' correlation with each other,

$$P^{2h}(k) = \iint dm_1 dm_2\, n(m_1) n(m_2) \left(\frac{m_1 m_2}{\tilde{\rho}^2}\right) u(k|m_1) u(k|m_2) P^{hh}(k|m_1, m_2), \tag{4.38}$$

where $P^{hh}(k, m_1, m_2)$ is the halo-halo power spectrum, and can be approximated using the linear matter power spectrum,

$$P^{hh}(k, |m_1, m_2) \approx \prod_{i=1}^{2} b_i(m_i) P^{\text{lin}}(k), \tag{4.39}$$

and going to orders beyond linear may yield better accuracy.

The higher order correlation functions, e.g. the bi- and trispectrum, can be constructed in a similar fashion using a sum of $1, 2, \ldots, n$-halo contributions. I omit the expressions for these as they are quite cumbersome, but they are presented in e.g. Ref. [762].

4.3 Halos in Simulations

As mentioned in the previous section, the perturbative approaches to computing halo statistics are generally checked against, if not calibrated with, non-linear numerical simulations. The same is true for the halo density profiles, where these are analytical expressions chosen to match the density profiles that show up in simulations.

While the halos themselves emerge directly from the gravitational interactions in the simulations, extracting this information from the simulation data is not a trivial operation, and in particular there are additional wrinkles for simulations of dark matter models beyond the standard cold dark matter paradigm. There are a variety of different software packages for this purpose [722, 794–822].

Historically, these halo finders generally fall into one of two types. The Friends-of-Friends (FoF) method [798], and the spherical overdensity method [722]. The former being based on the proximity of N-body particles to each other, while the latter is based on computing the density field from such particles.

The basic principle of the FoF method is very simple, and makes use of only two parameters: the linking length and the minimum group size. In a simplified view, the algorithm looks through the particles in the N-body simulations and for each one computes the distance to its neighbouring particles. A FoF group is found when a group of particles exceeds the minimum group size where none of the members are further from another member particle than the lining length, i.e. any particle no further than the linking length from a member particle will also be a member. They can in principle be linked to the group through only a single other particle, hence the name "Friends-of-Friends". Commonly chosen values for the minimum group size and linking length are 32 particles and 20% of the average interparticle spacing, respectively, as these are found to give physically meaningful results [742].

In practice, a naive implementation of the algorithm as described would be very computationally inefficient, so much effort has been put into writing better optimised versions, making smarter choices about which particles to compute the distances between, etc. In modern simulations, where the memory requirements of a simulation are much too large for a single computation node, a key concern is also efficiency in sharing information between nodes. Determining whether the particles of a FoF group are spread across multiple nodes is an important component, as inter-node MPI communication can easily become a computational bottleneck if not taken into account. This is typically done by making use of the "tree" computed for the gravity solver in many N-body codes [742, 802, 805, 823, 824]. Many modern halo finders use a FoF approach, including Rockstar, VELOCIraptor and the built-in halo finding in Gadget-4 [742, 795, 800, 805]

An issue with the FoF method is, that a particle is either connected to a group, or not. Thus, it cannot be used to identify substructure. Another is the danger of spurious linking of two "blobs" via a linking bridge, where a very narrow strip of particles, technically within the linking length of each other, connect two otherwise separate groups [806]. These issues do not present themselves in the spherical overdensity method. In this method, peaks in the dark matter density are identified, then the mean density inside a sphere around the density peak is computed. If the density is above a threshold value, the sphere is expanded, and the process is repeated until the density falls below the threshold. Again, there are different ways to optimise this scheme, as well as computing the density. This method is also used by multiple modern halo finders, such as Amiga and ASOHF [805, 806, 809, 821].

Identifying substructure inside a main halo is also an important task for modern halo finders, e.g. identifying galaxies inside a galaxy cluster, or satellites of a galaxy. This is not really feasible with FoF and must be done using the dark matter density (or potential). In practice, a hybrid approach is often used where the primary group finding is done using FoF, after which a density/potential based approach is used to find substructure within each FoF group. This limits the scope for computing the density field, bringing computational efficiency. A prime example of this is the FoF/SubFind implementation in Gadget-4 [742]. SubFind identifies density peaks within a FoF group and computes the local density field within an expanding region[5] until it reaches a saddle-point. Since the particles within this region may not be gravitationally bound to the subhalo, but rather to the parent halo, and just happen to pass through the volume of the subhalo at the time, a gravitational unbinding procedure is applied. The gravitational potential of the subhalo is computed using the particles inside the volume. The subhalo centre is located at the most bound particle, and its velocity is the mean velocity of its constituent particles. Computing the velocities of the particles in the frame comoving with the halo, it can be checked if they are gravitationally bound to the subhalo or not. Particles with positive energy are successively removed from the halo and the potential recomputed, until only bound particles remain. If the number is larger than the chosen minimum required for a subhalo, it is accepted [811].

Some implementations [795, 800] make use of 6D phase space clustering information to identify substructure, essentially using FoF in the full phase space rather than only in the three spatial dimensions. This is particularly useful for identifying member particles of distinct substructures close to large density peaks of host halos, as the density differential might not be large. Sometimes the gravitational unbinding step is omitted, which makes it slightly harder to physically interpret the results [742].

[5] SubFind uses an excursion set method rather than just an expanding sphere, but the general principle is the same.

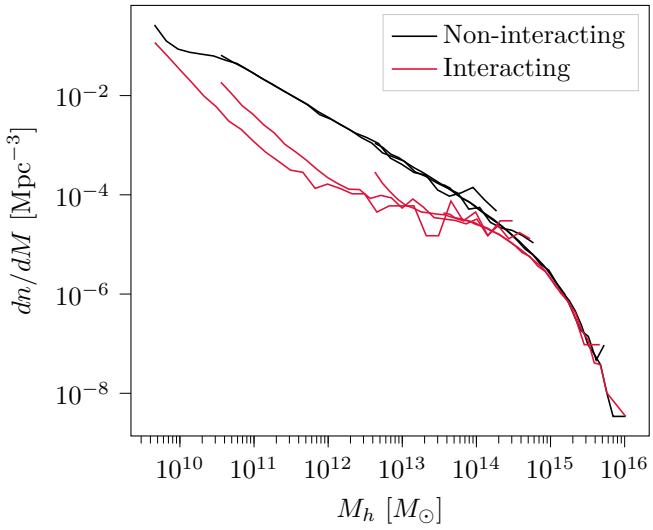

Figure 4.3: *The halo mass function obtained from N-body simulations using the Friends-of-Friends method. The data uses a suite of N-body simulations with $N = 512^3$ particles in a set of boxes of side length $L = 50$, 100, 500, and $1000\,h/\mathrm{Mpc}$. The Interacting curve uses the dark matter-neutrino interaction model described in Chapter 5. It is clear that the interacting model shows a spurious enhancement of the number of halos close to the lower end of the simulations' halo mass resolution.*

4.4 Beyond Cold Dark Matter

As always, things get more complicated when moving beyond the non-interacting cold dark matter paradigm. In N-body simulations, models beyond cold dark matter can generally be separated into two categories, those that behave like cold dark matter at late times, thus only requiring modified initial conditions, and those whose behaviour requires specific extra modelling.

In the former category, we find models of dark matter interacting with light species, such as photons and neutrinos, as well as warm dark matter[6]. The fact that these interaction types do not need to be modeled in the late universe is of course not a given, but follows from modelling at the linear level, and finding that for all interaction strengths allowed by CMB and BAO data (assuming that the interacting species makes up 100% of the dark matter), the interaction would become suppressed long before the initialization time of an N-body simulation, see e.g. Chapters 5 to 7 and Refs. [379, 659, 661].

These interacting scenarios are therefore fairly straightforward to investigate in N-body simulations, as the simulation software does not need to be modified to account for new physics. They can be explored by merely passing the linear matter power spectrum of the model to the initial condition generator. The discretized density of N-body simulations does offer some challenges for models with suppressed small-scale structure, such as warm dark matter and models interacting with relativistic species. Namely, it has been found that the dark matter particles will form spurious halos at small halo masses in these models [827–829], as illustrated in Fig. 4.3.

One possible (but inefficient) way of "solving" this problem is by increasing the number of particles and hence the mass resolution, thus moving the spurious halos to smaller masses. This is of course not a real solution, since the spurious halos are still there, but they might be shifted out of the mass range relevant to a given study. An equivalent solution is to run multiple simulations with different box sizes and stitch the halo mass functions together, cutting off the low-mass tail

[6] Warm dark matter can require slightly more involved modifications to the initial conditions to account for the thermal velocity [237, 825, 826].

of each one, where the spurious halos are. This method is used in Chapter 7. Both of these are unfortunately computationally inefficient, as the mass scale of the spurious halos only scales as $N^{-1/3}$ [827]. These halos can be removed through postprocessing [828], but this has the usual problems associated with post-processing, namely that it does not necessarily account for any dynamical effects they might have had on the simulation. Another way to escape this problem is using a sheet-based method, rather than traditional N-body. However, this approach becomes prohibitively expensive when densities in the cores of halos are large enough. A possible solution is a mixed approach where high density regions are treated with particles and low density regions with a sheet approach [829–833].

In the category of models requiring modifications to the physics in the simulation software, we find dark matter whose late-time behaviour deviates from the cold dark matter paradigm, such as self interacting dark matter and decaying dark matter. If dark matter decays, it needs to have a lifetime long enough that it can survive on cosmological timescales. Decaying dark matter at late times can have two distinct effects on structure formation: if the dark matter decays to a lighter but still massive state, the particle could receive a velocity kick, essentially becoming warm dark matter at late times, this type of scenario is investigated in e.g. Refs. [834–837]. Alternatively, the dark matter might decay into radiation, thus lowering the late time matter density and increasing the radiation density, which is investigated in e.g. Refs. [838–841]. Late-time decaying dark matter scenarios have been suggested as solutions to both the core-cusp and missing satellite problems, and the H_0 and σ_8 tensions.

Self-interacting dark matter is also a very popular subject of investigations [360, 361, 365, 842–850]. In particular, it has been suggested as a solution to the core-cusp and missing satellite problems, as simulations of self-interacting dark matter generally leads to cored rather than cuspy halo centres, as well as fewer satellite galaxies.

There is not a single unified implementation of self-interaction in N-body codes, but several different methods exist. As the N-body particles do not directly correspond to the "physical" particle physics particles, the method must reproduce the large-scale effects of the physics, conceptually similarly to baryonic physics. Two widely used implementations are those of GIZMO [365, 734, 851] and AREPO [745, 746, 852]. Both use a probabilistic method to determine if a dark matter particle will have an interaction with a neighbour in a given timestep [844].

The GIZMO implementation's probability for an interaction between particles i and j is given through,

$$P_{ij} = \left(\frac{\sigma}{m}\right) m_i v_{ij} g_{ij} \delta t, \tag{4.40}$$

where σ and m are the particle physics cross-section and particle mass, m_i is the N-body particle mass of particle i, v_{ij} is the N-BODY particles' relative velocity, and g_{ij} is a number density factor accounting for the fact that each N-body particles represents a smoothed density. Finally, δt is the length of the timestep. To determine if a scattering occurs, a random number is drawn from a uniform distribution between 0 and 1, which is compared to the scattering probability P_{ij} If an interaction happens, the particles are each given a velocity kick consistent with elastic scattering, with the scattering angles isotropic in the centre of mass frame of the particles and the outgoing particles moving in opposite directions.

The expression for the AREPO implementation of this scattering probability is quite similar,

$$P_{ij} = \left(\frac{\sigma}{m}\right) m_i v_{ij} W(r_{ij}, h_i) \delta t, \tag{4.41}$$

which is calculated for the k nearest neighbouring particles, with a default $k = 32 \pm 5$ [844]. The function $W(r_{ij}, h_i)$ is the cubic spline kernel, with h_i being the smoothing length enclosing particle i's nearest k particles. Again, a random number, x, is drawn from a uniform distribution

to determine if a scattering happens, however, here the pair of scattering particles is determined afterwards. The k neighbours are sorted by the distance to particle i, and the scattering will take place with the first particle l satisfying,

$$x \leq \sum_{j}^{l} P_{ij}, \tag{4.42}$$

with j increasing with increasing particle separation. The scattering then happens similarly to in the GIZMO implementation, as an isotropic elastic scattering.

It is found that these two methods agree to around $\sim 30\%$ for computing a halo density profile, and can confidently differentiate between different orders of magnitude in the cross-section σ/m [844].

As specific framework for connecting such phenomenological dark matter scattering to particle physics models is the so-called ETHOS (effective theory of structure formation) [663, 664, 853–859]. This offers an effective framework in which an array of different particle physics models can be described using a set of effective parameters. In particular, this includes models in which dark matter interacts with a massless dark radiation species through some mediator, which would also effectively lead to self-interactions between the dark matter particles. This also yields a consistent way of computing the linear initial conditions, where many studies of interacting dark matter have merely used standard cold dark matter initial conditions. In practice, the works using ETHOS have generally used the self-interaction implementation of AREPO for the non-linear evolution.

4.5 Neutrinos and other hot dark matter

Being effectively non-interacting, neutrinos of nonzero mass are essentially a type of hot dark matter. They have been shown to be much too light to compose the majority of the dark matter in the standard picture, but they can (and should, according to the Standard Model), form a subdominant component. Standard Model neutrinos are expected to have a relic density of $10^{-3} \leq \Omega_\nu \leq 0.03$ [860], which may be small, but is not necessarily negligible, especially with modern and future cosmological surveys, several of which have the cosmological detection of the neutrino mass as an explicit goal [171, 861–865].

To make use of such precise measurements, accurate predictions are necessary, and that means including the effects of neutrinos in the nonlinear modelling. There are also hopes to detect the relic neutrino background with the PTOLEMY experiment [866–868], which would require accurate calculations of the local neutrino density to make predictions for detection.

Perhaps the conceptually simplest way to model neutrinos nonlinearly is as N-body particles, but with smaller masses and larger velocities than the regular cold dark matter particles [869]. This presents some challenges, however, especially at early times when the velocities might be very large. This would require the simulation to take very small timesteps, greatly increasing the computational requirements, and even then, the large thermal velocities might lead to Poisson noise on small scales.

Another method is evolving the neutrinos as a fluid on a grid, which allows a perturbative approach and can be much cheaper computationally than full N-body particles. However, if perturbative, it may not fully capture the nonlinear effects, and it is impossible to resolve bound structures and scales smaller than the grid [870, 871]. Nevertheless, this approach can be very effective for computing quantities like the power spectrum [733, 872]. A class of these types of simulations is known as linear response. Here, the neutrinos are evolved through linear

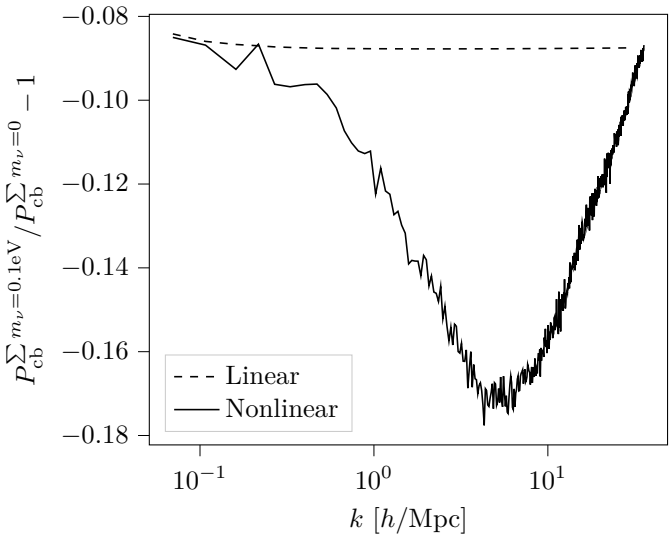

Figure 4.4: *An illustration of the so-called neutrino spoon, a nonlinear effect on the shape of the matter power spectrum, which shows a spoon-like suppression compared to the case of massless neutrinos that cannot be obtained from linear calculations. Results shown here at redshift $z = 3$ and a degenerate neutrino hierarchy with $\sum m_\nu = 0.1$ eV, computed with CONCEPT [718, 733].*

perturbation theory, but are able to feel the nonlinear potential from the nonlinearly clustering matter, and the effect of linearly evolved neutrinos feeds back into the nonlinear matter evolution. This can yield highly accurate predictions for the cold- and total matter power spectra and reasonable results for the neutrinos [731, 873–875].

A "third" method attempts to circumvent the shortcomings of the N-body and fluid methods by essentially combining them in a hybrid method. Here, neutrinos are modelled using computationally cheaper methods in the early universe while their velocities are large and clustering small, e.g. perturbatively as fluids [860]. Then, at later times in the simulations, these are converted to N-body particles initialised with appropriate thermal velocities and evolved normally. This method also makes it possible to split the neutrinos into separate momentum bins, and only convert those with the smallest momenta, and hence most affected by nonlinear clustering [860, 871, 876].

Of course, these schemes are not necessarily tied to neutrinos, but can be used for any particle species that acts as hot dark matter, i.e. a species that has a large thermal velocity at early times and low mass. An example could be axions too heavy to act as fuzzy dark matter. Here, some modifications to the initial conditions may be in order to match early time axion simulations, and the distribution function is Bose-Einstein rather than Fermi-Dirac. Other non-thermal distributions could also be considered.

4.6 Beyond Dark Matter

Another (very important) complication to non-linear structure formation is baryons. Since they interact much more strongly than dark matter, and have a range of important processes, such as gas cooling, star formation, and supernova explosions, they are quite computationally demanding. There are multiple ways of handling the inclusion of baryons, but again they can be roughly separated into two categories: in-simulation modelling, where the baryonic matter is handled as part of the simulation, or post-processing, where the simulation output is populated with

baryonic matter based on the dark matter distribution. The former has the advantage of allowing for back-reaction on the dark matter distribution from the baryons, at the cost of being much more computationally demanding. However, there is still significant uncertainties related to the modelling of baryons in cosmological simulations [151]. One way of dealing with this uncertainty is through the use of different implementations of baryon physics, such as in the CAMELS simulation suite [150, 877, 878], which makes use of the AREPO-based IllustrisTNG model [879, 880] and the GIZMO-based Simba model [881].

Cosmological simulations including baryons in their modelling generally use some form of smoothed particle hydrodynamics, where the simulation uses smoothed particles to represent the gas distribution. They can involve a variety of gas physics, including multiple cooling channels, star formation and feedback, supernovae and black holes [151, 734, 745, 746, 879–882]. For appropriate gas temperatures and densities, star formation occurs, leading to feedback from stars and supernovae heating the gas and changing the chemical composition. In the end, this produces galaxies with e.g. realistic stellar populations, which can be compared to observations.

Getting accurate modelling of the behaviour of baryons is absolutely crucial to make inferences from data about nonlinear structures, as all we really are able to observe comes from baryons.[7] Even gravitational lensing, which gives a direct measurement of the gravitational potential, requires light emitted by baryons to experience the lensing. To make the right conclusions from current and next generation surveys of e.g. Lyman-α, 21cm and galaxies, we need to understand the modelling of baryonic physics.

The uncertainty on implementations of the baryons yields an additional wrinkle to using simulations for investigating the nature of dark matter, as some effects of e.g. interacting dark matter models may be degenerate with the effects of including baryons [843].

Post-processing is generally a computationally cheaper solution than on-the-fly hydrodynamics, and thus offer a good alternative. Based on models of halo occupation, the halo catalogs of dark matter only simulations can be populated with galaxies, so their baryonic signatures can be extracted. This uses semi-analytic models of galaxy evolution and is often referred to as SAG. Generally, these methods will rely on the merger trees of the halos, a list of their progenitor halos and when mergers happened, in order to better estimate the history and evolution of a given halo, and thus how it would look at the time of observation. Examples of this type of models are Galform [883–888], Shark [889], SAGE [890], and Galacticus [891].

Galform in particular also allows the generation of entirely synthetic merger trees and galaxy populations using only a halo model, thus circumventing the need for expensive N-body simulations. This can also counter the problems of spurious small-scale structure in simulations of models with suppressed small-scale power, described in greater detail in Chapter 7.

[7] It could perhaps be argued that gravitational waves emitted from merging black holes are not truly emitted by baryonic matter, but unless these black holes are primordial, they would be the remnants of massive stars, thus requiring accurate stellar modelling.

Part II

Research Works

CHAPTER 5

A linear treatment of dark matter-neutrino scattering

While the standard cold dark matter paradigm fits the data to a large extent, it is not particularly theoretically satisfying. It does not a priori offer any clues to how it came to exist, or any connections to the Standard Model of particle physics. As it is, it offers merely an ad-hoc way of describing the data.

Neutrinos are similarly a part of the Standard Model that leaves open questions, in particular how they gain their mass. Interacting only weakly with other particles, they share some similarity with dark matter. It is always tempting to try to solve two problems at once, and indeed a possible connection has been suggested an origin of neutrino masses [892].

Of course, there is an effectively infinite possibility space for new particle physics models that could, potentially, offer a solution. Investigating every such theory in full rigorous detail would be a career's worth of work for multiple researchers, so I have taken a different path.

Rather than working on a full UV-complete theory for dark matter, I have applied an effective model with a phenomenological scattering between dark matter and neutrinos, which could arise from any number of underlying theories. It is therefore possible to collectively probe their cosmological consequences, and thus also their viability, using just a phenomenological implementation.

The work reproduced in this chapter offers the first full linear treatment of dark matter-neutrino scattering that includes neutrino masses. As cosmological surveys approach the sensitivity required to measure neutrino masses, it is prudent to include them in both linear and non-linear modelling. The effective treatment presented in this chapter thus also forms the basis of my later work on the analyses in Chapters 6 and 7.

The full Boltzmann hierarchy for dark matter-massive neutrino interactions

Markus R. Mosbech,[a] Celine Boehm,[a] Steen Hannestad,[b] Olga Mena,[c] Julia Stadler,[d] and Yvonne Y. Y. Wong[e]

[a]School of Physics, University of Sydney, Camperdown, NSW 2006, Australia
Sydney Consortium for Particle Physics and Cosmology

[b]Department of Physics and Astronomy, Aarhus University, DK-8000 Aarhus C, Denmark

[c]IFIC, Universidad de Valencia-CSIC, 46071, Valencia, Spain

[d]Max Planck Institute for Extraterrestrial Physics, Giessenbachstraße 1, 85748 Garching, Germany

[e]School of Physics, The University of New South Wales, Sydney NSW 2052, Australia,
Sydney Consortium for Particle Physics and Cosmology

Abstract: The impact of dark matter-neutrino interactions on the measurement of the cosmological parameters has been investigated in the past in the context of massless neutrinos exclusively. Here we revisit the role of a neutrino-dark matter coupling in light of ongoing cosmological tensions by implementing the full Boltzmann hierarchy for three massive neutrinos. Our tightest 95% CL upper limit on the strength of the interactions, parameterized via $u_\chi = \frac{\sigma_0}{\sigma_{Th}} \left(\frac{m_\chi}{100\mathrm{GeV}}\right)^{-1}$, is $u_\chi \leq 3.34 \cdot 10^{-4}$, arising from a combination of Planck TTTEEE data, Planck lensing data and SDSS BAO data. This upper bound is, as expected, slightly higher than previous results for interacting massless neutrinos, due to the correction factor associated with neutrino masses. We find that these interactions significantly relax the lower bounds on the value of σ_8 that is inferred in the context of ΛCDM from the Planck data, leading to agreement within 1-2σ with weak lensing estimates of σ_8, as those from KiDS-1000. However, the presence of these interactions barely affects the value of the Hubble constant H_0.

5.1 Introduction

The cosmological ΛCDM model is tremendously successful in describing scales ranging from the cosmological volume to the sizes of galaxies. In its most basic form, it depends on six free parameters only, five of which are determined to better than 1% accuracy to date [16]. In particular Cosmic Microwave Background data (CMB), together with measurements of the universe's Large Scale Structure (LSS), allow for such precise constraints. Present data is well described by the minimal parameterization of the ΛCDM model, which treats neutrinos either as massless particles or sets their masses to the minimum value allowed by neutrino oscillations, $m_\nu \sim 0.06\,\mathrm{eV}$ [893]. Cosmology already imposes the tightest limits available on the neutrino mass scale: $m_\nu \leq 0.241\,\mathrm{eV}$ from the CMB alone and $m_\nu \leq 0.120\,\mathrm{eV}$ from a joint analysis of CMB and Baryonic Acoustic Oscillations (BAO) [16], both at 95% CL. These constraints surpass not only the current sensitivity of kinematic terrestrial neutrino-mass experiments, such as KATRIN [894]

(which currently reports a 95% CL upper limit of $m_\nu \leq 1.1\,\mathrm{eV}$ [895]), but also future prospects, which plan to improve the present limit to 0.2 eV. Planned LSS surveys [171, 174, 896] will further increase the sensitivity to $\sim 0.02\,\mathrm{eV}$ and thus provide hope for a cosmological detection of neutrino masses [897, 898].

Constraints on the neutrino mass from CMB and LSS, however, depend on the cosmological scenario considered, and alternatives to the minimal ΛCDM scenario are attractive for a number of reasons. ΛCDM faces challenges in effectively describing structures on sub-galactic scales [147, 899–903] as well as tensions between different experiments. Most notably, there is a disagreement at more than 4σ [130, 904] between the value of H_0 determined from early [5, 696, 905–908] and late-type [139, 909–911] cosmological probes, with the latter favouring higher values. Another tension is the discrepancy in σ_8/S_8 clustering parameter between Planck CMB data and other measurements from weak lensing surveys [140, 142, 912]. Apart from new physics, instrumental effects have been brought forward to explain the discrepancy [135]. Finally, the ΛCDM model remains a phenomenological description where the nature of two of its principal components, dark matter (DM) and dark energy, are still unknown.

Complementary to collider searches and direct detection efforts, the microscopic properties of DM can be investigated from cosmological observations, by relaxing the assumptions of a cold, collisionless single fluid. Models of warm DM [145, 162, 165, 237, 381–383, 389, 392], self-interacting DM [352, 356, 360–369] and DM interactions with baryons [352, 355, 356, 370–372, 374], photons [144, 148, 149, 352, 353, 356, 357, 359, 371, 372, 375–379], neutrinos [352, 356, 378, 660, 913–915] or dark radiation [663, 916–923] have therefore received plenty of attention in the literature. Recently, the case of DM simultaneously interacting with multiple other species has also been considered [659]. In the context of DM-neutrino interactions, however, only the massless limit has been implemented, making it e.g. impossible to simultaneously derive constraints on the interaction strength of three interacting neutrinos and their mass scale. To the best knowledge of the authors, no previous study has re-derived the full Boltzmann hierarchy for massive neutrinos in the presence of interactions with dark matter.

In light of the imminent improvements on the neutrino mass scale from cosmological observations, we consider it timely to update the formalism for DM-ν interactions. Here, we present the full Boltzmann hierarchy for massive neutrinos interacting with DM through a constant scattering term (similar to e.g. Thomson scattering) and its implementation in the Boltzmann solver CLASS [67]. The modified CLASS version developed for this paper can be used to create initial conditions for N-body simulations, which study the effect of DM-ν interactions on smaller scales[1]. We use our results to update constraints on the neutrino interaction rate from cosmological observations through a MCMC approach using the publicly available code MontePython [924, 925]. For a minimal neutrino mass scale of 0.06 eV, we find that the correct treatment of the neutrino mass slightly loosens the bounds on the cross-section, due to the appearance of an momentum-dependent factor p^2/E^2 in the scattering term.

The structure of the paper is as follows. In Section 5.2 we review the linearized relativistic Boltzmann equations for ΛCDM, then we present the modification from DM-ν interactions in Section 5.3. The impact on the CMB and on the matter power spectrum are discussed in Section 5.4, together with the parameter constraints obtained from current cosmological observations. We conclude in Section 5.5. The detailed derivation of the modified Boltzmann equations and the accuracy of its numerical implementation are presented in Section 5.A and Section 5.B, respectively. We shall also illustrate the results for all the cosmological parameters considered in this work in Section 5.C.

[1] Our code is publicly available under `https://github.com/MarkMos/CLASS_nu-DM`

5.2 The Boltzmann equation

For a large fraction of its evolution history, the universe is well-described by the linearised Boltzmann equations. Beginning in a very homogeneous state with only minor deviations, the linear Boltzmann treatment works extremely well, until the onset of nonlinear structure formation in the late universe.

The basis of the framework is the relativistic Boltzmann equation, as presented in e.g. references [163, 926]

$$P^\alpha \frac{\partial f}{\partial x^\alpha} - \Gamma^\gamma_{\alpha\beta} P^\alpha P^\beta \frac{\partial f}{\partial P^\gamma} = m \left(\frac{\partial f}{\partial \tau}\right)_C , \tag{5.1}$$

which describes the evolution of the distribution function f for a given species with mass m, defined through the number of particles in a phase-space volume element

$$f(\mathbf{x}, \mathbf{P}, \tau) dx^1 dx^2 dx^3 dP^1 dP^2 dP^3 = dN , \tag{5.2}$$

where x^i are the comoving coordinates and P^i their canonical momentum conjugate. We can then define the perturbation to the distribution function, Ψ, using the comoving momentum $\mathbf{p}$,

$$f(\mathbf{x}, \mathbf{p}, \tau) = f_0(p) \left[1 + \Psi(\mathbf{x}, \mathbf{p}, \tau)\right] . \tag{5.3}$$

The Boltzmann equation retains the gauge freedom of general relativity, so it is necessary to solve it in a specific gauge. The Boltzmann equation for Ψ, reads, in the Newtonian gauge, as

$$\frac{\partial \Psi}{\partial \tau} + i \frac{p}{E} \left(\mathbf{k} \cdot \hat{\mathbf{n}}\right) \Psi + \frac{d \ln f^{(0)}(p)}{d \ln p} \left[\dot{\phi} - i \frac{E}{p} \left(\hat{\mathbf{k}} \cdot \hat{\mathbf{n}}\right) \psi\right] = \frac{1}{f_0} \left(\frac{\partial f}{\partial \tau}\right)_C , \tag{5.4}$$

where ϕ and ψ are the gauge fields of the Newtonian gauge, E and p are particle energy and comoving momentum and $\hat{\mathbf{n}}$ is the unit vector pointing in the direction of the momentum.

For most standard species, it is possible to perform a Legendre decomposition and integrate analytically over the particle momentum p and then evolve the integrated quantities (e.g. δ, θ). However such a simplification is not possible for massive neutrinos. The fact that they have a small but nonzero mass, means they are not inherently ultrarelativistic (like photons) or nonrelativistic (like baryons or cold dark matter (CDM)) and prevents the use of various approximations. Instead, it is required to solve the hierarchy in a momentum-dependent way. In practice, this is done by separately solving the hierarchy for a set of momentum bins, as described in e.g. [163, 635].

The Boltzmann equations for conventional cold dark matter are very simple, since it only interacts gravitationally. In the Newtonian gauge, the dark matter fluid is described by the equations

$$\dot{\delta}_{\rm cdm} = -\theta_{\rm cdm} + 3\dot{\phi} , \tag{5.5a}$$

$$\dot{\theta}_{\rm cdm} = -\frac{\dot{a}}{a} \theta_{\rm cdm} + k^2 \psi . \tag{5.5b}$$

The non-interacting Boltzmann hierarchy for massive neutrinos in the Conformal Newtonian gauge (using the conventions of reference [163]) are:

$$\frac{\partial \Psi_0}{\partial \tau} = -\frac{pk}{E_\nu(p)} \Psi_1 - \dot{\phi} \frac{d \ln f^{(0)}(p)}{d \ln p} , \tag{5.6a}$$

$$\frac{\partial \Psi_1}{\partial \tau} = \frac{1}{3} \frac{pk}{E_\nu(p)} \left(\Psi_0 - 2\Psi_2\right) - \frac{E_\nu(p)\, k}{3p} \psi \frac{d \ln f^{(0)}(p)}{d \ln p} , \tag{5.6b}$$

$$\frac{\partial \Psi_l}{\partial \tau} = \frac{1}{2l+1} \frac{pk}{E_\nu(p)} \left(l \Psi_{l-1} - (l+1) \Psi_{l+1}\right) , \quad l \geq 2 . \tag{5.6c}$$

5.3 Modified Boltzmann equations in presence of neutrino-dark matter interactions

We introduce a new interaction between massive neutrinos and a dark matter species similarly to the case of massless neutrinos or photons interacting with dark matter [658, 660, 661, 915].

We shall assume a constant cross-section scattering between the massive neutrinos (ν) and the DM particles (χ), where the total neutrino energy is much smaller than the DM mass. This corresponds to a mass-degeneracy between the mediator and the dark matter particle [220, 352]. Solving the scattering integral for a massive neutrino with momentum p:

$$C(p) = \frac{1}{E_\nu(\mathbf{p})} \int \frac{d^3\mathbf{p}'}{(2\pi)^3\, 2E_\nu(\mathbf{p}')} \frac{d^3\mathbf{q}}{(2\pi)^3\, 2E_\chi(\mathbf{q})} \frac{d^3\mathbf{q}'}{(2\pi)^3\, 2E_\chi(\mathbf{q}')} (2\pi)^4 |M|^2 \times \delta^4(q + p - q' - p') \left[g(\mathbf{q}')\, f(\mathbf{p}')\, (1 - f(\mathbf{p})) - g(\mathbf{q})\, f(\mathbf{p})\, (1 - f(\mathbf{p}'))\right], \quad (5.7)$$

yields the collision term

$$C(p) = \frac{\sigma_0 n_\chi p^2}{E_\nu^2(p)} \left[f_0^{(1)}(p) + \frac{1}{2} f_2^{(1)}(p)\, P_2(\mu) - f^{(1)}(p,\mu) - v_\chi \mu E_\nu(p) \frac{df^{(0)}(p)}{dp} \right], \quad (5.8)$$

from which we can define a momentum-dependent interaction rate

$$C_\chi(p) \equiv \frac{a\sigma_0 n_\chi p^2}{E_\nu^2(p)} \ . \quad (5.9)$$

The extra factor of a originates from the use of comoving coordinates and conformal time. The cross section can be re-parameterized using

$$u_{\nu\chi} = \frac{\sigma_0}{\sigma_{\rm Th}} \left(\frac{m_\chi}{100\,\mathrm{GeV}} \right)^{-1}, \quad (5.10)$$

the interaction rate is then given by

$$C_\chi = a\, u_{\nu\chi} \frac{\sigma_{\rm Th} \rho_\chi}{100\,\mathrm{GeV}} \frac{p^2}{E_\nu^2} \ . \quad (5.11)$$

The modifications to the Boltzmann hierarchy for massive neutrinos are gauge independent and consist of adding a collision term to the Euler equation and a damping term to the higher moments:

$$\frac{\partial \Psi_1}{\partial \tau} = [...] - C_\chi \frac{v_\chi E_\nu(p)}{3 f^{(0)}(p)} \frac{df^{(0)}(p)}{dp} - C_\chi \Psi_1 \ , \quad (5.12a)$$

$$\frac{\partial \Psi_2}{\partial \tau} = [...] - \frac{9}{10} C_\chi \Psi_2 \ , \quad (5.12b)$$

$$\frac{\partial \Psi_l}{\partial \tau} = [...] - C_\chi \Psi_l, \quad l \geq 3 \ , \quad (5.12c)$$

where [...] represents the standard terms of the non-interacting case, omitted for clarity. Note that the $l = 0$ equation is unmodified, as the interaction does not transfer energy at linear order.

The corresponding Boltzmann equations for DM are usually presented after being integrated over momentum. An integrated term has to be added to the θ_χ-equation,

$$\begin{aligned} \dot\theta_\chi &= [...] + K_\chi \frac{3}{4} k \frac{\int p^2 dp\, p f^{(0)}(p)\, C_\chi(p) \left(\frac{\theta_\chi E_\nu(p)}{3 k f^{(0)}(p)} \frac{df^{(0)}(p)}{dp} + \Psi_1 \right)}{\int p^2 dp\, p f^{(0)}(p)} \ , \\ &= [...] + K_\chi \dot\mu_\chi\, (\theta_\nu - \theta_\chi) \ , \end{aligned} \quad (5.13)$$

with [...] representing the terms of the standard non-interacting DM equation, $\dot{\mu}_\nu$ is the interaction rate in terms of a ν-DM opacity, as in e.g. [915]. Since the integral in Eq. (5.13) cannot be solved analytically, we do not offer an explicit definition of $\dot{\mu}_\nu$, but merely present it to serve as an interpretation of the integral. K_χ is the momentum conservation factor, given by

$$K_\chi \equiv \frac{\rho_\nu + P_\nu}{\rho_\chi} = \frac{(1+w_\nu)\rho_\nu}{\rho_\chi} \ , \tag{5.14}$$

It is similar to the $R = \frac{4\rho_\gamma}{3\rho_b}$ found in the Thomson scattering term for baryons but not identical due to the fact that w_ν is not always 1/3. Note that in our numerical code, v_χ can be expressed as $v_\chi = \theta_\chi/k$. For a detailed derivation of the interaction term and the Boltzmann hierarchy, see Section 5.A. It is also worth noting that CLASS does not always solve the full momentum-dependent hierarchy. In some regimes a fluid approximation is used instead, which greatly lowers computation time. In Section 5.B we describe how we consistently treat the momentum-dependent interaction rate $C_\chi(p)$ in this regime.

In our numerical implementation, the interacting species χ is included as a new species, independently of the non-interacting CDM component, and therefore allowing for only a fraction of the dark matter to interact with neutrinos. However, all of the results presented in this work are based on a scenario with 100% of the dark matter being the interacting species χ. Additionally, our framework allows for different cross sections for the different neutrino species, albeit the results presented here were obtained for three massive neutrino species with identical coupling to χ. While in our publicly available modified CLASS version we have only implemented the interaction in the Newtonian gauge, the inclusion in the synchronous gauge would be straightforward.

5.4 Numerical results

The largest impact of the interaction is on the matter power spectrum, as illustrated in Fig. 5.1, where the matter power spectrum is depicted for a range of u_χ-values. The main effect is a damping on small scales, with the scale of the threshold for damping depending on u_χ. The shape of the damped power spectrum is qualitatively similar to the results for massless neutrinos, see e.g. [662, 913, 915].

The effect on the CMB is illustrated in Fig. 5.2, see also references [660, 913, 915]. As carefully explained in [915, 927], the CMB temperature anisotropies are mainly generated by the coupled baryon-photon fluid. This fluid is normally affected separately by the neutrinos and the dark matter components, because of their different behaviour: that is, neutrinos free stream and dark matter clusters slowly. The solution to the system can be separated into slow modes and fast modes [928, 929], where the baryon-photon fluid and neutrinos fall into the former category and DM into the latter. This means that, in the non-interacting case, only the neutrinos will have significant gravitational interactions with the baryon-photon fluid. However, when the DM couples strongly enough to neutrinos, it will also experience oscillations and will contribute to the fast modes. This effect will significantly affect the CMB spectrum, leading to a gravitational boosting effect, which enhances the peaks. Additionally, if the neutrinos and DM are tightly coupled, their lower sound speed compared to the baryon-photon fluid will cause a drag effect, leading to a lightly smaller acoustic scale, causing the CMB peaks to be shifted slightly towards higher multipoles l.

We run our MCMC chains varying the six usual ΛCDM cosmological parameters, i.e. the baryon and cold dark matter physical densities $\omega_b \equiv \Omega_b h^2$ and $\omega_{DM} \equiv \Omega_{DM} h^2$, the angular size of the sound horizon at last-scattering $100 * \theta_s$, the optical depth to reionization τ and the amplitude and tilt of the primordial scalar power spectrum (represented by $\ln 10^{10} A_s$ and n_s

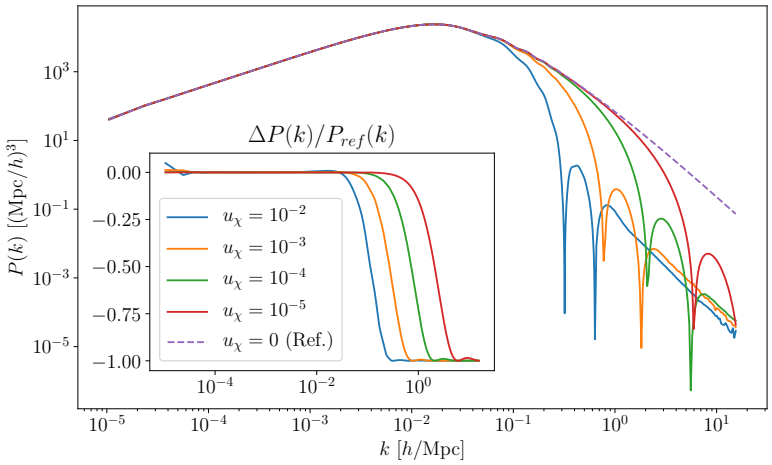

Figure 5.1: *Matter power spectrum for different values of u_χ in a fiducial cosmology using Planck 2018 parameters [5], the insert panel shows relative difference, compared to the non-interacting case.*

Parameter	Prior
ω_b	Flat, unbounded
ω_{DM}	Flat, unbounded
$100 * \theta_s$	Flat, unbounded
$\ln 10^{10} A_s$	Flat, unbounded
n_s	Flat, unbounded
τ_{reio}	Flat, $\tau_{reio} \geq 0.004$
u_χ	Flat, $u_\chi \geq 0$
$\sum m_\nu$	Flat, $\sum m_\nu \geq 0.06$ eV

Table 5.1: *MCMC parameters and priors.*

respectively) in addition to the interaction parameter u_χ. We have also run cases varying the sum of neutrino masses, assuming a degenerate mass hierarchy. While we know from neutrino oscillations that this is not the correct model, the difference should be negligible for our purposes [930]. We have further ensured that this is the case by running CLASS with all three mass hierarchies (normal, inverted, degenerate) for a set of different masses and comparing the output for the different hierarchies, confirming that the difference between the hierarchies is negligible in the region of interest. We use combinations of three different datasets for our MCMC. All our runs make use of the Planck 2018 CMB temperature plus high and low multipole polarization measurements, i.e. the TTTEEE dataset (using the likelihoods highl_TTTEEE, lowl_TT, and lowl_EE), which we refer to as *Planck* or *TTTEEE*. Some runs also include the Planck 2018 CMB lensing power spectrum reconstructed from the CMB temperature four-point function , referred to as *Lensing* [931]. Finally, in some runs we shall also use BAO observations, specifically from BOSS DR12 [696] and combined quasar and Lyman-α data from eBOSS DR14 [932–934], denoted as *BAO*. Notice, from the matter power spectrum results depicted in Fig. 5.1, that the impact of DM-interacting massive neutrinos is very similar to the one observed in non-cold dark matter models, see e.g. [385, 935] and references therein. For instance, mixed (cold plus warm) or fuzzy dark matter scenarios, or models with keV sterile neutrinos, will lead to a very similar small-scale suppression of the matter power spectrum to the one obtained here. In this regard, high resolution observations of the Lyman-α forest, i.e. of the absorption lines produced by the

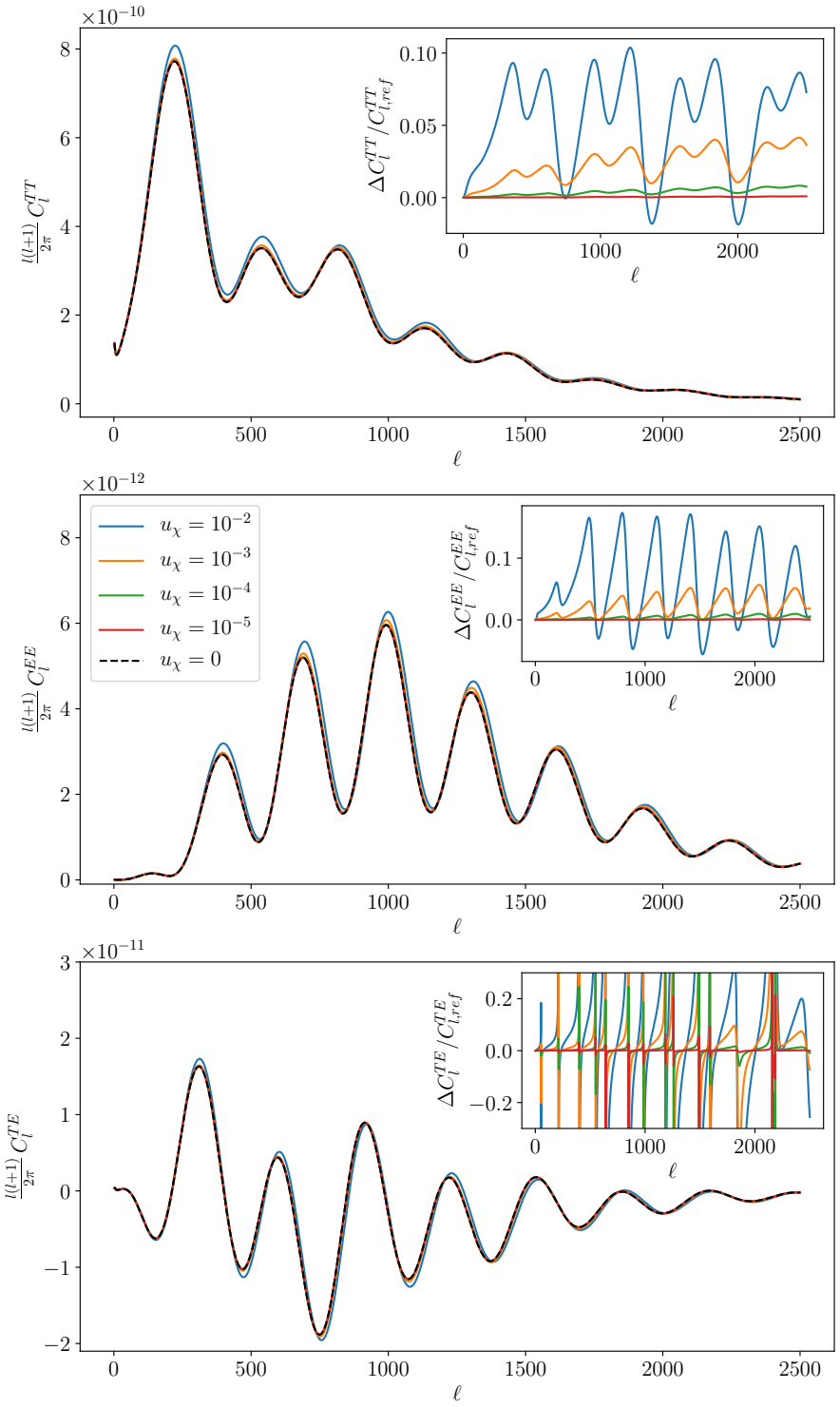

Figure 5.2: *CMB TT, EE and TE power spectra for different values of u_χ in a fiducial cosmology using Planck 2018 parameters [5]. The insert panels show the relative differences compared to the non-interacting case.*

	Planck TTTEEE	Planck + Lensing	Planck + BAO	Planck + Lensing + BAO
$100\,\omega_b$	$2.25^{+0.02}_{-0.04}$	$2.23^{+0.03}_{-0.03}$	$2.23^{+0.04}_{-0.01}$	$2.25^{+0.02}_{-0.03}$
ω_{DM}	$0.120^{+0.003}_{-0.002}$	$0.121^{+0.002}_{-0.003}$	$0.119^{+0.00}_{-0.002}$	$0.119^{+0.002}_{-0.002}$
$100\,\theta_s$	$1.0416^{+0.0014}_{-0.0001}$	$1.0421^{+0.0008}_{-0.0007}$	$1.0418^{+0.0012}_{-0.0002}$	$1.0419^{+0.0010}_{-0.0003}$
$\ln 10^{10} A_s$	$3.05^{+0.03}_{-0.04}$	$3.04^{+0.03}_{-0.03}$	$3.04^{+0.04}_{-0.03}$	$3.04^{+0.04}_{-0.02}$
n_s	$0.963^{+0.009}_{-0.011}$	$0.964^{+0.008}_{-0.011}$	$0.970^{+0.004}_{-0.014}$	$0.966^{+0.007}_{-0.010}$
τ_{reio}	$0.056^{+0.015}_{-0.018}$	$0.051^{+0.020}_{-0.012}$	$0.055^{+0.017}_{-0.014}$	$0.056^{+0.018}_{-0.013}$
u_χ	$4.21 \cdot 10^{-4}$	$3.55 \cdot 10^{-4}$	$3.85 \cdot 10^{-4}$	$3.40 \cdot 10^{-4}$
H_0 [km/s/Mpc]	$67.4^{+1.1}_{-1.4}$	$67.1^{+1.3}_{-0.9}$	$67.8^{+1.0}_{-0.9}$	$67.8^{+0.8}_{-1.0}$
σ_8	$0.81^{+0.01}_{-0.07}$	$0.80^{+0.02}_{-0.05}$	$0.80^{+0.02}_{-0.06}$	$0.80^{+0.02}_{-0.06}$

Table 5.2: *Best fit values with 95% confidence limits for the case of constant neutrino mass, except for u_χ, where only the 95% CL upper limit is shown.*

	Planck TTTEEE	Planck + Lensing	Planck + BAO	Planck + Lensing + BAO
$100\,\omega_b$	$2.24^{+0.03}_{-0.04}$	$2.24^{+0.03}_{-0.03}$	$2.25^{+0.03}_{-0.03}$	$2.24^{+0.03}_{-0.03}$
ω_{DM}	$0.120^{+0.003}_{-0.003}$	$0.120^{+0.004}_{-0.001}$	$0.120^{+0.002}_{-0.003}$	$0.119^{+0.002}_{-0.002}$
$100\,\theta_s$	$1.0420^{+0.0009}_{-0.0005}$	$1.0419^{+0.0010}_{-0.0005}$	$1.0419^{+0.0011}_{-0.0004}$	$1.0419^{+0.0010}_{-0.0004}$
$\ln 10^{10} A_s$	$3.05^{+0.03}_{-0.04}$	$3.04^{+0.04}_{-0.02}$	$3.03^{+0.05}_{-0.02}$	$3.05^{+0.03}_{-0.03}$
n_s	$0.963^{+0.009}_{-0.012}$	$0.965^{+0.006}_{-0.014}$	$0.966^{+0.008}_{-0.009}$	$0.967^{+0.007}_{-0.010}$
τ_{reio}	$0.055^{+0.016}_{-0.016}$	$0.0528^{+0.019}_{-0.012}$	$0.048^{+0.026}_{-0.006}$	$0.057^{+0.017}_{-0.014}$
u_χ	$3.97 \cdot 10^{-4}$	$3.83 \cdot 10^{-4}$	$3.83 \cdot 10^{-4}$	$3.34 \cdot 10^{-4}$
$\sum m_\nu$ [eV]	0.33	0.26	0.15	0.14
H_0 [km/s/Mpc]	$67.2^{+1.2}_{-3.3}$	$67.3^{+0.9}_{-2.9}$	$67.5^{+1.2}_{-0.9}$	$67.6^{+1.0}_{-1.0}$
σ_8	$0.80^{+0.01}_{-0.09}$	$0.79^{+0.03}_{-0.06}$	$0.80^{+0.02}_{-0.07}$	$0.81^{+0.01}_{-0.06}$

Table 5.3: *Best fit values with 95% confidence limits for the case of varying neutrino mass, except for u_χ and $\sum m_\nu$, where 95% CL upper limits are shown.*

distribution of the intergalactic neutral hydrogen along different line of sights to distant quasars, can potentially discern among the different possible non-cold dark matter scenarios [145, 387] and also set very strong bounds on each of them. These observations could therefore further constrain the DM-interacting neutrino schemes explored here. Another possible avenue for further structure formation constraints is milky way satellites, which has been used to constrain WDM and dark matter-dark radiation interaction in e.g. [148, 149, 359]. Since larger values of the cross section are associated with lower values of σ_8 (see Fig. 5.4), a tighter constrain on u_χ would limit the model's ability to ease the σ_8 tension.

Tables 5.2 and 5.3 show the best fit values with 95% CL limits for constant and varying neutrino mass, respectively. For u_χ and $\sum m_\nu$, 95% CL upper limits are shown.

We find the correlation between u_χ and most of the ΛCDM parameters to be weak at most, but there seems to be a slight correlation with θ_s and anticorrelation with n_s. We show the posteriors for u_χ and $\sum m_\nu$ in Fig. 5.3. The two-dimensional posterior has the characteristic quarter-ellipse shape, as data bounds both parameters from above. It is evident that there is a significant difference in the upper bound on the neutrino mass depending on whether BAO data is used, regardless of whether neutrinos are interacting or not. The interaction strength u_χ shows no such strong dependence on datasets. In Section 5.C we provide a list of figures illustrating all the correlations in two-dimensional plots, which also include the one-dimensional posterior probabilities.

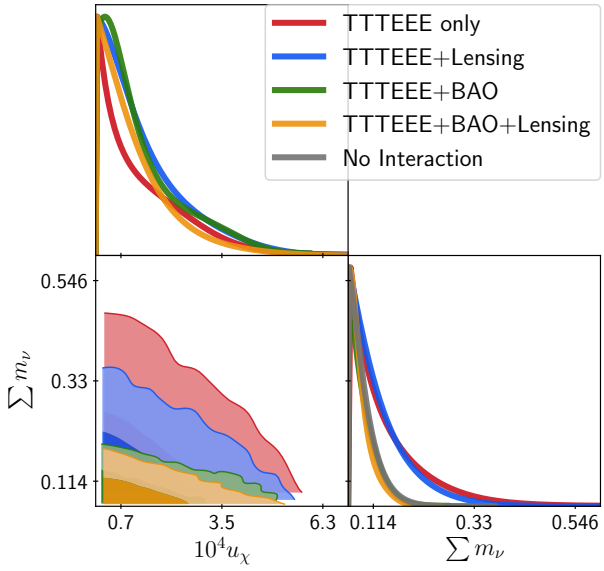

Figure 5.3: *One-dimensional posterior probability distributions for u_χ and $\sum m_\nu$ for different combination of datasets and two-dimensional 68% and 95% CL allowed regions in the (u_χ,$\sum m_\nu$) plane. The 'Non-Interacting' posterior uses all the three datasets, that is, Planck CMB TTTEEE+ Planck CMB Lensing + BAO.*

Our 95% CL upper limits on the interaction cross section are slightly weaker than those previously found for massless neutrinos, see e.g. [660, 662, 936]. This was expected, as the main effect of the mass on the interaction term is through the p^2/E^2-term, which can only make the interaction weaker, allowing for a larger value of u_χ. It is also worth noting that we have used a flat prior for u_χ, while previous studies have sometimes used Jeffreys or logarithmic priors, which can make a difference[936]. An initial guess for the upper limit of u_χ was found by running a shorter chain with a logarithmic prior to obtain an appropriate scale for the MCMC step size and the starting point.

Another interesting issue to explore is how the interaction affects H_0 and σ_8, as there is currently tension in the field concerning the values of these two parameters. They are calculated as derived parameters in our MCMC chains and their posterior distributions are depicted in Fig. 5.4. Note that there is no real correlation between u_χ and H_0, and therefore this interaction does not offer a solution to the H_0-tension. The main effect on H_0 comes from Ω_Λ, which is set indirectly by enforcing flatness. Thus the lower dark matter abundance in the chains using BAO data is compensated with an increase in Ω_Λ and by extension H_0. However, these differences are almost negligible. On the other hand, σ_8 shows a strong dependence on u_χ, a stronger interaction yielding a lower σ_8, which may help in this tension, especially because this easing of the σ_8-tension comes without exacerbating the H_0-tension [131]. The weak-lensing-devoted KiDS-1000 survey finds $\sigma_8 = 0.76^{+0.025}_{-0.020}$ [142], which is slightly lower than our best fit, but consistent within our 1σ lower limit for some of our data combinations and consistent with our 2σ lower limits for all data combinations, see Tables 5.2 and 5.3. It is also clear from looking at the significant overlap with the KiDS-1000 results shown in Fig. 5.4. Comparing to the non-interacting case, it is evident that there is no change in H_0 in the allowed parameter space, but the allowed range for σ_8 is significantly enlarged.

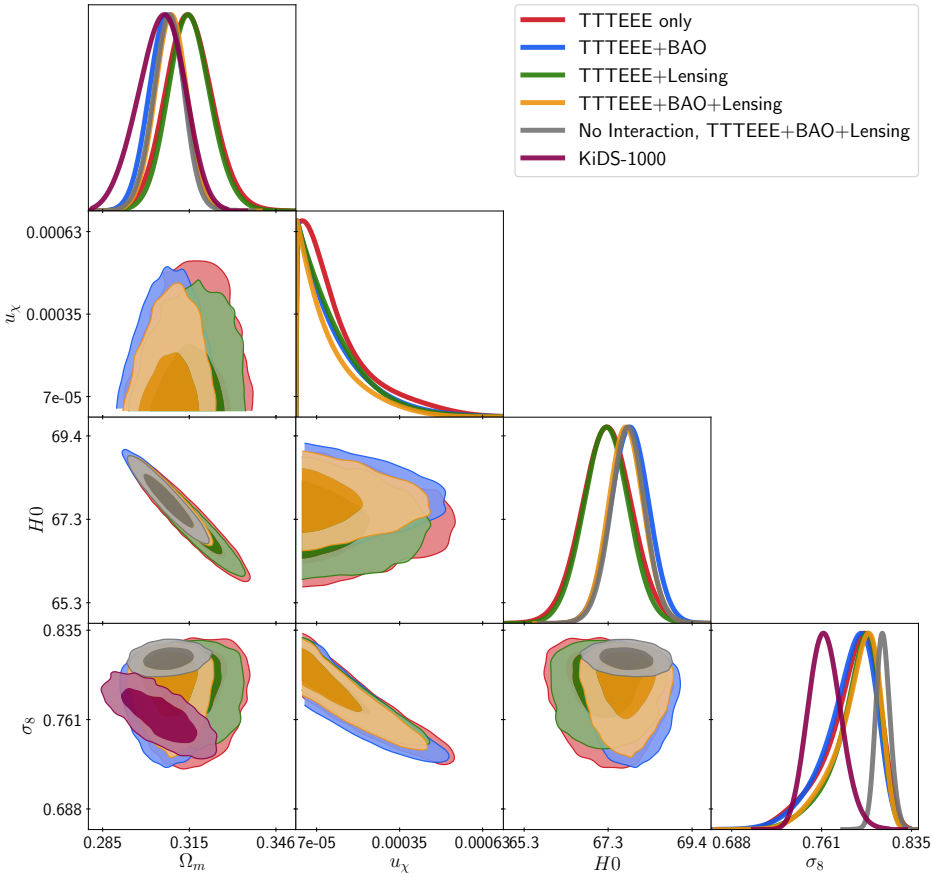

Figure 5.4: *One-dimensional posterior probability distributions for the most interesting parameters for different combination of datasets and two-dimensional* 68% *and* 95% *CL allowed regions. Note the very strong correlation between* u_χ *and* σ_8*. In the interacting case, the viable range for* σ_8 *is significantly larger than in standard* ΛCDM *and clearly overlaps with the KiDS-1000 allowed region, see text for details. KiDS-1000 here refers to the full 3x2pt analysis with cosmic shear + galaxy galaxy lensing + galaxy clustering, plotted from the publicly available multinest chains of [142].*

5.5 Conclusions

We have presented a complete Boltzmann hierarchy for massive neutrinos interacting with cold dark matter, using a momentum independent scattering cross section (similar to e.g. Thomson scattering). As a novelty, we have also accounted for non-zero neutrino masses in the derivation, which means updating the Boltzmann hierarchy. We have implemented this interaction in the Boltzmann code CLASS, which we have used together with the MCMC sampler MontePython to infer upper limits for the interaction strength u_χ, using Planck 2018 data [5, 16] as well as SDSS BAO data from galaxies, Lyα and quasars [696, 932–934]. Our implementation yields results similar to previous work for the effect on the CMB and matter power spectra. However, we generally find slightly looser upper bounds for the interaction strength u_χ than previous work developed under the approximation of massless neutrinos. This is in good agreement with our expectations, since a new factor proportional to p^2/E^2 will appear in the interaction rate. This in turn suppresses the interaction compared to the case of massless neutrinos with the same u_χ. A slightly larger u_χ is therefore needed to obtain the same effect on observables, yielding a slightly looser upper limit.

We also find that the interaction does not appreciably change the upper bound on the sum

of neutrino masses compared to the non-interacting case, meaning that the usual cosmological neutrino bounds are robust even in the presence of this type of non-standard interactions. Concerning the current cosmological tensions, we do not find any significant change to the value of the Hubble constant H_0 in the interacting case. However, very interestingly, the interaction case shows an appreciable decrease in the value of σ_8, bringing it more in line with the values reported by the weak lensing surveys KiDS-1000 [142] and DES [140, 912] among others, which report a significantly lower value than Planck. Here the interaction offers a hint to a potential solution, since it eases the σ_8-tension without exacerbating the H_0-tension, which is often an issue [131]. Future cosmological observations will further constrain the neutrino and dark matter sector interactions, shedding light on the microphysics of these two invisible components of our universe.

acknowledgments

The authors acknowledge the Sydney Informatics Hub and the use of the University of Sydney's high performance computing cluster, Artemis, some numerical results presented in this work were obtained at the Centre for Scientific Computing, Aarhus.[2]. O.M. is supported by the Spanish grants FPA2017-85985-P, PROMETEO/2019/083 and by the European ITN project HIDDeN (H2020-MSCA-ITN-2019//860881-HIDDeN).

[2] `http://phys.au.dk/forskning/cscaa/`

Appendix

5.A Derivation

We assume that the DM-particle is much heavier than the neutrino and completely nonrelativistic. This means that we can use approximations similar to those used when deriving the Thompson scattering terms.

The neutrino distribution function obeys the Boltzmann equation

$$\frac{d}{dt} f\left(\mathbf{x}, \mathbf{p}, t\right) = C\left[f\left(\mathbf{x}, \mathbf{p}, t\right)\right]. \tag{5.15}$$

The left-hand side has been well described in the literature. In the standard case of noninteracting massive neutrinos, the right-hand side is zero, but when introducing an interaction with dark matter, a collision term appears. The form of this term will be derived in the following section. We will proceed in a fashion very similar to the derivation of the first-order Thompson scattering term in [651].

5.A.1 The Collision Term

We do not assume any quantum statistics for the DM particles, and thus do not introduce any Pauli-blocking or stimulated emission terms for them. The collision term is then determined by the integral

$$\begin{aligned} C(p) = \frac{1}{E_\nu(\mathbf{p})} \int \frac{d^3\mathbf{p}'}{(2\pi)^3 2E_\nu(\mathbf{p}')} \frac{d^3\mathbf{q}}{(2\pi)^3 2E_\chi(\mathbf{q})} \frac{d^3\mathbf{q}'}{(2\pi)^3 2E_\chi(\mathbf{q}')} (2\pi)^4 |M|^2 \\ \times \delta^4(q + p - q' - p') \left[g(\mathbf{q}')\, f(\mathbf{p}')\, (1 - f(\mathbf{p})) - g(\mathbf{q})\, f(\mathbf{p})\, (1 - f(\mathbf{p}'))\right], \end{aligned} \tag{5.16}$$

where p and q denote the momenta of neutrinos and DM particles respectively. Unprimed quantities are initial state values and primed quantities are final state values. f and g are the distribution functions of neutrinos and DM particles respectively and E_i is the total energy of a particle of species i, given as usual by

$$E_i = \sqrt{m_i^2 + p_i^2}\,. \tag{5.17}$$

Finally $|M|^2$ is the matrix element squared of the interaction.

We perform the $\mathbf{q}'$ integral using the spatial part of the δ-function, yielding

$$\begin{aligned} C(p) = \frac{1}{8E_\nu(\mathbf{p})} \int \frac{d^3\mathbf{p}'}{(2\pi)^3 E_\nu(\mathbf{p}')} \frac{d^3\mathbf{q}}{(2\pi)^3 E_\chi(\mathbf{q})} \\ \times \frac{(2\pi)^4 |M|^2}{(2\pi)^3 E_\chi(\mathbf{q} + \mathbf{p} - \mathbf{p}')} \delta(E_\chi(\mathbf{q}) + E_\nu(\mathbf{p}) - E_\chi(\mathbf{q} + \mathbf{p} - \mathbf{p}') - E_\nu(\mathbf{p}')) \\ \times \left[g(\mathbf{q} + \mathbf{p} - \mathbf{p}')\, f(\mathbf{p}')\, (1 - f(\mathbf{p})) - g(\mathbf{q})\, f(\mathbf{p})\, (1 - f(\mathbf{p}'))\right], \end{aligned} \tag{5.18}$$

Because the DM particles are so much heavier than the neutrinos, the energy transfer will be very small. We expand the DM energies in the δ-function. To the first order,

$$E_\chi(\mathbf{q}) = \sqrt{m_\chi^2 + q^2} \simeq m_\chi + \frac{q^2}{2m_\chi}, \tag{5.19}$$

thus

$$\begin{aligned}\delta(E_\chi(\mathbf{q})+E_\nu(\mathbf{p})-E_\chi(\mathbf{q}+\mathbf{p}-\mathbf{p}')-E_\nu(\mathbf{p}'))\\ \simeq\delta\left(m_\chi+\frac{q^2}{m_\chi}+E_\nu(\mathbf{p})-m_\chi-\frac{q^2}{m_\chi}-\frac{(\mathbf{p}-\mathbf{p}')^2}{2m_\chi}-\frac{(\mathbf{p}-\mathbf{p}')\cdot\mathbf{q}}{m_\chi}-E_\nu(\mathbf{p}')\right)\\ =\delta\left(E_\nu(\mathbf{p})-E_\nu(\mathbf{p}')-\frac{(\mathbf{p}-\mathbf{p}')^2}{2m_\chi}-\frac{(\mathbf{p}-\mathbf{p}')\cdot\mathbf{q}}{m_\chi}\right).\end{aligned}\tag{5.20}$$

We then expand the δ-function in terms of the energy transfer. To the first order,

$$\begin{aligned}\delta\left(E_\nu(\mathbf{p})-E_\nu(\mathbf{p}')-\frac{(\mathbf{p}-\mathbf{p}')^2}{2m_\chi}-\frac{(\mathbf{p}-\mathbf{p}')\cdot\mathbf{q}}{m_\chi}\right)=&\delta(E_\nu(\mathbf{p})-E_\nu(\mathbf{p}'))\\ &+\left[\frac{(\mathbf{p}-\mathbf{p}')^2}{2m_\chi}+\frac{(\mathbf{p}-\mathbf{p}')\cdot\mathbf{q}}{m_\chi}\right]\\ &\times\frac{\partial\delta(E_\nu(\mathbf{p})-E_\nu(\mathbf{p}'))}{\partial E_\nu(\mathbf{p}')}.\end{aligned}\tag{5.21}$$

We can then change the variable of differentiation to p', using

$$\frac{d}{dp}E_\nu(\mathbf{p})=\frac{p}{E_\nu(\mathbf{p})},$$

so

$$\frac{\partial\delta(E_\nu(\mathbf{p})-E_\nu(\mathbf{p}'))}{\partial E_\nu(\mathbf{p}')}=\frac{\partial\delta(E_\nu(\mathbf{p})-E_\nu(\mathbf{p}'))}{\partial p'}\frac{E_\nu(\mathbf{p}')}{p'}.\tag{5.22}$$

The collision integral is then expressed as

$$\begin{aligned}C(p)=\frac{1}{8E_\nu(\mathbf{p})}\int\frac{d^3\mathbf{p}'}{(2\pi)^3E_\nu(\mathbf{p}')}\frac{d^3\mathbf{q}}{(2\pi)^3E_\chi(\mathbf{q})}\frac{(2\pi)^4|M|^2}{(2\pi)^3E_\chi(\mathbf{q}+\mathbf{p}-\mathbf{p}')}\\ \times\left\{\delta(E_\nu(\mathbf{p})-E_\nu(\mathbf{p}'))+\left[\frac{(\mathbf{p}-\mathbf{p}')^2}{2m_\chi}+\frac{(\mathbf{p}-\mathbf{p}')\cdot\mathbf{q}}{m_\chi}\right]\frac{\partial\delta(E_\nu(\mathbf{p})-E_\nu(\mathbf{p}'))}{\partial p'}\frac{E_\nu(\mathbf{p}')}{p'}\right\}\\ \times\left[g(\mathbf{q}+\mathbf{p}-\mathbf{p}')\,f(\mathbf{p}')\,(1-f(\mathbf{p}))-g(\mathbf{q})\,f(\mathbf{p})\,(1-f(\mathbf{p}'))\right].\end{aligned}\tag{5.23}$$

Under the assumption that the DM temperature is extremely low, the distribution function is

$$g(\mathbf{q})\simeq n_\chi\,(2\pi)^3\,\delta^3(\mathbf{q}-m_\chi\mathbf{v}_\chi)\,,\tag{5.24}$$

fulfilling the normalisation condition that

$$n_\chi=\int\frac{d^3\mathbf{q}}{(2\pi)^3}g(\mathbf{q})\,.$$

This allows only two values of $\mathbf{q}$ to give nonzero contributions to the collision integral:

$$\begin{aligned}g(\mathbf{q})\to\mathbf{q}=m_\chi\mathbf{v}_\chi,\\ g(\mathbf{q}+\mathbf{p}-\mathbf{p}')\to\mathbf{q}=m_\chi\mathbf{v}_\chi+\mathbf{p}'-\mathbf{p}.\end{aligned}$$

The collision integral is then expressed as

$$C(p)=\frac{1}{8E_\nu(\mathbf{p})}\int\frac{d^3\mathbf{p}'}{(2\pi)^3E_\nu(\mathbf{p}')}\frac{(2\pi)^4|M|^2}{(2\pi)^3E_\chi(m_\chi\mathbf{v}_\chi)}\Big[A+B\Big]\,,\tag{5.25}$$

with the A term corresponding to $\mathbf{q} = m_\chi \mathbf{v}_\chi$ and the B term corresponding to $\mathbf{q} = m_\chi \mathbf{v}_\chi + \mathbf{p}' - \mathbf{p}$. Then

$$\begin{aligned} A =& \frac{1}{E_\chi(m_\chi \mathbf{v}_\chi + \mathbf{p} - \mathbf{p}')} \\ & \times \left\{ \delta(E_\nu(\mathbf{p}) - E_\nu(\mathbf{p}')) + \left[\frac{(\mathbf{p}-\mathbf{p}')^2}{2m_\chi} + \frac{(\mathbf{p}-\mathbf{p}')\cdot m_\chi \mathbf{v}_\chi}{m_\chi} \right] \frac{\partial \delta(E_\nu(\mathbf{p}) - E_\nu(\mathbf{p}'))}{\partial p'} \frac{E_\nu(\mathbf{p}')}{p'} \right\} \\ & \times \left[g(m_\chi \mathbf{v}_\chi + \mathbf{p} - \mathbf{p}')\, f(\mathbf{p}')\,(1 - f(\mathbf{p})) - n_\chi f(\mathbf{p})\,(1 - f(\mathbf{p}')) \right] , \end{aligned} \tag{5.26}$$

and

$$\begin{aligned} B =& \frac{1}{E_\chi(m_\chi \mathbf{v}_\chi - \mathbf{p} + \mathbf{p}')} \\ & \times \left\{ \delta(E_\nu(\mathbf{p}) - E_\nu(\mathbf{p}')) + \left[\frac{(\mathbf{p}-\mathbf{p}')^2}{2m_\chi} + \frac{(\mathbf{p}-\mathbf{p}')\cdot (m_\chi \mathbf{v}_\chi + \mathbf{p}' - \mathbf{p})}{m_\chi} \right] \frac{\partial \delta(E_\nu(\mathbf{p}) - E_\nu(\mathbf{p}'))}{\partial p'} \frac{E_\nu(\mathbf{p}')}{p'} \right\} \\ & \times \left[n_\chi f(\mathbf{p}')\,(1 - f(\mathbf{p})) - g(m_\chi \mathbf{v}_\chi - \mathbf{p} + \mathbf{p}')\, f(\mathbf{p})\,(1 - f(\mathbf{p}')) \right] . \end{aligned} \tag{5.27}$$

We throw away all terms $\propto \frac{1}{m_\chi}$, leading to

$$\begin{aligned} C(p) = & \frac{1}{8E_\nu(\mathbf{p})} \int \frac{d^3\mathbf{p}'}{(2\pi)^3 E_\nu(\mathbf{p}')} \frac{(2\pi)^4 |M|^2}{(2\pi)^3 E_\chi(m_\chi \mathbf{v}_\chi)} \\ & \times \left\{ \delta(E_\nu(\mathbf{p}) - E_\nu(\mathbf{p}')) + (\mathbf{p}-\mathbf{p}')\cdot \mathbf{v}_\chi \frac{E_\nu(\mathbf{p}')}{p'} \frac{\partial \delta(E_\nu(\mathbf{p}) - E_\nu(\mathbf{p}'))}{\partial p'} \right\} \\ & \times \left[\frac{1}{E_\chi(m_\chi \mathbf{v}_\chi + \mathbf{p} - \mathbf{p}')} \left[g(m_\chi \mathbf{v}_\chi + \mathbf{p} - \mathbf{p}')\, f(\mathbf{p}')\,(1 - f(\mathbf{p})) - n_\chi f(\mathbf{p})\,(1 - f(\mathbf{p}')) \right] \right. \\ & \left. + \frac{1}{E_\chi(m_\chi \mathbf{v}_\chi - \mathbf{p} + \mathbf{p}')} \left[n_\chi f(\mathbf{p}')\,(1 - f(\mathbf{p})) - g(m_\chi \mathbf{v}_\chi - \mathbf{p} + \mathbf{p}')\, f(\mathbf{p})\,(1 - f(\mathbf{p}')) \right] \right]. \end{aligned} \tag{5.28}$$

We split the neutrino distribution function is a zeroth-order and a first-order part:

$$f(\mathbf{p}) = f^{(0)}(p) + f^{(1)}(\mathbf{p}) ,$$

where the zeroth-order part is independent of the momentum direction. Hence,

$$\begin{aligned} C(p) = & \frac{1}{8E_\nu(\mathbf{p})} \int \frac{d^3\mathbf{p}'}{(2\pi)^3 E_\nu(\mathbf{p}')} \frac{(2\pi)^4 |M|^2}{(2\pi)^3 E_\chi(m_\chi \mathbf{v}_\chi)} \\ & \times \left\{ \delta(E_\nu(\mathbf{p}) - E_\nu(\mathbf{p}')) + (\mathbf{p}-\mathbf{p}')\cdot \mathbf{v}_\chi \frac{E_\nu(\mathbf{p}')}{p'} \frac{\partial \delta(E_\nu(\mathbf{p}) - E_\nu(\mathbf{p}'))}{\partial p'} \right\} \\ & \times \left[\frac{1}{E_\chi(m_\chi \mathbf{v}_\chi + \mathbf{p} - \mathbf{p}')} \left[g(m_\chi \mathbf{v}_\chi + \mathbf{p} - \mathbf{p}') \left\{ f^{(0)}(p') + f^{(1)}(\mathbf{p}') \right\} \left(1 - \left\{ f^{(0)}(p) + f^{(1)}(\mathbf{p}) \right\} \right) \right. \right. \\ & \left. - n_\chi \left\{ f^{(0)}(p) + f^{(1)}(\mathbf{p}) \right\} \left(1 - \left\{ f^{(0)}(p') + f^{(1)}(\mathbf{p}') \right\} \right) \right] \\ & + \frac{1}{E_\chi(m_\chi \mathbf{v}_\chi - \mathbf{p} + \mathbf{p}')} \left[n_\chi \left\{ f^{(0)}(p') + f^{(1)}(\mathbf{p}') \right\} \left(1 - \left\{ f^{(0)}(p) + f^{(1)}(\mathbf{p}) \right\} \right) \right. \\ & \left. \left. - g(m_\chi \mathbf{v}_\chi - \mathbf{p} + \mathbf{p}') \left\{ f^{(0)}(p) + f^{(1)}(\mathbf{p}) \right\} \left(1 - \left\{ f^{(0)}(p') + f^{(1)}(\mathbf{p}') \right\} \right) \right] \right]. \end{aligned} \tag{5.29}$$

For the sake of simplicity, this can be written in terms of for phase-space terms, $\delta 1$, $\delta 2$, $\partial\delta 1$, $\partial\delta 2$,

$$C(p) = \frac{1}{8E_\nu(\mathbf{p})}\int \frac{d^3\mathbf{p}'}{(2\pi)^3 E_\nu(\mathbf{p}')}\frac{(2\pi)^4|M|^2}{(2\pi)^3 E_\chi(m_\chi \mathbf{v}_\chi)}\Bigg[\\ \delta(E_\nu(\mathbf{p}) - E_\nu(\mathbf{p}'))\,[\delta 1 + \delta 2] \\ + (\mathbf{p}-\mathbf{p}')\cdot\mathbf{v}_\chi \frac{E_\nu(\mathbf{p}')}{p'}\frac{\partial\delta(E_\nu(\mathbf{p}) - E_\nu(\mathbf{p}'))}{\partial p'}\,[\partial\delta 1 + \partial\delta 2]\Bigg]. \quad (5.30)$$

The only terms multiplied with the δ-function that will be nonzero, are those that fulfil the condition $E_\nu(\mathbf{p}) = E_\nu(\mathbf{p}')$, hence $|\mathbf{p}| = |\mathbf{p}'|$ and $f^{(0)}(p') \to f^{(0)}(p)$. Since, the δ-function is a zeroth-order term, zeroth-order and first-order terms are kept in $\delta 1$ and $\delta 2$.

Writing out $\delta 1$,

$$\delta 1 = \frac{1}{E_\chi(m_\chi\mathbf{v}_\chi + \mathbf{p} - \mathbf{p}')}\Bigg[g(m_\chi\mathbf{v}_\chi + \mathbf{p} - \mathbf{p}') \\ \left(f^{(0)}(p) + f^{(1)}(\mathbf{p}') - \left(f^{(0)}(p)\right)^2 - f^{(1)}(\mathbf{p}')\,f^{(1)}(\mathbf{p}) - f^{(0)}(p)\left(f^{(1)}(\mathbf{p}) + f^{(1)}(\mathbf{p}')\right)\right) \\ - n_\chi\left(f^{(0)}(p) + f^{(1)}(\mathbf{p}) - \left(f^{(0)}(p)\right)^2 - f^{(1)}(\mathbf{p})\,f^{(1)}(\mathbf{p}') - f^{(0)}(p)\left(f^{(1)}(\mathbf{p}) + f^{(1)}(\mathbf{p}')\right)\right)\Bigg], \quad (5.31)$$

the $f^{(1)}(\mathbf{p})\,f^{(1)}(\mathbf{p}')$-terms are discarded, since they are second-order. It is evident that if $\mathbf{p} = \mathbf{p}'$, the two terms are identical, leading to $\delta 1 = 0$. For all other values of $\mathbf{p}'$, we have $g(m_\chi\mathbf{v}_\chi + \mathbf{p} - \mathbf{p}') = 0$, thus the nonzero contributions yield

$$\delta 1 = \frac{n_\chi}{E_\chi(m_\chi\mathbf{v}_\chi + \mathbf{p} - \mathbf{p}')}\left(\left(f^{(0)}(p)\right)^2 + f^{(0)}(p)\left(f^{(1)}(\mathbf{p}) + f^{(1)}(\mathbf{p}')\right) - f^{(0)}(p) - f^{(1)}(\mathbf{p})\right). \quad (5.32)$$

Using the same arguments, we get

$$\delta 2 = \frac{n_\chi}{E_\chi(m_\chi\mathbf{v}_\chi - \mathbf{p} + \mathbf{p}')}\left(f^{(0)}(p) + f^{(1)}(\mathbf{p}') - \left(f^{(0)}(p)\right)^2 - f^{(0)}(p)\left(f^{(1)}(\mathbf{p}) + f^{(1)}(\mathbf{p}')\right)\right). \quad (5.33)$$

The $\partial\delta 1$ and $\partial\delta 2$ terms are multiplied with a first-order term, hence, only their zeroth-order terms are kept. However, there is no δ-function to set $|\mathbf{p}| = |\mathbf{p}'|$. By the same arguments as used for $\delta 1$ and $\delta 2$ we obtain

$$\partial\delta 1 = -\frac{n_\chi}{E_\chi(m_\chi\mathbf{v}_\chi + \mathbf{p} - \mathbf{p}')}\left(f^{(0)}(p) - f^{(0)}(p)\,f^{(0)}(p')\right), \quad (5.34)$$

$$\partial\delta 2 = \frac{n_\chi}{E_\chi(m_\chi\mathbf{v}_\chi - \mathbf{p} + \mathbf{p}')}\left(f^{(0)}(p') - f^{(0)}(p)\,f^{(0)}(p')\,.\right) \quad (5.35)$$

Since the DM particles are very nonrelativistic, we can make the approximation that $E_\chi \simeq m_\chi$. This allows us to reduce the terms:

$$\delta 1 + \delta 2 = \frac{n_\chi}{m_\chi}\left(f^{(1)}(\mathbf{p}') - f^{(1)}(\mathbf{p})\right) \quad (5.36)$$

$$\partial\delta 1 + \partial\delta 2 = \frac{n_\chi}{m_\chi}\left(f^{(0)}(p') - f^{(0)}(p)\right). \quad (5.37)$$

We can then write the collision integral as

$$C(p) = \frac{n_\chi}{8E_\nu(\mathbf{p})\, m_\chi^2} \int \frac{d^3\mathbf{p}'}{(2\pi)^3\, E_\nu(\mathbf{p}')} \frac{(2\pi)^4 |M|^2}{(2\pi)^3} \Bigg[\delta(E_\nu(\mathbf{p}) - E_\nu(\mathbf{p}')) \left[f^{(1)}(\mathbf{p}') - f^{(1)}(\mathbf{p}) \right] + (\mathbf{p} - \mathbf{p}') \cdot \mathbf{v}_\chi \frac{E_\nu(\mathbf{p}')}{p'} \frac{\partial \delta(E_\nu(\mathbf{p}) - E_\nu(\mathbf{p}'))}{\partial p'} \left[f^{(0)}(p') - f^{(0)}(p) \right] \Bigg]. \quad (5.38)$$

We then split up the integral in an angular and a magnitude part

$$C(p) = \frac{n_\chi}{8E_\nu(\mathbf{p})\, m_\chi^2} \int \frac{dp' d\Omega p'^2}{(2\pi)^3\, E_\nu(\mathbf{p}')} \frac{(2\pi)^4 |M|^2}{(2\pi)^3} \Bigg[\delta(E_\nu(\mathbf{p}) - E_\nu(\mathbf{p}')) \left[f^{(1)}(\mathbf{p}') - f^{(1)}(\mathbf{p}) \right] + (\mathbf{p} - \mathbf{p}') \cdot \mathbf{v}_\chi \frac{E_\nu(\mathbf{p}')}{p'} \frac{\partial \delta(E_\nu(\mathbf{p}) - E_\nu(\mathbf{p}'))}{\partial p'} \left[f^{(0)}(p') - f^{(0)}(p) \right] \Bigg] \quad (5.39)$$

We define the polar axis to be in the same direction as the DM velocity, i.e.

$$\mu = \hat{\mathbf{v}}_\chi \cdot \hat{\mathbf{p}} \qquad \text{and} \qquad \mu' = \hat{\mathbf{v}}_\chi \cdot \hat{\mathbf{p}}'.$$

We assume the matrix element to have the same form as the one used for Thompson scattering,

$$|M|^2 = 6\pi\sigma_0 m_\chi^2 \left(1 + \cos^2\theta\right), \quad (5.40)$$

where

$$\cos\theta = \hat{\mathbf{p}} \cdot \hat{\mathbf{p}}' \ ,$$

and σ_0 is some constant.

The angular part of the collision integral can then be expressed in terms of μ' and ϕ,

$$C(p) = \frac{6\pi\,(2\pi)^4\,\sigma_0 n_\chi}{(2\pi)^3\,(2\pi)^3\,8E_\nu(\mathbf{p})} \int \frac{dp' p'^2}{E_\nu(\mathbf{p}')} \Bigg[\delta(E_\nu(\mathbf{p}) - E_\nu(\mathbf{p}')) \int_{-1}^{1} d\mu' \left[f^{(1)}(\mathbf{p}') - f^{(1)}(\mathbf{p}) \right] \int_0^{2\pi} d\phi' \left(1 + (\hat{\mathbf{p}} \cdot \hat{\mathbf{p}}')^2\right) + \frac{E_\nu(\mathbf{p}')\, v_\chi}{p'} \frac{\partial \delta(E_\nu(\mathbf{p}) - E_\nu(\mathbf{p}'))}{\partial p'} \left[f^{(0)}(p') - f^{(0)}(p) \right] \int_{-1}^{1} d\mu' \left[\mu p - \mu' p'\right] \int_0^{2\pi} d\phi' \left(1 + (\hat{\mathbf{p}} \cdot \hat{\mathbf{p}}')^2\right) \Bigg]. \quad (5.41)$$

We assume a cosmology with azimuthal symmetry, hence $f^{(1)}(\mathbf{p}')$ depends only on μ' and not ϕ. We solve the ϕ-integral by rewriting the integrand in terms of Legendre polynomials, just as in reference [651],

$$+ (\hat{\mathbf{p}} \cdot \hat{\mathbf{p}}')^2 = \frac{4}{3}\left(1 + \frac{1}{2} P_2\left(\hat{\mathbf{p}} \cdot \hat{\mathbf{p}}'\right)\right)$$

then using the addition theorem of the spherical harmonics

$$\int_0^{2\pi} d\phi P_2\left(\hat{\mathbf{p}} \cdot \hat{\mathbf{p}}'\right) = 2\pi P_2\left(\hat{\mathbf{p}} \cdot \hat{\mathbf{v}}_\chi\right) P_2\left(\hat{\mathbf{p}}' \cdot \hat{\mathbf{v}}_\chi\right) = 2\pi P_2(\mu) P_2(\mu')$$

We can also use the definition of the moments of the distribution function,

$$f_l(p) = \int_{-1}^{1} \frac{d\mu}{2} P_l(\mu) f(p, \mu). \quad (5.42)$$

This allows us to do the μ' and ϕ integrals, resulting in

$$C(p) = \frac{\pi\,(2\pi)^4\,\sigma_0 n_\chi 4\pi}{(2\pi)^3\,(2\pi)^3\,E_\nu(\mathbf{p})}\int\frac{dp'p'^2}{E_\nu(p')}\Bigg[\delta(E_\nu(p)-E_\nu(p'))\left(f_0^{(1)}(p')+\frac{1}{2}f_2^{(1)}(p')\,P_2(\mu)-f^{(1)}(p,\mu)\right) + \frac{E_\nu(p')\,v_\chi p\mu}{p'}\frac{\partial\delta(E_\nu(p)-E_\nu(p'))}{\partial p'}\left[f^{(0)}(p')-f^{(0)}(p)\right]\Bigg]. \quad (5.43)$$

The first part of the integral is easily done using the delta function,

$$\int\frac{dp'p'^2}{E_\nu(\mathbf{p}')}\delta(E_\nu(\mathbf{p})-E_\nu(\mathbf{p}'))\left(f_0^{(1)}(p')+\frac{1}{2}f_2^{(1)}(p')\,P_2(\mu)-f^{(1)}(p,\mu)\right) = \frac{p^2}{E_\nu(\mathbf{p})}\left(f_0^{(1)}(p)+\frac{1}{2}f_2^{(1)}(p)\,P_2(\mu)-f^{(1)}(p,\mu)\right). \quad (5.44)$$

The second part of the integral is done with integration by parts

$$\begin{aligned}\int dp'p'v_\chi p\mu\left(f^{(0)}(p')-f^{(0)}(p)\right)&\frac{\partial\delta(E_\nu(p)-E_\nu(p'))}{\partial p'}\\ &= v_\chi p\mu\Bigg(\left[p'\left(f^{(0)}(p')-f^{(0)}(p)\right)\delta(E_\nu(p)-E_\nu(p'))\right]_{p'=0}^{p'=\infty}\\ &\quad-\int dp'\left(f^{(0)}(p')-f^{(0)}(p)\right)\delta(E_\nu(p)-E_\nu(p'))\\ &\quad-\int dp'p'\frac{\partial f^{(0)}(p')}{\partial p'}\delta(E_\nu(p)-E_\nu(p'))\Bigg)\\ &= -v_\chi p^2\mu\frac{\partial f^{(0)}(p)}{\partial p}.\end{aligned} \quad (5.45)$$

Inserting these yields the collision term

$$C(p) = \frac{\pi\,(2\pi)^4\,\sigma_0 n_\chi 4\pi}{(2\pi)^3\,(2\pi)^3}\left[\frac{p2}{E_\nu(p)}\left(f_0^{(1)}(p)+\frac{1}{2}f_2^{(1)}(p)\,P_2(\mu)-f^{(1)}(p,\mu)\right)-\frac{v_\chi p^2\mu}{E_\nu(p)}\frac{df^{(0)}(p)}{dp}\right], \quad (5.46)$$

which reduces to

$$C(p) = \frac{\sigma_0 n_\chi p^2}{E_\nu^2(p)}\left[f_0^{(1)}(p)+\frac{1}{2}f_2^{(1)}(p)\,P_2(\mu)-f^{(1)}(p,\mu)-v_\chi\mu E_\nu(p)\,\frac{df^{(0)}(p)}{dp}\right]. \quad (5.47)$$

5.A.2 The Boltzmann Hierarchy

We will now derive the Boltzmann hierarchy for massive neutrinos with DM interactions, proceeding in a fashion similar to reference [163]. Their Boltzmann equation in the synchronous gauge is

$$\frac{\partial\Psi}{\partial\tau}+i\frac{p}{E_\iota(p)}\left(\mathbf{k}\cdot\hat{\mathbf{n}}\right)\Psi+\frac{d\ln f^{(0)}(p)}{d\ln p}\left[\dot\eta-\frac{\dot h+6\dot\eta}{2}\left(\hat{\mathbf{k}}\cdot\hat{\mathbf{n}}\right)^2\right] = \frac{a\sigma_0 n_\chi p^2}{E_\nu^2(p)}\left[\Psi_0(p)+\frac{1}{2}\Psi_2(p)\,P_2(\mu)-\Psi(p,\mu)-\frac{v_\chi\mu E_\nu(p)}{f^{(0)}(p)}\frac{df^{(0)}(p)}{dp}\right], \quad (5.48)$$

with $\hat{\mathbf{n}}$ being the unit vector in the direction of p and the usual definition of Ψ,

$$f(p) = f^{(0)}(p)\,(1+\Psi).$$

We cannot analytically integrate over all momenta, so we write Ψ as a Legendre series,

$$\Psi(\mathbf{k},\hat{\mathbf{n}},p,\tau)=\sum_{l=0}^{\infty}(-i)^l\,(2l+1)\,\Psi_l(\mathbf{k},p,\tau)\,P_l\Big(\hat{\mathbf{k}}\cdot\hat{\mathbf{n}}\Big)\,. \tag{5.49}$$

Because the velocity $\mathbf{v}_\chi$ is irrotational, its Fourier transform is parallel to $\mathbf{k}$, hence $\hat{\mathbf{v}}_\chi\cdot\hat{\mathbf{n}}=\hat{\mathbf{k}}\cdot\hat{\mathbf{n}}=\mu$. For brevity, we define the interaction rate

$$C_\chi(p)\equiv\frac{a\sigma_0 n_\chi p^2}{E_\nu^2(p)}. \tag{5.50}$$

The zeroth moment of the differential equation is then

$$\begin{aligned}\frac{\partial\Psi_0}{\partial\tau}=&\int_{-1}^{1}\frac{d\mu}{2}\Bigg\{\\&C_\chi(p)\left[\Psi_0(p)+\frac{1}{2}\Psi_2(p)\,P_2(\mu)-\Psi(p,\mu)-\frac{v_\chi\mu E_\nu(p)}{f^{(0)}(p)}\frac{df^{(0)}(p)}{dp}\right]\\&-i\frac{pk}{E_\nu(p)}\mu\Psi-\frac{d\ln f^{(0)}(p)}{d\ln p}\left[\dot\eta-\frac{\dot h+6\dot\eta}{2}\mu^2\right]\Bigg\}\\=&-\frac{pk}{E_\nu(p)}\Psi_1(p)+\frac{1}{6}\dot h\frac{d\ln f^{(0)}(p)}{d\ln p},\end{aligned} \tag{5.51}$$

the same as for the noninteracting case. The parts of the integrals not associated with the interaction will also always yield the same as the standard case, so there is no reason to calculate them again. The first moment is then

$$\begin{aligned}\frac{\partial\Psi_1}{\partial\tau}=&\frac{pk}{3E_\nu(p)}\left(\Psi_0(p)-2\Psi_2(p)\right)\\&+\int_{-1}^{1}\frac{d\mu}{2}C_\chi(p)\left[\Psi_0(p)\,\mu+\frac{1}{2}\Psi_2(p)\,P_2(\mu)\,\mu-\Psi(p,\mu)\,\mu-\frac{v_\chi\mu^2E_\nu(p)}{f^{(0)}(p)}\frac{df^{(0)}(p)}{dp}\right]\\=&\frac{1}{3}\frac{pk}{E_\nu(p)}\left(\Psi_0(p)-2\Psi_2(p)\right)-C_\chi(p)\frac{v_\chi E_\nu(p)}{3f^{(0)}(p)}\frac{df^{(0)}(p)}{dp}-C_\chi(p)\Psi_1(p).\end{aligned} \tag{5.52}$$

Following the same method for the second moment, we get

$$\frac{\partial\Psi_2}{\partial\tau}=\frac{1}{5}\frac{pk}{E_\nu(p)}\left(2\Psi_1(p)-3\Psi_3(p)\right)-\left(\frac{\dot h}{15}+\frac{2\dot\eta}{5}\right)\frac{d\ln f^{(0)}(p)}{d\ln p}-\frac{9}{10}C_\chi(p)\Psi_2(p). \tag{5.53}$$

The $C_\chi\Psi$-term will just become a $C_\chi\Psi_l$-term for higher l, acting as a damping term. The form of the higher-l moments is thus

$$\frac{\partial\Psi_l}{\partial\tau}=\frac{1}{2l+1}\frac{pk}{E_\nu(p)}\left(l\Psi_{l-1}-(l+1)\Psi_{l+1}\right)-C_\chi(p)\Psi_l(p) \tag{5.54}$$

5.B Fluid Approximation

The publicly available Bolztmann solver code CLASS uses a fluid approximation for the non cold dark matter-species [635], which is used for massive neutrinos, to minimize the computational time. In that approximation, the full integral over momentum-space is not performed, instead the hierarchy is truncated at $l_{\max}=2$ and the continuity, Euler, and shear equations are calculated directly instead of performing an integral over the momentum. Since the interaction rate C_χ is

momentum-dependent, see Eq. (5.11), the expression must be adapted to use some approximation suited to this particular regime.

In the regime where CLASS uses the fluid approximation to evolve δ_ν, θ_ν, and σ_ν, rather than the full momentum hierarchies, the interaction term acts both as a collision and a damping term, similarly to the Thomson scattering case. The shapes of these terms are independent of the gauge, yielding the modified equations:

$$\dot{\theta}_\nu = [...] + \widetilde{C}_\chi(w)\,(\theta_\chi - \theta_\nu)\,, \qquad \dot{\sigma}_\nu = [...] - \frac{9}{10}\widetilde{C}_\chi(w)\sigma_\nu,$$

where [...] represents the usual terms present in the non-interacting case, as described in [635]. The interaction rate does not change the number of neutrinos or facilitate any appreciable energy transport between species, so no modification to the δ_ν-equation is made.

Since the momentum dependence of the interaction rate is $\propto \frac{p^2}{E^2}$, it is reasonable to assume that the integrated rate $\widetilde{C}_\chi$ is related to the equation of state parameter w, as both are integrated quantities dependent on the ratio between the kinetic and total energies. However, the relationship between $\widetilde{C}_\chi$ and w is highly non-trivial. We extract it numerically by calculating both $\widetilde{C}_\chi$ and w for a range of temperatures. On the other hand, such a relation turns out to be independent of the particle mass, mildly simplifying the interacting scenario. The relationship between $\widetilde{C}_\chi$ and w is well approximated by

$$\widetilde{C}_\chi(w) = S_\chi \left[A\,(3w)^B + Cw\right]\,, \tag{5.55}$$

where S_χ contains all the factors that do not depend on the momentum p,

$$S_\chi = a u_{\nu\chi} \frac{\sigma_{\rm Th}\rho_\chi}{100\,{\rm GeV}}. \tag{5.56}$$

The parameters A, B, and C have the following values:

$$A = 1.52116\,, \quad B = 0.50884\,, \quad C = -1.56422\,,$$

which provides a very good fit.

The approximation introduces an error into the CMB and matter power spectra, which is important to quantize. The effect on the CMB power spectra is on the order of 0.01%, and therefore completely negligible. Concerning the matter power spectrum in the interacting scenario there is some error at very small scales. Nevertheless these scales are well beyond the linear regime probed here. The error on the matter power spectrum is mostly related to the exact shape of the oscillatory features, as illustrated in Fig. 5.5. Note that the regime where the discrepancy is largest falls well outside the area probed by our MCMC, as we use a maximum scale $k_{max} = 1$. The largest discrepancy is therefore $\sim 5\%$ at $k \to 1$. In order to ensure that the error from the fluid approximation does not introduce a significant bias in our MCMC results, we have recalculated a few selected points using high-precision settings, without the fluid approximation, to probe that the χ^2 shows the same behavior as the one obtained using the approximations, obtaining insignificant changes to the likelihood. We therefore conclude that the error with normal precision settings remains within very acceptable limits.

5.C Parameter correlations

For completeness, we present here the two-dimensional contour plots and the one-dimensional posterior distribution plots from our MCMC runs showing all varied parameters, see Figs. 5.6 to 5.8. Figure 5.6 shows the posterior distributions computed using Planck TTTEEE data exclusively, comparing the results obtained after fixing the neutrino to $\sum m_\nu = 0.066$ eV to the

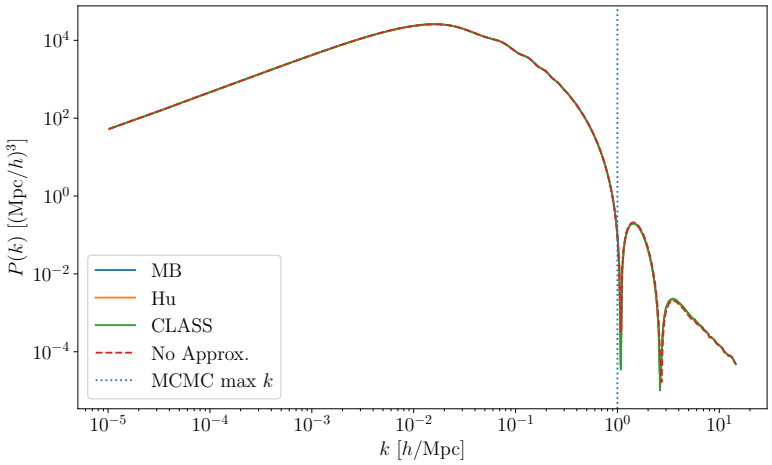

Figure 5.5: *The matter power spectrum computed with the different prescriptions in in CLASS for evolving the shear, σ_ν, in the truncated spectrum, as well as the case of using the full hierarchy. MB is the standard Ma and Bertschinger approach [163], Hu is an approach by Wayne Hu [632] and CLASS is a new approach introduced in the CLASS code, all three are detailed in references [67, 635]. Cosmological parameters are set to their best fit value from MCMC with Planck 2018TTTEEE, except for $u_\chi = 4.2 \cdot 10^{-4}$, which is set to its 2σ upper limit. It is clear that the approximations yield very similar results.*

results assuming a free varying neutrino mass with the prior $\sum m_\nu \geq 0.06$ eV. The latter yields a 2σ upper limit of $\sum m_\nu \leq 0.339$ eV. A clear correlation between the interaction strength u_χ and several cosmological parameters, most notably θ_s and n_s, can be noticed from this figure .

Figure 5.7 shows the case of a fixed neutrino mass $\sum m_\nu = 0.066$ eV, using different combinations of datasets to constrain parameters. The general trends are similar to the non-interacting case, the addition of BAO data lowers the estimated value of ω_{DM}, while raising ω_b and n_s, however, these shifts are not significant. It is interesting to note that the addition of lensing data helps in constraining u_χ more strongly. Nevertheless the constraints on the cosmological parameters are generally very similar, which may also indicate that they are dominated by their determination from Planck 2018 TTTEEE data.

Finally, Fig. 5.8 compares the cases of interacting, non-interacting, fixed m_ν and free m_ν. Note that the interacting case mildly favors a larger value of θ_s and a lower value of n_s. This also matches what can be expected from their correlations with u_χ. Results for the non-interacting case were obtained by running chains with the same parameters and datasets, but setting u_χ to 0.

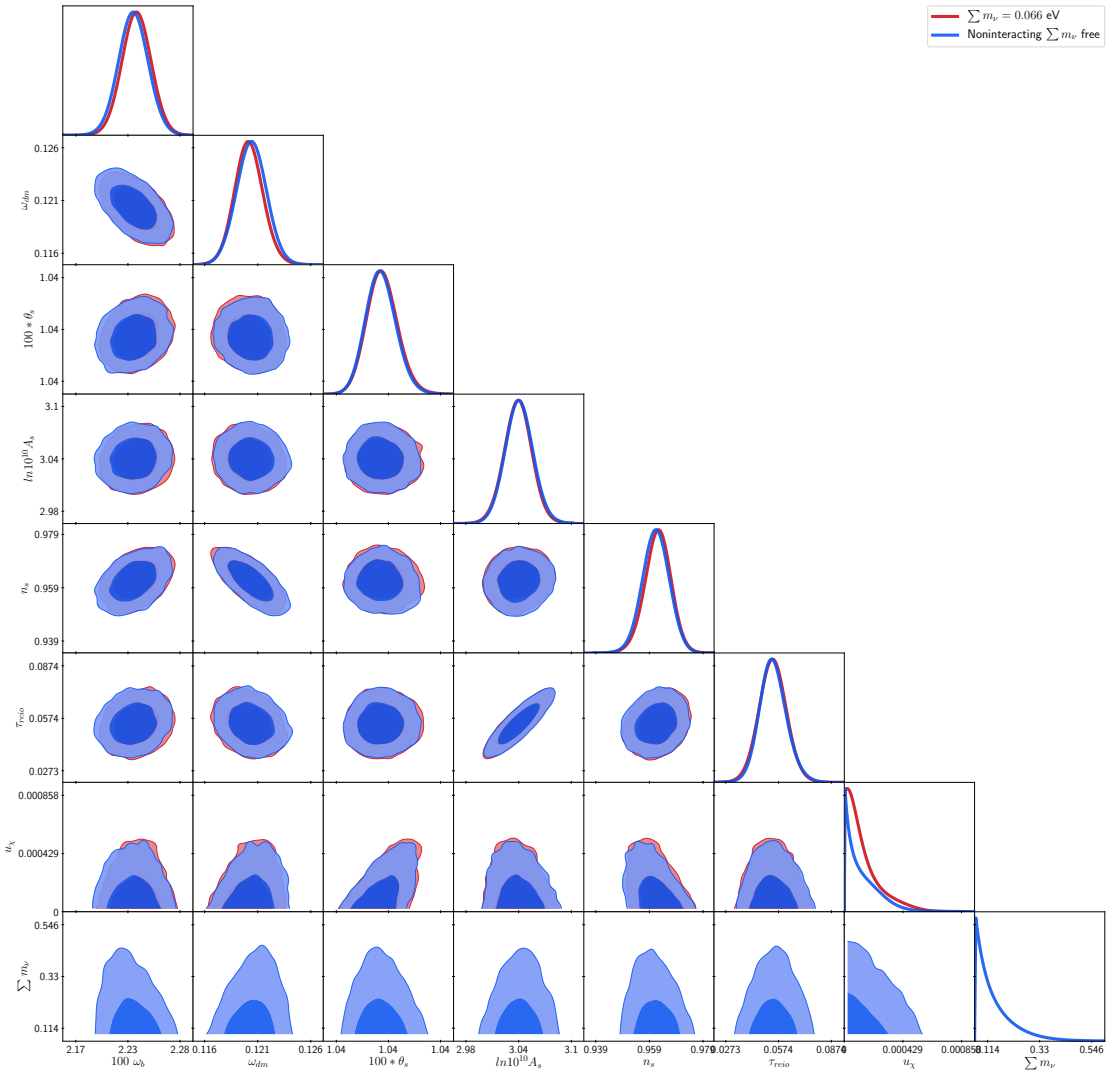

Figure 5.6: *One and two-dimensional probability posterior distributions computed using exclusively Planck TTTEEE data, comparing the results for a fixed neutrino mass* $\sum m_\nu = 0.066$ *eV and a freely varying neutrino mass with the prior* $\sum m_\nu \geq 0.06$ *eV.*

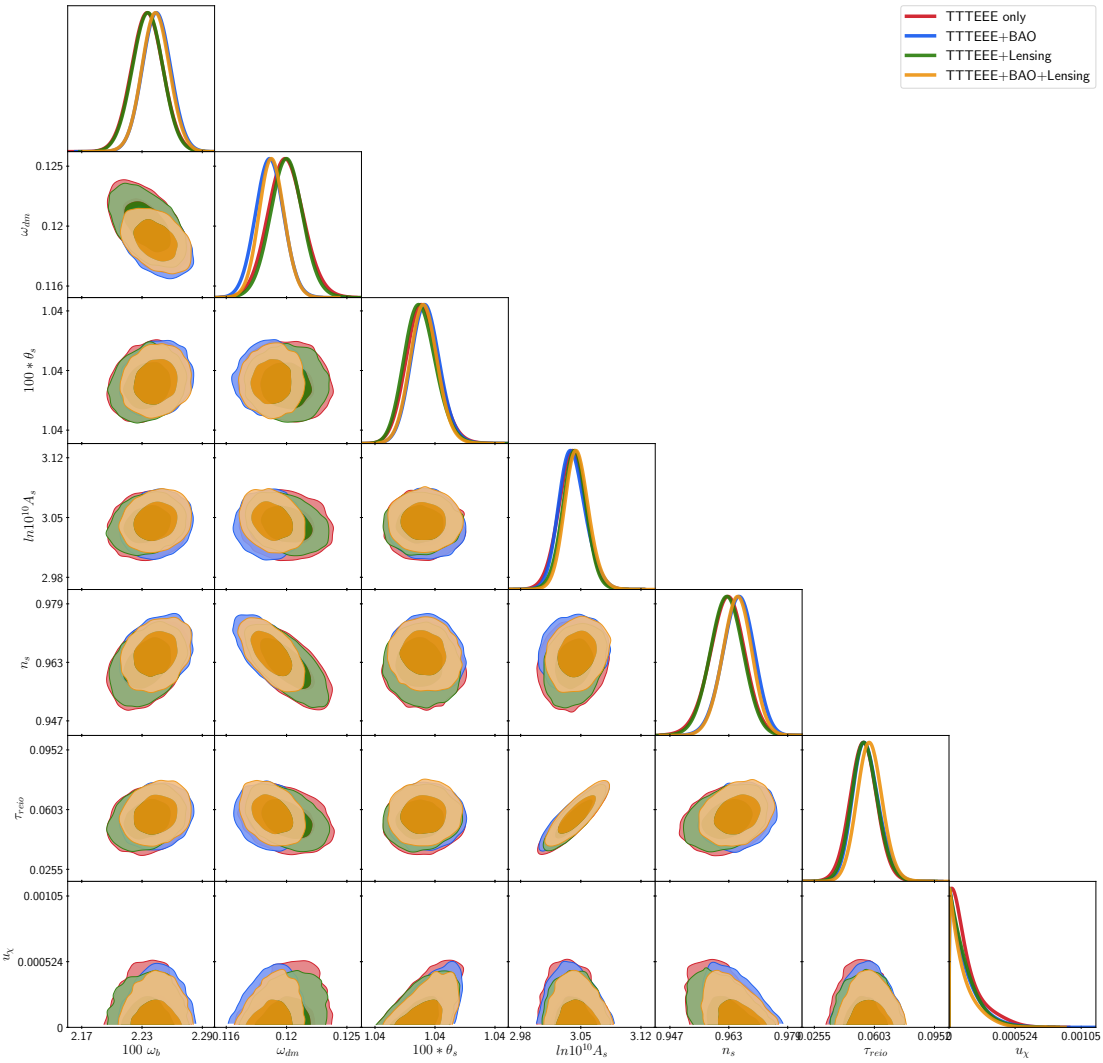

Figure 5.7: *One and two-dimensional probability posterior distributions computed using a fixed neutrino mass* $\sum m_\nu = 0.066$ *eV for different combinations of datasets.*

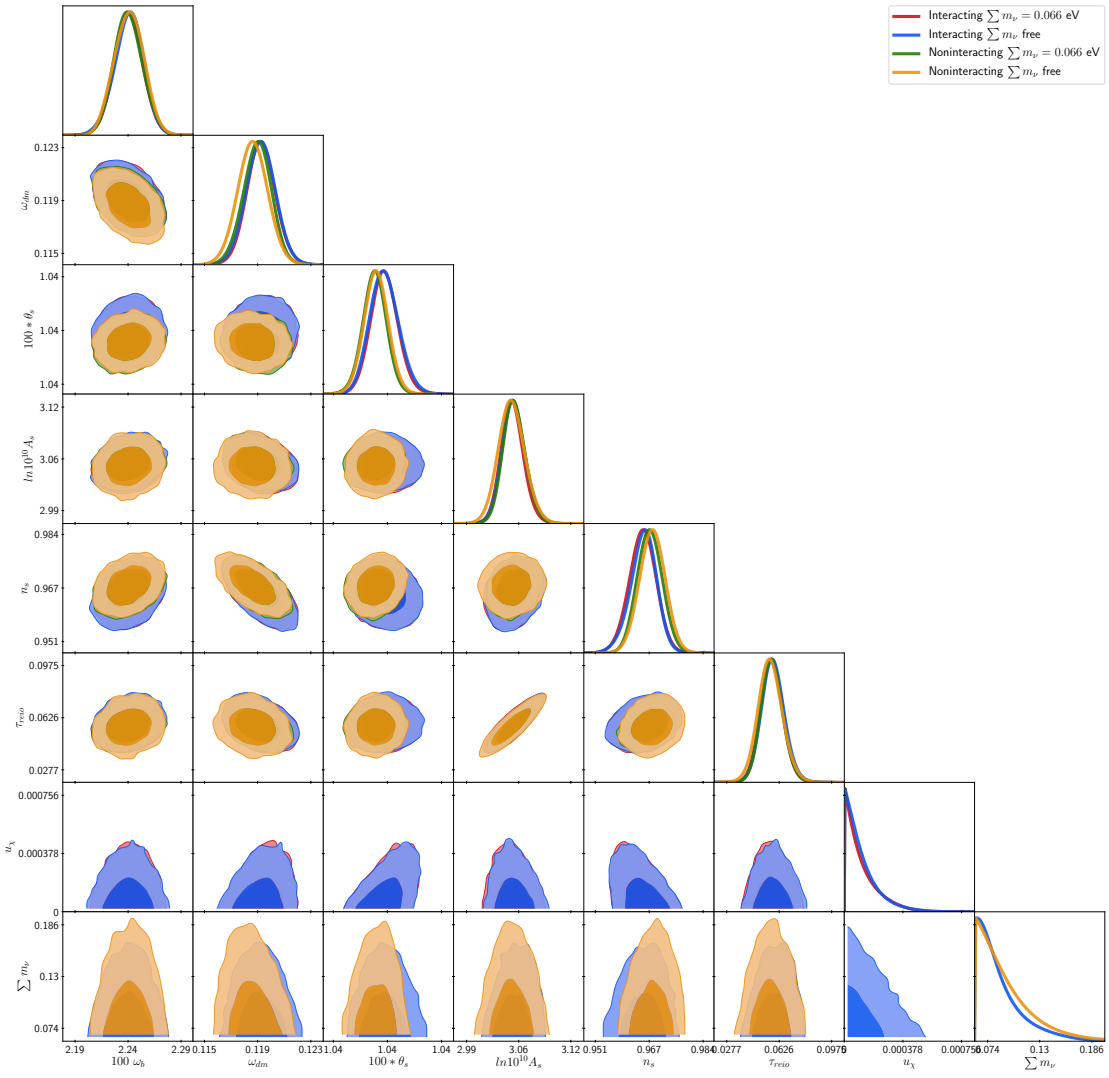

Figure 5.8: *Comparison of the one and two-dimensional probability posterior distributions using a fixed neutrino mass* $\sum m_\nu = 0.066$ *eV and using* $\sum m_\nu$ *as a free parameter, for the interacting and non-interacting scenarios. These are computed using our full range of datasets,* TTTEEE+BAO+lensing.

CHAPTER 6

Investigating the nature of dark matter with 21cm signals

Building on the analysis of Chapter 5, it is interesting to take the investigation of this scenario further, into the nonlinear regime in particular. As constraints on models beyond cold dark matter become stronger, the regime where viable models can be tested moves to smaller scales, necessitating a nonlinear treatment.

Many different dark matter scenarios offer to help alleviate the tensions in ΛCDM, or just provide a model beyond cold dark matter, but so far, it has only been possible to put constraints on these models. In the event of a detection of e.g. a matter power spectrum with suppression on small scales, this could still be described by a multitude of models, and it may be hard to distinguish between e.g. warm and interacting dark matter.

In the work presented in this chapter, I use nonlinear N-body simulations to quantify the difference in predictions between warm and interacting models, offering both a description for when constraints on one can be generalised to others, as well as, crucially, what is necessary to distinguish between such models. In particular, the simulations show that the signatures of early-time dark matter interactions get washed out by nonlinear structure formation, so high-redshift measurements of small-scale structure will be necessary to make such distictions.

Probing dark matter interactions with 21cm observations

Markus R. Mosbech[a] *Celine Boehm*[a] *Yvonne Y. Y. Wong*[b]

[a]School of Physics, University of Sydney, Camperdown, NSW 2006, Australia
ARC Centre of Excellence for Dark Matter Particle Physics
Sydney Consortium for Particle Physics and Cosmology
[b]School of Physics, The University of New South Wales, Sydney NSW 2052, Australia,
Sydney Consortium for Particle Physics and Cosmology

Abstract: Similarly to warm dark matter which features a cut-off in the matter power spectrum due to free-streaming, many interacting dark matter models predict a suppression of the matter power spectrum on small length scales through collisional damping. Forecasts for 21cm line intensity mapping have shown that an instrument like the SKA will be able to probe a suppression of power in warm dark matter scenarios in a statistically significant way. Here we investigate the implications of these findings on interacting dark matter scenarios, particularly dark matter-neutrino interactions, which we use as an example. Using a suite of cosmological N-body simulations, we demonstrate that interacting scenarios show a suppression of the non-linear power spectrum similar to warm dark matter models. This implies that 21cm line intensity mapping will be able to set the strongest limits yet on dark matter-neutrino scattering, improving the constraints by two orders of magnitude over current Lyman-α bounds, and by four orders of magnitude over cosmic microwave background and baryon acoustic oscillations limits. However, to distinguish between warm dark matter and interacting scenarios, our simulations show that percent-level precision measurements of the matter power spectrum at redshifts $z \gtrsim 15$ are necessary, as the key features of interacting scenarios are washed out by non-linear evolution at later times.

6.1 Introduction

The universe on large scales seems to be well described by the simple cosmological ΛCDM. The model reproduces to a high accuracy the statistical properties of both the cosmic microwave background (CMB) anisotropies and the large-scale matter distribution—including the baryon acoustic oscillations (BAO)—using only six parameters [16, 937, 938]. However, this simplicity comes at a price: in order to achieve concordance with observations, the model must invoke two mysterious components, namely, dark matter and dark energy. The standard assumptions for these are, respectively, a collisionless massive particle—the so-called Cold Dark Matter (CDM)—and a cosmological constant (Λ). Many particle physics models have been designed to include a viable particle candidate for the dark matter; similarly, there is no shortage of gravity theories capable of mimicking the phenomenology of a cosmological constant. However, there is no consensus yet on the nature of either component [939–941].

Focusing on the dark matter question, we note that generic CDM particle candidates predict structures on all length scales. However, we cannot preclude the possibility that structures may not be present on small length scales not yet accessible to observations. Indeed, several classes of dark matter scenarios predict exactly that. The warm dark matter (WDM) scenarios, for example, are typically characterised by a relatively low particle mass (in the low keV range). Such light masses enable the free-streaming of these particles to erase the primordial seeds for cosmological structure formation, thus leading to a heavily suppressed number of small-scale structures relative to the CDM case [145, 162, 165, 237, 381–383, 389, 391, 392].

Another interesting possibility are the interacting dark matter (IDM) scenarios, wherein the interaction of the DM—with other constituents of the universe or with itself—persists until the primordial nucleosynthesis epoch or later. This class of DM also predicts a loss of small-scale structures on cosmologically testable scales, but through collisional damping rather than free-streaming. In addition, IDM scenarios predict the appearance of dark acoustic oscillations, as has been demonstrated in the linear regime of evolution, a strong distinguishing feature of this class of DM scenarios from the classic WDM. A variety of IDM scenarios has been investigated in the literature. These include interactions of DM with itself [352, 356, 360–369], with baryons [352, 355, 356, 370–372, 374, 665–668], with photons [144, 148, 149, 352, 353, 356, 357, 359, 371, 372, 375–379, 658, 942], as well as with neutrinos [1, 352, 356, 378, 660, 661, 913–915, 943] and more recently with a dark sector radiation species [663, 916–923].

While both WDM and IDM are often invoked as a possible solution to the observational challenges confronting ΛCDM on small scales [132], we emphasise that, ultimately, the way to acquire a complete picture of the fundamental nature of dark matter is to reconstruct the matter power spectrum down to the smallest scales and at the highest redshifts possible. Indeed, although both WDM and IDM predict a damped power spectrum in the linear regime and IDM scenarios have additional tell-tale features, the evolution of structure formation in the non-linear regime tends to erase these differences, bringing the observable effects of these scenarios closer to the CDM predictions with time [358]. Hence, the closer the observations are to probing the linear regime of evolution, the better they would be for distinguishing between these scenarios and possibly confirming the particle nature of dark matter.

As technology advances and ever better experiments are built, we gain access to more powerful probes to constrain deviations from ΛCDM (or perhaps even rule out ΛCDM itself). In this work, we confirm that measurements of the matter power spectrum $P(k)$ at high redshifts will be a key observable to probe the existence of dark matter interactions and show that 21cm intensity mapping, which traces neutral hydrogen—commonly denoted HI—through its emission from a hyperfine transition to its ground state, will provide a critical tool to do so. Although the all-sky average signal, including redshift information, has already been measured by EDGES [944], which can also be used to constrain dark matter interactions [942], its lack of angular resolution does not allow for intensity mapping. The Square Kilometre Array (SKA), however, will have a much better resolution than EDGES and its measurements of the 21cm emission intensity as a function of the angular position will yield density maps similar to maps of the CMB anisotropies [945–949]. Together with redshift information out to $z \sim 25$, these angular maps will enable the 3D reconstruction of the distribution of emitters in the sky [84], and as such SKA will be an ideal instrument to help distinguish between different types of dark matter scenarios.

To make our predictions, we perform a suite of numerical simulations using the public code GADGET-4 [742], for several WDM and IDM scenarios as well as CDM which we use as reference. In the case of IDM, we use as a generic example a DM-neutrino scattering scenario, as this can

help probe very weak dark matter interactions with the Standard Model and might also be related to the neutrino mass generation mechanism [892]. The linear evolution of this IDM scenario is computed using a modified version of CLASS [67, 635] described in Ref. [1], which includes the full Boltzmann hierarchy for massive neutrinos interacting with a heavy dark matter species. Our simulations show that, while the small-scale suppression of the IDM matter power spectrum remains—thereby making the scenario distinguishable from CDM—the dark acoustic oscillations that characterise IDM are washed out by non-linear growth at late times, particularly at redshifts $z \lesssim 10$. The predictions of IDM at late times should therefore resemble those of WDM. Thus, like for the WDM scenarios studied in Ref. [390, 950], one expects future 21 cm data to set a limit on the IDM damping scale. Here, we show that using these data would improve the constraints on the elastic DM-neutrino scattering cross section by two orders of magnitude with respect to the Lyman-α constraints [943] and four orders of magnitude with respect to CMB+BAO bounds [1].

To quantify just how well future matter power spectrum measurements will be able to distinguish between IDM and WDM scenarios, we investigate also the predictions of these scenarios at higher redshifts. For IDM interaction strengths tuned to mimic as closely as possible the linear predictions of specific WDM masses, we find that the non-linear matter power spectra of these two classes of DM scenarios match to a few percent or better at $z \lesssim 10$. Therefore, to distinguish them, one would need percent-level precise measurements at redshifts $z \gtrsim 15$, i.e., just before the dark acoustic oscillations in the matter power spectrum become completely washed out.

The structure of this work is as follows. In Section 6.2 we present the interacting and warm dark matter scenarios we wish to investigate, while in Section 6.3 we provide a short overview of the 21cm emission and how the signal is predicted. Section 6.4 presents a comparison of our interacting and warm dark matter initial conditions and a description of our N-body simulations. We present the results of our N-body simulations in Section 6.5. Section 6.6 contains our conclusions.

6.2 Dark matter scenarios

We present in this section the interacting dark matter and warm dark matter scenarios investigated in this work. We describe in particular their linear evolution, which is in turn used to set the initial conditions for our numerical simulations in Section 6.4.

6.2.1 Interacting dark matter

Our IDM analysis is based on the DM-neutrino interaction scenario presented in Ref. [1]. In this scenario, the dark matter scatters elastically with three Standard Model neutrinos with nonzero masses and the scattering cross-section σ_0 is taken to be independent of temperature. This phenomenological description is similar to the Thomson scattering process of electrons and photons, and the effective parameter that controls the phenomenology is normally given in the form [357]

$$u_{\nu\chi} \equiv \frac{\sigma_0}{\sigma_{\rm Th}} \left(\frac{m_\chi}{100\,{\rm GeV}}\right)^{-1}, \tag{6.1}$$

where $\sigma_{\rm Th} \approx 6.65 \times 10^{-29}\,{\rm m}^2$ is the Thomson scattering cross-section, and m_χ is the dark matter particle mass.

Introducing an elastic scattering interaction between DM particles and neutrinos leads to a suppression of the power spectrum through collisional damping, i.e., the collisions between DM particles and neutrinos prevent the gravitational collapse of structures below the diffusion scale set by the interaction strength $u_{\nu\chi}$. This process is similar to the scattering between baryons and

photons, which prevents baryons from collapsing to form structures until they are released from the photons' drag at $z \approx 1020$. Just as photon-baryon interactions set up acoustic oscillations in both the photon and the baryonic fluctuations, the competition between the force of gravity and the pressure exerted by the coupled DM-neutrino fluid will imprint oscillations in both the DM and neutrino power spectra. This is the so-called "dark acoustic oscillations" [373].

For relatively weak interaction strengths compatible with current cosmological observations, the DM-neutrino interaction decouples well before recombination, i.e., $z \gtrsim 1100$. After DM-neutrino decoupling, we take both the neutrino and DM populations to be completely collisionless species. We have previously described in Ref. [1] the linear evolution of cosmological perturbations in this scenario and implemented it in a modified version of CLASS. Here, we shall use the output of this linear evolution at $z = 99$ as initial conditions for collisionless DM simulations.

Note that neutrinos may or may not be already kinetically decoupled when the dark matter stops being influenced by its interactions with neutrinos, depending on the value of the mass and interaction cross-sections. In particular, for MeV DM particles and when the neutrino kinetic decoupling is with electrons, neutrinos can transfer their free-streaming to the dark matter fluctuations through their collisions with the DM particles due to the shear ratio of the DM-to-neutrino number densities. This damping mode can be particularly efficient and was considered in [661] in great detail. However, this so-called"mixed damping" is a special case of collisional damping and, as such, will not be explicitly considered in the present work.

Lastly, we expect our findings to be generalisable to other types of dark matter interactions that suppress the matter power spectrum at small scales. We have explicitly checked this for dark matter interacting with photons, following the prescriptions of Ref. [379] and the implementation in CLASS described in Ref. [659]. Any scattering between the 21cm photons and dark matter is suppressed and can thus be safely neglected, making the numerical modelling of the 21cm signal essentially the same as for dark matter-neutrino interactions. In the case of dark matter-baryon interactions, however, the impact of the interaction on the baryon temperature and its influence on the global 21cm signal would need to be taken into account. Such a study was recently performed in Ref. [671], putting strong constraints on millicharged dark matter.

6.2.2 Warm dark matter

Warm dark matter also suppresses structure formation on small scales, but the physics behind this suppression is fundamentally different from collisional damping caused by DM scattering. In WDM scenarios, DM particles with large initial velocities and negligible interaction free-stream away from initial overdensities of small spatial extents over a time scale much shorter than the gravitational collapse time scale. This free-streaming prevents gravitational collapse and hence the formation of structures on scales below a so-called free-streaming scale [162, 237]. For a thermally produced WDM, the free-streaming scale is determined by the temperature-mass ratio of the particle species.

The free-streaming suppression in the linear matter power spectrum should in principle be computed in the same way as we track massive Standard-Model neutrinos. However, it has been known for some time that the WDM power spectrum $P_{\rm WDM}(k)$ can be captured quite neatly by a fitting function of the form [237]

$$P_{\rm WDM}(k) = T^2(k) P_{\rm CDM}(k), \tag{6.2}$$

where $P_{\rm CDM}(k)$ is the equivalent CDM power spectrum in the same cosmology modulo the DM content, and

$$T(k) = \left(1 + (\alpha k)^{2\nu}\right)^{-5/\nu} \tag{6.3}$$

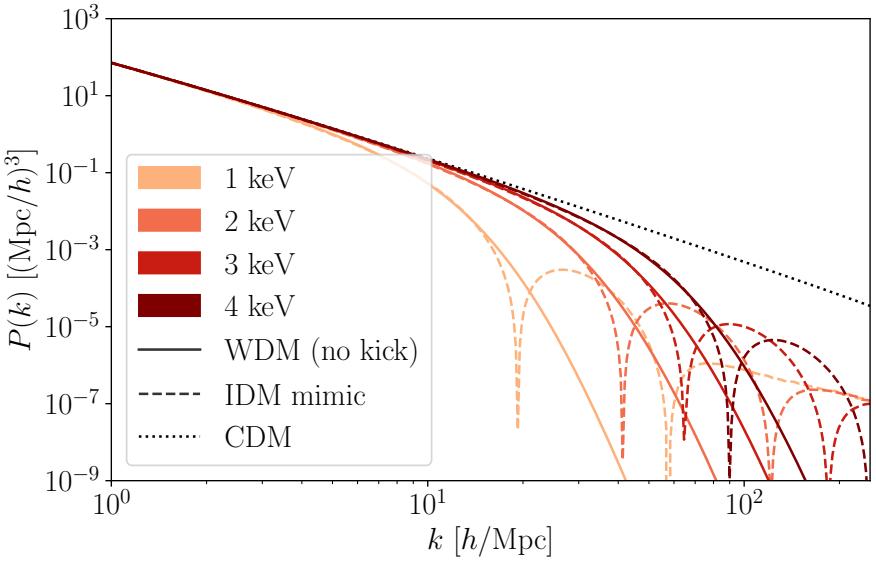

Figure 6.1: *The matter power spectrum for several WDM (solid lines) and IDM (dahsed lines) scenarios, as well as for a reference non-interacting CDM cosmology (dotted line). Note that the relevant scales of impact are much smaller, i.e., occur at much large wave numbers k, than, e.g., the BAO scale.*

is the suppression transfer function, with index $\nu = 1.12$ determined from a fit to computational outcomes. For a given present-day reduced dark matter density $\Omega_{\rm WDM}$ and assuming a thermally-produced WDM, the damping scale α is given by

$$\alpha = 0.049 \left(\frac{1\text{keV}}{m_{\rm WDM}}\right)^{1.11} \left(\frac{\Omega_{\rm WDM}}{0.25}\right)^{0.25} \left(\frac{h}{0.7}\right)^{1.22} h^{-1}\text{Mpc}, \tag{6.4}$$

where $m_{\rm WDM}$ is the WDM particle mass, and h is the dimensionless Hubble parameter. The numerical values of the indices have again been determined from fits [237].

$m_{\rm WDM}$	Mimic $u_{\nu\chi}$	Mimic $u_{\gamma\chi}$
1 keV	$8.5 \cdot 10^{-7}$	$4.0 \cdot 10^{-7}$
2 keV	$1.75 \cdot 10^{-7}$	$9.0 \cdot 10^{-8}$
3 keV	$7.0 \cdot 10^{-8}$	$3.5 \cdot 10^{-8}$
4 keV	$3.6 \cdot 10^{-8}$	$1.8 \cdot 10^{-8}$

Table 6.1: *List of $u_{\nu\chi}$ and $u_{\gamma\chi}$ [379, 659] values mimicking each WDM particle mass, in terms of their linear matter power spectrum predictions.*

Figure 6.1 shows the WDM linear power spectrum for a range of $m_{\rm WDM}$ values. In addition, we display on the same figure predictions of IDM scenarios with the interaction strengths $u_{\nu\chi}$ tuned to mimic the WDM linear power spectrum at $z = 0$ to $< 5\%$-accuracy at $k \leq 0.75 k_{\rm osc}$, where $k_{\rm osc}$ is the scale of the first oscillation (see Table 6.1). Beyond the matching region the IDM scenarios all begin to show their characteristic dark acoustic oscillations, making their linear predictions drastically different from those of WDM scenarios. This is illustrated in detail in Fig. 6.2.

6.3 The 21cm emission line

The 21cm line is an electromagnetic spectral line emitted from a spin-flip transition in neutral hydrogen (HI) between the two levels of a hyperfine splitting in the 1s state. The transition is

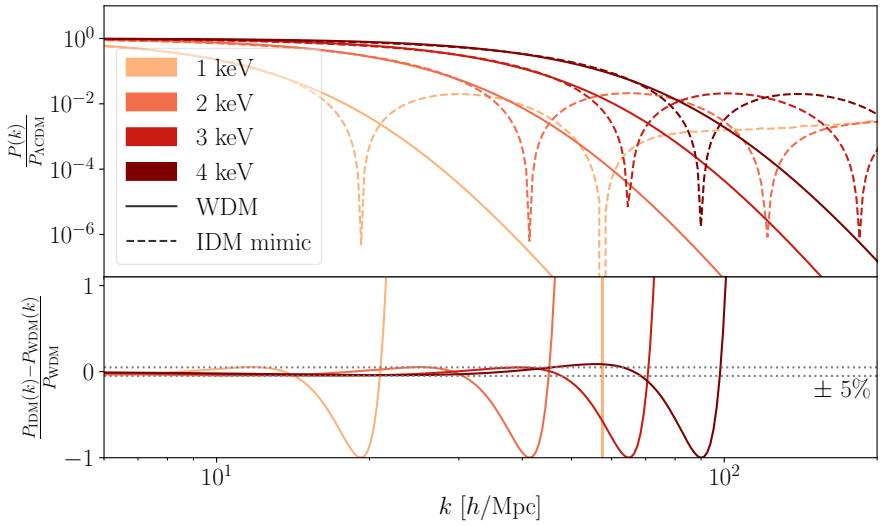

Figure 6.2: *Suppression in the linear matter power spectrum for several WDM and IDM cosmologies relative to a reference ΛCDM cosmology described by the same parameters (except in the DM sector). as well as the relative difference between them. The bottom panel shows the relative difference between the same WDM scenarios and the IDM scenarios tuned to mimic them.*

usually deemed forbidden under laboratory conditions, but is nonetheless possible to observe in astronomical settings if there is a sufficient abundance of neutral hydrogen.

In the context of standard cosmology after recombination, some 75% of the universe's baryon content comes in the form of HI. After they have been released by the CMB from the baryon drag at $z \approx 1020$ and cooled sufficiently, the higher-energy triplet state can be excited from the singlet ground state by background photons, collisions between hydrogen atoms, or via an intermediate state after excitation from Lyman-α photons [946]. The ratio of atoms in the two energy levels is usually parameterised in terms of a "spin temperature" T_s,

$$\frac{n_1}{n_0} \equiv 3 \exp\{(-T_*/T_S)\}, \tag{6.5}$$

where $T_* = 0.068\,\mathrm{K} = 5.9 \cdot 10^{-6}$ eV corresponds to the transition energy between the two states, and the factor of 3 accounts for the degeneracy of the triplet state.

Because of the multitude of processes, such as those listed above, that can alter the spin distribution, the evolution of the ratio n_1/n_0 and hence the spin temperature T_S is generally highly non-trivial. Crucially, however, if the spin temperature is higher than the CMB background temperature, i.e., $T_S \gtrsim T_{\mathrm{CMB}}$, then the 21cm line is observable against the CMB background as a net emission, while the opposite case of $T_s \lesssim T_{\mathrm{CMB}}$ results in net absorption. This variation of T_S relative to T_{CMB} leads to variations in the intensity of the global 21cm signal against the CMB back light as a function of redshift, normally expressed in terms of the differential brightness temperature [946],

$$\delta T_b(z) = \frac{T_S - T_{\mathrm{CMB}}}{1+z} \left(1 - \exp\{(-\tau_{\nu_0})\}\right), \tag{6.6}$$

where τ_{ν_0} is the optical depth at the 21cm frequency ν_0. Measurements of the gloabl $\delta T_b(z)$ can therefore serve as a powerful probe of processes that affect the evolution of the HI content of the universe, from standard effects such as the onset of star formation, to non-standard interactions between hydrogen and the dark sector. See, for example, Ref. [951] for investigations of the latter in relation to the EDGES result.

Furthermore, because the spatial distribution of the underlying dark matter density field is inhomogeneous, the HI density and hence the 21cm signal intensity must also trace this inhomogeneity to a large extent. The 21cm signal can therefore be used to map structures through line intensity mapping. In this endeavour, the intensity of the 21cm line is measured for locations across the sky, similarly to the construction of a CMB map. The mapping does not require individual sources to be resolved, but provides a tracer for the density of atomic hydrogen, which is itself a (biased) tracer of structures. Because the emission is a well-defined line, the redshift can be measured precisely, thereby allowing the distance to be inferred. Together with the angular information, this distance measurement will allow us to reconstruct in 3D the spatial distribution of the HI in the early universe, from which to infer the underlying DM density field.

6.3.1 Predicting the 21cm signal

In order to predict the 21cm power spectrum for a given cosmological model, it is usually necessary to perform some kind of numerical simulations. The authors of Refs. [390, 952], for example, modelled the non-linear evolution of DM and baryons using hydrodynamic N-body simulations and then populated the simulation box with HI following two different schemes, namely, a halo-based method and a particle-based method. The former assumes all neutral hydrogen to be located in halos, with an amount pro-rata the halo mass, and the total of neutral hydrogen at $z \sim 3$–5 is normalised to the observed value of $\Omega_{\rm HI} = 10^{-3}$, though this is subject to uncertainty [953]. The latter assigns neutral hydrogen to every gas particle in the simulation, based on the gas particle's density and internal energy, as well as whether it is star-forming. These two methods should generally bracket the possible distributions of HI, with the halo-based method overestimating the clustering and the particle-based method underestimating it.

Then, assuming further that the 21cm emission intensity traces the HI density $\rho_{\rm HI}$ exactly, the differential brightness temperature everywhere in the box $\delta T_b(z, \mathbf{x})$ can be estimated from the simulation outcome via

$$\delta T_b(z, \mathbf{x}) = \overline{\delta T_b}(z) \frac{\rho_{\rm HI}(z, \mathbf{x})}{\bar{\rho}_{\rm HI}(z)}, \tag{6.7}$$

with mean HI density $\bar{\rho}_{\rm HI}$ is the mean HI, and a mean brightness temperature given by

$$\overline{\delta T_b}(z, \mathbf{x}) = 23.88\, \bar{x}_{\rm HI} \left(\frac{\Omega_b h^2}{0.02}\right) \sqrt{\frac{0.15}{\Omega_m h^2} \frac{(1+z)}{10}}\ \text{mK}, \tag{6.8}$$

where Ω_b is the reduced baryon density, Ω_m the reduced matter density, and $\bar{x}_{\rm HI} \equiv \bar{\rho}_{\rm HI}/\bar{\rho}_{\rm H}$ is the mean neutral hydrogen fraction in the simulation box.

Reference [390] found that, at redshifts $z \approx 3$–5 when the 21cm emitting HI atoms are mainly found in halos, the brightness temperature power spectrum for WDM scenarios show an enhanced amplitude on the scales probed by SKA, $0.3 \lesssim k/[h/\text{Mpc}] \lesssim 60$, relative to the reference CDM scenario. This effect is stronger for smaller WDM masses and can be explained by the fact that WDM cosmologies contain fewer halos for HI to cluster in, so that for a fixed total amount of HI, halos that do manage to form must contain more hydrogen. The SKA1-LOW should be able to measure this effect with $\mathcal{O}(1000)$ hours of observation, which would make it possible to rule out thermal warm dark matter masses up to 4 keV, or conversely, confirm a deviation from standard ΛCDM cosmology [390]. Since our IDM scenario also predicts a suppression of low-mass halo formation in much the same fashion as WDM, a quick inspection of Table 6.1 would suggest that the same measurement could also be used to rule out DM-neutrino interaction strengths up to $u_{\nu\chi} \approx 3.6 \cdot 10^{-8}$. We shall investigate in more detail, via a suite of collisionless N-body simulations, how well these WDM bounds translate to IDM cosmologies. Both ΛCDM and models

beyond have also been investigated with simulations using more advanced hydrodynamics in, e.g., the THESAN project [953].

Note that there are also fast alternatives to hydrodynamic simulations capable of predicting the 21cm power spectrum to a reasonable accuracy. For example, the 21cmFAST code [954–959], itself built upon the DexM [960], uses a combination of first-order Lagrangian perturbation theory and excursion sets to generate 3D realisations of HI field. The method is fast enough that a Markov Chain Monte Carlo analysis is feasible using the 21CMMC tool [955]. Following this approach, Ref. [961] argues that warm dark matter masses up to 8 keV can be constrained by the global 21cm signal with an EDGES-like experiment, and up to 14 keV by the small-scale 21cm power spectrum using HERA [82].

6.4 Comparing interacting and warm dark matter scenarios

Provided that the particle velocity is not too large, the late-time (i.e., $z \lesssim 100$) evolution of a WDM cosmology should be very similar to that of a previously interacting but now decoupled IDM cosmology tuned to give matching linear predictions in the manner described in Section 6.2. As a direct consequence of the suppressed linear power on small scales—whether due to free-streaming or collisional damping—the onset of gravitational collapse into structures would be similarly delayed relative to the standard CDM case. Thus, for an IDM scenario with no late-time interaction with baryons and photons, WDM forecasts should be directly translatable to the case of IDM—as we have proposed to do at the end of Section 6.3.1—without the need to recompute the hydrodynamic evolution of the baryons and/or the HI distribution. This is convenient, as forecasts for how well SKA can distinguish between CDM and WDM cosmolgies via the 21cm brightness temperature power spectrum at $z \approx 3$–5 already exist [390], as discussed above in Section 6.3.1.

What remains to be done is therefore two-fold. First, we need to confirm that non-linear evolution does tend to bring closer together the gross predictions of a WDM scenario to that of an IDM scenario tuned to match as closely as possible the former's linear predictions. Second, what observable differences between the two cosmologies remain, and hence whether the SKA can help distinguish WDM from IDM. To this end, we perform a suite of collisionless N-body simulations for several WDM and IDM cosmologies, paying particular attention to the high-redshift ($z \gtrsim 10$) predictions, where the differences between them are most likely to remain. We describe briefly the simulation settings below. The simulation results are presented in Section 6.5.

6.4.1 Simulation settings

We perform collisionless N-body simulations using the public code GADGET-4 [742], modified to include massive neutrino density perturbations as a linear response as per Ref. [732]. We adopt almost the same simulation settings and cosmological parameters as those used in Ref. [390]. That is, we use 512^3 DM particles, a comoving box of side length $30\,h^{-1}$Mpc, and the cosmological parameters given in Table 6.2.

We initialise our simulations at redshift $z_{\rm in} = 99$, using the linear spectrum output evolved with a modified version of CLASS [1] in the case of IDM. In the case of WDM, we use a standard ΛCDM linear power spectrum output from CLASS, modulated with the transfer function Eq. (6.3) as per Eq. (6.2). As discussed in Section 6.2, the IDM initial power spectrum can be chosen to mimic the suppression scales of a chosen WDM scenario to $\lesssim 5\%$ accuracy before the onset of dark acoustic oscillations at larger wave numbers k. The inclusion of massive neutrinos with $\sum m_\nu \approx 0.06$ eV spread equally amongst three species only has a small effect on structure

	Parameter	Value
Matter density	Ω_m	0.3175
Baryon density	Ω_b	0.049
Neutrino density	Ω_ν	0.00157
Spectral index	n_s	1
Dimensionless Hubble parameter	h	0.6711
Amplitude of primordial power spectrum	A_s	$2.206342 \cdot 10^{-9}$

Table 6.2: *Common cosmological parameter values used in our N-body simulations.*

formation, and should therefore not appreciably affect the 21cm predictions in the presence of the more dominant effects of interactions or WDM; we have included it in our simulations only as a matter of internal consistency for the IDM scenarios.

The information contained in the linear power spectrum of a chosen cosmology is translated into an initial displacement and kick for each N-body particle in the simulation box using the usual Zel'dovich approximation. In the case of WDM, we note that the authors of Ref. [390] also folded the thermal velocity dispersion of the WDM particles into the initial conditions, by adding to each N-body particle an extra thermal velocity kick drawn randomly from a relativistic Fermi-Dirac distribution, $f(v) = (e^{v/\bar{V}_{\rm WDM}} + 1)^{-1}$, where, assuming the WDM to constitute the entire dark matter content, the mean velocity $\bar{V}_{\rm WDM}$ is given by [237, 390]

$$\bar{V}_{\rm WDM} = 0.012\,(1+z)\left(\frac{\Omega_{\rm WDM}}{0.3}\right)^{1/3}\left(\frac{h}{0.65}\right)^{2/3}\left(\frac{1\,\text{keV}}{m_{\rm WDM}}\right)^{4/3}\text{km/s}. \tag{6.9}$$

This thermal velocity has sometimes been neglected in the literature because of the large amount of Poisson noise it generates in the simulation volume at early times, which may render the subsequent simulation outcome unreliable on small scales [826]. On the other hand, omitting the thermal kick could mean that we are missing important physics related to the thermal velocity [237, 827, 872, 962, 963]. We therefore perform two sets of WDM simulations in this work, one set including the thermal kick, and one set omitting it.

Lastly, to quantify the degree of convergence of our 512^3-particle simulations, we perform a set of high-resolution comparison simulations using $(1024)^3$ particles. We find that there is evidence of unphysical Poisson noise effects at large wave numbers k. However, up to the scales of interest these effects are relatively small effect compared with the overall suppression trend expected of WDM and IDM scenario, as shown in Fig. 6.3.

6.5 Simulation results

Figures 6.4, 6.5, and 6.6 summarise our simulation results in a set of matter power spectra at various redshifts.

The first key takeaway is that non-linear evolution causes the difference between CDM, WDM, and IDM cosmologies to diminish with time. This is well illustrated in Fig. 6.4, where it is evident that despite significant differences at early times ($z \gtrsim 15$), the late-time ($z \lesssim 5$) matter power spectra of these different cosmologies differ only by a few percent. Endowing WDM particles with a thermal velocity kick does not significantly alter the outcome, apart from adding Poisson noise at large wave numbers k, as was also noted in Ref. [826]. It is therefore clear that high-precision measurements at high redshifts are a key part of constraining departures from CDM.

Focusing on the $z = 3$–5 matter power spectra shown in Fig. 6.5, we see that a maximum 10%–60% suppression remains for the WDM and IDM cosmologies relative to the reference

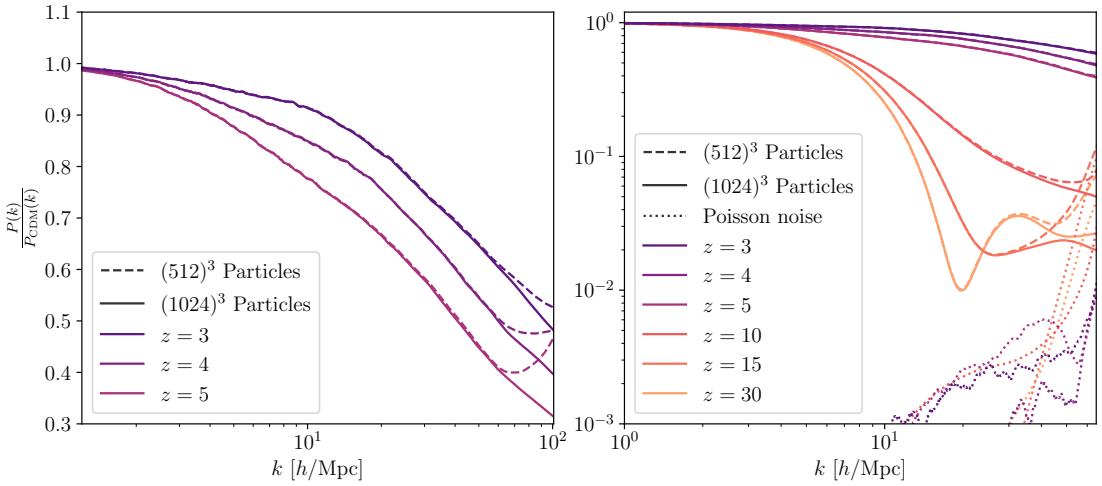

Figure 6.3: *The suppression of the matter power spectrum for the mimic 1 keV interacting scenario relative to ΛCDM at selected redshifts, simulated using two different resolutions. For easy comparison, the wave number ranges have been chose to correspond to those in Fig. 6.5 in the left panel and to Fig. 6.4 in the right panel. While it is clear that the upturn at large wave numbers in the 512^3-particle simulation is due to the limited number of particles, the general suppression trend continues monotonically to high k at redshifts z =3–5 in the k-range of interest. The oscillatory behaviour is also resolved at $z = 30$, and to a lesser extent at $z = 15$, at both simulation resolutions.*

CDM case in the wave number range $0.3 \lesssim k/[h/\mathrm{Mpc}] \lesssim 60$ to be probed by SKA. However, non-linear evolution has completely washed out the characteristic oscillatory features of IDM cosmologies, leading to power spectrum predictions that differ from those of WDM scenarios only by a few percent. Importantly though, the difference between WDM and IDM at these redshifts appears to be smaller than the free-streaming or collision damping suppression of the small-scale power spectrum itself relative to CDM. This means we should also expect the 21cm brightness temperature power spectrum of IDM cosmologies to be characterised by an enhancement in the amplitude relative to the CDM case, where the enhancement increases with interaction strength $u_{\nu\chi}$ in a manner directly relatable to WDM masses via Table 6.1.[1] Thus we arrive at our second key takeaway: constraints on WDM masses from non-linear structure measurements at $z \approx 3$–5 can be immediately translated to constraints on the equivalent $u_{\nu\chi}$. As demonstrated in Ref. [390], observations by SKA1-LOW can constrain WDM masses to $m_{\mathrm{WDM}} \gtrsim 4$ keV, which translates into a limit of $u_{\nu\chi} \lesssim 3.6 \cdot 10^{-8}$ for IDM. The strongest constraint on $u_{\nu\chi}$ at the time of writing is $u_{\nu\chi} \lesssim 8 \cdot 10^{-6}$ [943] obtained from the Lyman-α forest. Thus, 21cm intensity mapping by SKA1-LOW could improve upon current cosmological constraints on IDM scenarios by at least two orders of magnitude.

Our findings also imply that, in order to distinguish between IDM and WDM, higher-redshift observations are necessary. Indeed, as shown in Fig. 6.6 (and verified at a higher simulation

[1] Note that our CDM and WDM power spectra are not an exact match to those found in Ref. [390]. Specifically, we see a slightly greater small-scale suppression of power in the WDM cosmologies relative to the reference ΛCDM model. For example the right panel of Fig. 6.5 shows a 60% suppression in the 1 keV WDM scenario at $k = 100\,h/\mathrm{Mpc}$ and $z = 5$; the equivalent result of Ref. [390], displayed in their Fig. 1, finds a 40% suppression. The slightly different n_s values adopted in the simulations may have contributed to the discrepancy. However, the most likely explanation is that, unlike Ref. [390], we have not accorded baryons a hydrodynamical treatment, but merely lumped them together with the DM as one single collisionless species. This is undoubtedly a drastic simplification. However, for the purpose of demonstrating that the collisionless dark matter in both WDM and IDM cosmologies evolve similarly, it is a sufficient treatment. Furthermore, because neither the WDM nor the IDM has direct, non-gravitational interactions with baryons, full hydrodynamical simulations of these cosmologies should not change the qualitative conclusion that WDM and IDM are phenomenologically very similar at $z \approx 3$–5.

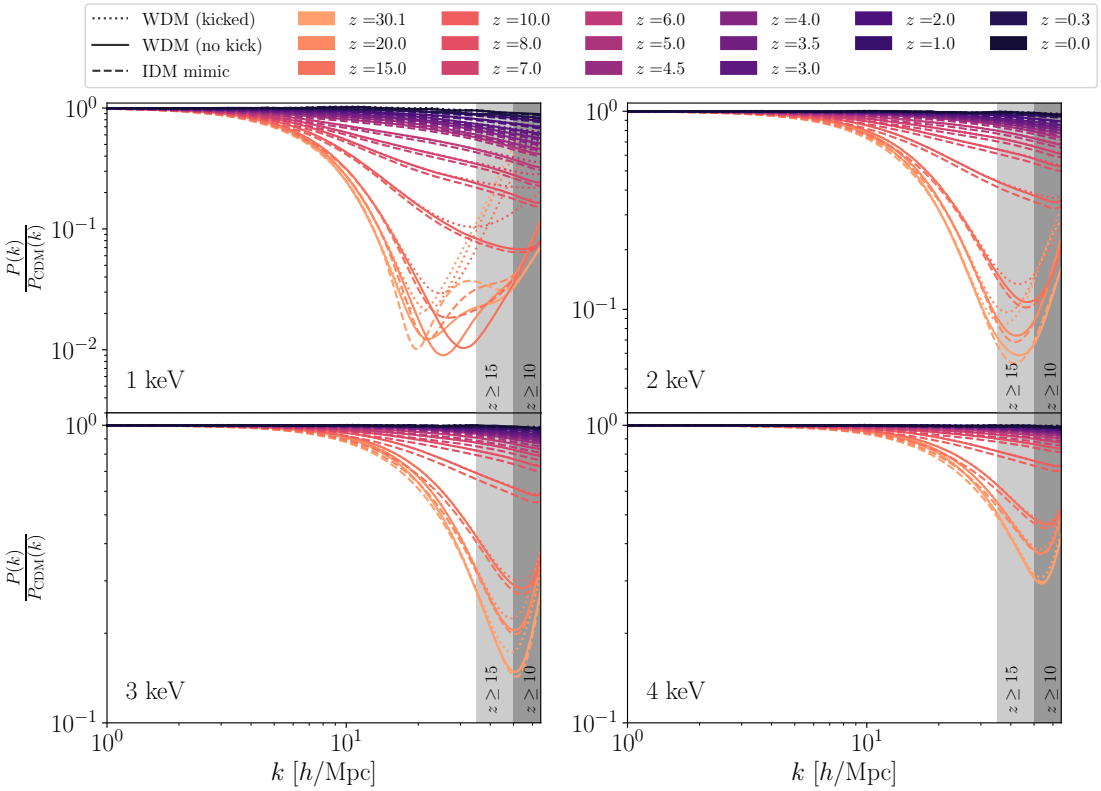

Figure 6.4: *The IDM and WDM matter power spectra relative to a reference ΛCDM power spectrum at a range of redshifts for various WDM masses. The upturn at large wave numbers k at high redshifts ($z \gtrsim 15$) seen in all cases is due to Poisson noise from a limited number of simulation particles. The shaded regions indicate where this noise kicks in at the specified redshifts. The WDM cosmologies have been simulated in two different ways: including a thermal velocity kick for the N-body particles, and excluding it. That the former leads to even more Poisson noise is evident.*

resolution in Fig. 6.7 for the 1 keV and $u_\chi = 8.5 \cdot 10^{-7}$ cases), the characteristic dark acoustic oscillations of IDM become discernible at $z \gtrsim 15$, and are, for a fixed redshift, more evident for larger interaction strengths $u_{\nu\chi}$, i.e., smaller equivalent WDM masses. The latter effect is due largely to the dark acoustic acoustic oscillations appearing on smaller length scales as we decrease $u_{\nu\chi}$, where non-linear dynamics kicks in at an earlier time. If we were to decrease $u_{\nu\chi}$ even further to values outside of the range investigated in this work, we would expect the dark acoustic oscillations to be pushed into a k region below the resolution of these simulations; to numerically probe these cases would necessitate dedicated high-resolution simulations.

However, even with the simulations performed for this work, we are able to give conservative estimates of the precision needed in $P(k)$ measurements to distinguish between WDM and IDM scenarios. For the strongest interactions investigated, $u_{\nu\chi} \approx 8.5 \cdot 10^{-7}$, only $\sim 10\%$ and $\sim 20\%$ precision is needed at $z \sim 15$ and $z \sim 30$, respectively, to distinguish it from a WDM cosmology with $m_{\rm WDM} \approx 1$ keV. For the weaker $u_{\nu\chi} \approx 1.75 \cdot 10^{-7}$ and its $m_{\rm WDM} \approx 2$ keV equivalent, the precision requirements for distinction tighten to $\sim 5\%$ and $\sim 10\%$. Even greater precision would be required for weaker interactions/larger $m_{\rm WDM}$, or we would need to observe at even higher redshifts and/or larger wave numbers.

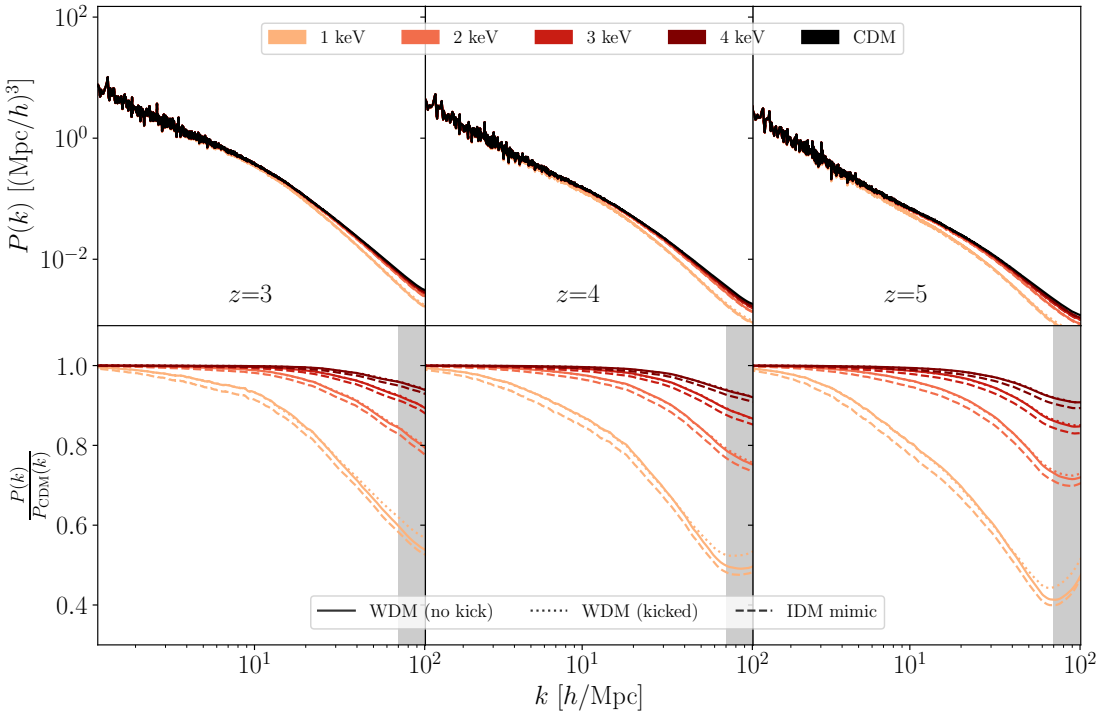

Figure 6.5: *The CDM, WDM, and IDM matter power spectra at redshifts $z = 3$, 4, 5, the same redshifts investigated in Ref. [390], for various WDM masses. We show also in the bottom panels the WDM and IDM power spectra normalised to the reference CDM prediction. The shaded regions indicate where Poisson noise kicks in at the specified redshifts.*

6.6 Conclusions

Using a suite of collisionless N-body simulations, we have shown in this work that the observable consequences of interacting dark matter cosmologies closely mimic those of warm dark matter scenarios at redshifts $z \lesssim 10$. This means that cosmological observations at these redshifts sensitive to WDM properties must also be able to probe IDM in a similar manner, and forecasts for future WDM constraints should be easily adaptable to constraints on IDM.

Specifically, we have considered the constraining power of future 21cm line intensity mapping by SKA in the context of a DM-neutrino interaction scenario. Previous works in the literature showed that the 21cm brightness temperature power spectrum as will be measured by SKA1-LOW will be able to constrain the WDM mass to $m_{\rm WDM} \lesssim 4$ keV [390] with $\mathcal{O}(1000)$ hours of observation. The analysis of Ref. [961] forecasted constraints that are even stronger by up to a factor of 3.5. Through mapping IDM to WDM simulation outcomes, we find the more conservative $m_{\rm WDM} \lesssim 4$ eV can be translated to an upper limit on the DM-neutrino interaction strength of $u_{\nu\chi} \lesssim 3.6 \cdot 10^{-8}$. This represents a forecasted improvement of more than two orders of magnitude with respect to the current constraint from the Lyman-α forest [943], and will likewise tighten by four orders of magnitude current bounds from CMB+BAO [1].

While the observable similarity between WDM and IDM at $z \lesssim 10$ makes it a plus in terms of computational convenience, at the same time it also detracts from our ability to distinguish between these two classes of models observationally. Indeed, we find that in order to obtain a "smoking gun" signal for an IDM scenario, it is necessary to observe the matter power spectrum at redshifts $z \gtrsim 15$ to a precision of ∼2–10%, depending on the interaction strength, before the characteristic dark acoustic oscillations of this type of scenarios become completely washed out

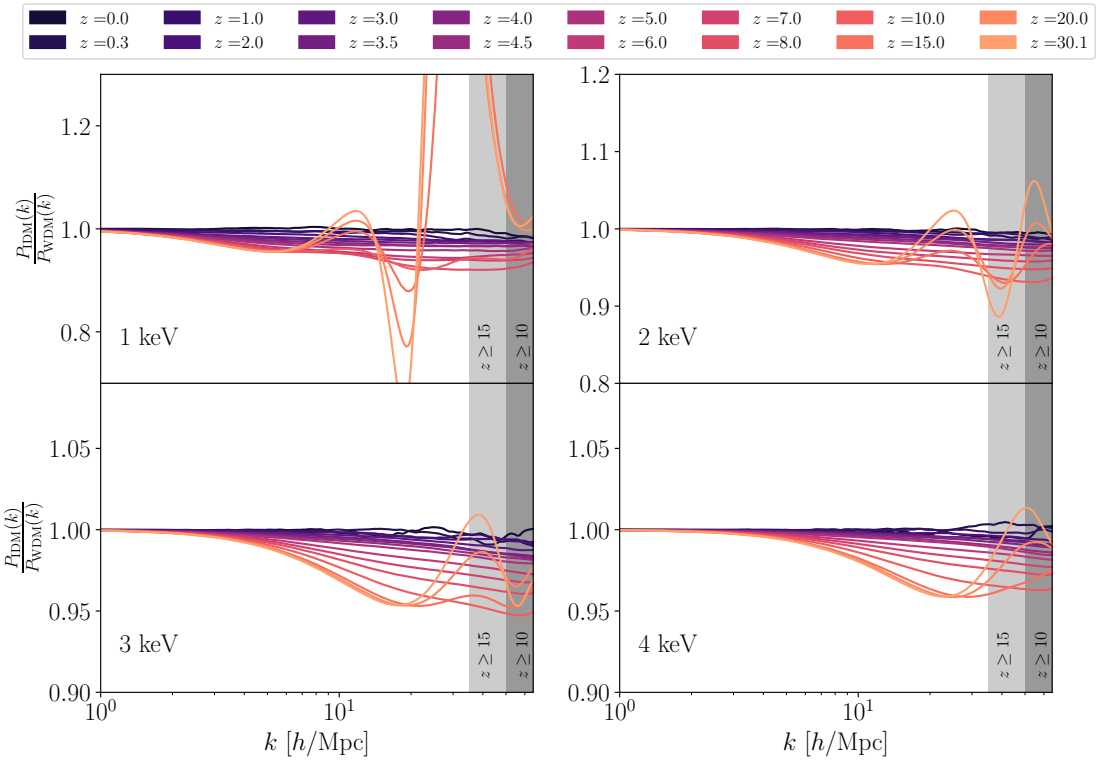

Figure 6.6: *Matter power spectra of several IDM cosmologies at a range of redshifts, relative to the WDM cosmologies they have been tuned to mimic. As we decrease the interaction strength/increase the WDM mass, the difference between WDM and the mimicking IDM cosmologies become increasing difficult to probe, because the characteristic dark acoustic oscillations now appear on smaller and hence more non-linear scales. The shaded regions indicate where Poisson noise kicks in at the specified redshifts.*

by non-linear evolution. The weaker the interaction, the more stringent the redshift and precision requirements, as the characteristic dark acoustic oscillations get pushed out to smaller and more non-linear scales with decreasing interaction strength.

The SKA should be able to probe the 21cm signal out to $z \gtrsim 25$ [84, 388] and therefore has the potential to make the distinction between WDM and IDM. Observing at such high redshifts also offers another advantage over lower redshifts: it allows us to bypass the uncertainties introduced by astrophysics in the form of feedback from star formation, supernovae, and galaxy formation, which are important effects at $z \lesssim 10$. At earlier times, the hydrogen found in filaments also has a higher relative importance [952] compared to halos, changing the dependence of the 21cm power spectrum on the halo number, and the HI-to-DM bias at these redshifts would need to be well-modelled. Such predictions would require a dedicated study beyond the scope of this paper, and is therefore left for future work.

Note added: While we were finalising this manuscript, Ref. [964] appeared on the arXiv which explores a very similar scenario. Their conclusions are that SKA1-LOW observations of the 21cm signal at $z = 8$ will be able to constrain the DM-neutrino interaction strength to $u_{\nu\chi} \lesssim 6.6 \cdot 10^{-7}$. This forecasted bound is weaker than our prediction of $u_{\nu\chi} \lesssim 3.6 \cdot 10^{-8}$, and is likely due to a different set of detection criteria used to derive the constraint.

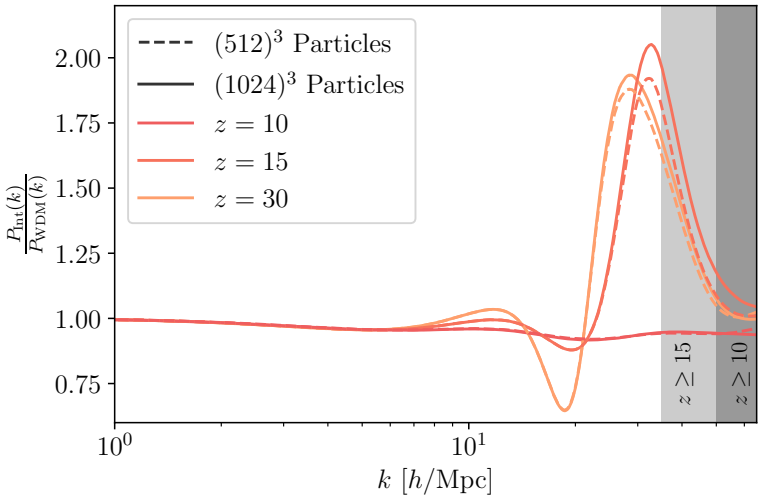

Figure 6.7: *Matter power spectra of the mimic 1 keV IDM cosmology at a range of redshifts, relative to the 1 keV WDM cosmology it has been tuned to mimic, from our standard $N = 512^3$ particle simulations and a set of higher-resolution $N = 1024^3$ simulations. The good agreement between different N runs confirms that the observed oscillations are a physical effect. The shaded regions indicate where Poisson noise kicks in at the specified redshifts in the $N = 512^3$ particle simulations.*

Acknowledgments

We thank Joe Chen for useful discussions on the implementation of thermal velocities. Y^{3}W is supported in part by the Australian Government through the Australian Research Council's Future Fellowship (project FT180100031). This research includes computations using the computational cluster Katana supported by Research Technology Services at UNSW Sydney. Part of this work was performed on the OzSTAR national facility at Swinburne University of Technology. The OzSTAR program receives funding in part from the Astronomy National Collaborative Research Infrastructure Strategy (NCRIS) allocation provided by the Australian Government.

CHAPTER 7

Probing the nature of dark matter with gravitational waves

With cosmological models beyond ΛCDM generally approaching the standard ΛCDM predictions at late times,[1] it is necessary to probe high redshifts to look for discrepancies. Such observations are subject to difficult foreground modelling and other possible systematics, so it would be useful to have a different type of probe, whose systematics would at least be different.

In the work included as this chapter, we present such a new probe in the form of gravitational waves from compact binary mergers. The rate of mergers is dependent on the cosmic star formation rate, which in turn depends on the structure formation seeded by dark matter. We show how dark matter models with suppressed small-scale structure, such as the one described in Chapter 5, affect the halo and galaxy populations, and in turn the rate of compact binary mergers over cosmological timescales.

This shows that with upcoming gravitational wave telescopes, binary merger events will be a viable avenue for probing small scale structure at high redshifts, with an accuracy that will only improve with our understanding of galaxy formation and evolution.

Following our work, others have presented similar analyses of how gravitational waves can help up learn more about their host galaxies [965].

[1] As necessitated by the fact that ΛCDM matches late time observations well.

Gravitational-wave event rates as a new probe for dark matter microphysics

Markus R. Mosbech[a] *Alexander C. Jenkins*[b] *Sownak Bose*[c] *Celine Boehm*[a] *Mairi Sakellariadou*[d] *Yvonne Y. Y. Wong*[e]

[a]School of Physics, The University of Sydney, Camperdown NSW 2006, Australia
ARC Centre of Excellence for Dark Matter Particle Physics
Sydney Consortium for Particle Physics and Cosmology

[b]Department of Physics and Astronomy, University College London, London WC1E 6BT, United Kingdom

[c]Institute for Computational Cosmology, Department of Physics, Durham University, Durham DH1 3LE, United Kingdom

[d]Theoretical Particle Physics and Cosmology Group, Physics Department, King's College London, University of London, Strand, London WC2R 2LS, United Kingdom

[e]School of Physics, The University of New South Wales, Sydney NSW 2052, Australia, Sydney Consortium for Particle Physics and Cosmology

Abstract: We show that gravitational waves have the potential to unravel the microphysical properties of dark matter due to the dependence of the binary black hole merger rate on cosmic structure formation, which is itself highly dependent on the dark matter scenario. In particular, we demonstrate that suppression of small-scale structure—such as that caused by interacting, warm, or fuzzy dark matter—leads to a significant reduction in the rate of binary black hole mergers at redshifts $z \gtrsim 5$. This shows that future gravitational-wave observations will provide a new probe of physics beyond ΛCDM.

7.1 Introduction

The standard ΛCDM model of cosmology has been posited to explain a range of observations spanning the largest observable scales to the scale of galaxies. Its success at explaining these data relies on two mysterious components: dark energy in the form of a cosmological constant (Λ) and dark matter (DM). Dark matter, in particular, is key to explaining the formation and evolution of structures such as galaxies and clusters of galaxies in the late-time Universe.

Present observations on supergalactic scales are compatible with the hypothesis that the dark matter is cold—i.e., the particles have vanishingly small thermal velocities. In this cold dark matter (CDM) model, the particles also do not have significant non-gravitational interactions [16, 357, 966]; these requirements can be satisfied by particle-like dark matter of typical mass $\gtrsim$ keV, or wave-like dark matter of mass $\gtrsim 10^{-22}$ eV. However, the key to determining the fundamental nature of dark matter lies in subgalactic scales at large redshifts. This is because the onset of nonlinear structure formation can be very sensitive to the microphysics of the dark matter [352,

356, 358]. In turn, any probe that could shed light on this epoch of structure formation would also provide valuable insights into the nature of dark matter [390, 967].

There are three classes of phenomenological particle-like and wave-like dark matter scenarios that generically predict small-scale signatures that differ from the predictions of standard CDM. The first, warm dark matter (WDM) scenario usually assumes negligible interactions but has a small DM particle mass in the low keV range that allows these particles to free-stream out of small-scale perturbations [145, 162, 165, 237, 380–383, 389, 391, 392]. The second, interacting dark matter (IDM) scenario makes no strong assumption about the particle mass but endows the DM particle with non-negligible interactions (see Section 7.2 for details). The third, fuzzy dark matter (FDM) scenario comprises a condensate of ultra-light DM particles of mass $\sim 10^{-22}$–10^{-21} eV whose collective behaviour is wave-like [394, 968–970]. As shown in Fig. 7.1, although the details differ between WDM, IDM, and FDM, all three scenarios predict a cutoff in the linear matter power spectrum at large wave numbers k, a feature that is often invoked as a possible solution to the claimed "small-scale crisis", a long-standing set of discrepancies where simulations predict more small-scale structures than observed [147].

In this *Letter* we present a new observational probe of dark matter microphysics, namely the merger rate of stellar-mass binary black holes (BBHs) throughout cosmic time.[2] With the recent advent of gravitational-wave astronomy, advanced interferometers like LIGO [971] and Virgo [972] have already detected dozens of BBHs [481, 482]. Next-generation observatories such as Einstein Telescope [973] and Cosmic Explorer [974] will be capable of detecting nearly *all* stellar-mass binary black holes in the observable Universe [975], extending the reach of gravitational-wave astronomy out to the beginning of cosmic star formation. The space-based interferometer LISA [495] will also provide a great deal of complementary low-frequency information about this population. The abundances of these systems at different epochs encode the star formation, chemical enrichment, and other baryonic processes occurring within dark matter haloes. As we demonstrate below, *the BBH merger rate is highly sensitive to the suppression of small-scale structure induced by dark matter microphysics*, as this in turn inhibits star formation and reduces the BBH yield, particularly at redshifts $z \gtrsim 5$.

In the following, we use as a working example a DM-neutrino interacting scenario [1, 352, 356, 378, 660, 661, 913–915, 943] to demonstrate quantitatively the potential of the BBH merger rate to probe cosmologies with suppressed small-scale structure. A brief description of this IDM scenario is given in Section 7.2. Our analysis pipeline, shown in Fig. 7.2, is as follows. We compute the linear matter power spectrum of an IDM cosmology using CLASS [1, 67, 635], which is then fed into the semi-analytic model of structure formation GALFORM [883, 888] to produce synthetic realisations of galactic populations, as described in Section 7.3. Concurrently, we perform an N-body simulation of the IDM cosmology using the GADGET-4 code [732, 742], initialised with the same linear input, in order to cross-check the halo mass functions predicted by GALFORM. Finally, the star formation rate and stellar metallicities computed by GALFORM are fed into the binary population synthesis code COMPAS [977–979], described in Section 7.4, which computes the gravitational-wave event rate. Our results and conclusions are presented in Section 7.5.

Note that while we have chosen to focus on a specific IDM scenario, we expect our general conclusions to remain valid for other dark matter scenarios that predict qualitatively similar suppression of small-scale power, as nonlinear evolution at $z \lesssim 10$ tends to wash out their detailed features [2]. These include WDM and to some extent FDM as already illustrated in Fig. 7.1,

[2] We focus here on stellar-mass BBHs (and therefore Hz-band detectors such as LIGO, Virgo, Einstein Telescope, and Cosmic Explorer) because the physics underpinning their merger rates is much better understood at present than that of the supermassive BBHs probed by GW searches at lower frequencies (principally by pulsar timing arrays).

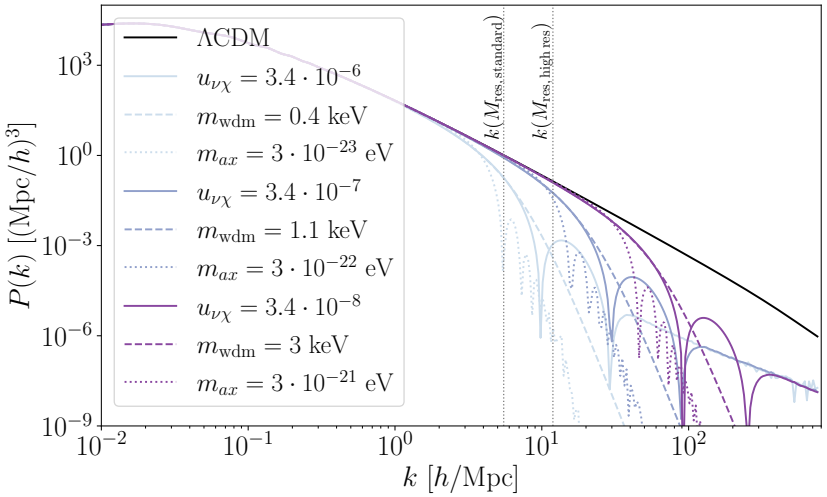

Figure 7.1: *Linear matter power spectra for several DM-neutrino interacting scenarios of varying interaction strength $u_{\nu\chi}$, along with predictions of their "equivalent" FDM and thermal WDM scenarios characterised by their respective particle masses, m_{ax} and $m_{\rm wdm}$, tuned to give a similar small-scale suppression. The FDM power spectra have been computed using AxionCAMB [441, 976]; the WDM power spectra are derived from the ΛCDM power spectrum filtered with a transfer function [237]. Vertical lines indicate rough k-scales corresponding to the mass resolutions used in GALFORM.*

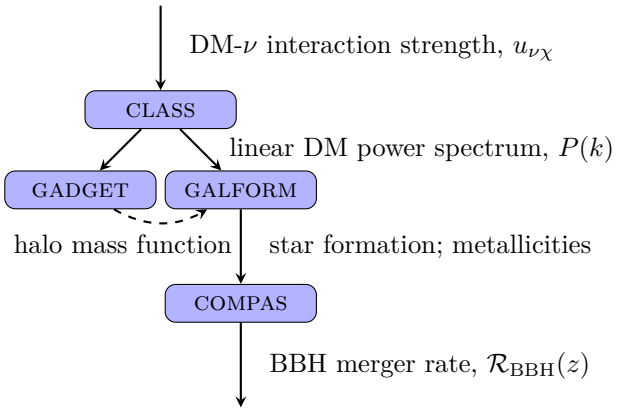

Figure 7.2: *An illustration of our pipeline. Linear power spectra of IDM scenarios are computed using CLASS, which are then fed into GADGET and GALFORM as initial conditions. The GALFORM output is cross-checked with the halo mass function from GADGET and fed into COMPAS, which computes the gravitational-wave event rate.*

as well as DM interactions with itself [352, 356, 360–369], with photons [144, 148, 149, 352, 353, 356, 357, 359, 371, 372, 375–379, 658], baryons [352, 355, 356, 370–372, 374, 665–668], and dark radiation [373, 663, 855, 916–923, 980]. The FDM and baryon-IDM models may need more detailed analysis to confirm that their impact on baryons on subgalactic scales does not fundamentally differ from CDM.

7.2 Interacting dark matter

We consider the case in which the dark matter scatters elastically with (massive) neutrinos, via a constant, velocity-independent cross-section σ_0 as described in [1]. This kind of interaction can

be realised in some particle physics theories beyond the Standard Model [197, 220, 358, 892]. From the phenomenological perspective, however, the cosmological dynamics of this interaction can be captured by a single parameter, the interaction strength, normally parameterised in terms of the dimensionless quantity [1, 353, 660, 661]

$$u_{\nu\chi} \equiv \frac{\sigma_0}{\sigma_{\rm Th}} \left(\frac{m_\chi}{100\,{\rm GeV/c^2}} \right)^{-1}, \tag{7.1}$$

where m_χ is the DM mass, σ_0 the interaction cross-section, and $\sigma_{\rm Th} \approx 6.65 \times 10^{-29}\,{\rm m}^2$ is the Thomson scattering cross-section. The case of DM-massive neutrino interaction was previously implemented in the Einstein-Boltzmann solver CLASS [67, 635] in [1], which we use in this work to generate the linear matter power spectra for our IDM scenarios.

As noted earlier, the interaction suppresses the matter power spectrum below a certain scale, similar to the predictions of WDM scenarios. As collisions occur between dark matter and neutrinos, the former is prevented from collapsing to form structures, leading to a suppressed linear matter power through collisional damping. This type of damping is physically distinct from free-streaming in WDM scenarios, where the large initial velocities result in the WDM particles escaping from initial overdensities. It is also distinct from the damping seen in FDM scenarios, which arises from quantum pressure hindering gravitational collapse. In general, the stronger the coupling, the later the DM decouples from the neutrinos and hence the larger the scales affected (see Fig. 7.1). Observe also that IDM scenarios predict in addition prominent acoustic oscillations at higher wavenumbers. The origin of these acoustic oscillations is analogous to the baryon acoustic oscillations (BAO) from the coupling of photons and baryons at early times, and the scale at which the oscillations appear is again governed by the dark matter and neutrino decoupling times.

Cosmic microwave background (CMB) anisotropy and BAO measurements currently constrain the DM-neutrino interaction strength to $u_{\nu\chi} \lesssim 10^{-4}$ (95% C.L.) [1]. Including Lyman-α forest measurements strengthens the bound to $u_{\nu\chi} \lesssim 10^{-5}$ (95% C.L.), albeit with an apparent $\sim 3\sigma$ preference for a non-zero value centred around $u_{\nu\chi} \sim 5 \times 10^{-5}$ [943] (although other studies claim to rule out WDM with similar suppression [981, 982]). Given these constraints on $u_{\nu\chi}$, the interaction only occurs at appreciable rates at redshifts $z \gg 1000$. At $z \lesssim 1000$, the DM particles are effectively collisionless and cold as in standard CDM, and hence amenable to standard N-body simulations of nonlinear structure formation.

7.3 Simulating structure formation

Our modelling of nonlinear structure is based on a combination of semi-analytic computations and N-body simulations. We use the semi-analytic model of structure formation GALFORM, first introduced in [883], which provides a flexible and computationally inexpensive way to produce synthetic realisations of galactic populations in a cosmological setting. The latest version [888] includes a large variety of astrophysical processes [884–887] to accurately model galaxy formation and evolution.

We generate merger trees using the Monte Carlo technique described in [886] (which is itself based on the extended Press-Schechter (EPS) theory, and is calibrated to the results of N-body simulations). In models in which the linear power spectrum $P(k)$ has a cutoff, as in our IDM scenario, a small correction is required to the EPS formalism: to obtain the variance of the density field $\sigma(M_{\rm h})$, $P(k)$ needs to be convolved with a sharp k-space filter rather than with the real-space top-hat filter used for CDM [772]. Using our Monte-Carlo technique rather than N-body simulations to generate merger trees has the advantage that IDM scenarios can be studied

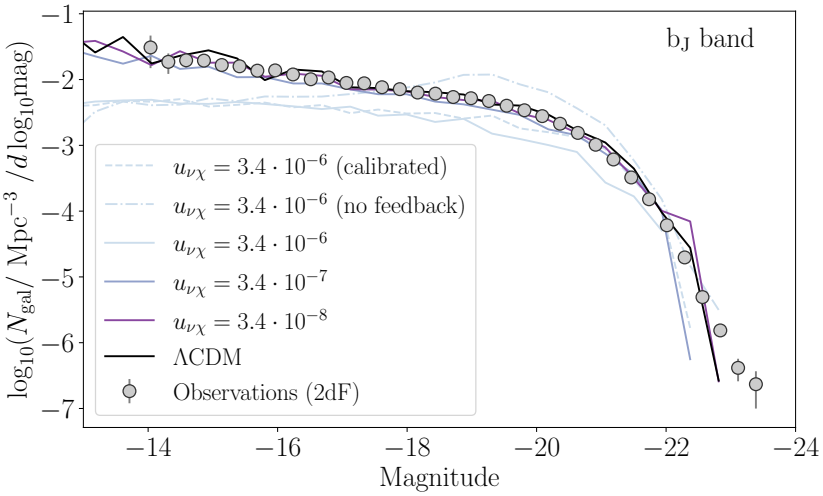

Figure 7.3: *Galaxy luminosity functions in the b_J band for several IDM scenarios of different interaction strengths. Observational data are from the 2dF survey [983]. It is evident that while the more weakly-interacting IDM scenarios and ΛCDM are roughly consistent with observations, the $u_{\nu\chi} \sim 10^{-6}$ case deviates significantly, and even in the case with feedback turned off, cannot reproduce the low luminosity tail, despite overpredicting at high luminosities. This corresponds to a slightly weaker interaction than the preferred value of $u_{\nu\chi} = 5.5^{+2.6}_{1.1} \times 10^{-6}$ from [943]. We do not show even more strongly-interacting IDM scenarios, as these deviate from observations even further.*

at minimum computational expense while avoiding the complication of spurious fragmentation in filaments that occurs in N-body simulations with a resolved cutoff in $P(k)$ (e.g., [827, 828]).

We calibrate the astrophysical parameters in GALFORM to obtain the best possible fit to observational data for ΛCDM. In particular, we adjust parameters controlling the strength of supernova feedback to achieve the best possible match to the $z = 0$ galaxy luminosity functions in the b_J and K-bands, using observational data from [983, 984]. We find that for IDM scenarios with $u_{\nu\chi} < 10^{-6}$, the same parameters used for ΛCDM provide an equally good fit to the observational data. For $u_{\nu\chi} \gtrsim 10^{-6}$, however, the feedback strength (as a function of halo mass) has to be reduced significantly to obtain the best possible fit. As shown in Fig. 7.3, this is still a worse fit than for the more weakly-interacting scenarios, particularly for galaxies fainter than -19$^{\rm th}$ magnitude. We find that it is impossible for scenarios with $u_{\nu\chi} \gtrsim 10^{-5}$ to produce realistic galaxy distributions, since even with all astrophysical feedback mechanisms suppressing galaxy formation turned off, not enough galaxies are produced. The failure to reproduce the observed galaxy luminosity functions at $z = 0$ therefore already poses a stronger constraint on $u_{\nu\chi}$ than the previous tightest bounds from Lyman-α and rules out the preferred value of $u_{\nu\chi} = 5.5^{+2.6}_{1.1} \times 10^{-6}$ found in [943].

To ensure the validity of our GALFORM results, we compute the merger trees with two different mass resolution settings, which determine the smallest tracked progenitor halos. As shown in Fig. 7.4, our "standard" resolution is well below the minimum halo mass expected to form in IDM models with interaction strength $u_{\nu\chi} > 10^{-6}$. For the models with weaker interactions ($u_{\nu\chi} \leq 10^{-7}$), the resolution is not high enough to capture the formation of the smallest haloes, though it does capture a large part of the suppression in the $u_{\nu\chi} \sim 10^{-7}$ case. This motivates our choice of the "high" resolution halo merger trees. Conveniently, this corresponds nearly exactly with the atomic hydrogen cooling limit, which marks the lowest mass haloes expected to form stars [985]. This means that, although even our high-resolution halo merger trees don't resolve the smallest haloes expected to form in the models with $u_{\nu\chi} < 10^{-7}$, we are still able to capture

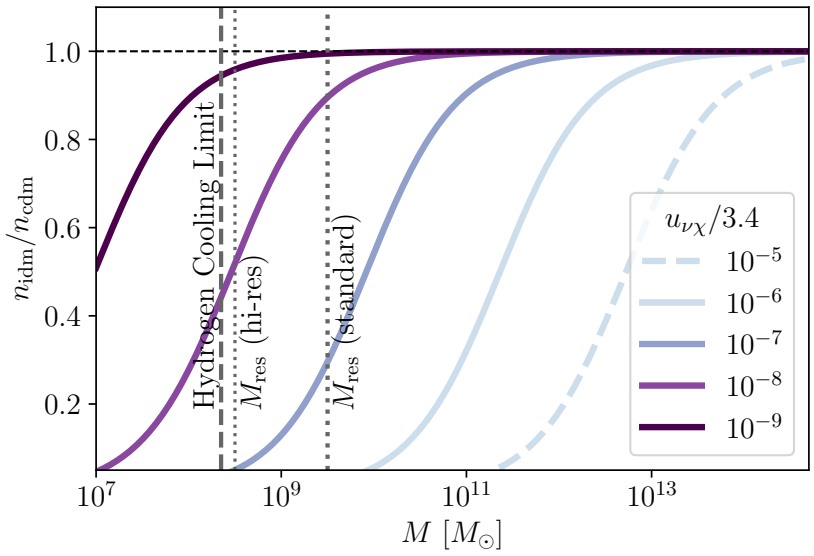

Figure 7.4: *The suppression of the halo mass function, as described by Eq.* (7.2)*, for a range of interaction strengths. The dotted lines show the mass resolution of our* GALFORM *merger trees for both the standard and high-resolution settings, while the dashed line shows the atomic hydrogen cooling limit, below which star formation is not expected [985].*

the majority of the star formation expected to occur in these models.

To ensure that GALFORM accurately predicts the halo mass function of the IDM scenarios, we cross-check it by performing N-body simulations using a version of GADGET-4 [742] modified to include the effects of massive neutrinos [732] and initialised with the matter power spectra of the IDM scenarios of Fig. 7.1. See Section 7.3.1 for details of our N-body simulations. We find that the GALFORM and N-body results are compatible with each other to the $\sim \mathcal{O}(10\%)$ level in the mass range over which we generate merger trees using the Monte Carlo technique.

7.3.1 N-body simulations and the halo mass function

Our simulations are performed using a modified version of GADGET-4 [742], which includes massive neutrinos via the SUPEREASY linear response method of [732]. GADGET-4 is a massively parallel N-body code supporting both collisionless (gravity-only) simulations and hydrodynamical simulations for baryonic matter and star formation. We restrict ourselves to collisionless simulations, which suffice for the purpose of cross-checking the GALFORM halo mass function output. Initial conditions are generated at $z = 49$ using the built-in NGENIC implementation, with linear matter power spectra from our modified version of CLASS as input. For interaction strengths allowed by current cosmological data, dark matter-neutrino decoupling happens at redshifts $z \gg 1000$, well before the simulation initialisation time. Thus, the interaction affects non-linear structure formation only through initial conditions, and there is no need to modify the main body of GADGET-4 itself.

To probe the effects of our IDM scenario at a range of scales, we run our simulations using $N = 512^3$ particles in several different box sizes, $(50\,\mathrm{Mpc})^3$, $(100\mathrm{Mpc})^3$, $(500\mathrm{Mpc})^3$, and $(1\mathrm{Gpc})^3$, for different values of the interaction strength $u_{\nu\chi}$, including a non-interacting ($u_{\nu\chi} = 0$) set. All other cosmological parameters are kept fixed to the CMB+BAO best-fit values found in [1]. We also perform a set of simulations using the best-fit parameters found in [943], which is phenomenologically similar to our $u_{\nu\chi} = 3.4 \times 10^{-6}$ scenario.

We use the friends-of-friends algorithm to identify haloes in our simulations. For halo

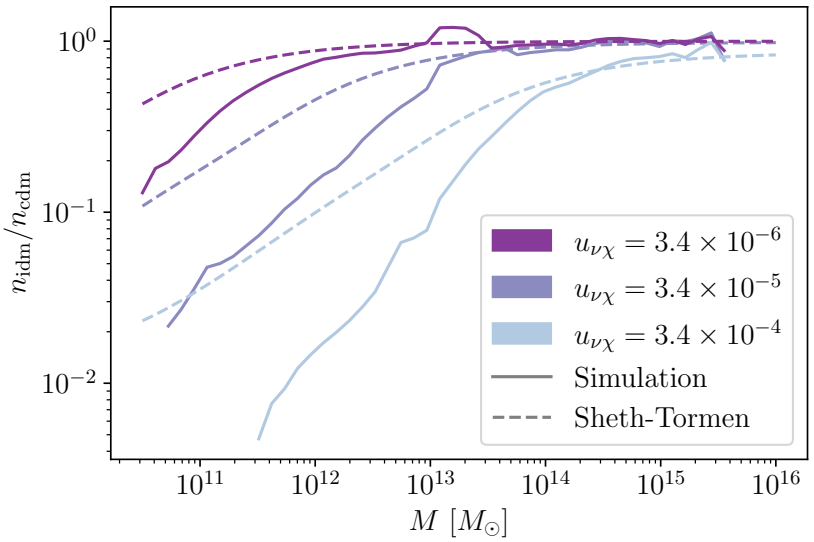

Figure 7.5: *IDM halo mass function $n_{\rm idm}$ normalised to a reference CDM mass function $n_{\rm cdm}$ for various interacting strengths $u_{\nu\chi}$, computed from N-body simulations (solid lines) and the Sheth-Tormen formalism (dashed lines). The choice of $u_{\nu\chi} = 3.4 \times 10^{-4}$ has been motivated by the CMB+BAO constraint found in Ref. [1]. It is evident that the standard Sheth-Tormen halo mass function does not provide a good description of our simulation results.*

masses we use the convention M_{200c}, i.e., the mass contained within a sphere with mean density 200 times the critical density of the universe. The haloes from each simulation are sorted into 30 evenly-spaced logarithmic mass bins to obtain the halo number density per mass bin, i.e., the halo mass function. As is well described in the literature (see, e.g., [827–829, 831, 986]), the halo mass function of cosmologies with a small-scale cut-off exhibits unphysical discreteness effects on small scales (relative to the box size). We therefore conservatively choose to disregard the low-mass end of each halo mass function thus constructed, cutting it off just above the scale at which discreteness effects become evident. Then, to produce a halo mass function that spans a range of mass scales, we simply stitch together the pieces obtained from our different box-size runs.

We have attempted to describe the IDM halo mass functions semi-analytically using the Sheth-Tormen mass function, with the IDM linear matter power spectra as input and a real-space spherical tophat filter for smoothing. However, as is evident in Fig. 7.5, the Sheth-Tormen mass function thus constructed fails to capture the low-mass suppression relative to the CDM case seen in our N-body simulation results. We therefore forego the Sheth-Tormen approach completely, opting instead to use a fitting function to describe the suppression relative to the CDM case.

We find the following fitting function to serve the purpose well:

$$\frac{n_{\rm idm}}{n_{\rm cdm}} = \frac{1}{1 + \left(\frac{M_\beta}{M}\right)^\alpha}, \tag{7.2}$$

where $M_\beta \equiv (4\pi)\bar{\rho}_m / 3k_\beta^{-3}$ is the mass corresponding to the wave number k_β at which the linear matter power spectrum of an IDM scenario is suppressed by $\beta\%$ relative to the CDM case, $\bar{\rho}_m$ is the comoving mean matter density, and the parameters α and β are to be determined by fitting Eq. (7.2) to our N-body results. The fit is achieved by forming and then minimising a

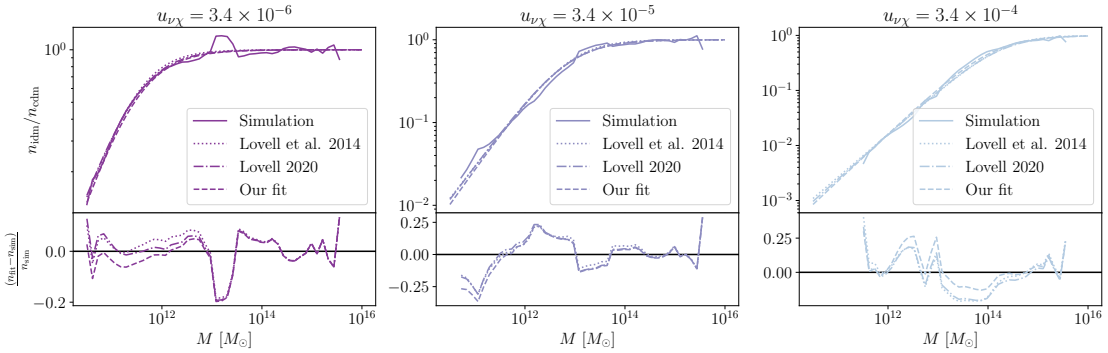

Figure 7.6: *IDM halo mass function $n_{\rm idm}$ normalised to a reference CDM mass function $n_{\rm cdm}$ for three interacting strengths $u_{\nu\chi}$. Solid lines denote results from N-body simulations; dashed lines represent our fitting function Eq.* (7.2)*; dotted and dot-dash lines are two fitting functions from Refs. [828, 987]. The bottom panel of each plot shows the fractional residuals of the three fitting functions.*

$u_{\nu\chi}$	$M_{10}/M_\odot$	k_{10}/h Mpc^{-1}
3.4×10^{-4}	1.0×10^{14}	0.17
3.4×10^{-5}	5.3×10^{12}	0.46
3.4×10^{-6}	2.3×10^{11}	1.3
3.4×10^{-7}	8.3×10^{9}	4.0
3.4×10^{-8}	2.9×10^{8}	12
3.4×10^{-9}	9.6×10^{6}	38

Table 7.1: *IDM interacting strengths and the corresponding suppression mass scale M_β that appears in the fitting function Eq.* (7.2) *for the halo mass function. We find $\beta = 10$ to be the best-fit value against simulation results. k_{10} is the corresponding k-scale.*

figure-of-merit (FoM) of the form

$$\mathrm{FoM} = \sum_M \left(\log_{10} \left(\frac{n_{\rm idm}}{n_{\rm cdm}} \right)_{\rm fit} - \log_{10} \left(\frac{n_{\rm idm}}{n_{\rm cdm}} \right)_{\text{N-body}} \right)^2 , \tag{7.3}$$

and fitting Eq. (7.2) to our $u_{\nu\chi} = 3.4 \times 10^{-4}$, 3.4×10^{-5}, and 3.4×10^{-6} simulation results simultaneously.

We find the best-fit values to be $\alpha = 0.9$ and $\beta = 10$. The fit is displayed against simulation results in Fig. 7.6. We also give in Table 7.1 the M_{10} values corresponding to several interacting strengths $u_{\nu\chi}$. To confirm the robustness of the fit, we test the fitting function Eq. (7.2) against simulations at several low $u_{\nu\chi}$ values outside of the calibration range, and find the fit to be accurate to better than $\sim 10\%$.

Finally, we remark that extended Press-Schechter formalism used in GALFORM does not exactly use our fitting function, but produces a halo mass function that matches it to the same or better precision, as the fitting function matches the simulations.

7.4 Gravitational-wave event rates

Our key observable is the redshift-dependent BBH merger rate density $\mathcal{R}_{\rm BBH}(z)$. In principle we could also use our simulations to study the merger rates of binary neutron stars and black hole-neutron star binaries; however, these are only detectable at lower redshifts due to their smaller masses and correspondingly weaker gravitational-wave signals. They are thus a less sensitive as a probe of the high-redshift suppression effects we are interested in.

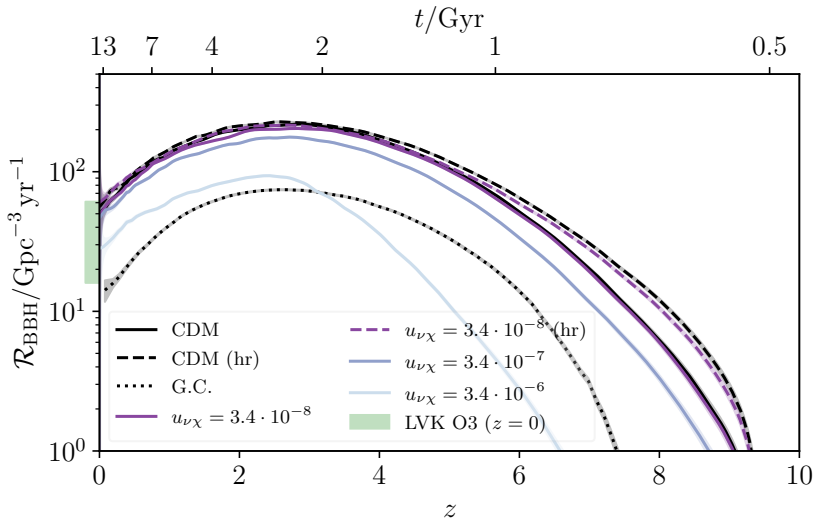

Figure 7.7: *The binary black hole merger rate density over cosmic time, as predicted by our pipeline for ΛCDM and a range of IDM scenarios. The local $z = 0$ rate (90% C.L.) inferred from LIGO/Virgo observations [991] is shown as a green band. Curves marked "hr" are high resolution, meaning that the* GALFORM *merger trees are tracked to smaller progenitor masses. The curve marked "G.C." is the contribution from globular clusters in the non-interacting scenario.*

Stellar-mass BBH mergers are thought to form primarily through isolated binary evolution, in which massive binary stars end their lives as black holes and radiate orbital energy through gravitational-wave emission until they eventually merge, generating an observable gravitational-wave event [988]. The BBH merger rate is thus essentially a delayed tracer of star formation, whose normalisation depends on the efficiency with which massive binary stars are converted into BBHs. This efficiency is mostly determined by the stellar metallicity (i.e., the fraction of the stellar mass that is in elements heavier than helium).

We model the merger rate using the binary population synthesis code COMPAS [977–979], which generates a synthetic BBH population by sampling individual stellar binaries from initial mass and metallicity distributions and evolving them over cosmic time. COMPAS tracks the stellar and orbital evolution of each binary, accounting for a range of physical processes such as stellar winds, mass transfer, BH formation at the end of each star's lifetime, and subsequent shrinking of the orbit via gravitational-wave radiation reaction. We use a COMPAS dataset of 20 million evolved binaries (resulting in ≈ 0.7 million BBHs) presented in [977], which is publicly available at [989]. This gives us the BBH formation efficiency as a function of initial mass and metallicity, as well as the delay time between star formation and BBH merger. By combining this with a model for the star formation rate density and metallicity distribution as functions of redshift, we can use the COMPAS "cosmic integration" module [990] to average over the synthetic population and obtain the cosmic BBH merger rate. These inputs are typically phenomenological models chosen to fit low-redshift observational data. In our case, we instead use the star formation rates and metallicity distributions generated by GALFORM, allowing us to model how the BBH rate changes as we vary the underlying dark matter model.

Our key results for the BBH merger rate are shown in Fig. 7.7. In addition to the baseline ΛCDM case, we consider a range of IDM models with $u_{\nu\chi} = 3.4 \times \{10^{-6}, 10^{-7}, 10^{-8}\}$ (recall that models with stronger DM-ν interactions than this are unable to reproduce the galaxy luminosity function data shown in Fig. 7.3). The factor of 3.4 comes from the CMB+BAO limits in [1]; we

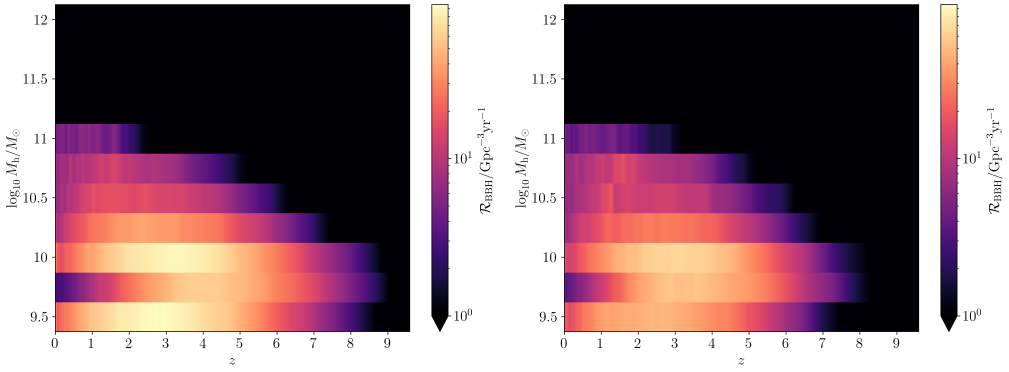

Figure 7.8: *BBH merger rate as a function of redshift and host halo mass, in both the (standard-resolution) CDM case and the* $u_{\nu\chi} \sim 10^{-7}$ *case.*

have chosen interaction strength values that are whole factors of 10 smaller. The rates that we obtain depend on the mass resolution of our GALFORM merger trees, with finer resolution allowing us to access additional star formation taking place in smaller haloes, resulting in a greater total number of BBHs. Most of the results shown in Fig. 7.7 use a benchmark mass resolution of $M_{\rm h} \geq 10^{9.5}\,M_\odot$, but we additionally show results for CDM and for $u_{\nu\chi} = 3.4 \times 10^{-8}$ at a finer resolution of $M_{\rm h} \geq 10^{8.5}\,M_\odot$. At this mass resolution, we are able to resolve the majority of the star formation in the Universe (under the assumption that it takes place through the cooling of atomic hydrogen), except for that from the ultrafaint dwarf population. We do not anticipate these galaxies to contribute significantly to the overall BBH merger rate.

One limitation of our approach is that COMPAS only accounts for BBHs formed through isolated binary evolution, neglecting other sub-dominant formation channels such as dynamical capture in dense stellar environments [988, 992] (globular clusters [993], nuclear star clusters [994], etc.) or in AGN disks [995], as well as the possible presence of primordial BBHs [568]. However, these additional merger channels can be safely neglected in a first analysis, as they are expected to be sub-dominant compared to the contribution from isolated binary evolution. For example, Fig. 7.7 shows the contribution from dynamical BBH assembly in globular clusters, as calculated in [996] by combining cluster N-body simulations [997] with a semi-analytical cosmological model of globular cluster abundances [998]. We see that the rate of BBH mergers from globular clusters is subdominant at all redshifts, justifying our focus here on isolated binary evolution. In principle, however, one could incorporate sub-dominant channels such as these into our analysis with additional modelling, e.g., so that we capture the suppression of globular cluster abundances due to IDM.

7.4.1 BBH merger rate as a function of host halo mass

The advantage of our proposed method for constraining dark matter models is that it allows us to target the high-redshift, low-mass haloes that are most strongly suppressed in these models. This is highlighted in Fig. 7.8, where we break the total redshift-dependent BBH merger rate down into bins in halo mass for CDM and for an IDM model with $u_{\nu\chi} \sim 10^{-7}$. We see that the strongest contribution to the observed merger rate, across all redshifts, comes from light haloes, $M_{\rm h} \lesssim 10^{10}\,M_\odot$. These are precisely the haloes that are suppressed for DM-ν interactions on the order of $u_{\nu\chi} \sim 10^{-7}$ (c.f. Fig. 7.4), which explains why the BBH merger rate is a useful probe of this suppression.

In particular, we see in Fig. 7.8 that the suppression is most apparent at high redshifts,

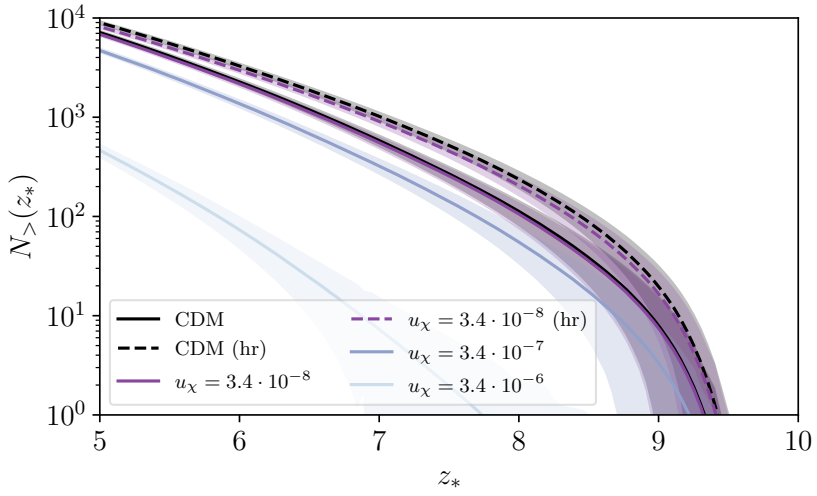

Figure 7.9: *Expected number of BBH mergers observed with estimated redshift larger than z_*, using one year of observations with a third-generation interferometer network (Einstein Telescope plus two Cosmic Explorers), taking into account the forecast redshift uncertainty and signal-to-noise for the expected BBH population. The shaded regions show the statistical uncertainty (99% C.L.) due to Poisson fluctuations in the number of BBHs, and 'hr' means high resolution, signifying that the* GALFORM *merger trees are tracked to smaller progenitor masses.*

$z \gtrsim 7$. This again highlights the advantages of our method, as galaxies in these light haloes are challenging to observe directly at such high redshift, even with JWST. For instance, at $z \gtrsim 7$ the observational limit for JWST assuming a Hubble Ultra Deep Field-like survey is around $M_\star \sim 10^{7.5}\,M_\odot$, or $M_\mathrm{h} \sim 10^{9-10}\,M_\odot$ [999, 1000] depending on the stellar-to-halo mass relation assumed. Even under the assumption of this optimistic scenario, the BBH merger rate technique allows us, in principle, to probe halo masses one to two orders of magnitude lower.

7.4.2 Future gravitational-wave detection forecasts

In order to convince ourselves that these differences in the high-z BBH merger rate will be detectable with future gravitational-wave observatories, we compute forecasts for the expected number of BBHs, $N_>(z_*)$, detected above a given threshold redshift z_*, as well as the expected uncertainty in this quantity due to Poisson fluctuations in the number of BBHs at each redshift as well as redshift measurement errors. (This is based on the "cut-and-count" method discussed in [1001].) We assume one year of observations with a third-generation interferometer network consisting of Einstein Telescope [1002] and two Cosmic Explorers [1003], accounting for the detection efficiency and redshift uncertainty associated with this network. As shown in Fig. 7.9, we can clearly distinguish between the different $N_>(z_*)$ predictions, allowing us to confirm or rule out a small-scale suppression of the scale caused by DM-neutrino interactions down to the level of $u_{\nu\chi} \sim 10^{-7}$.

Figure 7.9 clearly demonstrates that the main limitation to the cosmological information we can extract from future gravitational-wave detections is not statistical uncertainty, but systematics associated with modelling choices. In particular, since the observational study of BBHs is still at an early stage, there are numerous astrophysical uncertainties associated with the stellar physics that governs isolated binary evolution. We return to this issue later in this section, where we investigate the impact of these uncertainties and show that they are not degenerate with the DM suppression effect.

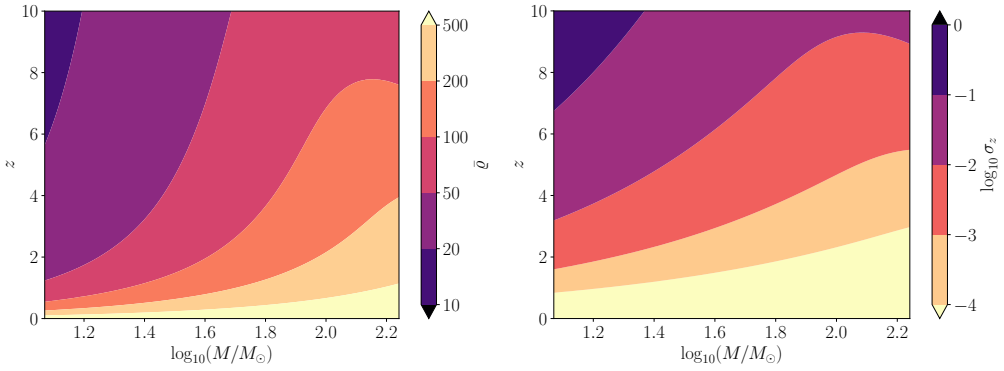

Figure 7.10: *Left panel: mean signal-to-noise ratio* $\bar{\varrho} = \sqrt{(h|h)}$ *of equal-mass non-spinning BBHs detected with our third-generation interferometer network, as a function of redshift* z *and total source-frame mass* M*. Right panel: forecast redshift uncertainty* $\sigma_z = \sqrt{(F^{-1})_{zz}}$ *for the same parameter space. The mass range in both panels is truncated at the boundaries of our broken-power-law mass distribution (*$12\,M_\odot < M < 174\,M_\odot$*).*

Our key observable quantity is constructed as follows: we choose some redshift threshold z_*, and define $N_>(z_*)$ as the number of detected BBHs whose best-fit inferred redshift falls above this threshold, $\hat{z} > z_*$. Our results show that different dark matter scenarios will predict different values of $N_>$. We can predict whether these models are distinguishable in a given observational scenario by forecasting the corresponding uncertainty on $N_>$.

It is straightforward to write down the mean value of this quantity,

$$\begin{aligned}\bar{N}_>(z_*) = T_{\rm obs} \int_0^\infty {\rm d}z\, \frac{{\rm d}V}{{\rm d}z} \frac{\bar{\mathcal{R}}(z)}{1+z} \\ \times \int {\rm d}\boldsymbol{\theta}\, p_{\rm pop}(\boldsymbol{\theta}|z) P_{\rm det}(z,\boldsymbol{\theta}) P_>(z,\boldsymbol{\theta}|z_*).\end{aligned} \tag{7.4}$$

Here, $T_{\rm obs}$ is the total observing time, V is the comoving volume as a function of redshift, $\bar{\mathcal{R}}$ is the mean BBH merger rate density as a function of redshift, $\boldsymbol{\theta}$ is a vector of BBH parameters (masses, spins, etc.) with population distribution $p_{\rm pop}(\boldsymbol{\theta}|z)$ (which we allow to evolve over redshift), $P_{\rm det}(z,\boldsymbol{\theta})$ is the probability of detecting a BBH with parameters $\boldsymbol{\theta}$ at redshift z, and $P_>(z,\boldsymbol{\theta}|z_*)$ is the probability of inferring a best-fit redshift greater than z_* for the same BBH, the width of which encapsulates redshift measurement uncertainties for a given GW detector network. We describe how to calculate each of these probabilities below.

In order to calculate the variance of $N_>$, we assume that the number, n, of BBH signals emitted from a comoving volume V in a source-frame time $T = T_{\rm obs}/(1+z)$ is a Poisson random variable with mean $\bar{n} = VT\bar{\mathcal{R}}$. We further assume that Poissonian fluctuations in the BBH rate at different redshifts are uncorrelated with each other. This allows us to write the covariance matrix between these BBH number counts as

$${\rm Cov}[n(z), n(z')] = \delta(z-z'){\rm Var}[n(z)] = \delta(z-z')\bar{n}(z). \tag{7.5}$$

We thus find that

$$\begin{aligned}{\rm Var}[N_>(z_*)] = T_{\rm obs} \int_0^\infty {\rm d}z\, \frac{{\rm d}V}{{\rm d}z} \frac{\bar{\mathcal{R}}(z)}{1+z} \\ \times \left[\int {\rm d}\boldsymbol{\theta}\, p_{\rm pop}(\boldsymbol{\theta}|z) P_{\rm det}(z,\boldsymbol{\theta}) P_>(z,\boldsymbol{\theta}|z_*)\right]^2,\end{aligned} \tag{7.6}$$

which shows that $N_>$ is *not* itself Poissonian, since its mean and variance are unequal so long as the $\boldsymbol{\theta}$ integral is not equal to unity.

We assume the BBH signals are detected using a matched-filter search, in which the detection statistic is a noise-weighted inner product of the data d with the signal template h,

$$(d,h) \equiv 4\,\mathrm{Re}\int_0^\infty \mathrm{d}f\,\frac{\tilde{d}(f)\tilde{h}^*(f)}{S(f)}, \tag{7.7}$$

with $S(f)$ the noise power spectral density of the detector. In Gaussian noise, the signal-to-noise ratio (SNR) ϱ of the search is then approximately a Gaussian random variable with unit variance and mean $\bar{\varrho} = \sqrt{(h,h)}$; so for example, having $\bar{\varrho} = 5$ would constitute a 5σ detection in this idealised scenario. In reality, the noise is not Gaussian, and we require a larger SNR in order to confidently discriminate a BBH from various non-Gaussian noise transients. A commonly-adopted detection threshold is $\bar{\varrho} \geq 8$. We can therefore write the detection probability as

$$\begin{aligned} P_\mathrm{det}(z,\boldsymbol{\theta}) &= \int_8^\infty \frac{\mathrm{d}\varrho}{\sqrt{2\pi}}\exp\left[-\frac{1}{2}(\varrho - \bar{\varrho}(z,\boldsymbol{\theta}))^2\right] \\ &= \frac{1}{2}\left[1 + \mathrm{erf}\left(\frac{\bar{\varrho}(z,\boldsymbol{\theta}) - 8}{\sqrt{2}}\right)\right], \end{aligned} \tag{7.8}$$

which interpolates between (almost) zero for faint signals and (almost) one for strong signals, with a characteristic width set by the randomness of the observed SNR.

We approximate the redshift inference using a Fisher forecast. The Fisher matrix for parameters θ_i (including z) of the signal model $h(\theta_i)$ is given by

$$F_{ij} \equiv \left(\frac{\partial h}{\partial\theta_i}, \frac{\partial h}{\partial\theta_j}\right). \tag{7.9}$$

In the strong-signal limit, the inferred redshift $\hat{z}$ is a Gaussian random variable with mean equal to the true redshift z, and standard deviation given by the inverse Fisher matrix,

$$\sigma_z(z,\boldsymbol{\theta}) = \sqrt{(F^{-1})_{zz}}. \tag{7.10}$$

We therefore have

$$P_>(z,\boldsymbol{\theta}|z_*) = \frac{1}{2}\left[1 + \mathrm{erf}\left(\frac{z - z_*}{\sqrt{2}\sigma_z}\right)\right], \tag{7.11}$$

which interpolates between (almost) zero for nearby BBHs and (almost) one for distant BBHs, with a width set by σ_z.

In order to evaluate the expected SNR $\bar{\varrho}$ and the redshift uncertainty σ_z, we need a signal model $h(\boldsymbol{\theta}, z)$. For this, we use the phenomenological hybrid waveform model of [1004]. For simplicity, we assume that the BBHs are all equal-mass and non-spinning (as is approximately true for most of the BBHs detected by LIGO/Virgo thus far [482]), and we average out all of the extrinsic parameters (sky location, polarisation angle, inclination, etc.). This reduces the number of relevant parameters to just two: the redshift z and the total mass M. In terms of these parameters, the frequency-domain waveform model can be written as

$$\begin{aligned} \tilde{h}(f) &= \mathrm{e}^{\mathrm{i}\Psi(f)}\left(\frac{\pi}{30}\right)^{1/2}\frac{(GM)^2}{2r}(\pi GMf_\mathrm{merge})^{-7/6} \\ &\quad\times\begin{cases} (f/f_\mathrm{merge})^{-7/6} & f < f_\mathrm{merge} \\ (f/f_\mathrm{merge})^{-2/3} & f_\mathrm{merge} \leq f < f_\mathrm{ring} \\ \frac{(f_\mathrm{ring}/f_\mathrm{merge})^{-2/3} f_\mathrm{width}^2}{(f-f_\mathrm{ring})^2 + f_\mathrm{width}^2} & f_\mathrm{ring} \leq f < f_\mathrm{cut} \end{cases}, \\ \Psi(f) &= \varphi_0 + \sum_{k=0}^{7}\psi_k(\pi GMf)^{(k-5)/3}, \end{aligned} \tag{7.12}$$

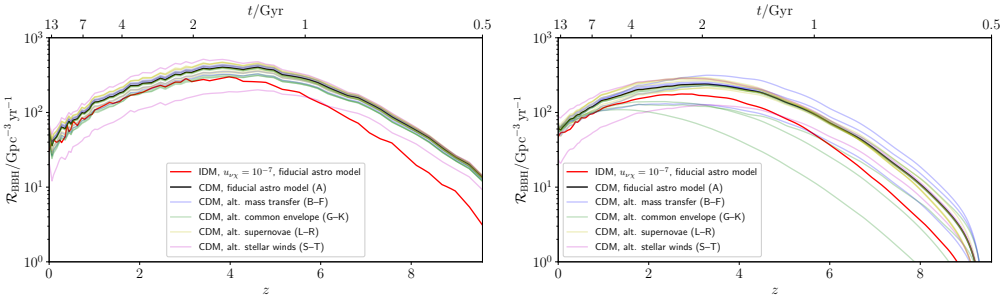

Figure 7.11: *Formation rate (left panel) and merger rate (right panel) of BBHs in 21 different scenarios: a fiducial CDM model, an IDM model with $u_{\nu\chi} \sim 10^{-7}$ and fiducial astrophysical settings, and 19 alternative CDM models in which various* COMPAS *parameters are varied.*

where $f_{\rm merge}$, $f_{\rm ring}$, $f_{\rm cut}$, $f_{\rm width}$, φ_0, and $\{\psi_k\}$ are all constants given in [1004]. This expression is appropriate for $z \to 0$; in order to generalise to arbitrary redshift we simply replace $r \to d_L(z)$ (with d_L the luminosity distance), $M \to (1+z)M$, and $f \to f/(1+z)$ for all of the frequencies.

We can now use this waveform to compute the expected SNR $\bar{\varrho}$ and the redshift uncertainty σ_z (the latter of which involves computing and inverting the 2×2 Fisher matrix for the mass and redshift), as shown in Fig. 7.10. The final missing ingredient to calculate $N_>$ and its variance is the population distribution of the BBH masses, for which we use the best-fit broken-power-law model from [1005], which transitions from a shallow $m^{-1.58}$ power law at low masses ($5.9\,M_\odot < m < 41\,M_\odot$) to a steeper one, $m^{-5.59}$, at large masses ($41\,M_\odot < m < 87\,M_\odot$). Here m is the source-frame mass of each individual black hole, so $M = 2(1+z)m$.

7.4.3 Varying astrophysical model parameters

While our results show that the high-z BBH merger rate is sensitive to DM microphysics, it undoubtedly also depends on the astrophysical modelling choices we have made in our pipeline. In order to investigate the extent to which variations in these choices are degenerate with the DM suppression effect, we use the COMPAS simulation data from [1006] (publicly available at [1007]), consisting of 19 alternative models in which the binary stellar evolution modelling is systematically modified, isolating the effects of mass transfer, common envelopes, supernovae, and stellar winds. We focus on modifications to COMPAS modelling choices rather than those in GALFORM, as the latter are currently much more tightly constrained by fitting to observational data. In fact, the predictive power of the GALFORM model is enhanced by the fact that the same set of parameters that show consistency with low redshift observational data also predict reasonably accurate galaxy abundances at high redshift (relevant to the epochs of interest in this paper) across multiple wavelengths [1008–1010].

In Fig. 7.11 we show the BBH formation rate and merger rate in 21 different scenarios: our fiducial CDM model ("A"), 19 alternative CDM models ("B"–"T") with alternative modelling of binary stellar evolution, and a fiducial IDM model with $u_{\nu\chi} = 3.4 \times 10^{-7}$. We see that the IDM model is clearly distinguished from the other 20 models in terms of its BBH *formation* rate, with a characteristic high-z suppression relative to these other models. However, the distinction between IDM and the other alternative models is blurred when considering the BBH *merger* rate, which we can understand as being due to the way these models modify the distribution of delay times between formation and merger.

Nonetheless, a more detailed analysis reveals that IDM is still distinguishable from the alternative models, even if we only have access to the BBH merger rate. To demonstrate this, we

define a parameterised merger rate model,

$$\mathcal{R}(z, \{\theta_i\}) = \mathcal{R}_{\rm A}(z) + \sum_i \theta_i [\mathcal{R}_i(z) - \mathcal{R}_{\rm A}(z)], \tag{7.13}$$

where the index i labels models IDM, B, C, ..., T. The case where $\theta_i = 0$ for all i corresponds to our fiducial model A, while having $\mathcal{R}$ equal to a particular alternative model corresponds to $\theta_i = 1$ for that case and $= 0$ otherwise. Between these special points in parameter space, (7.13) linearly interpolates between the 21 different models. We can therefore investigate the degeneracy between the different models by carrying out a Fisher analysis on the θ_i parameters. We stress that this is not intended to represent a realistic model of the BBH merger rate over the full space of astrophysical model parameters (this would require us to carry out simulations for a large number of points sampled from the 20+ dimensional parameter space, which is prohibitively expensive), but rather to provide an approximate tool for assessing the degeneracy of IDM suppression with astrophysical modelling choices.

To perform our Fisher analysis for the parameters $\{\theta_i\}$, we imagine sorting a large number of observed BBHs into redshift bins, and counting the number $N(z)$ in each bin.[3] We model these counts with a Gaussian likelihood,

$$-2\mathcal{L}(N|\{\theta_i\}) = \sum_{z\in\text{bins}} \frac{1}{\sigma_z^2} \big[N(z) - \bar{N}(z, \{\theta_i\})\big]^2 + \text{const.}, \tag{7.14}$$

where the mean count in each bin, $\bar{N}(z)$, is calculated from (7.4) using the parameterised merger rate (7.13), and the variance σ_z^2 is calculated from (7.6) using the fiducial rate $\mathcal{R}_{\rm A}$. (Recall that this variance includes redshift measurement errors.) The Fisher matrix is then

$$F_{ij} = \sum_{z\in\text{bins}} \frac{1}{\sigma_z^2} \big[\bar{N}_i(z) - \bar{N}_{\rm A}(z)\big] \big[\bar{N}_j(z) - \bar{N}_{\rm A}(z)\big]. \tag{7.15}$$

In Fig. 7.12 we show the covariance matrix, $\text{Cov}(\theta_i, \theta_j) = (F^{-1})_{ij}$, computed from Eq. (7.15) using 38 redshift bins of width $\Delta z = 0.25$ over the range $z \in [0, 9.25]$, assuming one year of observations with a third-generation GW interferometer network as described in the main text. We are particularly interested in the on-diagonal elements of this matrix, which indicate the measurement variance for each of the θ_i; roughly speaking, a variance significantly smaller than unity for a given model indicates that the BBH merger rate in that model can be distinguished from all other models with one year of data. We find that $\text{Var}(\theta_{\rm IDM}) \approx 0.18$, so that the DM suppression effect is *not* degenerate with the other models considered here, at least for an interaction strength of $u_{\nu\chi} \sim 10^{-7}$; in fact, IDM is the only model in which this is the case, indicating that the alternative models B–T are all degenerate with each other. This variance corresponds to a $\sim 2.3\sigma$ detection of the IDM suppression after one year of observations. Since the Fisher information grows linearly with observation time (see Eq. (7.4) and Eq. (7.6)), this implies a 5σ detection with $\sim 4.6\,\text{yr}$ of data.

7.5 Summary and conclusion

We have investigated the suppression of the merger rate of binary black holes in scenarios where dark matter scatters off of neutrinos, taking this as an example of a broader family of dark matter models in which structure is suppressed on small scales. Our predictions are based on

[3] These number counts are related to the "cut-and-count" quantity $N_>$ from the previous section by $N(z) = N_>(z_{\rm min}) - N_>(z_{\rm max})$, where $z_{\rm max}$, $z_{\rm min}$ are the upper and lower edges of bin z.

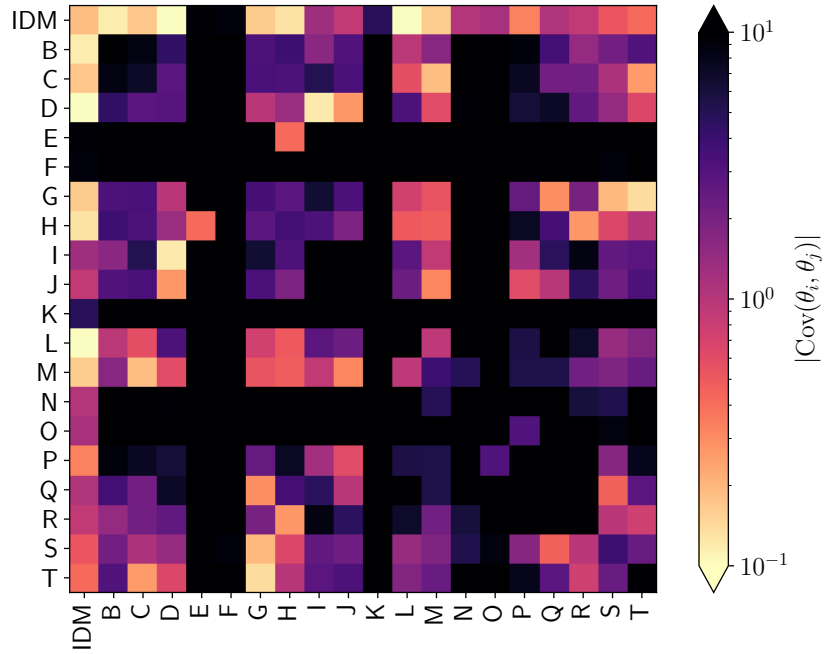

Figure 7.12: *Covariance of the θ_i parameters defined in* (7.13) *based on the Gaussian Fisher matrix Eq.* (7.15)*, assuming one year of observations with a third-generation GW interferometer network.*

a simulation pipeline (c.f. Fig. 7.2) that captures all of the crucial physical ingredients of the problem, from the initial (linear) matter power spectra, through the formation and evolution of galaxies, to a population of merging BBHs. Our key results are shown in Figs. 7.7 and 7.9, which respectively show the suppression of the BBH merger rate and demonstrate that this suppression will be detectable with next-generation gravitational-wave observatories.

All of the dark matter scenarios we consider are consistent with the local ($z = 0$) merger rate inferred by LIGO/Virgo, $\mathcal{R}_{\mathrm{BBH}}(z = 0) = [16\text{–}61]\,\mathrm{Gpc}^{-3}\,\mathrm{yr}^{-1}$ [482], with only a small suppression ($\lesssim 20\%$) of this local rate in the $u_{\nu\chi} \leq 3.4 \times 10^{-7}$ IDM scenarios compared to ΛCDM. At higher redshifts, however, we see that their differences become increasingly significant. Physically this reflects that most star formation takes place in smaller haloes at these early epochs, and these smaller haloes are where the effects of DM interactions are most pronounced. Even for interactions as weak as $u_{\nu\chi} = 3.4 \times 10^{-8}$ there is a small but visible difference from CDM in the predictions from our high-resolution simulations. Decreasing the interaction strength further down to $u_{\nu\chi} = 3.4 \times 10^{-9}$, however, makes the suppression scale so small that there are very few star-forming haloes that are missing compared to ΛCDM, and consequently the BBH merger rate for this scenario is essentially indistinguishable from that in ΛCDM.

To confirm that the different dark matter models can indeed be distinguished in this way, we have carried out a Fisher forecast for the redshift-dependent BBH number count $N_{>}(z_*)$, as shown in Fig. 7.9. We find that future observations with Einstein Telescope and Cosmic Explorer will allow us to confirm or rule out suppression caused by DM-neutrino interactions down to the level of $u_{\nu\chi} \sim 10^{-7}$.

The main challenge for this method is the significant astrophysical uncertainties in the modelling. We stress however that there is good reason to be optimistic regarding these systematic uncertainties: any changes to the binary evolution model will have an impact at *all* redshifts and should therefore have minimal degeneracy with the specific high-redshift suppression we

are targeting. We envisage that the very large numbers of BBHs detected by third-generation interferometers at low redshifts will be able to pin down the astrophysical modelling, allowing us to use the high-redshift tail as a sensitive probe of structure formation and dark matter. We demonstrate this explicitly by investigating 19 alternative COMPAS models [1006]; we find that the suppression effect from IDM (at the level of $u_{\nu\chi} \sim 10^{-7}$) can be confidently distinguished from each of these alternatives with next-generation GW observations. Similarly, we anticipate that uncertainties associated with the GALFORM modelling governing star formation and chemical enrichment will be reduced by comparing against future low-redshift observational data for faint galaxies, as well as high-redshift observations with, e.g., the James Webb Space Telescope [83], leaving little degeneracy with DM microphysics.

To conclude, we have shown that the binary black hole merger rate has the potential to become an important probe of deviations from the ΛCDM model, particularly the suppression of structure from dark matter interactions. As a by-product of our analysis, we have shown that dark matter–neutrino interactions with $u_{\nu\chi} \gtrsim 10^{-6}$ are already strongly in tension with the observed abundance of faint galaxies. With the next generation of gravitational-wave observatories probing the gravitational-wave event rate out to the earliest epochs of star formation, it will be possible to strengthen these constraints by another order of magnitude or more, giving us highly sensitive information about the earliest stages of nonlinear structure formation.

Author Contributions

The idea for this project was proposed by CB, MS and ACJ. MM performed the N-body simulations, halo-finding, and halo mass function analysis with input from YW, SB computed the galaxy populations, and ACJ made the gravitational-wave predictions. All authors contributed to every stage of the paper, including the writing.

Acknowledgments

The authors would like to thank Joe Silk for useful discussions, and Ilya Mandel for helpful correspondence about COMPAS. MS thanks the University of Sydney for its hospitality during the early stages of this project. ACJ was supported by the Science and Technology Facilities Council through the UKRI Quantum Technologies for Fundamental Physics Programme [grant number ST/T005904/1]. SB is supported by the UK Research and Innovation (UKRI) Future Leaders Fellowship [grant number MR/V023381/1]. MS is supported in part by the Science and Technology Facility Council (STFC), United Kingdom, under the research grant ST/P000258/1. Y^{3}W is supported in part by the Australian Government through the Australian Research Council's Future Fellowship (project FT180100031). The authors acknowledge the Sydney Informatics Hub and the use of the University of Sydney's high-performance computing cluster, Artemis. This work used the DiRAC@Durham facility managed by the Institute for Computational Cosmology on behalf of the STFC DiRAC HPC Facility (www.dirac.ac.uk). The equipment was funded by BEIS capital funding via STFC capital grants ST/P002293/1, ST/R002371/1 and ST/S002502/1, Durham University and STFC operations grant ST/R000832/1. DiRAC is part of the National e-Infrastructure. This work was partly enabled by the UCL Cosmoparticle Initiative. Simulations in this paper made use of the COMPAS rapid binary population synthesis code (version 02.21.00), which is freely available at `http://github.com/TeamCOMPAS/COMPAS`. This paper has an Einstein Telescope number ET-0171A-22.

CHAPTER 8

The evolution of extended primordial black hole distributions

As described in Section 2.3, primordial black holes represent an interesting and well-motivated alternative to particle dark matter, and even if not the main component, a sub-dominant population of primordial black holes could have interesting consequences.

One scenario of particular significance would be the possibility to observe the final moments of an evaporating black hole, the so-called explosion. Due to the large energies, and the fact that such a black hole would emit any particles coupled to gravity with mass below this energy, it could offer a window to particles beyond the standard model [1011]. This could even potentially generate dark matter particles [507].

Since a monochromatic mass distribution would have to be incredibly fine-tuned to allow for evaporations finishing today, it is much more reasonable to expect an extended mass distribution at formation with a non-negligible population formed at $M_{\rm crit}$.

To determine the rate of explosions today, we therefore develeoped a simple formalism for computing the evolved mass distribution from its initial shape, which could conveniently also be used to set constraints on the allowed population using gamma rays from the galactic centre, in addition to computing the expected distance to the closest exploding black holes for realistic populations.

Effects of Hawking evaporation on PBH distributions

Markus R. Mosbech[a] *Zachary S. C. Picker*[a]

[a]School of Physics, University of Sydney, Camperdown, NSW 2006, Australia
ARC Centre of Excellence for Dark Matter Particle Physics
Sydney Consortium for Particle Physics and Cosmology

Abstract: Primordial black holes (PBHs) may lose mass by Hawking evaporation. For sufficiently small PBHs, they may lose a large portion of their formation mass by today, or evaporate completely if they form with mass $M < M_{\rm crit} \sim 5\times10^{14}$ g. We investigate the effect of this mass loss on extended PBH distributions, showing that the shape of the distribution is significantly changed between formation and today. We reconsider the γ-ray constraints on PBH dark matter in the Milky Way center with a correctly 'evolved' lognormal distribution, and derive a semi-analytic time-dependent distribution which can be used to accurately project monochromatic constraints to extended distribution constraints. We also derive the rate of black hole explosions in the Milky Way per year, finding that although there can be a significant number, it is extremely unlikely to find one close enough to Earth to observe. Along with a more careful argument for why monochromatic PBH distributions are unlikely to source an exploding PBH population today, we (unfortunately) conclude that we are unlikely to witness any PBH explosions.

8.1 Introduction

Primordial black holes (PBHS) [463–465, 1012] are one of the earliest and most intriguing dark matter candidates. With the recent direct observations of black holes [473, 483, 1013], PBHs could be considered to be back in the limelight as a popular dark matter candidate. However, the fraction $f_{\rm PBH}$ of the dark matter energy density in PBHs is constrained by a wide range of observations across the PBH mass spectrum [180, 470]. Typically, these constraints are given for *monochromatic* black hole mass distributions, but there has been growing interest in studying extended mass distributions. Constraints for extended distributions differ nontrivially from the monochromatic case, and these distributions are often predicted to arise from the physical processes which form PBHs [614–616, 618, 619, 1014]—for instance, the lognormal distribution may serve as a reasonable fit to the mass functions produced by the collapse of large inflationary density perturbations [597, 598, 617–621, 1015]. Not only are extended distributions probably more accurate for modelling PBHs, but the resulting phenomenology of the black holes may additionally explain several interesting cosmological questions besides dark matter [1014].

Black holes are understood to have a temperature proportional to the surface gravity at the horizon and so lose mass by Hawking radiation [542, 543]. The black holes radiate a thermal spectrum consisting of all particles with a mass below this surface temperature, with emission

rate,

$$\frac{d^2N_i}{dtdE} = \frac{1}{2\pi}\sum_{\rm dof}\frac{\Gamma_i(E,M,a^*)}{e^{E'/T}\pm 1}\ , \tag{8.1}$$

where N_i is the number of particles emitted, Γ_i is the 'greybody factor', E' is the energy of the particle (including the BH spin), a^* is the reduced spin parameter, the sum is over the degrees of freedom of the particle (including color and helicity), and the $\pm$ sign accounts for fermions and bosons respectively. For large black holes, mass loss from Hawking evaporation is negligible over their lifetime. For sufficiently small black holes, however, the effect of Hawking evaporation is large. These PBHs may lose a significant portion of their mass by today, or evaporate completely (possibly leaving some small remnant behind). Black holes which evaporate exactly with the lifetime of the universe are called 'critical mass' black holes, forming with a mass $M_{\rm crit}\sim 5\times 10^{14}$g [1016]. In this paper we will explore the effect that Hawking evaporation has on extended PBH distributions. Throughout, we use the public code BlackHawk [551, 1017] to calculate lifetimes and emission spectra of the primordial black holes.

Since black holes of different masses evaporate at different rates, extended mass distributions evolve non-trivially from their formation time until today. That means that a distribution which is e.g. lognormal at PBH formation, has quite a different shape today—we will refer to this as the 'evolved' distribution, which we derive explicitly. Often, constraints on extended distributions are derived by 'adapting' the monochromatic constraints with a kind of interpolation [614]. However, it was pointed out in Ref. [618] that this method does not work for small PBH masses, for the above reason—the distribution changes over time. We show that using the correct evolved distribution, however, allows us to still use the method of Ref. [614] to derive correct constraints. In particular, we rederive the constraints on galactic center γ-rays [613] detected by HESS and Fermi [1018–1020] for a lognormal extended distribution, showing the rather large effect of properly evolving the PBH distribution (and agreeing with the isotropic γ-ray constraints found numerically in Ref. [618]).

In the final portion of this paper, we investigate the 'exploding' tail of the tiniest black holes in the evolving distribution, and calculate the rate of black hole explosions over time. We find that there can be a significant number of black hole explosions in the Milky Way every year—however, for currently unconstrained mass distributions, the expected distance to the nearest black hole explosion from Earth is sufficiently large that the photon flux is probably too small to witness one of these transient events without exceptional luck. Nonetheless, it is interesting to consider the possible signal from such an event—since black holes evaporate with the entire particle spectrum, witnessing such an explosion could have profound science consequences [542, 543, 1011, 1021].

8.2 Evolving PBH distributions

With the increased interest in primordial black holes in recent years, constraining extended distributions has become a more pressing task. In Ref. [614], Carr et al. derived the constraints on extended distributions by interpolating the constraints on monochromatic PBH distributions. In Ref. [618], Arbey et al. argue that this method will not work for small black holes, since Hawking evaporation changes the PBH mass distribution between formation and today. Arbey et al. rederived the PBH constrains from isotropic gamma rays numerically, by simulating the evaporation of a number of black holes using the program BlackHawk [551, 1017]. Here, we will show that the method of Ref. [614] can still be applied for evolved distributions, as long as one uses the correct distribution at relevant epochs. We show how to derive this distribution and later rederive the galactic center γ-ray bounds.

Extended Distributions: We define the fraction of total PBHs in the range $[M, M + \mathrm{d}M]$ as,

$$\phi(M) \equiv \frac{1}{n_{\rm BH}} \frac{\mathrm{d}n(M)}{\mathrm{d}M} \ , \tag{8.2}$$

where $n_{\rm BH}$ is the total PBH number density and $n(M)$ is the number density of PBHs in the mass range $[M, M + \mathrm{d}M]$. The physical interpretation of ϕ is that if you had a population of a certain number of black holes, the fraction of this population in a particular mass range (by number) can be found by integrating ϕ over the mass range. This is to be compared to the often-used definition $\psi \equiv M\mathrm{d}n/\mathrm{d}M$, which would give the fraction of energy density in some mass range. Defining the quantity as in Eq. (8.2) is perhaps more useful in our case because Hawking evaporation occurs for each black hole separately, rather than to the black hole population as a whole. Then $\phi(M)$, at PBH formation, would be normalized as,

$$\int \mathrm{d}M \ \phi(M) = 1 \ , \tag{8.3}$$

and we could compute,

$$\rho_{\rm BH} = n_{\rm BH} \int \mathrm{dM} \ M\phi(M) \ , \tag{8.4}$$

for some choice of volume V. However, we are interested in the time evolution of this distribution. In this case, the fraction of black holes in the range $[M, M + \mathrm{d}M]$ at a particular time has two arguments, $\phi(M, t)$. We assume that the initial distribution $\mathrm{d}n(M)/\mathrm{d}M$ is fixed by whatever physics produces the PBHs, and from then on is able to evolve. Then the fraction at a particular time is given by,

$$\phi(M, t) = \phi(M_0(M, t), t_0) \frac{\mathrm{d}M_0(M, t)}{\mathrm{d}M} \ , \tag{8.5}$$

where $M_0(M, t)$ is the formation mass corresponding to a black hole of mass M at time t, and t_0 is the time of formation. The second term can be thought of as a change of variable, since we need to preserve $\phi(M)\mathrm{d}M = \phi(M_0)\mathrm{d}M_0$.

Finally, we will assume the black holes have no spin or charge (the arguments will not change drastically with the inclusion of this complication). Also, although black holes of different sizes form at different epochs in the early universe, accounting for this properly will only have a minuscule effect on the distribution, since we are considering black hole evolution times on the scale of the age of the universe. For simplicity, we can then define the time of formation as $t = 0$.

Black hole mass loss equations: The Hawking mass-loss equation [544] is given by,

$$\frac{dM}{dt} = -\frac{\hbar c^4}{G^2} \frac{\alpha}{M^2}, \tag{8.6}$$

where α is a coefficient determined by the particle species the black hole can emit at a particular mass. A black hole will spend the majority of its lifetime near its initial mass, so $\alpha \approx \alpha_0$ is a sufficiently good approximation for our purposes and allows for the analytic solution of the differential equation,

$$M(t) = \left(M_0^3 - 3\alpha_0 \frac{\hbar c^4}{G^2} t \right)^{1/3}, \qquad t \leq \tau. \tag{8.7}$$

This equation can trivially be inverted to calculate the initial mass M_0 for a black hole of mass M at time t after formation:

$$M_0(M, t) = \left(M^3 + 3\alpha_0 \frac{\hbar c^4}{G^2} t \right)^{1/3} . \tag{8.8}$$

However, determining α_0 is generally complicated. One could use the 'classical' value $\alpha_{\rm classical} = 1/15360\pi$, but this is not particularly accurate, since it only accounts for photon emission. In order to proceed semi-analytically, we use the approximation $\alpha_0 = \alpha_{\rm eff}$, which we define as,

$$\alpha_{\rm eff} \equiv \frac{G^2}{\hbar c^4}\frac{M_0^3}{3\tau} \ , \tag{8.9}$$

where τ is the black hole lifetime, calculated numerically with BlackHawk. This means that $\alpha_{\rm eff}$ guarantees we obtain the correct lifetime for any initial mass. We find that using this effective parameter instead of the numerical value gives a correct evolved mass to within a few percent at all times for the majority of initial masses. We show a plot of $\alpha_{\rm eff}$ in Fig. 8.1, which must be derived numerically. The numerical solution can be roughly approximated with the following function, fit with a χ^2 regression:

$$\alpha_{\rm eff,fit} = \begin{cases} c_1 + c_2 M_0^p & M_0 \lesssim 10^{18} g \\ 2.011 \times 10^{-4} & M_0 \gtrsim 10^{18} g \end{cases} \ , \tag{8.10}$$

where $c_1 = -0.3015$, $c_2 = 0.3113$, and $p = -0.0008$ and the value for $M_0 \gtrsim 10^{18}$g is taken from Ref. [544]. This fit is also shown in Fig. 8.1 and may be useful if one requires an analytic solution.

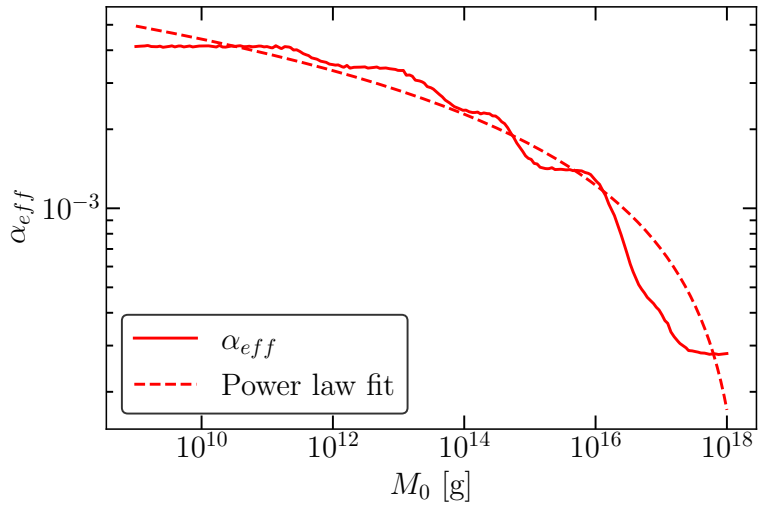

Figure 8.1: *$\alpha_{\rm eff}$ as a function of initial black hole mass, with the power law fit given by Eq.* (8.10).

The evolved distribution: Combining Eqs. (8.5) and (8.8), we find the time-dependent evolved distribution,

$$\boxed{\begin{aligned}\phi(M,t) &= \phi(M_0(M,t),t_0) \\ &\quad \times M^2\left(M^3 + \alpha_{\rm eff}(M_0(M,t))\frac{\hbar c^4}{G^2}t\right)^{-2/3}\end{aligned}} \tag{8.11}$$

We highlight this equation to emphasize its general utility—anyone wishing to study extended PBH distributions which are affected by Hawking radiation can straightforwardly use this result. If one wishes to study a different kind of mass change, such as by accretion in the early universe, however, the second term would need to be modified according to the mass-change equations for that physical process.

There are a few subtleties which should be addressed. Firstly, $n_{\rm BH}$ in Eq. (8.2) is defined at the black hole formation time. Since some black holes will completely evaporate, this means that the integral in Eq. (8.3) will be less than one as time goes on, a portion of the integral is lost, covering the low mass tail which reaches $M = 0$ before the time t. Secondly, two black holes with different initial masses, but which have eventually evaporated, will not be distinguishable (since there is nothing to distinguish)—so one must be careful when applying Eq. (8.8) for fully evaporated black holes.

It would certainly be interesting to additionally examine the evolution of the distribution from mergers, although it would not be trivial to calculate. The PBH-binary parameter distribution from even a monochromatic distribution [564, 566, 1022] is already somewhat complicated, and performing this calculation with an extended mass distribution is well beyond the scope of this paper, if it is even analytically tractable (and it is difficult to intuit which way the bounds would shift, after including this effect).

The monochromatic stability constraint: Finally, it is worth touching on an important point related to the evolution of specifically monochromatic distributions. It is often stated that 'black holes with masses $m < M_{\rm crit}$ cannot be the dark matter, since they evaporate before today'. This statement is technically true, when considering the mass at formation. But there remains the question—can a monochromatic distribution with mass slightly larger than the critical mass leave behind a sizeable population today of very tiny black holes? Constraints from Hawking emissions already do exist for such a population. However, this question can be answered on more theoretical grounds, without reference to specific observations. This is important since in scenarios where the PBHs are not modelled as Schwarzschild or Kerr black holes, we may not be able to rely on such constraints [567], so the point is worth making explicitly.

Consider the scenario where there is a remnant population today of black holes of masses $m < M_{\rm crit}$. If the black holes had mass 1.1×10^{11} g, the mass of these black holes at formation would have been 7.4×10^{14} g (very close to the critical mass). However, if the population had mass 1.1×10^{14} g today, the initial mass would have been just 7.5×10^{14} g. Clearly, there is extremely little difference between these two initial populations. For these two examples, we can compute $\Delta M_{\rm init}/M_{\rm crit} \sim 0.01$—so there is roughly a 1% difference in formation mass for a three orders-of-magnitude difference in black hole mass today. As a result, we have a kind of 'stability' constraint on a theory which predicts a specific range of black holes today with $M < M_{\rm crit}$, since it is so sensitive to the initial conditions—the precision required to source such a population would be smaller than the theoretical and observational uncertainties in our calculation. Essentially, we can not expect to find a rapidly evaporating monochromatic distribution of black holes today.

8.3 γ-ray constraints

For demonstrative purposes, we will recompute the γ-ray constraints from the galactic center using a lognormal distribution as a toy model. Although these constraints have been computed before [613, 614, 618], it is useful to show how our Eq. (8.11) can be used to convert monochromatic constraints to extended distribution constraints without extensive numerical calculations.

The lognormal distribution: The lognormal distribution is given by,

$$\frac{{\rm d}n(M)}{{\rm d}M} = \frac{n_{\rm BH}}{\sqrt{2\pi}\sigma M} \exp\left\{\left(-\frac{(\ln(M/M_*))^2}{2\sigma^2}\right)\right\} . \tag{8.12}$$

This distribution is relatively well-motivated, since many physically realistic processes (such as the collapse of density perturbations sourced by some inflationary scenario) are reasonably fit by a lognormal distribution [597, 598, 617–620, 1015], although Ref. [621] for example predicts a deviation from lognormal for the low-mass tail.

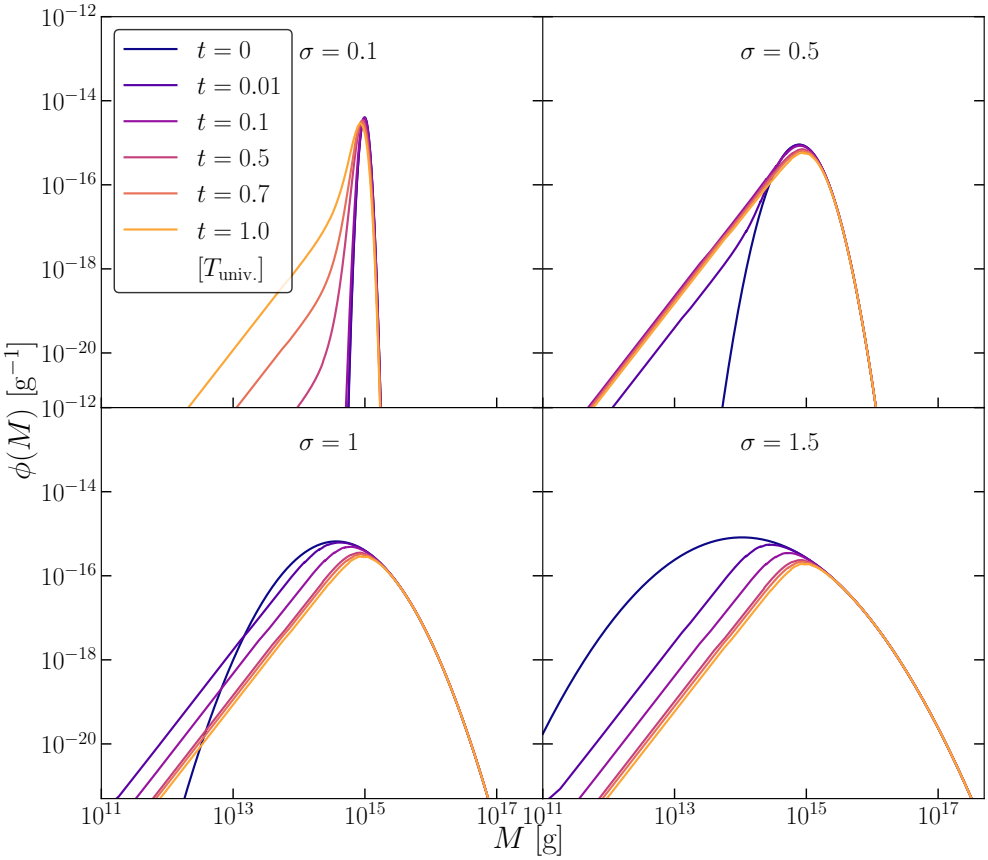

Figure 8.2: *Four PBH extended distributions with $M_* = 10^{15}$ g and different standard deviations σ are evolved, with line colour denoting evolution time. Note that t is in units of the age of the universe.*

Figure 8.2 shows the effect of Hawking radiation on lognormally distributed PBHs. The extended distribution at a particular time is properly modified by Eq. (8.11), leading to a significantly altered shape. Specifically, the low-mass tail tends towards a slope $\propto M^2$, leading to a suppression of masses around the peak, but an enhancement at much lower masses. In fact, Eq. (8.11) provides a simple explanation for this shape, in both the lower- and higher-mass regimes regimes. For $M^3 \gg \alpha_{\rm eff} \frac{\hbar c^4}{G^2} t$, the second term is suppressed, leading to an essentially unchanged distribution. Conversely, when $M^3 \ll \alpha_{\rm eff} \frac{\hbar c^4}{G^2} t$, the second term dominates, scaling $\propto M^2$. Since evolved PBHs with small masses originate at almost the same initial mass, $\phi(M_0, t_0)$ and $\alpha_{\rm eff}(M_0)$ become essentially constant in M, and the evolved distribution becomes $\propto M^2$. This agrees with the low-mass tail findings in Ref. [613]. This analysis is independent of the initial distribution, and will hold as long as $\phi(M_0, t_0)$ does not vary extremely quickly in mass.

Calculating the gamma-ray flux: The γ-ray flux from an extended distribution of black holes is given by,

$$\frac{d^2 N_\gamma}{dE dt}(E) = \int dM \frac{df}{dM} \frac{d^2 N_\gamma}{dE dt}(M, E) \ . \tag{8.13}$$

Since the gamma-ray emission from low-mass black holes is much larger than for more massive PBHs, the low-mass tail of $\phi(M)$ becomes very important, as was noted in Ref. [618].

We use this to compute the expected flux in γ-rays, Φ, from the galactic centre, using

$$\frac{d\Phi_\gamma}{dE}(E) = f_{\rm pbh}\frac{D}{\bar{M}}\frac{d^2N_\gamma}{dEdt}(E), \tag{8.14}$$

where $\bar{M}$ is the initial mean PBH mass, and D is the D-factor commonly used for decaying dark matter predictions [326], given by,

$$D = \int dl d\Omega\, \rho_{\rm dm}\ . \tag{8.15}$$

In Fig. 8.3 we show the expected spectrum from the galactic centre, using the Navarro–Frenk–White

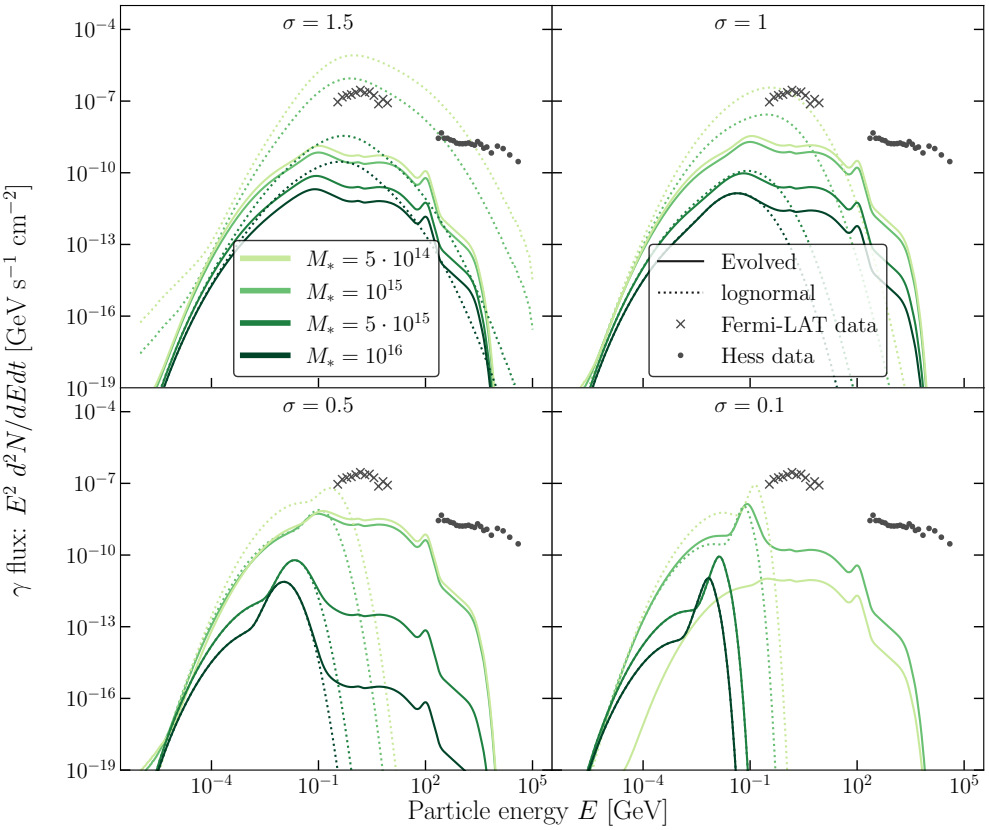

Figure 8.3: *The expected gamma-ray spectrum from the galactic centre for sixteen extended distributions of varying mass and standard deviation with $f_{\rm pbh} = 10^{-8}$, alongside measured fluxes from HESS [1018] (black dots) and Fermi-LAT data [1019, 1020] (black crosses). The thick lines correspond to distributions correctly evolved as in Eq.* (8.11)*, while the dotted lines correspond to a naive 'unevolved' distribution.*

(NFW) dark matter profile [790] for the PBHs, contrasted with the spectrum for a lognormal PBH distribution which does not evolve. Note that for evolved distributions, we use $f_{\rm pbh}$ to refer to the PBH fraction of dark matter at formation. For distributions with significant portions of low-mass PBHs, part of that mass would be evaporated away by later times. The correct use of the evolved distribution significantly alters the shape of the gamma-ray spectrum, showing both significantly smaller fluxes in some areas of the spectrum and larger fluxes in others..

Gamma-ray constraints: By requiring that the emission from PBHs does not exceed the

observed flux from the galactic centre, we can constrain $f_{\rm pbh}$ for a specific distribution. An alternative method for doing this was proposed in [614], which does not require computing the expected signal from a given distribution, but instead adapts the constraints on monochromatic distributions. We find that using this 'adapted' method, but with our correctly evolved distribution, agrees excellently with the bounds computed numerically by simulating an initial PBH distribution and computing the γ-ray spectrum. In addition, the correctly evolved bounds are very similar to those derived in Ref. [618] for isotropic γ-rays [1].

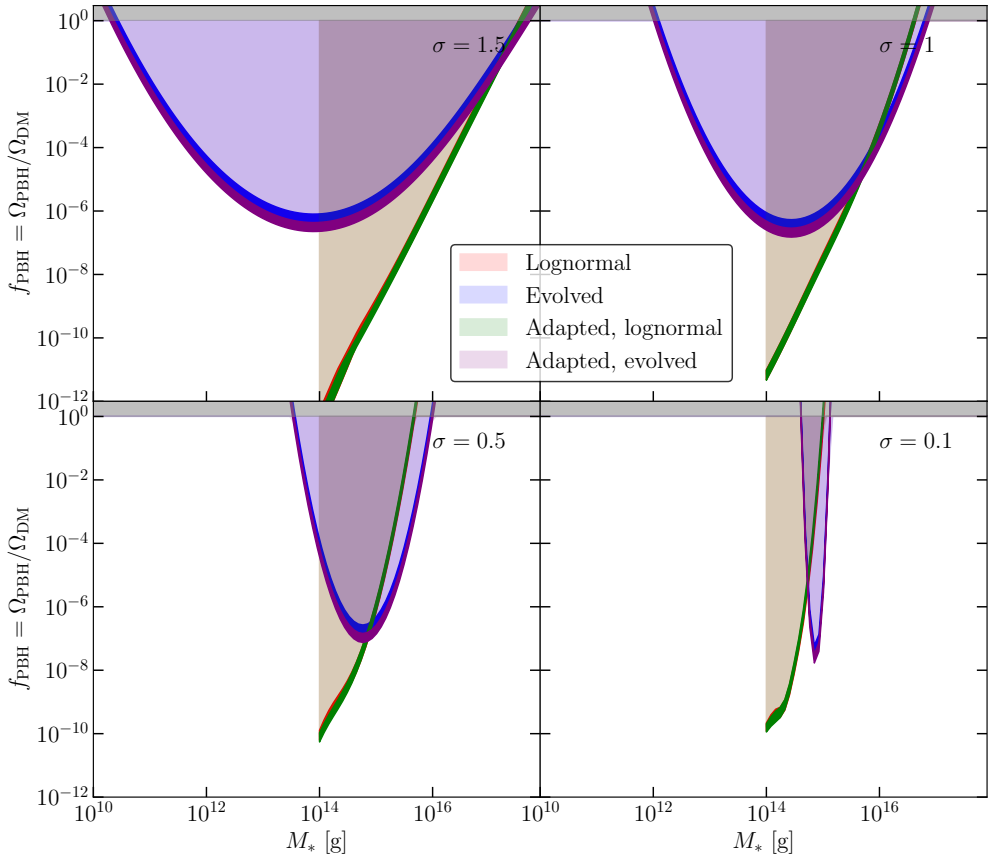

Figure 8.4: *Bounds on $f_{\rm pbh}$ from galactic centre γ-ray observations for extended distributions with central mass M_* and four values of σ, comparing the the 'naive' lognormal and properly evolved distributions. The thickness of the borders accounts for observational uncertainty. 'Adapted' curves are obtained from monochromatic constraints using the method of Ref. [614].*

The bounds are shown in Fig. 8.4. The first 'lognormal' bound is for the naive unevolved distribution. The second 'evolved' bound is numerically calculated from the γ-ray spectrum of black holes, distributed with our evolved spectrum today Eq. (8.11). The 'adapted' bound refers to the bound obtained using the method from Ref. [614], where the monochromatic constraints are interpolated to form the extended distribution bounds. The 'adapted, evolved' bound is calculated using the same method, but with the correct evolved distribution Eq. (8.11). In each case, the actual bound is placed by requiring that the predicted flux be smaller than the flux measured by HESS and Fermi-LAT. We can see that the adapted method is perfectly compatible with the numerical results, but only when the evolved distribution of Eq. (8.11) is used.

[1] We choose not to reproduce these particular bounds, however, since the extragalactic flux must be integrated back in time—a slightly more complicated task when the distribution itself is evolving.

The bounds for the evolved distribution are loosened for small values of M_* because a large fraction of that population would have evaporated already, and thus would have no impact on the γ-rays from the galactic centre. A different early universe probe, such as BBN or CMB anisotropies, would be needed to constrain these PBHs. The unevolved lognormal bounds must be arbitrarily cutoff at 10^{14} g, since it would not be consistent to have a lognormal distribution *today* consisting of tiny, rapidly-evaporating black holes, similar to the discussion at the end of Section 8.2.

8.4 Black hole explosions

The end of life of an evaporating black hole is not entirely known [1023]. However, at least down to extremely small masses, it should be the case that the black holes will get hotter and brighter, emitting a huge spectrum of particles. For convenience, we call this end-of-life phenomenon an 'explosion', although we will not comment on whether or not the black hole is completely exhausted, or leaves behind some kind of remnant.

The gamma-ray background created by evaporating PBHs is not the only way to search for these exploding black holes. An observation of the burst of gamma-rays produced by a single black hole evaporation would be very exciting, since all possible particle species are emitted. We could not only probe the Standard Model more clearly, but we could possibly make statements about dark matter and beyond-the-Standard Model physics [1011, 1021]. Unfortunately, it does not appear that there is any evidence for such an observation so far [1024–1026]. We will show in this section that this result is not surprising. While we have already argued that a monochromatic population barely above $M_{\rm crit}$ is not theoretically sound, an extended distribution of PBHs would produce a population of exploding black holes today. However, we show that this population cannot be sufficiently large that we would expect to see any bursts near enough to Earth.

For convenience we will again use the toy lognormal distribution as in Section 8.3. However, since the low-mass tail of the distribution generically scales as $\propto M^2$ regardless of the distribution, our findings here are somewhat general.

Likelihood of witnessing a PBH explosion: In Fig. 8.5 we show the black hole explosion rate per unit mass of PBH matter from the evolved PBH distributions. We can see that there is actually quite a large quantity of explosions per year, even for very small $f_{\rm pbh}$. However, and unfortunately, the distance between these explosions is still probably too small for observation from Earth—see Fig. 8.6, where we plot the average distance between these explosions as a function of the distribution parameters and $f_{\rm pbh}$.

As a representative observation, we can examine the γ-ray flux from one of these transient events. In the last year of the black hole's life, at a distance of $\sim$0.01 parsec, we only expect to detect 1 photon per square cm per year. In order to observe a single photon from an explosion with Fermi[2], for example, the black hole would then need to be within a distance of ~ 100 AU. A single photon, however, is hardly a positive detection. Ten detected photons would require the black hole be only as far as ~ 35 AU ($\sim 10^{-4}$ pc), placing it firmly inside our solar system. One such event, unless we happen to be very lucky, could only occur with PBH fractions which are already well excluded—in the monochromatic case, it would be excluded by the argument at the end of Section 8.2, whereas the extended distributions are ruled out by the arguments in Section 8.3.

[2]Assuming an effective area of 10^4 cm^2 for the relevant energies[599].

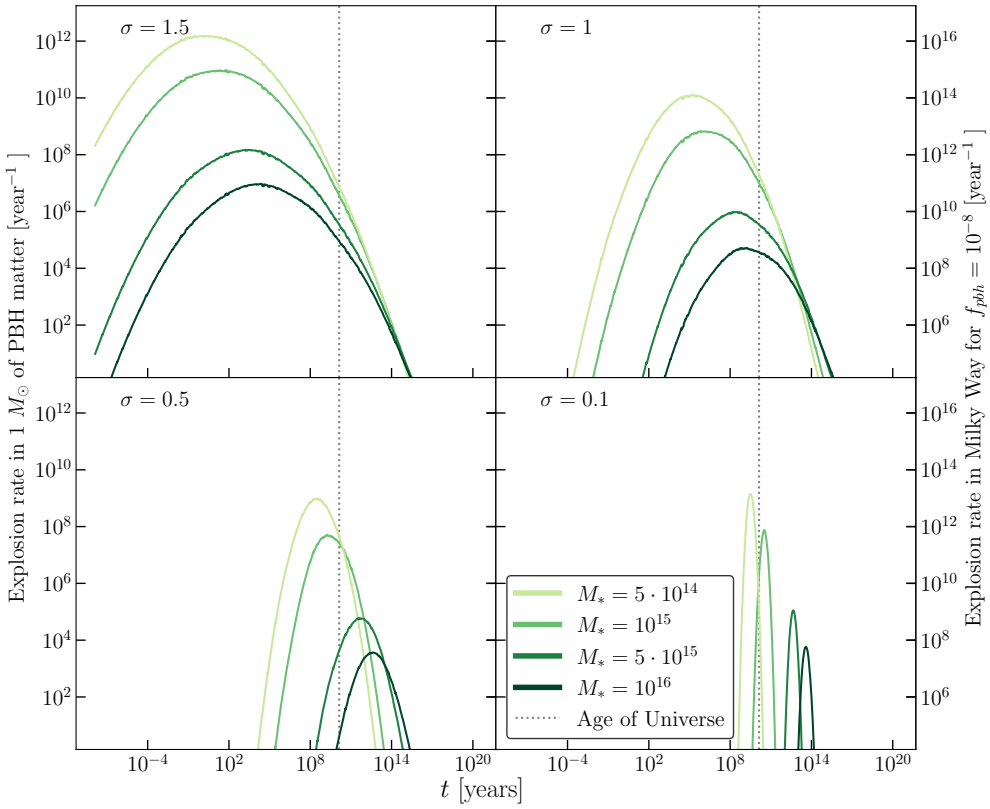

Figure 8.5: *The explosion rate of PBHs over time for sixteen distributions with varying values of σ and central mass M_* and $f_{\text{PBH}} \sim 10^{-8}$. The rate is given in terms of number of explosions per solar mass of PBHs. The second vertical axis gives the explosion rate in yearly numbers for the Milky Way.*

Perhaps there is some more creative way to observe these explosions as transient events which we have not considered—after all, the entire particle spectrum is produced. However, for the moment, it does not appear that we will be witnessing any black hole explosions anytime soon.

Energy injection from explosions: A different way of determining the presence of such explosions could be via the energy injected into the interstellar medium. A conservative estimate of the energy emitted from PBHs in a given year is $\sim 10^{11}$ g (10^{32} ergs) per explosion, neglecting the emission from PBHs with more than a year of life left. As shown in Fig. 8.5, the explosion rate in a Milky Way-like galaxy can vary greatly over time, depending on the initial distribution. Assuming a Milky Way explosion rate of 10^{10} per year, this is 10^{42} ergs emitted per year, of which a large portion is in photons. In a similar naive analysis, a supernova will generally release $\sim 10^{51}$ ergs [1027, 1028]. If the supernova rate is one every 10 to 100 years in a MW-like galaxy, this means that supernovae will inject $\sim 10^7$ times more energy over that timespan compared to the black hole explosions, making it unlikely that we could constrain the PBH fraction this way. However, there may be some morphological differences, as a supernova will be very localised, whereas the energy injection from PBH explosions will be distributed with the halo density profile, and with roughly 'continuous' emission. Additionally, supernovae are often tied to star formation, since many supernova progenitors are short-lived high-mass stars, whereas PBH explosions are completely independent of star formation, and could even happen before stars are formed. A more thorough analysis of the energy injection by PBH explosions would be interesting, but

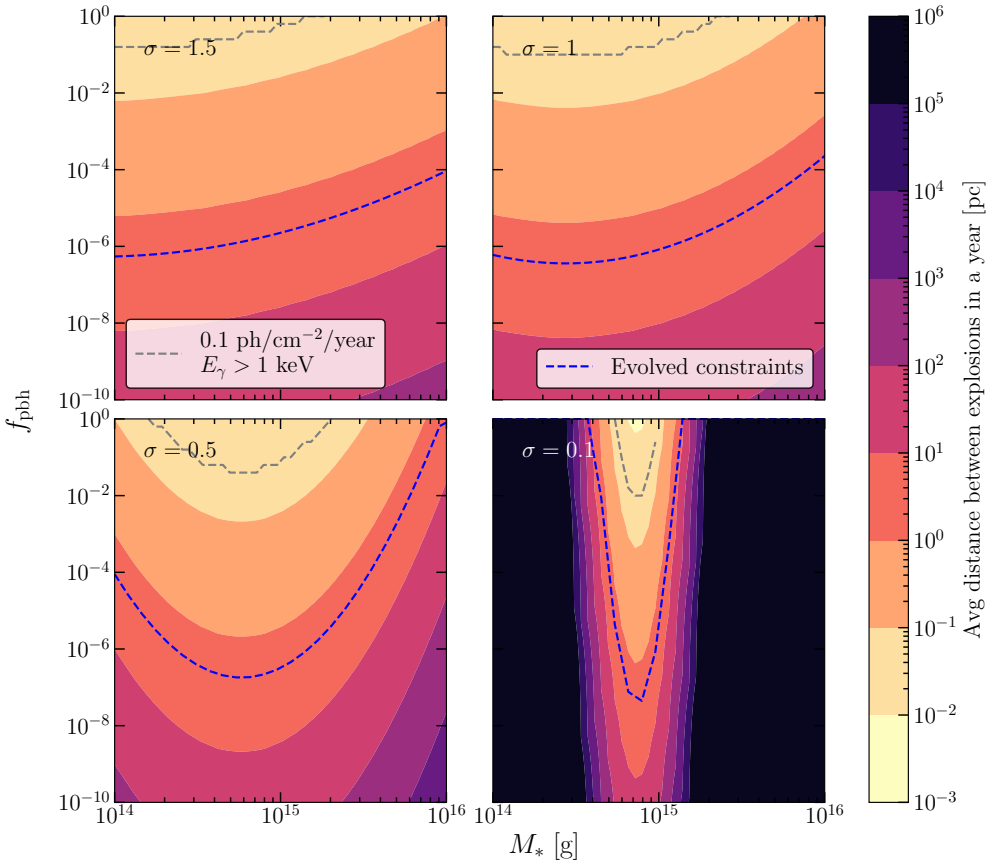

Figure 8.6: *The average distance between black hole explosions for evolved distributions with varying central mass M_* and four values of σ. The dotted grey line gives the distance that would correspond to a observed photon flux of* 0.1 photons cm^{-2} yr^{-1}.

beyond the scope of this paper.

8.5 Conclusions

Small black holes can lose a significant fraction of their mass via Hawking radiation. Distributions of small black holes therefore evolve over time, as black holes shrink and even explode. We showed that for monochromatic distributions, it is extremely unlikely to find a population today which is rapidly evaporating, since the initial mass would have to be extremely fine-tuned to a small value above this critical mass. However, extended distributions centered near the critical mass would source a population of evaporating black holes. We demonstrated how to derive this distribution today, and that using the correctly evolved distributions, the method of recasting monochromatic constraints into extended constraints [614] is applicable even for evolving distributions. We then calculated the rate of PBH explosions for a lognormal distribution near the critical mass. Unfortunately, we found that although there can be a significant quantity of these explosions, they are on average sufficiently far from Earth that we do not expect to see them.

Primordial black holes are experiencing something of a renaissance today, in large part due to the exciting observations of black holes from a wide range of sources, such as gravitational waves and very-long-baseline interferometry. As our understanding of their origins and astrophysics improves, the need to properly model extended mass distributions becomes more pressing.

During the preparation of this paper, a similar treatment of the evolved mass distribution was published in the context of PBH bubbles as cosmological standard timers [1029]. We find that our results agree well.

Acknowledgements

We would like to thank Celine Boehm, Archil Kobakhidze, and Ciaran O'Hare for many useful discussions and insights throughout the research and writing of this paper.

Funding

The authors are funded by The University of Sydney.

CHAPTER 9

Conclusions

Dark matter remains a mysterious component in our model for the universe, but it is not hopeless. As is demonstrated here, our understanding of its dynamics and the effects on observables is ever growing, as is the sensitivity of our particle experiments to detect any interactions with the Standard Model, as well as our astrophysical observations, measuring any impact of its microphysics.

Our frameworks for describing dark matter models and computing their consequences are continually evolving, improving in precision and finding new avenues to search for signatures. This work collects and presents my contributions to the common efforts to determine the nature of dark matter, building on the work previously done, and hopefully acting as a foundation for future investigations.

Introducing in Chapter 5 the full Boltzmann hierarchy for dark matter interacting with neutrinos of non-zero mass presents a natural continuation of others' previous work with the massless neutrino approximation [661].The inclusion of neutrino masses in cosmological analyses is of increasing importance as experimental sensitivities improve, and the linear theory framework presented serves as a solid basis further nonlinear study, as in Chapters 6 and 7, or Refs. [943, 964].

As new experiments and observatories are built, the parameter space where the impact of dark matter can be investigated grows larger. If we, as cosmologists, truly wish to understand the nature of dark matter, rather than just make every improving band-aid solutions to ΛCDM, it is necessary to determine how to distinguish different dark matter models. In Chapter 6 we present nonlinear structure predictions for dark matter models including interactions with relativistic species, which we compare and contrast with similar warm dark matter models as well as standard cold dark matter. Our findings indicate that such different models with suppressed small scale structure could be nearly indistinguishable in late time observations, but offer hope that the next generations of observatories may be of use. In particular, the possibility of resolving 3d structure at high redshift, using intensity mapping of the 21 cm neutral hydrogen line, may offer a window into the regime where such dark matter models have not yet been homogenised. This is an area ripe for further study, in particular calling for follow-up studies with high-resolution treatment of the baryonic physics at these times.

New types of experiments can also yield entirely new observables, and ways of investigating dark matter. One such recently opened avenue is through gravitational wave astronomy, as described in Chapter 7. With the rate of gravitational wave events determined by the cosmological

star formation history, it is, albeit indirectly, sensitive to the underlying structure formation history, and thus the dark matter model. We have shown how the redshift dependent compact binary merger rate can provide independent measurements of structure formation, and with the next generation of interferometers may be able to set competitive limits on dark matter models with suppressed small scale structure.

Finally, Chapter 8 presents an analysis of primordial black holes as an alternative dark matter model, or as a subdominant component. The particular focus is on extended mass distributions, giving a simple framework for computing the modern day evolution of any initial mass distribution at formation. This offers potential both for setting constraints on extended distribution based on local measurements, such as the included galactic centre gamma ray analysis, as well as for computing rates of black hole explosions at present times. The observation of such an event could be tremendously educational, as it could provide a probe of any particle coupled to gravity, including dark matter, if the primordial black holes form only a subdominant component. Unfortunately our findings show that for the considered log-normal distribution, we are unlikely to observe such an event, but the framework presented makes it simple to compute predictions for any other distributions.

As such, this thesis represents a modest collection of contributions to our general understanding of dark matter, in particular on the topic of cosmological probes of dark matter-neutrino interactions, but also shining a light on the possibilities of future observations for constraining, and distinguishing between, dark matter models beyond the standard cold dark matter paradigm.

Bibliography

[1] Markus R. Mosbech et al. "The Full Boltzmann Hierarchy for Dark Matter-Massive Neutrino Interactions". In: *Journal of Cosmology and Astroparticle Physics* 2021.03 (Mar. 2021), p. 066. ISSN: 1475-7516. DOI: 10.1088/1475-7516/2021/03/066. arXiv: 2011.04206.

[2] Markus R. Mosbech, Celine Boehm and Yvonne Y. Y. Wong. "Probing Dark Matter Interactions with 21cm Observations". In: *Journal of Cosmology and Astroparticle Physics* 2023.03 (1st Mar. 2023), p. 047. ISSN: 1475-7516. DOI: 10.1088/1475-7516/2023/03/047. arXiv: 2207.03107.

[3] Markus R. Mosbech et al. *Gravitational-Wave Event Rates as a New Probe for Dark Matter Microphysics*. 2nd Aug. 2022. DOI: 10.48550/arXiv.2207.14126. arXiv: 2207.14126. URL: http://arxiv.org/abs/2207.14126 (visited on 03/08/2022). preprint.

[4] Markus R. Mosbech and Zachary S. C. Picker. "Effects of Hawking Evaporation on PBH Distributions". In: *SciPost Physics* 13.4 (25th Oct. 2022), p. 100. ISSN: 2542-4653. DOI: 10.21468/SciPostPhys.13.4.100. arXiv: 2203.05743.

[5] Planck Collaboration et al. "Planck 2018 Results. VI. Cosmological Parameters". In: *Astronomy & Astrophysics* 641 (Sept. 2020), A6. ISSN: 0004-6361, 1432-0746. DOI: 10.1051/0004-6361/201833910. arXiv: 1807.06209.

[6] Plato et al. *Plato in Twelve Volumes: With an English Translation*. 12 vols. Loeb Classical Library. London, Cambridge: W. Heinemann ; Harvard University Press, 1914.

[7] V. C. Rubin, W. K. Ford Jr. and N. Thonnard. "Rotational Properties of 21 SC Galaxies with a Large Range of Luminosities and Radii, from NGC 4605 (R=4kpc) to UGC 2885 (R=122kpc)." In: *The Astrophysical Journal* 238 (1st June 1980), pp. 471–487. ISSN: 0004-637X. DOI: 10.1086/158003.

[8] Vera C. Rubin and W. Kent Ford Jr. "Rotation of the Andromeda Nebula from a Spectroscopic Survey of Emission Regions". In: *The Astrophysical Journal* 159 (1st Feb. 1970), p. 379. ISSN: 0004-637X. DOI: 10.1086/150317.

[9] A. Bosma. "21-Cm Line Studies of Spiral Galaxies. I. Observations of the Galaxies NGC 5033, 3198, 5055, 2841, and 7331." In: *The Astronomical Journal* 86 (1st Dec. 1981), pp. 1791–1824. ISSN: 0004-6256. DOI: 10.1086/113062.

[10] A. Bosma. "21-Cm Line Studies of Spiral Galaxies. II. The Distribution and Kinematics of Neutral Hydrogen in Spiral Galaxies of Various Morphological Types." In: *The Astronomical Journal* 86 (1st Dec. 1981), pp. 1825–1846. ISSN: 0004-6256. DOI: 10.1086/113063.

[11] A. Bosma. "The Distribution and Kinematics of Neutral Hydrogen in Spiral Galaxies of Various Morphological Types". PhD thesis. Groningen University, Mar. 1978. URL: https://ui.adsabs.harvard.edu/abs/1978PhDT.....195B/abstract (visited on 03/04/2023).

[12] A. Bosma and P. C. van der Kruit. "The Local Mass-to-Light Ratio in Spiral Galaxies." In: *Astronomy and Astrophysics* 79 (1st Nov. 1979), pp. 281–286. ISSN: 0004-6361.

[13] J. G. de Swart, G. Bertone and J. van Dongen. "How Dark Matter Came to Matter". In: *Nature Astronomy* 1.3 (2nd Mar. 2017), p. 0059. ISSN: 2397-3366. DOI: 10.1038/s41550-017-0059. arXiv: 1703.00013 [astro-ph, physics:gr-qc, physics:hep-ph, physics:physics].

[14] Adam G. Riess et al. "Observational Evidence from Supernovae for an Accelerating Universe and a Cosmological Constant". In: *The Astronomical Journal* 116.3 (1st Sept. 1998), pp. 1009–1038. ISSN: 0004-6256. DOI: 10.1086/300499. arXiv: astro-ph/9805201.

[15] S. Perlmutter et al. "Measurements of Ω and Λ from 42 High-Redshift Supernovae". In: *The Astrophysical Journal* 517.2 (1st June 1999), pp. 565–586. ISSN: 0004-637X, 1538-4357. DOI: 10.1086/307221. arXiv: astro-ph/9812133.

[16] Planck Collaboration et al. "Planck 2018 Results. I. Overview and the Cosmological Legacy of Planck". In: *Astronomy & Astrophysics* 641 (Sept. 2020), A1. ISSN: 0004-6361, 1432-0746. DOI: 10.1051/0004-6361/201833880. arXiv: 1807.06205.

[17] E. Komatsu et al. "Seven-Year Wilkinson Microwave Anisotropy Probe (WMAP) Observations: Cosmological Interpretation". In: *The Astrophysical Journal Supplement Series* 192.2 (1st Feb. 2011), p. 18. ISSN: 0067-0049. DOI: 10.1088/0067-0049/192/2/18. arXiv: 1001.4538 [astro-ph].

[18] J. M. Kovac et al. "Detection of Polarization in the Cosmic Microwave Background Using DASI". In: *Nature* 420.6917 (Dec. 2002), pp. 772–787. ISSN: 0028-0836, 1476-4687. DOI: 10.1038/nature01269. arXiv: astro-ph/0209478.

[19] Planck Collaboration et al. "Planck 2015 Results - I. Overview of Products and Scientific Results". In: *Astronomy & Astrophysics* 594 (Oct. 2016), A1. ISSN: 0004-6361, 1432-0746. DOI: 10.1051/0004-6361/201527101. arXiv: 1502.01582 [astro-ph].

[20] Daniel J. Eisenstein et al. "Detection of the Baryon Acoustic Peak in the Large-Scale Correlation Function of SDSS Luminous Red Galaxies". In: *The Astrophysical Journal* 633.2 (10th Nov. 2005), pp. 560–574. ISSN: 0004-637X, 1538-4357. DOI: 10.1086/466512. arXiv: astro-ph/0501171.

[21] Shaun Cole et al. "The 2dF Galaxy Redshift Survey: Power-spectrum Analysis of the Final Dataset and Cosmological Implications". In: *Monthly Notices of the Royal Astronomical Society* 362.2 (11th Sept. 2005), pp. 505–534. ISSN: 00358711, 13652966. DOI: 10.1111/j.1365-2966.2005.09318.x. arXiv: astro-ph/0501174.

[22] William Thomson Kelvin. *Baltimore Lectures on Molecular Dynamics and the Wave Theory of Light*. London, Baltimore: C.J. Clay and Sons; Publication agency of the Johns Hopkins University, 1904. 703 pp. URL: https://catalog.hathitrust.org/Record/011929196 (visited on 02/08/2022).

[23] J. C. Kapteyn. "First Attempt at a Theory of the Arrangement and Motion of the Sidereal System". In: *The Astrophysical Journal* 55 (1st May 1922), p. 302. ISSN: 0004-637X. DOI: 10.1086/142670.

[24] K. Lundmark. "Über Die Bestimmung Der Entfernungen, Dimensionen, Massen Und Dichtigkeit Fur Die Nächstgelegenen Anagalacktischen Sternsysteme." In: *Meddelanden fran Lunds Astronomiska Observatorium Serie I* 125 (1st Jan. 1930), pp. 1–13.

[25] J. H. Oort. "The Force Exerted by the Stellar System in the Direction Perpendicular to the Galactic Plane and Some Related Problems". In: *Bulletin of the Astronomical Institutes of the Netherlands* 6 (1st Aug. 1932), p. 249. ISSN: 0365-8910.

[26] F. Zwicky. "Die Rotverschiebung von Extragalaktischen Nebeln". In: *Helvetica Physica Acta* 6 (1st Jan. 1933), pp. 110–127. ISSN: 0018-0238.

[27] Heinz Andernach and Fritz Zwicky. *English and Spanish Translation of Zwicky's (1933) The Redshift of Extragalactic Nebulae*. 5th Nov. 2017. arXiv: 1711.01693 [astro-ph]. URL: http://arxiv.org/abs/1711.01693 (visited on 24/04/2023). preprint.

[28] F. Zwicky. "On the Masses of Nebulae and of Clusters of Nebulae". In: *The Astrophysical Journal* 86 (1st Oct. 1937), p. 217. ISSN: 0004-637X. DOI: 10.1086/143864.

[29] Horace W. Babcock. "The Rotation of the Andromeda Nebula". In: *Lick Observatory Bulletin* 498 (1st Jan. 1939), pp. 41–51. ISSN: 0075-9317. DOI: 10.5479/ADS/bib/1939LicOB.19.41B.

[30] K. C. Freeman. "On the Disks of Spiral and S0 Galaxies". In: *The Astrophysical Journal* 160 (1st June 1970), p. 811. ISSN: 0004-637X. DOI: 10.1086/150474.

[31] Albert Einstein. "Kosmologische Betrachtungen Zur Allgemeinen Relativitätstheorie". In: *Sitzungsberichte der Königlich Preußischen Akademie der Wissenschaften (Berlin* (1st Jan. 1917), pp. 142–152.

[32] A. Friedman. "Über die Krümmung des Raumes". In: *Zeitschrift für Physik* 10.1 (1st Dec. 1922), pp. 377–386. ISSN: 0044-3328. DOI: 10.1007/BF01332580.

[33] G. Lemaître. "Un Univers Homogène de Masse Constante et de Rayon Croissant Rendant Compte de La Vitesse Radiale Des Nébuleuses Extra-Galactiques". In: *Annales de la Société Scientifique de Bruxelles* 47 (1st Jan. 1927), pp. 49–59.

[34] Edwin Hubble. "A Relation between Distance and Radial Velocity among Extra-Galactic Nebulae". In: *Proceedings of the National Academy of Sciences* 15.3 (15th Mar. 1929), pp. 168–173. DOI: 10.1073/pnas.15.3.168.

[35] Ian Steer. "Who Discovered Universe Expansion?" In: *Nature* 490.7419 (Oct. 2012), pp. 176–176. ISSN: 1476-4687. DOI: 10.1038/490176c. arXiv: 1212.1359 [astro-ph, physics:physics].

[36] Steven Weinberg. "The Cosmological Constant Problem". In: *Reviews of Modern Physics* 61.1 (1st Jan. 1989), pp. 1–23. DOI: 10.1103/RevModPhys.61.1.

[37] Super-Kamiokande Collaboration et al. "Evidence for Oscillation of Atmospheric Neutrinos". In: *Physical Review Letters* 81.8 (24th Aug. 1998), pp. 1562–1567. ISSN: 0031-9007, 1079-7114. DOI: 10.1103/PhysRevLett.81.1562. arXiv: hep-ex/9807003.

[38] SNO Collaboration et al. "Direct Evidence for Neutrino Flavor Transformation from Neutral-Current Interactions in the Sudbury Neutrino Observatory". In: *Physical Review Letters* 89.1 (13th June 2002), p. 011301. DOI: 10.1103/PhysRevLett.89.011301. arXiv: nucl-ex/0204008.

[39] H. E. S. Velten, R. F. vom Marttens and W. Zimdahl. "Aspects of the Cosmological "Coincidence Problem"". In: *The European Physical Journal C* 74.11 (22nd Nov. 2014), p. 3160. ISSN: 1434-6052. DOI: 10.1140/epjc/s10052-014-3160-4. arXiv: 1410.2509.

[40] Fred C. Adams and Gregory Laughlin. "A Dying Universe: The Long-Term Fate and Evolutionof Astrophysical Objects". In: *Reviews of Modern Physics* 69.2 (1st Apr. 1997), pp. 337–372. DOI: 10.1103/RevModPhys.69.337. arXiv: astro-ph/9701131.

[41] Jianming Zhang et al. "A Preliminary Study about Gravitational Wave Radiation and Cosmic Heat Death". In: *Monthly Notices of the Royal Astronomical Society* 502.2 (1st Apr. 2021), pp. 2787–2792. ISSN: 0035-8711. DOI: 10.1093/mnras/stab226. arXiv: 2102.12054.

[42] M E Caplan. "Black Dwarf Supernova in the Far Future". In: *Monthly Notices of the Royal Astronomical Society* 497.4 (1st Oct. 2020), pp. 4357–4362. ISSN: 0035-8711. DOI: 10.1093/mnras/staa2262. arXiv: 2008.02296.

[43] G. Lemaître. "The Beginning of the World from the Point of View of Quantum Theory". In: *Nature* 127.3210 (3210 May 1931), pp. 706–706. ISSN: 1476-4687. DOI: 10.1038/127706b0.

[44] Abbé Georges Lemaître. "The Expanding Universe". In: *General Relativity and Gravitation* 29.5 (1st May 1997), pp. 641–680. ISSN: 1572-9532. DOI: 10.1023/A:1018855621348.

[45] Helge Kragh. "'The Wildest Speculation of All': Lemaître and the Primeval-Atom Universe". In: *Georges Lemaître: Life, Science and Legacy*. Ed. by Rodney D. Holder and Simon Mitton. Astrophysics and Space Science Library. Berlin, Heidelberg: Springer, 2012, pp. 23–38. ISBN: 978-3-642-32254-9. DOI: 10.1007/978-3-642-32254-9_3. URL: https://doi.org/10.1007/978-3-642-32254-9_3 (visited on 24/08/2022).

[46] Alan H. Guth. "Inflationary Universe: A Possible Solution to the Horizon and Flatness Problems". In: *Physical Review D* 23.2 (15th Jan. 1981), pp. 347–356. DOI: 10.1103/PhysRevD.23.347.

[47] A. D. Linde. "A New Inflationary Universe Scenario: A Possible Solution of the Horizon, Flatness, Homogeneity, Isotropy and Primordial Monopole Problems". In: *Physics Letters B* 108.6 (4th Feb. 1982), pp. 389–393. ISSN: 0370-2693. DOI: 10.1016/0370-2693(82)91219-9.

[48] A. A. Starobinsky. "A New Type of Isotropic Cosmological Models without Singularity". In: *Physics Letters B* 91.1 (24th Mar. 1980), pp. 99–102. ISSN: 0370-2693. DOI: 10.1016/0370-2693(80)90670-X.

[49] A. A. Starobinsky. "Dynamics of Phase Transition in the New Inflationary Universe Scenario and Generation of Perturbations". In: *Physics Letters B* 117.3 (11th Nov. 1982), pp. 175–178. ISSN: 0370-2693. DOI: 10.1016/0370-2693(82)90541-X.

[50] B S Ryden. *Introduction to Cosmology*. Addison-Wesley, 2003. ISBN: 978-0-8053-8912-8.

[51] Kaloian D. Lozanov. "Lectures on Reheating after Inflation". 9th July 2019. URL: http://arxiv.org/abs/1907.04402.

[52] Planck Collaboration et al. "Planck 2015 Results. XX. Constraints on Inflation". In: *Astronomy & Astrophysics* 594 (Oct. 2016), A20. ISSN: 0004-6361, 1432-0746. DOI: 10.1051/0004-6361/201525898. arXiv: 1502.02114.

[53] Ralph A. Alpher, James W. Follin and Robert C. Herman. "Physical Conditions in the Initial Stages of the Expanding Universe". In: *Physical Review* 92.6 (15th Dec. 1953), pp. 1347–1361. DOI: 10.1103/PhysRev.92.1347.

[54] Richard H. Cyburt, Brian D. Fields, Keith A. Olive and Tsung-Han Yeh. "Big Bang Nucleosynthesis: 2015". In: *Reviews of Modern Physics* 88.1 (23rd Feb. 2016), p. 015004. ISSN: 0034-6861, 1539-0756. DOI: 10.1103/RevModPhys.88.015004. arXiv: 1505.01076 [astro-ph].

[55] Brian D. Fields, Paolo Molaro and Subir Sarkar. "Big-Bang Nucleosynthesis". In: *Chinese Physics C* 38.9 (Aug. 2014), p. 090001. ISSN: 1674-1137. DOI: 10.1088/1674-1137/38/9/090001. arXiv: 1412.1408 [astro-ph].

[56] G. Gamow. "The Evolution of the Universe". In: *Nature* 162.4122 (4122 Oct. 1948), pp. 680–682. ISSN: 1476-4687. DOI: 10.1038/162680a0.

[57] S. W. Hawking and R. J. Tayler. "Helium Production in an Anisotropic Big-Bang Cosmology". In: *Nature* 209.5030 (5030 Mar. 1966), pp. 1278–1279. ISSN: 1476-4687. DOI: 10.1038/2091278a0.

[58] Chushiro Hayashi. "Proton-Neutron Concentration Ratio in the Expanding Universe at the Stages Preceding the Formation of the Elements". In: *Progress of Theoretical Physics* 5.2 (1st Mar. 1950), pp. 224–235. ISSN: 0033-068X. DOI: 10.1143/ptp/5.2.224.

[59] P. J. E. Peebles. "Primeval Helium Abundance and the Primeval Fireball". In: *Physical Review Letters* 16.10 (7th Mar. 1966), pp. 410–413. DOI: 10.1103/PhysRevLett.16.410.

[60] P. J. E. Peebles. "Primordial Helium Abundance and the Primordial Fireball. II". In: *The Astrophysical Journal* 146 (1st Nov. 1966), p. 542. ISSN: 0004-637X. DOI: 10.1086/148918.

[61] Robert V. Wagoner. "Big-Bang Nucleosynthesis Revisited". In: *The Astrophysical Journal* 179 (1st Jan. 1973), pp. 343–360. ISSN: 0004-637X. DOI: 10.1086/151873.

[62] Daniel Baumann. *Cosmology*. Cambridge: Cambridge University Press, 2022. ISBN: 978-1-108-83807-8. DOI: 10.1017/9781108937092.

[63] Scott Dodelson. *Modern Cosmology*. Amsterdam: Academic Press, 2003. ISBN: 978-0-12-219141-1. DOI: 10.1016/B978-0-12-219141-1.X5019-0.

[64] Cyril Pitrou, Alain Coc, Jean-Philippe Uzan and Elisabeth Vangioni. "A New Tension in the Cosmological Model from Primordial Deuterium?" In: *Monthly Notices of the Royal Astronomical Society* 502.2 (10th Feb. 2021), pp. 2474–2481. ISSN: 0035-8711, 1365-2966. DOI: 10.1093/mnras/stab135. arXiv: 2011.11320 [astro-ph, physics:nucl-th].

[65] Cyril Pitrou, Alain Coc, Jean-Philippe Uzan and Elisabeth Vangioni. "Precision Big Bang Nucleosynthesis with Improved Helium-4 Predictions". In: *Physics Reports* 754 (Sept. 2018), pp. 1–66. ISSN: 03701573. DOI: 10.1016/j.physrep.2018.04.005. arXiv: 1801.08023 [astro-ph, physics:nucl-th].

[66] Brian D. Fields. "The Primordial Lithium Problem". In: *Annual Review of Nuclear and Particle Science* 61.1 (23rd Nov. 2011), pp. 47–68. ISSN: 0163-8998, 1545-4134. DOI: 10.1146/annurev-nucl-102010-130445. arXiv: 1203.3551.

[67] Diego Blas, Julien Lesgourgues and Thomas Tram. "The Cosmic Linear Anisotropy Solving System ({CLASS). Part {II: Approximation Schemes". In: *Journal of Cosmology and Astroparticle Physics* 2011.7 (July 2011), pp. 34–34. DOI: 10.1088/1475-7516/2011/07/034. arXiv: 1104.2933.

[68] Yacine Ali-Haïmoud and Christopher M Hirata. "HyRec: A Fast and Highly Accurate Primordial Hydrogen and Helium Recombination Code". In: *Physical Review D* 83.4 (Feb. 2011), pp. 043513–043513. ISSN: 1550-7998, 1550-2368. DOI: 10.1103/PhysRevD.83.043513. arXiv: 1011.3758.

[69] P. J. E. Peebles. "Recombination of the Primeval Plasma". In: *The Astrophysical Journal* 153 (1st July 1968), p. 1. ISSN: 0004-637X. DOI: 10.1086/149628.

[70] Sara Seager et al. "How Exactly Did the Universe Become Neutral?" In: *The Astrophysical Journal Supplement Series* 128.2 (June 2000), pp. 407–430. ISSN: 0067-0049, 1538-4365. DOI: 10.1086/313388. arXiv: astro-ph/9912182.

[71] S Seager, D D Sasselov and D Scott. "A New Calculation of the Recombination Epoch". In: *The Astrophysical Journal* 523.1 (Sept. 1999), pp. L1–L5. ISSN: 0004637X. DOI: 10.1086/312250. arXiv: astro-ph/9909275.

[72] Nanoom Lee and Yacine Ali-Haïmoud. "HYREC-2: A Highly Accurate Sub-Millisecond Recombination Code". In: *Physical Review D* 102.8 (13th Oct. 2020), p. 083517. ISSN: 2470-0010, 2470-0029. DOI: 10.1103/PhysRevD.102.083517. arXiv: 2007.14114.

[73] J. R. Shaw and J. Chluba. "Precise Cosmological Parameter Estimation Using CosmoRec". In: *Monthly Notices of the Royal Astronomical Society* 415.2 (1st Aug. 2011), pp. 1343–1354. ISSN: 00358711. DOI: 10.1111/j.1365-2966.2011.18782.x. arXiv: 1102.3683 [astro-ph].

[74] F. Hoyle. "On the Fragmentation of Gas Clouds Into Galaxies and Stars." In: *The Astrophysical Journal* 118 (1st Nov. 1953), p. 513. ISSN: 0004-637X. DOI: 10.1086/145780.

[75] Rennan Barkana and Abraham Loeb. "In the Beginning: The First Sources of Light and the Reionization of the Universe". In: *Physics Reports* 349.2 (July 2001), pp. 125–238. ISSN: 03701573. DOI: 10.1016/S0370-1573(01)00019-9. arXiv: astro-ph/0010468.

[76] Volker Bromm and Naoki Yoshida. "The First Galaxies". In: *Annual Review of Astronomy and Astrophysics* 49.1 (22nd Sept. 2011), pp. 373–407. ISSN: 0066-4146, 1545-4282. DOI: 10.1146/annurev-astro-081710-102608. arXiv: 1102.4638 [astro-ph].

[77] Ralf S. Klessen and Simon C. O. Glover. *The First Stars: Formation, Properties, and Impact*. 22nd Mar. 2023. arXiv: 2303.12500 [astro-ph]. URL: http://arxiv.org/abs/2303.12500 (visited on 31/03/2023). preprint.

[78] Abraham Loeb and Rennan Barkana. "The Reionization of the Universe by the First Stars and Quasars". In: *Annual Review of Astronomy and Astrophysics* 39.1 (Sept. 2001), pp. 19–66. ISSN: 0066-4146, 1545-4282. DOI: 10.1146/annurev.astro.39.1.19. arXiv: astro-ph/0010467.

[79] Piero Madau and Mark Dickinson. "Cosmic Star Formation History". In: *Annual Review of Astronomy and Astrophysics* 52.1 (18th Aug. 2014), pp. 415–486. ISSN: 0066-4146, 1545-4282. DOI: 10.1146/annurev-astro-081811-125615. arXiv: 1403.0007 [astro-ph].

[80] L. V. E. Koopmans et al. "The Cosmic Dawn and Epoch of Reionization with the Square Kilometre Array". In: *Proceedings of Advancing Astrophysics with the Square Kilometre Array — PoS(AASKA14)*. 29th May 2015, p. 001. DOI: 10.22323/1.215.0001. arXiv: 1505.07568 [astro-ph]. URL: http://arxiv.org/abs/1505.07568 (visited on 31/03/2023).

[81] Garrelt Mellema et al. "Reionization and the Cosmic Dawn with the Square Kilometre Array". In: *Experimental Astronomy* 36.1-2 (Aug. 2013), pp. 235–318. ISSN: 0922-6435, 1572-9508. DOI: 10.1007/s10686-013-9334-5. arXiv: 1210.0197 [astro-ph].

[82] David R. DeBoer et al. "Hydrogen Epoch of Reionization Array (HERA)". In: *Publications of the Astronomical Society of the Pacific* 129.974 (1st Apr. 2017), p. 045001. ISSN: 0004-6280, 1538-3873. DOI: 10.1088/1538-3873/129/974/045001. arXiv: 1606.07473.

[83] Jonathan P. Gardner et al. "The James Webb Space Telescope". In: *Space Science Reviews* 123.4 (Apr. 2006), pp. 485–606. ISSN: 0038-6308, 1572-9672. DOI: 10.1007/s11214-006-8315-7. arXiv: astro-ph/0606175.

[84] A. Weltman et al. "Fundamental Physics with the Square Kilometre Array". In: *Publications of the Astronomical Society of Australia* 37 (2020), e002. ISSN: 1323-3580, 1448-6083. DOI: 10.1017/pasa.2019.42. arXiv: 1810.02680 [astro-ph, physics:hep-ph].

[85] Square Kilometre Array Cosmology Science Working Group et al. "Cosmology with Phase 1 of the Square Kilometre Array; Red Book 2018: Technical Specifications and Performance Forecasts". In: *Publications of the Astronomical Society of Australia* 37 (2020), e007. ISSN: 1323-3580, 1448-6083. DOI: 10.1017/pasa.2019.51. arXiv: 1811.02743 [astro-ph].

[86] Anirudh Chiti et al. "An Extended Halo around an Ancient Dwarf Galaxy". In: *Nature Astronomy* 5.4 (Apr. 2021), pp. 392–400. ISSN: 2397-3366. DOI: 10.1038/s41550-020-01285-w. arXiv: 2012.02309.

[87] Pablo F. de Salas and Axel Widmark. "Dark Matter Local Density Determination: Recent Observations and Future Prospects". In: *Reports on Progress in Physics* 84.10 (1st Oct. 2021), p. 104901. ISSN: 0034-4885, 1361-6633. DOI: 10.1088/1361-6633/ac24e7. arXiv: 2012.11477.

[88] Timothy Clifton, Pedro G. Ferreira, Antonio Padilla and Constantinos Skordis. "Modified Gravity and Cosmology". In: *Physics Reports*. Modified Gravity and Cosmology 513.1 (1st Mar. 2012), pp. 1–189. ISSN: 0370-1573. DOI: 10.1016/j.physrep.2012.01.001. arXiv: 1106.2476.

[89] Constantinos Skordis and Tom Złośnik. "Gravitational Alternatives to Dark Matter with Tensor Mode Speed Equaling the Speed of Light". In: *Physical Review D* 100.10 (7th Nov. 2019), p. 104013. DOI: 10.1103/PhysRevD.100.104013. arXiv: 1905.09465.

[90] Constantinos Skordis and Tom Złośnik. "New Relativistic Theory for Modified Newtonian Dynamics". In: *Physical Review Letters* 127.16 (15th Oct. 2021), p. 161302. DOI: 10.1103/PhysRevLett.127.161302. arXiv: 2007.00082.

[91] G. Hinshaw et al. "Nine-Year Wilkinson Microwave Anisotropy Probe (WMAP) Observations: Cosmological Parameter Results". In: *The Astrophysical Journal Supplement Series* 208.2 (20th Sept. 2013), p. 19. ISSN: 0067-0049, 1538-4365. DOI: 10.1088/0067-0049/208/2/19. arXiv: 1212.5226 [astro-ph].

[92] Planck Collaboration et al. "Planck 2015 Results. XIII. Cosmological Parameters". In: *Astronomy & Astrophysics* 594 (Oct. 2016), A13. ISSN: 0004-6361, 1432-0746. DOI: 10.1051/0004-6361/201525830. arXiv: 1502.01589 [astro-ph].

[93] Richard H. Cyburt, Brian D. Fields and Keith A. Olive. "Primordial Nucleosynthesis in Light of WMAP". In: *Physics Letters B* 567.3-4 (Aug. 2003), pp. 227–234. ISSN: 03702693. DOI: 10.1016/j.physletb.2003.06.026. arXiv: astro-ph/0302431.

[94] Ryan Cooke et al. "Precision Measures of the Primordial Abundance of Deuterium". In: *The Astrophysical Journal* 781.1 (3rd Jan. 2014), p. 31. ISSN: 0004-637X, 1538-4357. DOI: 10.1088/0004-637X/781/1/31. arXiv: 1308.3240.

[95] Brian D. Fields, Keith A. Olive, Tsung-Han Yeh and Charles Young. "Big-Bang Nucleosynthesis After Planck". In: *Journal of Cosmology and Astroparticle Physics* 2020.03 (3rd Mar. 2020), pp. 010–010. ISSN: 1475-7516. DOI: 10.1088/1475-7516/2020/03/010. arXiv: 1912.01132.

[96] C. L. Bennett et al. "The Microwave Anisotropy Probe (MAP) Mission". In: *The Astrophysical Journal* 583.1 (20th Jan. 2003), pp. 1–23. ISSN: 0004-637X, 1538-4357. DOI: 10.1086/345346. arXiv: astro-ph/0301158.

[97] D. N. Spergel et al. "First Year Wilkinson Microwave Anisotropy Probe (WMAP) Observations: Determination of Cosmological Parameters". In: *The Astrophysical Journal Supplement Series* 148.1 (Sept. 2003), pp. 175–194. ISSN: 0067-0049, 1538-4365. DOI: 10.1086/377226. arXiv: astro-ph/0302209.

[98] C. L. Bennett et al. "Nine-Year Wilkinson Microwave Anisotropy Probe (WMAP) Observations: Final Maps and Results". In: *The Astrophysical Journal Supplement Series* 208.2 (20th Sept. 2013), p. 20. ISSN: 0067-0049, 1538-4365. DOI: 10.1088/0067-0049/208/2/20. arXiv: 1212.5225 [astro-ph].

[99] The Planck Collaboration. *The Scientific Programme of Planck*. 4th Apr. 2006. arXiv: astro-ph/0604069. URL: http://arxiv.org/abs/astro-ph/0604069 (visited on 03/04/2023). preprint.

[100] F. Villa et al. "The Planck Telescope". In: *AIP Conference Proceedings*. Vol. 616. 2002, pp. 224–228. DOI: 10.1063/1.1475633. arXiv: astro-ph/0112173. URL: http://arxiv.org/abs/astro-ph/0112173 (visited on 03/04/2023).

[101] Planck Collaboration et al. "Planck 2013 Results. XVI. Cosmological Parameters". In: *Astronomy & Astrophysics* 571 (Nov. 2014), A16. ISSN: 0004-6361, 1432-0746. DOI: 10.1051/0004-6361/201321591. arXiv: 1303.5076 [astro-ph].

[102] W. J. G. de Blok et al. "High-Resolution Rotation Curves and Galaxy Mass Models from THINGS". In: *The Astronomical Journal* 136.6 (1st Dec. 2008), pp. 2648–2719. ISSN: 0004-6256, 1538-3881. DOI: 10.1088/0004-6256/136/6/2648. arXiv: 0810.2100 [astro-ph].

[103] Jo Bovy. "Galpy: A Python Library for Galactic Dynamics". In: *The Astrophysical Journal Supplement Series* 216.2 (3rd Feb. 2015), p. 29. ISSN: 1538-4365. DOI: 10.1088/0067-0049/216/2/29. arXiv: 1412.3451 [astro-ph].

[104] Gaia Collaboration et al. "Gaia Data Release 2: Kinematics of Globular Clusters and Dwarf Galaxies around the Milky Way". In: *Astronomy & Astrophysics* 616 (Aug. 2018), A12. ISSN: 0004-6361, 1432-0746. DOI: 10.1051/0004-6361/201832698. arXiv: 1804.09381 [astro-ph].

[105] Giuseppina Battaglia, Amina Helmi and Maarten Breddels. "Internal Kinematics and Dynamical Models of Dwarf Spheroidal Galaxies around the Milky Way". In: *New Astronomy Reviews* 57.3-4 (Sept. 2013), pp. 52–79. ISSN: 13876473. DOI: 10.1016/j.newar.2013.05.003. arXiv: 1305.5965 [astro-ph].

[106] J. T. Kleyna, M. I. Wilkinson, N. W. Evans and G. Gilmore. "Dark Matter in Dwarf Spheroidals II: Observations and Modelling of Draco". In: *Monthly Notices of the Royal Astronomical Society* 330.4 (Mar. 2002), pp. 792–806. ISSN: 00358711, 13652966. DOI: 10.1046/j.1365-8711.2002.05155.x. arXiv: astro-ph/0109450.

[107] Pieter van Dokkum et al. "Spatially-Resolved Stellar Kinematics of the Ultra Diffuse Galaxy Dragonfly 44. I. Observations, Kinematics, and Cold Dark Matter Halo Fits". In: *The Astrophysical Journal* 880.2 (30th July 2019), p. 91. ISSN: 1538-4357. DOI: 10.3847/1538-4357/ab2914. arXiv: 1904.04838 [astro-ph].

[108] Matthew G. Walker. "Dark Matter in the Milky Way's Dwarf Spheroidal Satellites". In: 2013, pp. 1039–1089. DOI: 10.1007/978-94-007-5612-0_20. arXiv: 1205.0311 [astro-ph]. URL: http://arxiv.org/abs/1205.0311 (visited on 04/04/2023).

[109] Matthias Bartelmann and Peter Schneider. "Weak Gravitational Lensing". In: *Physics Reports* 340.4-5 (Jan. 2001), pp. 291–472. ISSN: 03701573. DOI: 10.1016/S0370-1573(00)00082-X. arXiv: astro-ph/9912508.

[110] Marusa Bradac et al. "Strong and Weak Lensing United III: Measuring the Mass Distribution of the Merging Galaxy Cluster 1E0657-56". In: *The Astrophysical Journal* 652.2 (Dec. 2006), pp. 937–947. ISSN: 0004-637X, 1538-4357. DOI: 10.1086/508601. arXiv: astro-ph/0608408.

[111] Douglas Clowe et al. "A Direct Empirical Proof of the Existence of Dark Matter". In: *The Astrophysical Journal* 648.2 (10th Sept. 2006), pp. L109–L113. ISSN: 0004-637X, 1538-4357. DOI: 10.1086/508162. arXiv: astro-ph/0608407.

[112] Arthur Stanley Eddington. *Space, Time and Gravitation: An Outline of the General Relativity Theory*. Cambridge: University Press, 1920 [eBook 2009]. 218 pp. ISBN: 978-0-521-33709-0. URL: https://www.gutenberg.org/ebooks/29782 (visited on 03/04/2023).

[113] Peter Schneider, Jürgen Ehlers and Emilio E. Falco. *Gravitational Lenses*. Red. by I. Appenzeller et al. Astronomy and Astrophysics Library. Berlin, Heidelberg: Springer Berlin Heidelberg, 1992. ISBN: 978-3-540-66506-9 978-3-662-03758-4. DOI: 10.1007/978-3-662-03758-4. URL: http://link.springer.com/10.1007/978-3-662-03758-4 (visited on 03/04/2023).

[114] Peter Schneider. *Extragalactic Astronomy and Cosmology: An Introduction*. Second Edition. Berlin, Heidelberg: Springer Berlin Heidelberg, 2015. 637 pp. ISBN: 978-3-642-54082-0 978-3-642-54083-7. DOI: 10.1007/978-3-642-54083-7. URL: https://link.springer.com/10.1007/978-3-642-54083-7.

[115] Matthias Bartelmann et al. "Arc Statistics with Realistic Cluster Potentials. IV. Clusters in Different Cosmologies". In: *Astronomy and Astrophysics* 330 (15th July 1997), pp. 1–9. ISSN: 0004-6361. DOI: 10.48550/arXiv.astro-ph/9707167. arXiv: astro-ph/9707167.

[116] David J. Lagattuta et al. "Lens Modeling Abell 370: Crowning the Final Frontier Field with MUSE". In: *Monthly Notices of the Royal Astronomical Society* 469.4 (Aug. 2017), pp. 3946–3964. ISSN: 0035-8711, 1365-2966. DOI: 10.1093/mnras/stx1079. arXiv: 1611.01513 [astro-ph].

[117] Marceau Limousin, Benjamin Beauchesne and Eric Jullo. "Dark Matter in Galaxy Clusters: A Parametric Strong Lensing Approach". In: *Astronomy & Astrophysics* 664 (Aug. 2022), A90. ISSN: 0004-6361, 1432-0746. DOI: 10.1051/0004-6361/202243278. arXiv: 2202.02992 [astro-ph].

[118] Guillaume Mahler et al. "Precision Modeling of JWST's First Cluster Lens SMACSJ0723.3-7327". In: *The Astrophysical Journal* 945.1 (1st Mar. 2023), p. 49. ISSN: 0004-637X, 1538-4357. DOI: 10.3847/1538-4357/acaea9. arXiv: 2207.07101 [astro-ph].

[119] Masamune Oguri, Cristian E. Rusu and Emilio E. Falco. "The Stellar and Dark Matter Distributions in Elliptical Galaxies from the Ensemble of Strong Gravitational Lenses". In: *Monthly Notices of the Royal Astronomical Society* 439.3 (11th Apr. 2014), pp. 2494–2504. ISSN: 1365-2966, 0035-8711. DOI: 10.1093/mnras/stu106. arXiv: 1309.5408 [astro-ph].

[120] Johan Richard et al. "Abell 370 Revisited: Refurbished Hubble Imaging of the First Strong Lensing Cluster". In: *Monthly Notices of the Royal Astronomical Society: Letters* 402.1 (1st Feb. 2010), pp. L44–L48. ISSN: 1745-3933, 1745-3925. DOI: 10.1111/j.1745-3933.2009.00796.x. arXiv: 0910.5553 [astro-ph].

[121] J. Richard et al. "Mass and Magnification Maps for the Hubble Space Telescope Frontier Fields Clusters: Implications for High Redshift Studies". In: *Monthly Notices of the Royal Astronomical Society* 444.1 (11th Oct. 2014), pp. 268–289. ISSN: 0035-8711, 1365-2966. DOI: 10.1093/mnras/stu1395. arXiv: 1405.3303 [astro-ph].

[122] G. Soucail et al. "The Giant Arc in A 370 : Spectroscopic Evidence for Gravitational Lensing from a Source at Z=0.724." In: *Astronomy and Astrophysics* 191 (1st Feb. 1988), pp. L19–L21. ISSN: 0004-6361.

[123] T. Treu. "Strong Lensing by Galaxies". In: *Annual Review of Astronomy and Astrophysics* 48.1 (1st Aug. 2010), pp. 87–125. ISSN: 0066-4146, 1545-4282. DOI: 10.1146/annurev-astro-081309-130924. arXiv: 1003.5567 [astro-ph].

[124] J. Anthony Tyson, Greg P. Kochanski and Ian P. Dell'Antonio. "Detailed Mass Map of CL0024+1654 from Strong Lensing". In: *The Astrophysical Journal* 498.2 (10th May 1998), pp. L107–L110. ISSN: 0004637X. DOI: 10.1086/311314. arXiv: astro-ph/9801193.

[125] H. Wang et al. "Constraining the Multi-Scale Dark-Matter Distribution in CASSOWARY 31 with Strong Gravitational Lensing and Stellar Dynamics". In: *Astronomy & Astrophysics* 668 (Dec. 2022), A162. ISSN: 0004-6361, 1432-0746. DOI: 10.1051/0004-6361/202243600. arXiv: 2203.13759 [astro-ph].

[126] M. Bartelmann and P. Schneider. "Gravitational Lensing by Large-Scale Structures". In: *Astronomy and Astrophysics* 248 (1st Aug. 1991), pp. 349–353. ISSN: 0004-6361.

[127] Henk Hoekstra, Howard K. C. Yee and Michael D. Gladders. "Properties of Galaxy Dark Matter Halos from Weak Lensing". In: *The Astrophysical Journal* 606.1 (May 2004), pp. 67–77. ISSN: 0004-637X, 1538-4357. DOI: 10.1086/382726. arXiv: astro-ph/0306515.

[128] Nick Kaiser and Gordon Squires. "Mapping the Dark Matter with Weak Gravitational Lensing". In: *The Astrophysical Journal* 404 (Feb. 1993), p. 441. ISSN: 0004-637X, 1538-4357. DOI: 10.1086/172297.

[129] Peter Schneider. "Detection of (Dark) Matter Concentrations via Weak Gravitational Lensing". In: *Monthly Notices of the Royal Astronomical Society* 283 (1st Dec. 1996), pp. 837–853. ISSN: 0035-8711. DOI: 10.1093/mnras/283.3.837. arXiv: astro-ph/9601039.

[130] Eleonora Di Valentino et al. "Cosmology Intertwined II: The Hubble Constant Tension". In: *Astroparticle Physics* 131 (Sept. 2021), p. 102605. ISSN: 09276505. DOI: 10.1016/j.astropartphys.2021.102605. arXiv: 2008.11284.

[131] Eleonora Di Valentino et al. "Cosmology Intertwined III: $f \sigma_8$ and S_8". In: *Astroparticle Physics* 131 (Sept. 2021), p. 102604. ISSN: 09276505. DOI: 10.1016/j.astropartphys.2021.102604. arXiv: 2008.11285.

[132] Leandros Perivolaropoulos and Foteini Skara. "Challenges for ΛCDM: An Update". In: *New Astronomy Reviews* 95 (Dec. 2022), p. 101659. ISSN: 13876473. DOI: 10.1016/j.newar.2022.101659. arXiv: 2105.05208 [astro-ph, physics:gr-qc, physics:hep-ph, physics:hep-th].

[133] Guido D'Amico, Leonardo Senatore, Pierre Zhang and Henry Zheng. "The Hubble Tension in Light of the Full-Shape Analysis of Large-Scale Structure Data". In: *Journal of Cosmology and Astroparticle Physics* 2021.05 (1st May 2021), p. 072. ISSN: 1475-7516. DOI: 10.1088/1475-7516/2021/05/072. arXiv: 2006.12420 [astro-ph, physics:gr-qc, physics:hep-ph].

[134] Eleonora Di Valentino et al. "In the Realm of the Hubble Tension—a Review of Solutions". In: *Classical and Quantum Gravity* 38.15 (22nd July 2021), p. 153001. ISSN: 0264-9381, 1361-6382. DOI: 10.1088/1361-6382/ac086d. arXiv: 2103.01183.

[135] G. Efstathiou. *A Lockdown Perspective on the Hubble Tension (with Comments from the SH0ES Team)*. 26th July 2020. arXiv: 2007.10716 [astro-ph]. URL: http://arxiv.org/abs/2007.10716. preprint.

[136] Nils Schöneberg et al. "The H_0 Olympics: A Fair Ranking of Proposed Models". In: *Physics Reports* 984 (Oct. 2022), pp. 1–55. ISSN: 03701573. DOI: 10.1016/j.physrep.2022.07.001. arXiv: 2107.10291 [astro-ph, physics:hep-ph, physics:hep-th].

[137] Adam G. Riess et al. "A 3% Solution: Determination of the Hubble Constant with the Hubble Space Telescope and Wide Field Camera 3". In: *The Astrophysical Journal* 730.2 (1st Apr. 2011), p. 119. ISSN: 0004-637X, 1538-4357. DOI: 10.1088/0004-637X/730/2/119. arXiv: 1103.2976 [astro-ph].

[138] Adam G. Riess et al. "A 2.4% Determination of the Local Value of the Hubble Constant". In: *The Astrophysical Journal* 826.1 (21st July 2016), p. 56. ISSN: 1538-4357. DOI: 10.3847/0004-637X/826/1/56. arXiv: 1604.01424 [astro-ph].

[139] Adam G. Riess et al. "Large Magellanic Cloud Cepheid Standards Provide a 1% Foundation for the Determination of the Hubble Constant and Stronger Evidence for Physics beyond \ensuremath\LambdaCDM". In: *The Astrophysical Journal* 876.1 (1st May 2019), p. 85. ISSN: 0004-637X, 1538-4357. DOI: 10.3847/1538-4357/ab1422. arXiv: 1903.07603 [astro-ph].

[140] DES Collaboration et al. "Dark Energy Survey Year 1 Results: Cosmological Constraints from Galaxy Clustering and Weak Lensing". In: *Physical Review D* 98.4 (27th Aug. 2018), p. 043526. ISSN: 2470-0010, 2470-0029. DOI: 10.1103/PhysRevD.98.043526. arXiv: 1708.01530 [astro-ph].

[141] Tilman Tröster et al. "Cosmology from Large-Scale Structure: Constraining ΛCDM with BOSS". In: *Astronomy & Astrophysics* 633 (Jan. 2020), p. L10. ISSN: 0004-6361, 1432-0746. DOI: 10.1051/0004-6361/201936772. arXiv: 1909.11006 [astro-ph].

[142] Catherine Heymans et al. "KiDS-1000 Cosmology: Multi-probe Weak Gravitational Lensing and Spectroscopic Galaxy Clustering Constraints". In: *Astronomy & Astrophysics* 646 (Feb. 2021), A140. ISSN: 0004-6361, 1432-0746. DOI: 10.1051/0004-6361/202039063. arXiv: 2007.15632 [astro-ph].

[143] Maria Archidiacono et al. "Linear Scale Bounds on Dark Matter-Dark Radiation Interactions and Connection with the Small Scale Crisis of Cold Dark Matter". In: *Journal of Cosmology and Astroparticle Physics* 2017.11 (Nov. 2017), pp. 10–10. DOI: 10.1088/1475-7516/2017/11/010. arXiv: 1706.06870.

[144] James A. D. Diacoumis and Yvonne Y. Y. Wong. "Using CMB Spectral Distortions to Distinguish between Dark Matter Solutions to the Small-Scale Crisis". In: *Journal of Cosmology and Astroparticle Physics* 2017.09 (8th Sept. 2017), pp. 011–011. ISSN: 1475-7516. DOI: 10.1088/1475-7516/2017/09/011. arXiv: 1707.07050 [astro-ph, physics:hep-ph].

[145] Matteo Viel, George D. Becker, James S. Bolton and Martin G. Haehnelt. "Warm Dark Matter as a Solution to the Small Scale Crisis: New Constraints from High Redshift Lyman-alpha Forest Data". In: *Physical Review D* 88.4 (5th Aug. 2013), p. 043502. ISSN: 1550-7998, 1550-2368. DOI: 10.1103/PhysRevD.88.043502. arXiv: 1306.2314 [astro-ph].

[146] David H Weinberg et al. "Cold Dark Matter: Controversies on Small Scales". In: *Proceedings of the National Academy of Sciences* 112.40 (6th Oct. 2015), pp. 12249–12255. ISSN: 0027-8424, 1091-6490. DOI: 10.1073/pnas.1308716112. arXiv: 1306.0913 [astro-ph].

[147] James S Bullock and Michael Boylan-Kolchin. "Small-Scale Challenges to the ΛCDM Paradigm". In: *Annual Review of Astronomy and Astrophysics* 55.1 (18th Aug. 2017), pp. 343–387. ISSN: 0066-4146, 1545-4282. DOI: 10.1146/annurev-astro-091916-055313. arXiv: 1707.04256 [astro-ph, physics:hep-ph].

[148] C. Boehm et al. "Using the Milky Way Satellites to Study Interactions between Cold Dark Matter and Radiation". In: *Monthly Notices of the Royal Astronomical Society: Letters* 445.1 (21st Nov. 2014), pp. L31–L35. ISSN: 1745-3933, 1745-3925. DOI: 10.1093/mnrasl/slu115. arXiv: 1404.7012.

[149] J. A. Schewtschenko et al. "Dark Matter-Radiation Interactions: The Structure of Milky Way Satellite Galaxies". In: *Monthly Notices of the Royal Astronomical Society* 461.3 (Sept. 2016), pp. 2282–2287. DOI: 10.1093/mnras/stw1078. arXiv: 1512.06774.

[150] Francisco Villaescusa-Navarro et al. "The CAMELS Project: Cosmology and Astrophysics with MachinE Learning Simulations". In: *The Astrophysical Journal* 915.1 (1st July 2021), p. 71. ISSN: 0004-637X, 1538-4357. DOI: 10.3847/1538-4357/abf7ba. arXiv: 2010.00619 [astro-ph].

[151] Raul E. Angulo and Oliver Hahn. "Large-Scale Dark Matter Simulations". In: *Living Reviews in Computational Astrophysics* 8.1 (Dec. 2022), p. 1. ISSN: 2367-3621, 2365-0524. DOI: 10.1007/s41115-021-00013-z. arXiv: 2112.05165.

[152] Gianfranco Bertone, ed. *Particle Dark Matter*. Cambridge: Cambridge University Press, 2010. ISBN: 978-0-511-77073-9. DOI: 10.1017/CBO9780511770739. URL: http://ebooks.cambridge.org/ref/id/CBO9780511770739.

[153] Leszek Roszkowski, Enrico Maria Sessolo and Sebastian Trojanowski. "WIMP Dark Matter Candidates and Searches - Current Status and Future Prospects". In: *Reports on Progress in Physics* 81.6 (1st June 2018), p. 066201. ISSN: 0034-4885, 1361-6633. DOI: 10.1088/1361-6633/aab913. arXiv: 1707.06277.

[154] Howard Baer, Ki-Young Choi, Jihn E. Kim and Leszek Roszkowski. "Dark Matter Production in the Early Universe: Beyond the Thermal WIMP Paradigm". In: *Physics Reports* 555 (Feb. 2015), pp. 1–60. ISSN: 03701573. DOI: 10.1016/j.physrep.2014.10.002. arXiv: 1407.0017 [astro-ph, physics:hep-ph].

[155] R. Cowsik and J. McClelland. "Gravity of Neutrinos of Nonzero Mass in Astrophysics". In: *The Astrophysical Journal* 180 (1st Feb. 1973), pp. 7–10. ISSN: 0004-637X. DOI: 10.1086/151937.

[156] J. R. Bond, G. Efstathiou and J. Silk. "Massive Neutrinos and the Large-Scale Structure of the Universe". In: *Physical Review Letters* 45.24 (15th Dec. 1980), pp. 1980–1984. DOI: 10.1103/PhysRevLett.45.1980.

[157] S. Tremaine and J. E. Gunn. "Dynamical Role of Light Neutral Leptons in Cosmology". In: *Physical Review Letters* 42.6 (1979). Ed. by M. A. Srednicki, pp. 407–410. DOI: 10.1103/PhysRevLett.42.407.

[158] Jaan Einasto. *Dark Matter*. 19th Oct. 2010. DOI: 10.48550/arXiv.0901.0632. arXiv: 0901.0632. URL: http://arxiv.org/abs/0901.0632 (visited on 17/11/2022). preprint.

[159] E. L. Wright et al. "Interpretation of the Cosmic Microwave Background Radiation Anisotropy Detected by the COBE Differential Microwave Radiometer". In: *The Astrophysical Journal* 396 (1st Sept. 1992), p. L13. ISSN: 0004-637X. DOI: 10.1086/186506.

[160] David O. Caldwell and Rabindra N. Mohapatra. "Neutrino Mass Explanations of Solar and Atmospheric Neutrino Deficits and Hot Dark Matter". In: *Physical Review D* 48.7 (1st Oct. 1993), pp. 3259–3263. DOI: 10.1103/PhysRevD.48.3259.

[161] G. Dvali, Q. Shafi and R. Schaefer. "Large Scale Structure and Supersymmetric Inflation without Fine Tuning". In: *Physical Review Letters* 73.14 (3rd Oct. 1994), pp. 1886–1889. ISSN: 0031-9007. DOI: 10.1103/PhysRevLett.73.1886. arXiv: hep-ph/9406319.

[162] Scott Dodelson and Lawrence M Widrow. "Sterile Neutrinos as Dark Matter". In: *Physical Review Letters* 72.1 (3rd Jan. 1994), pp. 17–20. ISSN: 0031-9007. DOI: 10.1103/PhysRevLett.72.17. arXiv: hep-ph/9303287.

[163] Chung-Pei C.-P. Ma and Edmund Bertschinger. "Cosmological Perturbation Theory in the Synchronous and Conformal Newtonian Gauges". In: *The Astrophysical Journal* 455 (Dec. 1995), p. 7. ISSN: 0004-637X, 1538-4357. DOI: 10.1086/176550. arXiv: astro-ph/9506072.

[164] Z. Berezhiani and R. N. Mohapatra. "Reconciling Present Neutrino Puzzles: Sterile Neutrinos as Mirror Neutrinos". In: *Physical Review D* 52.11 (1st Dec. 1995), pp. 6607–6611. ISSN: 0556-2821. DOI: 10.1103/PhysRevD.52.6607. arXiv: hep-ph/9505385.

[165] Kevork Abazajian, George M. Fuller and Mitesh Patel. "Sterile Neutrino Hot, Warm, and Cold Dark Matter". In: *Physical Review D* 64.2 (31st May 2001), p. 023501. ISSN: 0556-2821, 1089-4918. DOI: 10.1103/PhysRevD.64.023501. arXiv: astro-ph/0101524.

[166] Julien Lesgourgues and Sergio Pastor. "Massive Neutrinos and Cosmology". In: *Physics Reports* 429.6 (Mar. 2006), pp. 307–379. ISSN: 03701573. DOI: 10.1016/j.physrep.2006.04.001. arXiv: astro-ph/0603494.

[167] Simeon Bird, Matteo Viel and Martin G. Haehnelt. "Massive Neutrinos and the Non-linear Matter Power Spectrum". In: *Monthly Notices of the Royal Astronomical Society* 420.3 (1st Mar. 2012), pp. 2551–2561. ISSN: 00358711. DOI: 10.1111/j.1365-2966.2011.20222.x. arXiv: 1109.4416.

[168] K. N. Abazajian et al. "Neutrino Physics from the Cosmic Microwave Background and Large Scale Structure". In: *Astroparticle Physics* 63 (Mar. 2015), pp. 66–80. ISSN: 09276505. DOI: 10.1016/j.astropartphys.2014.05.014. arXiv: 1309.5383.

[169] eBOSS Collaboration et al. "The Completed SDSS-IV Extended Baryon Oscillation Spectroscopic Survey: Cosmological Implications from Two Decades of Spectroscopic Surveys at the Apache Point Observatory". In: *Physical Review D* 103.8 (28th Apr. 2021), p. 083533. ISSN: 2470-0010, 2470-0029. DOI: 10.1103/PhysRevD.103.083533. arXiv: 2007.08991.

[170] DES Collaboration et al. "Dark Energy Survey Year 3 Results: Cosmological Constraints from Galaxy Clustering and Weak Lensing". In: *Physical Review D* 105.2 (13th Jan. 2022), p. 023520. ISSN: 2470-0010, 2470-0029. DOI: 10.1103/PhysRevD.105.023520. arXiv: 2105.13549.

[171] R. Laureijs et al. *Euclid Definition Study Report*. 14th Oct. 2011. DOI: 10.48550/arXiv.1110.3193. arXiv: 1110.3193. URL: http://arxiv.org/abs/1110.3193 (visited on 09/08/2022). preprint.

[172] Jan Hamann, Steen Hannestad and Yvonne Y. Y. Wong. "Measuring Neutrino Masses with a Future Galaxy Survey". In: *Journal of Cosmology and Astroparticle Physics* 2012.11 (26th Nov. 2012), pp. 052–052. ISSN: 1475-7516. DOI: 10.1088/1475-7516/2012/11/052. arXiv: 1209.1043.

[173] B. Sartoris et al. "Next Generation Cosmology: Constraints from the Euclid Galaxy Cluster Survey". In: *Monthly Notices of the Royal Astronomical Society* 459.2 (21st June 2016), pp. 1764–1780. ISSN: 0035-8711, 1365-2966. DOI: 10.1093/mnras/stw630. arXiv: 1505.02165.

[174] DESI Collaboration et al. *The DESI Experiment Part I: Science,Targeting, and Survey Design*. 13th Dec. 2016. DOI: 10.48550/arXiv.1611.00036. arXiv: 1611.00036. URL: http://arxiv.org/abs/1611.00036 (visited on 09/08/2022). preprint.

[175] Michael E. Levi et al. *The Dark Energy Spectroscopic Instrument (DESI)*. 24th July 2019. DOI: 10.48550/arXiv.1907.10688. arXiv: 1907.10688. URL: http://arxiv.org/abs/1907.10688 (visited on 17/11/2022). preprint.

[176] The Simons Observatory Collaboration et al. "The Simons Observatory: Science Goals and Forecasts". In: *Journal of Cosmology and Astroparticle Physics* 2019.02 (27th Feb. 2019), pp. 056–056. ISSN: 1475-7516. DOI: 10.1088/1475-7516/2019/02/056. arXiv: 1808.07445.

[177] B. J. Carr, Kazunori Kohri, Yuuiti Sendouda and Jun'ichi Yokoyama. "New Cosmological Constraints on Primordial Black Holes". In: *Physical Review D* 81.10 (10th May 2010), p. 104019. ISSN: 1550-7998, 1550-2368. DOI: 10.1103/PhysRevD.81.104019. arXiv: 0912.5297.

[178] Bernard Carr and Joseph Silk. "Primordial Black Holes as Generators of Cosmic Structures". In: *Monthly Notices of the Royal Astronomical Society* 478.3 (Aug. 2018), pp. 3756–3775. DOI: 10.1093/MNRAS/STY1204. arXiv: 1801.00672.

[179] Bernard Carr and Florian Kuhnel. "Primordial Black Holes as Dark Matter: Recent Developments". In: *Annual Review of Nuclear and Particle Science* 70.1 (19th Oct. 2020), pp. 355–394. ISSN: 0163-8998, 1545-4134. DOI: 10.1146/annurev-nucl-050520-125911. arXiv: 2006.02838.

[180] Bernard Carr, Kazunori Kohri, Yuuiti Sendouda and Jun'ichi Yokoyama. "Constraints on Primordial Black Holes". In: *Reports on Progress in Physics* 84.11 (1st Nov. 2021), p. 116902. ISSN: 0034-4885, 1361-6633. DOI: 10.1088/1361-6633/ac1e31. arXiv: 2002.12778.

[181] Jonathan L. Feng. *The WIMP Paradigm: Theme and Variations*. 5th Dec. 2022. DOI: 10.48550/arXiv.2212.02479. arXiv: 2212.02479. URL: http://arxiv.org/abs/2212.02479 (visited on 20/01/2023). preprint.

[182] Gerard Jungman, Marc Kamionkowski and Kim Griest. "Supersymmetric Dark Matter". In: *Physics Reports* 267.5-6 (Mar. 1996), pp. 195–373. ISSN: 03701573. DOI: 10.1016/0370-1573(95)00058-5. arXiv: hep-ph/9506380.

[183] S. Dimopoulos, S. Raby and Frank Wilczek. "Supersymmetry and the Scale of Unification". In: *Physical Review D* 24.6 (15th Sept. 1981), pp. 1681–1683. DOI: 10.1103/PhysRevD.24.1681.

[184] Heinz Pagels and Joel R. Primack. "Supersymmetry, Cosmology, and New Physics at Teraelectronvolt Energies". In: *Physical Review Letters* 48.4 (25th Jan. 1982), pp. 223–226. DOI: 10.1103/PhysRevLett.48.223.

[185] John Ellis et al. "Supersymmetric Relics from the Big Bang". In: *Nuclear Physics B* 238.2 (1984), pp. 453–476. DOI: 10.1016/0550-3213(84)90461-9.

[186] Toby Falk, Keith A Olive and Mark Srednicki. "Heavy Sneutrinos as Dark Matter". In: *Physics Letters B* 339.3 (Nov. 1994), pp. 248–251. ISSN: 03702693. DOI: 10.1016/0370-2693(94)90639-4. arXiv: hep-ph/9409270.

[187] Stephen P. Martin. "A Supersymmetry Primer". In: vol. 18. July 1998, pp. 1–98. DOI: 10.1142/9789812839657_0001. arXiv: hep-ph/9709356. URL: http://arxiv.org/abs/hep-ph/9709356 (visited on 20/01/2023).

[188] Yael Shadmi and Yuri Shirman. "Dynamical Supersymmetry Breaking". In: *Reviews of Modern Physics* 72.1 (1st Jan. 2000), pp. 25–64. ISSN: 0034-6861, 1539-0756. DOI: 10.1103/RevModPhys.72.25. arXiv: hep-th/9907225.

[189] Chiara Arina and Nicolao Fornengo. "Sneutrino Cold Dark Matter, a New Analysis: Relic Abundance and Detection Rates". In: *Journal of High Energy Physics* 2007.11 (13th Nov. 2007), pp. 029–029. ISSN: 1029-8479. DOI: 10.1088/1126-6708/2007/11/029. arXiv: 0709.4477.

[190] John Preskill, Mark B. Wise and Frank Wilczek. "Cosmology of the Invisible Axion". In: *Physics Letters B* 120.1 (6th Jan. 1983), pp. 127–132. ISSN: 0370-2693. DOI: 10.1016/0370-2693(83)90637-8.

[191] David J. E. Marsh. "Axion Cosmology". In: *Physics Reports* 643 (July 2016), pp. 1–79. ISSN: 03701573. DOI: 10.1016/j.physrep.2016.06.005. arXiv: 1510.07633.

[192] YA. B. Zeldovich. "Survey of Modern Cosmology". In: *Advances in Astronomy and Astrophysics*. Ed. by ZDENĚK Kopal. Vol. 3. Elsevier, 1st Jan. 1965, pp. 241–379. DOI: 10.1016/B978-1-4831-9921-4.50011-9. URL: https://www.sciencedirect.com/science/article/pii/B9781483199214500119 (visited on 20/01/2023).

[193] Hong-Yee Chiu. "Symmetry Between Particle and Antiparticle Populations in the Universe". In: *Physical Review Letters* 17.13 (26th Sept. 1966), pp. 712–714. DOI: 10.1103/PhysRevLett.17.712.

[194] G Steigman. "Cosmology Confronts Particle Physics". In: *Annual Review of Nuclear and Particle Science* 29.1 (1st Dec. 1979), pp. 313–338. ISSN: 0163-8998. DOI: 10.1146/annurev.ns.29.120179.001525.

[195] Robert J. Scherrer and Michael S. Turner. "On the Relic, Cosmic Abundance of Stable, Weakly Interacting Massive Particles". In: *Physical Review D* 33.6 (15th Mar. 1986), pp. 1585–1589. DOI: 10.1103/PhysRevD.33.1585.

[196] Robert J. Scherrer and Michael S. Turner. "Erratum: On the Relic, Cosmic Abundance of Stable, Weakly Interacting Massive Particles". In: *Physical Review D* 34.10 (15th Nov. 1986), pp. 3263–3263. DOI: 10.1103/PhysRevD.34.3263.

[197] C. Boehm and Pierre Fayet. "Scalar Dark Matter Candidates". In: *Nuclear Physics B* 683.1-2 (Apr. 2004), pp. 219–263. ISSN: 05503213. DOI: 10.1016/j.nuclphysb.2004.01.015. arXiv: hep-ph/0305261.

[198] Martin Bauer and Tilman Plehn. *Yet Another Introduction to Dark Matter: The Particle Physics Approach*. Vol. 959. Lecture Notes in Physics. Cham: Springer International Publishing, 2019. ISBN: 978-3-030-16233-7 978-3-030-16234-4. DOI: 10.1007/978-3-030-16234-4. arXiv: 1705.01987. URL: http://arxiv.org/abs/1705.01987 (visited on 09/02/2023).

[199] C. Boehm, T. A. Ensslin and J. Silk. "Can Annihilating Dark Matter Be Lighter than a Few GeVs?" In: *Journal of Physics G: Nuclear and Particle Physics* 30.3 (1st Mar. 2004), pp. 279–285. ISSN: 0954-3899, 1361-6471. DOI: 10.1088/0954-3899/30/3/004. arXiv: astro-ph/0208458.

[200] Giorgio Arcadi et al. "The Waning of the WIMP? A Review of Models, Searches, and Constraints". In: *The European Physical Journal C* 78.3 (Mar. 2018), p. 203. ISSN: 1434-6044, 1434-6052. DOI: 10.1140/epjc/s10052-018-5662-y. arXiv: 1703.07364.

[201] J. Aalbers et al. "DARWIN: Towards the Ultimate Dark Matter Detector". 22nd June 2016. URL: https://arxiv.org/abs/1606.07001v1 (visited on 31/01/2023).

[202] E. Aprile et al. "Dark Matter Search Results from a One Tonne$\times$Year Exposure of XENON1T". In: *Physical Review Letters* 121.11 (12th Sept. 2018), p. 111302. ISSN: 0031-9007, 1079-7114. DOI: 10.1103/PhysRevLett.121.111302. arXiv: 1805.12562.

[203] The XENON collaboration et al. "Projected WIMP Sensitivity of the XENONnT Dark Matter Experiment". In: *Journal of Cosmology and Astroparticle Physics* 2020.11 (16th Nov. 2020), pp. 031–031. ISSN: 1475-7516. DOI: 10.1088/1475-7516/2020/11/031. arXiv: 2007.08796.

[204] Yue Meng et al. "Dark Matter Search Results from the PandaX-4T Commissioning Run". In: *Physical Review Letters* 127.26 (23rd Dec. 2021), p. 261802. ISSN: 0031-9007, 1079-7114. DOI: 10.1103/PhysRevLett.127.261802. arXiv: 2107.13438.

[205] J. Aalbers et al. *First Dark Matter Search Results from the LUX-ZEPLIN (LZ) Experiment*. 27th Oct. 2022. DOI: 10.48550/arXiv.2207.03764. arXiv: 2207.03764. URL: http://arxiv.org/abs/2207.03764 (visited on 31/01/2023). preprint.

[206] Jim Alexander et al. *Dark Sectors 2016 Workshop: Community Report*. 30th Aug. 2016. DOI: 10.48550/arXiv.1608.08632. arXiv: 1608.08632. URL: http://arxiv.org/abs/1608.08632 (visited on 31/01/2023). preprint.

[207] Yang Bai, Patrick J. Fox and Roni Harnik. "The Tevatron at the Frontier of Dark Matter Direct Detection". In: *Journal of High Energy Physics* 2010.12 (Dec. 2010), p. 48. ISSN: 1029-8479. DOI: 10.1007/JHEP12(2010)048. arXiv: 1005.3797.

[208] Jessica Goodman et al. "Constraints on Dark Matter from Colliders". In: *Physical Review D* 82.11 (27th Dec. 2010), p. 116010. ISSN: 1550-7998, 1550-2368. DOI: 10.1103/PhysRevD.82.116010. arXiv: 1008.1783.

[209] Patrick J. Fox, Roni Harnik, Joachim Kopp and Yuhsin Tsai. "LEP Shines Light on Dark Matter". In: *Physical Review D* 84.1 (22nd July 2011), p. 014028. ISSN: 1550-7998, 1550-2368. DOI: 10.1103/PhysRevD.84.014028. arXiv: 1103.0240.

[210] Jessica Goodman et al. "Constraints on Light Majorana Dark Matter from Colliders". In: *Physics Letters B* 695.1-4 (Jan. 2011), pp. 185–188. ISSN: 03702693. DOI: 10.1016/j.physletb.2010.11.009. arXiv: 1005.1286.

[211] Patrick J. Fox, Roni Harnik, Joachim Kopp and Yuhsin Tsai. "Missing Energy Signatures of Dark Matter at the LHC". In: *Physical Review D* 85.5 (30th Mar. 2012), p. 056011. ISSN: 1550-7998, 1550-2368. DOI: 10.1103/PhysRevD.85.056011. arXiv: 1109.4398.

[212] Jalal Abdallah et al. "Simplified Models for Dark Matter Searches at the LHC". In: *Physics of the Dark Universe* 9–10 (Sept. 2015), pp. 8–23. ISSN: 22126864. DOI: 10.1016/j.dark.2015.08.001. arXiv: 1506.03116.

[213] CMS Collaboration. "Search for Dark Matter, Extra Dimensions, and Unparticles in Monojet Events in Proton-Proton Collisions at Sqrt(s) = 8 TeV". In: *The European Physical Journal C* 75.5 (May 2015), p. 235. ISSN: 1434-6044, 1434-6052. DOI: 10.1140/epjc/s10052-015-3451-4. arXiv: 1408.3583.

[214] ATLAS Collaboration. "Search for Dark Matter and Other New Phenomena in Events with an Energetic Jet and Large Missing Transverse Momentum Using the ATLAS Detector". In: *Journal of High Energy Physics* 2018.1 (Jan. 2018), p. 126. ISSN: 1029-8479. DOI: 10.1007/JHEP01(2018)126. arXiv: 1711.03301.

[215] Daniel Abercrombie et al. "Dark Matter Benchmark Models for Early LHC Run-2 Searches: Report of the ATLAS/CMS Dark Matter Forum". In: *Physics of the Dark Universe* 27 (Jan. 2020), p. 100371. ISSN: 22126864. DOI: 10.1016/j.dark.2019.100371. arXiv: 1507.00966.

[216] Fermi-LAT Collaboration. "Searching for Dark Matter Annihilation from Milky Way Dwarf Spheroidal Galaxies with Six Years of Fermi-LAT Data". In: *Physical Review Letters* 115.23 (30th Nov. 2015), p. 231301. ISSN: 0031-9007, 1079-7114. DOI: 10.1103/PhysRevLett.115.231301. arXiv: 1503.02641.

[217] The Fermi-LAT Collaboration. "The Fermi Galactic Center GeV Excess and Implications for Dark Matter". In: *The Astrophysical Journal* 840.1 (4th May 2017), p. 43. ISSN: 1538-4357. DOI: 10.3847/1538-4357/aa6cab. arXiv: 1704.03910.

[218] The Cherenkov Telescope Array Consortium et al. *Science with the Cherenkov Telescope Array*. Mar. 2019. DOI: 10.1142/10986. arXiv: 1709.07997. URL: http://arxiv.org/abs/1709.07997 (visited on 31/01/2023).

[219] M. Aguilar et al. "The Alpha Magnetic Spectrometer (AMS) on the International Space Station: Part II — Results from the First Seven Years". In: *Physics Reports*. The Alpha Magnetic Spectrometer (AMS) on the International Space Station: Part II - Results from the First Seven Years 894 (7th Feb. 2021), pp. 1–116. ISSN: 0370-1573. DOI: 10.1016/j.physrep.2020.09.003.

[220] Andrés Olivares-Del Campo, Céline Boehm, Sergio Palomares-Ruiz and Silvia Pascoli. "Dark Matter-Neutrino Interactions through the Lens of Their Cosmological Implications". In: *Physical Review D* 97.7 (30th Apr. 2018), p. 075039. ISSN: 2470-0010, 2470-0029. DOI: 10.1103/PhysRevD.97.075039. arXiv: 1711.05283.

[221] John McDonald. "Thermally Generated Gauge Singlet Scalars as Self-Interacting Dark Matter". In: *Physical Review Letters* 88.9 (15th Feb. 2002), p. 091304. ISSN: 0031-9007, 1079-7114. DOI: 10.1103/PhysRevLett.88.091304. arXiv: hep-ph/0106249.

[222] Lawrence J. Hall, Karsten Jedamzik, John March-Russell and Stephen M. West. "Freeze-In Production of FIMP Dark Matter". In: *Journal of High Energy Physics* 2010.3 (Mar. 2010), p. 80. ISSN: 1029-8479. DOI: 10.1007/JHEP03(2010)080. arXiv: 0911.1120.

[223] Nicolás Bernal et al. "The Dawn of FIMP Dark Matter: A Review of Models and Constraints". In: *International Journal of Modern Physics A* 32.27 (30th Sept. 2017), p. 1730023. ISSN: 0217-751X, 1793-656X. DOI: 10.1142/S0217751X1730023X. arXiv: 1706.07442.

[224] Alexander Kusenko. "Sterile Neutrinos, Dark Matter, and the Pulsar Velocities in Models with a Higgs Singlet". In: *Physical Review Letters* 97.24 (12th Dec. 2006), p. 241301. ISSN: 0031-9007, 1079-7114. DOI: 10.1103/PhysRevLett.97.241301. arXiv: hep-ph/0609081.

[225] Kalliopi Petraki and Alexander Kusenko. "Dark-Matter Sterile Neutrinos in Models with a Gauge Singlet in the Higgs Sector". In: *Physical Review D* 77.6 (13th Mar. 2008), p. 065014. ISSN: 1550-7998, 1550-2368. DOI: 10.1103/PhysRevD.77.065014. arXiv: 0711.4646.

[226] Xiaoyong Chu, Thomas Hambye and Michel H. G. Tytgat. "The Four Basic Ways of Creating Dark Matter Through a Portal". In: *Journal of Cosmology and Astroparticle Physics* 2012.05 (28th May 2012), pp. 034–034. ISSN: 1475-7516. DOI: 10.1088/1475-7516/2012/05/034. arXiv: 1112.0493.

[227] Clifford Cheung, Gilly Elor, Lawrence J. Hall and Piyush Kumar. "Origins of Hidden Sector Dark Matter I: Cosmology". In: *Journal of High Energy Physics* 2011.3 (Mar. 2011), p. 42. ISSN: 1029-8479. DOI: 10.1007/JHEP03(2011)042. arXiv: 1010.0022.

[228] Clifford Cheung, Gilly Elor, Lawrence J. Hall and Piyush Kumar. "Origins of Hidden Sector Dark Matter II: Collider Physics". In: *Journal of High Energy Physics* 2011.3 (Mar. 2011), p. 85. ISSN: 1029-8479. DOI: 10.1007/JHEP03(2011)085. arXiv: 1010.0024.

[229] Carlos E. Yaguna. "The Singlet Scalar as FIMP Dark Matter". In: *Journal of High Energy Physics* 2011.8 (Aug. 2011), p. 60. ISSN: 1029-8479. DOI: 10.1007/JHEP08(2011)060. arXiv: 1105.1654.

[230] Mattias Blennow, Enrique Fernandez-Martinez and Bryan Zaldivar. "Freeze-in through Portals". In: *Journal of Cosmology and Astroparticle Physics* 2014.01 (3rd Jan. 2014), pp. 003–003. ISSN: 1475-7516. DOI: 10.1088/1475-7516/2014/01/003. arXiv: 1309.7348.

[231] Giorgio Arcadi, Pradipta Ghosh, Yann Mambrini and Mathias Pierre. "Re-Opening Dark Matter Windows Compatible with a Diphoton Excess". In: *Journal of Cosmology and Astroparticle Physics* 2016.07 (5th July 2016), pp. 005–005. ISSN: 1475-7516. DOI: 10.1088/1475-7516/2016/07/005. arXiv: 1603.05601.

[232] Kunio Kaneta, Hye-Sung Lee and Seokhoon Yun. "Portal Connecting Dark Photons and Axions". In: *Physical Review Letters* 118.10 (9th Mar. 2017), p. 101802. ISSN: 0031-9007, 1079-7114. DOI: 10.1103/PhysRevLett.118.101802. arXiv: 1611.01466.

[233] K. N. Abazajian et al. *Light Sterile Neutrinos: A White Paper*. 18th Apr. 2012. DOI: 10.48550/arXiv.1204.5379. arXiv: 1204.5379 [astro-ph, physics:hep-ex, physics:hep-ph, physics:nucl-ex, physics:nucl-th]. URL: http://arxiv.org/abs/1204.5379 (visited on 07/03/2023). preprint.

[234] R. Barbieri and A. Dolgov. "Bounds on Sterile Neutrinos from Nucleosynthesis". In: *Physics Letters B* 237.3 (22nd Mar. 1990), pp. 440–445. ISSN: 0370-2693. DOI: 10.1016/0370-2693(90)91203-N.

[235] A. D. Dolgov. "Neutrinos in the Early Universe". In: *Sov. J. Nucl. Phys.* 33 (1981), pp. 700–706.

[236] Aneesh Manohar. "Statistical Mechanics of Oscillating Neutrinos". In: *Physics Letters B* 186.3 (12th Mar. 1987), pp. 370–374. ISSN: 0370-2693. DOI: 10.1016/0370-2693(87)90310-8.

[237] Paul Bode, Jeremiah P. Ostriker and Neil Turok. "Halo Formation in Warm Dark Matter Models". In: *The Astrophysical Journal* 556.1 (20th July 2001), pp. 93–107. ISSN: 0004-637X, 1538-4357. DOI: 10.1086/321541. arXiv: astro-ph/0010389.

[238] J. R. Bond, A. S. Szalay and M. S. Turner. "Formation of Galaxies in a Gravitino-Dominated Universe". In: *Physical Review Letters* 48.23 (7th June 1982), pp. 1636–1639. DOI: 10.1103/PhysRevLett.48.1636.

[239] Daniel J. H. Chung, Edward W. Kolb and Antonio Riotto. "Nonthermal Supermassive Dark Matter". In: *Physical Review Letters* 81.19 (9th Nov. 1998), pp. 4048–4051. ISSN: 0031-9007, 1079-7114. DOI: 10.1103/PhysRevLett.81.4048. arXiv: hep-ph/9805473.

[240] Masaaki Fujii and K. Hamaguchi. "Non-Thermal Dark Matter via Affleck-Dine Baryogenesis and Its Detection Possibility". In: *Physical Review D* 66.8 (3rd Oct. 2002), p. 083501. ISSN: 0556-2821, 1089-4918. DOI: 10.1103/PhysRevD.66.083501. arXiv: hep-ph/0205044.

[241] Edward W. Kolb, Daniel J. H. Chung and Antonio Riotto. "WIMPZILLAS!" In: *AIP Conference Proceedings*. Vol. 484. arXiv, 1999, pp. 91–105. DOI: 10.1063/1.59655. arXiv: hep-ph/9810361. URL: http://arxiv.org/abs/hep-ph/9810361 (visited on 07/03/2023).

[242] W. B. Lin, D. H. Huang, X. Zhang and R. Brandenberger. "Non-Thermal Production of WIMPs and the Sub-Galactic Structure of the Universe". In: *Physical Review Letters* 86.6 (5th Feb. 2001), pp. 954–957. ISSN: 0031-9007, 1079-7114. DOI: 10.1103/PhysRevLett.86.954. arXiv: astro-ph/0009003.

[243] Xiangdong Shi and George M. Fuller. "A New Dark Matter Candidate: Non-thermal Sterile Neutrinos". In: *Physical Review Letters* 82.14 (5th Apr. 1999), pp. 2832–2835. ISSN: 0031-9007, 1079-7114. DOI: 10.1103/PhysRevLett.82.2832. arXiv: astro-ph/9810076.

[244] Carlos Blanco, Bahaa Elshimy, Rafael F. Lang and Robert Orlando. "Models of Ultra-Heavy Dark Matter Visible to Macroscopic Mechanical Sensing Arrays". In: *Physical Review D* 105.11 (23rd June 2022), p. 115031. ISSN: 2470-0010, 2470-0029. DOI: 10.1103/PhysRevD.105.115031. arXiv: 2112.14784.

[245] The Windchime Collaboration et al. *Snowmass 2021 White Paper: The Windchime Project*. 14th Mar. 2022. DOI: 10.48550/arXiv.2203.07242. arXiv: 2203.07242. URL: http://arxiv.org/abs/2203.07242 (visited on 15/02/2023). preprint.

[246] Mark W. Goodman and Edward Witten. "Detectability of Certain Dark Matter Candidates". In: *Physical Review D* 31.12 (15th June 1985). Ed. by M. A. Srednicki, pp. 3059–3063. DOI: 10.1103/PhysRevD.31.3059.

[247] Marc Schumann. "Direct Detection of WIMP Dark Matter: Concepts and Status". In: *Journal of Physics G: Nuclear and Particle Physics* 46.10 (1st Oct. 2019), p. 103003. ISSN: 0954-3899, 1361-6471. DOI: 10.1088/1361-6471/ab2ea5. arXiv: 1903.03026.

[248] Jennifer M. Gaskins. "A Review of Indirect Searches for Particle Dark Matter". In: *Contemporary Physics* 57.4 (Oct. 2016), pp. 496–525. ISSN: 0010-7514, 1366-5812. DOI: 10.1080/00107514.2016.1175160. arXiv: 1604.00014.

[249] Carlos Pérez de los Heros. "Status, Challenges and Directions in Indirect Dark Matter Searches". In: *Symmetry* 12.10 (8th Oct. 2020), p. 1648. ISSN: 2073-8994. DOI: 10.3390/sym12101648. arXiv: 2008.11561.

[250] P. Jean et al. "Early SPI/INTEGRAL Measurements of Galactic 511 keV Line Emission from Positron Annihilation". In: *Astronomy & Astrophysics* 407.3 (Sept. 2003), pp. L55–L58. ISSN: 0004-6361, 1432-0746. DOI: 10.1051/0004-6361:20031056. arXiv: astro-ph/0309484.

[251] Celine Boehm, Dan Hooper, Joseph Silk and Michel Casse. "MeV Dark Matter: Has It Been Detected?" In: *Physical Review Letters* 92.10 (12th Mar. 2004), p. 101301. ISSN: 0031-9007, 1079-7114. DOI: 10.1103/PhysRevLett.92.101301. arXiv: astro-ph/0309686.

[252] Ryan J. Wilkinson, Aaron C. Vincent, Céline Bœhm and Christopher McCabe. "Ruling out the Light Weakly Interacting Massive Particle Explanation of the Galactic 511 keV Line". In: *Physical Review D* 94.10 (28th Nov. 2016), p. 103525. ISSN: 2470-0010, 2470-0029. DOI: 10.1103/PhysRevD.94.103525. arXiv: 1602.01114.

[253] Particle Data Group et al. "Review of Particle Physics". In: *Progress of Theoretical and Experimental Physics* 2022.8 (8th Aug. 2022), p. 083C01. ISSN: 2050-3911. DOI: 10.1093/ptep/ptac097.

[254] M. C. Smith et al. "The RAVE Survey: Constraining the Local Galactic Escape Speed". In: *Monthly Notices of the Royal Astronomical Society* 379.2 (1st Aug. 2007), pp. 755–772. ISSN: 0035-8711, 1365-2966. DOI: 10.1111/j.1365-2966.2007.11964.x. arXiv: astro-ph/0611671.

[255] Nikhil Anand, A. Liam Fitzpatrick and W. C. Haxton. "Model-Independent WIMP Scattering Responses and Event Rates: A Mathematica Package for Experimental Analysis". In: *Physical Review C* 89.6 (25th June 2014), p. 065501. ISSN: 0556-2813, 1089-490X. DOI: 10.1103/PhysRevC.89.065501. arXiv: 1308.6288.

[256] A. Liam Fitzpatrick et al. "The Effective Field Theory of Dark Matter Direct Detection". In: *Journal of Cosmology and Astroparticle Physics* 2013.02 (5th Feb. 2013), pp. 004–004. ISSN: 1475-7516. DOI: 10.1088/1475-7516/2013/02/004. arXiv: 1203.3542 [astro-ph, physics:hep-ph].

[257] Govinda Adhikari et al. "An Experiment to Search for Dark-Matter Interactions Using Sodium Iodide Detectors". In: *Nature* 564.7734 (Dec. 2018), pp. 83–86. ISSN: 1476-4687. DOI: 10.1038/s41586-018-0739-1. arXiv: 1906.01791.

[258] R. Ajaj et al. "Search for Dark Matter with a 231-Day Exposure of Liquid Argon Using DEAP-3600 at SNOLAB". In: *Physical Review D* 100.2 (24th July 2019), p. 022004. ISSN: 2470-0010, 2470-0029. DOI: 10.1103/PhysRevD.100.022004. arXiv: 1902.04048.

[259] D. S. Akerib et al. "Results from a Search for Dark Matter in the Complete LUX Exposure". In: *Physical Review Letters* 118.2 (11th Jan. 2017), p. 021303. ISSN: 0031-9007, 1079-7114. DOI: 10.1103/PhysRevLett.118.021303. arXiv: 1608.07648.

[260] C. Amole et al. "Dark Matter Search Results from the PICO-60 C$_3$F$_8$ Bubble Chamber". In: *Physical Review Letters* 118.25 (23rd June 2017), p. 251301. ISSN: 0031-9007, 1079-7114. DOI: 10.1103/PhysRevLett.118.251301. arXiv: 1702.07666.

[261] C. Amole et al. "Improved Dark Matter Search Results from PICO-2L Run 2". In: *Physical Review D* 93.6 (21st Mar. 2016), p. 061101. ISSN: 2470-0010, 2470-0029. DOI: 10.1103/PhysRevD.93.061101. arXiv: 1601.03729.

[262] E. Aprile et al. "Search for Coherent Elastic Scattering of Solar 8B Neutrinos in the XENON1T Dark Matter Experiment". In: *Physical Review Letters* 126.9 (1st Mar. 2021), p. 091301. ISSN: 0031-9007, 1079-7114. DOI: 10.1103/PhysRevLett.126.091301. arXiv: 2012.02846.

[263] E. Aprile et al. "Search for Light Dark Matter Interactions Enhanced by the Migdal Effect or Bremsstrahlung in XENON1T". In: *Physical Review Letters* 123.24 (13th Dec. 2019), p. 241803. ISSN: 0031-9007, 1079-7114. DOI: 10.1103/PhysRevLett.123.241803. arXiv: 1907.12771.

[264] R. Bernabei et al. "First Model Independent Results from DAMA/LIBRA-phase2". In: *Nuclear Physics and Atomic Energy* 19.4 (25th Dec. 2018), pp. 307–325. ISSN: 1818331X, 20740565. DOI: 10.15407/jnpae2018.04.307. arXiv: 1805.10486.

[265] Julien Billard et al. "Direct Detection of Dark Matter – APPEC Committee Report". In: *Reports on Progress in Physics* 85.5 (1st May 2022), p. 056201. ISSN: 0034-4885, 1361-6633. DOI: 10.1088/1361-6633/ac5754. arXiv: 2104.07634.

[266] J. Billard, L. Strigari and E. Figueroa-Feliciano. "Implication of Neutrino Backgrounds on the Reach of next Generation Dark Matter Direct Detection Experiments". In: *Physical Review D* 89.2 (27th Jan. 2014), p. 023524. ISSN: 1550-7998, 1550-2368. DOI: 10.1103/PhysRevD.89.023524. arXiv: 1307.5458.

[267] PandaX-II Collaboration et al. "Dark Matter Results From 54-Ton-Day Exposure of PandaX-II Experiment". In: *Physical Review Letters* 119.18 (30th Oct. 2017), p. 181302. ISSN: 0031-9007, 1079-7114. DOI: 10.1103/PhysRevLett.119.181302. arXiv: 1708.06917.

[268] NEWS-G. Collaboration et al. "First Results from the NEWS-G Direct Dark Matter Search Experiment at the LSM". In: *Astroparticle Physics* 97 (Jan. 2018), pp. 54–62. ISSN: 09276505. DOI: 10.1016/j.astropartphys.2017.10.009. arXiv: 1706.04934.

[269] CRESST Collaboration et al. "First Results from the CRESST-III Low-Mass Dark Matter Program". In: *Physical Review D* 100.10 (25th Nov. 2019), p. 102002. ISSN: 2470-0010, 2470-0029. DOI: 10.1103/PhysRevD.100.102002. arXiv: 1904.00498.

[270] EDELWEISS Collaboration et al. "Improved EDELWEISS-III Sensitivity for Low-Mass WIMPs Using a Profile Likelihood Approach". In: *The European Physical Journal C* 76.10 (Oct. 2016), p. 548. ISSN: 1434-6044, 1434-6052. DOI: 10.1140/epjc/s10052-016-4388-y. arXiv: 1607.03367.

[271] Ciaran A. J. O'Hare. "Fog on the Horizon: A New Definition of the Neutrino Floor for Direct Dark Matter Searches". In: *Physical Review Letters* 127.25 (16th Dec. 2021), p. 251802. ISSN: 0031-9007, 1079-7114. DOI: 10.1103/PhysRevLett.127.251802. arXiv: 2109.03116.

[272] Christopher Savage, Graciela Gelmini, Paolo Gondolo and Katherine Freese. "Compatibility of DAMA/LIBRA Dark Matter Detection with Other Searches". In: *Journal of Cosmology and Astroparticle Physics* 2009.04 (14th Apr. 2009), pp. 010–010. ISSN: 1475-7516. DOI: 10.1088/1475-7516/2009/04/010. arXiv: 0808.3607.

[273] SuperCDMS Collaboration et al. "Search for Low-Mass Dark Matter with CDMSlite Using a Profile Likelihood Fit". In: *Physical Review D* 99.6 (15th Mar. 2019), p. 062001. ISSN: 2470-0010, 2470-0029. DOI: 10.1103/PhysRevD.99.062001. arXiv: 1808.09098.

[274] The DarkSide Collaboration et al. "Low-Mass Dark Matter Search with the DarkSide-50 Experiment". In: *Physical Review Letters* 121.8 (23rd Aug. 2018), p. 081307. ISSN: 0031-9007, 1079-7114. DOI: 10.1103/PhysRevLett.121.081307. arXiv: 1802.06994.

[275] J. Billard et al. "In Situ Measurement of the Electron Drift Velocity for Upcoming Directional Dark Matter Detectors". In: *Journal of Instrumentation* 9.01 (28th Jan. 2014), P01013–P01013. ISSN: 1748-0221. DOI: 10.1088/1748-0221/9/01/P01013. arXiv: 1305.2360.

[276] C. Boehm et al. "How High Is the Neutrino Floor?" In: *Journal of Cosmology and Astroparticle Physics* 2019.01 (21st Jan. 2019), pp. 043–043. ISSN: 1475-7516. DOI: 10.1088/1475-7516/2019/01/043. arXiv: 1809.06385.

[277] A. Gütlein et al. "Solar and Atmospheric Neutrinos: Background Sources for the Direct Dark Matter Searches". In: *Astroparticle Physics* 34.2 (Sept. 2010), pp. 90–96. ISSN: 09276505. DOI: 10.1016/j.astropartphys.2010.06.002. arXiv: 1003.5530.

[278] Jocelyn Monroe and Peter Fisher. "Neutrino Backgrounds to Dark Matter Searches". In: *Physical Review D* 76.3 (30th Aug. 2007), p. 033007. ISSN: 1550-7998, 1550-2368. DOI: 10.1103/PhysRevD.76.033007. arXiv: 0706.3019.

[279] Ciaran A. J. O'Hare. "Dark Matter Astrophysical Uncertainties and the Neutrino Floor". In: *Physical Review D* 94.6 (26th Sept. 2016), p. 063527. ISSN: 2470-0010, 2470-0029. DOI: 10.1103/PhysRevD.94.063527. arXiv: 1604.03858.

[280] Louis E. Strigari. "Neutrino Coherent Scattering Rates at Direct Dark Matter Detectors". In: *New Journal of Physics* 11.10 (16th Oct. 2009), p. 105011. ISSN: 1367-2630. DOI: 10.1088/1367-2630/11/10/105011. arXiv: 0903.3630.

[281] J. D. Vergados and H. Ejiri. "Can Solar Neutrinos Be a Serious Background in Direct Dark Matter Searches?" In: *Nuclear Physics B* 804.1-2 (Nov. 2008), pp. 144–159. ISSN: 05503213. DOI: 10.1016/j.nuclphysb.2008.06.004. arXiv: 0805.2583.

[282] E. Aprile et al. "First Dark Matter Search Results from the XENON1T Experiment". In: *Physical Review Letters* 119.18 (30th Oct. 2017), p. 181301. ISSN: 0031-9007, 1079-7114. DOI: 10.1103/PhysRevLett.119.181301. arXiv: 1705.06655.

[283] XENON Collaboration et al. *First Dark Matter Search with Nuclear Recoils from the XENONnT Experiment*. 26th Mar. 2023. arXiv: 2303.14729 [astro-ph, physics:hep-ex, physics:hep-ph, physics:physics]. URL: http://arxiv.org/abs/2303.14729 (visited on 20/04/2023). preprint.

[284] R Bernabei et al. "Searching for WIMPs by the Annual Modulation Signature". In: *Physics Letters B* 424.1 (2nd Apr. 1998), pp. 195–201. ISSN: 0370-2693. DOI: 10.1016/S0370-2693(98)00172-5.

[285] Andrzej K. Drukier, Katherine Freese and David N. Spergel. "Detecting Cold Dark-Matter Candidates". In: *Physical Review D* 33.12 (15th June 1986), pp. 3495–3508. DOI: 10.1103/PhysRevD.33.3495.

[286] Katherine Freese, Mariangela Lisanti and Christopher Savage. "Annual Modulation of Dark Matter: A Review". In: *Reviews of Modern Physics* 85.4 (1st Nov. 2013), pp. 1561–1581. ISSN: 0034-6861, 1539-0756. DOI: 10.1103/RevModPhys.85.1561. arXiv: 1209.3339.

[287] Katherine Freese, Joshua Frieman and Andrew Gould. "Signal Modulation in Cold-Dark-Matter Detection". In: *Physical Review D* 37.12 (15th June 1988), pp. 3388–3405. DOI: 10.1103/PhysRevD.37.3388.

[288] S. P. Ahlen et al. "Limits on Cold Dark Matter Candidates from an Ultralow Background Germanium Spectrometer". In: *Physics Letters B* 195.4 (17th Sept. 1987), pp. 603–608. ISSN: 0370-2693. DOI: 10.1016/0370-2693(87)91581-4.

[289] R. Bernabei et al. "The DAMA/LIBRA Apparatus". In: *Nuclear Instruments and Methods in Physics Research Section A: Accelerators, Spectrometers, Detectors and Associated Equipment* 592.3 (July 2008), pp. 297–315. ISSN: 01689002. DOI: 10.1016/j.nima.2008.04.082. arXiv: 0804.2738.

[290] R. Bernabei et al. *Dark Matter: DAMA/LIBRA and Its Perspectives*. 2nd Sept. 2022. DOI: 10.48550/arXiv.2209.00882. arXiv: 2209.00882. URL: http://arxiv.org/abs/2209.00882 (visited on 16/02/2023). preprint.

[291] R. Bernabei et al. "Final Model Independent Result of DAMA/LIBRA-phase1". In: *The European Physical Journal C* 73.12 (Dec. 2013), p. 2648. ISSN: 1434-6044, 1434-6052. DOI: 10.1140/epjc/s10052-013-2648-7. arXiv: 1308.5109.

[292] R. Bernabei et al. "First Results from DAMA/LIBRA and the Combined Results with DAMA/NaI". In: *The European Physical Journal C* 56.3 (Aug. 2008), pp. 333–355. ISSN: 1434-6044, 1434-6052. DOI: 10.1140/epjc/s10052-008-0662-y. arXiv: 0804.2741.

[293] R. Bernabei et al. "On a Further Search for a Yearly Modulation of the Rate in Particle Dark Matter Direct Search". In: *Physics Letters B* 450.4 (25th Mar. 1999), pp. 448–455. ISSN: 0370-2693. DOI: 10.1016/S0370-2693(99)00091-X.

[294] R. Bernabei et al. "New Results from DAMA/LIBRA". In: *The European Physical Journal C* 67.1-2 (May 2010), pp. 39–49. ISSN: 1434-6044, 1434-6052. DOI: 10.1140/epjc/s10052-010-1303-9. arXiv: 1002.1028.

[295] R Bernabei et al. "Search for WIMP Annual Modulation Signature: Results from DAMA/NaI-3 and DAMA/NaI-4 and the Global Combined Analysis". In: *Physics Letters B* 480.1 (4th May 2000), pp. 23–31. ISSN: 0370-2693. DOI: 10.1016/S0370-2693(00)00405-6.

[296] M. Antonello et al. "The SABRE Project and the SABRE PoP". In: *The European Physical Journal C* 79.4 (Apr. 2019), p. 363. ISSN: 1434-6044, 1434-6052. DOI: 10.1140/epjc/s10052-019-6860-y. arXiv: 1806.09340.

[297] E. Barberio et al. "The SABRE South Experiment at the Stawell Underground Physics Laboratory". In: *PoS* ICHEP2022 (Nov. 2022), p. 1127. DOI: 10.22323/1.414.1127.

[298] I. Bolognino. *The SABRE South Experiment at the Stawell Underground Physics Laboratory*. 5th Nov. 2022. DOI: 10.48550/arXiv.2211.03016. arXiv: 2211.03016. URL: http://arxiv.org/abs/2211.03016 (visited on 16/02/2023). preprint.

[299] Giulia D'Imperio et al. "The SABRE Experiment for Dark Matter Search". In: *PoS* ICHEP2018 (2019), p. 653. DOI: 10.22323/1.340.0653.

[300] M. J. Zurowski. "Status of the SABRE South Experiment at the Stawell Underground Physics Laboratory". In: *Nuclear Instruments and Methods in Physics Research Section A: Accelerators, Spectrometers, Detectors and Associated Equipment* 1045 (1st Jan. 2023), p. 167585. ISSN: 0168-9002. DOI: 10.1016/j.nima.2022.167585.

[301] COSINUS Collaboration et al. "Results from the First Cryogenic NaI Detector for the COSINUS Project". In: *Journal of Instrumentation* 12.11 (8th Nov. 2017), P11007–P11007. ISSN: 1748-0221. DOI: 10.1088/1748-0221/12/11/P11007. arXiv: 1705.11028.

[302] COSINUS collaboration et al. "Results of the First NaI Scintillating Calorimeter Prototypes by COSINUS". In: *Journal of Physics: Conference Series* 1342.1 (1st Jan. 2020), p. 012099. ISSN: 1742-6588, 1742-6596. DOI: 10.1088/1742-6596/1342/1/012099. arXiv: 1711.01482.

[303] Natalia Di Marco et al. "A NaI-based Cryogenic Scintillating Calorimeter: Status and Results of the COSINUS Project". In: *Proceedings of Neutrino Oscillation Workshop — PoS(NOW2018)*. Neutrino Oscillation Workshop. Vol. 337. SISSA Medialab, 24th Apr. 2019, p. 097. DOI: 10.22323/1.337.0097. URL: https://pos.sissa.it/337/097 (visited on 21/02/2023).

[304] Felix Kahlhoefer et al. "Model-Independent Comparison of Annual Modulation and Total Rate with Direct Detection Experiments". In: *Journal of Cosmology and Astroparticle Physics* 2018.05 (30th May 2018), pp. 074–074. ISSN: 1475-7516. DOI: 10.1088/1475-7516/2018/05/074. arXiv: 1802.10175.

[305] Vanessa Zema. "COSINUS: A NaI-based Cryogenic Calorimeter for Direct Dark Matter Search". In: *Il Nuovo Cimento C* 42.5 (2020), p. 228. ISSN: 03905551, 03905551. DOI: 10.1393/ncc/i2019-19228-1.

[306] Y. Kanemitsu et al. "Purification of the NaI(Tl) Crystal for Dark Matter Search Project PICOLON". In: *Journal of Physics: Conference Series* 1468.1 (Feb. 2020), p. 012054. ISSN: 1742-6596. DOI: 10.1088/1742-6596/1468/1/012054.

[307] K. Fushimi et al. "PICOLON Dark Matter Search Project". In: *Journal of Physics: Conference Series* 2156.1 (1st Dec. 2021), p. 012045. ISSN: 1742-6588, 1742-6596. DOI: 10.1088/1742-6596/2156/1/012045. arXiv: 2112.10116.

[308] J. Amaré et al. "ANAIS-112 Status: Two Years Results on Annual Modulation". In: *Journal of Physics: Conference Series* 1468.1 (1st Feb. 2020), p. 012014. ISSN: 1742-6588, 1742-6596. DOI: 10.1088/1742-6596/1468/1/012014. arXiv: 1910.13365.

[309] J. Amare et al. "Analysis of Backgrounds for the ANAIS-112 Dark Matter Experiment". In: *The European Physical Journal C* 79.5 (May 2019), p. 412. ISSN: 1434-6044, 1434-6052. DOI: 10.1140/epjc/s10052-019-6911-4. arXiv: 1812.01377.

[310] J. Amare et al. "Annual Modulation Results from Three-Year Exposure of ANAIS-112". In: *Physical Review D* 103.10 (27th May 2021), p. 102005. ISSN: 2470-0010, 2470-0029. DOI: 10.1103/PhysRevD.103.102005. arXiv: 2103.01175.

[311] J. Amaré et al. "First Results on Dark Matter Annual Modulation from ANAIS-112 Experiment". In: *Physical Review Letters* 123.3 (16th July 2019), p. 031301. ISSN: 0031-9007, 1079-7114. DOI: 10.1103/PhysRevLett.123.031301. arXiv: 1903.03973.

[312] J. Amaré et al. "Performance of ANAIS-112 Experiment after the First Year of Data Taking". In: *The European Physical Journal C* 79.3 (Mar. 2019), p. 228. ISSN: 1434-6044, 1434-6052. DOI: 10.1140/epjc/s10052-019-6697-4. arXiv: 1812.01472.

[313] G. Adhikari et al. *An Induced Annual Modulation Signature in COSINE-100 Data by DAMA/LIBRA's Analysis Method*. 10th Aug. 2022. DOI: 10.48550/arXiv.2208.05158. arXiv: 2208.05158. URL: http://arxiv.org/abs/2208.05158 (visited on 21/02/2023). preprint.

[314] G. Adhikari et al. "Initial Performance of the COSINE-100 Experiment". In: *The European Physical Journal C* 78.2 (Feb. 2018), p. 107. ISSN: 1434-6044, 1434-6052. DOI: 10.1140/epjc/s10052-018-5590-x. arXiv: 1710.05299.

[315] G. Adhikari et al. "Searching for Low-Mass Dark Matter via Migdal Effect in COSINE-100". In: *Physical Review D* 105.4 (22nd Feb. 2022), p. 042006. ISSN: 2470-0010, 2470-0029. DOI: 10.1103/PhysRevD.105.042006. arXiv: 2110.05806.

[316] G. Adhikari et al. "Strong Constraints from COSINE-100 on the DAMA Dark Matter Results Using the Same Sodium Iodide Target". In: *Science Advances* 7.46 (12th Nov. 2021), eabk2699. ISSN: 2375-2548. DOI: 10.1126/sciadv.abk2699. arXiv: 2104.03537.

[317] COSINE-100 Collaboration et al. "COSINE-100 and DAMA/LIBRA-phase2 in WIMP Effective Models". In: *Journal of Cosmology and Astroparticle Physics* 2019.06 (25th June 2019), pp. 048–048. ISSN: 1475-7516. DOI: 10.1088/1475-7516/2019/06/048. arXiv: 1904.00128.

[318] COSINE-100 Collaboration et al. "Search for a Dark Matter-Induced Annual Modulation Signal in NaI(Tl) with the COSINE-100 Experiment". In: *Physical Review Letters* 123.3 (16th July 2019), p. 031302. ISSN: 0031-9007, 1079-7114. DOI: 10.1103/PhysRevLett.123.031302. arXiv: 1903.10098.

[319] COSINE-100 Collaboration et al. "Three-Year Annual Modulation Search with COSINE-100". In: *Physical Review D* 106.5 (14th Sept. 2022), p. 052005. ISSN: 2470-0010, 2470-0029. DOI: 10.1103/PhysRevD.106.052005. arXiv: 2111.08863.

[320] B. J. Park et al. "Development of Ultra-Pure NaI(Tl) Detectors for the COSINE-200 Experiment". In: *The European Physical Journal C* 80.9 (Sept. 2020), p. 814. ISSN: 1434-6044, 1434-6052. DOI: 10.1140/epjc/s10052-020-8386-8. arXiv: 2004.06287.

[321] E. Baracchini et al. *CYGNO: A CYGNUs Collaboration 1 M3 Module with Optical Readout for Directional Dark Matter Search*. 24th Sept. 2019. DOI: 10.48550/arXiv.1901.04190. arXiv: 1901.04190. URL: http://arxiv.org/abs/1901.04190 (visited on 24/02/2023). preprint.

[322] C. A. J. O'Hare et al. *Recoil Imaging for Directional Detection of Dark Matter, Neutrinos, and Physics beyond the Standard Model*. 17th July 2022. DOI: 10.48550/arXiv.2203.05914. arXiv: 2203.05914. URL: http://arxiv.org/abs/2203.05914 (visited on 24/02/2023). preprint.

[323] S. E. Vahsen et al. *CYGNUS: Feasibility of a Nuclear Recoil Observatory with Directional Sensitivity to Dark Matter and Neutrinos*. 22nd Dec. 2020. DOI: 10.48550/arXiv.2008.12587. arXiv: 2008.12587. URL: http://arxiv.org/abs/2008.12587 (visited on 24/02/2023). preprint.

[324] Sven E. Vahsen, Ciaran A. J. O'Hare and Dinesh Loomba. "Directional Recoil Detection". In: *Annual Review of Nuclear and Particle Science* 71.1 (21st Sept. 2021), pp. 189–224. ISSN: 0163-8998, 1545-4134. DOI: 10.1146/annurev-nucl-020821-035016. arXiv: 2102.04596.

[325] Ciaran A. J. O'Hare et al. "Particle Detection and Tracking with DNA". In: *The European Physical Journal C* 82.4 (8th Apr. 2022), p. 306. ISSN: 1434-6052. DOI: 10.1140/epjc/s10052-022-10264-6. arXiv: 2105.11949.

[326] N. W. Evans, J. L. Sanders and Alex Geringer-Sameth. "Simple J-factors and D-factors for Indirect Dark Matter Detection". In: *Physical Review D* 93.10 (12th May 2016), p. 103512. ISSN: 2470-0010, 2470-0029. DOI: 10.1103/PhysRevD.93.103512. arXiv: 1604.05599.

[327] Celine Boehm, Matthew J. Dolan and Christopher McCabe. "A Weighty Interpretation of the Galactic Centre Excess". In: *Physical Review D* 90.2 (22nd July 2014), p. 023531. ISSN: 1550-7998, 1550-2368. DOI: 10.1103/PhysRevD.90.023531. arXiv: 1404.4977.

[328] Paolo Gondolo and Joseph Silk. "Dark Matter Annihilation at the Galactic Center". In: *Physical Review Letters* 83.9 (30th Aug. 1999), pp. 1719–1722. ISSN: 0031-9007, 1079-7114. DOI: 10.1103/PhysRevLett.83.1719. arXiv: astro-ph/9906391.

[329] Lisa Goodenough and Dan Hooper. *Possible Evidence For Dark Matter Annihilation In The Inner Milky Way From The Fermi Gamma Ray Space Telescope*. 11th Nov. 2009. DOI: 10.48550/arXiv.0910.2998. arXiv: 0910.2998. URL: http://arxiv.org/abs/0910.2998 (visited on 28/02/2023). preprint.

[330] Dan Hooper and Lisa Goodenough. "Dark Matter Annihilation in The Galactic Center As Seen by the Fermi Gamma Ray Space Telescope". In: *Physics Letters B* 697.5 (Mar. 2011), pp. 412–428. ISSN: 03702693. DOI: 10.1016/j.physletb.2011.02.029. arXiv: 1010.2752.

[331] Dan Hooper and Tim Linden. "On The Origin Of The Gamma Rays From The Galactic Center". In: *Physical Review D* 84.12 (20th Dec. 2011), p. 123005. ISSN: 1550-7998, 1550-2368. DOI: 10.1103/PhysRevD.84.123005. arXiv: 1110.0006.

[332] Thomas Lacroix, Celine Boehm and Joseph Silk. "Probing a Dark Matter Density Spike at the Galactic Center". In: *Physical Review D* 89.6 (27th Mar. 2014), p. 063534. ISSN: 1550-7998, 1550-2368. DOI: 10.1103/PhysRevD.89.063534. arXiv: 1311.0139.

[333] Dan Hooper et al. "Possible Evidence for MeV Dark Matter In Dwarf Spheroidals". In: *Physical Review Letters* 93.16 (13th Oct. 2004), p. 161302. ISSN: 0031-9007, 1079-7114. DOI: 10.1103/PhysRevLett.93.161302. arXiv: astro-ph/0311150.

[334] A. Albert et al. "Dark Matter Limits From Dwarf Spheroidal Galaxies with The HAWC Gamma-Ray Observatory". In: *The Astrophysical Journal* 853.2 (1st Feb. 2018), p. 154. ISSN: 1538-4357. DOI: 10.3847/1538-4357/aaa6d8. arXiv: 1706.01277.

[335] VERITAS Collaboration et al. "Dark Matter Constraints from a Joint Analysis of Dwarf Spheroidal Galaxy Observations with VERITAS". In: *Physical Review D* 95.8 (5th Apr. 2017), p. 082001. ISSN: 2470-0010, 2470-0029. DOI: 10.1103/PhysRevD.95.082001. arXiv: 1703.04937.

[336] Marco Cirelli, Paolo Panci and Pasquale D. Serpico. "Diffuse Gamma Ray Constraints on Annihilating or Decaying Dark Matter after Fermi". In: *Nuclear Physics B* 840.1-2 (Nov. 2010), pp. 284–303. ISSN: 05503213. DOI: 10.1016/j.nuclphysb.2010.07.010. arXiv: 0912.0663.

[337] The Fermi-LAT collaboration et al. "Constraints on the Galactic Halo Dark Matter from Fermi-LAT Diffuse Measurements". In: *The Astrophysical Journal* 761.2 (20th Dec. 2012), p. 91. ISSN: 0004-637X, 1538-4357. DOI: 10.1088/0004-637X/761/2/91. arXiv: 1205.6474.

[338] Pasquale D. Serpico and Gabrijela Zaharijas. "Optimal Angular Window for Observing Dark Matter Annihilation from the Galactic Center Region: The Case of Gamma-Ray Lines". In: *Astroparticle Physics* 29.6 (July 2008), pp. 380–385. ISSN: 09276505. DOI: 10.1016/j.astropartphys.2008.04.001. arXiv: 0802.3245.

[339] Felix Stoehr et al. "Dark Matter Annihilation in the Halo of the Milky Way". In: *Monthly Notices of the Royal Astronomical Society* 345.4 (11th Nov. 2003), pp. 1313–1322. ISSN: 0035-8711, 1365-2966. DOI: 10.1046/j.1365-2966.2003.07052.x. arXiv: astro-ph/0307026.

[340] Lars Bergstrom, Joakim Edsjo and Piero Ullio. "Spectral Gamma-ray Signatures of Cosmological Dark Matter Annihilation". In: *Physical Review Letters* 87.25 (28th Nov. 2001), p. 251301. ISSN: 0031-9007, 1079-7114. DOI: 10.1103/PhysRevLett.87.251301. arXiv: astro-ph/0105048.

[341] The Fermi-LAT collaboration et al. "Constraints on Cosmological Dark Matter Annihilation from the Fermi-LAT Isotropic Diffuse Gamma-Ray Measurement". In: *Journal of Cosmology and Astroparticle Physics* 2010.04 (15th Apr. 2010), pp. 014–014. ISSN: 1475-7516. DOI: 10.1088/1475-7516/2010/04/014. arXiv: 1002.4415.

[342] Mattia Fornasa and Miguel A. Sanchez-Conde. "The Nature of the Diffuse Gamma-Ray Background". In: *Physics Reports* 598 (Oct. 2015), pp. 1–58. ISSN: 03701573. DOI: 10.1016/j.physrep.2015.09.002. arXiv: 1502.02866.

[343] Emiliano Sefusatti et al. "Extragalactic Gamma-Ray Signal from Dark Matter Annihilation: An Appraisal". In: *Monthly Notices of the Royal Astronomical Society* 441.3 (12th May 2014), pp. 1861–1878. ISSN: 0035-8711, 1365-2966. DOI: 10.1093/mnras/stu686. arXiv: 1401.2117.

[344] Pasquale D. Serpico, Emiliano Sefusatti, Michael Gustafsson and Gabrijela Zaharijas. "Extragalactic Gamma-Ray Signal from Dark Matter Annihilation: A Power Spectrum Based Computation". In: *Monthly Notices of the Royal Astronomical Society: Letters* 421.1 (Mar. 2012), pp. L87–L91. ISSN: 17453925. DOI: 10.1111/j.1745-3933.2011.01212.x. arXiv: 1109.0095.

[345] Piero Ullio, Lars Bergstrom, Joakim Edsjo and Cedric Lacey. "Cosmological Dark Matter Annihilations into Gamma-Rays - a Closer Look". In: *Physical Review D* 66.12 (17th Dec. 2002), p. 123502. ISSN: 0556-2821, 1089-4918. DOI: 10.1103/PhysRevD.66.123502. arXiv: astro-ph/0207125.

[346] Marco Cirelli et al. "PPPC 4 DM ID: A Poor Particle Physicist Cookbook for Dark Matter Indirect Detection". In: *Journal of Cosmology and Astroparticle Physics* 2011.03 (31st Mar. 2011), pp. 051–051. ISSN: 1475-7516. DOI: 10.1088/1475-7516/2011/03/051. arXiv: 1012.4515.

[347] Paolo Ciafaloni et al. "Weak Corrections Are Relevant for Dark Matter Indirect Detection". In: *Journal of Cosmology and Astroparticle Physics* 2011.03 (9th Mar. 2011), pp. 019–019. ISSN: 1475-7516. DOI: 10.1088/1475-7516/2011/03/019. arXiv: 1009.0224.

[348] Pietro Baratella et al. "PPPC 4 DMnu: A Poor Particle Physicist Cookbook for Neutrinos from DM Annihilations in the Sun". In: *Journal of Cosmology and Astroparticle Physics* 2014.03 (27th Mar. 2014), pp. 053–053. ISSN: 1475-7516. DOI: 10.1088/1475-7516/2014/03/053. arXiv: 1312.6408.

[349] Mathieu Boudaud, Marco Cirelli, Gaëlle Giesen and Pierre Salati. "A Fussy Revisitation of Antiprotons as a Tool for Dark Matter Searches". In: *Journal of Cosmology and Astroparticle Physics* 2015.05 (8th May 2015), pp. 013–013. ISSN: 1475-7516. DOI: 10.1088/1475-7516/2015/05/013. arXiv: 1412.5696.

[350] Jatan Buch, Marco Cirelli, Gaëlle Giesen and Marco Taoso. "PPPC 4 DM Secondary: A Poor Particle Physicist Cookbook for Secondary Radiation from Dark Matter". In: *Journal of Cosmology and Astroparticle Physics* 2015.09 (11th Sept. 2015), pp. 037–037. ISSN: 1475-7516. DOI: 10.1088/1475-7516/2015/09/037. arXiv: 1505.01049.

[351] Gilly Elor, Nicholas L. Rodd, Tracy R. Slatyer and Wei Xue. "Model-Independent Indirect Detection Constraints on Hidden Sector Dark Matter". In: *Journal of Cosmology and Astroparticle Physics* 2016.06 (10th June 2016), pp. 024–024. ISSN: 1475-7516. DOI: 10.1088/1475-7516/2016/06/024. arXiv: 1511.08787.

[352] C. Bœhm, P. Fayet and R. Schaeffer. "Constraining Dark Matter Candidates from Structure Formation". In: *Physics Letters B* 518.1-2 (Oct. 2001), pp. 8–14. ISSN: 03702693. DOI: 10.1016/S0370-2693(01)01060-7. arXiv: astro-ph/0012504.

[353] Ryan J. Wilkinson, Julien Lesgourgues and Céline Boehm. "Using the CMB Angular Power Spectrum to Study Dark Matter-photon Interactions". In: *Journal of Cosmology and Astroparticle Physics* 2014.04 (28th Apr. 2014), p. 026. ISSN: 1475-7516. DOI: 10.1088/1475-7516/2014/04/026. arXiv: 1309.7588.

[354] Celine Boehm, Pierre Fayet and Richard Schaeffer. "Constraining the Strength of Dark Matter Interactions from Structure Formation". In: *Dark Matter in Astro- and Particle Physics. Proceedings, 4th Heidelberg International Conference*. DARK 2002. Cape Town, South Africa: arXiv, 23rd May 2002, pp. 333–344. DOI: 10.48550/arXiv.astro-ph/0205406. arXiv: astro-ph/0205406. URL: http://arxiv.org/abs/astro-ph/0205406 (visited on 28/02/2023).

[355] Xuelei Chen, Steen Hannestad and Robert J. Scherrer. "Cosmic Microwave Background and Large Scale Structure Limits on the Interaction between Dark Matter and Baryons". In: *Physical Review D* 65.12 (13th June 2002), p. 123515. ISSN: 0556-2821, 1089-4918. DOI: 10.1103/PhysRevD.65.123515. arXiv: astro-ph/0202496.

[356] Celine Boehm and R. Schaeffer. "Constraints on Dark Matter Interactions from Structure Formation: Damping Lengths". In: *Astronomy & Astrophysics* 438.2 (Aug. 2005), pp. 419–442. ISSN: 0004-6361, 1432-0746. DOI: 10.1051/0004-6361:20042238. arXiv: astro-ph/0410591.

[357] Celine Boehm, Alain Riazuelo, Steen H. Hansen and Richard Schaeffer. "Interacting Dark Matter Disguised as Warm Dark Matter". In: *Physical Review D* 66.8 (14th Oct. 2002), p. 083505. ISSN: 0556-2821, 1089-4918. DOI: 10.1103/PhysRevD.66.083505. arXiv: astro-ph/0112522.

[358] Celine Boehm, H. Mathis, J. Devriendt and Joseph Silk. "Non-Linear Evolution of Suppressed Dark Matter Primordial Power Spectra". In: *Monthly Notices of the Royal Astronomical Society* 360.1 (June 2005), pp. 282–287. DOI: 10.1111/j.1365-2966.2005.09032.x. arXiv: astro-ph/0309652.

[359] J. A. Schewtschenko et al. "Dark Matter-Radiation Interactions: The Impact on Dark Matter Haloes". In: *Monthly Notices of the Royal Astronomical Society* 449.4 (1st June 2015), pp. 3587–3596. ISSN: 0035-8711, 1365-2966. DOI: 10.1093/mnras/stv431. arXiv: 1412.4905.

[360] Eric D. Carlson, Marie E. Machacek and Lawrence J. Hall. "Self-Interacting Dark Matter". In: *The Astrophysical Journal* 398 (1992), pp. 43–52. DOI: 10.1086/171833.

[361] Andrew A. de Laix, Robert J. Scherrer and Robert K. Schaefer. "Constraints on Self-Interacting Dark Matter". In: *Astrophys. J.* 452 (Oct. 1995), p. 495. ISSN: 0004-637X, 1538-4357. DOI: 10.1086/176322. arXiv: astro-ph/9502087.

[362] David N Spergel and Paul J Steinhardt. "Observational Evidence for Self-Interacting Cold Dark Matter". In: *Physical Review Letters* 84.17 (24th Apr. 2000), pp. 3760–3763. ISSN: 0031-9007, 1079-7114. DOI: 10.1103/PhysRevLett.84.3760. arXiv: astro-ph/9909386.

[363] Romeel Dave, David N. Spergel, Paul J. Steinhardt and Benjamin D. Wandelt. "Halo Properties in Cosmological Simulations of Self-Interacting Cold Dark Matter". In: *The Astrophysical Journal* 547.2 (Feb. 2001), pp. 574–589. ISSN: 0004-637X, 1538-4357. DOI: 10.1086/318417. arXiv: astro-ph/0006218.

[364] Peter Creasey et al. "Spreading out and Staying Sharp – Creating Diverse Rotation Curves via Baryonic and Self-Interaction Effects". In: *Monthly Notices of the Royal Astronomical Society* 468.2 (June 2017), pp. 2283–2295. ISSN: 0035-8711, 1365-2966. DOI: 10.1093/mnras/stx522. arXiv: 1612.03903 [astro-ph].

[365] Miguel Rocha et al. "Cosmological Simulations with Self-Interacting Dark Matter I: Constant Density Cores and Substructure". In: *Monthly Notices of the Royal Astronomical Society* 430.1 (21st Mar. 2013), pp. 81–104. ISSN: 1365-2966, 0035-8711. DOI: 10.1093/mnras/sts514. arXiv: 1208.3025 [astro-ph, physics:hep-ph].

[366] Stacy Y. Kim, Annika H. G. Peter and David Wittman. "In the Wake of Dark Giants: New Signatures of Dark Matter Self Interactions in Equal Mass Mergers of Galaxy Clusters". In: *Monthly Notices of the Royal Astronomical Society* 469.2 (Aug. 2017), pp. 1414–1444. ISSN: 0035-8711, 1365-2966. DOI: 10.1093/mnras/stx896. arXiv: 1608.08630 [astro-ph].

[367] Ran Huo, Manoj Kaplinghat, Zhen Pan and Hai-Bo Yu. "Signatures of Self-Interacting Dark Matter in the Matter Power Spectrum and the CMB". In: *Physics Letters B* 783 (Aug. 2018), pp. 76–81. ISSN: 03702693. DOI: 10.1016/j.physletb.2018.06.024. arXiv: 1709.09717 [astro-ph, physics:hep-ph].

[368] Maxim Markevitch et al. "Direct Constraints on the Dark Matter Self-Interaction Cross-Section from the Merging Galaxy Cluster 1E0657-56". In: *The Astrophysical Journal* 606.2 (10th May 2004), pp. 819–824. ISSN: 0004-637X, 1538-4357. DOI: 10.1086/383178. arXiv: astro-ph/0309303.

[369] Scott W. Randall et al. "Constraints on the Self-Interaction Cross-Section of Dark Matter from Numerical Simulations of the Merging Galaxy Cluster 1E 0657-56". In: *The Astrophysical Journal* 679.2 (June 2008), pp. 1173–1180. ISSN: 0004-637X, 1538-4357. DOI: 10.1086/587859. arXiv: 0704.0261 [astro-ph].

[370] Cora Dvorkin, Kfir Blum and Marc Kamionkowski. "Constraining Dark Matter-Baryon Scattering with Linear Cosmology". In: *Physical Review D* 89.2 (27th Jan. 2014), p. 023519. ISSN: 1550-7998, 1550-2368. DOI: 10.1103/PhysRevD.89.023519. arXiv: 1311.2937.

[371] A. D. Dolgov, S. L. Dubovsky, G. I. Rubtsov and I. I. Tkachev. "Constraints on Millicharged Particles from Planck". In: *Physical Review D* 88.11 (2nd Dec. 2013), p. 117701. ISSN: 1550-7998, 1550-2368. DOI: 10.1103/PhysRevD.88.117701. arXiv: 1310.2376 [astro-ph, physics:hep-ph].

[372] Francis-Yan Cyr-Racine and Kris Sigurdson. "The Cosmology of Atomic Dark Matter". In: *Physical Review D* 87.10 (20th May 2013), p. 103515. ISSN: 1550-7998, 1550-2368. DOI: 10.1103/PhysRevD.87.103515. arXiv: 1209.5752 [astro-ph, physics:hep-ph].

[373] Francis-Yan Cyr-Racine, Roland de Putter, Alvise Raccanelli and Kris Sigurdson. "Constraints on Large-Scale Dark Acoustic Oscillations from Cosmology". In: *Physical Review D* 89.6 (17th Mar. 2014), p. 063517. ISSN: 1550-7998, 1550-2368. DOI: 10.1103/PhysRevD.89.063517. arXiv: 1310.3278.

[374] A. A. Prinz et al. "Search for Millicharged Particles at SLAC". In: *Physical Review Letters* 81.6 (10th Aug. 1998), pp. 1175–1178. ISSN: 0031-9007, 1079-7114. DOI: 10.1103/PhysRevLett.81.1175. arXiv: hep-ex/9804008.

[375] Kris Sigurdson et al. "Dark-Matter Electric and Magnetic Dipole Moments". In: *Physical Review D* 73.8 (2004), p. 083501. ISSN: 1550-7998, 1550-2368. DOI: 10.1103/PhysRevD.70.083501,10.1103/PhysRevD.73.089903. arXiv: astro-ph/0406355.

[376] Miguel Escudero et al. "Exploring Dark Matter Microphysics with Galaxy Surveys". In: *Journal of Cosmology and Astroparticle Physics* 2015.9 (10th Sept. 2015), p. 034. ISSN: 1475-7516. DOI: 10.1088/1475-7516/2015/9/034,10.1088/1475-7516/2015/09/034. arXiv: 1505.06735 [astro-ph, physics:hep-ph].

[377] Samuel D. McDermott, Hai-Bo Yu and Kathryn M. Zurek. "Turning off the Lights: How Dark Is Dark Matter?" In: *Physical Review D* 83.6 (9th Mar. 2011), p. 063509. ISSN: 1550-7998, 1550-2368. DOI: 10.1103/PhysRevD.83.063509. arXiv: 1011.2907 [astro-ph, physics:hep-ph].

[378] Yacine Ali-Haïmoud, Jens Chluba and Marc Kamionkowski. "Constraints on Dark Matter Interactions with Standard Model Particles from CMB Spectral Distortions". In: *Physical Review Letters* 115.7 (14th Aug. 2015), p. 071304. ISSN: 0031-9007, 1079-7114. DOI: 10.1103/PhysRevLett.115.071304. arXiv: 1506.04745 [astro-ph, physics:hep-ph].

[379] Julia Stadler and Céline Bœhm. "Constraints on γ-CDM Interactions Matching the Planck Data Precision". In: *Journal of Cosmology and Astroparticle Physics* 2018.10 (4th Oct. 2018), pp. 009–009. ISSN: 1475-7516. DOI: 10.1088/1475-7516/2018/10/009. arXiv: 1802.06589 [astro-ph].

[380] Sownak Bose et al. "The Copernicus Complexio: Statistical Properties of Warm Dark Matter Haloes". In: *Monthly Notices of the Royal Astronomical Society* 455.1 (1st Jan. 2016), pp. 318–333. ISSN: 0035-8711, 1365-2966. DOI: 10.1093/mnras/stv2294. arXiv: 1507.01998 [astro-ph].

[381] Alexey Boyarsky, Julien Lesgourgues, Oleg Ruchayskiy and Matteo Viel. "Lyman-Alpha Constraints on Warm and on Warm-plus-Cold Dark Matter Models". In: *Journal of Cosmology and Astroparticle Physics* 2009.05 (20th May 2009), p. 012. ISSN: 1475-7516. DOI: 10.1088/1475-7516/2009/05/012. arXiv: 0812.0010 [astro-ph, physics:hep-ph].

[382] Alexey Boyarsky, Oleg Ruchayskiy and Mikhail Shaposhnikov. "The Role of Sterile Neutrinos in Cosmology and Astrophysics". In: *Annual Review of Nuclear and Particle Science* 59.1 (1st Nov. 2009), pp. 191–214. ISSN: 0163-8998, 1545-4134. DOI: 10.1146/annurev.nucl.010909.083654. arXiv: 0901.0011 [astro-ph, physics:hep-ph].

[383] A.D. Dolgov and S.H. Hansen. "Massive Sterile Neutrinos as Warm Dark Matter". In: *Astropart. Phys.* 16.3 (Jan. 2002), pp. 339–344. ISSN: 09276505. DOI: 10.1016/S0927-6505(01)00115-3. arXiv: hep-ph/0009083.

[384] Wolfgang Enzi et al. "Joint Constraints on Thermal Relic Dark Matter from Strong Gravitational Lensing, the Lyman-α Forest, and Milky Way Satellites". In: *Monthly Notices of the Royal Astronomical Society* 506.4 (13th Aug. 2021), pp. 5848–5862. ISSN: 0035-8711, 1365-2966. DOI: 10.1093/mnras/stab1960. arXiv: 2010.13802 [astro-ph].

[385] A. Garzilli, A. Magalich, O. Ruchayskiy and A. Boyarsky. "How to Constrain Warm Dark Matter with the Lyman α Forest". In: *Monthly Notices of the Royal Astronomical Society* 502.2 (9th Feb. 2021), pp. 2356–2363. ISSN: 0035-8711, 1365-2966. DOI: 10.1093/mnras/stab192. arXiv: 1912.09397 [astro-ph, physics:hep-ph].

[386] Simon Knapen, Tongyan Lin and Kathryn M. Zurek. "Light Dark Matter: Models and Constraints". In: *Physical Review D* 96.11 (26th Dec. 2017), p. 115021. ISSN: 2470-0010, 2470-0029. DOI: 10.1103/PhysRevD.96.115021. arXiv: 1709.07882 [hep-ph].

[387] Riccardo Murgia, Vid Iršič and Matteo Viel. "Novel Constraints on Non-Cold (Non-Thermal) Dark Matter from Lyman-α Forest Data". In: *Physical Review D* 98.8 (31st Oct. 2018), p. 083540. ISSN: 2470-0010, 2470-0029. DOI: 10.1103/PhysRevD.98.083540. arXiv: 1806.08371.

[388] Michael Sitwell, Andrei Mesinger, Yin-Zhe Ma and Kris Sigurdson. "The Imprint of Warm Dark Matter on the Cosmological 21-Cm Signal". In: *Monthly Notices of the Royal Astronomical Society* 438.3 (1st Mar. 2014), pp. 2664–2671. ISSN: 0035-8711, 1365-2966. DOI: 10.1093/mnras/stt2392. arXiv: 1310.0029 [astro-ph].

[389] Matteo Viel et al. "Constraining Warm Dark Matter Candidates Including Sterile Neutrinos and Light Gravitinos with WMAP and the Lyman-alpha Forest". In: *Physical Review D* 71.6 (31st Mar. 2005), p. 063534. ISSN: 1550-7998, 1550-2368. DOI: 10.1103/PhysRevD.71.063534. arXiv: astro-ph/0501562.

[390] Isabella P. Carucci, Francisco Villaescusa-Navarro, Matteo Viel and Andrea Lapi. "Warm Dark Matter Signatures on the 21cm Power Spectrum: Intensity Mapping Forecasts for SKA". In: *Journal of Cosmology and Astroparticle Physics* 2015.07 (29th July 2015), pp. 047–047. ISSN: 1475-7516. DOI: 10.1088/1475-7516/2015/07/047. arXiv: 1502.06961 [astro-ph].

[391] Steen H. Hansen, Julien Lesgourgues, Sergio Pastor and Joseph Silk. "Constraining the Window on Sterile Neutrinos as Warm Dark Matter". In: *Monthly Notices of the Royal Astronomical Society* 333.3 (1st July 2002), pp. 544–546. ISSN: 0035-8711, 1365-2966. DOI: 10.1046/j.1365-8711.2002.05410.x. arXiv: astro-ph/0106108.

[392] Takehiko Asaka, Steve Blanchet and Mikhail Shaposhnikov. "The νMSM, Dark Matter and Neutrino Masses". In: *Physics Letters B* 631.4 (Dec. 2005), pp. 151–156. ISSN: 03702693. DOI: 10.1016/j.physletb.2005.09.070. arXiv: hep-ph/0503065.

[393] Francesca Chadha-Day, John Ellis and David J. E. Marsh. "Axion Dark Matter: What Is It and Why Now?" In: *Science Advances* 8.8 (23rd Feb. 2022). DOI: 10.1126/sciadv.abj3618. arXiv: 2105.01406.

[394] Lam Hui. "Wave Dark Matter". In: *Annual Review of Astronomy and Astrophysics* 59.1 (8th Sept. 2021), pp. 247–289. ISSN: 0066-4146, 1545-4282. DOI: 10.1146/annurev-astro-120920-010024. arXiv: 2101.11735.

[395] Jihn E. Kim and Gianpaolo Carosi. *Axions and the Strong CP Problem*. 3rd Mar. 2009. DOI: 10.1103/RevModPhys.82.557,10.1103/RevModPhys.91.049902. arXiv: 0807.3125. URL: http://arxiv.org/abs/0807.3125 (visited on 02/03/2023). preprint.

[396] R D Peccei and Helen R Quinn. "$\mathrm{CP$ Conservation in the Presence of Pseudoparticles". In: *Physical Review Letters* 38.25 (20th June 1977), pp. 1440–1443. DOI: 10.1103/PhysRevLett.38.1440.

[397] R D Peccei and Helen R Quinn. "Constraints Imposed by $\mathrm{CP$ Conservation in the Presence of Pseudoparticles". In: *Physical Review D* 16.6 (15th Sept. 1977), pp. 1791–1797. DOI: 10.1103/PhysRevD.16.1791.

[398] Steven Weinberg. "A New Light Boson?" In: *Physical Review Letters* 40.4 (23rd Jan. 1978), pp. 223–226. DOI: 10.1103/PhysRevLett.40.223.

[399] F. Wilczek. "Problem of Strong P and T Invariance in the Presence of Instantons". In: *Physical Review Letters* 40.5 (30th Jan. 1978), pp. 279–282. DOI: 10.1103/PhysRevLett.40.279.

[400] R. J. Crewther, P. Di Vecchia, G. Veneziano and E. Witten. "Chiral Estimate of the Electric Dipole Moment of the Neutron in Quantum Chromodynamics". In: *Physics Letters B* 88.1 (3rd Dec. 1979), pp. 123–127. ISSN: 0370-2693. DOI: 10.1016/0370-2693(79)90128-X.

[401] R. J. Crewther, P. Di Vecchia, G. Veneziano and E. Witten. "Erratum: Chiral Estimate of the Electric Dipole Moment of the Neutron in Quantum Chromodynamics: R.J. Crewther, P. Di Vecchia. G. Veneziano and E. Witten Phys. Lett. 88B (1979) 123." In: *Physics Letters B* 91.3 (21st Apr. 1980), p. 487. ISSN: 0370-2693. DOI: 10.1016/0370-2693(80)91025-4.

[402] C. Abel et al. "Measurement of the Permanent Electric Dipole Moment of the Neutron". In: *Physical Review Letters* 124.8 (28th Feb. 2020), p. 081803. ISSN: 0031-9007, 1079-7114. DOI: 10.1103/PhysRevLett.124.081803. arXiv: 2001.11966 [hep-ex, physics:nucl-ex, physics:physics].

[403] C. A. Baker et al. "An Improved Experimental Limit on the Electric Dipole Moment of the Neutron". In: *Physical Review Letters* 97.13 (27th Sept. 2006), p. 131801. ISSN: 0031-9007, 1079-7114. DOI: 10.1103/PhysRevLett.97.131801. arXiv: hep-ex/0602020.

[404] Georg G. Raffelt. "Astrophysical Axion Bounds". In: *Axions: Theory, Cosmology, and Experimental Searches*. Ed. by Markus Kuster, Georg Raffelt and Berta Beltrán. Lecture Notes in Physics. Berlin, Heidelberg: Springer, 2008, pp. 51–71. ISBN: 978-3-540-73518-2. DOI: 10.1007/978-3-540-73518-2_3. arXiv: hep-ph/0611350.

[405] Jihn E. Kim. "Weak-Interaction Singlet and Strong $\mathrm{CP$ Invariance". In: *Physical Review Letters* 43.2 (9th July 1979), pp. 103–107. DOI: 10.1103/PhysRevLett.43.103.

[406] M. A. Shifman, A. I. Vainshtein and V. I. Zakharov. "Can Confinement Ensure Natural CP Invariance of Strong Interactions?" In: *Nuclear Physics B* 166.3 (28th Apr. 1980), pp. 493–506. ISSN: 0550-3213. DOI: 10.1016/0550-3213(80)90209-6.

[407] Michael Dine, Willy Fischler and Mark Srednicki. "A Simple Solution to the Strong CP Problem with a Harmless Axion". In: *Physics Letters B* 104.3 (27th Aug. 1981), pp. 199–202. ISSN: 0370-2693. DOI: 10.1016/0370-2693(81)90590-6.

[408] A. R. Zhitnitsky. "On Possible Suppression of the Axion Hadron Interactions." In: *Sov. J. Nucl. Phys.* 31 (1980), p. 260.

[409] Ciaran O'Hare. *Cajohare/AxionLimits: AxionLimits*. July 2020. DOI: 10.5281/zenodo.3932430.

[410] ADMX Collaboration et al. "Search for "Invisible" Axion Dark Matter in the $3.3\text{-}4.2~{\mu}$eV Mass Range". In: *Physical Review Letters* 127.26 (23rd Dec. 2021), p. 261803. ISSN: 0031-9007, 1079-7114. DOI: 10.1103/PhysRevLett.127.261803. arXiv: 2110.06096.

[411] K. M. Backes et al. "A Quantum-Enhanced Search for Dark Matter Axions". In: *Nature* 590.7845 (11th Feb. 2021), pp. 238–242. ISSN: 0028-0836, 1476-4687. DOI: 10.1038/s41586-021-03226-7. arXiv: 2008.01853.

[412] C. Bartram et al. *Dark Matter Axion Search Using a Josephson Traveling Wave Parametric Amplifier*. 15th Oct. 2021. arXiv: 2110.10262. URL: http://arxiv.org/abs/2110.10262 (visited on 03/03/2023). preprint.

[413] T. Braine et al. "Extended Search for the Invisible Axion with the Axion Dark Matter Experiment". In: *Physical Review Letters* 124.10 (11th Mar. 2020), p. 101303. ISSN: 0031-9007, 1079-7114. DOI: 10.1103/PhysRevLett.124.101303. arXiv: 1910.08638.

[414] N. Crisosto et al. "ADMX SLIC: Results from a Superconducting LC Circuit Investigating Cold Axions". In: *Physical Review Letters* 124.24 (17th June 2020), p. 241101. ISSN: 0031-9007, 1079-7114. DOI: 10.1103/PhysRevLett.124.241101. arXiv: 1911.05772.

[415] N. Du et al. "A Search for Invisible Axion Dark Matter with the Axion Dark Matter Experiment". In: *Physical Review Letters* 120.15 (9th Apr. 2018), p. 151301. ISSN: 0031-9007, 1079-7114. DOI: 10.1103/PhysRevLett.120.151301. arXiv: 1804.05750.

[416] HAYSTAC Collaboration et al. *New Results from HAYSTAC's Phase II Operation with a Squeezed State Receiver*. 26th Jan. 2023. arXiv: 2301.09721. URL: http://arxiv.org/abs/2301.09721 (visited on 03/03/2023). preprint.

[417] I. Stern. *ADMX Status*. 5th Jan. 2017. arXiv: 1612.08296. URL: http://arxiv.org/abs/1612.08296 (visited on 03/03/2023). preprint.

[418] The ADMX Collaboration et al. "A SQUID-based Microwave Cavity Search for Dark-Matter Axions". In: *Physical Review Letters* 104.4 (28th Jan. 2010), p. 041301. ISSN: 0031-9007, 1079-7114. DOI: 10.1103/PhysRevLett.104.041301. arXiv: 0910.5914.

[419] L. Zhong et al. "Results from Phase 1 of the HAYSTAC Microwave Cavity Axion Experiment". In: *Physical Review D* 97.9 (4th May 2018), p. 092001. ISSN: 2470-0010, 2470-0029. DOI: 10.1103/PhysRevD.97.092001. arXiv: 1803.03690.

[420] Junu Jeong et al. "Search for Invisible Axion Dark Matter with a Multiple-Cell Haloscope". In: *Physical Review Letters* 125.22 (25th Nov. 2020), p. 221302. ISSN: 0031-9007, 1079-7114. DOI: 10.1103/PhysRevLett.125.221302. arXiv: 2008.10141.

[421] Ohjoon Kwon et al. "First Results from Axion Haloscope at CAPP around 10.7 μeV". In: *Physical Review Letters* 126.19 (12th May 2021), p. 191802. ISSN: 0031-9007, 1079-7114. DOI: 10.1103/PhysRevLett.126.191802. arXiv: 2012.10764.

[422] S. Lee et al. "Axion Dark Matter Search around 6.7 μeV". In: *Physical Review Letters* 124.10 (13th Mar. 2020), p. 101802. ISSN: 0031-9007, 1079-7114. DOI: 10.1103/PhysRevLett.124.101802. arXiv: 2001.05102.

[423] Youngjae Lee et al. "Searching for Invisible Axion Dark Matter with an 18T Magnet Haloscope". In: *Physical Review Letters* 128.24 (17th June 2022), p. 241805. ISSN: 0031-9007, 1079-7114. DOI: 10.1103/PhysRevLett.128.241805. arXiv: 2206.08845.

[424] L. F. Abbott and P. Sikivie. "A Cosmological Bound on the Invisible Axion". In: *Physics Letters B* 120.1 (6th Jan. 1983), pp. 133–136. ISSN: 0370-2693. DOI: 10.1016/0370-2693(83)90638-X.

[425] Michael Dine and Willy Fischler. "The Not-so-Harmless Axion". In: *Physics Letters B* 120.1 (6th Jan. 1983), pp. 137–141. ISSN: 0370-2693. DOI: 10.1016/0370-2693(83)90639-1.

[426] Michael S. Turner. "Windows on the Axion". In: *Physics Reports* 197.2 (1st Dec. 1990), pp. 67–97. ISSN: 0370-1573. DOI: 10.1016/0370-1573(90)90172-X.

[427] J. Jaeckel, G. Rybka and L. Winslow. *Axion Dark Matter*. 1st Apr. 2022. DOI: 10.48550/arXiv.2203.14923. arXiv: 2203.14923. URL: http://arxiv.org/abs/2203.14923 (visited on 06/03/2023). preprint.

[428] Georg G. Raffelt. "Axions - Motivation, Limits and Searches". In: *Journal of Physics A: Mathematical and Theoretical* 40.25 (22nd June 2007), pp. 6607–6620. ISSN: 1751-8113, 1751-8121. DOI: 10.1088/1751-8113/40/25/S05. arXiv: hep-ph/0611118.

[429] S. Borsanyi et al. "Calculation of the Axion Mass Based on High-Temperature Lattice Quantum Chromodynamics". In: *Nature* 539.7627 (Nov. 2016), pp. 69–71. ISSN: 1476-4687. DOI: 10.1038/nature20115. arXiv: 1606.07494.

[430] Michael S. Turner. "Cosmic and Local Mass Density of "invisible" Axions". In: *Physical Review D* 33.4 (15th Feb. 1986), pp. 889–896. DOI: 10.1103/PhysRevD.33.889.

[431] T. W. B. Kibble. "Topology of Cosmic Domains and Strings". In: *Journal of Physics A: Mathematical and General* 9.8 (Aug. 1976), p. 1387. ISSN: 0305-4470. DOI: 10.1088/0305-4470/9/8/029.

[432] P. Sikivie. "Experimental Tests of the "Invisible" Axion". In: *Physical Review Letters* 51.16 (17th Oct. 1983), pp. 1415–1417. DOI: 10.1103/PhysRevLett.51.1415.

[433] Igor G. Irastorza and Javier Redondo. "New Experimental Approaches in the Search for Axion-like Particles". In: *Progress in Particle and Nuclear Physics* 102 (Sept. 2018), pp. 89–159. ISSN: 01466410. DOI: 10.1016/j.ppnp.2018.05.003. arXiv: 1801.08127.

[434] Yukio Fukuda, Toshiro Kohmoto, Shin-ichi Nakajima and Masakuzu Kunitomo. "Production and Detection of Axions by Using Optical Resonators". In: *Progress in Crystal Growth and Characterization of Materials* 33.1 (1st Jan. 1996), pp. 363–366. ISSN: 0960-8974. DOI: 10.1016/0960-8974(96)83672-2.

[435] F Hoogeveen and T Ziegenhagen. "Production and Detection of Light Bosons Using Optical Resonators". In: *Nuclear Physics B* 358.1 (8th July 1991), pp. 3–26. ISSN: 0550-3213. DOI: 10.1016/0550-3213(91)90528-6.

[436] Guido Mueller, Pierre Sikivie, D. B. Tanner and Karl van Bibber. "Detailed Design of a Resonantly-Enhanced Axion-Photon Regeneration Experiment". In: *Physical Review D* 80.7 (15th Oct. 2009), p. 072004. ISSN: 1550-7998, 1550-2368. DOI: 10.1103/PhysRevD.80.072004. arXiv: 0907.5387.

[437] Wayne Hu, Rennan Barkana and Andrei Gruzinov. "Cold and Fuzzy Dark Matter". In: *Physical Review Letters* 85.6 (7th Aug. 2000), pp. 1158–1161. ISSN: 0031-9007, 1079-7114. DOI: 10.1103/PhysRevLett.85.1158. arXiv: astro-ph/0003365.

[438] Lam Hui, Jeremiah P. Ostriker, Scott Tremaine and Edward Witten. "Ultralight Scalars as Cosmological Dark Matter". In: *Physical Review D* 95.4 (28th Feb. 2017), p. 043541. ISSN: 2470-0010, 2470-0029. DOI: 10.1103/PhysRevD.95.043541. arXiv: 1610.08297.

[439] Tessa Cookmeyer, Daniel Grin and Tristan L. Smith. "How Sound Are Our Ultra-Light Axion Approximations?" In: *Physical Review D* 101.2 (2nd Jan. 2020), p. 023501. ISSN: 2470-0010, 2470-0029. DOI: 10.1103/PhysRevD.101.023501. arXiv: 1909.11094 [astro-ph, physics:gr-qc, physics:hep-ph].

[440] Renée Hložek et al. "Future CMB Tests of Dark Matter: Ultra-Light Axions and Massive Neutrinos". In: *Physical Review D* 95.12 (8th June 2017), p. 123511. ISSN: 2470-0010, 2470-0029. DOI: 10.1103/PhysRevD.95.123511. arXiv: 1607.08208 [astro-ph, physics:hep-ph].

[441] Renée Hlozek, Daniel Grin, David J. E. Marsh and Pedro G. Ferreira. "A Search for Ultra-Light Axions Using Precision Cosmological Data". In: *Physical Review D* 91.10 (15th May 2015), p. 103512. ISSN: 1550-7998, 1550-2368. DOI: 10.1103/PhysRevD.91.103512. arXiv: 1410.2896.

[442] Virgile Dandoy, Thomas Schwetz and Elisa Todarello. "A Self-Consistent Wave Description of Axion Miniclusters and Their Survival in the Galaxy". In: *Journal of Cosmology and Astroparticle Physics* 2022.09 (1st Sept. 2022), p. 081. ISSN: 1475-7516. DOI: 10.1088/1475-7516/2022/09/081. arXiv: 2206.04619 [astro-ph, physics:hep-ph].

[443] Benedikt Eggemeier et al. "Axion Minivoids and Implications for Direct Detection". In: *Physical Review D* 107.8 (2023), p. 083510. DOI: 10.1103/PhysRevD.107.083510. arXiv: 2212.00560 [astro-ph, physics:hep-ph].

[444] Bradley J. Kavanagh, Thomas D. P. Edwards, Luca Visinelli and Christoph Weniger. "Stellar Disruption of Axion Miniclusters in the Milky Way". In: *Physical Review D* 104.6 (23rd Sept. 2021), p. 063038. ISSN: 2470-0010, 2470-0029. DOI: 10.1103/PhysRevD.104.063038. arXiv: 2011.05377 [astro-ph, physics:hep-ph].

[445] Hsi-Yu Schive, Tzihong Chiueh and Tom Broadhurst. "Cosmic Structure as the Quantum Interference of a Coherent Dark Wave". In: *Nature Physics* 10.7 (July 2014), pp. 496–499. ISSN: 1745-2473, 1745-2481. DOI: 10.1038/nphys2996. arXiv: 1406.6586 [astro-ph].

[446] Hsi-Yu Schive et al. "Understanding the Core-Halo Relation of Quantum Wave Dark Matter, ψDM, from 3D Simulations". In: *Physical Review Letters* 113.26 (30th Dec. 2014), p. 261302. ISSN: 0031-9007, 1079-7114. DOI: 10.1103/PhysRevLett.113.261302. arXiv: 1407.7762 [astro-ph].

[447] Malte Buschmann, Joshua W. Foster and Benjamin R. Safdi. "Early-Universe Simulations of the Cosmological Axion". In: *Physical Review Letters* 124.16 (24th Apr. 2020), p. 161103. ISSN: 0031-9007, 1079-7114. DOI: 10.1103/PhysRevLett.124.161103. arXiv: 1906.00967 [astro-ph, physics:hep-ph].

[448] Benedikt Eggemeier and Jens C. Niemeyer. "Formation and Mass Growth of Axion Stars in Axion Miniclusters". In: *Physical Review D* 100.6 (23rd Sept. 2019), p. 063528. ISSN: 2470-0010, 2470-0029. DOI: 10.1103/PhysRevD.100.063528. arXiv: 1906.01348 [astro-ph].

[449] Benedikt Eggemeier, Bodo Schwabe, Jens C. Niemeyer and Richard Easther. "Gravitational Collapse in the Post-Inflationary Universe". In: *Physical Review D* 105.2 (12th Jan. 2022), p. 023516. ISSN: 2470-0010, 2470-0029. DOI: 10.1103/PhysRevD.105.023516. arXiv: 2110.15109 [astro-ph, physics:hep-ph].

[450] David Ellis et al. "Structure of Axion Miniclusters". In: *Physical Review D* 106.10 (15th Nov. 2022), p. 103514. ISSN: 2470-0010, 2470-0029. DOI: 10.1103/PhysRevD.106.103514. arXiv: 2204.13187 [astro-ph, physics:hep-ph].

[451] Malcolm Fairbairn, David J. E. Marsh, Jérémie Quevillon and Simon Rozier. "Structure Formation and Microlensing with Axion Miniclusters". In: *Physical Review D* 97.8 (6th Apr. 2018), p. 083502. ISSN: 2470-0010, 2470-0029. DOI: 10.1103/PhysRevD.97.083502. arXiv: 1707.03310 [astro-ph, physics:hep-ph].

[452] Edward W. Kolb and Igor I. Tkachev. "Axion Miniclusters and Bose Stars". In: *Physical Review Letters* 71.19 (8th Nov. 1993), pp. 3051–3054. ISSN: 0031-9007. DOI: 10.1103/PhysRevLett.71.3051. arXiv: hep-ph/9303313.

[453] E. W. Kolb and I. I. Tkachev. "Femtolensing and Picolensing by Axion Miniclusters". In: *The Astrophysical Journal* 460.1 (20th Mar. 1996). ISSN: 0004637X. DOI: 10.1086/309962. arXiv: astro-ph/9510043.

[454] Ciaran A. J. O'Hare, Giovanni Pierobon, Javier Redondo and Yvonne Y. Y. Wong. "Simulations of Axion-like Particles in the Post-Inflationary Scenario". In: *Physical Review D* 105.5 (29th Mar. 2022), p. 055025. ISSN: 2470-0010, 2470-0029. DOI: 10.1103/PhysRevD.105.055025. arXiv: 2112.05117 [astro-ph, physics:hep-ph].

[455] Huangyu Xiao, Ian Williams and Matthew McQuinn. "Simulations of Axion Minihalos". In: *Physical Review D* 104.2 (13th July 2021), p. 023515. ISSN: 2470-0010, 2470-0029. DOI: 10.1103/PhysRevD.104.023515. arXiv: 2101.04177 [astro-ph, physics:hep-ph].

[456] Bodo Schwabe et al. "AxioNyx: Simulating Mixed Fuzzy and Cold Dark Matter". In: *Physical Review D* 102.8 (13th Oct. 2020), p. 083518. ISSN: 2470-0010, 2470-0029. DOI: 10.1103/PhysRevD.102.083518. arXiv: 2007.08256 [astro-ph].

[457] Philip F. Hopkins. "A Stable Finite-Volume Method for Scalar-Field Dark Matter". In: *Monthly Notices of the Royal Astronomical Society* 489.2 (21st Oct. 2019), pp. 2367–2376. ISSN: 0035-8711, 1365-2966. DOI: 10.1093/mnras/stz1922. arXiv: 1811.05583 [astro-ph].

[458] Philip Mocz et al. "Galaxy Formation with BECDM: I. Turbulence and Relaxation of Idealised Haloes". In: *Monthly Notices of the Royal Astronomical Society* 471.4 (Nov. 2017), pp. 4559–4570. ISSN: 0035-8711, 1365-2966. DOI: 10.1093/mnras/stx1887. arXiv: 1705.05845 [astro-ph].

[459] M. Nori and M. Baldi. "AX-GADGET: A New Code for Cosmological Simulations of Fuzzy Dark Matter and Axion Models". In: *Monthly Notices of the Royal Astronomical Society* 478.3 (11th Aug. 2018), pp. 3935–3951. ISSN: 0035-8711, 1365-2966. DOI: 10.1093/mnras/sty1224. arXiv: 1801.08144 [astro-ph].

[460] Bodo Schwabe, Jens C. Niemeyer and Jan F. Engels. "Simulations of Solitonic Core Mergers in Ultra-Light Axion Dark Matter Cosmologies". In: *Physical Review D* 94.4 (12th Aug. 2016), p. 043513. ISSN: 2470-0010, 2470-0029. DOI: 10.1103/PhysRevD.94.043513. arXiv: 1606.05151 [astro-ph, physics:gr-qc, physics:hep-th].

[461] Jan Veltmaat and Jens C. Niemeyer. "Cosmological Particle-in-Cell Simulations with Ultralight Axion Dark Matter". In: *Physical Review D* 94.12 (22nd Dec. 2016), p. 123523. ISSN: 2470-0010, 2470-0029. DOI: 10.1103/PhysRevD.94.123523. arXiv: 1608.00802 [astro-ph].

[462] Tak-Pong Woo and Tzihong Chiueh. "High-Resolution Simulation on Structure Formation with Extremely Light Bosonic Dark Matter". In: *The Astrophysical Journal* 697.1 (20th May 2009), pp. 850–861. ISSN: 0004-637X, 1538-4357. DOI: 10.1088/0004-637X/697/1/850. arXiv: 0806.0232 [astro-ph].

[463] Ya. B. Zel'dovich and I. D. Novikov. "The Hypothesis of Cores Retarded during Expansion and the Hot Cosmological Model". In: *Sov. Astron.* 10 (1966), p. 602.

[464] Stephen Hawking. "Gravitationally Collapsed Objects of Very Low Mass". In: *Mon. Not. Roy. Astron. Soc.* 152 (1971), p. 75.

[465] George F. Chapline. "Cosmological Effects of Primordial Black Holes". In: *Nature* 253.5489 (1975), pp. 251–252. DOI: 10.1038/253251a0.

[466] P. Meszaros. "Primeval Black Holes and Galaxy Formation". In: *Astronomy and Astrophysics* 38.1 (1975), pp. 5–13. ISSN: 0004-6361.

[467] Bernard Carr, Florian Kuhnel and Marit Sandstad. "Primordial Black Holes as Dark Matter". In: *Physical Review D* 94.8 (4th Oct. 2016), p. 083504. ISSN: 2470-0010, 2470-0029. DOI: 10.1103/PhysRevD.94.083504. arXiv: 1607.06077.

[468] Pablo Villanueva-Domingo, Olga Mena and Sergio Palomares-Ruiz. "A Brief Review on Primordial Black Holes as Dark Matter". In: *Frontiers in Astronomy and Space Sciences* 8 (28th May 2021), p. 681084. ISSN: 2296-987X. DOI: 10.3389/fspas.2021.681084. arXiv: 2103.12087.

[469] Bernard Carr and Florian Kuhnel. "Primordial Black Holes as Dark Matter Candidates". In: *SciPost Physics Lecture Notes* 48 (2nd May 2022), p. 48. ISSN: 2590-1990. DOI: 10.21468/SciPostPhysLectNotes.48. arXiv: 2110.02821.

[470] Anne M. Green and Bradley J. Kavanagh. "Primordial Black Holes as a Dark Matter Candidate". In: *Journal of Physics G: Nuclear and Particle Physics* 48.4 (July 2020), p. 043001. ISSN: 0954-3899, 1361-6471. DOI: 10.1088/1361-6471/abc534. arXiv: 2007.10722.

[471] Jérémy Auffinger. *Primordial Black Hole Constraints with Hawking Radiation – a Review*. 6th June 2022. DOI: 10.48550/arXiv.2206.02672. arXiv: 2206.02672. URL: http://arxiv.org/abs/2206.02672 (visited on 01/02/2023). preprint.

[472] Marc Oncins. *Constraints on PBH as Dark Matter from Observations: A Review*. 29th May 2022. DOI: 10.48550/arXiv.2205.14722. arXiv: 2205.14722. URL: http://arxiv.org/abs/2205.14722 (visited on 01/02/2023). preprint.

[473] The LIGO Scientific Collaboration and the Virgo Collaboration. "Observation of Gravitational Waves from a Binary Black Hole Merger". In: *Physical Review Letters* 116.6 (11th Feb. 2016), p. 061102. ISSN: 0031-9007, 1079-7114. DOI: 10.1103/PhysRevLett.116.061102. arXiv: 1602.03837.

[474] The LIGO Scientific Collaboration and the Virgo Collaboration. "GW151226: Observation of Gravitational Waves from a 22-Solar-Mass Binary Black Hole Coalescence". In: *Physical Review Letters* 116.24 (15th June 2016), p. 241103. ISSN: 0031-9007, 1079-7114. DOI: 10.1103/PhysRevLett.116.241103. arXiv: 1606.04855.

[475] The LIGO Scientific Collaboration et al. "GW170104: Observation of a 50-Solar-Mass Binary Black Hole Coalescence at Redshift 0.2". In: *Physical Review Letters* 118.22 (1st June 2017), p. 221101. ISSN: 0031-9007, 1079-7114. DOI: 10.1103/PhysRevLett.118.221101. arXiv: 1706.01812.

[476] The LIGO Scientific Collaboration et al. "GW170814: A Three-Detector Observation of Gravitational Waves from a Binary Black Hole Coalescence". In: *Physical Review Letters* 119.14 (6th Oct. 2017), p. 141101. ISSN: 0031-9007, 1079-7114. DOI: 10.1103/PhysRevLett.119.141101. arXiv: 1709.09660.

[477] The LIGO Scientific Collaboration et al. "Binary Black Hole Mergers in the First Advanced LIGO Observing Run". In: *Physical Review X* 6.4 (21st Oct. 2016), p. 041015. ISSN: 2160-3308. DOI: 10.1103/PhysRevX.6.041015. arXiv: 1606.04856.

[478] The LIGO Scientific Collaboration et al. "GW170608: Observation of a 19-Solar-Mass Binary Black Hole Coalescence". In: *The Astrophysical Journal* 851.2 (18th Dec. 2017), p. L35. ISSN: 2041-8213. DOI: 10.3847/2041-8213/aa9f0c. arXiv: 1711.05578.

[479] The LIGO Scientific Collaboration et al. "GWTC-1: A Gravitational-Wave Transient Catalog of Compact Binary Mergers Observed by LIGO and Virgo during the First and Second Observing Runs". In: *Physical Review X* 9.3 (4th Sept. 2019), p. 031040. ISSN: 2160-3308. DOI: 10.1103/PhysRevX.9.031040. arXiv: 1811.12907.

[480] R. Abbott et al. "GWTC-2: Compact Binary Coalescences Observed by LIGO and Virgo During the First Half of the Third Observing Run". In: *Physical Review X* 11.2 (9th June 2021), p. 021053. ISSN: 2160-3308. DOI: 10.1103/PhysRevX.11.021053. arXiv: 2010.14527.

[481] The LIGO Scientific Collaboration et al. *GWTC-2.1: Deep Extended Catalog of Compact Binary Coalescences Observed by LIGO and Virgo During the First Half of the Third Observing Run*. 10th May 2022. DOI: 10.48550/arXiv.2108.01045. arXiv: 2108.01045. URL: http://arxiv.org/abs/2108.01045 (visited on 01/02/2023). preprint.

[482] The LIGO Scientific Collaboration et al. *GWTC-3: Compact Binary Coalescences Observed by LIGO and Virgo During the Second Part of the Third Observing Run*. 17th Nov. 2021. DOI: 10.48550/arXiv.2111.03606. arXiv: 2111.03606. URL: http://arxiv.org/abs/2111.03606 (visited on 01/02/2023). preprint.

[483] The Event Horizon Telescope Collaboration. "First M87 Event Horizon Telescope Results. I. The Shadow of the Supermassive Black Hole". In: *The Astrophysical Journal Letters* 875.1 (26th June 2019), p. L1. ISSN: 2041-8205. DOI: 10.3847/2041-8213/ab0ec7. arXiv: 1906.11238.

[484] The Event Horizon Telescope Collaboration. "First M87 Event Horizon Telescope Results. IV. Imaging the Central Supermassive Black Hole". In: *The Astrophysical Journal Letters* 875.1 (26th June 2019), p. L4. ISSN: 2041-8205. DOI: 10.3847/2041-8213/ab0e85. arXiv: 1906.11241.

[485] Event Horizon Telescope Collaboration et al. "First Sagittarius A* Event Horizon Telescope Results. I. The Shadow of the Supermassive Black Hole in the Center of the Milky Way". In: *The Astrophysical Journal Letters* 930.2 (May 2022), p. L12. ISSN: 2041-8205. DOI: 10.3847/2041-8213/ac6674.

[486] Event Horizon Telescope Collaboration et al. "First Sagittarius A* Event Horizon Telescope Results. III. Imaging of the Galactic Center Supermassive Black Hole". In: *The Astrophysical Journal Letters* 930.2 (May 2022), p. L14. ISSN: 2041-8205. DOI: 10.3847/2041-8213/ac6429.

[487] J. R. Oppenheimer and G. M. Volkoff. "On Massive Neutron Cores". In: *Physical Review* 55.4 (15th Feb. 1939), pp. 374–381. DOI: 10.1103/PhysRev.55.374.

[488] Richard C. Tolman. "Static Solutions of Einstein's Field Equations for Spheres of Fluid". In: *Physical Review* 55.4 (15th Feb. 1939), pp. 364–373. DOI: 10.1103/PhysRev.55.364.

[489] The LIGO Scientific Collaboration et al. "Properties and Astrophysical Implications of the 150 Msun Binary Black Hole Merger GW190521". In: *The Astrophysical Journal* 900.1 (2nd Sept. 2020), p. L13. ISSN: 2041-8213. DOI: 10.3847/2041-8213/aba493. arXiv: 2009.01190.

[490] The LIGO Scientific Collaboration et al. *Search for Subsolar-Mass Black Hole Binaries in the Second Part of Advanced LIGO's and Advanced Virgo's Third Observing Run*. 2nd Dec. 2022. DOI: 10.48550/arXiv.2212.01477. arXiv: 2212.01477. URL: http://arxiv.org/abs/2212.01477 (visited on 01/02/2023). preprint.

[491] Alexander H. Nitz and Yi-Fan Wang. "Broad Search for Gravitational Waves from Subsolar-Mass Binaries through LIGO and Virgo's Third Observing Run". In: *Physical Review D* 106.2 (21st July 2022), p. 023024. ISSN: 2470-0010, 2470-0029. DOI: 10.1103/PhysRevD.106.023024. arXiv: 2202.11024.

[492] Khun Sang Phukon et al. *The Hunt for Sub-Solar Primordial Black Holes in Low Mass Ratio Binaries Is Open*. 24th May 2021. DOI: 10.48550/arXiv.2105.11449. arXiv: 2105.11449. URL: http://arxiv.org/abs/2105.11449 (visited on 01/02/2023). preprint.

[493] Gonzalo Morrás et al. *Analysis of a Subsolar-Mass Black Hole Trigger from the Second Observing Run of Advanced LIGO*. 27th Jan. 2023. DOI: 10.48550/arXiv.2301.11619. arXiv: 2301.11619. URL: http://arxiv.org/abs/2301.11619 (visited on 01/02/2023). preprint.

[494] Ville Vaskonen and Hardi Veermäe. "Did NANOGrav See a Signal from Primordial Black Hole Formation?" In: *Physical Review Letters* 126.5 (5th Feb. 2021), p. 051303. ISSN: 0031-9007, 1079-7114. DOI: 10.1103/PhysRevLett.126.051303. arXiv: 2009.07832.

[495] Pau Amaro-Seoane et al. *Laser Interferometer Space Antenna*. 23rd Feb. 2017. DOI: 10.48550/arXiv.1702.00786. arXiv: 1702.00786. URL: http://arxiv.org/abs/1702.00786 (visited on 01/02/2023). preprint.

[496] Juan García-Bellido. "Massive Primordial Black Holes as Dark Matter and Their Detection with Gravitational Waves". In: *Journal of Physics: Conference Series* 840 (May 2017), p. 012032. ISSN: 1742-6588, 1742-6596. DOI: 10.1088/1742-6596/840/1/012032. arXiv: 1702.08275.

[497] Paul H. Frampton. "Dark Matter Gravity Waves at LIGO and LISA". In: *Modern Physics Letters A* 34.16 (30th May 2019), p. 1950124. ISSN: 0217-7323, 1793-6632. DOI: 10.1142/S0217732319501244. arXiv: 1812.01468.

[498] K. G. Arun et al. "New Horizons for Fundamental Physics with LISA". In: *Living Reviews in Relativity* 25.1 (Dec. 2022), p. 4. ISSN: 2367-3613, 1433-8351. DOI: 10.1007/s41114-022-00036-9. arXiv: 2205.01597.

[499] Pierre Auclair et al. *Cosmology with the Laser Interferometer Space Antenna*. 11th Apr. 2022. DOI: 10.48550/arXiv.2204.05434. arXiv: 2204.05434. URL: http://arxiv.org/abs/2204.05434 (visited on 01/02/2023). preprint.

[500] Rachel Bean and Joao Magueijo. "Could Supermassive Black Holes Be Quintessential Primordial Black Holes?" In: *Physical Review D* 66.6 (19th Sept. 2002), p. 063505. ISSN: 0556-2821, 1089-4918. DOI: 10.1103/PhysRevD.66.063505. arXiv: astro-ph/0204486.

[501] Sébastien Clesse and Juan García-Bellido. "Massive Primordial Black Holes from Hybrid Inflation as Dark Matter and the Seeds of Galaxies". In: *Physical Review D* 92.2 (16th July 2015), p. 023524. ISSN: 1550-7998, 1550-2368. DOI: 10.1103/PhysRevD.92.023524. arXiv: 1501.07565.

[502] David Navidad Maeso et al. "Primordial Black Holes from Spectator Field Bubbles". In: *Journal of Cosmology and Astroparticle Physics* 02.02 (2022), p. 017. DOI: 10.1088/1475-7516/2022/02/017. arXiv: 2112.01505.

[503] Gia Dvali, Florian Kuhnel and Michael Zantedeschi. "Primordial Black Holes from Confinement". In: *Physical Review D* 104.12 (2nd Dec. 2021), p. 123507. ISSN: 2470-0010, 2470-0029. DOI: 10.1103/PhysRevD.104.123507. arXiv: 2108.09471.

[504] Huan Zhou et al. "Constraints on the Abundance of Supermassive Primordial Black Holes from Lensing of Compact Radio Sources". In: *Monthly Notices of the Royal Astronomical Society* 513.3 (12th May 2022), pp. 3627–3633. ISSN: 0035-8711, 1365-2966. DOI: 10.1093/mnras/stac915. arXiv: 2106.11705.

[505] Joaquim Iguaz Juan, Pasquale Serpico and Guillermo Franco Abellán. "The QCD Phase Transition behind a PBH Origin of LIGO/Virgo Events?" In: *Journal of Cosmology and Astroparticle Physics* 2022.07 (1st July 2022), p. 009. ISSN: 1475-7516. DOI: 10.1088/1475-7516/2022/07/009. arXiv: 2204.07027.

[506] Hooman Davoudiasl, Peter B. Denton and Julia Gehrlein. "Connecting the Extremes: A Story of Supermassive Black Holes and Ultralight Dark Matter". In: *Physical Review Letters* 128.8 (23rd Feb. 2022), p. 081101. ISSN: 0031-9007, 1079-7114. DOI: 10.1103/PhysRevLett.128.081101. arXiv: 2109.01678.

[507] Iason Baldes, Quentin Decant, Deanna C. Hooper and Laura Lopez-Honorez. "Non-Cold Dark Matter from Primordial Black Hole Evaporation". In: *Journal of Cosmology and Astroparticle Physics* 2020.08 (24th Aug. 2020), pp. 045–045. ISSN: 1475-7516. DOI: 10.1088/1475-7516/2020/08/045. arXiv: 2004.14773.

[508] Isabella Masina. "Dark Matter and Dark Radiation from Evaporating Primordial Black Holes". In: *The European Physical Journal Plus* 135.7 (9th July 2020), p. 552. ISSN: 2190-5444. DOI: 10.1140/epjp/s13360-020-00564-9. arXiv: 2004.04740.

[509] Andrew Cheek, Lucien Heurtier, Yuber F. Perez-Gonzalez and Jessica Turner. *Evaporation of Primordial Black Holes in the Early Universe: Mass and Spin Distributions*. 7th Dec. 2022. DOI: 10.48550/arXiv.2212.03878. arXiv: 2212.03878. URL: http://arxiv.org/abs/2212.03878 (visited on 01/02/2023). preprint.

[510] Andrew Cheek, Lucien Heurtier, Yuber F. Perez-Gonzalez and Jessica Turner. "Primordial Black Hole Evaporation and Dark Matter Production: I. Solely Hawking Radiation". In: *Physical Review D* 105.1 (21st Jan. 2022), p. 015022. ISSN: 2470-0010, 2470-0029. DOI: 10.1103/PhysRevD.105.015022. arXiv: 2107.00013.

[511] Andrew Cheek, Lucien Heurtier, Yuber F. Perez-Gonzalez and Jessica Turner. "Primordial Black Hole Evaporation and Dark Matter Production: II. Interplay with the Freeze-In/Out Mechanism". In: *Physical Review D* 105.1 (21st Jan. 2022), p. 015023. ISSN: 2470-0010, 2470-0029. DOI: 10.1103/PhysRevD.105.015023. arXiv: 2107.00016.

[512] S. W. Hawking, I. G. Moss and J. M. Stewart. "Bubble Collisions in the Very Early Universe". In: *Physical Review D* 26.10 (15th Nov. 1982), pp. 2681–2693. DOI: 10.1103/PhysRevD.26.2681.

[513] S. W. Hawking. "Black Holes from Cosmic Strings". In: *Physics Letters B* 231.3 (9th Nov. 1989), pp. 237–239. ISSN: 0370-2693. DOI: 10.1016/0370-2693(89)90206-2.

[514] Alexander Polnarev and Robert Zembowicz. "Formation of Primordial Black Holes by Cosmic Strings". In: *Physical Review D* 43.4 (15th Feb. 1991), pp. 1106–1109. DOI: 10.1103/PhysRevD.43.1106.

[515] Jaume Garriga, Alexander Vilenkin and Jun Zhang. "Black Holes and the Multiverse". In: *Journal of Cosmology and Astroparticle Physics* 2016.02 (25th Feb. 2016), pp. 064–064. ISSN: 1475-7516. DOI: 10.1088/1475-7516/2016/02/064. arXiv: 1512.01819.

[516] Heling Deng and Alexander Vilenkin. "Primordial Black Hole Formation by Vacuum Bubbles". In: *Journal of Cosmology and Astroparticle Physics* 2017.12 (28th Dec. 2017), pp. 044–044. ISSN: 1475-7516. DOI: 10.1088/1475-7516/2017/12/044. arXiv: 1710.02865.

[517] Heling Deng, Jaume Garriga and Alexander Vilenkin. "Primordial Black Hole and Wormhole Formation by Domain Walls". In: *Journal of Cosmology and Astroparticle Physics* 2017.04 (28th Apr. 2017), pp. 050–050. ISSN: 1475-7516. DOI: 10.1088/1475-7516/2017/04/050. arXiv: 1612.03753.

[518] B. J. Carr. "The Primordial Black Hole Mass Spectrum." In: *The Astrophysical Journal* 201 (1st Oct. 1975), pp. 1–19. ISSN: 0004-637X. DOI: 10.1086/153853.

[519] Misao Sasaki, Teruaki Suyama, Takahiro Tanaka and Shuichiro Yokoyama. "Primordial Black Holes - Perspectives in Gravitational Wave Astronomy -". In: *Classical and Quantum Gravity* 35.6 (22nd Mar. 2018), p. 063001. ISSN: 0264-9381, 1361-6382. DOI: 10.1088/1361-6382/aaa7b4. arXiv: 1801.05235.

[520] Anne M. Green. "Primordial Black Holes: Sirens of the Early Universe". In: vol. 178. 2015, pp. 129–149. DOI: 10.1007/978-3-319-10852-0_5. arXiv: 1403.1198.

[521] Tomohiro Harada, Chul-Moon Yoo and Kazunori Kohri. "Threshold of Primordial Black Hole Formation". In: *Physical Review D* 88.8 (28th Oct. 2013), p. 084051. ISSN: 1550-7998, 1550-2368. DOI: 10.1103/PhysRevD.88.084051. arXiv: 1309.4201.

[522] Tomohiro Harada, Chul-Moon Yoo and Kazunori Kohri. "Erratum: Threshold of Primordial Black Hole Formation [Phys. Rev. D 88, 084051 (2013)]". In: *Physical Review D* 89.2 (6th Jan. 2014), p. 029903. DOI: 10.1103/PhysRevD.89.029903.

[523] Jens C. Niemeyer and K. Jedamzik. "Near-Critical Gravitational Collapse and the Initial Mass Function of Primordial Black Holes". In: *Physical Review Letters* 80.25 (22nd June 1998), pp. 5481–5484. ISSN: 0031-9007, 1079-7114. DOI: 10.1103/PhysRevLett.80.5481. arXiv: astro-ph/9709072.

[524] Masaru Shibata and Misao Sasaki. "Black Hole Formation in the Friedmann Universe: Formulation and Computation in Numerical Relativity". In: *Physical Review D* 60.8 (8th Sept. 1999), p. 084002. ISSN: 0556-2821, 1089-4918. DOI: 10.1103/PhysRevD.60.084002. arXiv: gr-qc/9905064.

[525] Ilia Musco, John C. Miller, Luciano Rezzolla and ; "Computations of Primordial Black Hole Formation". In: *Classical and Quantum Gravity* 22.7 (7th Apr. 2005), pp. 1405–1424. ISSN: 0264-9381, 1361-6382. DOI: 10.1088/0264-9381/22/7/013. arXiv: gr-qc/0412063.

[526] Alexander G. Polnarev and Ilia Musco. "Curvature Profiles as Initial Conditions for Primordial Black Hole Formation". In: *Classical and Quantum Gravity* 24.6 (21st Mar. 2007), pp. 1405–1431. ISSN: 0264-9381, 1361-6382. DOI: 10.1088/0264-9381/24/6/003. arXiv: gr-qc/0605122.

[527] Ilia Musco, John C. Miller and Alexander G. Polnarev. "Primordial Black Hole Formation in the Radiative Era: Investigation of the Critical Nature of the Collapse". In: *Classical and Quantum Gravity* 26.23 (7th Dec. 2009), p. 235001. ISSN: 0264-9381, 1361-6382. DOI: 10.1088/0264-9381/26/23/235001. arXiv: 0811.1452.

[528] Tomohiro Nakama, Tomohiro Harada, A. G. Polnarev and Jun'ichi Yokoyama. "Identifying the Most Crucial Parameters of the Initial Curvature Profile for Primordial Black Hole Formation". In: *Journal of Cosmology and Astroparticle Physics* 2014.01 (24th Jan. 2014), pp. 037–037. ISSN: 1475-7516. DOI: 10.1088/1475-7516/2014/01/037. arXiv: 1310.3007.

[529] Ogan Özsoy and Gianmassimo Tasinato. *Inflation and Primordial Black Holes*. 24th Jan. 2023. DOI: 10.48550/arXiv.2301.03600. arXiv: 2301.03600. URL: http://arxiv.org/abs/2301.03600 (visited on 07/02/2023). preprint.

[530] A. G. Polnarev and M. Y. Khlopov. "Dustlike Stages in the Early Universe and Constraints on the Primordial Black-Hole Spectrum". In: *Soviet Astronomy* 26 (1st Aug. 1982), pp. 391–395. ISSN: 0038-5301.

[531] Tomohiro Harada et al. "Primordial Black Hole Formation in the Matter-Dominated Phase of the Universe". In: *The Astrophysical Journal* 833.1 (7th Dec. 2016), p. 61. ISSN: 1538-4357. DOI: 10.3847/1538-4357/833/1/61. arXiv: 1609.01588.

[532] Tomohiro Harada, Chul-Moon Yoo, Kazunori Kohri and Ken-Ichi Nakao. "Spins of Primordial Black Holes Formed in the Matter-Dominated Phase of the Universe". In: *Physical Review D* 96.8 (17th Oct. 2017), p. 083517. ISSN: 2470-0010, 2470-0029. DOI: 10.1103/PhysRevD.96.083517. arXiv: 1707.03595.

[533] Tomohiro Harada, Chul-Moon Yoo, Kazunori Kohri and Ken-Ichi Nakao. "Erratum: Spins of Primordial Black Holes Formed in the Matter-Dominated Phase of the Universe [Phys. Rev. D 96, 083517 (2017)]". In: *Physical Review D* 99.6 (28th Mar. 2019), p. 069904. DOI: 10.1103/PhysRevD.99.069904.

[534] Rouzbeh Allahverdi et al. "The First Three Seconds: A Review of Possible Expansion Histories of the Early Universe". In: *The Open Journal of Astrophysics* 4.1 (29th Jan. 2021), 10.21105/astro.2006.16182. ISSN: 2565-6120. DOI: 10.21105/astro.2006.16182. arXiv: 2006.16182.

[535] Joseph Silk and Michael S. Turner. "Double Inflation". In: *Physical Review D* 35.2 (15th Jan. 1987), pp. 419–428. DOI: 10.1103/PhysRevD.35.419.

[536] Lisa Randall, Marin Soljacic and Alan Guth. "Supernatural Inflation: Inflation from Supersymmetry with No (Very) Small Parameters". In: *Nuclear Physics B* 472.1-2 (July 1996), pp. 377–405. ISSN: 05503213. DOI: 10.1016/0550-3213(96)00174-5. arXiv: hep-ph/9512439.

[537] Juan Garcia-Bellido, Andrei Linde and David Wands. "Density Perturbations and Black Hole Formation in Hybrid Inflation". In: *Physical Review D* 54.10 (15th Nov. 1996), pp. 6040–6058. ISSN: 0556-2821, 1089-4918. DOI: 10.1103/PhysRevD.54.6040. arXiv: astro-ph/9605094.

[538] Masahiro Kawasaki, Tsutomu Takayama, Masahide Yamaguchi and Jun'ichi Yokoyama. "Power Spectrum of the Density Perturbations From Smooth Hybrid New Inflation Model". In: *Physical Review D* 74.4 (21st Aug. 2006), p. 043525. ISSN: 1550-7998, 1550-2368. DOI: 10.1103/PhysRevD.74.043525. arXiv: hep-ph/0605271.

[539] Masahiro Kawasaki, Alexander Kusenko, Yuichiro Tada and Tsutomu T. Yanagida. "PBH Dark Matter in Supergravity Inflation Models". In: *Physical Review D* 94.8 (26th Oct. 2016), p. 083523. ISSN: 2470-0010, 2470-0029. DOI: 10.1103/PhysRevD.94.083523. arXiv: 1606.07631.

[540] Keisuke Inomata et al. "Inflationary Primordial Black Holes for the LIGO Gravitational Wave Events and Pulsar Timing Array Experiments". In: *Physical Review D* 95.12 (8th June 2017), p. 123510. ISSN: 2470-0010, 2470-0029. DOI: 10.1103/PhysRevD.95.123510. arXiv: 1611.06130.

[541] Keisuke Inomata, Masahiro Kawasaki, Kyohei Mukaida and Tsutomu T. Yanagida. "Double Inflation as a Single Origin of Primordial Black Holes for All Dark Matter and LIGO Observations". In: *Physical Review D* 97.4 (14th Feb. 2018), p. 043514. ISSN: 2470-0010, 2470-0029. DOI: 10.1103/PhysRevD.97.043514. arXiv: 1711.06129.

[542] S. W. Hawking. "Black Hole Explosions". In: *Nature* 248 (1974), pp. 30–31. DOI: 10.1038/248030a0.

[543] S. W. Hawking. "Particle Creation by Black Holes". In: *Communications in Mathematical Physics* 43.3 (1975), pp. 199–220. DOI: 10.1007/BF02345020.

[544] Don N. Page. "Particle Emission Rates from a Black Hole: Massless Particles from an Uncharged, Nonrotating Hole". In: *Physical Review D* 13.2 (1976), pp. 198–206. DOI: 10.1103/PhysRevD.13.198.

[545] Don N. Page. "Particle Emission Rates from a Black Hole. II. Massless Particles from a Rotating Hole". In: *Physical Review D* 14.12 (1976), pp. 3260–3273. DOI: 10.1103/PhysRevD.14.3260.

[546] G. W. Gibbons and S. W. Hawking. "Cosmological Event Horizons, Thermodynamics, and Particle Creation". In: *Physical Review D* 15.10 (1977), pp. 2738–2751. DOI: 10.1103/PhysRevD.15.2738.

[547] Don N. Page. "Hawking Radiation and Black Hole Thermodynamics". In: *New Journal of Physics* 7 (29th Sept. 2005), pp. 203–203. ISSN: 1367-2630. DOI: 10.1088/1367-2630/7/1/203. arXiv: hep-th/0409024.

[548] Saul A. Teukolsky. "Rotating Black Holes: Separable Wave Equations for Gravitational and Electromagnetic Perturbations". In: *Physical Review Letters* 29.16 (1972), pp. 1114–1118. DOI: 10.1103/PhysRevLett.29.1114.

[549] Saul A. Teukolsky. "Perturbations of a Rotating Black Hole. I. Fundamental Equations for Gravitational, Electromagnetic, and Neutrino-Field Perturbations". In: *The Astrophysical Journal* 185 (Oct. 1973), pp. 635–635. DOI: 10.1086/152444.

[550] William H. Press and Saul A. Teukolsky. "Perturbations of a Rotating Black Hole. II. Dynamical Stability of the Kerr Metric". In: *The Astrophysical Journal* 185.9 (Oct. 1973), pp. 649–649. DOI: 10.1086/152445.

[551] Alexandre Arbey and Jérémy Auffinger. "BlackHawk: A Public Code for Calculating the Hawking Evaporation Spectra of Any Black Hole Distribution". In: *European Physical Journal C* 79.8 (Aug. 2019), pp. 1–57. ISSN: 1434-6044, 1434-6052. DOI: 10.1140/epjc/s10052-019-7161-1. arXiv: 1905.04268.

[552] Alexandre Arbey et al. "Hawking Radiation by Spherically-Symmetric Static Black Holes for All Spins: I – Teukolsky Equations and Potentials". In: *Physical Review D* 103.10 (7th May 2021), p. 104010. ISSN: 2470-0010, 2470-0029. DOI: 10.1103/PhysRevD.103.104010. arXiv: 2101.02951.

[553] Alexandre Arbey et al. "Hawking Radiation by Spherically-Symmetric Static Black Holes for All Spins: II – Numerical Emission Rates, Analytical Limits and New Constraints". In: *Physical Review D* 104.8 (4th Oct. 2021), p. 084016. ISSN: 2470-0010, 2470-0029. DOI: 10.1103/PhysRevD.104.084016. arXiv: 2107.03293.

[554] Martin Lemoine. "Moduli Constraints on Primordial Black Holes". In: *Physics Letters B* 481.2-4 (May 2000), pp. 333–338. ISSN: 03702693. DOI: 10.1016/S0370-2693(00)00469-X. arXiv: hep-ph/0001238.

[555] Sandeep Kumar Acharya and Rishi Khatri. "CMB and BBN Constraints on Evaporating Primordial Black Holes Revisited". In: *Journal of Cosmology and Astroparticle Physics* 2020.06 (8th June 2020), pp. 018–018. ISSN: 1475-7516. DOI: 10.1088/1475-7516/2020/06/018. arXiv: 2002.00898.

[556] Jens Chluba, Andrea Ravenni and Sandeep Kumar Acharya. "Thermalization of Large Energy Release in the Early Universe". In: *Monthly Notices of the Royal Astronomical Society* 498.1 (11th Oct. 2020), pp. 959–980. ISSN: 0035-8711, 1365-2966. DOI: 10.1093/mnras/staa2131. arXiv: 2005.11325.

[557] Matteo Lucca et al. "The Synergy between CMB Spectral Distortions and Anisotropies". In: *Journal of Cosmology and Astroparticle Physics* 2020.02 (Feb. 2020), pp. 026–026. ISSN: 1475-7516. DOI: 10.1088/1475-7516/2020/02/026. arXiv: 1910.04619.

[558] Patrick Stöcker, Michael Krämer, Julien Lesgourgues and Vivian Poulin. "Exotic Energy Injection with ExoCLASS: Application to the Higgs Portal Model and Evaporating Black Holes". In: *Journal of Cosmology and Astroparticle Physics* 2018.03 (Mar. 2018), pp. 018–018. ISSN: 1475-7516. DOI: 10.1088/1475-7516/2018/03/018. arXiv: 1801.01871.

[559] Harry Poulter et al. *CMB Constraints on Ultra-Light Primordial Black Holes with Extended Mass Distributions*. 15th July 2019. DOI: 10.48550/arXiv.1907.06485. arXiv: 1907.06485. URL: http://arxiv.org/abs/1907.06485 (visited on 07/02/2023). preprint.

[560] Basudeb Dasgupta, Ranjan Laha and Anupam Ray. "Neutrino and Positron Constraints on Spinning Primordial Black Hole Dark Matter". In: *Physical Review Letters* 125.10 (31st Aug. 2020), p. 101101. ISSN: 0031-9007, 1079-7114. DOI: 10.1103/PhysRevLett.125.101101. arXiv: 1912.01014.

[561] Vivian Poulin, Julien Lesgourgues and Pasquale D. Serpico. "Cosmological Constraints on Exotic Injection of Electromagnetic Energy". In: *Journal of Cosmology and Astroparticle Physics* 2017.03 (21st Mar. 2017), pp. 043–043. ISSN: 1475-7516. DOI: 10.1088/1475-7516/2017/03/043. arXiv: 1610.10051.

[562] B. Paczynski. "Gravitational Microlensing by the Galactic Halo". In: *The Astrophysical Journal* 304 (1st May 1986), p. 1. ISSN: 0004-637X. DOI: 10.1086/164140.

[563] Kim Griest. "Galactic Microlensing as a Method of Detecting Massive Compact Halo Objects". In: *The Astrophysical Journal* 366 (1991), pp. 412–421. ISSN: 0004-637X. DOI: 10.1086/169575.

[564] Takashi Nakamura, Misao Sasaki, Takahiro Tanaka and Kip S. Thorne. "Gravitational Waves from Coalescing Black Hole MACHO Binaries". In: *The Astrophysical Journal* 487.2 (1st Oct. 1997), pp. L139–L142. ISSN: 0004637X. DOI: 10.1086/310886. arXiv: astro-ph/9708060.

[565] Kunihito Ioka, Takeshi Chiba, Takahiro Tanaka and Takashi Nakamura. "Black Hole Binary Formation in the Expanding Universe — Three Body Problem Approximation —". In: *Physical Review D* 58.6 (27th Aug. 1998), p. 063003. ISSN: 0556-2821, 1089-4918. DOI: 10.1103/PhysRevD.58.063003. arXiv: astro-ph/9807018.

[566] Céline Boehm et al. "Eliminating the LIGO Bounds on Primordial Black Hole Dark Matter". In: *Journal of Cosmology and Astroparticle Physics* 2021.03 (Mar. 2021), p. 078. ISSN: 1475-7516. DOI: 10.1088/1475-7516/2021/03/078. arXiv: 2008.10743.

[567] Zachary S. C. Picker. "Navigating the Asteroid Field: New Evaporation Constraints for Primordial Black Holes as Dark Matter". 3rd Mar. 2021. URL: http://arxiv.org/abs/2103.02815 (visited on 13/05/2021).

[568] Simeon Bird et al. "Did LIGO Detect Dark Matter?" In: *Physical Review Letters* 116.20 (19th May 2016), p. 201301. ISSN: 0031-9007, 1079-7114. DOI: 10.1103/PhysRevLett.116.201301. arXiv: 1603.00464.

[569] Bradley J. Kavanagh, Daniele Gaggero and Gianfranco Bertone. "Black Holes' Dark Dress: On the Merger Rate of a Subdominant Population of Primordial Black Holes". In: *Physical Review D* 98.2 (25th July 2018), p. 023536. ISSN: 2470-0010, 2470-0029. DOI: 10.1103/PhysRevD.98.023536. arXiv: 1805.09034.

[570] Sai Wang, Yi-Fan Wang, Qing-Guo Huang and Tjonnie G. F. Li. "Constraints on the Primordial Black Hole Abundance from the First Advanced LIGO Observation Run Using the Stochastic Gravitational-Wave Background". In: *Physical Review Letters* 120.19 (10th May 2018), p. 191102. ISSN: 0031-9007, 1079-7114. DOI: 10.1103/PhysRevLett.120.191102. arXiv: 1610.08725 [astro-ph, physics:gr-qc, physics:hep-th].

[571] Christopher J. Moore, Robert H. Cole and Christopher P. L. Berry. "Gravitational-Wave Sensitivity Curves". In: *Classical and Quantum Gravity* 32.1 (8th Jan. 2015), p. 015014. ISSN: 0264-9381, 1361-6382. DOI: 10.1088/0264-9381/32/1/015014. arXiv: 1408.0740.

[572] Bradley J. Kavanagh. *Bradkav/PBHbounds: Release Version*. Version 1.0. Zenodo, Nov. 2019. DOI: 10.5281/zenodo.3538999. URL: https://doi.org/10.5281/zenodo.3538999.

[573] Pasquale D. Serpico, Vivian Poulin, Derek Inman and Kazunori Kohri. "Cosmic Microwave Background Bounds on Primordial Black Holes Including Dark Matter Halo Accretion". In: *Physical Review Research* 2.2 (26th May 2020), p. 023204. ISSN: 2643-1564. DOI: 10.1103/PhysRevResearch.2.023204. arXiv: 2002.10771.

[574] Steven Clark et al. "Planck Constraint on Relic Primordial Black Holes". In: *Physical Review D* 95.8 (14th Apr. 2017), p. 083006. ISSN: 2470-0010, 2470-0029. DOI: 10.1103/PhysRevD.95.083006. arXiv: 1612.07738.

[575] Shikhar Mittal, Anupam Ray, Girish Kulkarni and Basudeb Dasgupta. "Constraining Primordial Black Holes as Dark Matter Using the Global 21-Cm Signal with X-ray Heating and Excess Radio Background". In: *Journal of Cosmology and Astroparticle Physics* 2022.03 (1st Mar. 2022), p. 030. ISSN: 1475-7516. DOI: 10.1088/1475-7516/2022/03/030. arXiv: 2107.02190.

[576] Akash Kumar Saha and Ranjan Laha. "Sensitivities on Non-Spinning and Spinning Primordial Black Hole Dark Matter with Global 21 Cm Troughs". In: *Physical Review D* 105.10 (24th May 2022), p. 103026. ISSN: 2470-0010, 2470-0029. DOI: 10.1103/PhysRevD.105.103026. arXiv: 2112.10794.

[577] Benjamin V. Lehmann, Stefano Profumo and Jackson Yant. "The Maximal-Density Mass Function for Primordial Black Hole Dark Matter". In: *Journal of Cosmology and Astroparticle Physics* 2018.04 (3rd Apr. 2018), pp. 007–007. ISSN: 1475-7516. DOI: 10.1088/1475-7516/2018/04/007. arXiv: 1801.00808.

[578] A. Barnacka, J.-F. Glicenstein and R. Moderski. "New Constraints on Primordial Black Holes Abundance from Femtolensing of Gamma-Ray Bursts". In: *Physical Review D* 86.4 (2nd Aug. 2012), p. 043001. ISSN: 1550-7998, 1550-2368. DOI: 10.1103/PhysRevD.86.043001. arXiv: 1204.2056.

[579] Andrey Katz, Joachim Kopp, Sergey Sibiryakov and Wei Xue. "Femtolensing by Dark Matter Revisited". In: *Journal of Cosmology and Astroparticle Physics* 2018.12 (5th Dec. 2018), pp. 005–005. ISSN: 1475-7516. DOI: 10.1088/1475-7516/2018/12/005. arXiv: 1807.11495.

[580] Sunghoon Jung and TaeHun Kim. "GRB Lensing Parallax: Closing Primordial Black Hole Dark Matter Mass Window". In: *Physical Review Research* 2.1 (3rd Feb. 2020), p. 013113. ISSN: 2643-1564. DOI: 10.1103/PhysRevResearch.2.013113. arXiv: 1908.00078.

[581] Sunghoon Jung and Chang Sub Shin. "Gravitational-Wave Fringes at LIGO: Detecting Compact Dark Matter by Gravitational Lensing". In: *Physical Review Letters* 122.4 (30th Jan. 2019), p. 041103. ISSN: 0031-9007, 1079-7114. DOI: 10.1103/PhysRevLett.122.041103. arXiv: 1712.01396.

[582] Djuna Croon, David McKeen, Nirmal Raj and Zihui Wang. "Subaru through a Different Lens: Microlensing by Extended Dark Matter Structures". In: *Physical Review D* 102.8 (19th Oct. 2020), p. 083021. ISSN: 2470-0010, 2470-0029. DOI: 10.1103/PhysRevD.102.083021. arXiv: 2007.12697.

[583] Ranjan Laha, Julian B. Muñoz and Tracy R. Slatyer. "INTEGRAL Constraints on Primordial Black Holes and Particle Dark Matter". In: *Physical Review D* 101.12 (15th June 2020), p. 123514. ISSN: 2470-0010, 2470-0029. DOI: 10.1103/PhysRevD.101.123514. arXiv: 2004.00627.

[584] Kim Griest, Agnieszka M. Cieplak and Matthew J. Lehner. "Experimental Limits on Primordial Black Hole Dark Matter from the First Two Years of Kepler Data". In: *The Astrophysical Journal* 786.2 (25th Apr. 2014), p. 158. ISSN: 0004-637X, 1538-4357. DOI: 10.1088/0004-637X/786/2/158. arXiv: 1307.5798.

[585] Bo-Qiang Lu and Yue-Liang Wu. "Constraining Primordial Black Holes in Dark Matter with Kinematics of Dwarf Galaxies". In: *Physical Review D* 99.12 (25th June 2019), p. 123023. ISSN: 2470-0010, 2470-0029. DOI: 10.1103/PhysRevD.99.123023. arXiv: 1906.10463.

[586] Zu-Cheng Chen and Qing-Guo Huang. "Distinguishing Primordial Black Holes from Astrophysical Black Holes by Einstein Telescope and Cosmic Explorer". In: *Journal of Cosmology and Astroparticle Physics* 2020.08 (24th Aug. 2020), pp. 039–039. ISSN: 1475-7516. DOI: 10.1088/1475-7516/2020/08/039. arXiv: 1904.02396.

[587] Riccardo Murgia, Giulio Scelfo, Matteo Viel and Alvise Raccanelli. "Lyman-α Forest Constraints on Primordial Black Holes as Dark Matter". In: *Physical Review Letters* 123.7 (16th Aug. 2019), p. 071102. ISSN: 0031-9007, 1079-7114. DOI: 10.1103/PhysRevLett.123.071102. arXiv: 1903.10509.

[588] T. Blaineau et al. "New Limits from Microlensing on Galactic Black Holes in the Mass Range $10M_{\odot}". In: *Astronomy & Astrophysics* 664 (Aug. 2022), A106. ISSN: 0004-6361, 1432-0746. DOI: 10.1051/0004-6361/202243430. arXiv: 2202.13819.

[589] Zu-Cheng Chen, Chen Yuan and Qing-Guo Huang. "Pulsar Timing Array Constraints on Primordial Black Holes with NANOGrav 11-Year Data Set". In: *Physical Review Letters* 124.25 (22nd June 2020), p. 251101. ISSN: 0031-9007, 1079-7114. DOI: 10.1103/PhysRevLett.124.251101. arXiv: 1910.12239.

[590] Fabio Capela, Maxim Pshirkov and Peter Tinyakov. "Constraints on Primordial Black Holes as Dark Matter Candidates from Capture by Neutron Stars". In: *Physical Review D* 87.12 (21st June 2013), p. 123524. ISSN: 1550-7998, 1550-2368. DOI: 10.1103/PhysRevD.87.123524. arXiv: 1301.4984.

[591] Hiroko Niikura et al. "Constraints on Earth-mass Primordial Black Holes from OGLE 5-Year Microlensing Events". In: *Physical Review D* 99.8 (4th Apr. 2019), p. 083503. ISSN: 2470-0010, 2470-0029. DOI: 10.1103/PhysRevD.99.083503. arXiv: 1901.07120.

[592] Yi-Fan Wang, Qing-Guo Huang, Tjonnie G. F. Li and Shihong Liao. "Searching for Primordial Black Holes with Stochastic Gravitational-Wave Background in the Space-Based Detector Frequency Band". In: *Physical Review D* 101.6 (16th Mar. 2020), p. 063019. ISSN: 2470-0010, 2470-0029. DOI: 10.1103/PhysRevD.101.063019. arXiv: 1910.07397.

[593] Jeff A. Dror, Harikrishnan Ramani, Tanner Trickle and Kathryn M. Zurek. "Pulsar Timing Probes of Primordial Black Holes and Subhalos". In: *Physical Review D* 100.2 (12th July 2019), p. 023003. ISSN: 2470-0010, 2470-0029. DOI: 10.1103/PhysRevD.100.023003. arXiv: 1901.04490.

[594] A. Esteban-Gutiérrez et al. "Abundance of LIGO/Virgo Black Holes from Microlensing Observations of Quasars with Reverberation Mapping Size Estimates". In: *The Astrophysical Journal* 929.2 (1st Apr. 2022), p. 123. ISSN: 0004-637X, 1538-4357. DOI: 10.3847/1538-4357/ac57c5. arXiv: 2203.04777.

[595] Olga Mena, Sergio Palomares-Ruiz, Pablo Villanueva-Domingo and Samuel J. Witte. "Constraining the Primordial Black Hole Abundance with 21cm Cosmology". In: *Physical Review D* 100.4 (29th Aug. 2019), p. 043540. ISSN: 2470-0010, 2470-0029. DOI: 10.1103/PhysRevD.100.043540. arXiv: 1906.07735.

[596] Peter W. Graham, Surjeet Rajendran and Jaime Varela. "Dark Matter Triggers of Supernovae". In: *Physical Review D* 92.6 (9th Sept. 2015), p. 063007. ISSN: 1550-7998, 1550-2368. DOI: 10.1103/PhysRevD.92.063007. arXiv: 1505.04444.

[597] Ranjan Laha. "Primordial Black Holes as a Dark Matter Candidate Are Severely Constrained by the Galactic Center 511 keV γ -Ray Line". In: *Physical Review Letters* 123.25 (16th Dec. 2019), p. 251101. ISSN: 0031-9007, 1079-7114. DOI: 10.1103/PhysRevLett.123.251101. arXiv: 1906.09994.

[598] Mathieu Boudaud and Marco Cirelli. "Voyager 1 $e\pm$ Further Constrain Primordial Black Holes as Dark Matter". In: *Physical Review Letters* 122.4 (30th Jan. 2019), p. 041104. ISSN: 0031-9007, 1079-7114. DOI: 10.1103/PhysRevLett.122.041104. arXiv: 1807.03075.

[599] Adam Coogan, Logan Morrison and Stefano Profumo. "Direct Detection of Hawking Radiation from Asteroid-Mass Primordial Black Holes". In: *Physical Review Letters* 126.17 (28th Apr. 2021), p. 171101. ISSN: 0031-9007, 1079-7114. DOI: 10.1103/PhysRevLett.126.171101. arXiv: 2010.04797.

[600] Ville Vaskonen and Hardi Veermäe. "Lower Bound on the Primordial Black Hole Merger Rate". In: *Physical Review D* 101.4 (19th Feb. 2020), p. 043015. ISSN: 2470-0010, 2470-0029. DOI: 10.1103/PhysRevD.101.043015. arXiv: 1908.09752.

[601] Kai Liao, S.-B. Zhang, Zhengxiang Li and He Gao. "Constraints on Compact Dark Matter with Fast Radio Burst Observations". In: *The Astrophysical Journal Letters* 896.1 (1st June 2020), p. L11. ISSN: 2041-8205, 2041-8213. DOI: 10.3847/2041-8213/ab963e. arXiv: 2003.13349.

[602] Miguel Zumalacarregui and Uros Seljak. "Limits on Stellar-Mass Compact Objects as Dark Matter from Gravitational Lensing of Type Ia Supernovae". In: *Physical Review Letters* 121.14 (1st Oct. 2018), p. 141101. ISSN: 0031-9007, 1079-7114. DOI: 10.1103/PhysRevLett.121.141101. arXiv: 1712.02240.

[603] Masamune Oguri et al. "Understanding Caustic Crossings in Giant Arcs: Characteristic Scales, Event Rates, and Constraints on Compact Dark Matter". In: *Physical Review D* 97.2 (19th Jan. 2018), p. 023518. ISSN: 2470-0010, 2470-0029. DOI: 10.1103/PhysRevD.97.023518. arXiv: 1710.00148.

[604] Julien Manshanden et al. "Multi-Wavelength Astronomical Searches for Primordial Black Holes". In: *Journal of Cosmology and Astroparticle Physics* 2019.06 (11th June 2019), p. 026. ISSN: 1475-7516. DOI: 10.1088/1475-7516/2019/06/026. arXiv: 1812.07967.

[605] Philip Lu et al. "Constraining Primordial Black Holes with Dwarf Galaxy Heating". In: *The Astrophysical Journal Letters* 908.2 (July 2020), p. L23. ISSN: 2041-8205, 2041-8213. DOI: 10.3847/2041-8213/abdcb6. arXiv: 2007.02213.

[606] Andi Hektor et al. "Constraining Primordial Black Holes with the EDGES 21-Cm Absorption Signal". In: *Physical Review D* 98.2 (3rd July 2018), p. 023503. ISSN: 2470-0010, 2470-0029. DOI: 10.1103/PhysRevD.98.023503. arXiv: 1803.09697.

[607] The LIGO Scientific Collaboration et al. "Search for Sub-Solar Mass Ultracompact Binaries in Advanced LIGO's Second Observing Run". In: *Physical Review Letters* 123.16 (18th Oct. 2019), p. 161102. ISSN: 0031-9007, 1079-7114. DOI: 10.1103/PhysRevLett.123.161102. arXiv: 1904.08976 [astro-ph, physics:gr-qc].

[608] Miguel A. Monroy-Rodríguez and Christine Allen. "The End of the MACHO Era- Revisited: New Limits on MACHO Masses from Halo Wide Binaries". In: *The Astrophysical Journal* 790.2 (17th July 2014), p. 159. ISSN: 0004-637X, 1538-4357. DOI: 10.1088/0004-637X/790/2/159. arXiv: 1406.5169.

[609] Timothy D. Brandt. "Constraints on MACHO Dark Matter from Compact Stellar Systems in Ultra-Faint Dwarf Galaxies". In: *The Astrophysical Journal* 824.2 (21st June 2016), p. L31. ISSN: 2041-8213. DOI: 10.3847/2041-8205/824/2/L31. arXiv: 1605.03665.

[610] C. Alcock et al. "MACHO Project Limits on Black Hole Dark Matter in the 1-30 M_{solar} Range". In: *The Astrophysical Journal* 550.2 (1st Apr. 2001), pp. L169–L172. ISSN: 0004637X. DOI: 10.1086/319636. arXiv: astro-ph/0011506.

[611] Hyungjin Kim. "A Constraint on Light Primordial Black Holes from the Interstellar Medium Temperature". In: *Monthly Notices of the Royal Astronomical Society* 504.4 (July 2020), pp. 5475–5484. ISSN: 0035-8711, 1365-2966. DOI: 10.1093/mnras/stab1222. arXiv: 2007.07739.

[612] Steven Clark et al. "21cm Limits on Decaying Dark Matter and Primordial Black Holes". In: *Physical Review D* 98.4 (8th Aug. 2018), p. 043006. ISSN: 2470-0010, 2470-0029. DOI: 10.1103/PhysRevD.98.043006. arXiv: 1803.09390.

[613] B. J. Carr, Kazunori Kohri, Yuuiti Sendouda and Jun'ichi Yokoyama. "Constraints on Primordial Black Holes from the Galactic Gamma-Ray Background". In: *Physical Review D* 94.4 (12th Aug. 2016), p. 044029. ISSN: 2470-0010, 2470-0029. DOI: 10.1103/PhysRevD.94.044029. arXiv: 1604.05349.

[614] Bernard Carr et al. "Primordial Black Hole Constraints for Extended Mass Functions". In: *Physical Review D* 96.2 (14th July 2017), p. 023514. ISSN: 2470-0010, 2470-0029. DOI: 10.1103/PhysRevD.96.023514. arXiv: 1705.05567.

[615] Florian Kühnel and Katherine Freese. "Constraints on Primordial Black Holes with Extended Mass Functions". In: *Physical Review D* 95.8 (10th Apr. 2017), p. 083508. ISSN: 2470-0010, 2470-0029. DOI: 10.1103/PhysRevD.95.083508. arXiv: 1701.07223.

[616] Nicola Bellomo, José Luis Bernal, Alvise Raccanelli and Licia Verde. "Primordial Black Holes as Dark Matter: Converting Constraints from Monochromatic to Extended Mass Distributions". In: *Journal of Cosmology and Astroparticle Physics* 2018.01 (8th Jan. 2018), pp. 004–004. ISSN: 1475-7516. DOI: 10.1088/1475-7516/2018/01/004. arXiv: 1709.07467.

[617] Josh Calcino, Juan Garcia-Bellido and Tamara M. Davis. "Updating the MACHO Fraction of the Milky Way Dark Halo with Improved Mass Models". In: *Monthly Notices of the Royal Astronomical Society* 479.3 (2018), pp. 2889–2905. ISSN: 0035-8711, 1365-2966. DOI: 10.1093/mnras/sty1368. arXiv: 1803.09205.

[618] Alexandre Arbey, Jérémy Auffinger and Joseph Silk. "Constraining Primordial Black Hole Masses with the Isotropic Gamma Ray Background". In: *Physical Review D* 101.2 (22nd Jan. 2020), p. 023010. ISSN: 2470-0010, 2470-0029. DOI: 10.1103/PhysRevD.101.023010. arXiv: 1906.04750.

[619] Anne M. Green. "Microlensing and Dynamical Constraints on Primordial Black Hole Dark Matter with an Extended Mass Function". In: *Physical Review D* 94.6 (28th Sept. 2016), p. 063530. ISSN: 2470-0010, 2470-0029. DOI: 10.1103/PhysRevD.94.063530. arXiv: 1609.01143.

[620] Kristjan Kannike, Luca Marzola, Martti Raidal and Hardi Veermäe. "Single Field Double Inflation and Primordial Black Holes". In: *Journal of Cosmology and Astroparticle Physics* 2017.09 (12th Sept. 2017), pp. 020–020. ISSN: 1475-7516. DOI: 10.1088/1475-7516/2017/09/020. arXiv: 1705.06225.

[621] Andrew D. Gow, Christian T. Byrnes and Alex Hall. "Accurate Model for the Primordial Black Hole Mass Distribution from a Peak in the Power Spectrum". In: *Physical Review D* 105.2 (5th Jan. 2022), p. 023503. ISSN: 2470-0010, 2470-0029. DOI: 10.1103/PhysRevD.105.023503. arXiv: 2009.03204.

[622] Wayne Hu. "Concepts in CMB Anisotropy Formation". In: *The Universe at High-z, Large-Scale Structure and the Cosmic Microwave Background*. The Universe at High-z, Large-Scale Structure and the Cosmic Microwave Background. Ed. by Enrique Martínez-González and Jose Luis Sanz. Lecture Notes in Physics. Berlin, Heidelberg: Springer, 1996, pp. 207–239. ISBN: 978-3-540-68386-5. DOI: 10.1007/BFb0102588. arXiv: astro-ph/951113. URL: https://arxiv.org/abs/astro-ph/9511130v1.

[623] Steen Hannestad. "Neutrino Physics from Precision Cosmology". In: *Progress in Particle and Nuclear Physics* 65.2 (Oct. 2010), pp. 185–208. ISSN: 01466410. DOI: 10.1016/j.ppnp.2010.07.001. arXiv: 1007.0658.

[624] Eleonora Di Valentino, Stefano Gariazzo and Olga Mena. "On the Most Constraining Cosmological Neutrino Mass Bounds". In: *Physical Review D* 104.8 (1st Oct. 2021), p. 083504. ISSN: 2470-0010, 2470-0029. DOI: 10.1103/PhysRevD.104.083504. arXiv: 2106.15267.

[625] Yusuke Koshio, Gabriel D. Orebi Gann, Erin O'Sullivan and Irene Tamborra. *Snowmass 2021 Topical Group Report: Neutrinos from Natural Sources*. 16th Sept. 2022. DOI: 10.48550/arXiv.2209.04298. arXiv: 2209.04298. URL: http://arxiv.org/abs/2209.04298 (visited on 04/10/2022). preprint.

[626] Isabelle Tanseri et al. "Updated Neutrino Mass Constraints from Galaxy Clustering and CMB Lensing-Galaxy Cross-Correlation Measurements". In: *Journal of High Energy Astrophysics* 36 (Nov. 2022), pp. 1–26. ISSN: 22144048. DOI: 10.1016/j.jheap.2022.07.002. arXiv: 2207.01913 [astro-ph, physics:hep-ph].

[627] Eleonora di Valentino, Stefano Gariazzo and Olga Mena. "Model Marginalized Constraints on Neutrino Properties from Cosmology". In: *Physical Review D* 106.4 (31st Aug. 2022), p. 043540. ISSN: 2470-0010, 2470-0029. DOI: 10.1103/PhysRevD.106.043540. arXiv: 2207.05167.

[628] Hernán E. Noriega, Alejandro Aviles, Sebastien Fromenteau and Mariana Vargas-Magaña. "Fast Computation of Non-Linear Power Spectrum in Cosmologies with Massive Neutrinos". In: *Journal of Cosmology and Astroparticle Physics* 2022.11 (1st Nov. 2022), p. 038. ISSN: 1475-7516. DOI: 10.48550/arXiv.2208.02791. arXiv: 2208.02791.

[629] Steen Hannestad and Jes Madsen. "Neutrino Decoupling in the Early Universe". In: *Physical Review D* 52.4 (15th Aug. 1995), pp. 1764–1769. ISSN: 0556-2821. DOI: 10.1103/PhysRevD.52.1764. arXiv: astro-ph/9506015.

[630] Gary Steigman. "Neutrinos And Big Bang Nucleosynthesis". In: *Advances in High Energy Physics* 2012 (2012), pp. 1–24. ISSN: 1687-7357, 1687-7365. DOI: 10.1155/2012/268321. arXiv: 1208.0032.

[631] Julien Froustey and Cyril Pitrou. "Incomplete Neutrino Decoupling Effect on Big Bang Nucleosynthesis". In: *Physical Review D* 101.4 (18th Feb. 2020), p. 043524. ISSN: 2470-0010, 2470-0029. DOI: 10.1103/PhysRevD.101.043524. arXiv: 1912.09378.

[632] Wayne Hu. "Structure Formation with Generalized Dark Matter". In: *The Astrophysical Journal* 506.2 (20th Oct. 1998), pp. 485–494. ISSN: 0004-637X, 1538-4357. DOI: 10.1086/306274. arXiv: astro-ph/9801234.

[633] Michael Doran. "Speeding Up Cosmological Boltzmann Codes". In: *Journal of Cosmology and Astroparticle Physics* 2005.06 (28th June 2005), pp. 011–011. ISSN: 1475-7516. DOI: 10.1088/1475-7516/2005/06/011. arXiv: astro-ph/0503277.

[634] J. R. Bond and A. S. Szalay. "The Collisionless Damping of Density Fluctuations in an Expanding Universe". In: *The Astrophysical Journal* 274 (1st Nov. 1983), pp. 443–468. ISSN: 0004-637X. DOI: 10.1086/161460.

[635] Julien Lesgourgues and Thomas Tram. "The Cosmic Linear Anisotropy Solving System (CLASS) IV: Efficient Implementation of Non-Cold Relics". In: *Journal of Cosmology and Astroparticle Physics* 2011.09 (27th Sept. 2011), pp. 032–032. ISSN: 1475-7516. DOI: 10.1088/1475-7516/2011/09/032. arXiv: 1104.2935 [astro-ph].

[636] Cullan Howlett, Antony Lewis, Alex Hall and Anthony Challinor. "CMB Power Spectrum Parameter Degeneracies in the Era of Precision Cosmology". In: *Journal of Cosmology and Astroparticle Physics* 2012.04 (20th Apr. 2012), pp. 027–027. ISSN: 1475-7516. DOI: 10.1088/1475-7516/2012/04/027. arXiv: 1201.3654 [astro-ph].

[637] Antony Lewis and Anthony Challinor. "Evolution of Cosmological Dark Matter Perturbations". In: *Physical Review D* 66.2 (31st July 2002), p. 023531. ISSN: 0556-2821, 1089-4918. DOI: 10.1103/PhysRevD.66.023531. arXiv: astro-ph/0203507.

[638] Masatoshi Shoji and Eiichiro Komatsu. "Massive Neutrinos in Cosmology: Analytic Solutions and Fluid Approximation". In: *Physical Review D* 81.12 (June 2010), pp. 123516–123516. DOI: 10.1103/PhysRevD.81.123516. arXiv: 1003.0942.

[639] Masatoshi Shoji and Eiichiro Komatsu. "Erratum: Massive Neutrinos in Cosmology: Analytic Solutions and Fluid Approximation [Phys. Rev. D 81, 123516 (2010)]". In: *Physical Review D* 82.8 (Oct. 2010), p. 089901. DOI: 10.1103/PhysRevD.82.089901.

[640] P. J. E. Peebles. *Principles of Physical Cosmology*. Princeton: Princeton University Press, 1st Jan. 1993. ISBN: 978-0-691-20672-1. DOI: 10.1515/9780691206721.

[641] Christopher M. Hirata. "Two-Photon Transitions in Primordial Hydrogen Recombination". In: *Physical Review D* 78.2 (1st July 2008), p. 023001. ISSN: 1550-7998, 1550-2368. DOI: 10.1103/PhysRevD.78.023001. arXiv: 0803.0808.

[642] Eric R. Switzer and Christopher M. Hirata. "Primordial Helium Recombination I: Feedback, Line Transfer, and Continuum Opacity". In: *Physical Review D* 77.8 (30th Apr. 2008), p. 083006. ISSN: 1550-7998, 1550-2368. DOI: 10.1103/PhysRevD.77.083006. arXiv: astro-ph/0702143.

[643] Yacine Ali-Haïmoud and Christopher M. Hirata. "Ultrafast Effective Multi-Level Atom Method for Primordial Hydrogen Recombination". In: *Physical Review D* 82.6 (17th Sept. 2010), p. 063521. ISSN: 1550-7998, 1550-2368. DOI: 10.1103/PhysRevD.82.063521. arXiv: 1006.1355.

[644] J. A. Rubino-Martin, J. Chluba, W. A. Fendt and B. D. Wandelt. "Estimating the Impact of Recombination Uncertainties on the Cosmological Parameter Constraints from Cosmic Microwave Background Experiments". In: *Monthly Notices of the Royal Astronomical Society* 403.1 (21st Mar. 2010), pp. 439–452. ISSN: 00358711, 13652966. DOI: 10.1111/j.1365-2966.2009.16136.x. arXiv: 0910.4383.

[645] J. Chluba and R. M. Thomas. "Towards a Complete Treatment of the Cosmological Recombination Problem". In: *Monthly Notices of the Royal Astronomical Society* (Dec. 2010), no–no. ISSN: 00358711. DOI: 10.1111/j.1365-2966.2010.17940.x. arXiv: 1010.3631.

[646] Douglas Scott and Adam Moss. "Matter Temperature during Cosmological Recombination". In: *Monthly Notices of the Royal Astronomical Society* 397.1 (21st July 2009), pp. 445–446. ISSN: 00358711, 13652966. DOI: 10.1111/j.1365-2966.2009.14939.x. arXiv: 0902.3438.

[647] Wan Yan Wong, Adam Moss and Douglas Scott. "How Well Do We Understand Cosmological Recombination?" In: *Monthly Notices of the Royal Astronomical Society* 386.2 (May 2008), pp. 1023–1028. ISSN: 0035-8711, 1365-2966. DOI: 10.1111/j.1365-2966.2008.13092.x. arXiv: 0711.1357.

[648] P. J. E. Peebles and J. T. Yu. "Primeval Adiabatic Perturbation in an Expanding Universe". In: *Astrophys. J.* 162 (1970), pp. 815–836. DOI: 10.1086/150713.

[649] J. R. Bond and G. Efstathiou. "Cosmic Background Radiation Anisotropies in Universes Dominated by Nonbaryonic Dark Matter". In: *The Astrophysical Journal* 285 (1st Oct. 1984), pp. L45–L48. ISSN: 0004-637X. DOI: 10.1086/184362.

[650] J. R. Bond and G. Efstathiou. "The Statistics of Cosmic Background Radiation Fluctuations". In: *Monthly Notices of the Royal Astronomical Society* 226 (1st June 1987), pp. 655–687. ISSN: 0035-8711. DOI: 10.1093/mnras/226.3.655.

[651] Scott Dodelson and Jay M. Jubas. "Reionization and Its Imprint of the Cosmic Microwave Background". In: *The Astrophysical Journal* 439 (August Feb. 1995), p. 503. ISSN: 0004-637X, 1538-4357. DOI: 10.1086/175191. arXiv: astro-ph/9308019.

[652] Arthur Kosowsky. "Cosmic Microwave Background Polarization". In: *Annals of Physics* 246.1 (Feb. 1996), pp. 49–85. ISSN: 00034916. DOI: 10.1006/aphy.1996.0020. arXiv: astro-ph/9501045.

[653] Joseph Silk and Michael L. Wilson. "Residual Fluctuations in the Matter and Radiation Distribution After the Decoupling Epoch". In: *Physica Scripta* 21.5 (Jan. 1980), p. 708. ISSN: 1402-4896. DOI: 10.1088/0031-8949/21/5/022.

[654] M. L. Wilson and J. Silk. "On the Anisotropy of the Cosmological Background Matter and Radiation Distribution. I - The Radiation Anisotropy in a Spatially Flat Universe". In: *The Astrophysical Journal* 243 (1st Jan. 1981), pp. 14–25. ISSN: 0004-637X. DOI: 10.1086/158561.

[655] Antony Lewis, Anthony Challinor and Anthony Lasenby. "Efficient Computation of CMB Anisotropies in Closed FRW Models". In: *The Astrophysical Journal* 538.2 (Aug. 2000), pp. 473–476. ISSN: 0004-637X, 1538-4357. DOI: 10.1086/309179. arXiv: astro-ph/9911177.

[656] Francis-Yan Cyr-Racine and Kris Sigurdson. "Photons and Baryons before Atoms: Improving the Tight-Coupling Approximation". In: *Physical Review D* 83.10 (20th May 2011), p. 103521. ISSN: 1550-7998, 1550-2368. DOI: 10.1103/PhysRevD.83.103521. arXiv: 1012.0569.

[657] Cyril Pitrou. "The Tight-Coupling Approximation for Baryon Acoustic Oscillations". In: *Physics Letters B* 698.1 (Mar. 2011), pp. 1–5. ISSN: 03702693. DOI: 10.1016/j.physletb.2011.02.058. arXiv: 1012.0546.

[658] Julia Stadler, Céline Bœhm and Olga Mena. "Is It Mixed Dark Matter or Neutrino Masses?" In: *Journal of Cosmology and Astroparticle Physics* 2020.01 (17th Jan. 2020), pp. 039–039. ISSN: 1475-7516. DOI: 10.1088/1475-7516/2020/01/039. arXiv: 1807.10034.

[659] Niklas Becker et al. "Cosmological Constraints on Multi-Interacting Dark Matter". In: *Journal of Cosmology and Astroparticle Physics* 2021.02 (Oct. 2020), pp. 019–019. ISSN: 1475-7516. DOI: 10.1088/1475-7516/2021/02/019. arXiv: 2010.04074.

[660] Eleonora Di Valentino, Céline Bøehm, Eric Hivon and François R. Bouchet. "Reducing the H_0 and σ_8 Tensions with Dark Matter-neutrino Interactions". In: *Physical Review D* 97.4 (13th Feb. 2018), p. 043513. ISSN: 2470-0010, 2470-0029. DOI: 10.1103/PhysRevD.97.043513. arXiv: 1710.02559.

[661] Julia Stadler, Céline Boehm and Olga Mena. "Comprehensive Study of Neutrino-Dark Matter Mixed Damping". In: *Journal of Cosmology and Astroparticle Physics* 2019.08 (12th Aug. 2019), p. 014. ISSN: 1475-7516. DOI: 10.1088/1475-7516/2019/08/014. arXiv: 1903.00540.

[662] Julia Johanna Stadler. "How Dark Is Dark Matter? Robust Limits on Dark Matter - Radiation Interactions from Cosmological Observations". Doctoral. Durham University, 2019, p. 192. 192 pp. URL: http://etheses.dur.ac.uk/13334/.

[663] Maria Archidiacono et al. "Constraining Dark Matter – Dark Radiation Interactions with CMB, BAO, and Lyman-α". In: *Journal of Cosmology and Astroparticle Physics* 2019.10 (25th Oct. 2019), pp. 055–055. ISSN: 1475-7516. DOI: 10.1088/1475-7516/2019/10/055. arXiv: 1907.01496 [astro-ph].

[664] Francis-Yan Cyr-Racine et al. "ETHOS - An Effective Theory of Structure Formation: From Dark Particle Physics to the Matter Distribution of the Universe". In: *Physical Review D* 93.12 (28th June 2016), p. 123527. ISSN: 2470-0010, 2470-0029. DOI: 10.1103/PhysRevD.93.123527. arXiv: 1512.05344 [astro-ph, physics:hep-ph, physics:hep-th].

[665] Tracy R. Slatyer and Chih-Liang Wu. "Early-Universe Constraints on Dark Matter-Baryon Scattering and Their Implications for a Global 21cm Signal". In: *Physical Review D* 98.2 (13th July 2018), p. 023013. ISSN: 2470-0010, 2470-0029. DOI: 10.1103/PhysRevD.98.023013. arXiv: 1803.09734 [astro-ph, physics:hep-ph].

[666] Kimberly K. Boddy et al. "A Critical Assessment of CMB Limits on Dark Matter-Baryon Scattering: New Treatment of the Relative Bulk Velocity". In: *Physical Review D* 98.12 (10th Dec. 2018), p. 123506. ISSN: 2470-0010, 2470-0029. DOI: 10.1103/PhysRevD.98.123506. arXiv: 1808.00001 [astro-ph, physics:hep-ph].

[667] Kimberly K. Boddy and Vera Gluscevic. "First Cosmological Constraint on the Effective Theory of Dark Matter-Proton Interactions". In: *Physical Review D* 98.8 (8th Oct. 2018), p. 083510. ISSN: 2470-0010, 2470-0029. DOI: 10.1103/PhysRevD.98.083510. arXiv: 1801.08609 [astro-ph, physics:hep-ph].

[668] Weishuang Linda Xu, Cora Dvorkin and Andrew Chael. "Probing Sub-GeV Dark Matter-Baryon Scattering with Cosmological Observables". In: *Phys. Rev. D* 97.10 (29th May 2018), p. 103530. ISSN: 2470-0010, 2470-0029. DOI: 10.1103/PhysRevD.97.103530. arXiv: 1802.06788 [astro-ph, physics:hep-ph].

[669] Ely D Kovetz et al. "Tighter Limits on Dark Matter Explanations of the Anomalous EDGES 21cm Signal". In: *Physical Review D* 98.10 (28th Nov. 2018), p. 103529. ISSN: 2470-0010, 2470-0029. DOI: 10.1103/PhysRevD.98.103529. arXiv: 1807.11482 [astro-ph, physics:hep-ph, physics:hep-th].

[670] Julian B. Muñoz, Cora Dvorkin and Abraham Loeb. "21-Cm Fluctuations from Charged Dark Matter". In: *Physical Review Letters* 121.12 (21st Sept. 2018), p. 121301. ISSN: 0031-9007, 1079-7114. DOI: 10.1103/PhysRevLett.121.121301. arXiv: 1804.01092 [astro-ph, physics:hep-ph].

[671] Trey Driskell et al. "Structure Formation and the Global 21-Cm Signal in the Presence of Coulomb-like Dark Matter-Baryon Interactions". In: *Physical Review D* 106.10 (28th Nov. 2022), p. 103525. ISSN: 2470-0010, 2470-0029. DOI: 10.1103/PhysRevD.106.103525. arXiv: 2209.04499.

[672] N. Kaiser. "On the Spatial Correlations of Abell Clusters." In: *The Astrophysical Journal* 284 (1st Sept. 1984), pp. L9–L12. ISSN: 0004-637X. DOI: 10.1086/184341.

[673] J. M. Bardeen, J. R. Bond, N. Kaiser and A. S. Szalay. "The Statistics of Peaks of Gaussian Random Fields". In: *The Astrophysical Journal* 304 (1st May 1986), p. 15. ISSN: 0004-637X. DOI: 10.1086/164143.

[674] J. A. Peacock and S. J. Dodds. "Reconstructing the Linear Power Spectrum of Cosmological Mass Fluctuations". In: *Monthly Notices of the Royal Astronomical Society* 267.4 (15th Apr. 1994), pp. 1020–1034. ISSN: 0035-8711, 1365-2966. DOI: 10.1093/mnras/267.4.1020. arXiv: astro-ph/9311057.

[675] F. Bernardeau, S. Colombi, E. Gaztanaga and R. Scoccimarro. "Large-Scale Structure of the Universe and Cosmological Perturbation Theory". In: *Physics Reports* 367.1-3 (Sept. 2002), pp. 1–248. ISSN: 03701573. DOI: 10.1016/S0370-1573(02)00135-7. arXiv: astro-ph/0112551.

[676] Vincent Desjacques, Donghui Jeong and Fabian Schmidt. "Large-Scale Galaxy Bias". In: *Physics Reports* 733 (Feb. 2018), pp. 1–193. ISSN: 03701573. DOI: 10.1016/j.physrep.2017.12.002. arXiv: 1611.09787.

[677] H. J. Mo and S. D. M. White. "An Analytic Model for the Spatial Clustering of Dark Matter Haloes". In: *Monthly Notices of the Royal Astronomical Society* 282.2 (11th Sept. 1996), pp. 347–361. ISSN: 0035-8711, 1365-2966. DOI: 10.1093/mnras/282.2.347. arXiv: astro-ph/9512127.

[678] Neal Dalal, Martin White, J. Richard Bond and Alexander Shirokov. "Halo Assembly Bias in Hierarchical Structure Formation". In: *The Astrophysical Journal* 687.1 (Nov. 2008), pp. 12–21. ISSN: 0004-637X, 1538-4357. DOI: 10.1086/591512. arXiv: 0803.3453.

[679] Patrick McDonald and Arabindo Roy. "Clustering of Dark Matter Tracers: Generalizing Bias for the Coming Era of Precision LSS". In: *Journal of Cosmology and Astroparticle Physics* 2009.08 (17th Aug. 2009), pp. 020–020. ISSN: 1475-7516. DOI: 10.1088/1475-7516/2009/08/020. arXiv: 0902.0991.

[680] Valentin Assassi, Daniel Baumann, Daniel Green and Matias Zaldarriaga. "Renormalized Halo Bias". In: *Journal of Cosmology and Astroparticle Physics* 2014.08 (27th Aug. 2014), pp. 056–056. ISSN: 1475-7516. DOI: 10.1088/1475-7516/2014/08/056. arXiv: 1402.5916.

[681] Mehrdad Mirbabayi, Fabian Schmidt and Matias Zaldarriaga. "Biased Tracers and Time Evolution". In: *Journal of Cosmology and Astroparticle Physics* 2015.07 (21st July 2015), pp. 030–030. ISSN: 1475-7516. DOI: 10.1088/1475-7516/2015/07/030. arXiv: 1412.5169.

[682] Adi Nusser, Gustavo Yepes and Enzo Branchini. "Biasing Relation, Environmental Dependencies and Estimation of the Growth Rate from Star Forming Galaxies". In: *The Astrophysical Journal* 905.1 (11th Dec. 2020), p. 47. ISSN: 1538-4357. DOI: 10.3847/1538-4357/abc42f. arXiv: 2008.06541.

[683] Licia Verde et al. "The 2dF Galaxy Redshift Survey: The Bias of Galaxies and the Density of the Universe". In: *Monthly Notices of the Royal Astronomical Society* 335.2 (Sept. 2002), pp. 432–440. ISSN: 0035-8711, 1365-2966. DOI: 10.1046/j.1365-8711.2002.05620.x. arXiv: astro-ph/0112161.

[684] E. Gaztanaga, P. Norberg, C. M. Baugh and D. J. Croton. "Statistical Analysis of Galaxy Surveys-II. The 3-Point Galaxy Correlation Function Measured from the 2dFGRS". In: *Monthly Notices of the Royal Astronomical Society* 364.2 (Dec. 2005), pp. 620–634. ISSN: 0035-8711, 1365-2966. DOI: 10.1111/j.1365-2966.2005.09583.x. arXiv: astro-ph/0506249.

[685] J. Elvin-Poole et al. "Dark Energy Survey Year 1 Results: Galaxy Clustering for Combined Probes". In: *Physical Review D* 98.4 (27th Aug. 2018), p. 042006. ISSN: 2470-0010, 2470-0029. DOI: 10.1103/PhysRevD.98.042006. arXiv: 1708.01536.

[686] J. N. Fry. "The Evolution of Bias". In: *The Astrophysical Journal* 461.2 (20th Apr. 1996), p. L65. ISSN: 0004-637X. DOI: 10.1086/310006.

[687] Max Tegmark and P. J. E. Peebles. "The Time-Evolution of Bias". In: *The Astrophysical Journal* 500.2 (20th June 1998), pp. L79–L82. ISSN: 0004637X. DOI: 10.1086/311426. arXiv: astro-ph/9804067.

[688] Spyros Basilakos and Manolis Plionis. "Cosmological Evolution of Linear Bias". In: *The Astrophysical Journal* 550.2 (Apr. 2001), pp. 522–527. ISSN: 0004-637X, 1538-4357. DOI: 10.1086/319797. arXiv: astro-ph/0011265.

[689] Róbert Beck et al. "Hawaii Two-0: High-redshift Galaxy Clustering and Bias". In: *Monthly Notices of the Royal Astronomical Society* 493.2 (1st Apr. 2020), pp. 2318–2328. ISSN: 0035-8711, 1365-2966. DOI: 10.1093/mnras/staa432. arXiv: 1909.12854.

[690] J. Einasto, L. J. Liivamägi and M. Einasto. "The Time Evolution of Bias". In: *Monthly Notices of the Royal Astronomical Society* 518.2 (28th Nov. 2022), pp. 2164–2176. ISSN: 0035-8711, 1365-2966. DOI: 10.1093/mnras/stac3181. arXiv: 2209.06036.

[691] Alison L. Coil et al. "The DEEP2 Galaxy Redshift Survey: Clustering of Galaxies in Early Data". In: *The Astrophysical Journal* 609.2 (10th July 2004), pp. 525–538. ISSN: 0004-637X, 1538-4357. DOI: 10.1086/421337. arXiv: astro-ph/0305586.

[692] Alison L. Coil et al. "The DEEP2 Galaxy Redshift Survey: Color and Luminosity Dependence of Galaxy Clustering at Z~1". In: *The Astrophysical Journal* 672.1 (Jan. 2008), pp. 153–176. ISSN: 0004-637X, 1538-4357. DOI: 10.1086/523639. arXiv: 0708.0004.

[693] Patrick Simon and Stefan Hilbert. "CFHTLenS: Galaxy Bias as Function of Scale, Stellar Mass, and Colour. Conflicts with Predictions by Semi-Analytic Models". In: *Astronomy & Astrophysics* 646 (Feb. 2021), A71. ISSN: 0004-6361, 1432-0746. DOI: 10.1051/0004-6361/202038119. arXiv: 2012.12299.

[694] Nick Kaiser. "Clustering in Real Space and in Redshift Space". In: *Monthly Notices of the Royal Astronomical Society* 227.1 (1st July 1987), pp. 1–21. ISSN: 0035-8711. DOI: 10.1093/mnras/227.1.1.

[695] Will J. Percival et al. "Baryon Acoustic Oscillations in the Sloan Digital Sky Survey Data Release 7 Galaxy Sample". In: *Monthly Notices of the Royal Astronomical Society* 401.4 (1st Feb. 2010), pp. 2148–2168. ISSN: 00358711, 13652966. DOI: 10.1111/j.1365-2966.2009.15812.x. arXiv: 0907.1660.

[696] Shadab Alam et al. "The Clustering of Galaxies in the Completed SDSS-III Baryon Oscillation Spectroscopic Survey: Cosmological Analysis of the DR12 Galaxy Sample". In: *Monthly Notices of the Royal Astronomical Society* 470.3 (2017), pp. 2617–2652. ISSN: 0035-8711, 1365-2966. DOI: 10.1093/mnras/stx721. arXiv: 1607.03155.

[697] Ashley J. Ross et al. "The Clustering of Galaxies in the Completed SDSS-III Baryon Oscillation Spectroscopic Survey: Observational Systematics and Baryon Acoustic Oscillations in the Correlation Function". In: *Monthly Notices of the Royal Astronomical Society* 464.1 (1st Jan. 2017), pp. 1168–1191. ISSN: 0035-8711, 1365-2966. DOI: 10.1093/mnras/stw2372. arXiv: 1607.03145.

[698] Edward W. Kolb and Michael S. Turner. *The Early Universe*. Vol. 69. 1990. ISBN: 978-0-201-62674-2. DOI: 10.1201/9780429492860.

[699] Daniel J. Eisenstein and Wayne Hu. "Baryonic Features in the Matter Transfer Function". In: *The Astrophysical Journal* 496.2 (Apr. 1998), pp. 605–614. ISSN: 0004-637X, 1538-4357. DOI: 10.1086/305424. arXiv: astro-ph/9709112.

[700] Bruce A. Bassett and Renée Hlozek. *Baryon Acoustic Oscillations*. 27th Oct. 2009. DOI: 10.48550/arXiv.0910.5224. arXiv: 0910.5224. URL: http://arxiv.org/abs/0910.5224 (visited on 14/11/2022). preprint.

[701] Daniel J. Eisenstein, Wayne Hu and Max Tegmark. "Cosmic Complementarity: H_0 and Omega_m from Combining CMB Experiments and Redshift Surveys". In: *The Astrophysical Journal* 504.2 (10th Sept. 1998), pp. L57–L60. ISSN: 0004637X. DOI: 10.1086/311582. arXiv: astro-ph/9805239.

[702] D. J. Fixsen et al. "Cosmic Microwave Background Dipole Spectrum Measured by the COBE FIRAS Instrument". In: *The Astrophysical Journal* 420 (1st Jan. 1994), p. 445. ISSN: 0004-637X. DOI: 10.1086/173575.

[703] D. J. Fixsen et al. "The Cosmic Microwave Background Spectrum from the Full COBE/FIRAS Data Set". In: *The Astrophysical Journal* 473.2 (20th Dec. 1996), pp. 576–587. ISSN: 0004-637X, 1538-4357. DOI: 10.1086/178173. arXiv: astro-ph/9605054.

[704] D. J. Fixsen. "The Temperature of the Cosmic Microwave Background". In: *The Astrophysical Journal* 707.2 (20th Dec. 2009), pp. 916–920. ISSN: 0004-637X, 1538-4357. DOI: 10.1088/0004-637X/707/2/916. arXiv: 0911.1955.

[705] K. M. Gorski et al. "HEALPix – a Framework for High Resolution Discretization, and Fast Analysis of Data Distributed on the Sphere". In: *The Astrophysical Journal* 622.2 (Apr. 2005), pp. 759–771. ISSN: 0004-637X, 1538-4357. DOI: 10.1086/427976. arXiv: astro-ph/0409513.

[706] Andrea Zonca et al. "Healpy: Equal Area Pixelization and Spherical Harmonics Transforms for Data on the Sphere in Python". In: *Journal of Open Source Software* 4.35 (27th Mar. 2019), p. 1298. ISSN: 2475-9066. DOI: 10.21105/joss.01298.

[707] R. A. Sunyaev and Ya. B. Zeldovich. "Small-Scale Fluctuations of Relic Radiation". In: *Astrophysics and Space Science* 7 (1st Apr. 1970), pp. 3–19. ISSN: 0004-640X. DOI: 10.1007/BF00653471.

[708] R. A. Sunyaev and Ya. B. Zeldovich. "The Observations of Relic Radiation as a Test of the Nature of X-Ray Radiation from the Clusters of Galaxies". In: *Comments on Astrophysics and Space Physics* 4 (1st Nov. 1972), p. 173. ISSN: 0010-26790146-2970.

[709] R. A. Sunyaev and Ya. B. Zel'dovich. "Microwave Background Radiation as a Probe of the Contemporary Structure and History of the Universe". In: *Annual Review of Astronomy and Astrophysics* 18.1 (1980), pp. 537–560. DOI: 10.1146/annurev.aa.18.090180.002541.

[710] R. A. Sunyaev and Ya. B. Zeldovich. "The Velocity of Clusters of Galaxies Relative to the Microwave Background. The Possibility of Its Measurement". In: *Monthly Notices of the Royal Astronomical Society* 190.3 (1st Mar. 1980), pp. 413–420. ISSN: 0035-8711. DOI: 10.1093/mnras/190.3.413.

[711] Max Tegmark, Joseph Silk and Alain Blanchard. "On the Inevitability of Reionization: Implications for Cosmic Microwave Background Fluctuations". In: *The Astrophysical Journal* 420 (Jan. 1994), p. 484. ISSN: 0004-637X, 1538-4357. DOI: 10.1086/173579. arXiv: astro-ph/9307017.

[712] M. Birkinshaw. "The Sunyaev-Zel'dovich Effect". In: *Physics Reports* 310.2-3 (Mar. 1999), pp. 97–195. ISSN: 03701573. DOI: 10.1016/S0370-1573(98)00080-5. arXiv: astro-ph/9808050.

[713] J. Chluba and R. A. Sunyaev. "The Evolution of CMB Spectral Distortions in the Early Universe". In: *Monthly Notices of the Royal Astronomical Society* 419.2 (11th Jan. 2012), pp. 1294–1314. ISSN: 00358711. DOI: 10.1111/j.1365-2966.2011.19786.x. arXiv: 1109.6552.

[714] Hao Fu et al. "Unlocking the Synergy between CMB Spectral Distortions and Anisotropies". In: *Journal of Cosmology and Astroparticle Physics* 2021.12 (1st Dec. 2021), p. 050. ISSN: 1475-7516. DOI: 10.1088/1475-7516/2021/12/050. arXiv: 2006.12886.

[715] Uros Seljak and Matias Zaldarriaga. "A Line-of-Sight Integration Approach to Cosmic Microwave Background Anisotropies". In: *The Astrophysical Journal* 469 (Oct. 1996), pp. 437–437. ISSN: 0004-637X, 1538-4357. DOI: 10.1086/177793. arXiv: astro-ph/9603033.

[716] R. K. Sachs and A. M. Wolfe. "Perturbations of a Cosmological Model and Angular Variations of the Microwave Background". In: *The Astrophysical Journal* 147 (1st Jan. 1967), p. 73. ISSN: 0004-637X. DOI: 10.1086/148982.

[717] W. H. Press and E. T. Vishniac. "Tenacious Myths about Cosmological Perturbations Larger than the Horizon Size". In: *The Astrophysical Journal* 239 (1st July 1980), pp. 1–11. ISSN: 0004-637X. DOI: 10.1086/158083.

[718] Jeppe Dakin, Steen Hannestad and Thomas Tram. "The Cosmological Simulation Code $\scriptstyle{\rm CON{\rm CEPT\, 1.0$". In: *Monthly Notices of the Royal Astronomical Society* 513.1 (27th Apr. 2022), pp. 991–1014. ISSN: 0035-8711, 1365-2966. DOI: 10.1093/mnras/stac568. arXiv: 2112.01508 [astro-ph].

[719] S. J. Aarseth. "Dynamical Evolution of Clusters of Galaxies, I". In: *Monthly Notices of the Royal Astronomical Society* 126 (1st Jan. 1963), p. 223. ISSN: 0035-8711. DOI: 10.1093/mnras/126.3.223.

[720] Edmund Bertschinger. "Simulations of Structure Formation in the Universe". In: *Annual Review of Astronomy and Astrophysics* 36 (1998), pp. 599–654. ISSN: 0066-4146. DOI: 10.1146/annurev.astro.36.1.599.

[721] Erik Holmberg. "On the Clustering Tendencies among the Nebulae. II. a Study of Encounters Between Laboratory Models of Stellar Systems by a New Integration Procedure." In: *The Astrophysical Journal* 94 (1st Nov. 1941), p. 385. ISSN: 0004-637X. DOI: 10.1086/144344.

[722] William H. Press and Paul Schechter. "Formation of Galaxies and Clusters of Galaxies by Self-Similar Gravitational Condensation". In: *The Astrophysical Journal* 187 (1974), pp. 425–438. ISSN: 0004-637X. DOI: 10.1086/152650.

[723] S. von Hoerner. "Die Numerische Integration Des N-Körper-Problemes Für Sternhaufen. I". In: *Zeitschrift fur Astrophysik* 50 (1st Jan. 1960), pp. 184–214. ISSN: 0372-8331.

[724] S. von Hoerner. "Die Numerische Integration Des N-Körper-Problems Für Sternhaufen, II." In: *Zeitschrift fur Astrophysik* 57 (1st Jan. 1963), pp. 47–82. ISSN: 0372-8331.

[725] Tomoaki Ishiyama et al. "The Uchuu Simulations: Data Release 1 and Dark Matter Halo Concentrations". In: *Monthly Notices of the Royal Astronomical Society* 506.3 (3rd Aug. 2021), pp. 4210–4231. ISSN: 0035-8711, 1365-2966. DOI: 10.1093/mnras/stab1755. arXiv: 2007.14720 [astro-ph].

[726] Dylan Nelson et al. "The Illustris Simulation: Public Data Release". In: *Astronomy and Computing* 13 (Nov. 2015), pp. 12–37. ISSN: 22131337. DOI: 10.1016/j.ascom.2015.09.003. arXiv: 1504.00362 [astro-ph].

[727] Dylan Nelson et al. *The IllustrisTNG Simulations: Public Data Release*. 29th Jan. 2021. DOI: 10.48550/arXiv.1812.05609. arXiv: 1812.05609 [astro-ph]. URL: http://arxiv.org/abs/1812.05609 (visited on 09/03/2023). preprint.

[728] Ruediger Pakmor et al. *The MillenniumTNG Project: The Hydrodynamical Full Physics Simulation and a First Look at Its Galaxy Clusters*. 6th Dec. 2022. DOI: 10.48550/arXiv.2210.10060. arXiv: 2210.10060 [astro-ph]. URL: http://arxiv.org/abs/2210.10060 (visited on 25/04/2023). preprint.

[729] J. Adamek et al. *Euclid: Modelling Massive Neutrinos in Cosmology – a Code Comparison*. 22nd Nov. 2022. DOI: 10.48550/arXiv.2211.12457. arXiv: 2211.12457 [astro-ph]. URL: http://arxiv.org/abs/2211.12457 (visited on 09/03/2023). preprint.

[730] Julian Adamek, David Daverio, Ruth Durrer and Martin Kunz. "Gevolution: A Cosmological N-body Code Based on General Relativity". In: *Journal of Cosmology and Astroparticle Physics* 2016.07 (29th July 2016), pp. 053–053. ISSN: 1475-7516. DOI: 10.1088/1475-7516/2016/07/053. arXiv: 1604.06065 [astro-ph, physics:gr-qc, physics:physics].

[731] Joe Zhiyu Chen, Amol Upadhye and Yvonne Y. Y. Wong. "The Cosmic Neutrino Background as a Collection of Fluids in Large-Scale Structure Simulations". In: *Journal of Cosmology and Astroparticle Physics* 2021.03 (1st Mar. 2021), p. 065. ISSN: 1475-7516. DOI: 10.1088/1475-7516/2021/03/065. arXiv: 2011.12503 [astro-ph, physics:hep-ph].

[732] Joe Zhiyu Chen, Amol Upadhye and Yvonne Y. Y. Wong. "One Line to Run Them All: SuperEasy Massive Neutrino Linear Response in N-Body Simulations". In: *Journal of Cosmology and Astroparticle Physics* 2021.04 (1st Apr. 2021), p. 078. ISSN: 1475-7516. DOI: 10.1088/1475-7516/2021/04/078. arXiv: 2011.12504 [astro-ph, physics:hep-ph].

[733] Jeppe Dakin et al. "νcONCEPT: Cosmological Neutrino Simulations from the Non-Linear Boltzmann Hierarchy". In: *Journal of Cosmology and Astroparticle Physics* 2019.02 (26th Feb. 2019), pp. 052–052. ISSN: 1475-7516. DOI: 10.1088/1475-7516/2019/02/052. arXiv: 1712.03944 [astro-ph, physics:hep-ph].

[734] Philip F. Hopkins. "GIZMO: A New Class of Accurate, Mesh-Free Hydrodynamic Simulation Methods". In: *Monthly Notices of the Royal Astronomical Society* 450.1 (11th June 2015), pp. 53–110. ISSN: 0035-8711, 1365-2966. DOI: 10.1093/mnras/stv195. arXiv: 1409.7395 [astro-ph, physics:physics].

[735] Douglas Potter, Joachim Stadel and Romain Teyssier. "PKDGRAV3: Beyond Trillion Particle Cosmological Simulations for the next Era of Galaxy Surveys". In: *Computational Astrophysics and Cosmology* 4.1 (18th May 2017), p. 2. ISSN: 2197-7909. DOI: 10.1186/s40668-017-0021-1. arXiv: 1609.08621 [astro-ph].

[736] Eduardo Quintana-Miranda, Pierluigi Monaco and Luca Tornatore. *GrGadget: An N-body TreePM Relativistic Code for Cosmological Simulations*. 27th Jan. 2023. DOI: 10.48550/arXiv.2301.11854. arXiv: 2301.11854 [astro-ph]. URL: http://arxiv.org/abs/2301.11854 (visited on 09/03/2023). preprint.

[737] Matthieu Schaller et al. "SWIFT: SPH With Inter-dependent Fine-grained Tasking". In: *Astrophysics Source Code Library* (1st May 2018), ascl:1805.020.

[738] Matthieu Schaller, Pedro Gonnet, Aidan B. G. Chalk and Peter W. Draper. "SWIFT: Using Task-Based Parallelism, Fully Asynchronous Communication, and Graph Partition-Based Domain Decomposition for Strong Scaling on More than 100,000 Cores". In: *Proceedings of the Platform for Advanced Scientific Computing Conference*. 8th June 2016, pp. 1–10. DOI: 10.1145/2929908.2929916. arXiv: 1606.02738 [astro-ph]. URL: http://arxiv.org/abs/1606.02738 (visited on 09/03/2023).

[739] Aurel Schneider et al. "Matter Power Spectrum and the Challenge of Percent Accuracy". In: *Journal of Cosmology and Astroparticle Physics* 2016.04 (26th Apr. 2016), pp. 047–047. ISSN: 1475-7516. DOI: 10.1088/1475-7516/2016/04/047. arXiv: 1503.05920 [astro-ph].

[740] Volker Springel. "The Cosmological Simulation Code GADGET-2". In: *Monthly Notices of the Royal Astronomical Society* 364.4 (Dec. 2005), pp. 1105–1134. ISSN: 0035-8711, 1365-2966. DOI: 10.1111/j.1365-2966.2005.09655.x. arXiv: astro-ph/0505010.

[741] Volker Springel, Naoki Yoshida and Simon D. M. White. "GADGET: A Code for Collisionless and Gasdynamical Cosmological Simulations". In: *New Astronomy* 6.2 (Apr. 2001), pp. 79–117. ISSN: 13841076. DOI: 10.1016/S1384-1076(01)00042-2. arXiv: astro-ph/0003162.

[742] Volker Springel, Rüdiger Pakmor, Oliver Zier and Martin Reinecke. "Simulating Cosmic Structure Formation with the GADGET-4 Code". In: *Monthly Notices of the Royal Astronomical Society* 506.2 (22nd July 2021), pp. 2871–2949. ISSN: 0035-8711, 1365-2966. DOI: 10.1093/mnras/stab1855. arXiv: 2010.03567 [astro-ph].

[743] Joachim Gerhard Stadel. "Cosmological N-body Simulations and Their Analysis". 1st Jan. 2001, p. 3657. URL: https://ui.adsabs.harvard.edu/abs/2001PhDT.....21S (visited on 09/03/2023).

[744] Romain Teyssier. "Cosmological Hydrodynamics with Adaptive Mesh Refinement: A New High Resolution Code Called RAMSES". In: *Astronomy & Astrophysics* 385.1 (Apr. 2002), pp. 337–364. ISSN: 0004-6361, 1432-0746. DOI: 10.1051/0004-6361:20011817. arXiv: astro-ph/0111367.

[745] Rainer Weinberger, Volker Springel and Rüdiger Pakmor. "The Arepo Public Code Release". In: *The Astrophysical Journal Supplement Series* 248.2 (10th June 2020), p. 32. ISSN: 1538-4365. DOI: 10.3847/1538-4365/ab908c. arXiv: 1909.04667 [astro-ph, physics:physics].

[746] Volker Springel. "E Pur Si Muove: Galiliean-invariant Cosmological Hydrodynamical Simulations on a Moving Mesh". In: *Monthly Notices of the Royal Astronomical Society* 401.2 (11th Jan. 2010), pp. 791–851. ISSN: 00358711, 13652966. DOI: 10.1111/j.1365-2966.2009.15715.x. arXiv: 0901.4107 [astro-ph].

[747] P. P. Ewald. "Die Berechnung Optischer Und Elektrostatischer Gitterpotentiale". In: *Annalen der Physik* 369.3 (1921), pp. 253–287. ISSN: 1521-3889. DOI: 10.1002/andp.19213690304.

[748] Lars Hernquist, Francois R. Bouchet and Yasushi Suto. "Application of the Ewald Method to Cosmological N-Body Simulations". In: *The Astrophysical Journal Supplement Series* 75 (1st Feb. 1991), p. 231. ISSN: 0067-0049. DOI: 10.1086/191530.

[749] J. J. Monaghan and J. C. Lattanzio. "A Refined Particle Method for Astrophysical Problems". In: *Astronomy and Astrophysics* 149 (1st Aug. 1985), pp. 135–143. ISSN: 0004-6361.

[750] Walter Dehnen and Justin Read. "N-Body Simulations of Gravitational Dynamics". In: *The European Physical Journal Plus* 126.5 (May 2011), p. 55. ISSN: 2190-5444. DOI: 10.1140/epjp/i2011-11055-3. arXiv: 1105.1082 [astro-ph, physics:physics].

[751] A. G. Doroshkevich et al. "Two-Dimensional Simulation of the Gravitational System Dynamics and Formation of the Large-Scale Structure of the Universe". In: *Monthly Notices of the Royal Astronomical Society* 192.2 (1st Sept. 1980), pp. 321–337. ISSN: 0035-8711. DOI: 10.1093/mnras/192.2.321.

[752] Josh Barnes and Piet Hut. "A Hierarchical O(N Log N) Force-Calculation Algorithm". In: *Nature* 324.6096 (1st Dec. 1986), pp. 446–449. ISSN: 0028-0836, 1476-4687. DOI: 10.1038/324446a0.

[753] J. S. Bagla and Suryadeep Ray. "Performance Characteristics of TreePM Codes". In: *New Astronomy* 8.7 (Sept. 2003), pp. 665–677. ISSN: 13841076. DOI: 10.1016/S1384-1076(03)00056-3. arXiv: astro-ph/0212129.

[754] J. S. Bagla. "TreePM: A Code for Cosmological N-Body Simulations". In: *Journal of Astrophysics and Astronomy* 23.3-4 (Dec. 2002), pp. 185–196. ISSN: 0250-6335, 0973-7758. DOI: 10.1007/BF02702282. arXiv: astro-ph/9911025.

[755] Y. B. Zel'Dovich. "Gravitational Instability: An Approximate Theory for Large Density Perturbations". In: *Astronomy and Astrophysics* 5 (Mar. 1970), pp. 13–18. ISSN: 0004-6361.

[756] Cornelius Rampf and Oliver Hahn. "Shell-Crossing in a ΛCDM Universe". In: *Monthly Notices of the Royal Astronomical Society: Letters* 501.1 (5th Jan. 2021), pp. L71–L75. ISSN: 1745-3925, 1745-3933. DOI: 10.1093/mnrasl/slaa198. arXiv: 2010.12584 [astro-ph].

[757] Oliver Hahn and Tom Abel. "Multi-Scale Initial Conditions for Cosmological Simulations". In: *Monthly Notices of the Royal Astronomical Society* 415.3 (Mar. 2011), pp. 2101–2121. DOI: 10.1111/j.1365-2966.2011.18820.x. arXiv: 1103.6031.

[758] Adrian Jenkins and Stephen Booth. *Panphasia: A User Guide*. June 2013. DOI: 10.48550/arXiv.1306.5771. arXiv: 1306.5771. URL: http://arxiv.org/abs/1306.5771. preprint.

[759] Jerzy Neyman, Elizabeth L. Scott and C. D. Shane. "The Index of Clumpiness of the Distribution of Images of Galaxies." In: *The Astrophysical Journal Supplement Series* 1 (1st Dec. 1954), p. 269. ISSN: 0067-0049. DOI: 10.1086/190008.

[760] J. Neyman, E. L. Scott and C. D. Shane. "On the Spatial Distribution of Galaxies: A Specific Model." In: *The Astrophysical Journal* 117 (1st Jan. 1953), p. 92. ISSN: 0004-637X. DOI: 10.1086/145671.

[761] J. Neyman and E. L. Scott. "A Theory of the Spatial Distribution of Galaxies." In: *The Astrophysical Journal* 116 (1st July 1952), p. 144. ISSN: 0004-637X. DOI: 10.1086/145599.

[762] Asantha Cooray and Ravi Sheth. "Halo Models of Large Scale Structure". In: *Physics Reports* 372.1 (Dec. 2002), pp. 1–129. ISSN: 03701573. DOI: 10.1016/S0370-1573(02)00276-4. arXiv: astro-ph/0206508.

[763] Raul E. Angulo, Simon Foreman, Marcel Schmittfull and Leonardo Senatore. "The One-Loop Matter Bispectrum in the Effective Field Theory of Large Scale Structures". In: *Journal of Cosmology and Astroparticle Physics* 2015.10 (14th Oct. 2015), pp. 039–039. ISSN: 1475-7516. DOI: 10.1088/1475-7516/2015/10/039. arXiv: 1406.4143.

[764] Roger de Belsunce and Leonardo Senatore. "Tree-Level Bispectrum in the Effective Field Theory of Large-Scale Structure Extended to Massive Neutrinos". In: *Journal of Cosmology and Astroparticle Physics* 2019.02 (18th Feb. 2019), pp. 038–038. ISSN: 1475-7516. DOI: 10.1088/1475-7516/2019/02/038. arXiv: 1804.06849 [astro-ph].

[765] Jennifer E. Pollack, Robert E. Smith and Cristiano Porciani. "Modelling Large-Scale Halo Bias Using the Bispectrum". In: *Monthly Notices of the Royal Astronomical Society* 420.4 (11th Mar. 2012), pp. 3469–3489. ISSN: 00358711. DOI: 10.1111/j.1365-2966.2011.20279.x. arXiv: 1109.3458 [astro-ph].

[766] Rossana Ruggeri, Emanuele Castorina, Carmelita Carbone and Emiliano Sefusatti. "DEMNUni: Massive Neutrinos and the Bispectrum of Large Scale Structures". In: *Journal of Cosmology and Astroparticle Physics* 2018.03 (5th Mar. 2018), pp. 003–003. ISSN: 1475-7516. DOI: 10.1088/1475-7516/2018/03/003. arXiv: 1712.02334 [astro-ph].

[767] Roman Scoccimarro. "The Bispectrum: From Theory to Observations". In: *The Astrophysical Journal* 544.2 (Dec. 2000), pp. 597–615. ISSN: 0004-637X, 1538-4357. DOI: 10.1086/317248. arXiv: astro-ph/0004086.

[768] Roman Scoccimarro. "Fast Estimators for Redshift-Space Clustering". In: *Physical Review D* 92.8 (30th Oct. 2015), p. 083532. ISSN: 1550-7998, 1550-2368. DOI: 10.1103/PhysRevD.92.083532. arXiv: 1506.02729 [astro-ph].

[769] Emiliano Sefusatti, Martin Crocce, Roman Scoccimarro and Hugh Couchman. "Accurate Estimators of Correlation Functions in Fourier Space". In: *Monthly Notices of the Royal Astronomical Society* 460.4 (21st Aug. 2016), pp. 3624–3636. ISSN: 0035-8711, 1365-2966. DOI: 10.1093/mnras/stw1229. arXiv: 1512.07295 [astro-ph].

[770] Emiliano Sefusatti, Martin Crocce and Vincent Desjacques. "The Matter Bispectrum in N-body Simulations with Non-Gaussian Initial Conditions". In: *Monthly Notices of the Royal Astronomical Society* (May 2010). ISSN: 00358711, 13652966. DOI: 10.1111/j.1365-2966.2010.16723.x. arXiv: 1003.0007 [astro-ph].

[771] Thomas Tram et al. "The Intrinsic Matter Bispectrum in ΛCDM". In: *Journal of Cosmology and Astroparticle Physics* 2016.05 (25th May 2016), pp. 058–058. ISSN: 1475-7516. DOI: 10.1088/1475-7516/2016/05/058. arXiv: 1602.05933 [astro-ph, physics:gr-qc].

[772] Andrew J. Benson et al. "Dark Matter Halo Merger Histories beyond Cold Dark Matter – I. Methods and Application to Warm Dark Matter". In: *Monthly Notices of the Royal Astronomical Society* 428.2 (11th Jan. 2013), pp. 1774–1789. ISSN: 1365-2966, 0035-8711. DOI: 10.1093/mnras/sts159. arXiv: 1209.3018 [astro-ph].

[773] Steen Hannestad, Amol Upadhye and Yvonne Y. Y. Wong. "Spoon or Slide? The Non-Linear Matter Power Spectrum in the Presence of Massive Neutrinos". In: *Journal of Cosmology and Astroparticle Physics* 2020.11 (30th Nov. 2020), pp. 062–062. ISSN: 1475-7516. DOI: 10.1088/1475-7516/2020/11/062. arXiv: 2006.04995.

[774] J. R. Bond, S. Cole, G. Efstathiou and N. Kaiser. "Excursion Set Mass Functions for Hierarchical Gaussian Fluctuations". In: *The Astrophysical Journal* 379 (1st Oct. 1991), p. 440. ISSN: 0004-637X. DOI: 10.1086/170520.

[775] Cedric Lacey and Shaun Cole. "Merger Rates in Hierarchical Models of Galaxy Formation". In: *Monthly Notices of the Royal Astronomical Society* 262.3 (1st June 1993), pp. 627–649. ISSN: 0035-8711, 1365-2966. DOI: 10.1093/mnras/262.3.627.

[776] Ravi K. Sheth and Giuseppe Tormen. "Large Scale Bias and the Peak Background Split". In: *Monthly Notices of the Royal Astronomical Society* 308.1 (Sept. 1999), pp. 119–126. ISSN: 0035-8711, 1365-2966. DOI: 10.1046/j.1365-8711.1999.02692.x. arXiv: astro-ph/9901122.

[777] Suman Bhattacharya et al. "Mass Function Predictions Beyond LCDM". In: *The Astrophysical Journal* 732.2 (10th May 2011), p. 122. ISSN: 0004-637X, 1538-4357. DOI: 10.1088/0004-637X/732/2/122. arXiv: 1005.2239 [astro-ph].

[778] Rahul Biswas et al. *Effects of Massive Neutrinos and Dynamical Dark Energy on the Cluster Mass Function*. 30th Jan. 2019. DOI: 10.48550/arXiv.1901.10690. arXiv: 1901.10690 [astro-ph]. URL: http://arxiv.org/abs/1901.10690 (visited on 15/03/2023). preprint.

[779] Jacob Brandbyge, Steen Hannestad, Troels Haugboelle and Yvonne Y. Y. Wong. "Neutrinos in Non-linear Structure Formation - The Effect on Halo Properties". In: *Journal of Cosmology and Astroparticle Physics* 2010.09 (14th Sept. 2010), pp. 014–014. ISSN: 1475-7516. DOI: 10.1088/1475-7516/2010/09/014. arXiv: 1004.4105.

[780] Shaun Cole and Nick Kaiser. "Biased Clustering in the Cold Dark Matter Cosmogony." In: *Monthly Notices of the Royal Astronomical Society* 237 (1st Apr. 1989), pp. 1127–1146. ISSN: 0035-8711. DOI: 10.1093/mnras/237.4.1127.

[781] Ravi K. Sheth and Gerard Lemson. "Biasing and the Distribution of Dark Matter Haloes". In: *Monthly Notices of the Royal Astronomical Society* 304.4 (16th Apr. 1999), pp. 767–792. ISSN: 0035-8711, 1365-2966. DOI: 10.1046/j.1365-8711.1999.02378.x. arXiv: astro-ph/9808138.

[782] H. J. Mo, Y. P. Jing and S. D. M. White. "High-Order Correlations of Peaks and Halos: A Step toward Understanding Galaxy Biasing". In: *Monthly Notices of the Royal Astronomical Society* 284.1 (1st Jan. 1997), pp. 189–201. ISSN: 0035-8711, 1365-2966. DOI: 10.1093/mnras/284.1.189. arXiv: astro-ph/9603039.

[783] Roman Scoccimarro, Ravi K. Sheth, Lam Hui and Bhuvnesh Jain. "How Many Galaxies Fit in a Halo? Constraints on Galaxy Formation Efficiency from Spatial Clustering". In: *The Astrophysical Journal* 546.1 (Jan. 2001), pp. 20–34. ISSN: 0004-637X, 1538-4357. DOI: 10.1086/318261. arXiv: astro-ph/0006319.

[784] Lars Hernquist. "An Analytical Model for Spherical Galaxies and Bulges". In: *The Astrophysical Journal* 356 (1st June 1990), p. 359. ISSN: 0004-637X. DOI: 10.1086/168845.

[785] HongSheng Zhao. "Analytical Models For Galactic Nuclei". In: *Monthly Notices of the Royal Astronomical Society* 278.2 (11th Jan. 1996), pp. 488–496. ISSN: 0035-8711, 1365-2966. DOI: 10.1093/mnras/278.2.488. arXiv: astro-ph/9509122.

[786] Y. P. Jing and Yasushi Suto. "Triaxial Modeling of Halo Density Profiles with High-resolution N-body Simulations". In: *The Astrophysical Journal* 574.2 (Aug. 2002), pp. 538–553. ISSN: 0004-637X, 1538-4357. DOI: 10.1086/341065. arXiv: astro-ph/0202064.

[787] Ben Moore et al. "Cold Collapse and the Core Catastrophe". In: *Monthly Notices of the Royal Astronomical Society* 310.4 (Dec. 1999), pp. 1147–1152. ISSN: 0035-8711, 1365-2966. DOI: 10.1046/j.1365-8711.1999.03039.x. arXiv: astro-ph/9903164.

[788] Julio F. Navarro et al. "The Diversity and Similarity of Simulated Cold Dark Matter Halos". In: *Monthly Notices of the Royal Astronomical Society* 402.1 (11th Feb. 2010), pp. 21–34. ISSN: 00358711. DOI: 10.1111/j.1365-2966.2009.15878.x. arXiv: 0810.1522 [astro-ph].

[789] Julio F. Navarro et al. "The Inner Structure of LambdaCDM Halos III: Universality and Asymptotic Slopes". In: *Monthly Notices of the Royal Astronomical Society* 349.3 (Apr. 2004), pp. 1039–1051. ISSN: 00358711, 13652966. DOI: 10.1111/j.1365-2966.2004.07586.x. arXiv: astro-ph/0311231.

[790] Julio F. Navarro, Carlos S. Frenk and Simon D. M. White. "The Structure of Cold Dark Matter Halos". In: *The Astrophysical Journal* 462 (May 1996), p. 563. ISSN: 0004-637X, 1538-4357. DOI: 10.1086/177173. arXiv: astro-ph/9508025.

[791] Julio F. Navarro, Carlos S. Frenk and Simon D. M. White. "A Universal Density Profile from Hierarchical Clustering". In: *The Astrophysical Journal* 490.2 (Dec. 1997), pp. 493–508. ISSN: 0004-637X, 1538-4357. DOI: 10.1086/304888. arXiv: astro-ph/9611107.

[792] Volker Springel et al. "The Aquarius Project: The Subhalos of Galactic Halos". In: *Monthly Notices of the Royal Astronomical Society* 391.4 (21st Dec. 2008), pp. 1685–1711. ISSN: 00358711, 13652966. DOI: 10.1111/j.1365-2966.2008.14066.x. arXiv: 0809.0898 [astro-ph].

[793] C. Power et al. "The Inner Structure of LambdaCDM Halos I: A Numerical Convergence Study". In: *Monthly Notices of the Royal Astronomical Society* 338.1 (1st Jan. 2003), pp. 14–34. ISSN: 0035-8711, 1365-2966. DOI: 10.1046/j.1365-8711.2003.05925.x. arXiv: astro-ph/0201544.

[794] Dominique Aubert, Christophe Pichon and Stephane Colombi. "The Origin and Implications of Dark Matter Anisotropic Cosmic Infall on ~L* Haloes". In: *Monthly Notices of the Royal Astronomical Society* 352.2 (Aug. 2004), pp. 376–398. ISSN: 00358711, 13652966. DOI: 10.1111/j.1365-2966.2004.07883.x. arXiv: astro-ph/0402405.

[795] Peter S. Behroozi, Risa H. Wechsler and Hao-Yi Wu. "The Rockstar Phase-Space Temporal Halo Finder and the Velocity Offsets of Cluster Cores". In: *The Astrophysical Journal* 762.2 (10th Jan. 2013), p. 109. ISSN: 0004-637X, 1538-4357. DOI: 10.1088/0004-637X/762/2/109. arXiv: 1110.4372 [astro-ph].

[796] Edmund Bertschinger and James M. Gelb. "Cosmological N-Body Simulations". In: *Computers in Physics* 5.2 (Mar. 1991), pp. 164–179. ISSN: 0894-1866. DOI: 10.1063/1.4822978.

[797] James S. Bullock et al. "Profiles of Dark Haloes: Evolution, Scatter, and Environment". In: *Monthly Notices of the Royal Astronomical Society* 321.3 (1st Mar. 2001), pp. 559–575. ISSN: 0035-8711, 1365-2966. DOI: 10.1046/j.1365-8711.2001.04068.x. arXiv: astro-ph/9908159.

[798] M. Davis, G. Efstathiou, C. S. Frenk and S. D. M. White. "The Evolution of Large-Scale Structure in a Universe Dominated by Cold Dark Matter". In: *The Astrophysical Journal* 292 (1st May 1985), pp. 371–394. ISSN: 0004-637X. DOI: 10.1086/163168.

[799] Juerg Diemand, Michael Kuhlen and Piero Madau. "Early Supersymmetric Cold Dark Matter Substructure". In: *The Astrophysical Journal* 649.1 (20th Sept. 2006), pp. 1–13. ISSN: 0004-637X, 1538-4357. DOI: 10.1086/506377. arXiv: astro-ph/0603250.

[800] Pascal J. Elahi et al. "Hunting for Galaxies and Halos in Simulations with VELOCIraptor". In: *Publications of the Astronomical Society of Australia* 36 (2019), e021. ISSN: 1323-3580, 1448-6083. DOI: 10.1017/pasa.2019.12. arXiv: 1902.01010 [astro-ph].

[801] Jeffrey P Gardner, Andrew Connolly and Cameron McBride. "Enabling Knowledge Discovery in a Virtual Universe". In: *Proc. of the 2007 TeraGrid Symp.* Citeseer. 2007.

[802] Jeffrey P. Gardner, Andrew Connolly and Cameron McBride. *Enabling Rapid Development of Parallel Tree Search Applications*. 12th Sept. 2007. DOI: 10.48550/arXiv.0709.1967. arXiv: 0709.1967 [astro-ph]. URL: http://arxiv.org/abs/0709.1967 (visited on 20/03/2023). preprint.

[803] Stuart P. D. Gill, Alexander Knebe and Brad K. Gibson. "The Evolution of Substructure - I. A New Identification Method". In: *Monthly Notices of the Royal Astronomical Society* 351.2 (21st June 2004), pp. 399–409. ISSN: 0035-8711, 1365-2966. DOI: 10.1111/j.1365-2966.2004.07786.x. arXiv: astro-ph/0404258.

[804] Juhan Kim and Changbom Park. "A New Halo Finding Method for N-Body Simulations". In: *The Astrophysical Journal* 639.2 (10th Mar. 2006), pp. 600–616. ISSN: 0004-637X, 1538-4357. DOI: 10.1086/499761. arXiv: astro-ph/0401386.

[805] Alexander Knebe et al. "Haloes Gone MAD: The Halo-Finder Comparison Project". In: *Monthly Notices of the Royal Astronomical Society* 415.3 (11th Aug. 2011), pp. 2293–2318. ISSN: 00358711. DOI: 10.1111/j.1365-2966.2011.18858.x. arXiv: 1104.0949 [astro-ph].

[806] Steffen R. Knollmann and Alexander Knebe. "Ahf: Amiga's Halo Finder". In: *The Astrophysical Journal Supplement Series* 182.2 (1st June 2009), pp. 608–624. ISSN: 0067-0049, 1538-4365. DOI: 10.1088/0067-0049/182/2/608. arXiv: 0904.3662 [astro-ph].

[807] M. Maciejewski et al. "Phase-Space Structures II: Hierarchical Structure Finder". In: *Monthly Notices of the Royal Astronomical Society* 396.3 (1st July 2009), pp. 1329–1348. ISSN: 00358711, 13652966. DOI: 10.1111/j.1365-2966.2009.14825.x. arXiv: 0812.0288 [astro-ph].

[808] Mark C. Neyrinck, Nickolay Y. Gnedin and Andrew J. S. Hamilton. "VOBOZ: An Almost-Parameter-Free Halo-Finding Algorithm". In: *Monthly Notices of the Royal Astronomical Society* 356.4 (Feb. 2005), pp. 1222–1232. ISSN: 00358711, 13652966. DOI: 10.1111/j.1365-2966.2004.08505.x. arXiv: astro-ph/0402346.

[809] Susana Planelles and Vicent Quilis. "ASOHF: A New Adaptive Spherical Overdensity Halo Finder". In: *Astronomy and Astrophysics* 519 (Sept. 2010), A94. ISSN: 0004-6361, 1432-0746. DOI: 10.1051/0004-6361/201014214. arXiv: 1006.3205 [astro-ph].

[810] L. D. Shaw, J. Weller, J. P. Ostriker and P. Bode. "The Bound Mass of Substructures in Dark Matter Halos". In: *The Astrophysical Journal* 659.2 (20th Apr. 2007), pp. 1082–1095. ISSN: 0004-637X, 1538-4357. DOI: 10.1086/511849. arXiv: astro-ph/0603150.

[811] Volker Springel, Simon White, Giuseppe Tormen and Guinevere Kauffmann. "Populating a Cluster of Galaxies - I. Results at Z=0". In: *Monthly Notices of the Royal Astronomical Society* 328.3 (Dec. 2001), pp. 726–750. ISSN: 00358711, 13652966. DOI: 10.1046/j.1365-8711.2001.04912.x. arXiv: astro-ph/0012055.

[812] Jochen Weller, Jeremiah P. Ostriker, Paul Bode and Laurie Shaw. "Fast Identification of Bound Structures in Large N-body Simulations". In: *Monthly Notices of the Royal Astronomical Society* 364.3 (11th Dec. 2005), pp. 823–832. ISSN: 0035-8711, 1365-2966. DOI: 10.1111/j.1365-2966.2005.09602.x. arXiv: astro-ph/0405445.

[813] Martin White, J. D. Cohn and Renske Smit. "Cluster Galaxy Dynamics and the Effects of Large Scale Environment". In: *Monthly Notices of the Royal Astronomical Society* 408.3 (1st Nov. 2010), pp. 1818–1834. ISSN: 00358711. DOI: 10.1111/j.1365-2966.2010.17248.x. arXiv: 1005.3022 [astro-ph].

[814] Anna Balaudo, Francesca Calore, Valentina De Romeri and Fiorenza Donato. *HADES: A New Numerical Tool for the Determination of DM over-Densities*. 21st Dec. 2021. DOI: 10.48550/arXiv.2112.11138. arXiv: 2112.11138 [astro-ph]. URL: http://arxiv.org/abs/2112.11138 (visited on 20/03/2023). preprint.

[815] Sownak Bose et al. "Constructing High-Fidelity Halo Merger Trees in AbacusSummit". In: *Monthly Notices of the Royal Astronomical Society* 512.1 (16th Mar. 2022), pp. 837–854. ISSN: 0035-8711, 1365-2966. DOI: 10.1093/mnras/stac555. arXiv: 2110.11409 [astro-ph].

[816] Rodrigo Cañas et al. "Introducing a New, Robust Galaxy Finder Algorithm for Simulations". In: *Monthly Notices of the Royal Astronomical Society* 482.2 (11th Jan. 2019), pp. 2039–2064. ISSN: 0035-8711, 1365-2966. DOI: 10.1093/mnras/sty2725. arXiv: 1806.11417 [astro-ph].

[817] William H. Oliver, Pascal J. Elahi, Geraint F. Lewis and Chris Power. "The Hierarchical Structure of Galactic Haloes: Classification and Characterisation with Halo-OPTICS". In: *Monthly Notices of the Royal Astronomical Society* 501.3 (18th Jan. 2021), pp. 4420–4437. ISSN: 0035-8711, 1365-2966. DOI: 10.1093/mnras/staa3879. arXiv: 2012.04823 [astro-ph].

[818] Aidan Reilly et al. "Six Dimensional Streaming Algorithm for Cluster Finding in N-Body Simulations". In: *ASP Conference Series*. Astronomical Data Analysis Software and Systems XXIX. Vol. 527. Groningen, the Netherlands: Astronomical Society of the Pacific, 24th Dec. 2019, p. 155. ISBN: 978-1-58381-941-8. DOI: 10.48550/arXiv.1912.11432. arXiv: 1912.11432 [astro-ph]. URL: http://arxiv.org/abs/1912.11432 (visited on 20/03/2023).

[819] Jinsu Rhee, Pascal Elahi and Sukyoung K. Yi. "Performance Enhancement of Tree-based Friends-of-friend Galaxy-finder for High-resolution Simulations of Galaxy Formation". In: *The Astrophysical Journal* 927.1 (1st Mar. 2022), p. 129. ISSN: 0004-637X, 1538-4357. DOI: 10.3847/1538-4357/ac4239. arXiv: 2112.05269 [astro-ph].

[820] Shuangpeng Sun et al. "HIKER: A Halo-Finding Method Based on Kernel-Shift Algorithm". In: *Research in Astronomy and Astrophysics* 20.4 (1st Apr. 2020), p. 046. ISSN: 1674-4527. DOI: 10.1088/1674-4527/20/4/46. arXiv: 1909.13301 [astro-ph].

[821] David Vallés-Pérez, Susana Planelles and Vicent Quilis. "The Halo Finding Problem Revisited: A Deep Revision of the ASOHF Code". In: *Astronomy & Astrophysics* 664 (Aug. 2022), A42. ISSN: 0004-6361, 1432-0746. DOI: 10.1051/0004-6361/202243712. arXiv: 2205.02245 [astro-ph].

[822] Jiaxin Han et al. "HBT+: An Improved Code for Finding Subhalos and Building Merger Trees in Cosmological Simulations". In: *Monthly Notices of the Royal Astronomical Society* 474.1 (11th Feb. 2018), pp. 604–617. ISSN: 0035-8711, 1365-2966. DOI: 10.1093/mnras/stx2792. arXiv: 1708.03646 [astro-ph].

[823] Fabrice Roy, Vincent R. Bouillot and Yann Rasera. "pFoF: A Highly Scalable Halo-Finder for Large Cosmological Data Sets". In: *Astronomy & Astrophysics* 564 (Apr. 2014), A13. ISSN: 0004-6361, 1432-0746. DOI: 10.1051/0004-6361/201322555.

[824] Stephen Skory, Matthew J. Turk, Michael L. Norman and Alison L. Coil. "Parallel HOP: A Scalable Halo Finder for Massive Cosmological Data Sets". In: *The Astrophysical Journal Supplement Series* 191.1 (1st Nov. 2010), pp. 43–57. ISSN: 0067-0049, 1538-4365. DOI: 10.1088/0067-0049/191/1/43. arXiv: 1001.3411 [astro-ph].

[825] P. Colin, O. Valenzuela and V. Avila-Reese. "On the Structure of Dark Matter Halos at the Damping Scale of the Power Spectrum with and without Relict Velocities". In: *The Astrophysical Journal* 673.1 (20th Jan. 2008), pp. 203–214. ISSN: 0004-637X, 1538-4357. DOI: 10.1086/524030. arXiv: 0709.4027 [astro-ph].

[826] Matteo Leo, Carlton M. Baugh, Baojiu Li and Silvia Pascoli. "The Effect of Thermal Velocities on Structure Formation in N-body Simulations of Warm Dark Matter". In: *Journal of Cosmology and Astroparticle Physics* 2017.11 (13th Nov. 2017), pp. 017–017. ISSN: 1475-7516. DOI: 10.1088/1475-7516/2017/11/017. arXiv: 1706.07837.

[827] Jie Wang and Simon D. M. White. "Discreteness Effects in Simulations of Hot/Warm Dark Matter". In: *Monthly Notices of the Royal Astronomical Society* 380.1 (6th Aug. 2007), pp. 93–103. ISSN: 00358711, 13652966. DOI: 10.1111/j.1365-2966.2007.12053.x. arXiv: astro-ph/0702575.

[828] Mark R. Lovell et al. "The Properties of Warm Dark Matter Haloes". In: *Monthly Notices of the Royal Astronomical Society* 439.1 (21st Mar. 2014), pp. 300–317. ISSN: 1365-2966, 0035-8711. DOI: 10.1093/mnras/stt2431. arXiv: 1308.1399 [astro-ph].

[829] Jens Stücker, Raul E. Angulo, Oliver Hahn and Simon D. M. White. "Simulating the Complexity of the Dark Matter Sheet II: Halo and Subhalo Mass Functions for Non-Cold Dark Matter Models". In: *Monthly Notices of the Royal Astronomical Society* 509.2 (16th Nov. 2021), pp. 1703–1719. ISSN: 0035-8711, 1365-2966. DOI: 10.1093/mnras/stab3078. arXiv: 2109.09760.

[830] Tom Abel, Oliver Hahn and Ralf Kaehler. "Tracing the Dark Matter Sheet in Phase Space". In: *Monthly Notices of the Royal Astronomical Society* 427.1 (21st Nov. 2012), pp. 61–76. ISSN: 00358711, 13652966. DOI: 10.1111/j.1365-2966.2012.21754.x. arXiv: 1111.3944 [astro-ph].

[831] Raul E. Angulo, Oliver Hahn and Tom Abel. "The Warm DM Halo Mass Function below the Cut-off Scale". In: *Monthly Notices of the Royal Astronomical Society* 434.4 (1st Oct. 2013), pp. 3337–3347. ISSN: 0035-8711, 1365-2966. DOI: 10.1093/mnras/stt1246. arXiv: 1304.2406.

[832] Thierry Sousbie and Stéphane Colombi. "ColDICE: A Parallel Vlasov-Poisson Solver Using Moving Adaptive Simplicial Tessellation". In: *Journal of Computational Physics* 321 (Sept. 2016), pp. 644–697. ISSN: 00219991. DOI: 10.1016/j.jcp.2016.05.048. arXiv: 1509.07720 [astro-ph, physics:physics].

[833] Jens Stücker, Oliver Hahn, Raul E. Angulo and Simon D. M. White. "Simulating the Complexity of the Dark Matter Sheet I: Numerical Algorithms". In: *Monthly Notices of the Royal Astronomical Society* 495.4 (11th July 2020), pp. 4943–4964. ISSN: 0035-8711, 1365-2966. DOI: 10.1093/mnras/staa1468. arXiv: 1909.00008 [astro-ph].

[834] Annika H. G. Peter and Andrew J. Benson. "Dark-Matter Decays and Milky Way Satellite Galaxies". In: *Physical Review D* 82.12 (21st Dec. 2010), p. 123521. ISSN: 1550-7998, 1550-2368. DOI: 10.1103/PhysRevD.82.123521. arXiv: 1009.1912 [astro-ph, physics:hep-ph].

[835] Annika H. G. Peter, Christopher E. Moody and Marc Kamionkowski. "Dark-Matter Decays and Self-Gravitating Halos". In: *Physical Review D* 81.10 (3rd May 2010), p. 103501. ISSN: 1550-7998, 1550-2368. DOI: 10.1103/PhysRevD.81.103501. arXiv: 1003.0419 [astro-ph, physics:hep-ph].

[836] Mei-Yu Wang et al. "Lyman-Alpha Forest Constraints on Decaying Dark Matter". In: *Physical Review D* 88.12 (9th Dec. 2013), p. 123515. ISSN: 1550-7998, 1550-2368. DOI: 10.1103/PhysRevD.88.123515. arXiv: 1309.7354 [astro-ph, physics:hep-ph].

[837] Mei-Yu Wang et al. "Cosmological Simulations of Decaying Dark Matter: Implications for Small-scale Structure of Dark Matter Halos". In: *Monthly Notices of the Royal Astronomical Society* 445.1 (21st Nov. 2014), pp. 614–629. ISSN: 0035-8711, 1365-2966. DOI: 10.1093/mnras/stu1747. arXiv: 1406.0527.

[838] Jeppe Dakin, Steen Hannestad and Thomas Tram. "Fully Relativistic Treatment of Decaying Cold Dark Matter in N-Body Simulations". In: *Journal of Cosmology and Astroparticle Physics* 2019.06 (13th June 2019), pp. 032–032. ISSN: 1475-7516. DOI: 10.1088/1475-7516/2019/06/032. arXiv: 1904.11773.

[839] Steven J. Clark, Kyriakos Vattis and Savvas M. Koushiappas. "Cosmological Constraints on Late-Universe Decaying Dark Matter as a Solution to the H_0 Tension". In: *Physical Review D* 103.4 (23rd Feb. 2021), p. 043014. ISSN: 2470-0010, 2470-0029. DOI: 10.1103/PhysRevD.103.043014. arXiv: 2006.03678 [astro-ph, physics:hep-ph].

[840] Kari Enqvist, Seshadri Nadathur, Toyokazu Sekiguchi and Tomo Takahashi. "Decaying Dark Matter and the Tension in σ_8". In: *Journal of Cosmology and Astroparticle Physics* 2015.09 (29th Sept. 2015), pp. 067–067. ISSN: 1475-7516. DOI: 10.1088/1475-7516/2015/09/067. arXiv: 1505.05511 [astro-ph, physics:gr-qc, physics:hep-ph].

[841] Jonathan Hubert et al. "Decaying Dark Matter: Simulations and Weak-Lensing Forecast". In: *Journal of Cosmology and Astroparticle Physics* 2021.10 (1st Oct. 2021), p. 040. ISSN: 1475-7516. DOI: 10.1088/1475-7516/2021/10/040. arXiv: 2104.07675 [astro-ph].

[842] Andreas Burkert. "The Structure and Evolution of Weakly Self-Interacting Cold Dark Matter Halos". In: *The Astrophysical Journal* 534.2 (10th May 2000), pp. L143–L146. ISSN: 0004637X. DOI: 10.1086/312674. arXiv: astro-ph/0002409.

[843] Alex Fitts et al. "Dwarf Galaxies in CDM, WDM, and SIDM: Disentangling Baryons and Dark Matter Physics". In: *Monthly Notices of the Royal Astronomical Society* 490.1 (21st Nov. 2019), pp. 962–977. ISSN: 0035-8711, 1365-2966. DOI: 10.1093/mnras/stz2613. arXiv: 1811.11791 [astro-ph].

[844] Helen Meskhidze et al. "Comparing Implementations of Self-Interacting Dark Matter in the Gizmo and Arepo Codes". In: *Monthly Notices of the Royal Astronomical Society* 513.2 (6th May 2022), pp. 2600–2608. ISSN: 0035-8711, 1365-2966. DOI: 10.1093/mnras/stac1056. arXiv: 2203.06035 [astro-ph].

[845] Andrew B. Newman et al. "The Density Profiles of Massive, Relaxed Galaxy Clusters. I. The Total Density Over Three Decades in Radius". In: *The Astrophysical Journal* 765.1 (13th Feb. 2013), p. 24. ISSN: 0004-637X, 1538-4357. DOI: 10.1088/0004-637X/765/1/24. arXiv: 1209.1391 [astro-ph].

[846] Andrew B. Newman, Tommaso Treu, Richard S. Ellis and David J. Sand. "The Density Profiles of Massive, Relaxed Galaxy Clusters. II. Separating Luminous and Dark Matter in Cluster Cores". In: *The Astrophysical Journal* 765.1 (13th Feb. 2013), p. 25. ISSN: 0004-637X, 1538-4357. DOI: 10.1088/0004-637X/765/1/25. arXiv: 1209.1392 [astro-ph].

[847] Andrew Robertson et al. "Observable Tests of Self-Interacting Dark Matter in Galaxy Clusters: Cosmological Simulations with SIDM and Baryons". In: *Monthly Notices of the Royal Astronomical Society* 488.3 (21st Sept. 2019), pp. 3646–3662. ISSN: 0035-8711, 1365-2966. DOI: 10.1093/mnras/stz1815. arXiv: 1810.05649 [astro-ph].

[848] Andrew Robertson, Richard Massey and Vincent Eke. "What Does the Bullet Cluster Tell Us about Self-Interacting Dark Matter?" In: *Monthly Notices of the Royal Astronomical Society* 465.1 (11th Feb. 2017), pp. 569–587. ISSN: 0035-8711, 1365-2966. DOI: 10.1093/mnras/stw2670. arXiv: 1605.04307 [astro-ph].

[849] Ellen L. Sirks et al. "The Effects of Self-Interacting Dark Matter on the Stripping of Galaxies That Fall into Clusters". In: *Monthly Notices of the Royal Astronomical Society* 511.4 (10th Mar. 2022), pp. 5927–5935. ISSN: 0035-8711, 1365-2966. DOI: 10.1093/mnras/stac406. arXiv: 2109.03257 [astro-ph].

[850] Naoki Yoshida, Volker Springel, Simon D. M. White and Giuseppe Tormen. "Weakly Self-Interacting Dark Matter and the Structure of Dark Halos". In: *The Astrophysical Journal* 544.2 (1st Dec. 2000), pp. L87–L90. ISSN: 0004637X. DOI: 10.1086/317306. arXiv: astro-ph/0006134.

[851] Philip F. Hopkins et al. "FIRE-2 Simulations: Physics versus Numerics in Galaxy Formation". In: *Monthly Notices of the Royal Astronomical Society* 480.1 (11th Oct. 2018), pp. 800–863. ISSN: 0035-8711, 1365-2966. DOI: 10.1093/mnras/sty1690. arXiv: 1702.06148 [astro-ph].

[852] Mark Vogelsberger, Jesus Zavala and Abraham Loeb. "Subhaloes in Self-Interacting Galactic Dark Matter Haloes". In: *Monthly Notices of the Royal Astronomical Society* 423.4 (11th July 2012), pp. 3740–3752. ISSN: 00358711. DOI: 10.1111/j.1365-2966.2012.21182.x. arXiv: 1201.5892 [astro-ph].

[853] Sebastian Bohr et al. "ETHOS – An Effective Parametrization and Classification for Structure Formation: The Non-Linear Regime at $z\gtrsim5$". In: *Monthly Notices of the Royal Astronomical Society* 498.3 (22nd Sept. 2020), pp. 3403–3419. ISSN: 0035-8711, 1365-2966. DOI: 10.1093/mnras/staa2579. arXiv: 2006.01842 [astro-ph, physics:hep-ph].

[854] Sebastian Bohr, Jesús Zavala, Francis-Yan Cyr-Racine and Mark Vogelsberger. "The Halo Mass Function and Inner Structure of ETHOS Haloes at High Redshift". In: *Monthly Notices of the Royal Astronomical Society* 506.1 (6th July 2021), pp. 128–138. ISSN: 0035-8711, 1365-2966. DOI: 10.1093/mnras/stab1758. arXiv: 2101.08790 [astro-ph].

[855] Sownak Bose et al. "ETHOS - an Effective Theory of Structure Formation: Detecting Dark Matter Interactions through the Lyman-\ensuremath\alpha Forest". In: *Monthly Notices of the Royal Astronomical Society* 487.1 (21st July 2019), pp. 522–536. ISSN: 0035-8711, 1365-2966. DOI: 10.1093/mnras/stz1276. arXiv: 1811.10630 [astro-ph].

[856] Mark R. Lovell et al. "ETHOS – an Effective Theory of Structure Formation: Predictions for the High-Redshift Universe – Abundance of Galaxies and Reionization". In: *Monthly Notices of the Royal Astronomical Society* 477.3 (1st July 2018), pp. 2886–2899. ISSN: 0035-8711, 1365-2966. DOI: 10.1093/mnras/sty818. arXiv: 1711.10497 [astro-ph, physics:hep-ph].

[857] Mark R. Lovell, Jesús Zavala and Mark Vogelsberger. "ETHOS - an Effective Theory of Structure Formation: Formation of the First Haloes and Their Stars". In: *Monthly Notices of the Royal Astronomical Society* 485.4 (1st June 2019), pp. 5474–5489. ISSN: 0035-8711, 1365-2966. DOI: 10.1093/mnras/stz766. arXiv: 1812.04627 [astro-ph, physics:hep-ph].

[858] Julian B. Muñoz et al. "ETHOS – An Effective Theory of Structure Formation: Impact of Dark Acoustic Oscillations on Cosmic Dawn". In: *Physical Review D* 103.4 (8th Feb. 2021), p. 043512. ISSN: 2470-0010, 2470-0029. DOI: 10.1103/PhysRevD.103.043512. arXiv: 2011.05333 [astro-ph, physics:hep-ph].

[859] Mark Vogelsberger et al. "ETHOS - An Effective Theory of Structure Formation: Dark Matter Physics as a Possible Explanation of the Small-Scale CDM Problems". In: *Monthly Notices of the Royal Astronomical Society* 460.2 (1st Aug. 2016), pp. 1399–1416. ISSN: 0035-8711, 1365-2966. DOI: 10.1093/mnras/stw1076. arXiv: 1512.05349 [astro-ph].

[860] Joe Zhiyu Chen, Markus R. Mosbech, Amol Upadhye and Yvonne Y. Y. Wong. "Hybrid Multi-Fluid-Particle Simulations of the Cosmic Neutrino Background". In: *Journal of Cosmology and Astroparticle Physics* 2023.03 (Mar. 2023), p. 012. ISSN: 1475-7516. DOI: 10.1088/1475-7516/2023/03/012. arXiv: 2210.16012.

[861] Kevork N. Abazajian et al. *CMB-S4 Science Book, First Edition*. 9th Oct. 2016. DOI: 10.48550/arXiv.1610.02743. arXiv: 1610.02743 [astro-ph, physics:gr-qc, physics:hep-ph, physics:hep-th]. URL: http://arxiv.org/abs/1610.02743 (visited on 23/03/2023). preprint.

[862] Rupert Allison et al. "Towards a Cosmological Neutrino Mass Detection". In: *Physical Review D* 92.12 (23rd Dec. 2015), p. 123535. ISSN: 1550-7998, 1550-2368. DOI: 10.1103/PhysRevD.92.123535. arXiv: 1509.07471 [astro-ph].

[863] Luca Amendola et al. "Cosmology and Fundamental Physics with the Euclid Satellite". In: *Living Reviews in Relativity* 16.1 (Dec. 2013), p. 6. ISSN: 2367-3613, 1433-8351. DOI: 10.12942/lrr-2013-6. arXiv: 1206.1225 [astro-ph, physics:gr-qc, physics:hep-ph].

[864] William Giarè et al. "Cosmological Forecasts on Thermal Axions, Relic Neutrinos and Light Elements". In: *Monthly Notices of the Royal Astronomical Society* (18th Jan. 2022), stac126. ISSN: 0035-8711, 1365-2966. DOI: 10.1093/mnras/stac126. arXiv: 2110.00340 [astro-ph, physics:hep-ph].

[865] Michael Levi et al. *The DESI Experiment, a Whitepaper for Snowmass 2013*. 4th Aug. 2013. DOI: 10.48550/arXiv.1308.0847. arXiv: 1308.0847 [astro-ph]. URL: http://arxiv.org/abs/1308.0847 (visited on 23/03/2023). preprint.

[866] E. Baracchini et al. *PTOLEMY: A Proposal for Thermal Relic Detection of Massive Neutrinos and Directional Detection of MeV Dark Matter*. 6th Aug. 2018. DOI: 10.48550/arXiv.1808.01892. arXiv: 1808.01892 [astro-ph, physics:hep-ex, physics:physics]. URL: http://arxiv.org/abs/1808.01892 (visited on 24/03/2023). preprint.

[867] S. Betts et al. *Development of a Relic Neutrino Detection Experiment at PTOLEMY: Princeton Tritium Observatory for Light, Early-Universe, Massive-Neutrino Yield*. 26th Aug. 2013. DOI: 10.48550/arXiv.1307.4738. arXiv: 1307.4738 [astro-ph, physics:physics]. URL: http://arxiv.org/abs/1307.4738 (visited on 24/03/2023). preprint.

[868] PTOLEMY collaboration et al. "Neutrino Physics with the PTOLEMY Project: Active Neutrino Properties and the Light Sterile Case". In: *Journal of Cosmology and Astroparticle Physics* 2019.07 (31st July 2019), pp. 047–047. ISSN: 1475-7516. DOI: 10.1088/1475-7516/2019/07/047. arXiv: 1902.05508 [astro-ph, physics:hep-ex, physics:hep-ph].

[869] Jacob Brandbyge, Steen Hannestad, Troels Haugboelle and Bjarne Thomsen. "The Effect of Thermal Neutrino Motion on the Non-linear Cosmological Matter Power Spectrum". In: *Journal of Cosmology and Astroparticle Physics* 2008.08 (15th Aug. 2008), p. 020. ISSN: 1475-7516. DOI: 10.1088/1475-7516/2008/08/020. arXiv: 0802.3700 [astro-ph].

[870] Jacob Brandbyge and Steen Hannestad. "Grid Based Linear Neutrino Perturbations in Cosmological N-body Simulations". In: *Journal of Cosmology and Astroparticle Physics* 2009.05 (5th May 2009), pp. 002–002. ISSN: 1475-7516. DOI: 10.1088/1475-7516/2009/05/002. arXiv: 0812.3149 [astro-ph].

[871] Jacob Brandbyge and Steen Hannestad. "Resolving Cosmic Neutrino Structure: A Hybrid Neutrino N-body Scheme". In: *Journal of Cosmology and Astroparticle Physics* 2010.01 (13th Jan. 2010), pp. 021–021. ISSN: 1475-7516. DOI: 10.1088/1475-7516/2010/01/021. arXiv: 0908.1969 [astro-ph].

[872] Arka Banerjee and Neal Dalal. "Simulating Nonlinear Cosmological Structure Formation with Massive Neutrinos". In: *Journal of Cosmology and Astroparticle Physics* 2016.11 (7th Nov. 2016), pp. 015–015. ISSN: 1475-7516. DOI: 10.1088/1475-7516/2016/11/015. arXiv: 1606.06167.

[873] Shankar Agarwal and Hume A. Feldman. "The Effect of Massive Neutrinos on the Matter Power Spectrum". In: *Monthly Notices of the Royal Astronomical Society* (Oct. 2010), no–no. ISSN: 00358711. DOI: 10.1111/j.1365-2966.2010.17546.x. arXiv: 1006.0689 [astro-ph].

[874] Yacine Ali-Haïmoud and Simeon Bird. "An Efficient Implementation of Massive Neutrinos in Non-Linear Structure Formation Simulations". In: *Monthly Notices of the Royal Astronomical Society* 428.4 (1st Feb. 2013), pp. 3375–3389. ISSN: 0035-8711, 1365-2966. DOI: 10.1093/mnras/sts286. arXiv: 1209.0461 [astro-ph].

[875] Jia Liu et al. "MassiveNuS: Cosmological Massive Neutrino Simulations". In: *Journal of Cosmology and Astroparticle Physics* 2018.03 (29th Mar. 2018), pp. 049–049. ISSN: 1475-7516. DOI: 10.1088/1475-7516/2018/03/049. arXiv: 1711.10524 [astro-ph].

[876] Simeon Bird, Yacine Ali-Haïmoud, Yu Feng and Jia Liu. "An Efficient and Accurate Hybrid Method for Simulating Non-Linear Neutrino Structure". In: *Monthly Notices of the Royal Astronomical Society* 481.2 (1st Dec. 2018), pp. 1486–1500. ISSN: 0035-8711, 1365-2966. DOI: 10.1093/mnras/sty2376. arXiv: 1803.09854 [astro-ph].

[877] Francisco Villaescusa-Navarro et al. "The CAMELS Multifield Dataset: Learning the Universe's Fundamental Parameters with Artificial Intelligence". In: *The Astrophysical Journal Supplement Series* 259.2 (1st Apr. 2022), p. 61. ISSN: 0067-0049, 1538-4365. DOI: 10.3847/1538-4365/ac5ab0. arXiv: 2109.10915 [astro-ph].

[878] Francisco Villaescusa-Navarro et al. *The CAMELS Project: Public Data Release*. 4th Jan. 2022. DOI: 10.48550/arXiv.2201.01300. arXiv: 2201.01300 [astro-ph]. URL: http://arxiv.org/abs/2201.01300 (visited on 21/03/2023). preprint.

[879] Annalisa Pillepich et al. "Simulating Galaxy Formation with the IllustrisTNG Model". In: *Monthly Notices of the Royal Astronomical Society* 473.3 (21st Jan. 2018), pp. 4077–4106. ISSN: 0035-8711, 1365-2966. DOI: 10.1093/mnras/stx2656. arXiv: 1703.02970 [astro-ph].

[880] Rainer Weinberger et al. "Simulating Galaxy Formation with Black Hole Driven Thermal and Kinetic Feedback". In: *Monthly Notices of the Royal Astronomical Society* 465.3 (1st Mar. 2017), pp. 3291–3308. ISSN: 0035-8711, 1365-2966. DOI: 10.1093/mnras/stw2944. arXiv: 1607.03486 [astro-ph].

[881] Romeel Davé et al. "Simba: Cosmological Simulations with Black Hole Growth and Feedback". In: *Monthly Notices of the Royal Astronomical Society* 486.2 (21st June 2019), pp. 2827–2849. ISSN: 0035-8711, 1365-2966. DOI: 10.1093/mnras/stz937. arXiv: 1901.10203 [astro-ph].

[882] A. M. Beck et al. "An Improved SPH Scheme for Cosmological Simulations". In: *Monthly Notices of the Royal Astronomical Society* 455.2 (11th Jan. 2016), pp. 2110–2130. ISSN: 0035-8711, 1365-2966. DOI: 10.1093/mnras/stv2443. arXiv: 1502.07358 [astro-ph].

[883] S. Cole, C. G. Lacey, C. M. Baugh and C. S. Frenk. "Hierarchical Galaxy Formation". In: *Monthly Notices of the Royal Astronomical Society* 319 (Nov. 2000), pp. 168–204. DOI: 10.1046/j.1365-8711.2000.03879.x. arXiv: astro-ph/0007281.

[884] C. M. Baugh et al. "Can the Faint Submillimetre Galaxies Be Explained in the Λ Cold Dark Matter Model?" In: *Monthly Notices of the Royal Astronomical Society* 356 (Jan. 2005), pp. 1191–1200. DOI: 10.1111/j.1365-2966.2004.08553.x. arXiv: astro-ph/0406069.

[885] R. G. Bower et al. "Breaking the Hierarchy of Galaxy Formation". In: *Mon. Not. Roy. Astron. Soc.* 370 (Aug. 2006), pp. 645–655. DOI: 10.1111/j.1365-2966.2006.10519.x. arXiv: astro-ph/0511338.

[886] Hannah Parkinson, Shaun Cole and John Helly. "Generating Dark Matter Halo Merger Trees". In: *Monthly Notices of the Royal Astronomical Society* 383.2 (10th Dec. 2007), pp. 557–564. ISSN: 00358711. DOI: 10.1111/j.1365-2966.2007.12517.x. arXiv: 0708.1382.

[887] C. D. P. Lagos et al. "On the Impact of Empirical and Theoretical Star Formation Laws on Galaxy Formation". In: *Mon. Not. Roy. Astron. Soc.* 416 (Sept. 2011), pp. 1566–1584. DOI: 10.1111/j.1365-2966.2011.19160.x. arXiv: 1011.5506.

[888] Cedric G. Lacey et al. "A Unified Multiwavelength Model of Galaxy Formation". In: *Mon. Not. Roy. Astron. Soc.* 462.4 (Nov. 2016), pp. 3854–3911. DOI: 10.1093/mnras/stw1888. arXiv: 1509.08473.

[889] Claudia del P. Lagos et al. "Shark: Introducing an Open Source, Free and Flexible Semi-Analytic Model of Galaxy Formation". In: *Monthly Notices of the Royal Astronomical Society* 481.3 (11th Dec. 2018), pp. 3573–3603. ISSN: 0035-8711, 1365-2966. DOI: 10.1093/mnras/sty2440. arXiv: 1807.11180 [astro-ph].

[890] Darren J. Croton et al. "Semi-Analytic Galaxy Evolution (SAGE): Model Calibration and Basic Results". In: *The Astrophysical Journal Supplement Series* 222.2 (18th Feb. 2016), p. 22. ISSN: 1538-4365. DOI: 10.3847/0067-0049/222/2/22. arXiv: 1601.04709 [astro-ph].

[891] Andrew J. Benson. "Galacticus: A Semi-Analytic Model of Galaxy Formation". In: *New Astronomy* 17.2 (Feb. 2012), pp. 175–197. ISSN: 13841076. DOI: 10.1016/j.newast.2011.07.004. arXiv: 1008.1786 [astro-ph].

[892] Celine Boehm et al. "Is It Possible to Explain Neutrino Masses with Scalar Dark Matter?" In: *Physical Review D* 77.4 (15th Feb. 2008), p. 043516. ISSN: 1550-7998, 1550-2368. DOI: 10.1103/PhysRevD.77.043516. arXiv: hep-ph/0612228.

[893] Ivan Esteban et al. "Global Analysis of Three-Flavour Neutrino Oscillations: Synergies and Tensions in the Determination of Theta_23, delta_CP, and the Mass Ordering". In: *Journal of High Energy Physics* 2019.1 (Jan. 2019), p. 106. ISSN: 1029-8479. DOI: 10.1007/JHEP01(2019)106. arXiv: 1811.05487.

[894] KATRIN collaboration. *KATRIN: A next Generation Tritium Beta Decay Experiment with Sub-eV Sensitivity for the Electron Neutrino Mass*. 21st Sept. 2001. DOI: 10.48550/arXiv.hep-ex/0109033. arXiv: hep-ex/0109033. URL: http://arxiv.org/abs/hep-ex/0109033 (visited on 09/08/2022). preprint.

[895] M. Aker et al. "An Improved Upper Limit on the Neutrino Mass from a Direct Kinematic Method by KATRIN". In: *Physical Review Letters* 123.22 (Sept. 2019). DOI: 10.1103/PhysRevLett.123.221802. arXiv: 1909.06048.

[896] Mario G. Santos et al. *Cosmology with a SKA HI Intensity Mapping Survey*. 16th Jan. 2015. DOI: 10.48550/arXiv.1501.03989. arXiv: 1501.03989. URL: http://arxiv.org/abs/1501.03989 (visited on 09/08/2022). preprint.

[897] Andreu Font-Ribera et al. "DESI and Other Dark Energy Experiments in the Era of Neutrino Mass Measurements". In: *Journal of Cosmology and Astroparticle Physics* 2014.05 (19th May 2014), pp. 023–023. ISSN: 1475-7516. DOI: 10.1088/1475-7516/2014/05/023. arXiv: 1308.4164.

[898] Thejs Brinckmann et al. "The Promising Future of a Robust Cosmological Neutrino Mass Measurement". In: *Journal of Cosmology and Astroparticle Physics* 2019.01 (29th Jan. 2019), pp. 059–059. ISSN: 1475-7516. DOI: 10.1088/1475-7516/2019/01/059. arXiv: 1808.05955.

[899] Anatoly A. Klypin, Andrey V. Kravtsov, Octavio Valenzuela and Francisco Prada. "Where Are the Missing Galactic Satellites?" In: *The Astrophysical Journal* 522.1 (Sept. 1999), pp. 82–92. ISSN: 0004-637X, 1538-4357. DOI: 10.1086/307643. arXiv: astro-ph/9901240.

[900] Ben Moore et al. "Dark Matter Substructure in Galactic Halos". In: *The Astrophysical Journal* 524.1 (10th Oct. 1999), pp. L19–L22. ISSN: 0004637X. DOI: 10.1086/312287. arXiv: astro-ph/9907411.

[901] Ricardo A. Flores and Joel R. Primack. "Observational and Theoretical Constraints on Singular Dark Matter Halos". In: *The Astrophysical Journal* 427 (May 1994), p. L1. ISSN: 0004-637X, 1538-4357. DOI: 10.1086/187350. arXiv: astro-ph/9402004.

[902] Ben Moore. "Evidence against Dissipation-Less Dark Matter from Observations of Galaxy Haloes". In: *Nature* 370.6491 (6491 Aug. 1994), pp. 629–631. ISSN: 1476-4687. DOI: 10.1038/370629a0.

[903] Michael Boylan-Kolchin, James S. Bullock and Manoj Kaplinghat. "Too Big to Fail? The Puzzling Darkness of Massive Milky Way Subhaloes". In: *Monthly Notices of the Royal Astronomical Society: Letters* 415.1 (21st July 2011), pp. L40–L44. ISSN: 17453925. DOI: 10.1111/j.1745-3933.2011.01074.x. arXiv: 1103.0007.

[904] L. Verde, T. Treu and A. G. Riess. "Tensions between the Early and the Late Universe". In: *Nature Astronomy* 3.10 (July 2019), pp. 891–895. ISSN: 2397-3366. DOI: 10.1038/s41550-019-0902-0. arXiv: 1907.10625.

[905] DES Collaboration et al. "Dark Energy Survey Year 1 Results: A Precise H0 Measurement from DES Y1, BAO, and D/H Data". In: *Monthly Notices of the Royal Astronomical Society* 480.3 (1st Nov. 2018), pp. 3879–3888. ISSN: 0035-8711, 1365-2966. DOI: 10.1093/mnras/sty1939. arXiv: 1711.00403.

[906] Simone Aiola et al. "The Atacama Cosmology Telescope: DR4 Maps and Cosmological Parameters". In: *Journal of Cosmology and Astroparticle Physics* 2020.12 (30th Dec. 2020), pp. 047–047. ISSN: 1475-7516. DOI: 10.1088/1475-7516/2020/12/047. arXiv: 2007.07288.

[907] Florian Beutler et al. "The 6dF Galaxy Survey: Baryon Acoustic Oscillations and the Local Hubble Constant". In: *Monthly Notices of the Royal Astronomical Society* 416.4 (1st Oct. 2011), pp. 3017–3032. ISSN: 00358711. DOI: 10.1111/j.1365-2966.2011.19250.x. arXiv: 1106.3366 [astro-ph].

[908] Ashley J. Ross et al. "The Clustering of the SDSS DR7 Main Galaxy Sample I: A 4 per Cent Distance Measure at Z=0.15". In: *Monthly Notices of the Royal Astronomical Society* 449.1 (1st May 2015), pp. 835–847. ISSN: 1365-2966, 0035-8711. DOI: 10.1093/mnras/stv154. arXiv: 1409.3242 [astro-ph].

[909] Kenneth C. Wong et al. "H0LiCOW – XIII. A 2.4 per Cent Measurement of H0 from Lensed Quasars: 5.3σ Tension between Early- and Late-Universe Probes". In: *Monthly Notices of the Royal Astronomical Society* 498.1 (25th Sept. 2020), pp. 1420–1439. ISSN: 1365-2966, 0035-8711. DOI: 10.1093/mnras/stz3094. arXiv: 1907.04869.

[910] Wendy L. Freedman et al. "The Carnegie-Chicago Hubble Program. VIII. An Independent Determination of the Hubble Constant Based on the Tip of the Red Giant Branch". In: *The Astrophysical Journal* 882.1 (1st Sept. 2019), p. 34. ISSN: 0004-637X, 1538-4357. DOI: 10.3847/1538-4357/ab2f73. arXiv: 1907.05922.

[911] Caroline D. Huang et al. "Hubble Space Telescope Observations of Mira Variables in the SN Ia Host NGC 1559: An Alternative Candle to Measure the Hubble Constant". In: *The Astrophysical Journal* 889.1 (20th Jan. 2020), p. 5. ISSN: 1538-4357. DOI: 10.3847/1538-4357/ab5dbd. arXiv: 1908.10883.

[912] M. A. Troxel et al. "Dark Energy Survey Year 1 Results: Cosmological Constraints from Cosmic Shear". In: *Physical Review D* 98.4 (27th Aug. 2018), p. 043528. ISSN: 2470-0010, 2470-0029. DOI: 10.1103/PhysRevD.98.043528. arXiv: 1708.01538 [astro-ph].

[913] Gianpiero Mangano et al. "Cosmological Bounds on Dark-Matter-Neutrino Interactions". In: *Physical Review D* 74.4 (June 2006). DOI: 10.1103/PhysRevD.74.043517. arXiv: astro-ph/0606190.

[914] P. Serra et al. "Constraints on Neutrino-Dark Matter Interactions from Cosmic Microwave Background and Large Scale Structure Data". In: *Physical Review D* 81.4 (2nd Feb. 2010), p. 043507. ISSN: 1550-7998, 1550-2368. DOI: 10.1103/PhysRevD.81.043507. arXiv: 0911.4411.

[915] Ryan J. Wilkinson, Céline Bœhm and Julien Lesgourgues. "Constraining Dark Matter-Neutrino Interactions Using the CMB and Large-Scale Structure". In: *Journal of Cosmology and Astroparticle Physics* 2014.05 (12th May 2014), pp. 011–011. ISSN: 1475-7516. DOI: 10.1088/1475-7516/2014/05/011. arXiv: 1401.7597.

[916] Subinoy Das, Rajesh Mondal, Vikram Rentala and Srikanth Suresh. "On Dark Matter - Dark Radiation Interaction and Cosmic Reionization". In: *Journal of Cosmology and Astroparticle Physics* 2018.08 (30th Aug. 2018), p. 045. ISSN: 1475-7516. DOI: 10.1088/1475-7516/2018/08/045. arXiv: 1712.03976.

[917] David E. Kaplan, Gordan Z. Krnjaic, Keith R. Rehermann and Christopher M. Wells. "Atomic Dark Matter". In: *Journal of Cosmology and Astroparticle Physics* 2010.05 (19th May 2010), p. 021. ISSN: 1475-7516. DOI: 10.1088/1475-7516/2010/05/021. arXiv: 0909.0753.

[918] Roberta Diamanti et al. "Dark Radiation and Interacting Scenarios". In: *Physical Review D* 87.6 (7th Mar. 2013), p. 063509. ISSN: 1550-7998, 1550-2368. DOI: 10.1103/PhysRevD.87.063509. arXiv: 1212.6007.

[919] Manuel A. Buen-Abad, Gustavo Marques-Tavares and Martin Schmaltz. "Non-Abelian Dark Matter and Dark Radiation". In: *Physical Review D* 92.2 (27th July 2015), p. 023531. ISSN: 1550-7998, 1550-2368. DOI: 10.1103/PhysRevD.92.023531. arXiv: 1505.03542.

[920] Julien Lesgourgues, Gustavo Marques-Tavares and Martin Schmaltz. "Evidence for Dark Matter Interactions in Cosmological Precision Data?" In: *Journal of Cosmology and Astroparticle Physics* 2016.02 (16th Feb. 2016), pp. 037–037. ISSN: 1475-7516. DOI: 10.1088/1475-7516/2016/02/037. arXiv: 1507.04351.

[921] P. Ko, Natsumi Nagata and Yong Tang. "Hidden Charged Dark Matter and Chiral Dark Radiation". In: *Physics Letters B* 773 (Oct. 2017), pp. 513–520. DOI: 10.1016/j.physletb.2017.08.065. arXiv: 1706.05605.

[922] Miguel Escudero et al. "A Fresh Look into the Interacting Dark Matter Scenario". In: *Journal of Cosmology and Astroparticle Physics* 2018.06 (5th June 2018), p. 007. ISSN: 1475-7516. DOI: 10.1088/1475-7516/2018/06/007. arXiv: 1803.08427.

[923] Subinoy Das and Kris Sigurdson. "Cosmological Limits on Hidden Sector Dark Matter". In: *Physical Review D* 85.6 (14th Mar. 2012), p. 063510. ISSN: 1550-7998, 1550-2368. DOI: 10.1103/PhysRevD.85.063510. arXiv: 1012.4458.

[924] Thejs Brinckmann and Julien Lesgourgues. "MontePython 3: Boosted MCMC Sampler and Other Features". In: *Physics of the Dark Universe* 24 (Mar. 2019), p. 100260. ISSN: 22126864. DOI: 10.1016/j.dark.2018.100260. arXiv: 1804.07261.

[925] Benjamin Audren, Julien Lesgourgues, Karim Benabed and Simon Prunet. "Conservative Constraints on Early Cosmology: An Illustration of the Monte Python Cosmological Parameter Inference Code". In: *Journal of Cosmology and Astroparticle Physics* 2013.02 (4th Feb. 2013), pp. 001–001. ISSN: 1475-7516. DOI: 10.1088/1475-7516/2013/02/001. arXiv: 1210.7183.

[926] Isabel M. Oldengott, Cornelius Rampf and Yvonne Y. Y. Wong. "Boltzmann Hierarchy for Interacting Neutrinos I: Formalism". In: *Journal of Cosmology and Astroparticle Physics* 2015.04 (13th Apr. 2015), pp. 016–016. ISSN: 1475-7516. DOI: 10.1088/1475-7516/2015/04/016. arXiv: 1409.1577.

[927] Francis-Yan Cyr-Racine and Kris Sigurdson. "Limits on Neutrino-Neutrino Scattering in the Early Universe". In: *Physical Review D* 90.12 (29th Dec. 2014), p. 123533. ISSN: 1550-7998, 1550-2368. DOI: 10.1103/PhysRevD.90.123533. arXiv: 1306.1536.

[928] Steven Weinberg. *Cosmology*. Oxford University Press, 2008, p. 616. 616 pp. ISBN: 978-0-19-852682-7.

[929] Luc Voruz, Julien Lesgourgues and Thomas Tram. "The Effective Gravitational Decoupling between Dark Matter and the CMB". In: *Journal of Cosmology and Astroparticle Physics* 2014.03 (4th Mar. 2014), pp. 004–004. ISSN: 1475-7516. DOI: 10.1088/1475-7516/2014/03/004. arXiv: 1312.5301.

[930] Maria Archidiacono, Steen Hannestad and Julien Lesgourgues. "What Will It Take to Measure Individual Neutrino Mass States Using Cosmology?" In: *Journal of Cosmology and Astroparticle Physics* 2020.09 (10th Sept. 2020), pp. 021–021. ISSN: 1475-7516. DOI: 10.1088/1475-7516/2020/09/021. arXiv: 2003.03354.

[931] Planck Collaboration et al. "Planck 2018 Results. VIII. Gravitational Lensing". In: *Astronomy & Astrophysics* 641 (Sept. 2020), A8. ISSN: 0004-6361, 1432-0746. DOI: 10.1051/0004-6361/201833886. arXiv: 1807.06210.

[932] Michael Blomqvist et al. "Baryon Acoustic Oscillations from the Cross-Correlation of Ly α Absorption and Quasars in eBOSS DR14". In: *Astronomy & Astrophysics* 629 (Sept. 2019), A86. ISSN: 0004-6361, 1432-0746. DOI: 10.1051/0004-6361/201935641. arXiv: 1904.03430.

[933] Andrei Cuceu, James Farr, Pablo Lemos and Andreu Font-Ribera. "Baryon Acoustic Oscillations and the Hubble Constant: Past, Present and Future". In: *Journal of Cosmology and Astroparticle Physics* 2019.10 (17th Oct. 2019), pp. 044–044. ISSN: 1475-7516. DOI: 10.1088/1475-7516/2019/10/044. arXiv: 1906.11628.

[934] Victoria de Sainte Agathe et al. "Baryon Acoustic Oscillations at z = 2.34 from the Correlations of Ly α Absorption in eBOSS DR14". In: *Astronomy & Astrophysics* 629 (Sept. 2019), A85. ISSN: 0004-6361, 1432-0746. DOI: 10.1051/0004-6361/201935638. arXiv: 1904.03400.

[935] Riccardo Murgia et al. ""Non-cold" Dark Matter at Small Scales: A General Approach". In: *Journal of Cosmology and Astroparticle Physics* 2017.11 (24th Nov. 2017), pp. 046–046. ISSN: 1475-7516. DOI: 10.1088/1475-7516/2017/11/046. arXiv: 1704.07838.

[936] James A. D. Diacoumis and Yvonne Y. Y. Wong. "Prior Dependence of Cosmological Constraints on Dark Matter-Radiation Interactions". In: *Journal of Cosmology and Astroparticle Physics* 2019.05 (16th May 2019), pp. 025–025. ISSN: 1475-7516. DOI: 10.1088/1475-7516/2019/05/025. arXiv: 1811.11408.

[937] A. Amon et al. "Dark Energy Survey Year 3 Results: Cosmology from Cosmic Shear and Robustness to Data Calibration". In: *Physical Review D* 105.2 (13th Jan. 2022), p. 023514. ISSN: 2470-0010, 2470-0029. DOI: 10.1103/PhysRevD.105.023514. arXiv: 2105.13543 [astro-ph].

[938] DES Collaboration et al. "Dark Energy Survey Year 3 Results: A 2.7% Measurement of Baryon Acoustic Oscillation Distance Scale at Redshift 0.835". In: *Physical Review D* 105.4 (8th Feb. 2022), p. 043512. ISSN: 2470-0010, 2470-0029. DOI: 10.1103/PhysRevD.105.043512. arXiv: 2107.04646 [astro-ph].

[939] P. J. E. Peebles and Bharat Ratra. "The Cosmological Constant and Dark Energy". In: *Reviews of Modern Physics* 75.2 (22nd Apr. 2003), pp. 559–606. ISSN: 0034-6861, 1539-0756. DOI: 10.1103/RevModPhys.75.559. arXiv: astro-ph/0207347.

[940] Edmund J. Copeland, M. Sami and Shinji Tsujikawa. "Dynamics of Dark Energy". In: *International Journal of Modern Physics D* 15.11 (Nov. 2006), pp. 1753–1935. ISSN: 0218-2718, 1793-6594. DOI: 10.1142/S021827180600942X. arXiv: hep-th/0603057.

[941] Joshua Frieman, Michael Turner and Dragan Huterer. "Dark Energy and the Accelerating Universe". In: *Annual Review of Astronomy and Astrophysics* 46.1 (1st Sept. 2008), pp. 385–432. ISSN: 0066-4146, 1545-4282. DOI: 10.1146/annurev.astro.46.060407.145243. arXiv: 0803.0982 [astro-ph, physics:gr-qc, physics:hep-ph, physics:hep-th].

[942] Laura Lopez-Honorez, Olga Mena and Pablo Villanueva-Domingo. "Dark Matter Microphysics and 21 Cm Observations". In: *Physical Review D* 99.2 (22nd Jan. 2019), p. 023522. ISSN: 2470-0010, 2470-0029. DOI: 10.1103/PhysRevD.99.023522. arXiv: 1811.02716 [astro-ph].

[943] Deanna C. Hooper and Matteo Lucca. "Hints of Dark Matter-Neutrino Interactions in Lyman-\ensuremath\alpha Data". In: *Physical Review D* 105.10 (5th May 2022), p. 103504. ISSN: 2470-0010, 2470-0029. DOI: 10.1103/PhysRevD.105.103504. arXiv: 2110.04024.

[944] Raul A. Monsalve, Alan E. E. Rogers, Judd D. Bowman and Thomas J. Mozdzen. "Results from EDGES High-Band: I. Constraints on Phenomenological Models for the Global 21 Cm Signal". In: *The Astrophysical Journal* 847.1 (21st Sept. 2017), p. 64. ISSN: 1538-4357. DOI: 10.3847/1538-4357/aa88d1. arXiv: 1708.05817 [astro-ph].

[945] Matias Zaldarriaga, Steven Furlanetto and Lars Hernquist. "21 Centimeter Fluctuations from Cosmic Gas at High Redshifts". In: *The Astrophysical Journal* 608.2 (20th June 2004), pp. 622–635. ISSN: 0004-637X, 1538-4357. DOI: 10.1086/386327. arXiv: astro-ph/0311514.

[946] Jonathan R. Pritchard and Abraham Loeb. "21-Cm Cosmology". In: *Reports on Progress in Physics* 75.8 (1st Aug. 2012), p. 086901. ISSN: 0034-4885, 1361-6633. DOI: 10.1088/0034-4885/75/8/086901. arXiv: 1109.6012.

[947] Stefano Camera, Mario G. Santos, Pedro G. Ferreira and Luis Ferramacho. "Cosmology on Ultralarge Scales with Intensity Mapping of the Neutral Hydrogen 21 Cm Emission: Limits on Primordial Non-Gaussianity". In: *Physical Review Letters* 111.17 (22nd Oct. 2013), p. 171302. ISSN: 0031-9007, 1079-7114. DOI: 10.1103/PhysRevLett.111.171302. arXiv: 1305.6928 [astro-ph].

[948] Philip Bull, Pedro G. Ferreira, Prina Patel and Mario G. Santos. "Late-Time Cosmology with 21cm Intensity Mapping Experiments". In: *The Astrophysical Journal* 803.1 (9th Apr. 2015), p. 21. ISSN: 1538-4357. DOI: 10.1088/0004-637X/803/1/21. arXiv: 1405.1452 [astro-ph].

[949] Aviad Cohen, Anastasia Fialkov, Rennan Barkana and Matan Lotem. "Charting the Parameter Space of the Global 21-Cm Signal". In: *Monthly Notices of the Royal Astronomical Society* 472.2 (Dec. 2017), pp. 1915–1931. ISSN: 0035-8711, 1365-2966. DOI: 10.1093/mnras/stx2065. arXiv: 1609.02312 [astro-ph].

[950] Sambit K. Giri and Aurel Schneider. "Imprints of Fermionic and Bosonic Mixed Dark Matter on the 21-Cm Signal at Cosmic Dawn". In: *Physical Review D* 105.8 (22nd Apr. 2022), p. 083011. ISSN: 2470-0010, 2470-0029. DOI: 10.1103/PhysRevD.105.083011. arXiv: 2201.02210 [astro-ph].

[951] Sean Fraser et al. "The EDGES 21 Cm Anomaly and Properties of Dark Matter". In: *Physics Letters B* 785 (Oct. 2018), pp. 159–164. ISSN: 03702693. DOI: 10.1016/j.physletb.2018.08.035. arXiv: 1803.03245 [astro-ph, physics:hep-ph].

[952] Francisco Villaescusa-Navarro, Matteo Viel, Kanan K. Datta and T. Roy Choudhury. "Modeling the Neutral Hydrogen Distribution in the Post-Reionization Universe: Intensity Mapping". In: *Journal of Cosmology and Astroparticle Physics* 2014.09 (30th Sept. 2014), pp. 050–050. ISSN: 1475-7516. DOI: 10.1088/1475-7516/2014/09/050. arXiv: 1405.6713 [astro-ph].

[953] R. Kannan et al. "Introducing the THESAN Project: Radiation-Magnetohydrodynamic Simulations of the Epoch of Reionization". In: *Monthly Notices of the Royal Astronomical Society* 511.3 (23rd Feb. 2022), pp. 4005–4030. ISSN: 0035-8711, 1365-2966. DOI: 10.1093/mnras/stab3710. arXiv: 2110.00584.

[954] Bradley Greig and Andrei Mesinger. "21CMMC with a 3D Light-Cone: The Impact of the Co-Evolution Approximation on the Astrophysics of Reionisation and Cosmic Dawn". In: *Monthly Notices of the Royal Astronomical Society* 477.3 (1st July 2018), pp. 3217–3229. ISSN: 0035-8711, 1365-2966. DOI: 10.1093/mnras/sty796. arXiv: 1801.01592.

[955] Bradley Greig and Andrei Mesinger. "21CMMC: An MCMC Analysis Tool Enabling Astrophysical Parameter Studies of the Cosmic 21 Cm Signal". In: *Monthly Notices of the Royal Astronomical Society* 449.4 (1st June 2015), pp. 4246–4263. ISSN: 0035-8711, 1365-2966. DOI: 10.1093/mnras/stv571. arXiv: 1501.06576.

[956] Bradley Greig and Andrei Mesinger. "Simultaneously Constraining the Astrophysics of Reionisation and the Epoch of Heating with 21CMMC". In: *Proceedings of the International Astronomical Union* 12.S333 (Oct. 2017), pp. 18–21. ISSN: 1743-9213, 1743-9221. DOI: 10.1017/S1743921317011103. arXiv: 1705.03471.

[957] Andrei Mesinger, Steven Furlanetto and Renyue Cen. "21cmFAST: A Fast, Semi-Numerical Simulation of the High-Redshift 21-Cm Signal". In: *Monthly Notices of the Royal Astronomical Society* 411.2 (21st Feb. 2011), pp. 955–972. ISSN: 00358711. DOI: 10.1111/j.1365-2966.2010.17731.x. arXiv: 1003.3878.

[958] Julian B. Muñoz. "Robust Velocity-induced Acoustic Oscillations at Cosmic Dawn". In: *Physical Review D* 100.6 (26th Sept. 2019), p. 063538. ISSN: 2470-0010, 2470-0029. DOI: 10.1103/PhysRevD.100.063538. arXiv: 1904.07881.

[959] Julian B. Muñoz. "A Standard Ruler at Cosmic Dawn". In: *Physical Review Letters* 123.13 (26th Sept. 2019), p. 131301. ISSN: 0031-9007, 1079-7114. DOI: 10.1103/PhysRevLett.123.131301. arXiv: 1904.07868.

[960] Andrei Mesinger and Steven Furlanetto. "Efficient Simulations of Early Structure Formation and Reionization". In: *The Astrophysical Journal* 669.2 (10th Nov. 2007), pp. 663–675. ISSN: 0004-637X, 1538-4357. DOI: 10.1086/521806. arXiv: 0704.0946.

[961] Julian B. Muñoz, Cora Dvorkin and Francis Yan Cyr-Racine. "Probing the Small-Scale Matter Power Spectrum with Large-Scale 21-Cm Data". In: *Physical Review D* 101.6 (24th Mar. 2020), p. 063526. ISSN: 2470-0010, 2470-0029. DOI: 10.1103/PhysRevD.101.063526. arXiv: 1911.11144.

[962] V. Avila-Reese et al. "Formation and Structure of Halos in a Warm Dark Matter Cosmology". In: *The Astrophysical Journal* 559.2 (Oct. 2001), pp. 516–530. ISSN: 0004-637X, 1538-4357. DOI: 10.1086/322411. arXiv: astro-ph/0010525.

[963] Francisco Villaescusa-Navarro and Neal Dalal. "Cores and Cusps in Warm Dark Matter Halos". In: *Journal of Cosmology and Astroparticle Physics* 2011.03 (14th Mar. 2011), pp. 024–024. ISSN: 1475-7516. DOI: 10.1088/1475-7516/2011/03/024. arXiv: 1010.3008.

[964] Antara Dey, Arnab Paul and Supratik Pal. *Constraints on Dark Matter-Neutrino Interaction from 21-Cm Cosmology and Forecasts on SKA1-Low*. 6th July 2022. arXiv: 2207.02451 [astro-ph, physics:hep-ph]. URL: http://arxiv.org/abs/2207.02451 (visited on 25/04/2023). preprint.

[965] Liana Rauf, Cullan Howlett, Tamara M. Davis and Claudia D. P. Lagos. *Exploring Binary Black Hole Mergers and Host Galaxies with {\sc Shark and COMPAS*. 16th Feb. 2023. arXiv: 2302.08172 [astro-ph]. URL: http://arxiv.org/abs/2302.08172 (visited on 05/04/2023). preprint.

[966] Philip Bull et al. "Beyond ΛCDM: Problems, Solutions, and the Road Ahead". In: *Physics of the Dark Universe* 12 (June 2016), pp. 56–99. ISSN: 22126864. DOI: 10.1016/j.dark.2016.02.001. arXiv: 1512.05356 [astro-ph, physics:gr-qc, physics:hep-ph, physics:hep-th].

[967] Sukanya Chakrabarti et al. "Snowmass2021 Cosmic Frontier White Paper: Observational Facilities to Study Dark Matter". In: *2022 Snowmass Summer Study*. arXiv, 11th Mar. 2022. arXiv: 2203.06200 [astro-ph, physics:hep-ex, physics:hep-ph]. URL: http://arxiv.org/abs/2203.06200 (visited on 25/04/2023).

[968] Eric Armengaud et al. "Constraining the Mass of Light Bosonic Dark Matter Using SDSS Lyman-α Forest". In: *Monthly Notices of the Royal Astronomical Society* 471 (1st Nov. 2017), pp. 4606–4614. ISSN: 0035-8711. DOI: 10.1093/mnras/stx1870. arXiv: 1703.09126.

[969] Vid Iršič et al. "First Constraints on Fuzzy Dark Matter from Lyman-α Forest Data and Hydrodynamical Simulations". In: *Physical Review Letters* 119 (1st July 2017), p. 031302. ISSN: 0031-9007. DOI: 10.1103/PhysRevLett.119.031302. arXiv: 1703.04683.

[970] Adam Lidz and Lam Hui. "Implications of a Prereionization 21-Cm Absorption Signal for Fuzzy Dark Matter". In: *Physical Review D* 98 (1st July 2018), p. 023011. ISSN: 1550-79980556-2821. DOI: 10.1103/PhysRevD.98.023011. arXiv: 1805.01253.

[971] The LIGO Scientific Collaboration. "Advanced LIGO". In: *Classical and Quantum Gravity* 32.7 (9th Apr. 2015), p. 074001. ISSN: 0264-9381, 1361-6382. DOI: 10.1088/0264-9381/32/7/074001. arXiv: 1411.4547 [astro-ph, physics:gr-qc, physics:physics].

[972] F. Acernese et al. "Advanced Virgo: A Second-Generation Interferometric Gravitational Wave Detector". In: *Classical and Quantum Gravity* 32.2 (22nd Jan. 2015), p. 024001. ISSN: 0264-9381, 1361-6382. DOI: 10.1088/0264-9381/32/2/024001. arXiv: 1408.3978 [gr-qc, physics:physics].

[973] M Punturo et al. "The Einstein Telescope: A Third-Generation Gravitational Wave Observatory". In: *Classical and Quantum Gravity* 27.19 (7th Oct. 2010), p. 194002. ISSN: 0264-9381, 1361-6382. DOI: 10.1088/0264-9381/27/19/194002.

[974] David Reitze et al. "Cosmic Explorer: The U.S. Contribution to Gravitational-Wave Astronomy beyond LIGO". In: *Bulletin of the American Astronomical Society* 51.7 (Sept. 2019), p. 035. DOI: 10.48550/arXiv.1907.04833. arXiv: 1907.04833 [astro-ph, physics:gr-qc].

[975] T. Regimbau et al. "Digging Deeper: Observing Primordial Gravitational Waves below the Binary Black Hole Produced Stochastic Background". In: *Physical Review Letters* 118.15 (14th Apr. 2017), p. 151105. ISSN: 0031-9007, 1079-7114. DOI: 10.1103/PhysRevLett.118.151105. arXiv: 1611.08943 [astro-ph, physics:gr-qc].

[976] Daniel Grin, David J. E. Marsh and Renee Hlozek. *axionCAMB: Modification of the CAMB Boltzmann Code*. Mar. 2022.

[977] Jeff Riley et al. "Chemically Homogeneous Evolution: A Rapid Population Synthesis Approach". In: *Monthly Notices of the Royal Astronomical Society* 505.1 (28th May 2021), pp. 663–676. ISSN: 0035-8711, 1365-2966. DOI: 10.1093/mnras/stab1291. arXiv: 2010.00002 [astro-ph].

[978] Simon Stevenson et al. "Formation of the First Three Gravitational-Wave Observations through Isolated Binary Evolution". In: *Nature Communications* 8.1 (5th Apr. 2017), p. 14906. ISSN: 2041-1723. DOI: 10.1038/ncomms14906. arXiv: 1704.01352 [astro-ph, physics:gr-qc].

[979] Alejandro Vigna-Gómez et al. "On the Formation History of Galactic Double Neutron Stars". In: *Monthly Notices of the Royal Astronomical Society* 481.3 (1st Dec. 2018), pp. 4009–4029. ISSN: 0035-8711, 1365-2966. DOI: 10.1093/mnras/sty2463. arXiv: 1805.07974 [astro-ph].

[980] Mattias Blennow et al. "Asymmetric Dark Matter and Dark Radiation". In: *Journal of Cosmology and Astroparticle Physics* 2012.07 (10th July 2012), pp. 022–022. ISSN: 1475-7516. DOI: 10.1088/1475-7516/2012/07/022. arXiv: 1203.5803 [astro-ph, physics:hep-ph].

[981] Daniel Gilman et al. "Warm Dark Matter Chills out: Constraints on the Halo Mass Function and the Free-Streaming Length of Dark Matter with Eight Quadruple-Image Strong Gravitational Lenses". In: *Monthly Notices of the Royal Astronomical Society* 491 (1st Feb. 2020), pp. 6077–6101. ISSN: 0035-8711. DOI: 10.1093/mnras/stz3480. arXiv: 1908.06983.

[982] Nathalie Palanque-Delabrouille et al. "Hints, Neutrino Bounds, and WDM Constraints from SDSS DR14 Lyman-α and Planck Full-Survey Data". In: *Journal of Cosmology and Astroparticle Physics* 2020 (1st Apr. 2020), p. 038. ISSN: 1475-7516. DOI: 10.1088/1475-7516/2020/04/038. arXiv: 1911.09073.

[983] P. Norberg et al. "The 2dF Galaxy Redshift Survey: The B(J)-Band Galaxy Luminosity Function and Survey Selection Function". In: *Monthly Notices of the Royal Astronomical Society* 336.3 (1st Nov. 2002), pp. 907–931. ISSN: 0035-8711, 1365-2966. DOI: 10.1046/j.1365-8711.2002.05831.x. arXiv: astro-ph/0111011.

[984] S. P. Driver et al. "Galaxy And Mass Assembly (GAMA): The $0.013 < z < 0.1$ Cosmic Spectral Energy Distribution from 0.1 Micron to 1mm". In: *Monthly Notices of the Royal Astronomical Society* 427.4 (21st Dec. 2012), pp. 3244–3264. ISSN: 0035-8711, 1365-2966. DOI: 10.1111/j.1365-2966.2012.22036.x. arXiv: 1209.0259 [astro-ph].

[985] Alejandro Benitez-Llambay and Carlos Frenk. "The Detailed Structure and the Onset of Galaxy Formation in Low-Mass Gaseous Dark Matter Haloes". In: *Monthly Notices of the Royal Astronomical Society* 498.4 (29th Sept. 2020), pp. 4887–4900. ISSN: 0035-8711, 1365-2966. DOI: 10.1093/mnras/staa2698. arXiv: 2004.06124 [astro-ph].

[986] Oliver Hahn and Raul E. Angulo. "An Adaptively Refined Phase-Space Element Method for Cosmological Simulations and Collisionless Dynamics". In: *Monthly Notices of the Royal Astronomical Society* 455.1 (1st Jan. 2016), pp. 1115–1133. ISSN: 1365-2966, 0035-8711. DOI: 10.1093/mnras/stv2304. arXiv: 1501.01959 [astro-ph].

[987] Mark R. Lovell. "Towards a General Parametrization of the Warm Dark Matter Halo Mass Function". In: *The Astrophysical Journal* 897.2 (13th July 2020), p. 147. ISSN: 1538-4357. DOI: 10.3847/1538-4357/ab982a. arXiv: 2003.01125.

[988] Ilya Mandel and Alison Farmer. "Merging Stellar-Mass Binary Black Holes". In: *Physics Reports* 955 (Apr. 2022), pp. 1–24. ISSN: 03701573. DOI: 10.1016/j.physrep.2022.01.003. arXiv: 1806.05820 [astro-ph, physics:gr-qc].

[989] Jeff Riley et al. *Chemically Homogeneous Evolution: A Rapid Population Synthesis Approach*. 1st July 2021. DOI: 10.5281/zenodo.5595426.

[990] Coenraad J. Neijssel et al. "The Effect of the Metallicity-Specific Star Formation History on Double Compact Object Mergers". In: *Monthly Notices of the Royal Astronomical Society* 490.3 (11th Dec. 2019), pp. 3740–3759. ISSN: 0035-8711, 1365-2966. DOI: 10.1093/mnras/stz2840. arXiv: 1906.08136 [astro-ph].

[991] The LIGO Scientific Collaboration et al. *The Population of Merging Compact Binaries Inferred Using Gravitational Waves through GWTC-3*. 23rd Feb. 2022. DOI: 10.48550/arXiv.2111.03634. arXiv: 2111.03634. URL: http://arxiv.org/abs/2111.03634 (visited on 25/04/2023). preprint.

[992] LIGO Scientific Collaboration et al. "Predictions for the Rates of Compact Binary Coalescences Observable by Ground-based Gravitational-wave Detectors". In: *Classical and Quantum Gravity* 27.17 (7th Sept. 2010), p. 173001. ISSN: 0264-9381, 1361-6382. DOI: 10.1088/0264-9381/27/17/173001. arXiv: 1003.2480 [astro-ph, physics:gr-qc].

[993] Ryan O'Leary, Richard O'Shaughnessy and Frederic Rasio. "Dynamical Interactions and the Black Hole Merger Rate of the Universe". In: *Physical Review D* 76.6 (27th Sept. 2007), p. 061504. ISSN: 1550-7998, 1550-2368. DOI: 10.1103/PhysRevD.76.061504. arXiv: astro-ph/0701887.

[994] M. Coleman Miller and Vanessa M. Lauburg. "Mergers of Stellar-Mass Black Holes in Nuclear Star Clusters". In: *The Astrophysical Journal* 692.1 (10th Feb. 2009), pp. 917–923. ISSN: 0004-637X, 1538-4357. DOI: 10.1088/0004-637X/692/1/917. arXiv: 0804.2783 [astro-ph].

[995] B. McKernan et al. "Constraining Stellar-mass Black Hole Mergers in AGN Disks Detectable with LIGO". In: *The Astrophysical Journal* 866.1 (15th Oct. 2018), p. 66. ISSN: 1538-4357. DOI: 10.3847/1538-4357/aadae5. arXiv: 1702.07818 [astro-ph, physics:gr-qc].

[996] Carl L. Rodriguez and Abraham Loeb. "Redshift Evolution of the Black Hole Merger Rate from Globular Clusters". In: *The Astrophysical Journal* 866.1 (4th Oct. 2018), p. L5. ISSN: 2041-8213. DOI: 10.3847/2041-8213/aae377. arXiv: 1809.01152 [astro-ph].

[997] Carl L. Rodriguez, Pau Amaro-Seoane, Sourav Chatterjee and Frederic A. Rasio. "Post-Newtonian Dynamics in Dense Star Clusters: Highly-Eccentric, Highly-Spinning, and Repeated Binary Black Hole Mergers". In: *Physical Review D* 98.12 (10th Dec. 2018), p. 123005. ISSN: 2470-0010, 2470-0029. DOI: 10.1103/PhysRevD.98.123005. arXiv: 1712.04937 [astro-ph, physics:gr-qc].

[998] Kareem El-Badry et al. "The Formation and Hierarchical Assembly of Globular Cluster Populations". In: *Monthly Notices of the Royal Astronomical Society* 482.4 (1st Feb. 2019), pp. 4528–4552. ISSN: 0035-8711, 1365-2966. DOI: 10.1093/mnras/sty3007. arXiv: 1805.03652 [astro-ph].

[999] L. Y. Aaron Yung et al. "Semi-Analytic Forecasts for JWST - I. UV Luminosity Functions at z = 4 - 10". In: *Monthly Notices of the Royal Astronomical Society* 483.3 (1st Mar. 2019), pp. 2983–3006. ISSN: 0035-8711, 1365-2966. DOI: 10.1093/mnras/sty3241. arXiv: 1803.09761 [astro-ph].

[1000] Diana Khimey, Sownak Bose and Sandro Tacchella. "Degeneracies between Baryons and Dark Matter: The Challenge of Constraining the Nature of Dark Matter with JWST". In: *Monthly Notices of the Royal Astronomical Society* 506.3 (31st July 2021), pp. 4139–4150. ISSN: 0035-8711, 1365-2966. DOI: 10.1093/mnras/stab2019. arXiv: 2010.10520 [astro-ph].

[1001] Matteo Martinelli et al. "Dancing in the Dark: Detecting a Population of Distant Primordial Black Holes". In: *Journal of Cosmology and Astroparticle Physics* 2022.08 (1st Aug. 2022), p. 006. ISSN: 1475-7516. DOI: 10.1088/1475-7516/2022/08/006. arXiv: 2205.02639 [astro-ph, physics:gr-qc, physics:hep-th].

[1002] Michele Maggiore et al. "Science Case for the Einstein Telescope". In: *Journal of Cosmology and Astroparticle Physics* 2020.03 (24th Mar. 2020), pp. 050–050. ISSN: 1475-7516. DOI: 10.1088/1475-7516/2020/03/050. arXiv: 1912.02622 [astro-ph, physics:gr-qc].

[1003] Matthew Evans et al. *A Horizon Study for Cosmic Explorer: Science, Observatories, and Community*. 6th Oct. 2021. arXiv: 2109.09882 [astro-ph, physics:gr-qc]. URL: http://arxiv.org/abs/2109.09882 (visited on 25/04/2023). preprint.

[1004] P. Ajith et al. "Template Bank for Gravitational Waveforms from Coalescing Binary Black Holes: Nonspinning Binaries". In: *Physical Review D* 77.10 (14th May 2008), p. 104017. DOI: 10.1103/PhysRevD.77.104017. arXiv: 0710.2335.

[1005] The LIGO Scientific Collaboration et al. "Population Properties of Compact Objects from the Second LIGO-Virgo Gravitational-Wave Transient Catalog". In: *The Astrophysical Journal Letters* 913.1 (1st May 2021), p. L7. ISSN: 2041-8205, 2041-8213. DOI: 10.3847/2041-8213/abe949. arXiv: 2010.14533.

[1006] Floor S. Broekgaarden et al. "Impact of Massive Binary Star and Cosmic Evolution on Gravitational Wave Observations II: Double Compact Object Rates and Properties". In: *Monthly Notices of the Royal Astronomical Society* 516.4 (3rd Oct. 2022), pp. 5737–5761. ISSN: 0035-8711, 1365-2966. DOI: 10.1093/mnras/stac1677. arXiv: 2112.05763 [astro-ph].

[1007] Floor Broekgaarden. *BHBH Simulations from: Impact of Massive Binary Star and Cosmic Evolution on Gravitational Wave Observations II: Double Compact Object Mergers*. Version 1. 6th Nov. 2021. DOI: 10.5281/ZENODO.5651073.

[1008] Jun Hou, Carlos S. Frenk, Cedric G. Lacey and Sownak Bose. "Constraining SN Feedback: A Tug of War between Reionization and the Milky Way Satellites". In: *Monthly Notices of the Royal Astronomical Society* 463.2 (1st Dec. 2016), pp. 1224–1239. ISSN: 0035-8711, 1365-2966. DOI: 10.1093/mnras/stw2033. arXiv: 1512.04595 [astro-ph].

[1009] William Cowley et al. "Predictions for Deep Galaxy Surveys with JWST from ΛCDM". In: *Monthly Notices of the Royal Astronomical Society* 474.2 (21st Feb. 2018), pp. 2352–2372. ISSN: 0035-8711, 1365-2966. DOI: 10.1093/mnras/stx2897. arXiv: 1702.02146 [astro-ph].

[1010] William I. Cowley et al. "The Evolution of the UV-to-mm Extragalactic Background Light: Evidence for a Top-Heavy Initial Mass Function?" In: *Monthly Notices of the Royal Astronomical Society* 487.3 (11th Aug. 2019), pp. 3082–3101. ISSN: 0035-8711, 1365-2966. DOI: 10.1093/mnras/stz1398. arXiv: 1808.05208 [astro-ph].

[1011] Michael J. Baker and Andrea Thamm. "Probing the Particle Spectrum of Nature with Evaporating Black Holes". In: *SciPost Physics* 12.5 (9th May 2022), p. 150. ISSN: 2542-4653. DOI: 10.21468/SciPostPhys.12.5.150. arXiv: 2105.10506 [astro-ph, physics:hep-ph].

[1012] Bernard J. Carr and S.W. Hawking. "Black Holes in the Early Universe". In: *Monthly Notices of the Royal Astronomical Society* 168 (1974), pp. 399–415.

[1013] Kailash C. Sahu et al. "An Isolated Stellar-Mass Black Hole Detected Through Astrometric Microlensing". In: *The Astrophysical Journal* 933.1 (1st July 2022), p. 83. ISSN: 0004-637X, 1538-4357. DOI: 10.3847/1538-4357/ac739e. arXiv: 2201.13296 [astro-ph].

[1014] Bernard Carr, Sebastien Clesse, Juan Garcia-Bellido and Florian Kuhnel. "Cosmic Conundra Explained by Thermal History and Primordial Black Holes". In: *Physics of the Dark Universe* 31 (Jan. 2021), p. 100755. ISSN: 22126864. DOI: 10.1016/j.dark.2020.100755. arXiv: 1906.08217 [astro-ph, physics:gr-qc, physics:hep-ph, physics:hep-th].

[1015] William DeRocco and Peter W. Graham. "Constraining Primordial Black Hole Abundance with the Galactic 511 keV Line". In: *Physical Review Letters* 123.25 (16th Dec. 2019), p. 251102. ISSN: 0031-9007, 1079-7114. DOI: 10.1103/PhysRevLett.123.251102. arXiv: 1906.07740 [astro-ph, physics:hep-ph].

[1016] Jane H. MacGibbon, B. J. Carr and Don N. Page. "Do Evaporating Black Holes Form Photospheres?" In: *Physical Review D* 78.6 (15th Sept. 2008), p. 064043. ISSN: 1550-7998, 1550-2368. DOI: 10.1103/PhysRevD.78.064043. arXiv: 0709.2380 [astro-ph, physics:gr-qc, physics:hep-th].

[1017] Alexandre Arbey and Jérémy Auffinger. "Physics Beyond the Standard Model with BlackHawk v2.0". In: *The European Physical Journal C* 81.10 (Oct. 2021), p. 910. ISSN: 1434-6044, 1434-6052. DOI: 10.1140/epjc/s10052-021-09702-8. arXiv: 2108.02737.

[1018] H. E. S. S. collaboration et al. "Acceleration of Petaelectronvolt Protons in the Galactic Centre". In: *Nature* 531.7595 (24th Mar. 2016), pp. 476–479. ISSN: 0028-0836, 1476-4687. DOI: 10.1038/nature17147. arXiv: 1603.07730 [astro-ph].

[1019] Oscar Macias and Chris Gordon. "The Contribution of Cosmic Rays Interacting With Molecular Clouds to the Galactic Center Gamma-Ray Excess". In: *Physical Review D* 89.6 (11th Mar. 2014), p. 063515. ISSN: 1550-7998, 1550-2368. DOI: 10.1103/PhysRevD.89.063515. arXiv: 1312.6671 [astro-ph, physics:hep-ph].

[1020] Thomas Lacroix et al. "Spatial Morphology of the Secondary Emission in the Galactic Center Gamma-Ray Excess". In: *Physical Review D* 93.10 (20th May 2016), p. 103004. ISSN: 2470-0010, 2470-0029. DOI: 10.1103/PhysRevD.93.103004. arXiv: 1512.01846.

[1021] T. N. Ukwatta et al. "Primordial Black Holes: Observational Characteristics of The Final Evaporation". In: *Astroparticle Physics* 80 (July 2016), pp. 90–114. ISSN: 09276505. DOI: 10.1016/j.astropartphys.2016.03.007. arXiv: 1510.04372 [astro-ph].

[1022] Misao Sasaki, Teruaki Suyama, Takahiro Tanaka and Shuichiro Yokoyama. "Primordial Black Hole Scenario for the Gravitational-Wave Event GW150914". In: *Physical Review Letters* 117.6 (2nd Aug. 2016), p. 061101. ISSN: 0031-9007, 1079-7114. DOI: 10.1103/PhysRevLett.117.061101. arXiv: 1603.08338 [astro-ph, physics:gr-qc].

[1023] Pisin Chen, Yen Chin Ong and Dong-han Yeom. "Black Hole Remnants and the Information Loss Paradox". In: *Physics Reports* 603 (Nov. 2015), pp. 1–45. ISSN: 03701573. DOI: 10.1016/j.physrep.2015.10.007. arXiv: 1412.8366 [gr-qc, physics:hep-th].

[1024] Thomas Tavernier et al. "Limits on Primordial Black Hole Evaporation from H.E.S.S. Observations." In: *Proceedings of 37th International Cosmic Ray Conference — PoS(ICRC2021)*. 37th International Cosmic Ray Conference. Berlin, Germany - Online: Sissa Medialab, 8th July 2021, p. 518. DOI: 10.22323/1.395.0518. URL: https://pos.sissa.it/395/518 (visited on 25/04/2023).

[1025] Thomas Tavernier, Jean-Francois Glicenstein, Francois Brun and H.E.S.S. collaboration. "Search for Primordial Black Hole Evaporations with H.E.S.S." In: *Proceedings of 36th International Cosmic Ray Conference — PoS(ICRC2019)*. 36th International Cosmic Ray Conference. Madison, WI, U.S.A.: Sissa Medialab, 22nd July 2019, p. 804. DOI: 10.22323/1.358.0804. arXiv: 1909.01620 [astro-ph]. URL: http://arxiv.org/abs/1909.01620 (visited on 25/04/2023).

[1026] A. Albert et al. "Constraining the Local Burst Rate Density of Primordial Black Holes with HAWC". In: *Journal of Cosmology and Astroparticle Physics* 2020.04 (17th Apr. 2020), pp. 026–026. ISSN: 1475-7516. DOI: 10.1088/1475-7516/2020/04/026. arXiv: 1911.04356 [astro-ph, physics:hep-ex].

[1027] Bill Paxton et al. "Modules for Experiments in Stellar Astrophysics (MESA): Binaries, Pulsations, and Explosions". In: *The Astrophysical Journal Supplement Series* 220.1 (21st Sept. 2015), p. 15. ISSN: 1538-4365. DOI: 10.1088/0067-0049/220/1/15. arXiv: 1506.03146 [astro-ph].

[1028] H.-Thomas Janka, Tobias Melson and Alexander Summa. "Physics of Core-Collapse Supernovae in Three Dimensions: A Sneak Preview". In: *Annual Review of Nuclear and Particle Science* 66.1 (19th Oct. 2016), pp. 341–375. ISSN: 0163-8998, 1545-4134. DOI: 10.1146/annurev-nucl-102115-044747. arXiv: 1602.05576 [astro-ph, physics:hep-ph, physics:nucl-th].

[1029] Yi-Fu Cai, Chao Chen, Qianhang Ding and Yi Wang. *Cosmological Standard Timers from Unstable Primordial Relics*. 20th Dec. 2021. DOI: 10.48550/arXiv.2112.10422. arXiv: 2112.10422 [astro-ph, physics:gr-qc, physics:hep-ph, physics:hep-th]. URL: http://arxiv.org/abs/2112.10422. preprint.